

**GEOCHEMISTRY AND PETROGENESIS OF HIGH-MG
THOLEIITES AND LAMPROPHYRES IN THE VESTFOLD
HILLS, ANTARCTICA**

Hans - Michael Seitz

Dipl.- Geol. (TH Darmstadt)

Submitted in partial fulfilment of the requirements of the degree of Doctor of
Philosophy at the University of Tasmania

April 1991

This thesis contains no material which has been accepted for the award of any other degree or diploma in any University and, to the best of my knowledge and belief, contains no copy or paraphrase of material previously published or written by another person, except where due reference is made in the text of this thesis.

Hans -Michael Seitz

April, 1991

This thesis is dedicated to the memory of my father

Georg Friedrich Seitz

ACKNOWLEDGEMENTS

First I would like to thank my supervisor Professor David Green for initiating this project, for his support during my studies and for giving me the opportunity to visit Antarctica twice. A special thanks also to Dr. Gerhard Brey (Max-Planck Institut in Mainz), who encouraged me to go to Tasmania and for his support throughout my studies.

Thanks are also extended to the many people who have helped me during this project, especially:

- Dr. Russell Sweeney and Dr. Steven Eggins for fruitful discussions, support and encouragement, and for their most valuable friendships.

- Phil Robinson for his help with the XRF, Wieslaw Jablonski for his help with the electron microprobe, Simon Stephens for help in the lapidary laboratory, Penny Green for getting samples organized in the rock collection, Peter Cornish, Andrew Gillon and Vagn Jensen for help in the workshops at various times, June Pongratz, who gave me a lot of advice in drafting and computing, and to the invariably helpful secretaries Karyl Whelan, Jeanette Hankin and Christine Higgins.

- to various scientists for helpful discussions, including Dr. Christian Ballhaus, Dr. Simon Harley, Dr. Trevor Falloon, Dr. Joe Stolz, Dr. Wayne Taylor, Dr. Rick Varne, Dr. Tony Crawford, Dr. Garry Davidson, Dr. Bruce Gemmell, Dr. John Adam, Dr. Dave Huston, Dr. Ron Berry, Dr. Ross Large, and Dr. Reid Keays (University of Melbourne).

- to the graduate students of this department for their companionship, support and encouragement: Proto-Drs. Vanessa Guthrie and Richard Wedekind, to Sharon Adrichem, Ai Yang, Sjafra Dwipa, Khin Zaw, Ruth Lanyon, Geoff Nichols, Massimo Gasparon, Ingvar Sigurdson, Udi Hartono, Salman Palgunady, Anthea Hill, Micheal Roach, Greg Yaxley, Paul Kitto, Djojimherdjo Soetijoso, Memet Hermanto, Pol Choadumrong and Hannes Neugebauer with his helping hand on the 'LECO'.

- to various scientists, graduate students and 'normal' people who shared life with me in Antarctica, especially: Hans Hoek, Dr. Simon Harley, Dug Thost, Tubby Seton and Charly Wright.

I would also like to extend my general thanks to so many people in Tasmania who made my wife Sabine and I feel so much at home in Hobart and who made us learn English really quickly, special thanks to:

- Jenny & Cliff Edwards for 'adopting' us in their family
- Wendy, Sybil, Drew and Kirsty Edwards for a terrific friendship
- Louise Wright for her friendship and for being best 'first mate' on my 'huge' yacht 'Lotte'
- George Wilson for being a fantastic landlord (world's number one)
- Liz Frankham and her family
- Nigel Crocker, Simon Patterson and Ekkehard Steinbrink and many other musicians for sharing the world of music with me.
- Michael Tame for all his cooking and Mark Cutler for introducing us to backyard cricket.

Last not least I like to thank my mother for her support and my wife, Sabine for her love and care and for her help to finish this thesis in time.

Volley when you have to, volley when you must

Mark Cutler (1988)

CONTENTS

	<i>Page</i>
ACKNOWLEDGEMENTS	iv
LIST OF FIGURES	xiii
LIST OF TABLES	xvii
ABSTRACT	ixx

CHAPTER 1

GEOLOGICAL HISTORY OF THE VESTFOLD HILLS

1.1	INTRODUCTION	1
1.2	REGIONAL GEOLOGY OF THE VESTFOLD HILLS	3
1.2.1	Crustal Evolution	3
1.2.2	Deformation and Uplift History	6
1.2.3	Magmatic Episodes	7
1.3	EARLY TO MIDDLE PROTEROZOIC MAFIC DYKES - THEIR RELATIVE TIME OF EMPLACEMENT	10
1.3.1	Introduction	10
1.3.2	Identification of Dyke Suites and their Emplacement Sequence	10
1.4	MAFIC DYKES AND THEIR CLASSIFICATION	14
1.4.1	The 2350 Ma High-Mg Tholeiites	13
1.4.1	The 2350, 1800 and 1350 Ma Fe-rich Tholeiites	13
1.4.3	Lamprophyres	15
1.5	AIM OF STUDY	16

CHAPTER 2

ESTIMATION OF EMPLACEMENT PRESSURE FOR THE 2350 MA HIGH-MG THOLEIITIC SUITE

2.	INTRODUCTION	17
2.2	GEOBAROMETRY BASED ON ALUMINIUM EXCHANGE BETWEEN CLINOPYROXENE AND PLAGIOCLASE	18
2.2.1	Geobarometer	18
2.2.2	Application to Natural Assemblages	18
2.2.3	Dicussion	24
2.3	HIGH PRESSURE EXPERIMENTAL STUDIES OF LIQUIDUS PHASE FOR HIGH-MG THOLEIITE MAGMAS	25
2.3.1	Introduction	25
2.3.2	Discussion	
2.4	PRESSURE ESTIMATIONS USING ARGUMENTS OF MAGMATIC EVOLUTION AT VARIOUS PRESSURES	27
2.5	SUMMARY	31

CHAPTER 3

PETROGRAPHIC AND GEOCHEMICAL VARIATIONS IN A HIGH-MG THOLEIITIC DYKE WITH RESPECT TO CRUSTAL CONTAMINATION DURING ASCENT AND DIFFERENTIATION PROCESSES FOLLOWING EMPLACEMENT

3.1	INTRODUCTION	34
3.2	FIELD OBSERVATIONS	36
3.3	PETROGRAPHY AND MINERAL CHEMISTRY	37
3.4	MAJOR AND TRACE ELEMENT GEOCHEMISTRY	42
3.5	THE ROLE OF CRUSTAL ASSIMILATION IN PRODUCING GEOCHEMICAL VARIATIONS	51
3.6	CONCLUSIONS	55

CHAPTER 4

NORITIC RING COMPLEX

4.1	INTRODUCTION	60
4.2	PETROGRAPHY AND MINERAL CHEMISTRY	64
4.2.1	Homogeneous Norite	64
4.2.2	Mottled Norite	66
4.2.3	Rubbly Norite	67
4.2.4	Pyroxenite Nodules	68
4.2.5	Fine Grained Dykes	69
4.2.6	Late Stage Segregations	72
4.3	RELATIVE TIME OF EMPLACEMENT	73
4.5	TEMPERATURE AND PRESSURE OF EMPLACEMENT	75
4.5	LAYERING	81
4.5.1	Introduction	81
4.5.2	Layer Orientation	84
4.5.3	Petrography and Mineral Chemistry	84
4.5.4	Layer Genesis	89
4.6	MAJOR AND MINOR ELEMENT GEOCHEMISTRY	93
4.8	SUMMARY	106

CHAPTER 5

BASE METAL SULPIDES AND PLATINUM GROUP MINERAL OCCURRENCES IN THE RUBBLY NORITE

5.1	INTRODUCTION	111
5.2	PETROGRAPHY AND MINERAL CHEMISTRY	112
5.3	PLATINUM GROUP ELEMENT ABUNDANCES IN ROCK UNITS	117
5.3.1	Introduction	117
5.3.2	Platinum Group Element Geochemistry	118
5.3.2.1	<i>PGE Abundances in Basaltic Melts</i>	118
5.3.2.2	<i>PGE Abundances in the Vestfold Hills High-Mg Tholeiites</i>	119

5.4	DISCUSSION	131
5.5	SUMMARY	136

CHAPTER 6

GEOCHEMISTRY AND PETROGENESIS OF HIGH-MG THOLEIITES: PRIMARY MAGMAS OR PRODUCTS OF CRUSTAL CONTAMINATION ?

6.1	INTRODUCTION	139
6.2	WHOLE ROCK GEOCHEMISTRY	141
6.2.1	Major and Trace Element Geochemistry	141
6.3	CHEMICAL VARIATION WITHIN THE HIGH-MG THOLEIITIC SUITE	149
6.4	CRYSTAL FRACTIONATION	151
6.4.1	Summary	155
6.5	CRUSTAL CONTAMINATION	158
6.5.1	Introduction	158
6.5.2	Assimilation-Fractional Crystallization Model	159
6.5.3	Choice of Assimilant	160
6.5.4	Modelling	163
6.5.5	Discussion	167
6.6	HIGH-MG THOLEIITES, PRIMARY MAGMAS ?	169
6.7	PARTIAL MELTING	172
6.7.1	Introduction	172
6.7.2	Partial Melting Modelling	174
6.7.3	Implications for Source Compositions	179
6.7	SUMMARY	180

CHAPTER 7

LAMPROPHYRE DYKES

7.1	INTRODUCTION	182
7.2	PETROGRAPHY AND MINERAL CHEMISTRY	183
7.3	GEOCHEMISTRY	189
7.4	PETROGENESIS	197
7.4.1	Crystal Fractionation	197
7.4.2	Mixing	197
7.4.3	Partial Melting	201
7.5	SUMMARY	205

CHAPTER 8

ULTRAMAFIC XENOLITHS

8.1	INTRODUCTION	210
8.2	XENOLITH EMPLACEMENT IN PIPELIKE - BODIES	211
8.3	PETROGRAPHY AND MINERAL CHEMISTRY	214
8.3.1	Mineral Compositions and their Variations between Xenoliths	217
8.3.2	A Comparison with Spinel in Mantle Xenoliths Elsewhere	220
8.4	GEO THERMOMETRY	222
8.5	DISCUSSION	226
8.6	CONCLUSIONS	227

CHAPTER 9

SUMMARY

9	CONCLUSIONS	233
---	-------------	-----

10 APPENDIX
ANALYTICAL TECHNIQUES AND DATA BASE

10.1	WHOLE ROCK CHEMICAL ANALYSES	238
10.2	WHOLE ROCK ANALYSES	241
10.3	SULPHUR ANALYSES	241
10.4	PLATINUM GROUP ELEMENT (PGE) ANALYSES	242
10.5	MICROPROBE ANALYSES	242
10.6	SAMPLE CATALOGUE	243
10.7	DYKE BASE MAPS	243
REFERENCES		286

LIST OF FIGURES

	<i>Page</i>
Figure 1.1	Aerial view of central Vestfold Hills 2
Figure 1.2	Location map of East Antarctica and the Vestfold Hills 4
Figure 1.3	PTt-paths of the Vestfold Hills block 8
Figure 1.4	Flow-chart showing dyke emplacement sequence 12
Figure 2.1	Across dyke pressure variations 19
Figure 2.2	Al ₂ O ₃ versus SiO ₂ , Al ₂ O ₃ versus CaO distinguishing between chilled margins and dyke interiors 23
Figure 2.3	Estimated liquid compositions projected onto the plane Jd+CaTs - Qtz - Ol 29
Figure 2.4	Uplift history of the Vestfold Hill block 32
Figure 3.1	Photographs of dyke margins 36
Figure 3.2	Photomicrographs of chilled high-Mg tholeiite 49
Figure 3.3	Lindsley's graphical thermometer applied to the phenocryst assemblages of high-Mg tholeiite 40
Figure 3.4 A	MgO versus Zr and Al ₂ O ₃ versus Zr 44
Figure 3.4 B	Oxides plotted against Zr 45
Figure 3.5	Trace elements plotted against Zr 50
Figure 3.6	Spiderplot of chilled margins and dyke interiors from high-Mg tholeiite 52
Figure 3.7	REE pattern for high-Mg tholeiite distinguishing between chilled margin and dyke interior samples 53
Figure 4.1	Photographs of various norites and layering 62
Figure 4.2	Photomicrographs of norite 66
Figure 4.3	Al ₂ O ₃ , CaO and TiO ₂ versus Mg# showing variation in orthopyroxene and clinopyroxene 70
Figure 4.4	Lindley's graphical thermometer applied to various norites and associated fine grained dykes 75
Figure 4.5	Schematic view of layer intersections 83
Figure 4.6	Rosedigram showing layer orientations 85
Figure 4.7	Mineral distribution in layered norite 86
Figure 4.8	Plagioclase composition from the layer and Homogeneous Norite plotted onto Na - Ca - K diagrams 88
Figure 4.9	Schematic view of layering in the Homogeneous Norite 92
Figure 4.10	Oxides plotted versus MgO 95
Figure 4.11	Norite compositions projected onto the plane Jd+CaTs - Qtz - Ol and Di - Ol - Qtz 96
Figure 4.12	Trace elements plotted versus Zr 99

Figure 4.13	Spiderplot showing various norite types and associated fine grained dykes	100
Figure 4.14	REE pattern for norites and fine grained dykes	101
Figure 4.15	Spiderplot showing fractional crystallization model	104
Figure 5.1	Photomicrographs of sulphides	114
Figure 5.2	Sulpharsenides plotted onto FeAsS - NiAsS - CoAsS	116
Figure 5.3	PGE concentrations in natural silicate liquids	120
Figure 5.4	PGE abundances in high-Mg tholeiites from the Vestfold Hills	121
Figure 5.5	Pt, Pd, Ru and Ir plotted versus S	123
Figure 5.6 A	Chondrite normalized PGE patterns	125
Figure 5.6 B	Chondrite normalized PGE patterns	126
Figure 5.7	Chondrite normalized PGE patterns	127
Figure 5.8	Pd/Ir versus Ni/Cu	129
Figure 5.9	Ni/Cu versus Cu/Pd	130
Figure 5.10	PGE and S behaviour during fractionation	133
Figure 6.1	High-Mg theoleiite compositions projected onto the plane Jd+CaTs - Qtz - Ol	143
Figure 6.2	Spiderplots of various high-Mg tholeiite groups	146
Figure 6.3	(Rb/Ba) _N versus (Sr/Nd) _N discriminating various high-Mg tholeiite groups	146
Figure 6.4	REE pattern for high-Mg tholeiite groups	147
Figure 6.5	Spiderplot of chilled margins and dyke interiors from high-Mg tholeiite	150
Figure 6.6	Rb/Sr versus Sr	152
Figure 6.7	High-Mg theoleiite compositions projected onto the plane Jd+CaTs - Qtz - Ol	152
Figure 6.8	Spiderplot showing results from fractional crystallization model	156
Figure 6.9	Trace element patterns of Archaen and Proterozoic crust in comparison with high-Mg tholeiites	161
Figure 6.10	Spiderplot showing results from assimilation and crystallization fractional model	164
Figure 6.11	Ni, Cr and Sr versus Zr	166
Figure 6.12	Al ₂ O ₃ /CaO, Cr and Ni plotted against Mg#	170
Figure 6.13	Spiderplots - coparison of calculated and observed trace element abundances	176
Figure 6.14	Spiderplots showing the results from partial melting model	177
Figure 7.1	Photomicrographs of lamprophyres	184
Figure 7.2	Carbonate compositions	185
Figure 7.3	Lindley's graphical thermometer applied to Lamprophyres	188
Figure 7.4	TAS diagram	190

Figure 7.5	Major elements plotted against SiO ₂	192
Figure 7.6	Trace elements plotted against Zr	193
Figure 7.7	SiO ₂ and Mg# versus Zr	194
Figure 7.8	REE pattern for high-Mg tholeiite groups	195
Figure 7.9	CaO versus Al ₂ O ₃	198
Figure 7.10	Ratio/ratio plots (K/La vs Ba/Rb, K/La vs La/Nb, Ba/Rb vs Ti/Y)	199
Figure 7.11	REE showing results from partial melting model	202
Figure 7.12	Ba/Nb versus La/Nb	206
Figure 8.1	Schematic view of xenoliths bearing pipe in lamprophyre dyke	212
Figure 8.2	Photographs of xenoliths hosted by the lamprophyres	213
Figure 8.3	Photomicrographs of mantle xenoliths	215
Figure 8.4	Coexisting pyroxenes and olivine plotted onto the pyroxene quadrilateral	218
Figure 8.5	Spinel compositions plotted in Cr# versus Mg#	221
Figure 8.6	P-T estimate for mantle xenoliths from the Vestfold Hills	228

LIST OF TABLES

	<i>Page</i>
Table 1.1 Geological history	5
Table 2.1 Average Ca Tschermaks content showing variations between chilled margins and dyke interiors	20
Table 2.2 Estimated liquid compositions in equilibrium with olivine and orthopyroxene from chilled margin and interior samples	28
Table 2.3 Selected microprobe analyses of clinopyroxenes and plagioclase	33
Table 3.1 Calculated temperatures on samples 70536 and 70548	41
Table 3.2 Representative HMT whole rock analyses	43
Table 3.3 Results from least squares mixing calculation	47
Table 3.4 REE analyses	54
Table 3.5 Selected microprobe analyses of olivine, orthopyroxene, clinopyroxene, plagioclase and spinel	57
Table 4.1 Calculated temperature for various norites and associated fine grained dykes	79
Table 4.2 Representative Norite whole rock analyses	94
Table 4.3 Results from least squares mixing calculation	98
Table 4.4 REE analyses	102
Table 4.5 Mineral partition coefficients used in the fractional crystallization modelling	105
Table 4.6 Selected microprobe analyses of olivine, orthopyroxene, clinopyroxene, plagioclase and spinel	107
Table 5.1 Mineralization within the Rubbly Norite	113
Table 5.2 Selected microprobe analyses of sulphides, sulpharsenides and platinoides	137
Table 5.3 PGE and S analyses	138
Table 6.1 Representative HMT whole rock analyses	142
Table 6.2 REE analyses	148
Table 6.3 Results from least squares mixing calculation	153
Table 6.4 Parent high-Mg tholeiite magma and gneiss compositions	162
Table 6.5 Calculated parental magma compared with picrite and basaltic komatiite	165
Table 6.6 Whole rock compositions modelled by AFC	166
Table 6.7 Mineral distribution coefficients	175
Table 6.8 Mineral and melting modes	175
Table 6.9 Estimated source compositions	179
Table 7.1 Calculated temperatures for various lamprophyres	187

Table 7.2	Representative lamprophyre whole rock compositions	191
Table 7.3	REE analyses	196
Table 7.4	Results from least squares mixing calculation	200
Table 7.5	Mineral distribution coefficients	204
Table 7.6	Mineral mantle modes	204
Table 7.7	Selected mineral analyses	207
Table 8.1	Calculated temperature for various spinel harzburgites and spinel lherzolites	223
Table 8.2	Selected microprobe analyses of olivine, orthopyroxene, clinopyroxene, plagioclase and spinel	229

ABSTRACT

GEOCHEMISTRY AND PETROGENESIS OF HIGH-MG THOLEIITES AND LAMPROPHYRES IN THE VESTFOLD HILLS, ANTARCTICA

The Vestfold Hills, Antarctica, an ice-free region of *ca.* 400 km², is a well exposed terrane of deep Archaean and Proterozoic crust which has been strongly interfolded and transposed. Between 2350 and 1100 Ma a dense network of mafic dykes intruded at mid- to upper crustal depths. Crosscutting relationships distinguish 9 different dyke sets intruded in three magmatic episodes. These three episodes exhibit distinct directional trends suggesting rotation of the regional crustal stress field over the period 2350 to 1150 Ma. During the first magmatic episode high-Mg tholeiites were emplaced at about 2350 Ma together with Fe-rich tholeiites. A second magmatic period has been inferred at ~1800 Ma in which a further set of Fe-rich tholeiites was emplaced. Radiogenic dating of the 1800 Ma dykes is not well constrained and field observations from this study did not clarify the relationship of these dykes to the older (2350 Ma) Fe-rich tholeiites. A third magmatic episode, which occurred between 1350 and 1150 Ma, emplaced two sets of lamprophyric dykes and Fe-rich tholeiites, in at least four separate events.

Previous studies have concluded that the 2350 Ma old high-Mg tholeiites were emplaced at deep crustal levels (7 - 8 kbar). New pressure estimates based on aluminium exchange between clinopyroxene and plagioclase and on pressure dependent trends of magmatic evolution reveal that these dykes were more likely emplaced at considerably lower levels (< 5 kb), possibly as low as 1 -2 kbar. This

requires much faster uplift of the Vestfold Hills block, during the late Archaean and early Proterozoic, than previously thought.

The 2350 Ma high-Mg tholeiites can be divided into 3 geochemically distinct groups which are not related by simple crystal fractionation processes. The high SiO₂ and MgO, and low TiO₂ magmas and are enriched in platinum group elements and gold: all characteristic of siliceous high magnesian basalts (SHMB). A fundamental question arises as to whether these geochemical characteristics are primary features inherited from the mantle or whether the magmas have been modified through assimilation of continental crust. This has been assessed by evaluating the extent to which differentiation processes are able to account for geochemical variations within one of the largest dykes in the Vestfold Hills has been studied in detail. This dyke is found to be of virtual homogeneous composition, apart from some minor variations in major- and trace elements which are consistent with limited *in situ* differentiation. Major and minor element geochemistry shows no evidence exists for crustal contamination in this dyke.

A large noritic ring complex (*ca.* 7 - 8 km in diameter) is associated with the intrusion of the 2350 Ma high-Mg tholeiite suite. It consists of several partly isolated bodies which vary in width from 70 to 400 m. This complex comprises three lithological units: (1) *Homogeneous Norite*, the most uniform and voluminous unit, containing cumulus orthopyroxene with clinopyroxene and plagioclase as intercumulus phases, (2) the *Mottled Norite*, a unit characterized by large 1 - 2 cm plagioclase - alkali-feldspar aggregates, and (3) the *Rubbly Norite*, a less common variant, distinguished by patches of bronzitic orthopyroxene, cognate and inherited xenoliths, and globules of sulphide. The xenoliths are mostly orthopyroxenites but also include websterites, sapphirine-bearing fine-grained quartzite, and feldspathic gneiss. The sulphide-rich zones range in size from ~ 4 to 30 m in width, with extensions up to 400 m in length in the southern part of the complex. Evidence for multiple intrusion suggests the *Rubbly Norite* was subsequently emplaced into the *Homogeneous* and *Mottled Norite* units.

Major and trace element variations in the norite is consistent with orthopyroxene controlled differentiation, with orthopyroxene and sulphide accumulation in the *Rubbly Norite*.

Sulphides and associated PGE (platinum group element) mineralization occurring in the *Rubbly Norite* has been examined in detail. Elevated abundances of PGE occur in the high-Mg tholeiite suite compared to many basalts (e.g. MORB). This PGE enrichment is consistent with segregation of a sulphur-undersaturated basaltic melt, rich in PGE, from a refractory mantle. Subsequent sulphur saturation, probably at crustal levels, is responsible for the concentration of PGE in a sulphide melt.

During mid Proterozoic time (1350 - 1150 Ma) *lamprophyre* dykes were emplaced contemporaneously with Fe-rich tholeiites. Both suites crosscut one another, indicating at least four distinct magmatic events. The *lamprophyre* dykes occur throughout the Vestfold Hills but are volumetrically subordinate to the Fe-rich tholeiites. Trace element geochemistry indicates that they are not related by crystal fractionation of observed phenocryst phases. Rare earth element abundances require the derivation by variable small degree of partial melting of heterogeneous garnet peridotite sources.

Ultramafic xenoliths of various types, mainly *spinel harzburgites*, *spinel lherzolite* and *websterites*, occur in pipe-like bodies (ca. 2 by 5 m) within the *lamprophyres*. These represent samples of the uppermost Proterozoic mantle beneath the Vestfold Hills and are considered the likely mantle residues to the 2350 high-Mg tholeiites.

CHAPTER 1

GEOLOGICAL HISTORY OF THE VESTFOLD HILLS

1.1 INTRODUCTION

The East Antarctic Shield, which has been a relatively stable craton for the last 2.5 to 3.0 billion years, comprises mainly Archaean and Proterozoic terranes. Outcrops along the East Antarctic coast occur in Commonwealth Bay, the Bunger Hills, the Vestfold Hills, the Prince Charles Mountains and the Napier Complex of Enderby Land (Figure 1.2). During early to middle Proterozoic time mafic dyke swarms have intruded as distinct magmatic episodes into both Archaean and Proterozoic crust.

The Vestfold Hills, located at 69° S and 78° E in Princess Elizabeth Land, is an ice-free region of *ca.* 400 km². This region of low hills is cut by several fjords and is situated on the eastern shore of Prydz Bay. It is bordered by the Sørsdal Glacier to the south, the ice plateau to the east and north-east, and by the open sea to the west. Due to its excellent outcrop exposure it has been the subject of numerous studies over the last 30 years and is, together with the Napier Complex in Enderby Land and the coastal exposures near Mawson and near Syowa, one of the most studied areas of the Archaean cratonic crust in Antarctica.

The predominantly granulitic Archaean and Early Proterozoic crust of the Vestfold Hills is a well preserved terrane of uplifted deep continental crust which has been strongly deformed. Over a period of *ca.* 1300 Ma, mafic dykes of various compositions intruded at mid- to lower crustal levels. These dykes form a dense network with distinct orientations and crosscutting relationships (Figure 1.1). This



Figure 1.1

Aerial view of the central Vestfold Hills (*Long Fjord*) showing the dense network of Proterozoic mafic dykes. Scale: 1 : 50 000.

complex sequence of dyke emplacement can be used to constrain the pressure and temperature evolution with time of the Vestfold Hills.

1.2. REGIONAL GEOLOGY OF THE VESTFOLD HILLS

1.2.1. Crustal Evolution

The first geological mapping in the Vestfold Hills was undertaken in 1965 (McLeod et al., 1967). The Vestfold Hills are characterized by a series of east-west striking granulite facies gneiss units which are tectonically repeated from the north to the south. These gneiss units have been subdivided into four distinct groups (Oliver et al., 1982; Collerson et al., 1983 a); (1) a layered garnetiferous paragneiss (*Chelnok Supracrustals*), (2) a layered orthopyroxene - quartz - feldspar - gneiss of tonalitic composition (*Mossel Gneiss*), (3) a felsic orthogneiss of monzodioritic composition (*Crooked Lake Gneiss*), and (4) mafic granulites (*Tryne Metavolcanics*). Recent work has identified a fifth unit, the *Grace Lake Gneiss* (Black et al., 1990), which is a granodioritic gneiss occurring as pods and irregular sheets within the older gneiss units. The *Tryne Metavolcanics*, which together with the *Chelnok Supracrustals* are the oldest recognized rocks in the Vestfold Hill complex, are probably greater than 3000 Ma (Collerson et al., 1983 a). These mafic rocks occur within the gneisses as boudinaged xenoliths or tectonic intercalations up to 1 km in width. The *Mossel Gneiss*, which is a less extensive than the *Crooked Lake Gneiss*, is believed to be at least partly derived by partial melting from the *Tryne Metavolcanics* (Collerson et al., 1983 a). In the late Archaean, mafic dykes were intruded and subsequently became deformed, folded and boudinaged by a late Archaean to early Proterozoic metamorphic event.

Various dating techniques have been applied to determine ages of the Vestfold Hills rocks. Rb-Sr and Sm-Nd isotopic studies indicate middle to lower Archaean ages for the gneisses (Arriens, 1975; Collerson & Arriens, 1979; Collerson et al., 1983 a;

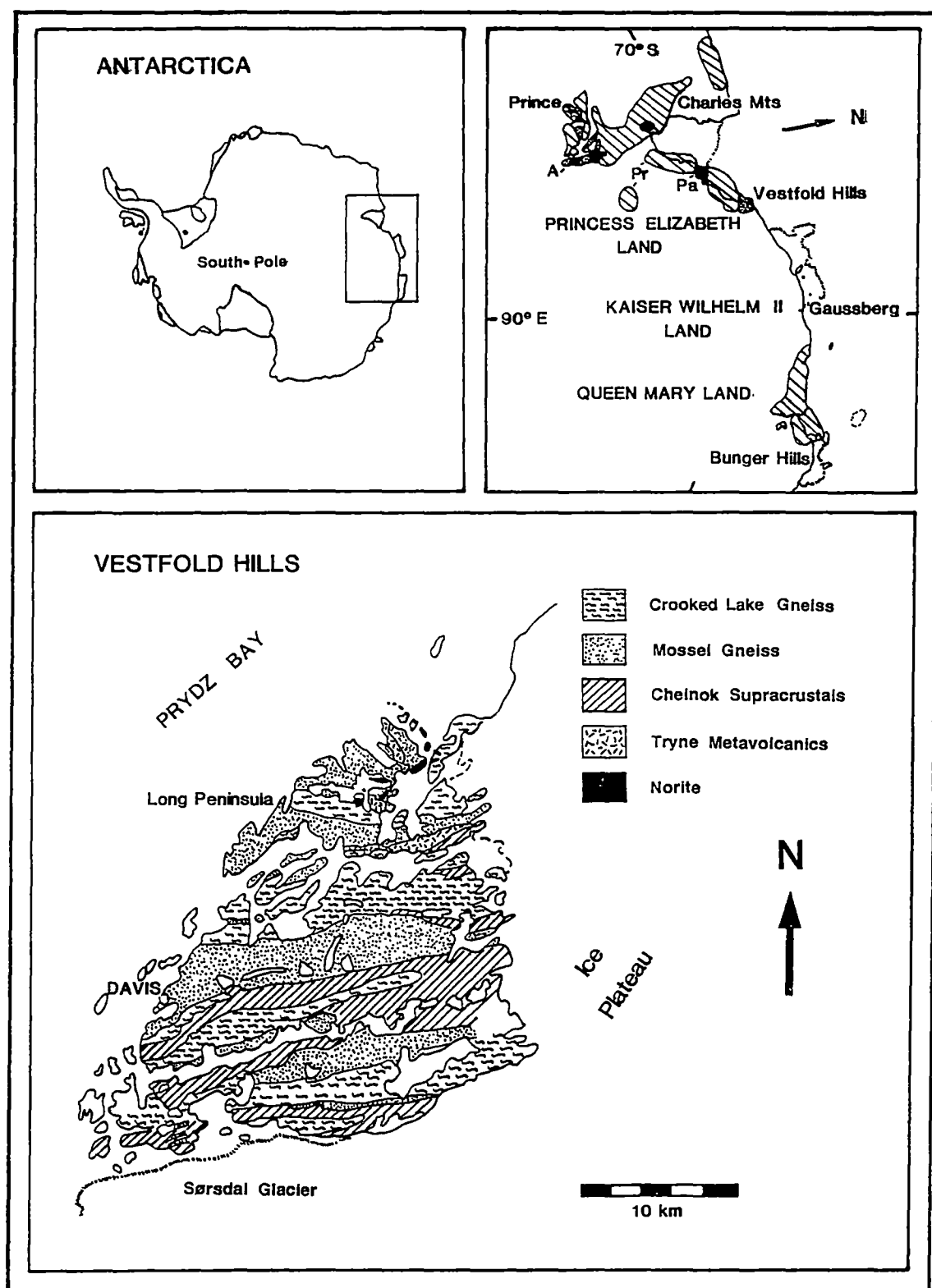


Figure 1.2

Maps of East Antarctica showing locations of metamorphic complexes of the Prince Charles Mountains, Bunge Hills and of the Vestfold Hills (Davis Station: 69° 35' S - 77° 58' E) in more detail. Abbreviations: A: Archaean rocks, Pr: Proterozoic rocks, Pa: Palaeozoic rock. Modified after Sheraton & Collerson (1984), James & Tingey (1983).

GEOLOGICAL HISTORY OF THE VESTFOLD HILLS AND PRYDZ BAY AREA

<i>Event</i>	<i>Metamorphism</i>	<i>Time Ma</i>	<i>Method</i>
Extrusion of <i>Tryne Metavolcanics</i> and deposition of <i>Chelnok Supracrustals</i>		> 3000	Rb-Sr Sm-Nd
High grade metamorphism and partial melting of <i>Tryne Metavolcanics</i> ;	Granulite facies	2800	
Intrusion of mafic dykes			
formation of <i>Mossel Gneiss</i> (mostly tonalitic) deformation (D1)		2526	U-Pb
Emplacement of <i>Crooked Lake Gneiss</i>		2500	U-Pb
Emplacement of <i>Grace Lake Gneiss</i>		2487	U-Pb
deformation (D2)			
deformation (D3)			
Emplacement of felsic dykes		2477	U-Pb
Mafic dyke swarms			
Intrusion of <i>high-Mg tholeiite dykes</i>		2350	Rb-Sr
<i>Fe-rich tholeiite dykes</i>			
Intrusion of <i>Fe-rich tholeiite dykes</i>		1800	Rb-Sr
Deposition of sediments; emplacement of granitic intrusives			
Intrusion of <i>Fe-rich tholeiite</i> and <i>lamprophyre dykes</i>		1350	Rb-Sr
Deposition of sediments			
Emplacement of tonalitic to granitic intrusives (Rauer Is.); high pressure metamorphism Rauer Is., Prydz Bay and southwestern area of the Vestfold Hills with minor deformational and thermal overprint in latter	Granulite facies	1100	
Intrusion of granitic pegmatites			
Intrusion of <i>lamprophyre dykes</i> (Rauer Islands)		500	
Rifting and separation of Antarctica from India, Madagascar and Africa		115 - 80	

Table 1.1 Modified after data from Collerson et al. (1983 a), Sheraton (1983), Sheraton et al. (1984), Oliver (1982), Black et al. (1990).

Sheraton et al., 1984). However, recent age determinations by the ion microprobe Zircon U-Pb technique (Kinny & Black, 1990; Black et al., 1990) require revision of the chronostratigraphy of some of these rock units (see Table 1.1 for summarized data).

1.2.2. Deformation and Uplift History

The Vestfold Hills have a complex late Archaean and Proterozoic deformational and thermal history, which has been described by Oliver et al. (1982), Parker et al. (1983) and Passchier et al. (1990). Two major high grade metamorphic events have been recognized in the Vestfold Block.

The first granulite facies event of the gneisses took place between 3000 - 2400 Ma under peak P-T conditions of 700° - 1000° C and 8 - 10 kbar (Collerson et al., 1983 b). Zircon ages determined by Black et al. (1990) suggest that the first deformation D₁ took place after emplacement of the *Mossel Gneiss* unit, at about 2500 Ma. The second deformation D₂ followed shortly after D₁ at about 2490 Ma and affected the *Grace Lake Gneiss*, which was emplaced syn-D₂. Data obtained by Black et al. (1990) indicate a much closer succession of D₁ and D₂ than previously proposed by Collerson et al. (1983 a), who separated these events by about one hundred million years. The intrusion of felsic dykes, at 2477 Ma, postdates the first granulite facies metamorphic event. These undeformed dykes exhibit chilled margins and baked contacts suggesting emplacement at elevated relatively cool crustal levels. This implies rapid uplift over a period of 50 Ma.

Evaluations of emplacement pressure estimates for the 2350 Ma old mafic dyke suites (Kuehner, 1987) infer deep crustal levels of about 7 - 8 kbar, whereas estimates for the 1350 Ma dyke suites indicate shallower crustal levels (4 - 5 kbar). These pressure estimates are critically re-evaluated in this study, particularly the evidence for deep emplacement of the 2350 Ma dykes.

The second granulite facies metamorphic event occurred after the emplacement of the youngest dyke suite, between 1100 - 600 Ma, at P-T conditions of 600° - 800° C

and 6 - 8 kbar. Based on temperature and pressure estimations for the Vestfold Hills (Collerson et al., 1983 a; Kuehner, 1987; Passchier et al., 1990) several PTt-paths have been proposed and are compiled in Figure 1.3. The more recent studies of Passchier et al. (1990) reveal that the presently exposed part of the Vestfold Hills was uplifted to shallow crustal levels prior to the emplacement of the youngest dyke suite. They observe pseudotachylytes predating the youngest dykes suites (1350 Ma), which indicate brittle faulting in the uppermost levels of the crust (probably around 3 kbar). Following emplacement of the later dykes, the southern part of the Vestfold Hills underwent a second metamorphic event which reached amphibolite to granulite facies conditions.

Since *ca.* 1000 Ma the Vestfold Hills block has probably undergone erosion controlled uplift. During the late Mesozoic (115 - 80 Ma), with the breakup of Gondwanaland, the East Antarctic Shield was separated from India, Madagascar and Africa.

1.2.3. Magmatic Episodes

Over a period of *ca.* 1300 Ma, from the early to middle Proterozoic time, mafic dykes of various compositions intruded into the Vestfold Block. All dykes postdate the first metamorphic event and in the northern part of the Vestfold Hills they show no sign of any deformational or thermal overprinting. Only in the south-western part of the Vestfold Hills has the late Proterozoic metamorphic event affected these dykes. This second granulite facies event produced high-pressure garnet-bearing assemblages, indicating metamorphic pressures between 6 and 7 kbar (Collerson et al., 1983 b; Kuehner, 1987).

The dyke suites have been emplaced during three magmatic episodes (Figure 1.4). The first episode is dominated by high-Mg tholeiites (olivine tholeiite and quartz tholeiite compositions), which occur throughout the Vestfold Hills and also in Napier Complex. Sheraton & Collerson (1983) previously classified these dykes as high-Mg tholeiites. Rb-Sr isochrons produce ages of 2350 ± 48 Ma and 2424 ± 72 Ma

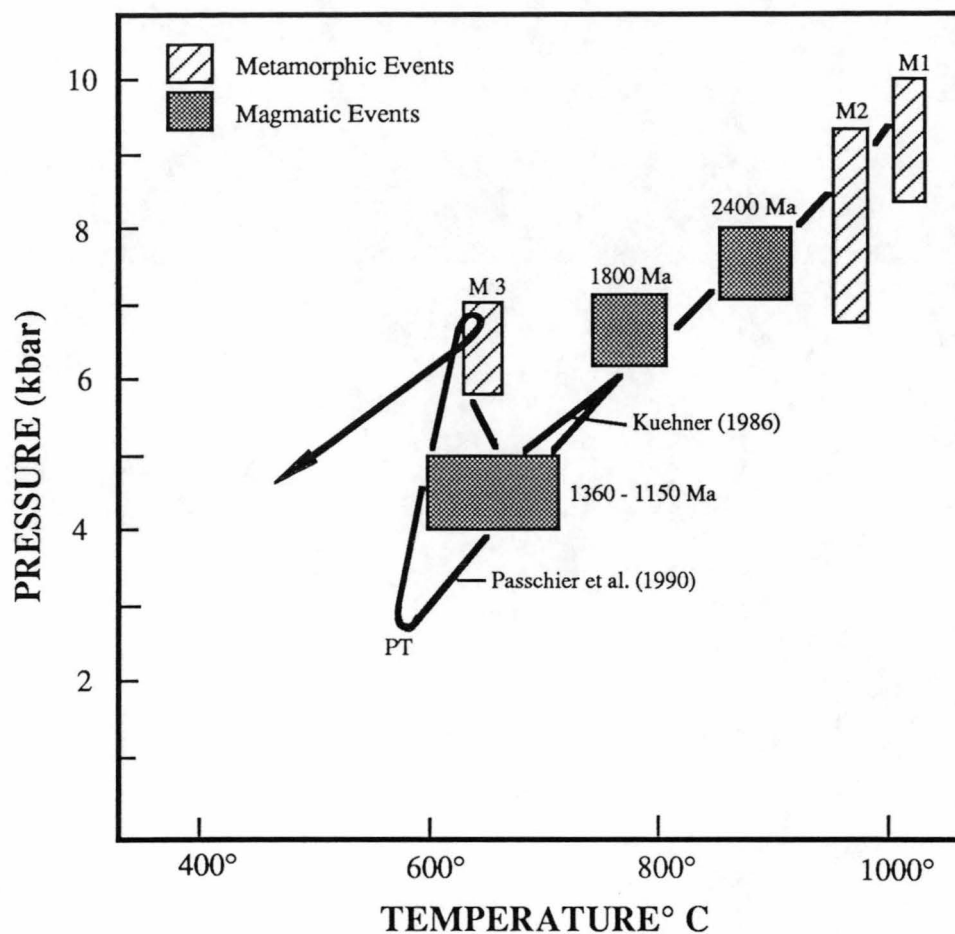


Figure 1.3

PTt-paths for the Vestfold Hills proposed by Kuehner (1986) and Passchier et al. (1990).

(Sheraton & Black, 1981; Collerson & Sheraton, 1986 b). In the more recent study of Kuehner (1987), this dyke suite has been subdivided, on the basis of crosscutting relationships, petrography and geochemistry, into two major groups. Dykes belonging to the first group are olivine- and orthopyroxene-phyric, whereas the second group has only orthopyroxene phenocrysts. Crosscutting relationships between these two groups indicate an older age for the first olivine + orthopyroxene-phyric group. Further subdivision has been made in the second group where two subgroups can be distinguished according to Rb enrichment and depletion trends, (Kuehner, 1987).

Emplacement of Fe-rich tholeiite dykes also occurred contemporaneously with intrusion of the high-Mg tholeiites (Kuehner, 1987). These have been subdivided by Kuehner (1986) into an older high-Ti subgroup and two younger subgroups, a low-Ti subgroup, and a plagioclase megacryst bearing subgroup. The Fe-rich tholeiites are geochemically distinct from the high-Mg tholeiites, and these two major dyke suites cannot be related by crystal fractionation or partial melting. Kuehner (1987) suggested they were derived by simultaneous tapping of at least two geochemically different mantle source regions.

Fe-rich tholeiite dykes were again emplaced during the later magmatic episodes. A small suite of dykes (group I tholeiites of Sheraton & Collerson, 1983) give an Rb-Sr isochron age of 1791 ± 62 Ma. These dyke group remains to be defined in terms of the more recent detailed sampling and definition of dyke groups based on crosscutting relationships (Kuehner, 1986 and this study).

Abundant dykes were emplaced during the final magmatic episode in the Vestfold Hills, which occurred between 1350 and 1150 Ma. These dyke suites have also been classified as Fe-rich tholeiites by Collerson & Sheraton (1986 b), who made a distinction between Group II and Group III tholeiites, both of which yield Rb-Sr isochron ages of 1374 ± 125 Ma. According to crosscut relationships and geochemical characteristics, Kuehner (1987) further subdivided these two groups into 10 subgroups. Lamprophyric dykes were also emplaced during the same magmatic episode. They are relatively widespread but are voluminously subordinate and seldom

exceed 1m in width. These lamprophyre dykes were believed to be the youngest intrusives in the Vestfold Block by Sheraton (1983), who compared them with lamprophyre dykes from the Rauer Islands, which were emplaced probably during the late Proterozoic. However, crosscut relationships between lamprophyre and tholeiite dykes, identified by this study, clearly reveal these lamprophyre dykes were emplaced during the 1350 Ma magmatic episode.

1.3 EARLY TO MIDDLE PROTEROZOIC MAFIC DYKES - THEIR RELATIVE TIME OF EMPLACEMENT

1.3.1 Introduction

Previous studies have established a complex emplacement history for the mafic dyke swarms of the Vestfold block. Major and trace element chemistry provided an important tool for distinguishing the different subgroups within dyke suites.

This study has brought additional information concerning dyke crosscutting relationships and the relative timing of the various dykes suites. This is to be used as the basis for a comprehensive analysis of the magma petrogenesis and tectothermal evolution of the Vestfold Hills. Several regions within the Vestfold Hills were identified and systematically mapped for this purpose, with particular emphasis being given to an area between *Taynaya Bay* and *Tryne Fjord*, where early to middle Proterozoic dykes are well exposed, including a large noritic ring complex and abundant 1350 - 1150 Ma lamprophyre dykes.

1.3.2 Identification of Dyke Suites and their Emplacement Sequence

Based on crosscut relationships it has been possible to distinguish 9 different dyke suites. These were intruded during the various magmatic episodes, each of which shows distinct directional trends. In all, four distinct emplacement-directions are recognized (see dyke base map), with the orientation of the successive dyke suites

rotating clockwise, suggesting a continuing rotation of the regional crustal stress field over the time period 2400 to 1300 Ma. This generalization omits the minor dykes associated locally with the noritic ring complex

The oldest, early Proterozoic high-Mg tholeiite dykes (2350 Ma) were emplaced in an \pm E-W direction. They are crosscut by NE - SW trending second generation of early Proterozoic high-Mg tholeiites, including dykes related to the norite complex tend to trend NE - SW trend. During the 1350 Ma events the earliest dykes, mainly Fe-rich tholeiites and subordinate lamprophyre dykes, were emplaced in a N - S direction. Intersections between these dykes are rare but the few which have been observed indicate older ages for the lamprophyre dykes. A second generation of lamprophyre dykes was identified crosscutting the older lamprophyre dykes and some younger tholeiites. The relationships among the youngest Fe-rich tholeiites (in which there are several subgroups) and with the latest lamprophyre dykes are not yet clear. Due to a tight NNE - SSW orientation for the youngest dyke suites, dyke intersections were not observed.

On the basis of observed crosscut relationships the following sequence of dyke emplacement is proposed.

DYKE SETS AND THEIR RELATIVE TIME OF EMPLACEMENT

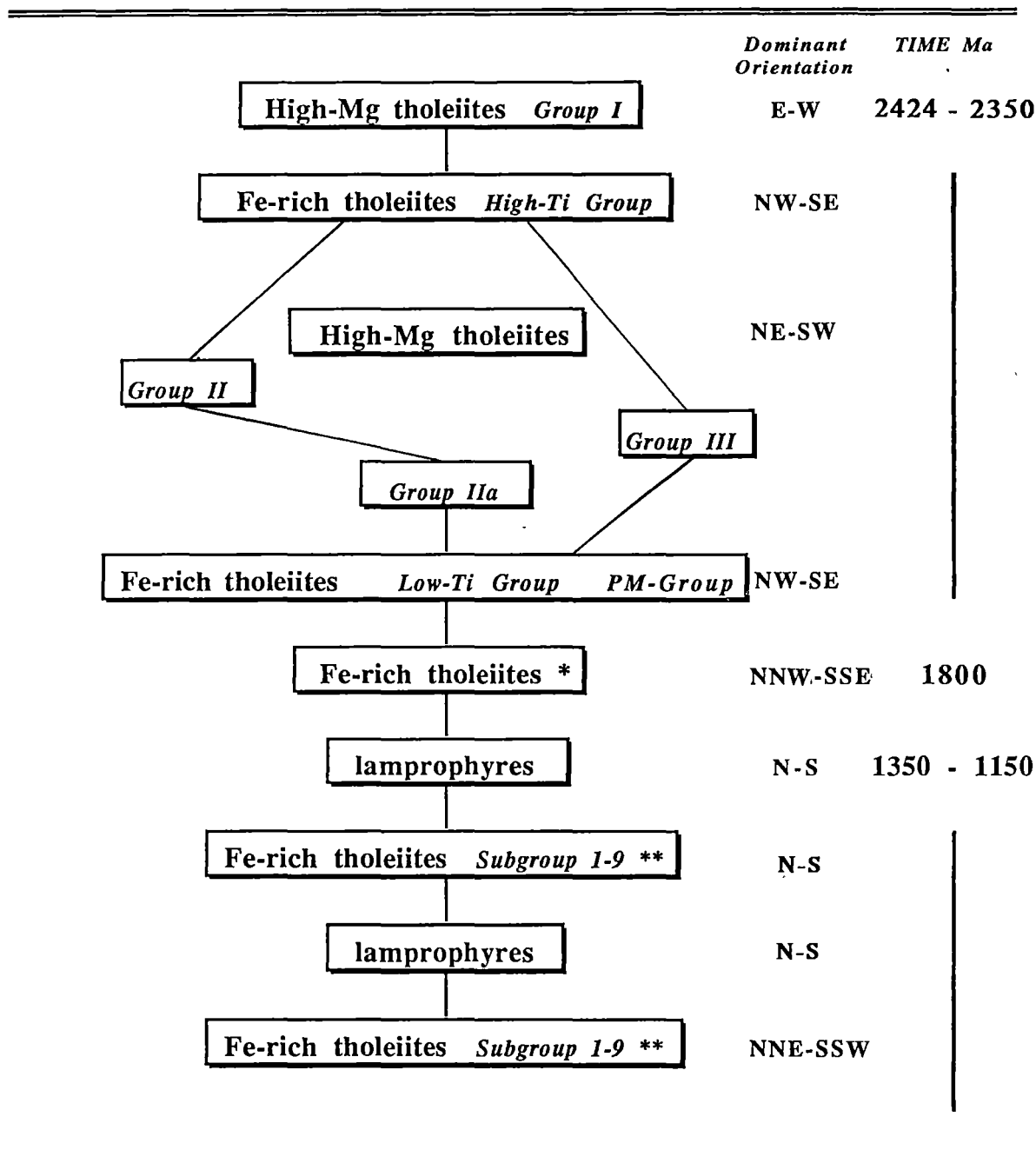


Figure 1.4

Proterozoic dyke sets in the Vestfold Hills and their emplacement in sequence. *The presence of the 1800 Ma dyke suite is not well established as these dykes share the same directional trend as the youngest 2350 Ma Fe-rich tholeiites. ** Emplacement in multiple stages (see text for discussion).

1.4 MAFIC DYKES AND THEIR CLASSIFICATIONS

This section summarizes the results and conclusions of previous workers, who classified some of the Vestfold Hills mafic dykes according to petrographical and geochemical features.

1.4.1 The 2350 Ma High-Mg Tholeiites

The oldest undeformed mafic dyke suite in the Vestfold Hills has been categorized as high-Mg tholeiites (Sheraton & Collerson, 1983; Kuehner, 1986) which has been emplaced in at least two distinct events (Kuehner, 1986). On the basis of petrographical and geochemical characteristics, Kuehner (1986, 1987) classified the dykes into three subgroups: (1) SGP I tholeiites, olivine + orthopyroxene-phyric samples with 'normal' $(\text{Sr})_N$ (normalized Sr), (2) SGP II tholeiites, orthopyroxene-phyric samples which are Rb-poor and depleted in $(\text{Sr})_N$ (3) orthopyroxene-phyric samples which are Pb-rich and depleted in $(\text{Sr})_N$. A noritic ring intrusion, first described by McLeod & Harding (1967), hosting enstatite nodules and sulphides, was classified as a SGP III tholeiite (Kuehner, 1986). Based on mineral chemistry and geochemical characteristics, Kuehner (1986, 1987) inferred that the three subgroups are not related to one another through fractionation and suggested derivation from three distinct primary liquids.

Based on isotopic data it was inferred that the high-Mg tholeiites have not experienced the process of crustal contamination (Sheraton & Black, 1981; Collerson & Sheraton, 1986; Kuehner, 1987).

1.4.2 The 2350, 1800 and 1350 Ma Fe-rich Tholeiites

Kuehner (1986) identified a Fe-rich tholeiitic dyke suite (herein high-Ti Fe-rich tholeiites), which postdates emplacement of the first generation of 2350 Ma high-Mg tholeiites and is crosscut by the second generation of high-Mg tholeiites. The final generation of 2350 Ma high-Mg tholeiites was followed by emplacement of the second Fe-rich tholeiitic suite. Crosscut relationships identified in this study confirmed the

existence of these dyke suites, however, it has not been possible to establish whether the 1800 Ma Fe-rich tholeiites are separated from the 2350 Ma Fe-rich tholeiites (Collerson & Sheraton, 1986 a) as these dykes suites both share the same directional trends (i. e. NW - SE). The time and geochemical relationships between these suites will require further study.

The 2350 Ma Fe-rich Tholeiites

Based on field relationships Kuehner (1986) inferred the oldest Fe-rich tholeiites to have an age of *ca.* 2420 Ma, whereas the two younger Fe-rich tholeiite dyke subgroups may or may not be considerably younger. Based on petrographical and geochemical features, Kuehner (1986) characterized three distinct groups within the Fe-rich tholeiite suite. The oldest Fe-rich tholeiite, which is crosscut by the second dyke set of the high-Mg suite, was named a high-Ti (HiTi) group. The two younger Fe-rich tholeiites from this suite, postdating the high-Mg tholeiitic dykes were divided into a low-Ti (LoTi) and Plagioclase Megacryst (PM) bearing group.

Major and trace element variations between HiTi and LoTi groups are explained by fractional crystallization (Kuehner, 1986). To explain the relative enrichment in P, LREE and Zr and depletion of TiO₂ in the LoTi group, Kuehner (1986) suggested open-system fractionation as a possible mechanism. Differences in the PM group could not be related to the HiTi or LoTi subgroup by fractional crystallization of the observed phenocryst assemblages. However, it was suggested that incompatible trace element and REE patterns, with the exception of K and Rb, indicate a common parental liquid for the PM and LoTi subgroups. The differences in major element compositions and the similarities in trace elements were interpreted as a result of a different P-T differentiation path for the PM subgroup on one hand and the HiTi and LoTi group on the other (Kuehner, 1986).

In comparison to the high-Mg tholeiites, the Fe-rich tholeiites are notably less siliceous, with the later being unable to be derived from the high-Mg tholeiites by simple crystal fractionation (Kuehner, 1986). Unfractionated LREE/HREE ratios of

the most mafic LoTi samples also suggest that the primary liquid to the Fe-rich tholeiite suite was derived from a primitive mantle source, which had not experienced previous melting or enrichment events. This contrasts with the LREE-enrichment nature of the high-Mg tholeiites and indicates that these separate 2350 Ma tholeiite suites cannot be derived from a single mantle source.

The 1350 Ma Fe-rich Tholeiites

Based on crosscutting relationships and directional trends within the 1350 Ma Fe-rich tholeiites two separate magmatic events can be identified. Kuehner (1986) further distinguished 9 chemical subgroups and showed that the major elements of these groups can be modelled by the crystal fractionation of observed phenocryst phases. However, the trace element and REE variations cannot be explained by simple crystal fractionation and more complex differentiation processes are required. Based on slight REE differences between the subgroups, Kuehner (1986) suggested the involvement of two separate mantle sources. He further pointed out that the cyclic variation in trace element concentrations with magma chamber processes, such as magma chamber replenishment, refilling, crystal fractionation as modelled by O'Hara (1977) and Langmuir (1980). Field observations made in this study (i.e. crosscutting relationships between Fe-rich tholeiites and lamprophyres) show that the emplacement of Fe-rich tholeiite dykes has occurred in more than two events.

1.4.3 Lamprophyres

Lamprophyric dykes are volumetrically subordinate compared to the tholeiites but are frequent throughout the Vestfold Hills. Their age relationship to the tholeiites has not been well established but e.g. Kuehner (1986) suggested contemporaneity with the 1350 Ma Fe-rich tholeiites. Little work has been done on this suite of rocks, including petrographical classification into olivine basalts, two alkali-olivine basalts and ankaramites (Collerson & Sheraton, 1986) or alternatively into monchiquites and camptonites (Mikhalsky & Andronikov, 1990, N.M. S. Rock pers. comm.).

1.5 AIM OF STUDY

The aim of this study is to examine the high-Mg tholeiites in detail, focussing upon their petrogenesis, with particular regard to assessing crustal contamination (Chapter 3 and 6) and a re-examination of the PTt - evolution path for the Vestfold Hills using a early high-Mg tholeiite to constrain emplacement pressure (Chapters 2). The large norite complex occurring in the Vestfold Hills is examined in Chapter 4 with the aim of understanding processes in magma chambers also with regard to PGE enrichments within the high-Mg tholeiite suite and the norite in particular (Chapter 5). The scope is extended in Chapters 7 and 8 to include the Proterozoic lamprophyre dykes and associated mantle xenoliths, which have not been examined in detail previously.

CHAPTER 2

ESTIMATION OF EMPLACEMENT PRESSURE FOR THE 2350 MA HIGH-MG SUITE

2.1 INTRODUCTION

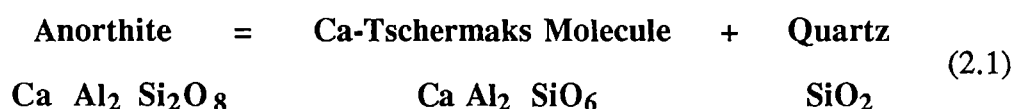
The depth of emplacement of the 2350 Ma old high-Mg tholeiites was previously suggested to be ~28 km (7 - 8 kbars): Kuehner (1986, 1987). This conclusion was derived from the occurrence of olivine and orthopyroxene phenocrysts and microphenocrysts in the chilled margins of these dykes and the reproduction of these phases as the liquidus assemblage in the bulk compositions corresponding to the chilled margins at pressures of 7 - 8 kbar (Kuehner, 1986). At higher pressure orthopyroxene is the sole liquidus phase and at lower pressure olivine is the liquidus phase. Use of clinopyroxene + plagioclase + quartz groundmass assemblages to estimate pressure, using the method of Ellis (1980), also yielded pressures of ~ 8 kbar (Kuehner, 1986, 1987).

The aim of this chapter is to critically examine the pressure estimations made by Kuehner (1986). This re-examination is based on the recognition that the chilled margins may contain phenocrysts or microphenocrysts crystallized at and transported from deeper levels (i.e. the pressure of crystallization of olivine and orthopyroxene from these compositions may be correctly estimated but this may have occurred at appreciably greater depth than the final emplacement and chilling of the dykes). (See Table 2.3 for sample numbers and Appendix 10.7 for sample locations).

2.2 GEOBAROMETRY BASED ON ALUMINIUM EXCHANGE BETWEEN CLINOPYROXENE AND PLAGIOCLASE

2.2.1 Geobarometer

The assemblage plagioclase - clinopyroxene - quartz is the only geobarometer applicable to the phase assemblages present in the high-Mg tholeiites. This geobarometer is based on aluminium exchange and can be expressed by the reaction:



It has been pointed out that the breakdown reaction of anorthite to Ca-Tschermaks and quartz has a minor temperature dependence under crustal conditions and the error is estimated to be within ± 1 kbar (Ellis, 1980; Ellis & Green, 1985). When applied to clinopyroxenes containing less than 0.35 Ca-Tschermaks molecule, the barometer gives pressures which agree reasonably well with experimental data (Ellis, 1980; Kuehner, 1986).

2.2.2 Application to Natural Assemblages

The high-Mg tholeiite dyke compositions are silica over-saturated and have modal quartz in their groundmasses, therefore it is appropriate to use the assemblage plagioclase + clinopyroxene + quartz as a geobarometer (Ellis, 1980). Uncertainty in use of this geobarometer may arise from zoned mineral compositions reflecting varying cooling rates within the dykes and from disequilibrium as indicated by the coexistence of olivine phenocrysts and quartz in the groundmass. It is therefore necessary to examine these assemblages from different parts of the dykes, which may have cooled at different rates, i.e. chilled margins and dyke interiors.

One of the largest high-Mg tholeiitic dykes in the Vestfold Hills has been sampled in detail with the purpose of monitoring across- and along- dyke variations.

CALCULATED PRESSURE VARIATIONS ACROSS A DYKE

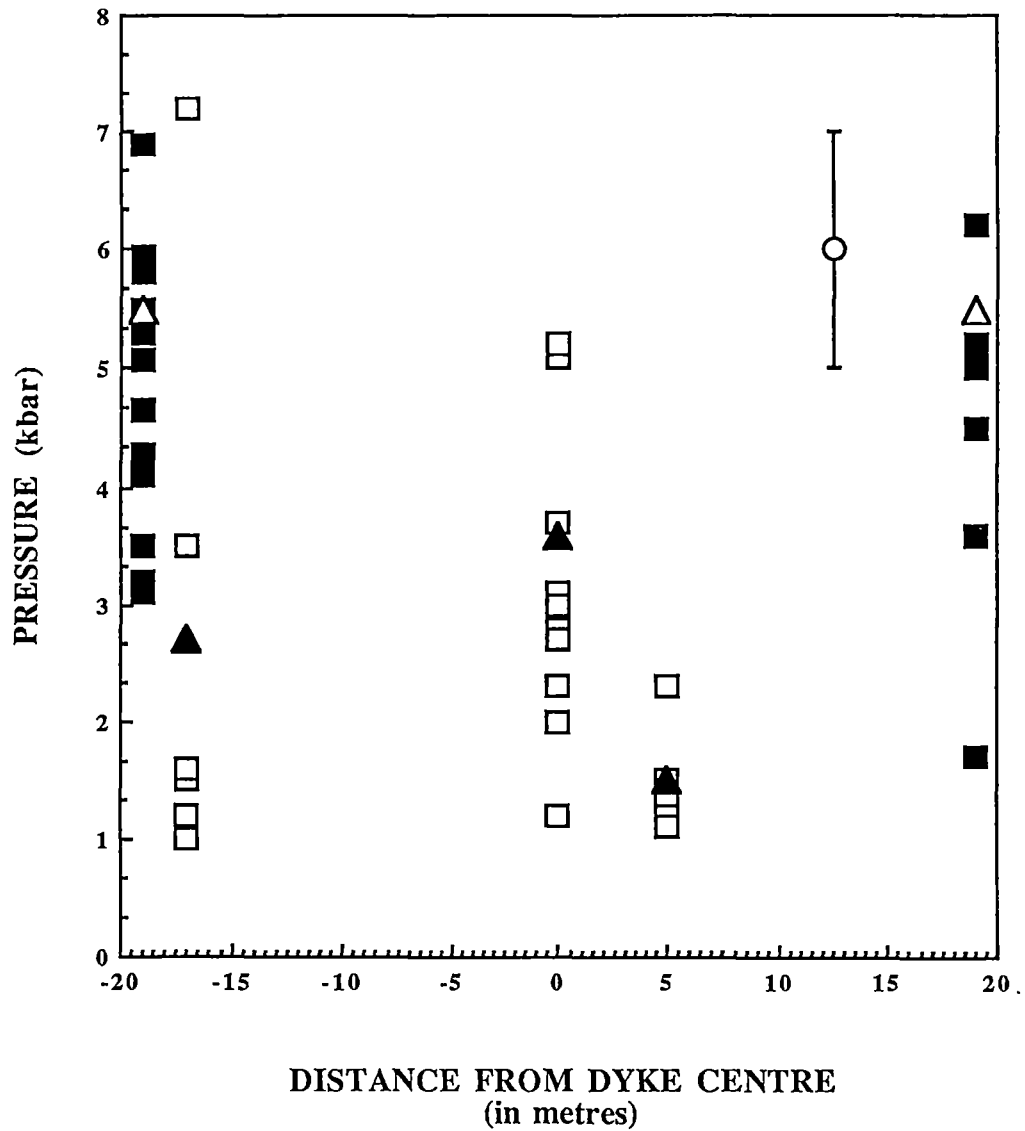


Figure 2.1

Calculated pressure based on aluminium exchange between clinopyroxene and plagioclase, versus distance from the dyke centre. Triangles indicate averaged pressures. Filled squares: chilled margins, open squares dyke interior, \bigcirc error bar (see text for details of calculation procedure).

Sample Location Rock Type	Chilled Margin High-Mg Tholeiite	Dyke Interior
	average	average
Ca Tschermaks	4.2	2.4
Anorthite	58.2	60.0
Albite	42.3	39.3
Temperature °C	Pressure (kbar)	Pressure (kbar)
1250	5.0	-
1200	5.3	0.5
1150	5.6	1.0
1100	6.0	1.5
1000	6.6	2.5
900	7.2	3.4
850	-	3.9
800	-	4.4

Table 2.1

Variation in pressure estimates occurring with variations in temperature for averaged Ca-Tschermaks content (mol%) in clinopyroxene, anorthite and albite in plagioclase (mol%) at chilled margins and dyke interiors. Corresponding clinopyroxene and plagioclase compositions are listed in Table 2.3.

This dyke has a width varying between 30 and 50 m, with fine grained chilled margins and a coarse grained interior. Microprobe analyses of clinopyroxene - plagioclase assemblages in contact with quartz were obtained from various samples across the dyke. The amount of Ca-Tschermaks molecule in the rims of calcic clinopyroxene was calculated following the method of Herzberg (1978) and used together with neighbouring Na-rich plagioclase compositions for the pressure calculations (see Table 2.1 and 2.3).

Calculated pressures are plotted in Figure 2.1 according to their relative position within the dyke. Temperature for chilled margins and dyke interior were obtained applying the two pyroxene thermometer of Wells (1977), Kretz (1982) and Bertrand & Mercier (1985) to coexisting ortho- and clinopyroxenes, using rim compositions only. For samples at or near chilled margins a temperature of 1150° C was used and for the dyke interiors a temperature of 900° C was used for the pressure calculations. It is notable that sample 70536, from the dyke centre, has a similar whole-rock composition to the chilled margin samples (e.g. 70533) indicating the dyke has not experienced significant geochemical differentiation (Table 2.2). The data in Figure 2.1 and Table 2.1 suggest that variations in calculated pressure correspond to sample location, both on a macro- and microscale. Samples from chilled margins (70533, 70538 and 70548) exhibit a similar range in calculated pressures (1.8 - 7 kbar), whereas pressures obtained from the dyke interior are significantly lower (1 - 5 kbar). In general each location within the dyke shows a wide range in pressure. It is notable that the basis of this barometer, the Ca-Tschermaks content of clinopyroxene, is also dependent on temperature and in particular on quenching rates (e.g. metastable aluminous clinopyroxenes are well-known to form by rapid quenching; Nesbitt, 1971; Goode & Moore, 1975). In order to evaluate the effect of temperature on calculated pressures, the geobarometer has been applied across a range of possible temperatures (see Table 2.1). Chilled margin samples are likely to record higher blocking temperatures (1100° and 1250 °C) than dyke interior samples (800° - 950° C), the application of suitable temperatures, as indicated by the boxes in Table 2.1, results in calculated pressures for

chilled margins from 5 to 6 kbar (1250° to 1100° C) and from 3 to 4 kbar (950° to 800°C) for the dyke interior samples. It becomes apparent that the application of this barometer is critically dependent upon the assumption of equilibrium between coexisting plagioclase, clinopyroxene and quartz, as well as temperature, pressure and cooling rate. Also shown in Table 2.1 is the compositional variation between the averaged endmembers at each sample location. While plagioclase exhibits a similar averaged composition in chilled and non-chilled samples, the averaged Ca-Tschemaks component in clinopyroxene diminishes by nearly 2 mol% in the dyke interior samples.

In Figure 2.2 Al₂O₃ content in clinopyroxenes is plotted against CaO and SiO₂, distinguishing between chilled margin samples and samples from the dyke interior. SiO₂ and Al₂O₃ show a poor negative correlation, while CaO and Al₂O₃ show no correlation.

In rapidly cooled magmas crystallization is commonly characterized by iron-enrichment trends in clinopyroxene and sodium-enrichment trends in zoned plagioclase. During rapid cooling limited opportunity exists for iron-magnesian and sodium-calcium fractionation between crystals and melt. Pyroxenes will tend to follow the well established 'quench trends' (e.g. Lofgren, 1980) within the pyroxene quadrilateral and such pyroxenes would be suspect for use in geobarometry. In more slowly cooled samples, limited iron-magnesium fractionation may develop and equilibrium among coexisting phases may be achieved. In selecting points for analysis giving sharp clinopyroxene to plagioclase contacts (commonly in ophitic to sub-ophitic texture) there appears to be avoidance of more Fe-rich compositions so that the data show a limited range of Mg# ($Mg\# = 100 \text{ Mg} / (\text{Mg} + \text{Fe}^{2+} + \text{Fe}^{3+})$) from 80 - 65 in dyke interior samples, with lesser range of Mg# (75 - 67) in chilled margin samples. There is a correlation between Mg# and CaO content so that more iron-rich clinopyroxenes are more subcalcic, which is consistent with clinopyroxene quench trends. However, there appears to be similar and a rather large variation in ^{IV}Si, ^{IV}Al, and calculated pyroxene endmembers (Figure 2.2 and Table 2.3) among clinopyroxenes analyzed from both chilled margin and dyke interior samples. There is

COMPOSITIONAL VARIATION IN CLINOPYROXENES

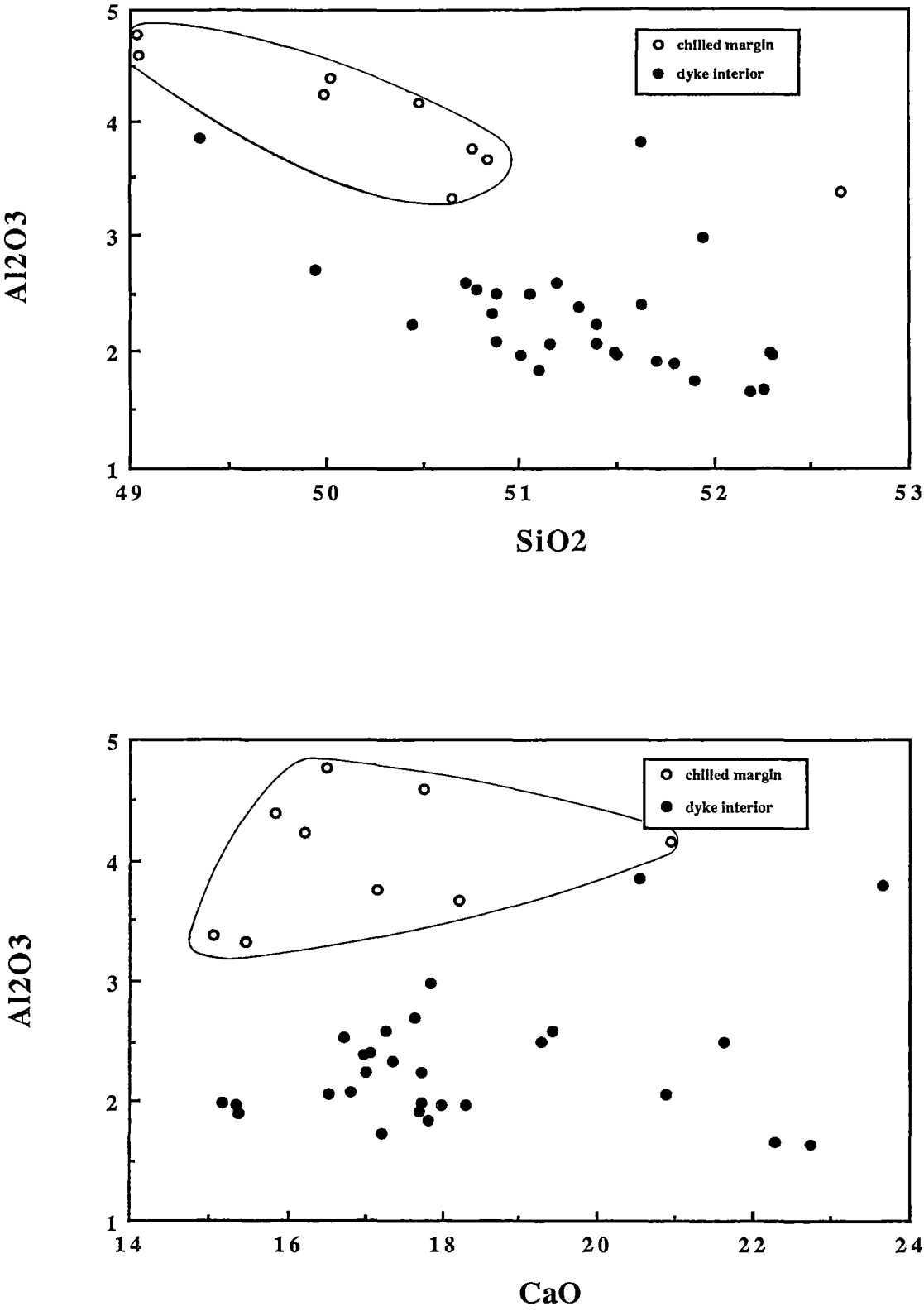


Figure 2.2
 Al_2O_3 content in clinopyroxene plotted against SiO_2 and CaO distinguishing between chilled margins and dyke interior samples.

no clear relationship between pyroxene end-member content and Mg# or quenched margins or dyke interior source. As noted above averaged Al_2O_3 contents emphasize the lower Al_2O_3 content present in the more slowly cooled dyke interior samples.

2.2.3 Discussion

A maximum pressure of *ca.* 7.5 kbar (Figure 2.1) obtained from aluminium exchange between plagioclase and clinopyroxene was calculated from two assemblages in one chilled margin sample, assuming a temperature of 1150° C. In contrast most pairs from the dyke interior samples give estimates of less than 4 kbar and eight pairs give pressures of less than 2 kbar. The average pressure in chilled margin samples is about 2 kbars higher than pressures calculated for the dyke interior. While the 7.5 kbar pressure is in agreement with the estimation of emplacement pressures based on experimental studies (Kuehner, 1986) to observed phenocryst phases in chilled margins, the presence of the low Al_2O_3 -content clinopyroxene, together with plagioclase + quartz, in the dyke interiors is quite inconsistent with such high pressures.

In interpreting the aluminous clinopyroxene + plagioclase + quartz assemblage of the groundmass of chilled margin samples as confirming the high pressure (7 - 8 kbar) emplacement of the high-Mg tholeiite dykes, Kuehner (1986, 1987) argued that this fine-grained mineralogy approached the ambient conditions of the country rock. It was inferred that these fine-grained mineral assemblages had equilibrated to existing metamorphic conditions. If correct, this interpretation would require that the coarser-grained, more slowly cooled mineral assemblages of the dyke interior should also record higher emplacement pressures. This is clearly not the case. This interpretation would require the retention of higher, igneous temperatures in dyke interiors (coarse grained assemblages) compared with lower devitrification temperatures (metamorphic temperatures) from the fine grained mineralogy. As has been described above, the situation is the reverse of this with a zoned, high temperature and metastable quench mineralogy being preserved in the chilled margins.

The new data indicate that the chilled margins have crystallized more Ca-Tschermaks-rich pyroxene, not because of high pressure emplacement, but because of rapid crystallization. It is notable that the more slowly cooled dyke interiors also retain igneous mineralogy including compositional zoning in minerals intergrown in ophitic and sub-ophitic textures. Application of the plagioclase + clinopyroxene + quartz geobarometer to these assemblages, particularly assuming high temperatures ($\sim 1000^{\circ}\text{C}$), yield pressure estimates as low as 1 - 2 kbar for some examples. Since the effect of quench crystallization and absence of coexisting quartz ($a_{\text{SiO}_2} < 1$) in chilled margins are to give increased Ca Tschermaks substitution and higher apparent pressures of crystallization, the preferred interpretation is that the depth of crystallization of the high-Mg tholeiite dykes is ≤ 4 kbar and maybe as low as 1 - 2 kbar (4 - 7 km).

2.3. IMPLICATIONS OF HIGH PRESSURE LIQUIDUS MINERALOGY OF THE HIGH-MG THOLEIITES

2.3.1 Introduction

Experimental studies of the liquidus phase relationships for a high-Mg tholeiite composition were carried out by Kuehner (1986) in attempt to reproduce the olivine-orthopyroxene phenocryst assemblages observed in the natural rocks. Olivine and orthopyroxene were found to be coexisting liquidus phases at 7.5 kbar and 1270°C , with olivine occurring as the sole liquidus phase at lower pressure and orthopyroxene the liquidus phase at higher pressure. It was argued that the sample composition studied experimentally, collected from the dyke margin, represents a liquid composition with Mg# 65 based on theoretical Fe - Mg exchange between orthopyroxene + liquid. Based on $K_D^{\text{cryst/liq}} = 0.3$ (Jaques & Green, 1979) an equilibrium orthopyroxene of Mg# 86.1 is predicted which is slightly higher than the composition of the most magnesian orthopyroxene (Mg# = 84.4) in the natural rock.

The most magnesian olivine observed by Kuehner (1986) has Mg# 78.5 which is not in equilibrium with the most magnesian orthopyroxene. Based on a $K_D^{Fe/Mg_{Ol/Opx}}$ value of 1.1 (Matsui & Nishazawa, 1974; Mori & Green, 1978; Jaques & Green, 1979), Kuehner (1986) further predicted an equilibrium olivine composition of Mg# 85. Samples analyzed in this study (collected from the same dyke) confirm the whole rock and orthopyroxene compositions of Kuehner, and establish the existence of magnesian olivines with Mg# up to 84.9, coexisting with orthopyroxene phenocrysts of Mg# 84.4, in accordance with Kuehners prediction.

2.3.2 Discussion

Experimental results suggest crystallization of observed orthopyroxene and olivine phenocrysts from a tholeiitic liquid under P-T conditions of 7.5 kbar and 1270° C (Kuehner, 1986). The results are in good agreement with chilled margin phenocryst compositions identified in the present study. The conclusion that the microphenocrysts of olivine and orthopyroxene represent equilibrium liquidus phases for the high-Mg tholeiite magma at 7.5 kbar, 1270° C is thus well founded.

Experimental studies are based on the most primitive phenocryst compositions obtained from a sample collected from the dyke margin. However, microprobe analyses show strong chemical zonation of orthopyroxene phenocrysts, especially in the slowly cooled dyke interior samples. Olivines on the other hand are always homogeneous, but become more Fe-rich in the dyke interior. The Fe-rich nature of olivine from the dyke interior, coexisting with zoned orthopyroxene with Mg-rich cores, may result from the more rapid intercrystalline diffusion of Fe and Mg in olivine relative to orthopyroxene (Jaques & Green, 1979), allowing olivine to re-equilibrate with the evolving liquid composition.

The preservation of magnesian orthopyroxene (Mg# 84.4) and olivine (Mg# 84.9) phenocryst assemblages in the chilled margins can be interpreted as a failure of the phenocrysts to achieve re-equilibration at local pressure conditions. Thus, it is suggested that the most magnesian natural phenocryst assemblages (in chilled margins)

do not represent P-T conditions of emplacement but the pressure and temperature of 7.5 kbar and 1270° C may represent the P-T conditions in a subjacent magma chamber in which the magma has been temporarily stored prior to the dyke emplacement.

2.4 PRESSURE ESTIMATIONS USING ARGUMENTS OF MAGMATIC EVOLUTION AT VARIOUS PRESSURES

Significant differences occur between the fractional crystallization path of a magma at 7.5 kbar and at 1 - 2 kbar. At 7.5 kbar olivine and orthopyroxene will co-precipitate in tholeiite compositions until joined by clinopyroxene and or plagioclase (Duncan & Green, 1980). The liquid will lie very close to the plagioclase - orthopyroxene join of the basalt tetrahedron (in projection from clinopyroxene, Figure 2.3). Consequently liquids at 7.5 kbar will evolve towards plagioclase, controlled largely by orthopyroxene and little or no olivine crystallization.

At 1 - 2 kbar compositions such as 70533 (chilled margin) or 70536 (interior), which lie close to the plagioclase - orthopyroxene join, will crystallize olivine only as a liquidus phase and evolve by olivine separation towards more quartz-normative compositions. As crystallization proceeds olivine will become more Fe-rich. In the case of ascending magma, magnesian orthopyroxene, crystallized at higher pressures, would be out of equilibrium and could show resorption and mantling by olivine. It may also show Fe/Mg exchange adjustment in attempt to remain in equilibrium with the decreasing Mg# of the evolving liquid.

It is thus possible to use the pressure-control on magmatic crystallization paths in two ways to constrain the depth of emplacement of the high-Mg tholeiite suite. Chilled margin compositions, if aphyric, may reveal the liquid line of descent. If liquids with Mg# < 65 plot well into the quartz-normative field they indicate low pressure and olivine control at P < 7.5 kbar. In addition they may, if sufficiently evolved crystallize an olivine + pigeonite + augite cotectic phase assemblage (Duncan & Green, 1980) and thus indicate crystallization near or below 2 kbar.

Sample No.	70533	Olivine	Orthopyroxene	Derivative
Mineral Modes (vol%)		5	11	
SiO ₂	51.80	39.92	53.48	52.93
TiO ₂	0.60		0.04	0.70
Al ₂ O ₃	11.36		1.56	13.08
Fe ₂ O ₃	1.16		0.86	1.26
FeO	9.40	14.58	9.82	9.25
MnO	0.19	0.17	0.21	0.19
MgO	12.36	44.84	29.79	9.19
CaO	9.28		2.45	10.56
Na ₂ O	1.74			2.03
K ₂ O	0.59			0.69
P ₂ O ₅	0.10			0.12
Total	98.58	98.58	98.21	100.00
Mg#	67.8	84.8	83.4	61.2
KD ol/Liq	0.38			0.29
KD opx/Liq	0.42			0.31

Sample No.	70536	Olivine	Orthopyroxene	Derivative
Mineral Modes (vol%)		3.5	14	
SiO ₂	52.83	39.18	53.32	54.13
TiO ₂	0.55		0.15	0.65
Al ₂ O ₃	11.52		2.52	13.74
Fe ₂ O ₃	1.12			1.38
FeO	9.05	17.25	11.27	8.45
MnO	0.19	0.10	0.26	0.18
MgO	11.56	43.10	29.29	7.32
CaO	9.32		2.56	11.03
Na ₂ O	1.81			2.23
K ₂ O	0.61			0.75
P ₂ O ₅	0.12			0.15
Total	98.68	99.63	99.37	100.00
Mg#	68.3	81.7	82.2	57.4
KD ol/Liq	0.47			0.30
KD opx/Liq	0.46			0.29

Table 2.2

Estimated liquid composition (Fe²⁺/Fe³⁺ = 0.1) in equilibrium with Mg# 84.8 olivine and Mg# 83.4 orthopyroxene (chilled margin 70533) and Mg# 81.7 olivine and Mg# 82.2 orthopyroxene (dyke centre 70536), using KD Fe/Mg crystal/liquid of 0.3 following Jaques & Green (1979). The amount of olivine and orthopyroxene fractionated from the natural assemblage to calculate equilibrium liquids are in agreement with observed mineral modes (determined by point counting). Olivine and orthopyroxene from chilled margin are in equilibrium with a liquid of Mg# 61.2, whereas those from the centre with a liquid of Mg# 57.4.

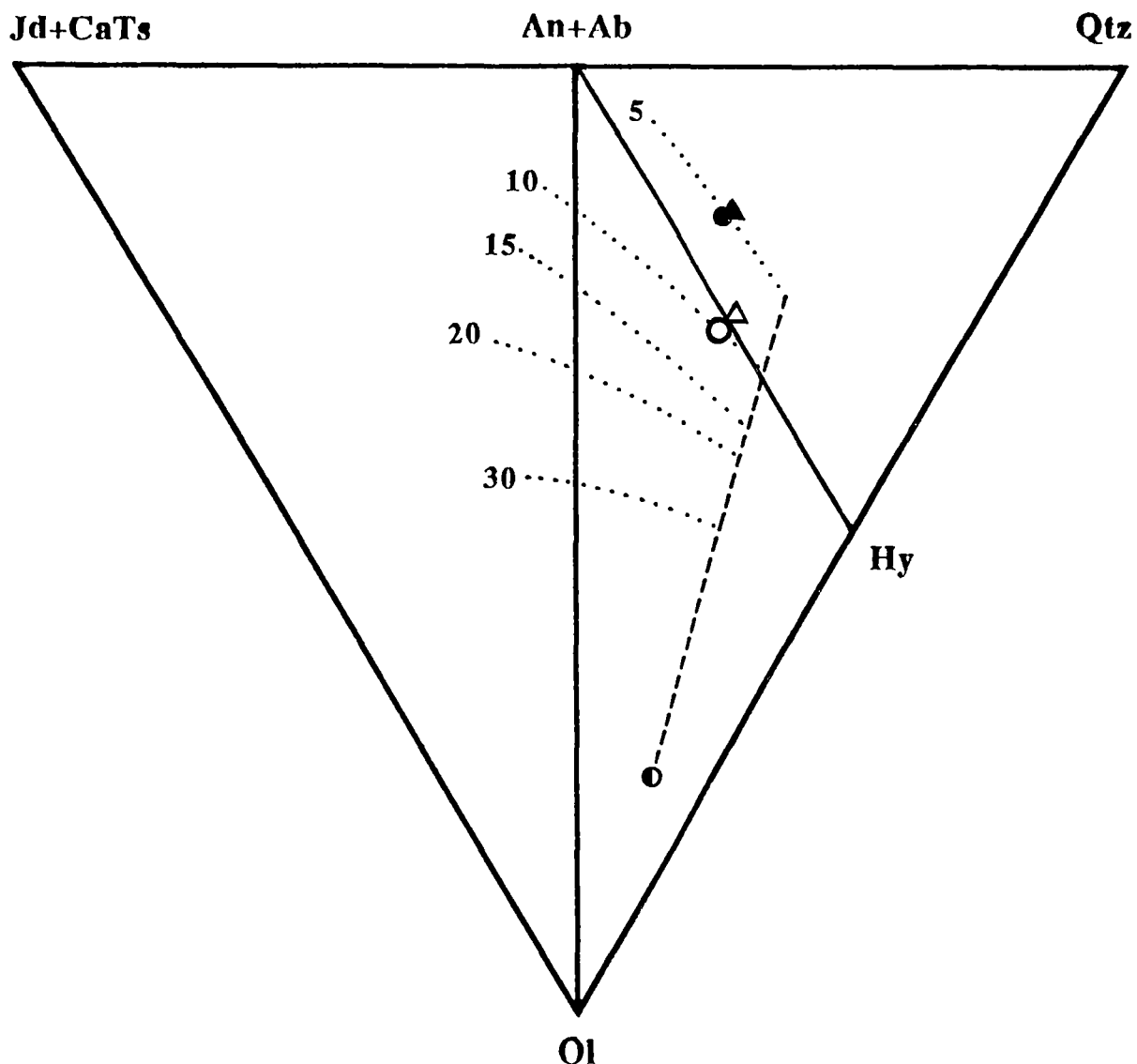


Figure 2.3

Calculated liquid compositions (solid symbols) in equilibrium with Mg# 81.7 olivine and Mg# 82.2 orthopyroxene, using a $K_D^{\text{cryst/liq}} = 0.3$ (Jaques & Green, 1979), are projected from diopside onto the Jd+CaTs - Qtz - Ol plane of the basalt tetrahedron following Falloon & Green (1988). Broken lines are olivine-orthopyroxene cotectics. **●** Hawaiian Pyrolite. Observed bulk rocks and olivine + orthopyroxene natural assemblages: **○** 70533 (chilled margin), **△** 70536 (dyke centre). Estimated liquids: **●** using chilled margin whole rock and phenocryst compositions, **▲** dyke interior whole rock and phenocryst compositions to calculate the equilibrium liquids.

A second approach is to use the olivine composition of the dyke interiors noting that these olivines are homogeneous and of composition Mg# 80 - 82. For example sample 70536, collected from a dyke centre, has a similar bulk composition to 70533 (chilled margin), but contains olivine phenocrysts which are too Fe-rich (Mg# 80 - 82) to be in equilibrium with a magma composition corresponding to the bulk rock composition, i.e. Mg# 68. Orthopyroxenes in sample 70536 are strongly zoned from Mg# 84.4 to Mg# 67 and rims are in part sub-calcic augite (Mg# 71.5).

Mineral modes (determined by point counting) for 70533 using olivine : orthopyroxene ratio 1 : 3 and $K_D^{Fe/Mg_{Ol/liq}} = 0.3$ (olivine Mg# = 84.8) gives a liquid composition with 1.8% normative quartz for chilled margin liquid in equilibrium with olivine of Mg# = 84.8. In contrast, dyke interior (70536) with mineral modes of 3.5% olivine and 14% orthopyroxene, constrained by $K_D^{Fe/Mg_{Ol/liq}} = 0.3$, yield calculated derivative liquids in equilibrium with olivine of Mg# = 81.7 with > 54 wt% SiO₂ and up to 5% normative quartz (Table 2.2).

The two contrasting inferences are reconciled by the postulate that the magma for the high-Mg tholeiite suite passed through a 'temporary storage' magma chamber at depth of ~28 km (7.5 kbar). The magma batches feeding the dykes crystallized small olivine and orthopyroxene crystals within or shortly after leaving this deep magma chamber and thus retain the signature of 7.5 kbar, 1270° C for their initial crystallization. However, the magma batches reach shallower levels before final quenching as the observed dyke interiors evolved to more siliceous liquids consistent with pressures < 5 kbar (Figure 2.3).

2.5 SUMMARY

Various methods of estimating pressure of emplacement of high-Mg tholeiites have been discussed in previous sections with the result that (1) these dykes were emplaced at low pressures and (2) previous high pressure estimates are incorrect due to rapid cooling and disequilibrium crystallization in chilled margins.

The geobarometer based on the aluminium exchange between clinopyroxene and plagioclase gives a range of pressures, corresponding to sample point location at macro- and micro-scale. It has also been shown that compositional variations in clinopyroxenes and olivines occur across the dyke, which has been interpreted as an effect of different cooling rates.

Assuming no within-dyke differentiation process (e.g. crystal fractionation or accumulation) it is suggested that mineral exchange geobarometers can only be applied to the more slowly cooled samples from the dyke interior to indicate emplacement pressures.

Estimated liquid compositions in equilibrium with Mg# 82 olivines, which are the most magnesian olivines commonly observed in the dyke interior, project close to the olivine-orthopyroxene cotectic at 5 kbar. These pressures were interpreted to represent maximum pressures of emplacement and are in agreement with maximum pressures yield from the barometry (based on aluminium exchange) for dyke interior samples.

In conclusion: The 2350 Ma old high-Mg tholeiitic dyke suite has been emplaced at low crustal levels no more than 3 - 5 kbars but possibly as low as 1 - 2 kbars. This pressure estimate is much lower than estimates from previous studies (7 - 8 kbar; Kuehner, 1986).

This also suggests that the Vestfold Hills block must have undergone a much faster uplift history in the early Proterozoic, being uplifted from deeper- into mid- to upper crustal levels. PTt-paths for the Vestfold Hills as concluded from previous work as well as the conclusions from this study are summarized in Figure 2.4.

UPLIFT HISTORY - VESTFOLD HILLS

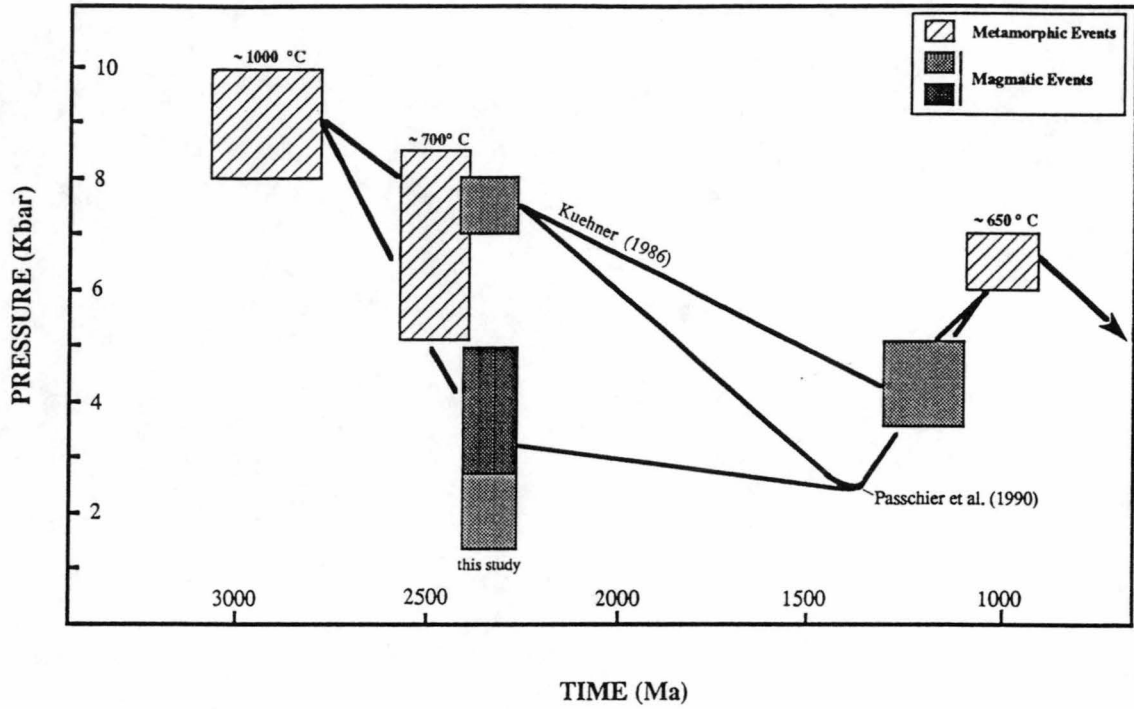


TABLE 2.3

SELECTED CLINOPYROXENE MICROPROBE ANALYSES

Sample No.	70536	70538				70536				70537			
Pos. of Anal.	rim-plag	rim-plag	rim-plag	rim-plag	rim-plag	rim-plag	rim-plag	rim-plag	rim-plag	rim-plag	rim-plag	rim-plag	rim-plag
Rock Type	High-Mg	Tholeiite	chilled margins					dyke centre		dyke interior			
SiO ₂	49.05	49.03	49.99	50.02	50.48	51.62	50.83	51.19	51.40	52.25	52.19	51.10	50.86
TiO ₂	0.59	0.48	0.45	0.57	0.57	0.00	0.41	0.25	0.02	0.28	0.60	0.29	0.66
Al ₂ O ₃	4.59	4.77	4.21	4.39	4.15	2.40	3.66	2.59	1.92	1.67	1.65	1.85	2.50
Cr ₂ O ₃	0.03	0.03	0.11	0.09	0.04	0.44	0.15	0.16	0.54	0.11	0.11	0.20	0.29
FeO	11.73	13.16	13.15	12.58	9.29	13.01	11.64	11.45	11.61	7.81	6.60	12.11	8.33
NiO	0.04	0.03	0.00	0.06	0.00	0.00	0.16	0.07	0.09	0.05	0.00	0.00	0.01
MnO	0.18	0.26	0.25	0.21	0.15	0.26	0.22	0.24	0.34	0.09	0.06	0.18	0.14
MgO	14.55	14.90	15.32	15.58	14.10	14.91	15.02	15.91	15.25	14.95	14.70	15.10	14.43
CaO	17.76	16.50	16.20	15.83	20.92	17.08	18.20	17.26	17.69	22.29	22.75	17.82	21.61
Na ₂ O	0.42	0.46	0.34	0.36	0.50	0.36	0.35	0.33	0.31	0.31	0.25	0.27	0.37
Total	98.94	99.61	100.02	99.69	100.20	100.08	100.65	99.46	99.17	99.79	98.90	98.91	99.23
Cations (6 ox)													
Si	1.846	1.836	1.865	1.868	1.869	1.932	1.885	1.914	1.938	1.939	1.952	1.930	1.904
Ti	0.017	0.013	0.013	0.016	0.016	0.000	0.011	0.007	0.000	0.008	0.017	0.008	0.019
Al	0.204	0.211	0.186	0.194	0.182	0.106	0.161	0.114	0.086	0.073	0.073	0.082	0.111
Cr	0.001	0.001	0.003	0.003	0.001	0.013	0.004	0.005	0.016	0.003	0.003	0.006	0.008
Fe ²⁺	0.269	0.289	0.330	0.331	0.205	0.363	0.293	0.296	0.321	0.190	0.202	0.327	0.198
Fe ³⁺	0.100	0.123	0.081	0.062	0.083	0.044	0.068	0.062	0.045	0.053	0.004	0.055	0.063
Mg	0.816	0.831	0.852	0.867	0.778	0.831	0.830	0.887	0.857	0.827	0.819	0.850	0.804
Ca	0.716	0.662	0.647	0.633	0.830	0.685	0.723	0.691	0.714	0.886	0.911	0.721	0.866
Na	0.031	0.034	0.024	0.026	0.036	0.026	0.025	0.024	0.023	0.022	0.018	0.020	0.027
Sum	4.000	4.000	4.000	4.000	4.000	4.000	4.000	4.000	4.000	4.000	4.000	4.000	4.000
Mg#	68.9	66.9	67.5	68.8	73.0	67.1	69.7	71.2	70.1	77.3	79.9	69.0	75.5
Endmembers													
Mg ₂ SiO ₆	40.8	41.6	42.6	43.4	38.9	41.6	41.5	44.3	42.8	41.3	41.0	42.5	40.2
Fe ₂ SiO ₆	13.5	14.4	16.5	16.5	10.2	18.1	14.7	14.8	16.1	9.5	10.1	16.4	9.9
Ca ₂ SiO ₆	29.0	25.6	26.2	25.9	35.8	30.8	31.0	30.6	32.6	41.6	44.0	33.0	39.4
NaAlSi ₃ O ₆	0.0	0.0	0.0	0.0	0.0	0.0	0.0	0.0	0.0	0.0	1.1	0.0	0.0
NaFeSi ₃ O ₆	3.0	3.3	2.1	2.4	3.5	1.4	2.1	1.9	0.7	1.9	0.4	1.4	1.9
NaCrSi ₃ O ₆	0.1	0.1	0.3	0.3	0.1	1.3	0.4	0.5	1.6	0.3	0.3	0.6	0.8
CaAl ₂ SiO ₆	5.1	4.7	5.0	6.2	5.1	3.7	4.5	2.9	2.3	1.2	1.4	1.3	1.5
CaFeAlSiO ₆	6.9	9.1	6.0	3.8	4.8	3.1	4.7	4.3	3.8	3.4	0.0	4.1	4.4
CaCrAlSiO ₆	0.0	0.0	0.0	0.0	0.0	0.0	0.0	0.0	0.0	0.0	0.0	0.0	0.0
CaTiAl ₂ O ₆	1.7	1.3	1.3	1.6	1.6	0.0	1.1	0.7	0.0	0.8	1.7	0.8	1.9
Total	100.0	100.0	100.0	100.0	100.0	100.0	100.0	100.0	100.0	100.0	100.0	100.0	100.0

SELECTED PLAGIOCLASE MICROPROBE ANALYSES

Sample No.	70548	70535				70536			
Pos. of Anal.	rim-cpx	rim-cpx	rim-cpx	rim-cpx	rim-cpx	rim-cpx	rim-cpx	rim-cpx	rim-cpx
Rock Type	High-Mg	Tholeiite	chilled margin		dyke interior			dyke centre	
SiO ₂	54.02	54.89	54.05	52.82	51.60	52.82	54.63	52.94	54.03
Al ₂ O ₃	28.80	27.74	28.52	29.05	30.05	29.05	29.79	30.72	29.26
FeO	0.31	0.71	0.46	0.27	0.24	0.27	0.41	0.29	0.38
MgO	0.04	0.57	0.03	0.03	0.00	0.03	0.07	0.02	0.00
CaO	11.63	11.60	11.40	12.20	13.57	12.20	12.54	13.47	12.46
Na ₂ O	4.83	5.10	4.88	4.48	3.91	4.48	4.30	3.85	4.42
K ₂ O	0.33	0.00	0.10	0.15	0.14	0.15	0.11	0.06	0.12
Total	99.97	100.60	99.44	98.99	99.51	98.99	101.85	101.34	100.67
Cations									
Si	2.449	2.491	2.461	2.420	2.360	2.420	2.432	2.372	2.433
Al	1.543	1.487	1.535	1.573	1.624	1.573	1.567	1.627	1.557
Ca	0.565	0.564	0.556	0.599	0.665	0.599	0.598	0.647	0.601
Na	0.425	0.448	0.431	0.398	0.347	0.398	0.371	0.334	0.386
K	0.019	0.000	0.006	0.009	0.008	0.009	0.006	0.003	0.007
Sum	5.001	4.990	4.989	4.997	5.005	4.997	4.974	4.983	4.985
Endmembers									
An	56.0	55.7	56.0	59.6	65.2	59.6	61.3	65.7	60.5
Ab	42.1	44.3	43.4	39.6	34.0	39.6	38.1	34.0	38.8
Or	1.9	0.0	0.6	0.8	0.8	0.8	0.6	0.3	0.7

Selected mineral analyses from chilled margins and dyke interiors of a single high-Mg tholeiite dyke. Mg# (silicates) = 100 Mg/(Mg + Fe total).
Fe determination as FeO: Fe³⁺ and Fe₂O₃ calculated from stoichiometry.

CHAPTER 3

PETROGRAPHIC AND GEOCHEMICAL VARIATIONS IN A HIGH-MG THOLEIITE DYKE WITH RESPECT TO CRUSTAL ASSIMILATION DURING ASCENT AND DIFFERENTIATION PROCESSES FOLLOWING EMPLACEMENT

3.1 INTRODUCTION

Crustal contamination can be responsible for significant changes to a magmas chemistry and related properties and to its crystallization. Establishing the extent to which this process has affected the Vestfold Hills dykes is paramount to achieving an understanding of their petrogenesis. The migration of magma from the upper mantle through heterogeneous crust gives rise to many possible sites and products of crustal contamination. The extent to which crustal contamination may occur will be dependent upon the relative physical and chemical properties of the magma and its crustal wall-rocks as well as factors such as the dimensions of a magma body and cooling rates. It is well established that very hot komatiitic or picritic magmas can interact extensively with their wall-rocks through melting and assimilation of crustal material (Huppert & Sparks, 1985), and that primitive, Mg-rich magmas are more susceptible to contamination than evolved, Mg-poor magmas. The magma flow regime is particularly important in determining whether wall-rock contamination will occur, with turbulent flow strongly favouring contamination and laminar flow inhibiting contamination. The occurrence of turbulent flow is promoted by low viscosities, nature of magma, temperature, phenocryst content and dyke width. In modelling magma flow conditions

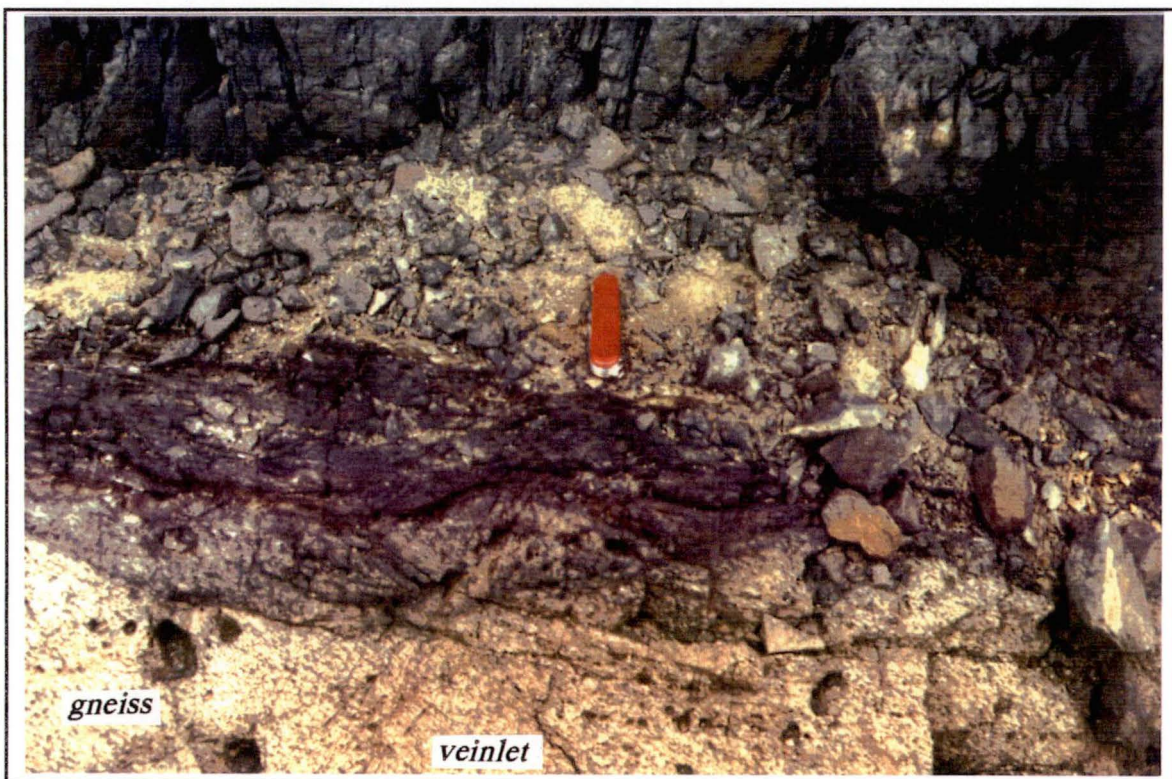
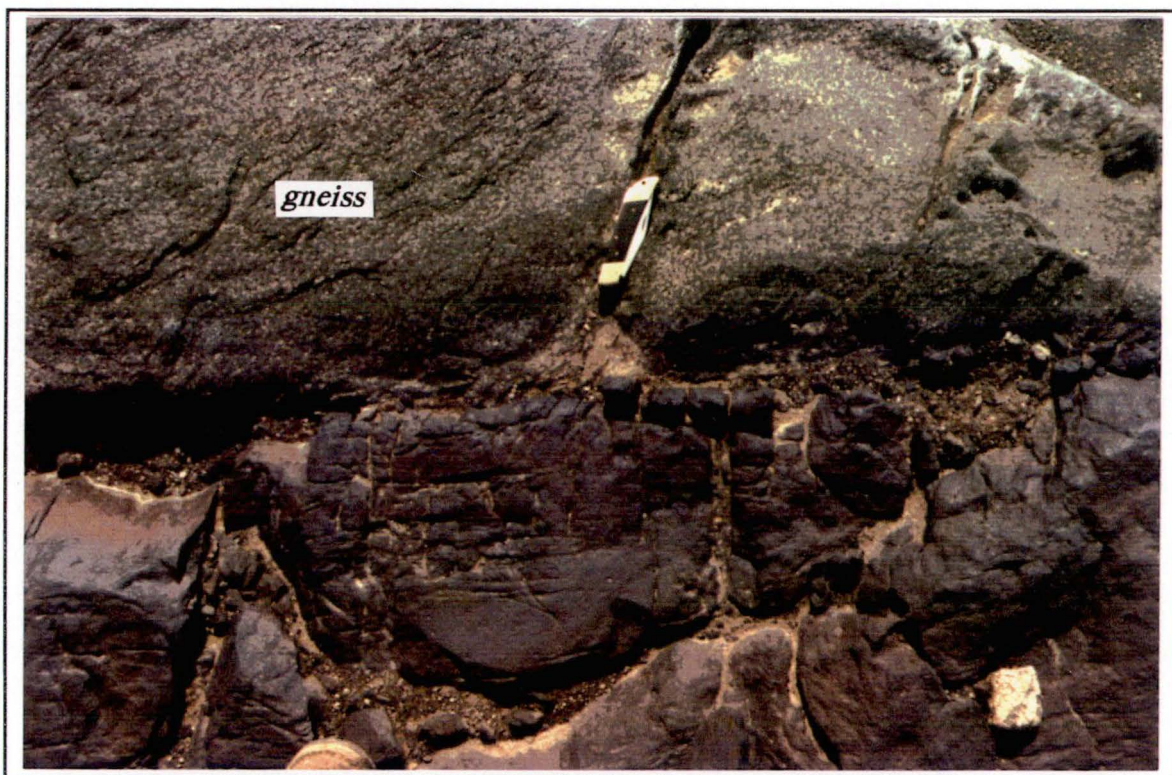


Figure 3.1

Dyke margins in contact with Crooked Lake Gneiss exhibiting a sharp contact and a well developed chilled margin (above) and a diffuse margin where the magma penetrated the country rock showing 'schlieren' texture (below). High-Mg tholeiite dyke south of Long Fjord.

Huppert & Sparks (1985) showed that a turbulent flow regime in a magma conduit will favour contamination, while a laminar flow regime will inhibit contamination.

It also has been shown that intrusive or extrusive magma bodies after their emplacement remain complex systems, where geochemical variations are due to locally restricted re-equilibration processes, crystal settling, fractional crystallization and other processes. Helz (1987) studied differentiation processes in Kilauea Iki Lava Lake, and Kalsbeck & Taylor (1986) showed geochemical variations in an 400 km long basic dyke and discussed the role of crustal contamination.

In order to evaluate the role of crustal assimilation in producing inhomogeneities in dykes from the Vestfold Hills area, one of the largest tholeiitic dykes (*ca.* 15 km and a width between 30 and 50 m) was systematically examined. This dyke belongs to the oldest recognized set of 2350 Ma high-Mg tholeiites. Sampling was undertaken both across the dyke, from the chilled margin to the centre, and along its entire length. This dyke was chosen because contamination was thought to be more likely to occur in larger magma bodies, where heat flux and magma flow rates will be relatively high.

The dyke dissects a variety of country rock types and can be followed along its E-W extension from the *Platcha* mylonite zone, into which it disappears, along the southern margin of *Long Fjord*, passing *Lied Bluff*, to *Soldat Island* (see dyke base map and compare Chapter 2).

3.2 FIELD EVIDENCE OF CRUSTAL CONTAMINATION

Throughout the Vestfold Hills and the dyke studied here in detail, field evidence for assimilation of crustal material by dykes is very limited. Dyke chilled margins were usually well defined (Figure 3.1), apart from the development of parallel schlieren structures within the country rock surrounding some dyke margins. These schlieren always occur beyond the dyke boundaries and are interpreted to be magma injected as small veinlets into the dyke wall rocks. These veinlets are mostly a couple of centimetres wide but do exceed one or two metres in several cases (Figure 3.1).

Crustal xenoliths in dykes are *very rare*. Where xenoliths are present at dyke margins, the magma surrounding these crustal xenoliths has been chilled and interaction does not appear to have occurred. The boundaries of xenoliths occurring in dyke centres, however, have been partially melted and assimilated by the intruding magma. In general the dyke-xenolith borders remain distinct and obvious evidence of mixing between magma host and xenolith is minimal. Despite the overall lack of field evidence for assimilation of crustal material at the depth of emplacement, prior contamination and local homogenization of the magma during ascent from depth, cannot be ruled out. The extensive sampling of the dyke undertaken here was designed to examine whether any such contamination had taken place.

3.3 PETROGRAPHY AND MINERAL CHEMISTRY

All samples of this large dyke are olivine and orthopyroxene phyric and samples from chilled margins are generally more altered than samples from the dyke interior. Anhedral olivine crystals in chilled margin samples are up to 0.6 mm in size and are always rimmed by kelyphite, comprising opaque minerals and orthopyroxene or are completely replaced by orthopyroxene and magnetite symplectites. Samples from the dyke centre frequently contain subhedral to anhedral olivine crystals up to 1.4 mm, which are mantled by orthopyroxenes. The mantling of olivine by orthopyroxene (without intergrown magnetite) reflects reaction of olivine with a more siliceous liquid and is important as an indication of pressure of equilibrium crystallization (Chapter 2).

Olivine phenocrysts show no zonation in Mg and Fe, revealing compositions of Mg# 82.5 in dyke interior samples and Mg# 85 in chilled margin samples. The modal abundance of olivine phenocrysts never exceeds 10 vol%.

Glomeroporphyritic clusters of euhedral orthopyroxene phenocrysts, up to 2 mm in size are more abundant than olivine, with modal abundances between 10 and 30 vol%. Subophitic textures are common, with small (0.1 - 0.3 mm) plagioclase laths being partly or entirely enclosed by orthopyroxenes (Figure 3.2). Compositions of

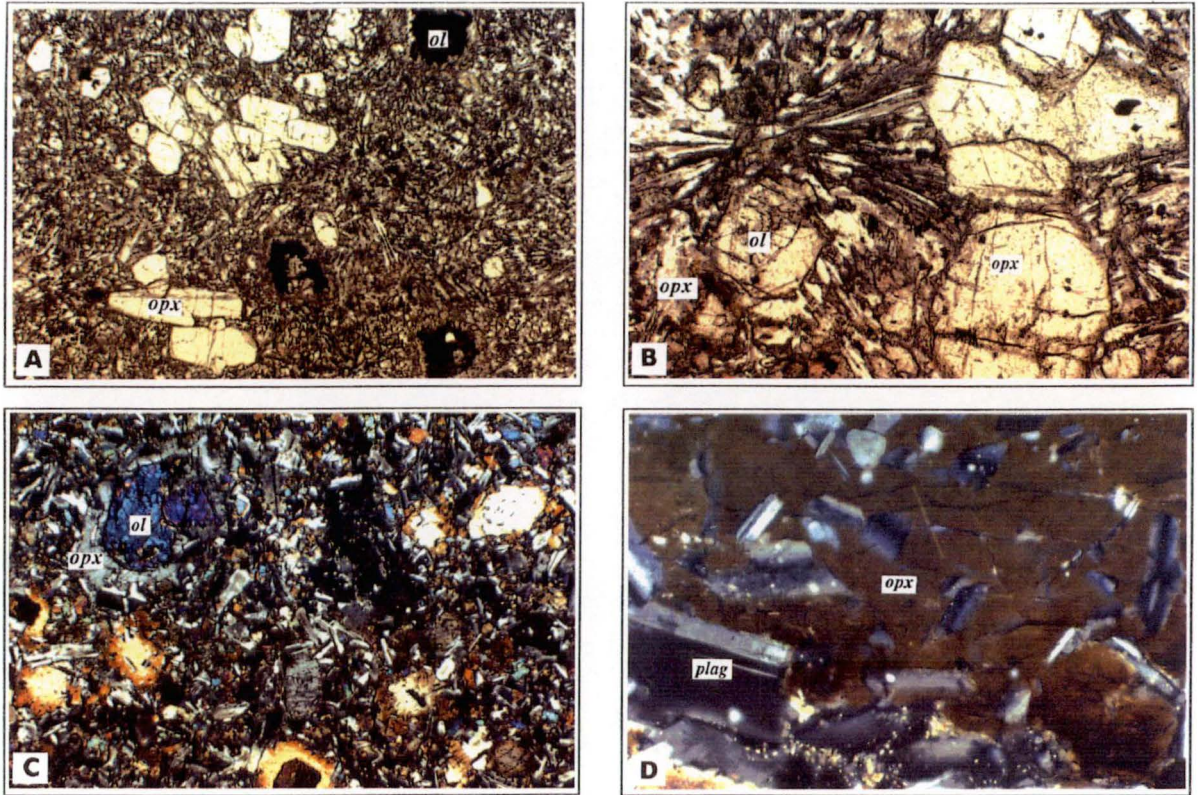


Figure 3.2

Photomicrographs of high-Mg tholeiite, showing chilled margin with orthopyroxene (*opx*) and olivine (*ol*) phenocrysts in a fine grained groundmass consisting mainly of clinopyroxene and plagioclase (A). Resorption of olivine (mantled by opaques and/or orthopyroxene) is shown in (A) and (B). Coarser grained dyke interior assemblages with orthopyroxene, plagioclase and myrmekite (C) and subophitic texture showing plagioclase (*plag*) laths partly or entirely enclosed in orthopyroxene (D). Scale: (A) 2.6 * 1.9 mm, (B) 1.3 * 0.95 mm, (C) 2.6 * 1.9 mm, (D) 0.65 * 0.45 mm.

enclosed plagioclase range from An 70.7 cores to An 61.5 rims. The orthopyroxene phenocrysts show strong zonation from Mg# 84.5 cores to Mg# 75 rims. Narrow (0.02 mm wide) inverted pigeonite rims occasionally occur around orthopyroxenes. Orthopyroxenes with inverted pigeonite rims in chilled margin samples have core Mg# values 84.4 for orthopyroxene and Mg# 71.4 for clinopyroxene exsolutions. Coexisting orthopyroxene phenocrysts (rim compositions) and adjacent clinopyroxene microphenocrysts from chilled margin samples give consistent temperatures around 1250° C using the geothermometers of Wells (1977), Kretz (1982), Lindsley (1983) and Bertrand & Mercier (1985) (see Table 3.1). The graphical thermometer of Lindsley (1983) gives higher temperatures for the clinopyroxene limb than for the orthopyroxene limb, ranging from 1100° up to 1250° C (Figure 3.3). Groundmass pyroxenes yield lower temperatures between 1128° to 1166° C, consistent with their more evolved, Fe-rich compositions.

Spinels are relatively common in the chilled margin samples but are absent in dyke interior samples. They occur as small (0.025 mm) euhedral to anhedral inclusions in orthopyroxene phenocrysts. Representative microprobe analyses are listed in Table 3.5. Spinels are unzoned and chrome-rich in character, with Cr# ($100 \text{ Cr}/(\text{Cr} + \text{Al})$) between 69.9 and 72.9.

The phenocrysts are embedded in a groundmass, consisting mainly of plagioclase, clinopyroxene and orthopyroxene in approximate abundance of 40, 20 and 10 vol%. Minor phases are biotite, apatite and opaques (magnetite, ilmenite and subordinate sulphides). Chilled margin samples and samples near the dyke margin have a fine grained groundmass which becomes gradually coarser towards the dyke centre (Figure 3.2). Groundmass orthopyroxenes have a wide range in composition with typically Mg# 65 in cores and becoming less magnesian (Mg# 59) towards the rim. Plagioclase is only present in the groundmass and has a compositional range of An 69.8 for core and An 47.1 for rims. As in other mafic dykes from the Vestfold Hills, plagioclase is mostly cloudy in appearance due to abundant, small ($< 1\mu\text{m}$) brown-greyish opaque inclusions (probably Fe-Ti oxides or sulphides) (see section

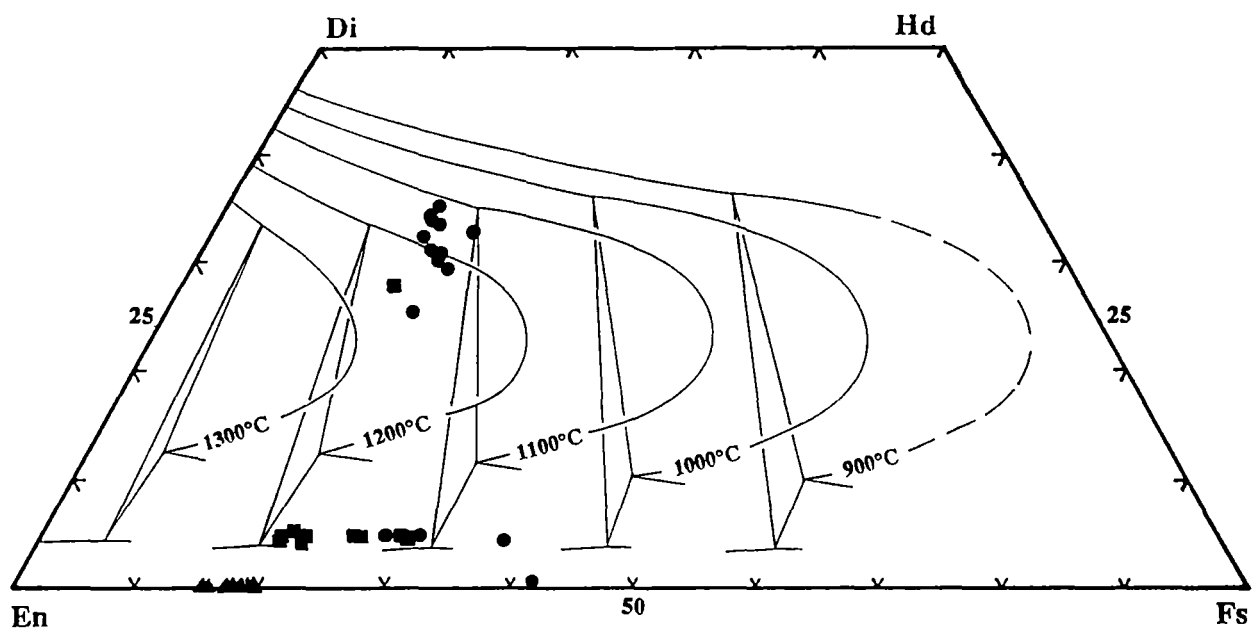


Figure 3.3

Graphical thermometer after Lindsley (1983) for 5 kbar. Projection shows coexisting clinopyroxene, orthopyroxene and olivine. Circles are rim compositions, squares are core compositions and triangles indicate olivines.

THERMOMETRY OF HIGH-MG THOLEIITE

Sample No. 70548

Sample Loc.: chilled margin

	cpx	opx	Thermometers	T°C
Si	1.892	1.940		
Ti	0.012	0.000	Bertrand & Mercier	1284
Al	0.129	0.051	Wells	1254
Cr	0.002	0.011	Kretz (>1080)	1264
Fe2+	0.268	0.502		
Fe3+	0.078	0.053		
Mn	0.000	0.012		
Mg	0.991	1.339		
Ca	0.611	0.089		
Na	0.017	0.000		
Sum	4.000	3.997		
Mg#	78.7	72.7		

Sample No. 70548

Sample Loc.: chilled margin

	cpx	opx	Thermometers	T°C
Si	1.885	1.910		
Ti	0.009	0.000	Bertrand & Mercier	1192
Al	0.135	0.083	Wells	1189
Cr	0.007	0.013	Kretz (>1080)	1195
Fe2+	0.214	0.540		
Fe3+	0.093	0.080		
Mn	0.000	0.010		
Mg	0.947	1.321		
Ca	0.689	0.041		
Na	0.021	0.000		
Sum	4.000	3.998		
Mg#	81.6	71.0		

Sample No. 70533

Sample Loc.: chilled margin

	cpx	opx	Thermometers	T°C
Si	1.985	1.951		
Ti	0.016	0.004	Bertrand & Mercier	1136
Al	0.076	0.064	Wells	1166
Cr	0.005	0.005	Kretz (>1080)	1128
Fe2+	0.276	0.611		
Fe3+	0.032	0.021		
Mn	0.000	0.011		
Mg	0.862	1.120		
Ca	0.727	0.213		
Na	0.020	0.000		
Sum	3.999	4.000		
Mg#	75.7	64.7		--

Table 3.1

Temperatures calculated from coexisting orthopyroxene and clinopyroxene pairs. Temperatures are calculated after Wells (1977), Kretz (1982) and Bertrand & Mercier (1985).

4.3.3). Plagioclase in samples near margins form variolitic textures, with individual laths up to 0.5 mm in size.

Coarser grained samples from the dyke centre are mostly more evolved and have crystallized alkali-feldspar-plagioclase-quartz myrmekite intergrowths as well as some interstitial quartz. Associated with the late stage crystallization of myrmekite is apatite, which grows in needles up to 0.3 mm in length. In sample 70553, the most evolved member of this dyke, plagioclase content increases up to 45 vol%, while quartz and alkali-feldspar myrmekite comprises up to 5 vol%. Orthopyroxene with rims of inverted pigeonite is the only phenocryst phase in the sample.

The petrographic variations described above are consistent along the strike of this dyke.

3.4 MAJOR AND TRACE ELEMENT GEOCHEMISTRY

Twenty-six samples were chosen for major and trace element geochemistry. The samples from cross sections of the dyke, taken at different localities along the dyke's length. Selected major and trace element analyses are listed in Table 3.2 (the complete data set are listed in Appendix 10.2).

With an average MgO content of 12 wt%, the dyke rock can be classified as an high-Mg tholeiite. Calculation of CIPW norms enables rocks to be classified according to their degree of Si-saturation. All samples are hypersthene normative with some being quartz-normative and others olivine-normative. This variation corresponds with across dyke sample locations, with chilled margin samples and those close to the dyke margin being olivine normative, changing to quartz normative compositions towards the dyke centre. SiO₂ content ranges between 50.5 and 53.9 wt%.

The major elements are plotted against Zr in Figure 3.4 A and B. MgO and Al₂O₃ define clear trends. Chilled margin samples are tightly clustered and generally have the more primitive, MgO-rich compositions, while most samples from the dyke centre are relatively evolved (lower MgO, higher Zr). The exceptions (samples 70570

REPRESENTATIVE HIGH-MG THOLEIITE WHOLE ROCK ANALYSES

Sample No.	70533	70536	70634	70553
Rock Type	HMT	HMT	HMT	HMT
Location	C.M.	D.I.	C.M.	D.I.
Major Elements				
SiO ₂	51.80	52.83	50.59	53.85
TiO ₂	0.60	0.55	0.57	0.69
Al ₂ O ₃	11.36	11.52	11.00	15.09
Fe ₂ O ₃	11.60	11.17	11.13	10.58
FeO	0.00	0.00	0.00	0.00
MnO	0.19	0.19	0.19	0.16
MgO	12.36	12.13	12.33	6.63
CaO	9.28	9.37	8.99	9.48
Na ₂ O	1.74	1.63	2.18	1.74
K ₂ O	0.59	0.61	0.71	0.93
P ₂ O ₅	0.10	0.10	0.11	0.10
LOI	0.14	-0.10	2.04	0.23
Total	99.76	100.00	99.84	99.48
Mg#	67.8	68.3	68.7	55.4
CIPW Norm wt%				
Qtz		1.31		7.27
Or	3.49	3.60	4.20	5.50
Ab	14.72	13.79	18.45	14.72
An	21.44	22.32	18.13	30.62
Lc				
Ne				
Cpx	19.39	19.04	20.83	12.97
Di	13.44	13.25	14.60	7.45
Hd	5.95	5.79	6.23	5.51
Opx	34.95	36.13	23.19	24.15
En	23.17	24.07	15.57	13.06
Fs	11.79	12.06	7.63	11.09
Ol	1.52		9.04	
Fo	0.97		5.87	
Fa	0.55		3.17	
Mt	1.68	1.62	1.62	1.54
Il	1.14	1.04	1.08	1.31
Ap	0.24	0.24	0.26	0.24
Trace Elements				
Ba	212	219	195	236
Rb	20	22	25	43
Nb	3	3	3	6
Sr	160	159	152	108
Zr	54	56	52	99
Y	18	15	16	25
La	8	9	7	17
Ce	16	14	15	31
Nd	10	9	8	13
Ni	311	262	301	119
Cr	1225	1093	1199	136
V	238	220	230	246
Sc	39	39	41	44

Table 3.2

Representative High-Mg Tholeiite (HMT) whole rock analyses from chilled margins (C.M.) and dyke interiors (D.I.).

High-Mg Tholeiite

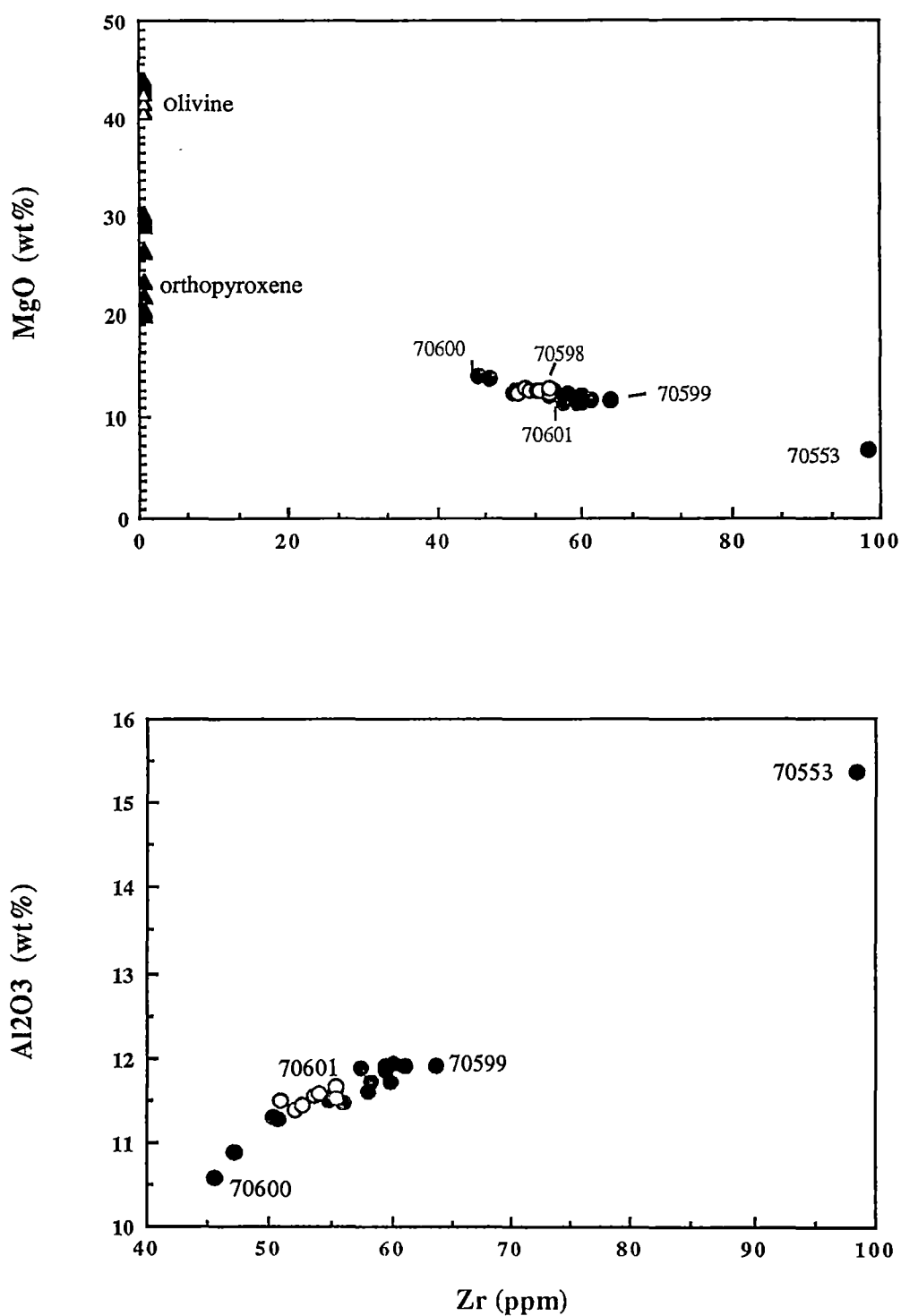


Figure 3.4 A

MgO and Al₂O₃ plotted against Zr. Open circles represent chilled margin sample and dots represent dyke interior samples (> 2 m from margins). Olivine compositions are shown as open triangles and orthopyroxene as filled triangles.

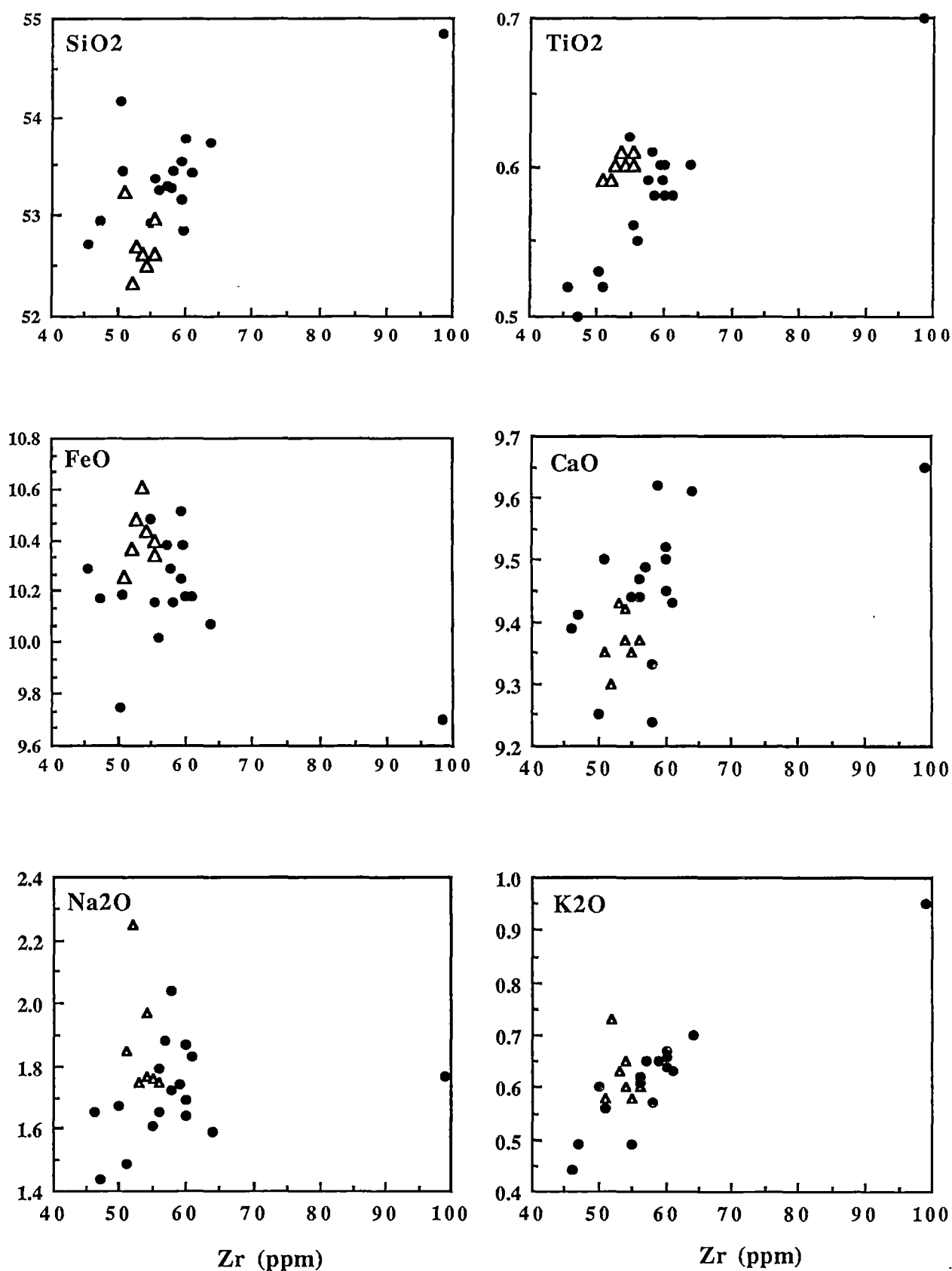


Figure 3.4 B

Selected oxides plotted against Zr as fractionation index. Triangles - chilled margins, dots - dyke interior samples.

and 70600) are notable and have the most primitive compositions in this intrusion.

Representative samples have been modelled by least-squares calculations (Le Maitre, 1980) to test whether the observed variations can be produced by the fractionation of observed phenocrysts from the chilled margin samples. Table 3.3 A shows the mixing of a chilled margin composition with 8.5% orthopyroxene, generating the most primitive member. The second most evolved composition (sample 70599) may be produced by 3.5% olivine fractionation from an intermediate chilled margin compositions (Table 3.3 C). Fractionating orthopyroxene instead of olivine from the second most evolved composition (Figure 3.3 B), a less satisfactory result is obtained (sum of squares: 2.1197). From petrographical observations, the compositions seem more likely to be controlled by orthopyroxene, rather than by olivine fractionation. As the whole rock compositions become more evolved, so the compositions are less readily explained by olivine and orthopyroxene fractionation. As Table 3.3 D reveals with a residual sum of squares of 3.359, it is not possible to generate the most evolved composition by extraction of an intermediate composition. Fractionating plagioclase, clinopyroxene, orthopyroxene and olivine from intermediate compositions (70599 and 70601), the most evolved composition can be generated (Figure 3.3 E and F).

While chilled samples preserve the parent magma composition, dyke interior samples which have cooled more slowly appear to behave as more complex systems, with fractional crystallization and flow differentiation occurring. The migration and accumulation of late stage liquids may be inferred in the occurrence of plagioclase and K-feldspar - quartz granophyric intergrowths. This is most likely to occur near the slowly cooled and crystallized dyke centre, resulting in the development of more varied bulk compositions enrichment and depletion in late stage liquids and/or accumulation and fractionation of phenocryst phases.

Trace element variations relative to Zr are shown in Figure 3.5. Both Ni and Cr content decrease (Figure 3.5) with increasing Zr, whereas the incompatible elements Rb, Ba, Sr and Nb increase systematically, with the exception of the most evolved

A				Estimated	
Sample No.	Reactant 70600	Product A 70598	Product B Opx core	Reactant	Difference
Description	most primitive	chilled margin	phenocryst		
SiO ₂	52.37	51.98	55.02	52.24	0.13
TiO ₂	0.52	0.59	0.06	0.55	-0.03
Al ₂ O ₃	10.50	11.43	1.25	10.57	-0.07
FeO	10.22	10.15	10.16	10.15	0.07
MgO	14.02	12.25	30.38	13.79	0.23
CaO	9.33	9.17	2.15	8.58	0.75
Na ₂ O	1.64	1.73	0.00	1.58	0.06
K ₂ O	0.44	0.57	0.00	0.52	-0.08
P ₂ O ₅	0.10	0.09	0.00	0.08	0.02
Total	99.14	97.96	99.02	98.06	1.08
Mass%	100.00	91.53	8.47		
Sum of squares					0.6621

B				Estimated	
Sample No.	Reactant 70598	Product A 70599	Product B Opx core	Reactant	Difference
Description	chilled margin	sec. most evol.	phenocryst		
SiO ₂	51.98	52.90	55.02	52.98	-1.00
TiO ₂	0.59	0.59	0.06	0.57	0.02
Al ₂ O ₃	11.43	11.71	1.25	11.32	0.11
FeO	10.15	9.10	10.16	9.14	1.01
MgO	12.25	11.40	30.38	12.10	0.15
CaO	9.17	9.38	2.15	9.11	0.06
Na ₂ O	1.73	1.55	0.00	1.49	0.24
K ₂ O	0.57	0.68	0.00	0.65	-0.08
P ₂ O ₅	0.09	0.12	0.00	0.12	-0.03
Total	97.96	97.43	99.02	97.48	0.48
Mass%	100.00	96.32	3.68		
Sum of squares					2.1197

C				Estimated	
Sample No.	Reactant 70598	Product A 70599	Product B Olivine	Reactant	Difference
Description	chilled margin	sec. most evol.	phenocryst		
SiO ₂	51.98	52.90	38.75	52.41	-0.43
TiO ₂	0.59	0.59	0.00	0.57	0.02
Al ₂ O ₃	11.43	11.71	0.00	11.30	0.13
FeO	10.15	9.10	17.18	9.38	0.77
MgO	12.25	11.40	43.95	12.54	-0.29
CaO	9.17	9.38	0.00	9.05	0.12
Na ₂ O	1.73	1.55	0.00	1.50	0.23
K ₂ O	0.57	0.68	0.00	0.66	-0.09
P ₂ O ₅	0.09	0.12	0.00	0.12	-0.03
Total	97.96	97.43	99.88	97.53	0.43
Mass%	100.00	96.51	3.49		
Sum of squares					0.9469

D		Product A	Product B	Product C	Estimated	
Sample No.	Reactant 70599	70553	Opx core	Olivine	Reactant	Difference
Description	sec. most evol.	most evolved	phenocryst	phenocryst		
SiO ₂	52.90	53.85	55.02	38.75	53.39	-0.49
TiO ₂	0.59	0.69	0.06	0.00	0.57	0.02
Al ₂ O ₃	11.71	15.09	1.25	0.00	12.56	-0.85
FeO	9.10	9.52	10.16	17.18	9.92	-0.82
MgO	11.40	6.63	30.38	43.95	11.44	-0.04
CaO	9.38	9.48	2.15	0.00	8.08	1.30
Na ₂ O	1.55	1.74	0.00	0.00	1.43	0.12
K ₂ O	0.68	0.93	0.00	0.00	0.76	-0.08
P ₂ O ₅	0.12	0.10	0.00	0.00	0.08	0.04
Total	97.43	98.03	99.02	99.88	98.23	-0.80
Mass%	100.00	82.08	13.83	4.09		
Sum of squares						3.3590

E		Product A	Product B	Product C	Product D	Product E	Estimated	
Sample No.	Reactant 70601	70553	Opx core	Olivine	Cpx	Plag	Reactant	Difference
Description	intermediate	most evolved	phenocryst	phenocryst	groundmass	groundmass		
SiO ₂	52.84	53.85	55.02	38.75	52.29	54.03	52.82	0.02
TiO ₂	0.55	0.69	0.06	0.00	0.28	0.00	0.49	0.06
Al ₂ O ₃	11.38	15.09	1.25	0.00	0.99	29.26	11.43	-0.05
FeO	9.94	9.52	10.16	17.18	11.37	0.38	9.90	0.04
MgO	12.43	6.63	30.38	43.95	15.99	0.00	12.43	0.00
CaO	9.37	9.48	2.15	0.00	17.72	12.46	9.38	-0.01
Na ₂ O	1.78	1.74	0.00	0.00	0.27	4.42	1.37	0.41
K ₂ O	0.61	0.93	0.00	0.00	0.00	0.12	0.61	0.00
P ₂ O ₅	0.11	0.10	0.00	0.00	0.00	0.00	0.07	0.04
Total	99.01	98.03	99.02	99.88	98.91	100.67	98.50	0.51
Mass%	100.00	65.01	6.29	10.45	13.63	4.62		
Sum of squares								0.1761

F		Product A	Product B	Product C	Product D	Product E	Estimated	
Sample No.	Reactant 70599	70553	Opx core	Olivine	Cpx	Plag	Reactant	Difference
Description	sec. most evol.	most evolved	phenocryst	phenocryst	groundmass	groundmass		
SiO ₂	52.90	53.85	55.02	38.75	52.29	54.03	53.19	-0.29
TiO ₂	0.59	0.69	0.06	0.00	0.28	0.00	0.49	0.10
Al ₂ O ₃	11.71	15.09	1.25	0.00	0.99	29.26	12.02	-0.31
FeO	9.10	9.52	10.16	17.18	11.37	0.38	9.49	-0.39
MgO	11.40	6.63	30.38	43.95	15.99	0.00	11.61	-0.21
CaO	9.38	9.48	2.15	0.00	17.72	12.46	9.60	-0.22
Na ₂ O	1.55	1.74	0.00	0.00	0.27	4.42	1.47	0.08
K ₂ O	0.68	0.93	0.00	0.00	0.00	0.12	0.60	0.08
P ₂ O ₅	0.12	0.10	0.00	0.00	0.00	0.00	0.06	0.06
Total	97.43	98.03	99.02	99.88	98.91	100.67	98.53	-1.10
Mass%	100.00	63.87	3.94	11.43	13.58	7.18		
Sum of squares								0.4503

Table 3.3

Least-squares mixing GENMIX (Le Maitre, 1980) calculation for various whole rock compositions, modelling major element variations within a single dyke.

sample (70553), which has Ba and Sr abundances falling well below the extrapolated trends. The extent and trend of these variations can be compared with the fractional crystallization results obtained by least squares modelling, using Rayleigh crystal fractionation equation:

$$C_l/C_o = F^{(D - 1)} \quad (3.1)$$

where C_l is the element concentration in liquid, C_o the original element concentration, F the weight proportion of melt and D the element distribution coefficient. Distribution coefficients taken from literature (Hart & Davis, 1978; Le Roex, 1980; Ewart & Taylor, 1969 and Hanson, 1977) and those calculated for Cr and Ni in orthopyroxene and olivine using percent crystal fractionation from GENMIX calculation, are in good agreement. The variations in Cr and Ni are best explained by orthopyroxene fractionation without involving olivine fractionation (see Figure 3.5).

In unchilled samples, Ti increases with increasing Zr suggesting ilmenite and magnetite have not played a role during fractionation. The modal content of ilmenite and magnetite increases from 2 vol% in the more primitive samples to about 8 - 10 vol% in the most evolved sample. In comparison to unchilled samples with similar Zr content, samples from the chilled margin have a higher Ti content - these are processes affecting Zr concentration or Ti/Zr which are not understood.

The relatively minor variations in trace element analyses observed in Figure 3.5, excluding sample 70553, are consistent with only minor *in situ* fractionation occurring within the dyke. The appreciable scatter observed for some of the elements plotted against Zr, is somewhat problematic but may result from variable degrees of crystal accumulation and melt migration on a local scale. Figure 3.5 illustrates increasing Nb, K, Rb, Y Sr and Ba concentrations with increasing fractionation, but depletion of Sr and Ba in the most evolved sample. Crystal fractionation may account for the change in Ba and Sr behaviour, as these elements are compatible in feldspar. With D_{Sr} values > 1, Sr will concentrate into crystallizing plagioclase and K-feldspar and therefore may

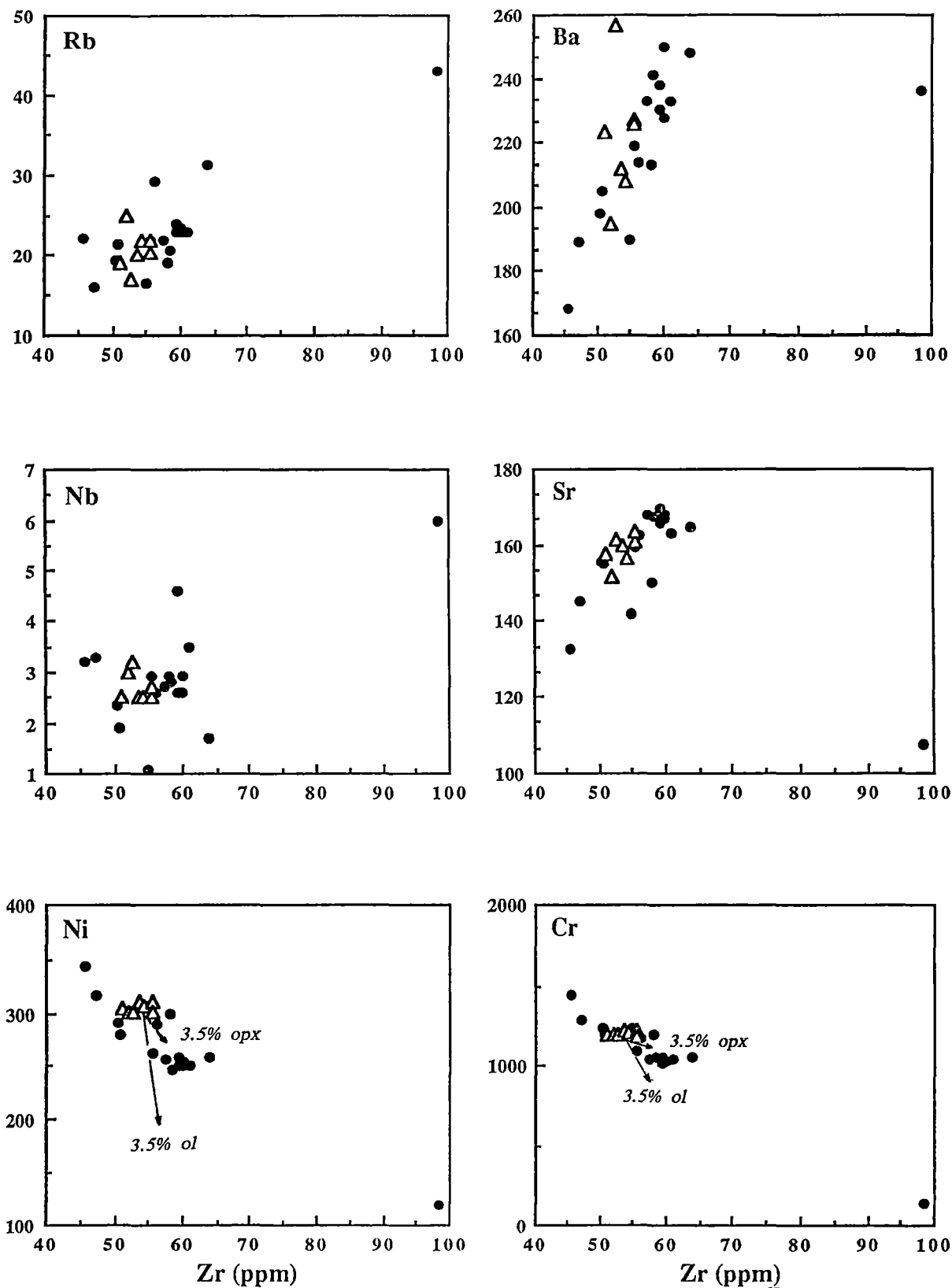


Figure 3.5

Selected trace elements plotted against Zr as a fractionation index, distinguishing between various chilled margins (triangles) and dyke interior samples (dots). Rayleigh model results are indicated by arrows.

become relatively depleted in late stage segregations. Least squares modelling of variations between intermediate and the most evolved composition (Figure 3.3 F) indicates plagioclase accounts for 20 % of the fractionating assemblage. This requires a $D_{\text{Sr}}^{\text{plag}} > 5$ if Sr is to be depleted by fractionation. Compared with distribution coefficients from the literature this required D_{Sr} is much too high. This may suggest that simple plagioclase fractionation is not responsible for the observed Sr variation. A more complex process, such as filter pressing could explain this variation, whereby plagioclase saturated residual liquid accumulates following migration through a plagioclase bearing matrix at a stage when the dyke was largely (e.g. 50%) crystalline.

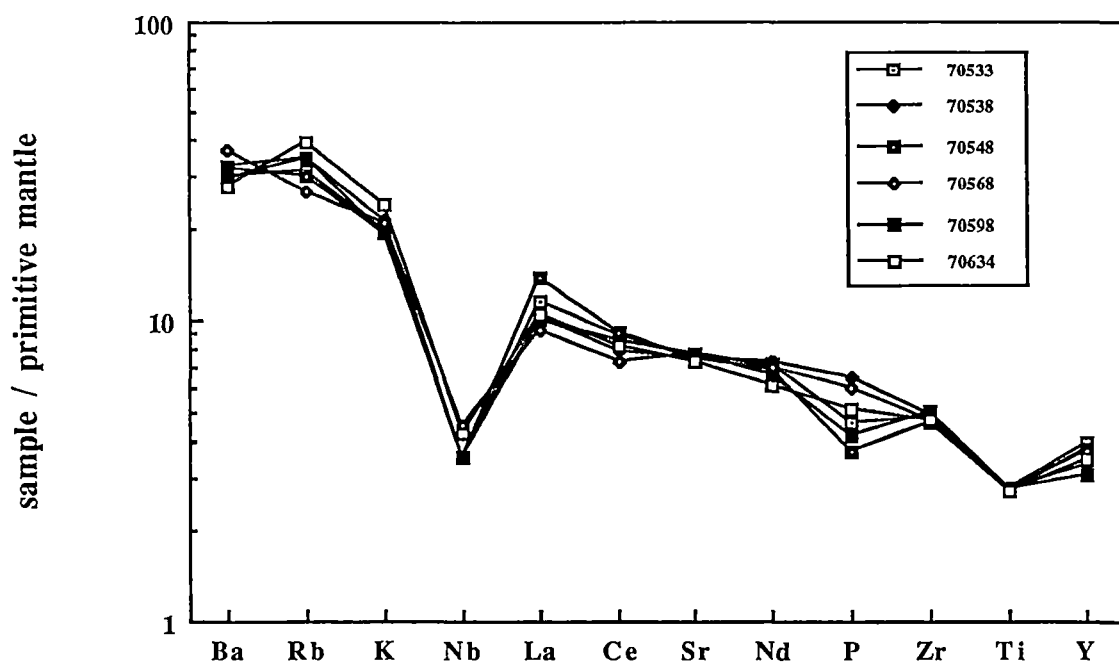
Multi element diagrams, normalized to primitive mantle, illustrate marked Nb depletion relative to other trace elements in all samples (Figure 3.6). Such anomalies in Nb are typical of continental tholeiites (e.g. Dupuy & Dostal, 1984). All the samples have nearly identical trace element patterns, with the exception of the most evolved and incompatible element-rich sample (70553), which has developed relative depletions in Sr, P and Ti.

The REE patterns (Figure 3.7) of these dykes (sample 70533 is not shown) are virtually identical with the slight variation in the patterns being within the range of analytical error. The lack of an Eu - anomaly supports previous arguments against the occurrence of plagioclase fractionation.

3.5. THE ROLE OF CRUSTAL ASSIMILATION IN PRODUCING GEOCHEMICAL VARIATION

The role of crustal contamination in the petrogenesis of continental tholeiites remains a controversial topic. It has been argued that crustal contamination is likely to play a significant role in the development of continental tholeiites (e.g. DePaolo, 1981; Huppert & Sparks, 1985). However, it has been demonstrated here that variations in major and trace element concentrations in the dyke examined here are accounted for by *in situ* fractionation processes.

HIGH-MG THOLEIITE - CHILLED MARGINS



HIGH-MG THOLEIITE - DYKE INTERIORS

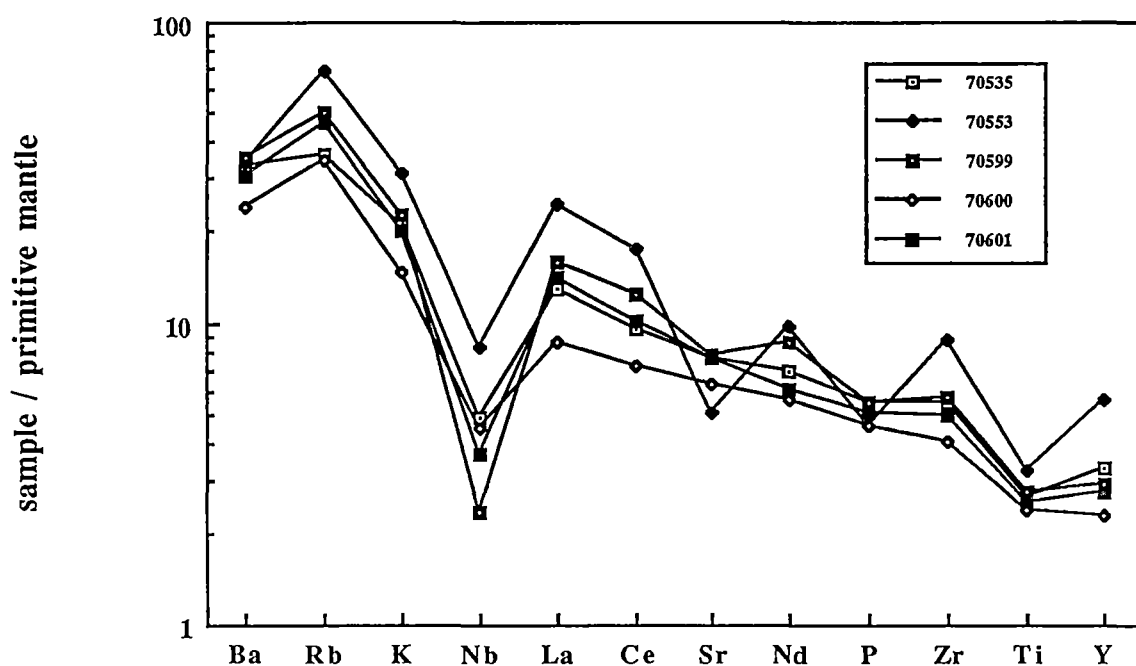


Figure 3.6

Incompatible element 'spidergrams' of chilled margins and dyke interiors, normalized to primitive mantle composition (Sun et al., 1989).

HIGH-MG THOLEIITE

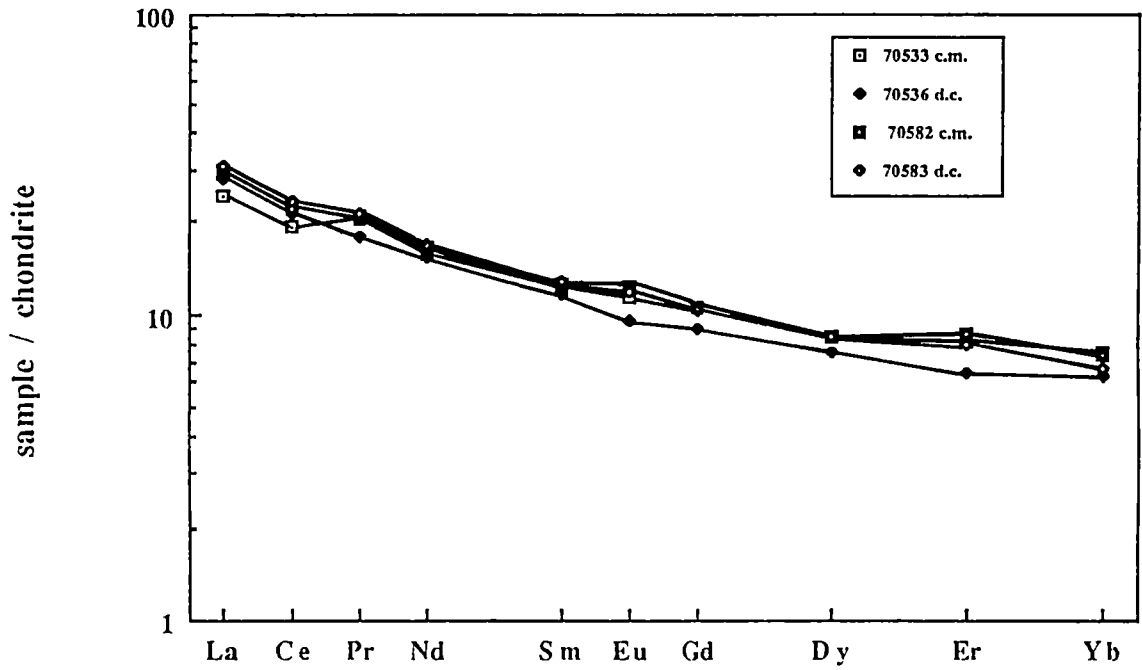


Figure 3.7

Chondrite normalized REE patterns (Leedy/1.2; Masuda et al. 1973; Taylor & Gorton, 1977) of chilled magin (c.m.) and dyke interior (d.c.) samples.

REE ANALYSES FROM HIGH-MG THOLEIITES

Sample No.	70533	70536	70582	70583
Rock Type	HMT	HMT	HMT	HMT
Sample Loc.:	c.m.	d.c.	c.m.	d.c.
REE / ppm				
La	7.8	8.9	9.4	9.9
Ce	15.6	17.2	18.0	19.0
Pr	2.4	2.1	2.4	2.5
Nd	9.3	9.1	9.8	10.1
Sm	2.4	2.2	2.4	2.5
Eu	0.8	0.7	0.9	0.9
Gd	2.7	2.3	2.7	2.7
Dy	2.7	2.4	2.7	2.8
Er	1.7	1.4	1.8	1.7
Yb	1.6	1.3	1.5	1.4
La/Yb	5.0	6.8	6.1	7.1

Table 3.4

Rare earth abundances in a high-Mg tholeiitic dyke from the central Vestfold Hills. Analyses were done following the method of Robinson et al. (1986). Concentrations are given in ppm.

Samples represent chilled margins (c.m.) and dyke centres (d.c.) from two cross sections. Abbreviation: HMT - high-Mg tholeiite

K, Rb, Ba and Sr are elements which are highly sensitive to crustal contamination. Only one chilled margin sample is slightly enriched in K and Rb but it is not enriched in Ba. Dupuy & Dostal, (1984) have proposed, that enrichment in K-group elements is a common characteristic of continental tholeiites, which may be inherited either from the subcontinental upper mantle or through the effects of crustal contamination.

Isotopic data from Collerson & Sheraton (1986) for the high-Mg suite in the Vestfold Hills only show minor variations in radiogenic ^{87}Sr and have very low initial ratios (0.7020 ± 0.0008). These data suggest crustal contamination is negligible (Sheraton & Black, 1981) but do not rule out possible contamination by lower continental crust which has low Sr_T . This will be discussed further in Chapter 6.

3.6. CONCLUSIONS

In situ differentiation processes account for much of the variations observed in the examined dyke. Crustal contamination during the emplacement of this dyke does not appear to have effected the geochemical signature of the magma. The existence of uncommon crustal xenoliths within dykes, plus the indication of a fast cooling history, suggests that assimilation of crustal material is not occurring on large scale. It can be argued that crustal contamination processes at relatively high levels of dyke emplacement (Chapter 2) are insignificant. Crustal contamination and magma homogenization at deeper crustal levels (i.e. lower crust), however, cannot be excluded. Nevertheless the overall homogeneity of this dyke over a strike length of 15 km suggests such deep contamination is not responsible for the overall geochemical character of this dyke. It is further concluded that a single chilled margin sample is adequate to characterize the parent magma geochemistry of this large dyke.

The data presented show that even small magma bodies, represented by this dyke, are dynamic systems in which significant geochemical differentiations may occur in situ. Significant variations in geochemistry may appear across such dykes, due to

prolonged cooling of dyke interiors allowing differentiation processes to take place. This may take the form of contemporaneous and post emplacement fractionation and accumulation of phenocrysts and of migration of accumulative of late stage residual liquids.

TABLE 3.5

SELECTED OLIVINE MICROPROBE ANALYSES

Sample No.	70533				70536			
Pos of Anal.	core	rim	core	core	core	rim-opx	core	rim-opx
Rock Type	High-Mg	Tholeiite, chilled margin			dyke centre			
SiO ₂	39.57	39.62	39.88	39.93	39.18	39.64	38.94	39.15
Cr ₂ O ₃	0.03	0.06	0.06	0.07	0.00	0.01	0.01	0.01
FeO	14.31	16.25	14.82	14.37	17.25	17.56	17.54	17.19
NiO	0.32	0.46	0.36	0.50	0.34	0.23	0.41	0.29
MnO	0.14	0.20	0.17	0.14	0.10	0.24	0.23	0.36
MgO	45.02	43.83	45.00	44.89	43.10	42.96	41.57	42.80
Total	99.38	100.43	100.29	99.89	99.96	100.63	98.71	99.81
Si	0.998	0.998	0.999	1.002	0.996	1.001	1.004	0.997
Cr	0.000	0.000	0.000	0.000	0.000	0.000	0.000	0.000
Fe	0.302	0.342	0.310	0.302	0.366	0.371	0.378	0.366
Ni	0.008	0.011	0.008	0.012	0.008	0.006	0.010	0.007
Mn	0.003	0.004	0.004	0.003	0.002	0.005	0.005	0.008
Mg	1.692	1.645	1.679	1.679	1.632	1.616	1.598	1.624
Sum	3.002	3.002	3.001	2.998	3.004	2.999	2.995	3.003
Mg#	84.9	82.8	84.4	84.8	81.7	81.3	80.9	81.6

SELECTED SPINEL MICROPROBE ANALYSES

Sample No.	70538							
Pos. of Anal.	core	rim	rim	rim	core	core	core	core
Rock Type	High Mg-Tholeiite, chilled margin							
SiO ₂	0.07	0.09	0.09	0.09	0.09	0.11	0.21	0.35
TiO ₂	0.09	0.14	0.09	0.05	0.13	0.10	0.12	0.14
Al ₂ O ₃	12.74	12.44	12.54	12.47	12.56	12.80	12.21	14.29
Cr ₂ O ₃	49.24	48.37	48.22	48.40	48.03	48.39	49.01	45.08
Fe ₂ O ₃	4.40	4.58	4.49	4.80	4.39	4.46	4.70	6.94
FeO	25.87	25.52	25.69	25.64	25.41	25.64	25.68	26.36
MnO	0.00	0.00	0.00	0.00	0.00	0.00	0.00	0.00
NiO	0.00	0.00	0.00	0.00	0.00	0.00	0.00	0.00
MgO	4.80	4.74	4.57	4.66	4.70	4.75	4.74	4.73
Total	97.20	95.89	95.70	96.10	95.31	96.24	96.66	97.88
Cations								
Ti	0.002	0.004	0.002	0.001	0.003	0.003	0.003	0.004
Al	0.524	0.519	0.525	0.520	0.527	0.532	0.507	0.583
Cr	1.356	1.351	1.351	1.350	1.349	1.345	1.362	1.230
Fe ³⁺	0.115	0.122	0.120	0.127	0.117	0.118	0.124	0.180
Fe ²⁺	0.753	0.754	0.761	0.756	0.755	0.754	0.755	0.761
Mn	0.000	0.000	0.000	0.000	0.000	0.000	0.000	0.000
Ni	0.000	0.000	0.000	0.000	0.000	0.000	0.000	0.000
Mg	0.249	0.250	0.241	0.245	0.249	0.249	0.248	0.243
Sum	3.000	3.000	3.000	3.000	3.000	3.000	3.000	3.000
Mg #	24.9	24.9	24.1	24.5	24.8	24.8	24.7	24.2
Chrome #	72.1	72.2	72.0	72.2	71.9	71.7	72.9	67.9
Ferric #	13.3	13.9	13.6	14.4	13.5	13.5	14.1	19.2

Selected mineral analyses from chilled margins and dyke interiors of a high-Mg tholeiite dyke.

Mg# (silicates) = 100 Mg/(Mg + Fe total). Mg# (spinel) = 100 Mg/(Mg + Fe²⁺), Cr# = 100 Cr/(Cr + Al), Fe determination as FeO: Fe³⁺ and Fe₂O₃ calculated from stoichiometry.

SELECTED ORTHOPYROXENE MICROPROBE ANALYSES

Sample No.	70548						70536					
Pos. of Anal.	core	rim	core	rim-cpx	core	GM rim	core	core	core	core	core	rim
Rock Type	High-Mg	Tholeiite,	chilled margin				dyke centre					
SiO ₂	55.00	52.91	54.84	54.86	53.48	49.30	53.14	53.54	53.58	53.14	51.41	
TiO ₂	0.13	0.12	0.12	0.14	0.04	0.58	0.11	0.11	0.10	0.11	0.24	
Al ₂ O ₃	2.60	1.97	1.79	2.04	1.56	2.10	1.95	1.63	1.70	1.95	1.45	
Cr ₂ O ₃	0.47	0.65	0.75	0.71	0.86	0.25	0.17	0.28	0.22	0.17	0.18	
FeO	10.11	16.43	11.49	9.91	9.82	25.16	14.25	13.21	13.04	14.25	20.30	
NiO	0.13	0.05	0.08	0.12	0.00	0.00	0.15	0.00	0.04	0.15	0.07	
MnO	0.22	0.22	0.17	0.20	0.21	0.48	0.30	0.28	0.18	0.30	0.38	
MgO	29.52	25.05	28.97	30.11	29.79	20.10	26.31	27.01	27.03	26.31	22.05	
CaO	2.78	2.79	2.36	2.76	2.45	0.46	2.55	2.47	2.49	2.55	2.20	
Total	100.96	100.19	100.57	100.85	98.20	98.43	98.93	98.52	98.38	98.93	98.29	
Cations (6 ox)												
Si	1.927	1.923	1.940	1.921	1.920	1.891	1.937	1.948	1.951	1.937	1.941	
Ti	0.003	0.003	0.003	0.004	0.001	0.017	0.003	0.003	0.003	0.003	0.007	
Al	0.108	0.085	0.075	0.084	0.066	0.095	0.084	0.070	0.073	0.084	0.065	
Cr	0.013	0.019	0.021	0.020	0.024	0.008	0.005	0.008	0.006	0.005	0.005	
Fe ²⁺	0.279	0.454	0.322	0.245	0.227	0.724	0.402	0.382	0.384	0.402	0.606	
Fe ³⁺	0.018	0.045	0.018	0.046	0.068	0.083	0.032	0.020	0.013	0.032	0.035	
Mn	0.007	0.007	0.005	0.006	0.006	0.016	0.009	0.009	0.006	0.009	0.012	
Mg	1.541	1.356	1.527	1.571	1.593	1.148	1.429	1.464	1.467	1.429	1.240	
Ca	0.105	0.109	0.089	0.103	0.094	0.019	0.099	0.096	0.097	0.099	0.089	
Sum	4.000	4.000	4.000	4.000	4.000	4.000	4.000	4.000	4.000	4.000	4.000	
Mg#	84.0	73.3	81.9	84.6	84.7	59.0	76.8	78.6	78.7	76.8	66.1	
Endmembers												
enstatite	79.4	69.1	78.1	80.0	80.4	58.2	72.8	74.6	74.8	72.8	63.0	
ferrosilite	15.3	25.4	17.4	14.8	14.9	40.9	22.1	20.5	20.2	22.1	32.5	
wollastonite	5.4	5.5	4.6	5.3	4.8	1.0	5.1	4.9	5.0	5.1	4.5	

SELECTED CLINOPYROXENE MICROPROBE ANALYSES

Sample No.	70538						70536					
Pos. of Anal.	rim-plag	rim-plag	rim-plag	rim-plag	rim-plag		rim-plag	rim-plag	core	rim-plag	exol-opx	rim-plag
Rock Type	High-Mg	Tholeiite,	chilled margin				dyke centre					
SiO ₂	51.49	51.13	49.99	50.48	50.75		51.58	51.19	51.01	49.05	50.84	49.03
TiO ₂	0.29	0.30	0.45	0.57	0.34		0.26	0.25	0.31	0.59	0.30	0.48
Al ₂ O ₃	1.99	3.88	4.21	4.15	3.75		2.00	2.59	3.81	4.59	3.56	4.77
Cr ₂ O ₃	0.06	0.17	0.11	0.04	0.09		0.19	0.16	0.47	0.03	0.46	0.03
FeO	13.57	10.75	13.15	9.29	12.00		12.29	11.45	10.67	11.73	12.49	13.16
NiO	0.00	0.03	0.00	0.00	0.04		0.00	0.07	0.00	0.04	0.00	0.03
MnO	0.18	0.21	0.25	0.15	0.23		0.20	0.24	0.20	0.18	0.26	0.26
MgO	16.49	17.42	15.32	14.10	15.42		16.26	15.91	17.78	14.55	17.50	14.90
CaO	15.18	15.82	16.20	20.92	17.16		17.04	17.26	15.02	17.76	13.42	16.50
Na ₂ O	0.25	0.24	0.34	0.50	0.35		0.24	0.33	0.24	0.42	0.37	0.46
Total	99.51	99.95	100.02	100.20	100.12		100.05	99.46	99.49	98.94	99.20	99.61
Cations (6 ox)												
Si	1.929	1.886	1.865	1.869	1.887		1.919	1.914	1.888	1.846	1.896	1.836
Ti	0.008	0.008	0.013	0.016	0.010		0.007	0.007	0.009	0.017	0.008	0.013
Al	0.088	0.169	0.186	0.182	0.165		0.088	0.114	0.166	0.204	0.157	0.211
Cr	0.002	0.005	0.003	0.001	0.003		0.005	0.005	0.014	0.001	0.014	0.001
Fe ²⁺	0.370	0.278	0.330	0.205	0.308		0.311	0.296	0.287	0.269	0.342	0.289
Fe ³⁺	0.055	0.054	0.081	0.083	0.065		0.072	0.062	0.044	0.100	0.048	0.123
Mg	0.921	0.957	0.852	0.778	0.854		0.901	0.887	0.981	0.816	0.972	0.831
Ca	0.609	0.625	0.647	0.830	0.683		0.679	0.691	0.596	0.716	0.536	0.662
Na	0.018	0.017	0.024	0.036	0.026		0.018	0.024	0.017	0.031	0.027	0.034
Sum	4.000	4.000	4.000	4.000	4.000		4.000	4.000	4.000	4.000	4.000	4.000
Mg#	68.4	74.3	67.5	73.0	69.6		70.2	71.2	74.8	68.9	71.4	66.9
Endmembers												
Mg ₂ Si ₂ O ₆	46.0	47.9	42.6	38.9	42.7		45.1	44.3	49.0	40.8	48.6	41.6
Fe ₂ Si ₂ O ₆	18.5	13.9	16.5	10.2	15.4		15.5	14.8	14.3	13.5	17.1	14.4
Ca ₂ Si ₂ O ₆	27.3	26.0	26.2	35.8	29.0		30.3	30.6	24.6	29.0	22.0	25.6
NaFeSi ₂ O ₆	1.6	1.2	2.1	3.5	2.3		1.2	1.9	0.3	3.0	1.3	3.3
NaCrSi ₂ O ₆	0.2	0.5	0.3	0.1	0.3		0.5	0.5	1.4	0.1	1.4	0.1
CaAl ₂ Si ₂ O ₆	1.7	5.5	5.0	5.1	5.2		0.7	2.9	5.5	5.1	5.3	4.7
CaFeAlSi ₂ O ₆	3.8	4.2	6.0	4.8	4.2		6.0	4.3	4.0	6.9	3.4	9.1
CaTiAl ₂ O ₆	0.8	0.8	1.3	1.6	1.0		0.7	0.7	0.9	1.7	0.8	1.3

SELECTED PLAGIOCLASE MICROPROBE ANALYSES

Sample No.	70548			70536									
Pos. of Anal.	rim-cpx	rim-cpx	rim-cpx	rim-cpx	rim-cpx	rim-cpx	rim-cpx	rim-cpx	rim-cpx	rim-cpx		core	incl-opx
Rock Type	High-Mg	Tholeiite	chilled margin	dyke centre									
SiO ₂	54.02	54.89	57.38	54.85	52.82	54.02	52.94	54.03	53.81	49.96	49.79		
Al ₂ O ₃	28.80	27.74	26.48	27.40	29.05	27.88	30.72	29.26	29.80	30.14	29.38		
FeO	0.31	0.71	0.17	0.55	0.27	0.35	0.29	0.38	0.22	0.40	1.22		
MgO	0.04	0.57	0.00	0.08	0.03	0.07	0.02	0.00	0.04	0.18	1.32		
CaO	11.63	11.60	9.01	10.62	12.20	11.56	13.47	12.46	12.56	14.06	13.31		
Na ₂ O	4.83	5.10	5.76	5.41	4.48	4.83	3.85	4.42	4.28	3.73	3.59		
K ₂ O	0.33	0.00	1.47	0.25	0.15	0.13	0.06	0.12	0.12	0.05	0.05		
Total	99.97	100.60	100.26	99.16	98.99	98.84	101.34	100.67	100.83	98.51	98.66		
Cations													
Si	2.449	2.491	2.581	2.507	2.420	2.475	2.372	2.433	2.417	2.323	2.351		
Al	1.543	1.487	1.407	1.480	1.573	1.509	1.627	1.557	1.581	1.656	1.639		
Ca	0.565	0.564	0.434	0.520	0.599	0.567	0.647	0.601	0.605	0.700	0.673		
Na	0.425	0.448	0.502	0.479	0.398	0.429	0.334	0.386	0.373	0.336	0.328		
K	0.019	0.000	0.084	0.015	0.009	0.008	0.003	0.007	0.007	0.003	0.003		
Sum	5.001	4.990	5.008	5.000	4.997	4.989	4.983	4.985	4.982	5.018	4.995		
Endmembers													
An	56.0	55.7	42.5	51.3	59.6	56.5	65.7	60.5	61.4	67.4	67.0		
Ab	42.1	44.3	49.2	47.2	39.6	42.7	34.0	38.8	37.9	32.3	32.7		
Or	1.9	0.0	8.3	1.5	0.8	0.8	0.3	0.7	0.7	0.3	0.3		

CHAPTER 4

NORITIC RING COMPLEX

4.1 INTRODUCTION

The noritic ring complex which occurs in the northern part of *Long Peninsula*, Vestfold Hills is a large intrusive dyke. This semicircular complex has a diameter of *ca.* 7 - 8 km and comprises several discrete bodies which vary in width from 70 to 400 m. Outcrops occur to the southwest of *Taynaya Bay*, on the western shore of *Tryne Fjord* and on the western part of *Snezhnyy Bay*, and can be traced along the *Tryne Islands* (e.g. Barrier and Bandits Island, see dyke base map). Bodies in the north, on the *Tryne Islands*, become progressively narrower in width westwards. The more voluminous southern branch continues through the western part of *Long Peninsula*, occurring in smaller pods along the southwestern extension of *Taynaya Bay* area and in elongated bodies extending to the western part of *Long Fjord* (*ca.* 1km SE of *Ace Lake*).

The norite complex was emplaced during early Proterozoic time and has intruded various Archaean orthogneiss units. The complex postdates the first dyke set of the high-Mg tholeiite suite, but predates subsequent dyke suites. The linking of this ring complex to the high-Mg tholeiitic suite is demonstrated by several dykes which may be traced into the complex. It remains uncertain, however, whether these dykes are feeders or whether the complex is their parent body. Contacts between the complex and the country rock are often sharp boundaries with the complex exhibiting chilled margins (Figure 4.1). Occasionally, 1 - 2 m wide schlieren structures occur within country rocks at the complex margins, reflecting partial melting and assimilation of

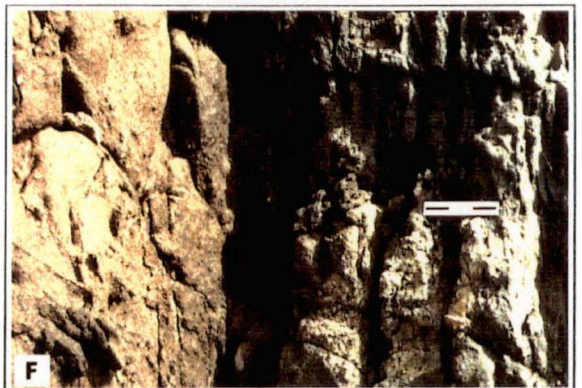
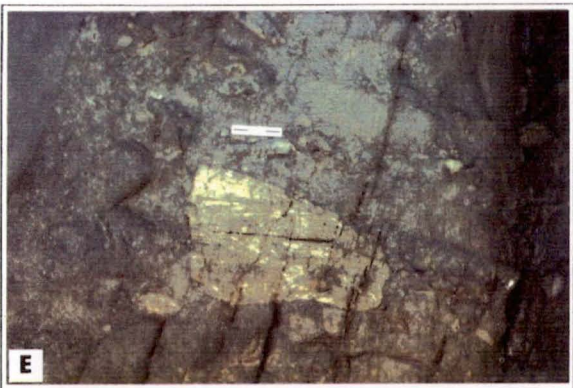
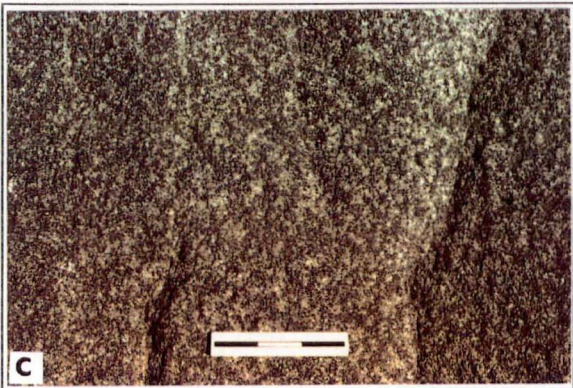
wall-rock (Figure 4.1). The margins of the ring complex dip steeply, between 60° and 90° and may be inclined inwards or outwards*.

The norite body was first recognized by McLeod & Harding (1967) and described in more detail by Kuehner (1986). In this study, the norite is divided into three distinct lithological units:

- (1) The *Homogeneous Norite*, the most voluminous unit, which contains orthopyroxene, clinopyroxene and plagioclase,
- (2) *Mottled Norite*, a unit characterized by large 1 - 2 cm plagioclase - alkali-feldspar aggregates, and
- (3) the *Rubbly Norite*, a less common variant which is distinguished by patches of bronzitic orthopyroxene, cognate and inherited xenoliths, and globules of sulphide.

Xenoliths occurring in the *Rubbly Norite* are mostly orthopyroxenites but also include websterite, sapphirine-bearing fine-grained quartzite and feldspathic gneiss. The sulphide-rich zones occur in most outcrops of the *Rubbly Norite* and vary in size from 4 - 6 m, up to 30 m in width and extending up to 400 m in length. The largest of these sulphide-bearing bodies occurs in the southern part of the complex. Contact relationships indicate that the *Rubbly Norite* is a late stage emplacement into the norite body.

* The terms ring dyke or ring complex are used here in a descriptive manner, with no genetic connotation.



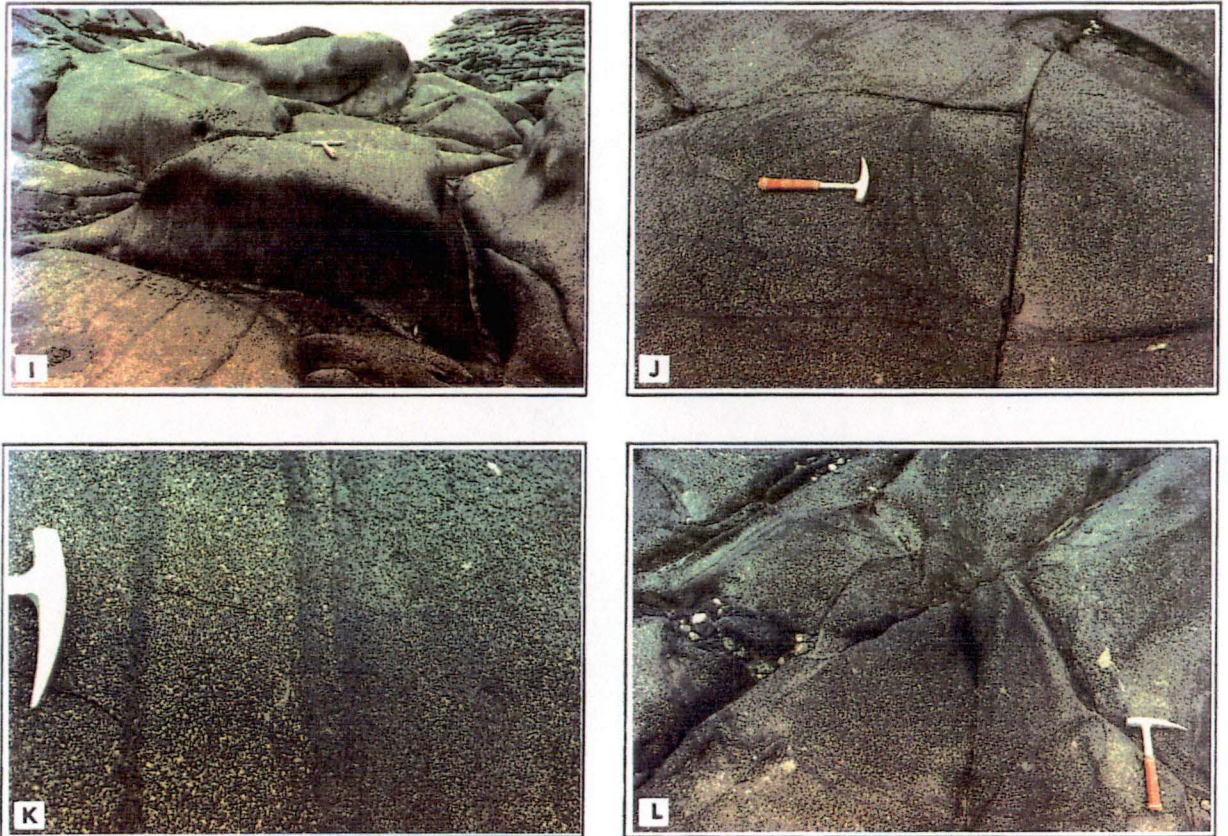


Figure 4.1

Photographs illustrating the various norite types and features of the norite ring complex (A) *Homogeneous Norite* showing sharp contact with country rock, (B) partial melting of country rock, exhibiting 'schlieren' textures, (C) *Mottled Norite* with 1 - 2 cm large aggregates of quartz-plagioclase-alkali-feldspar intergrowths. (D) sulphide-bearing *Rubbly Norite* (green colouring results from the weathering of Cu-Ni sulphides), (E) enstatite nodule in *Rubbly Norite*, (F) contact between *Homogeneous Norite* and *Rubbly Norite* hosting enstatite nodules, (G) and (H) late stage segregations (I) set of plagioclase layers running parallel to the strike of the complex, (J) curving layers with layer intersections, (K) plagioclase layer intersecting each other and (L) circular or cylindrical layering.

4.2 PETROGRAPHY AND MINERAL CHEMISTRY

4.2.1 Homogeneous Norite

The *Homogeneous Norite* constitutes approximately 80% of the exposure. It is macro- and microscopically uniform and in hand specimen appears as a medium to coarse grained rock dominated by orthopyroxene, with minor clinopyroxene and plagioclase.

Petrographically the rock is classified as an orthopyroxene orthocumulate with bronzitic orthopyroxenes up to 7 mm long. Orthopyroxenes are often rimmed by pigeonite (now inverted), with intercumulus phases consisting mainly of dusty plagioclase and clinopyroxene. The interstices between clinopyroxene and dusty plagioclase crystals (up to 2 mm) are occupied by late-stage alkali - feldspar - plagioclase granophyric intergrowths (0.4 - 1.0 mm in size). Other late crystallization products are brown biotite and light green chlorite which may partly rim the pyroxenes, apatite and Fe-Ti oxides, with the latter commonly exhibiting trellis textures formed by exsolution of ilmenite from magnetite (Figure 4.2). Occasionally, small (0.6 mm) euhedral zircons are observed in association with the late stage crystallization products.

Orthopyroxene crystals vary in abundance between 25 and 30 vol% (see Figure 4.2). They are strongly zoned with colourless cores and brown rims corresponding to a compositional zoning from Mg# 84 cores to Mg# 60. Most cores have Mg# in the range 76 - 80 while rim compositions markedly depending on the adjacent mineral. For instance, rims adjacent to clinopyroxene have Mg# 68 - 72 whereas rims in contact with plagioclase, or late stage assemblages, are more Fe-rich with Mg# 60 - 65. Al_2O_3 contents are consistently between 1.1 to 1.7 wt%, rarely exceed 2 wt%, and show no zoning. CaO generally increases from 1.0 to 2.2 wt% from core to rim, with the exception of some orthopyroxenes which have rim compositions as low as Mg# 60 and CaO contents as high as 1.6 wt%.

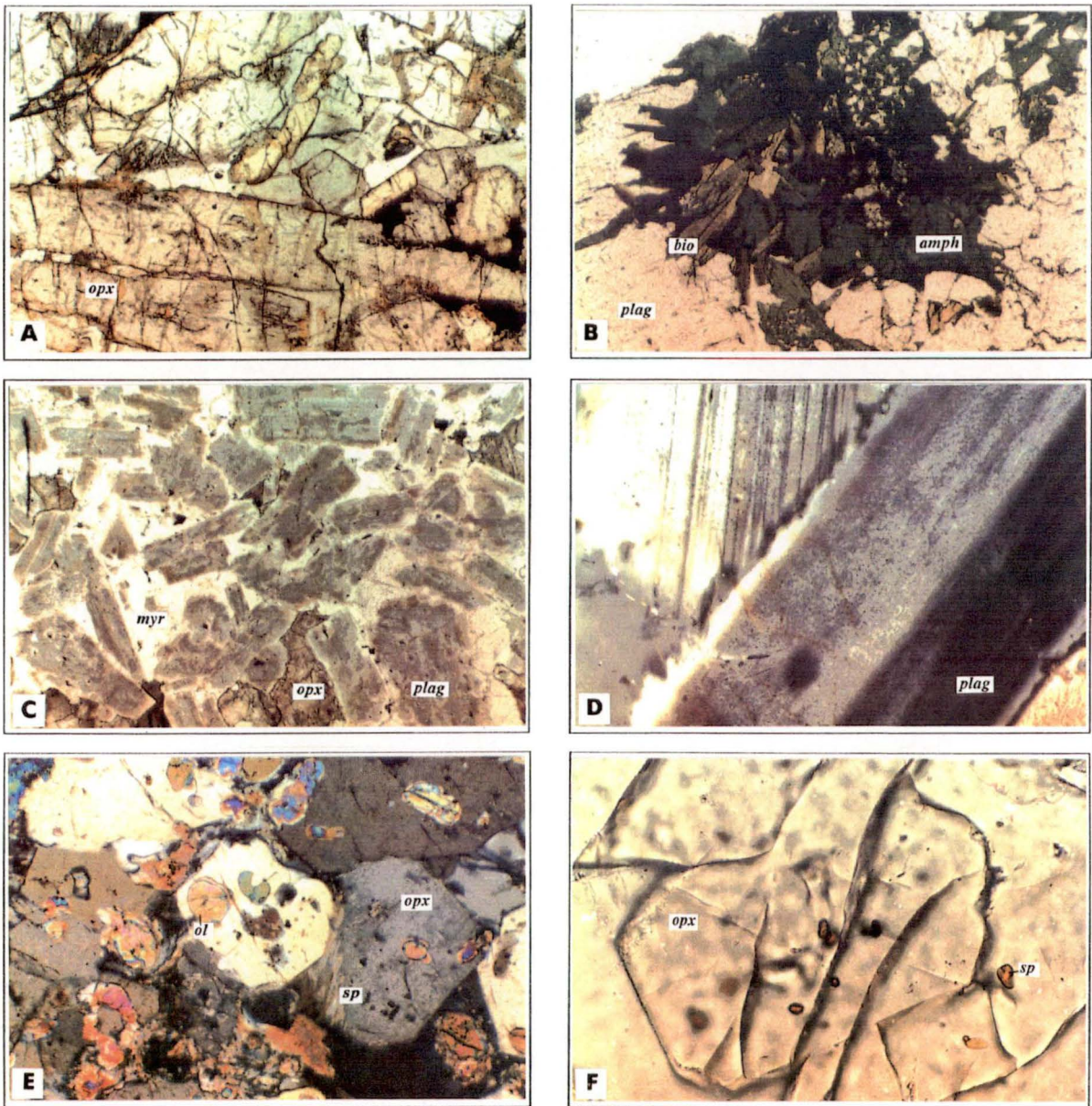


Figure 4.2

Photomicrographs of (A) cumulus orthopyroxene (*opx*) in the *Rubbly Norite* (2.6 * 1.9 mm), (B) late stage segregation showing aggregates of amphibole (*amph*) and biotite (*bio*) surrounded by quartz and feldspars (2.6 * 1.9 mm), (C) cloudy plagioclase (*plag*) surrounded by myrmekite (*myr*) occurring in plagioclase layer within the *Homogeneous Norite* (2.6 * 1.9 mm), (D) cloudy plagioclase - fine, ca. 1µm inclusions of Fe-oxides in plagioclase (0.35 * 0.25 mm), (E) spinel (*sp*) and olivine (*ol*) inclusions in enstatite (0.65 * 0.45 mm) and (F) spinel inclusions in enstatite nodule enclosed in large (3 - 4 cm) enstatite (0.35 * 0.25 mm).

The modal abundance of intercumulus clinopyroxene occasionally exceeds 10 vol%, which gives the norite a coarse grained appearance. The compositional variation of clinopyroxene is much more limited than orthopyroxene, with for example Mg# varying from 73.3 in cores to 61.5 at crystal rims. Where clinopyroxene is in contact with orthopyroxene, rims average Mg# 70.

Plagioclase is cloudy due to small opaque inclusions and is strongly zoned, usually from An₈₀ to An₅₀ though some plagioclase rim compositions are as sodic as An₃₂.

4.2.2 Mottled Norite

The *Mottled Norite* occurs as occasional narrow bands between the *Homogeneous Norite* and the *Rubbly Norite* and constitutes about 10% of the exposure. This rock type is most abundant in the southern outcrops of the *Taynaya Bay* region. It is distinguished from the *Homogeneous Norite* by its large, evenly distributed glomeroporphyritic aggregates of feldspars and quartz (Figure 4.1).

The crystal aggregates are granophyric intergrowths of orthoclase, quartz and plagioclase. These granophyric intergrowths occupy 15 - 20 vol%, compared to only 10 - 15 vol% in the *Homogeneous Norite*. The plagioclase intergrown with alkali-feldspar in these aggregates ranges in composition from An₅₂ to An₆₀, and the alkali-feldspar varies from Or₉₂ Ab_{7.2} An_{0.8} to Or₈₄ Ab_{13.6} An_{2.4}. Small (up to 2mm) apatite needles are also associated with these plagioclase - K-feldspar - quartz intergrowths.

Outside the crystal aggregates, the *Mottled Norite* is an orthocumulate with cumulus orthopyroxene (up to 8 mm) and is similar to the *Homogeneous Norite*. These crystals are strongly zoned from cores of Mg# 84.5 to the rims of Mg# 57. Subhedral orthopyroxene is often rimmed by inverted pigeonite. Intercumulus subhedral clinopyroxenes average 1.6 mm in size, and varying in composition from Mg# 78.5 to 64. The modal amount of this intercumulus clinopyroxene varies between 5 and 10 vol%. Biotite and chlorite are minor phases ranging between 1 and 3 vol%. Iron-titanium oxides and sulphides are also present but never exceed 2 vol%.

4.2.3 Rubbly Norite

The *Rubbly Norite* is the most heterogeneous norite unit and occurs in small elongate bodies at the outer margins of the ring complex. These bodies vary in size, from only a few metres in width up to 30 m. The largest body in the Taynaya Bay region (see dyke base map in appendix) reaches a maximum width of 20 m and extends over a linear distance of 400 m. The *Rubbly Norite* is characterized by bronzite-rich zones, which occur as irregular shaped concentrations and give the *Rubbly Norite* its typical brownish colour in hand specimen. This inhomogeneity is further enhanced by distinct greenish enstatite nodules up to 0.6 m in diameter (see Figure 4.1) and sulphide rich zones. On exposure to weathering, these sulphide-rich zones become an obvious green to reddish colour. In marginal zones, adjacent to country rocks, crustal xenoliths are common, and include both sapphirine and diopside bearing xenoliths.

Due to the heterogeneity of the *Rubbly Norite*, petrographic features are more complex than in the other norite units. The host *Rubbly Norite* (excluding pyroxene nodules and late stage segregations) is dominated by orthopyroxene which comprises up to 65 vol%. Euhedral to subhedral orthopyroxenes, sometimes exceeding 1 cm, form ortho- to adcumulates. The mineral chemistry of the orthopyroxenes is similar to that in the other norite units, ranging from Mg# 85 cores to Mg# 62 rims. Cores with Mg# near 83 have rim compositions of Mg# 72 - 75, adjacent to intercumulus clinopyroxenes. Thus, although intercumulus clinopyroxene is less abundant by ~ 5 vol% than in the other norite varieties, it has a similar compositional range. Inverted pigeonite rims on orthopyroxene are also common.

The amount of plagioclase decreases from 35 - 40 vol% in the *Homogeneous Norite* to 10 vol% in the *Rubbly Norite*. Compositions vary from An₆₈ cores to An₆₂ rims, though plagioclase intergrowths with K-feldspar are more sodic in character (An₅₀ to An₅₄). With decreasing plagioclase content in the *Rubbly Norite*, the granophyric patches become less abundant also (5 - 10 vol%). These intercumulus granophyric patches occupy areas up to 4 mm in diameter.

The *Rubbly Norite* is also characterized by a relative large abundance of opaque minerals. The modal amount of sulphide and Fe-Ti-oxide present is variable, ranging between 1 to 2 vol% and 15 vol%. The Fe-Ti oxides are always less abundant than sulphides, and usually comprise between 0.5 and 2 vol%. The main sulphide phases are pyrrhotite, chalcopyrite, pentlandite and bravoite, which have an average modal abundances of 3, 2, 1.5 and 0.5 vol% respectively. They occur in irregular-shaped aggregates consisting of anhedral crystals. Pentlandite is often exsolved as small anhedral blebs or patches in chalcopyrite. Associated with the sulphide mineralization are tiny PGE (Platinum Group Element) minerals.

The sulphides are mostly associated with plagioclase and other late stage phases, and to a lesser extent with pyroxenes. This suggests late-stage formation accompanying crystallization of the quartz-feldspar granophyric intergrowths. The specific characteristics of the sulphide and PGE mineralization in the high-Mg tholeiitic suite and in the *Rubbly Norite*, are discussed in Chapter 5.

4.2.4 Pyroxenite Nodules

Orthopyroxenite nodules are relatively abundant in the *Rubbly Norite* and vary in size from only few centimetres to more than half a metre (Figure 4.1). They are comprised of irregular aggregates of blocky orthopyroxene laths, which usually share the same crystallographic orientation. The crystal boundaries are often irregular in shape, with plagioclase, clinopyroxene, myrmekite and pale brown biotite occupying the interstices. Olivine is present within this interstitial assemblage in some samples. The larger orthopyroxene crystals have exsolved clinopyroxene. All pyroxene crystals are strongly zoned, from cores up to Mg# 91.9 to Fe-rich rims as low as Mg# 71. The most primitive orthopyroxene compositions have low CaO contents (0.35 to 0.75 wt%), which increase with decreasing MgO content, and low Al₂O₃ contents from 0.6 to 1.9 wt% (see Table 4.5). Kuehner (1986) described enstatite nodules from the same complex with Mg# up to 91.2 which were considered to be co-magmatic with the noritic magma. Orthopyroxenes from the nodules exhibit increasing CaO content with

decreasing Mg# and merge compositionally with those from the host norite (Kuehner, 1986, Kuehner, 1989). The highly magnesian and very low calcium cores (Mg# 91.9 and CaO < 0.2 wt%) may be exotic or xenocrystal to the noritic magma or may represent early higher temperature crystallization products. Due to the compositional overlap between orthopyroxenes from the nodules and the other norite types these enstatites are interpreted to be co-magmatic with the noritic magma.

Olivine crystals (up to 0.2 mm), occurring as inclusions in orthopyroxene, are less magnesian (Mg# 84 - 87) than their host orthopyroxene (Mg# 88 - 92). The most primitive olivine observed has a composition of Mg# 90. Inclusions of clinopyroxene are also common, and have Mg# up to 82. Clinopyroxenes adjacent to enstatite range in Mg# from 75 to 78, which is similar to the included clinopyroxenes. The most calcic plagioclase compositions range from An₇₀ to An₇₄, decreasing to An₅₄ rims adjacent intercumulus phases. Round spinels (up to 0.025 mm) occur as inclusions in enstatite (Figure 4.2). The light brown spinels are strongly zoned, with some having cores of Mg# 63 and Cr# 26 and rims of Mg# 40 and Cr# 70, and others having rims as magnesian as Mg# 74 and Cr# of 33.

4.2.5 Fine Grained Dykes

Dykes occurring in *Taynaya Bay* and *Tryne Fjord* region are in close proximity to the *Rubbly Norite* and are probably genetically related. The longest and best exposed example in the Taynaya Bay links two norite bodies which are *ca.* 1.5 km apart. It offshoots from the *Rubbly Norite* and exhibits an irregular zig-zag geometry (Hoek, 1991 in press). The norite body becomes progressively narrower towards the dyke offshoot, accompanied by progressively finer grain size. Enstatite nodules and sulphides associated with the *Rubbly Norite* become less abundant towards the dyke where they are absent. However, no clear contact between the dyke and the norite is observed and therefore their relationship is still equivocal (e.g. see sample 70623 on dyke base map).

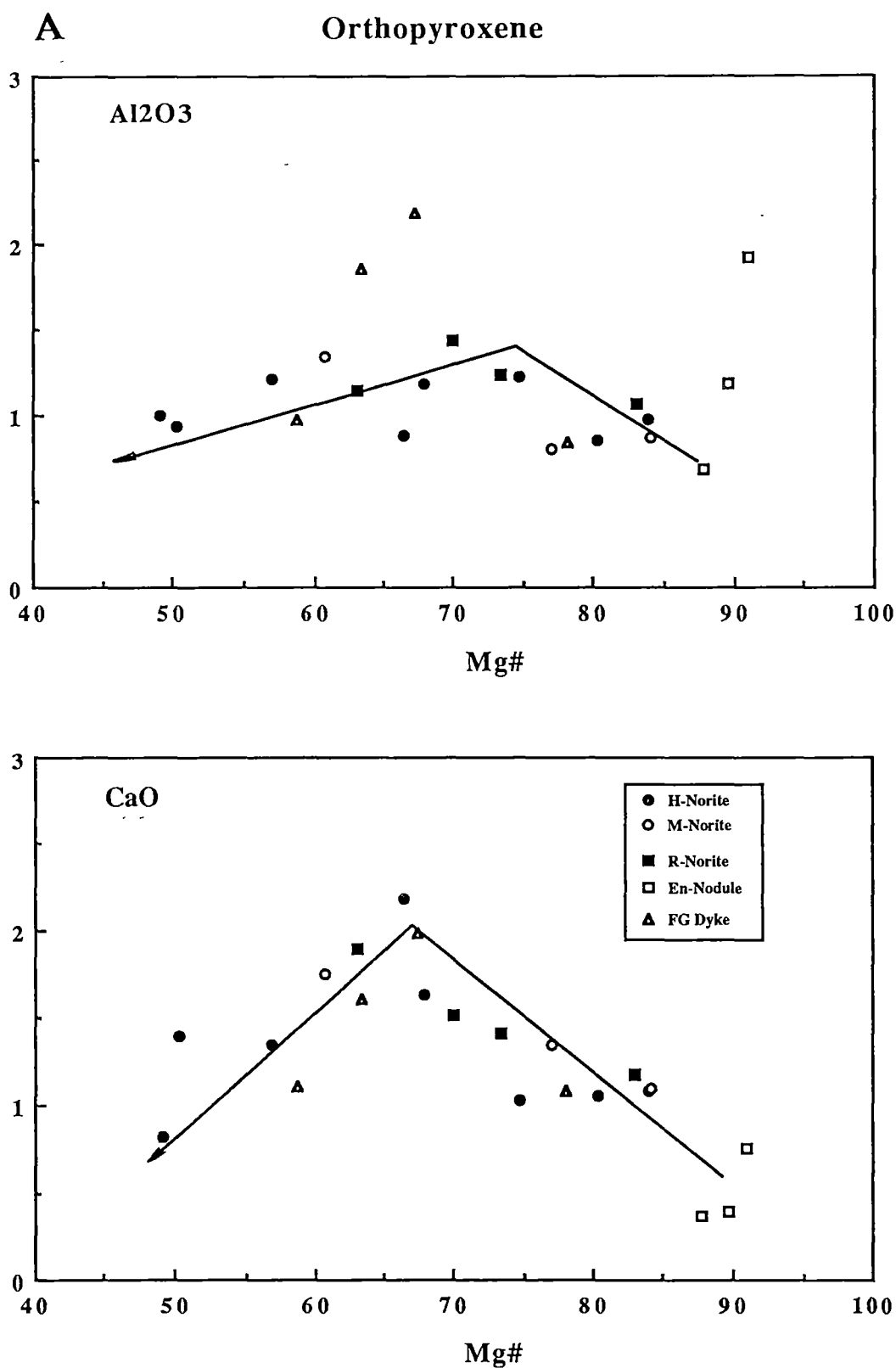
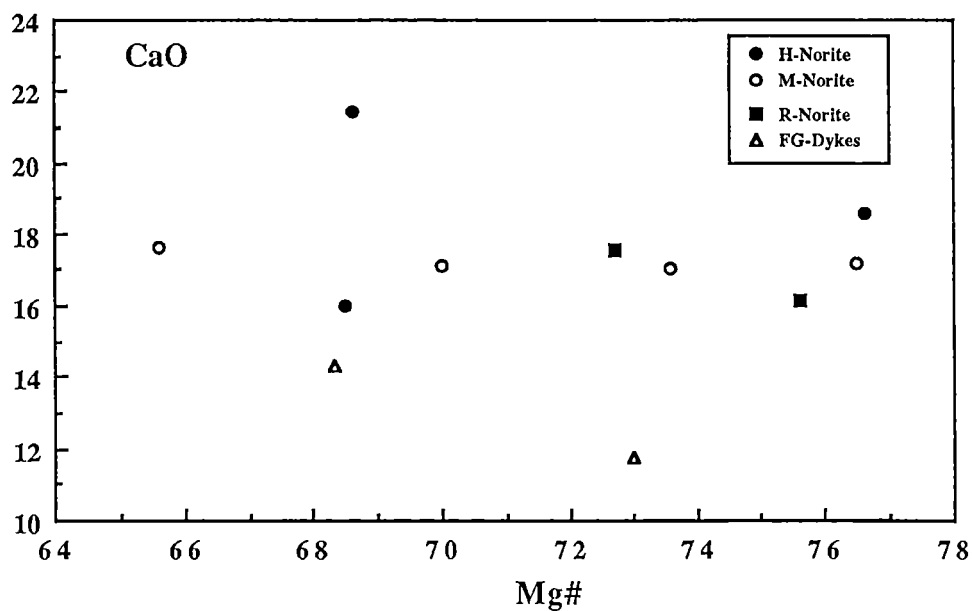
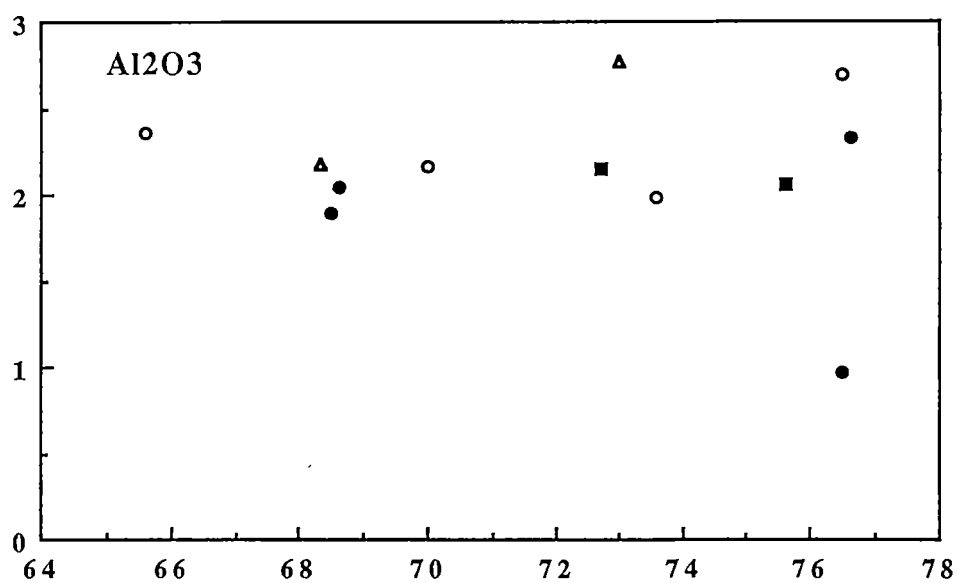
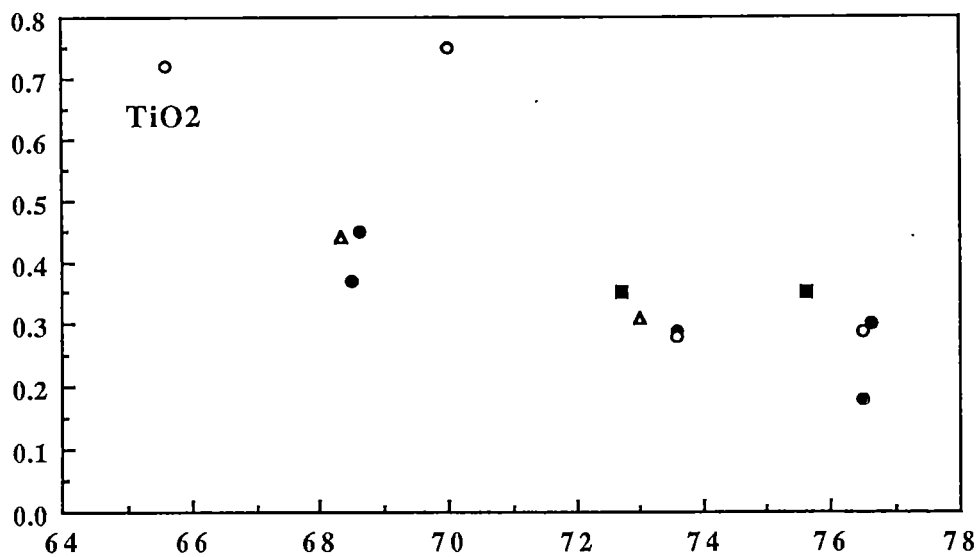


Figure 4.3

Mg# versus Al₂O₃ and CaO contents of orthopyroxenes (A) and Al₂O₃, CaO and TiO₂ contents of clinopyroxenes (B) in various norites. Vectors indicate crystallization of orthopyroxene only and orthopyroxene + clinopyroxene.

B Clinopyroxene



The finer grained dykes occurring in proximity to the norite, particularly the more slowly cooled dyke interiors, exhibit textural and mineralogical similarities to the norite bodies. The dykes are orthopyroxene phyric tholeiites with 15 - 25 vol% phenocrysts. Orthopyroxene occurs as euhedral phenocrysts up to 2.5 mm in length and commonly forms glomeroporphyritic clusters. Occasionally orthopyroxene is rimmed by clinopyroxene, which also occurs in the groundmass and as microphenocryst laths (5 - 10 vol%) up to 0.4 mm in length. Other groundmass phases are plagioclase, biotite, a granophyric intergrowth of quartz and alkali-feldspar, Fe-Ti oxides and sulphides. Plagioclase is the most abundant groundmass phase (*ca.* 50 vol%) with some laths reaching 1 mm in size. Plagioclase compositions are intermediate, ranging from An₅₃ to An₆₅. Magnetite, ilmenite and sulphides rarely exceed 2 vol%, with sulphides always being subordinate accessory phases.

Orthopyroxene in the fine grained dykes has pronounced zoning with cores of Mg # 83.3 and rims of Mg# 56. Clinopyroxene exsolution within the orthopyroxene rims ranges between Mg# between 62 and 70. These orthopyroxene and clinopyroxene compositions from the fine grained dykes and from various norite types are compared in Figure 4.3 A and B. Al₂O₃ in orthopyroxene is relatively constant, whereas CaO increases with increasing differentiation, from Mg# 92 - 68 and then decreases from Mg# 68 to 48. This inflection in CaO contents in orthopyroxene is consistent with the onset of clinopyroxene crystallization at Mg#_{opx} = 68. Al₂O₃ and CaO in clinopyroxene show no systematic variation with decreasing Mg#, whereas TiO₂ increases slightly. Orthopyroxene and clinopyroxene in the fine grained dykes overlap with these in the norite varieties apart from higher Al₂O₃ contents in some orthopyroxene. These relatively Al₂O₃-rich orthopyroxenes may result from more rapid crystallization in the fine grained dykes than in the norites.

4.2.6 Late Stage Segregations

Within the *Homogeneous Norite* late-stage segregations are common. They often occur as mushroom-like structures ranging from a couple of centimetres in diameter up

to 1m (Figure 4.1). The largest late stage-segregation, occurring on *Bandits Island*, has a diameter of *ca.* 10 - 15 m and occurs in the centre of the intrusion. It has a well defined structure, with distinct and steeply dipping borders to the host norite (Figure 4.1). These borders exhibit a *ca.* 5 cm wide transitional zone where abundant late-stage crystallization products occur within the norite. These products are mostly quartz-feldspar granophyric intergrowths, which have their highest concentration at the contact with the *Homogeneous Norite* and decrease inwards across the transition zone.

The mineralogy of the late-stage segregations is variable, but consists mainly of amphibole, feldspars and quartz. Some smaller segregations show strong mineral assemblage zonation, from amphibole, pyroxene and feldspar assemblages through amphibole-feldspar and biotite assemblages, to pegmatitic assemblages (Figure 4.2). Minor phases present in the late-stage segregations are apatite, sphene and Fe-Ti oxides, all of which are embedded in the large granophyric intergrowths. The amphibole bearing assemblages consist of pale green to blue-green tschermakite-rich hornblende, which can reach up to 5 mm in length. Both hornblende and biotite are iron-rich, with FeO contents of 23.7 wt% and 25.3 wt% respectively.

4.3 RELATIVE TIME OF EMPLACEMENT

The noritic ring complex postdates the intrusion of the olivine - orthopyroxene phyric high-Mg tholeiites. Contact relationships between the *Rubbly Norite* and the *Homogeneous Norite* suggest multiple intrusion within the norite (Figure 4.1). The borders between these norite types are always steep dipping, and field as well as microscopic observations suggest a sequence of emplacement in which the *Rubbly Norite* was the later body to be emplaced. The borders are characterized by a narrow contact zone (*ca.* 1 cm in width) consisting mainly of orthopyroxene, clinopyroxene and plagioclase. The grain size in this zone is much smaller (averaging between 0.2 and 0.5 mm) than in the adjacent norite units (1 - 3 mm). Orthopyroxenes are mostly euhedral and have compositions from Mg# 80 to 70, which is similar to

orthopyroxenes in both the *Rubbly* and *Homogeneous Norite*. Clinopyroxene and plagioclase compositions are also similar in all the norite bodies. However, plagioclase in the narrow contact zones is inclusion free in contrast with the cloudy plagioclase found elsewhere (section 4.5.3), and late-stage liquids are absent from the contact zone. The finer grain size, absence of granophyric intergrowths and inclusion free plagioclase, all suggest these zones have cooled rapidly and that the *Homogeneous* and *Rubbly Norite* have been emplaced in succession. A relative sharp contact between these fine grained zone and the *Homogeneous Norite* can be observed, while the contact with the *Rubbly Norite* is gradational, which suggests that this fine grained zone, belonging to the *Rubbly Norite* has been slightly quenched by the *Homogeneous Norite*. These observations, together with the presence of orthopyroxene accumulation in the *Rubbly Norite* suggest that the *Rubbly Norite* was emplaced after the *Homogeneous Norite*.

Contacts between the *Homogeneous Norite* and the *Mottled Norite* are gradational suggesting contemporaneous emplacement. The features which make the *Mottle Norite* distinguishable from the *Homogeneous Norite* are interpreted as in-situ differentiation processes following emplacement. Whereas sharp contacts are observed between the *Rubbly Norite* and both the *Mottled Norite* and *Homogeneous Norite*, borders between the *Homogeneous* and *Mottled Norite* are always gradational. Finally, observed fine grained dykes, which are petrographically distinctly different to the *Rubbly Norite*, appear to be related to the *Homogeneous Norite*.

4.4. PRESSURE AND TEMPERATURE OF NORITE EMPLACEMENT

Temperatures have been calculated using coexisting pyroxenes for the different norite units (Table 4.1) using the thermometers of Bertrand & Mercier (1985), Wells (1977), Kretz (1982) and Lindsley (1983). Results obtained using the different thermometers are in close agreement 1200° - 1250° C (Table 4.1), with the exception of temperatures obtained using the graphical thermometer of Lindsley (1983) which are often significantly lower (50° - 100° C; see Figure 4.4 A - F).

The relatively lower temperatures obtained for the ring dyke suggest it has cooled more slowly than the other high-Mg tholeiitic dykes in the Vestfold Hills to allow minerals to crystallize and reach equilibrium at lower temperatures. Alternatively these temperatures could reflect a lower magma temperatures for the ring dyke as it is more evolved than the olivine- and orthopyroxene-phyric tholeiites. However, some orthopyroxene - clinopyroxene pairs within the ring dyke preserve high magmatic temperatures, particularly pairs occurring in the margins of the ring complex. These pairs retain temperatures which are in good agreement with those in the chilled margins of the high-Mg tholeiitic dykes.

Norite emplacement temperature estimates can be based on the composition of cumulus orthopyroxene intergrown with cores of intercumulus clinopyroxene. These pairs, in the various norite units, give consistent temperatures between 1200° and 1250° C (see Table 4.1). The preservation of such high temperatures further suggests a relatively fast cooling history with little or no re-equilibration. Cumulus orthopyroxene have a compositional range from Mg# 85.9 to Mg# 76, suggesting no subsolidus homogenization, which can be commonly observed in cumulates (Wager et al., 1960).

Rims of intercumulus orthopyroxene - clinopyroxene pairs have equilibrated with the residual melt to much lower temperatures (800° - 900 °C; Table 4.1 and Figure 4.4 A - F). These differences confirm the relict magmatic characteristics of the rocks and are consistent with the retention of high temperatures in orthopyroxene and clinopyroxene cores.

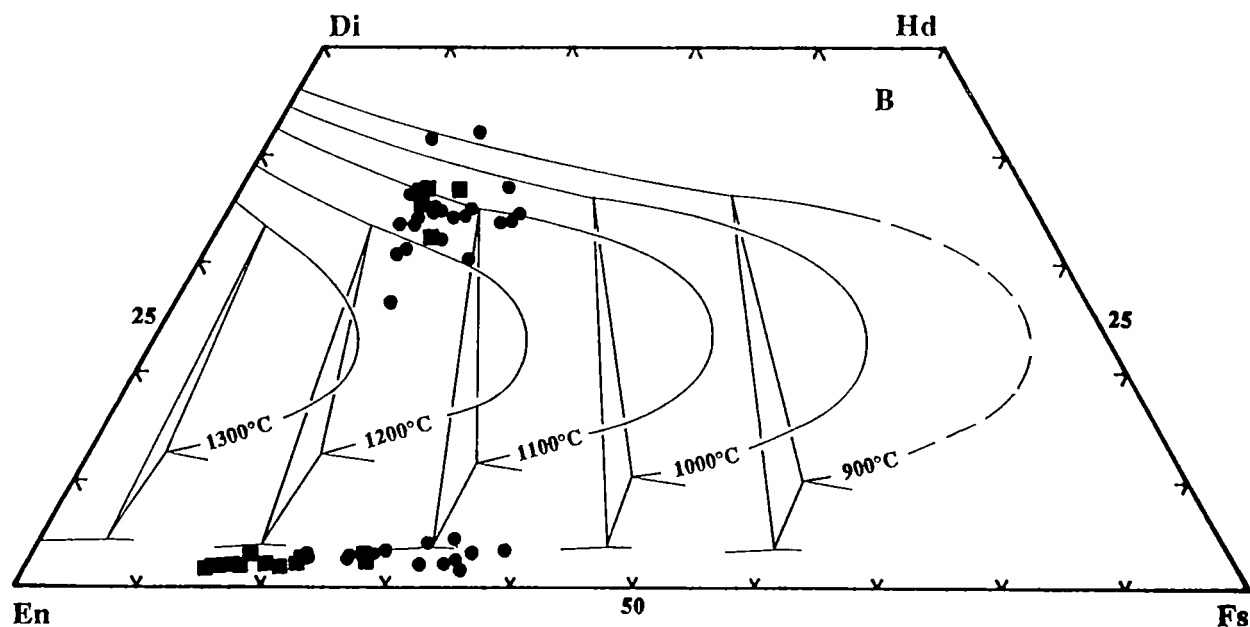
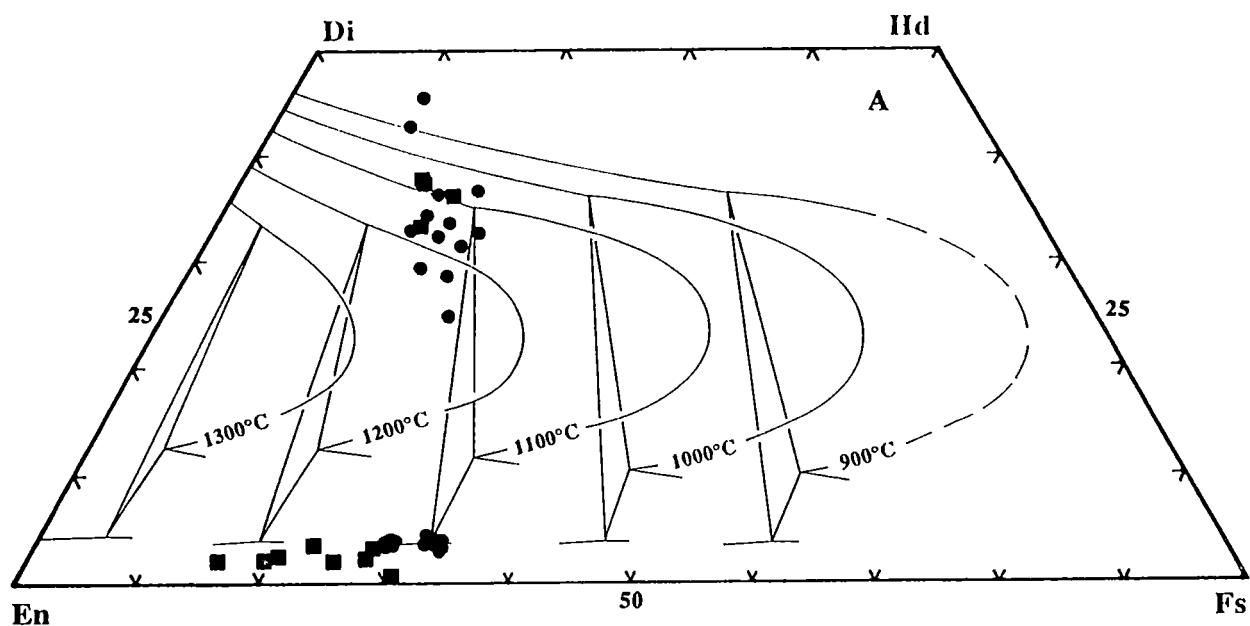
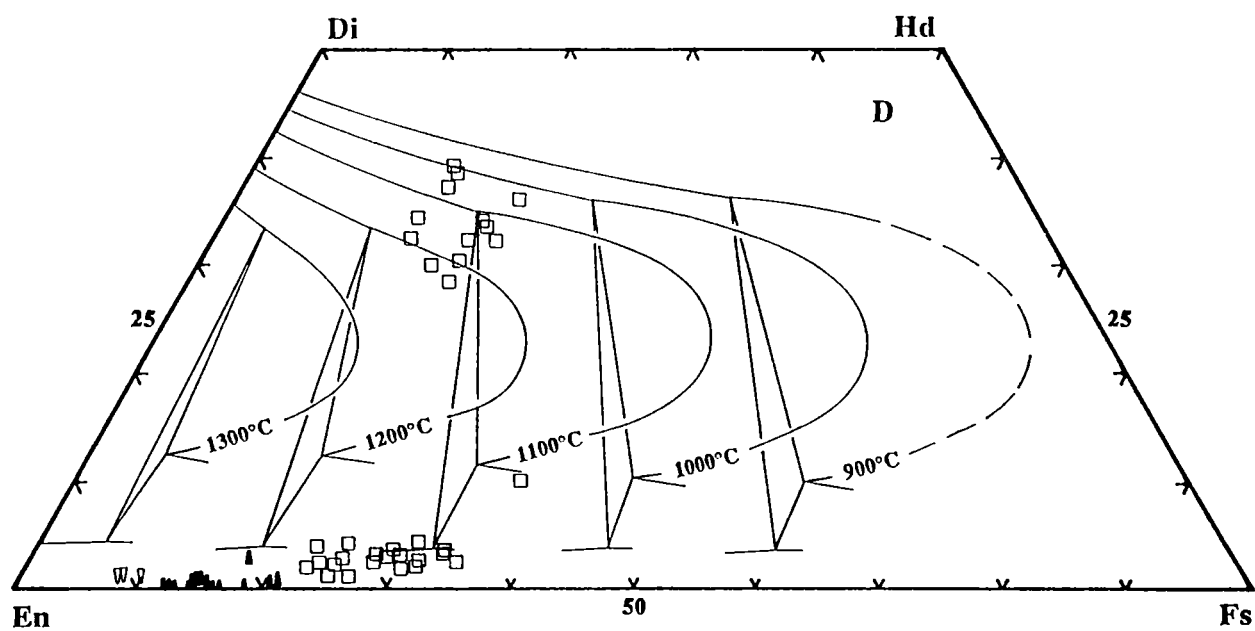
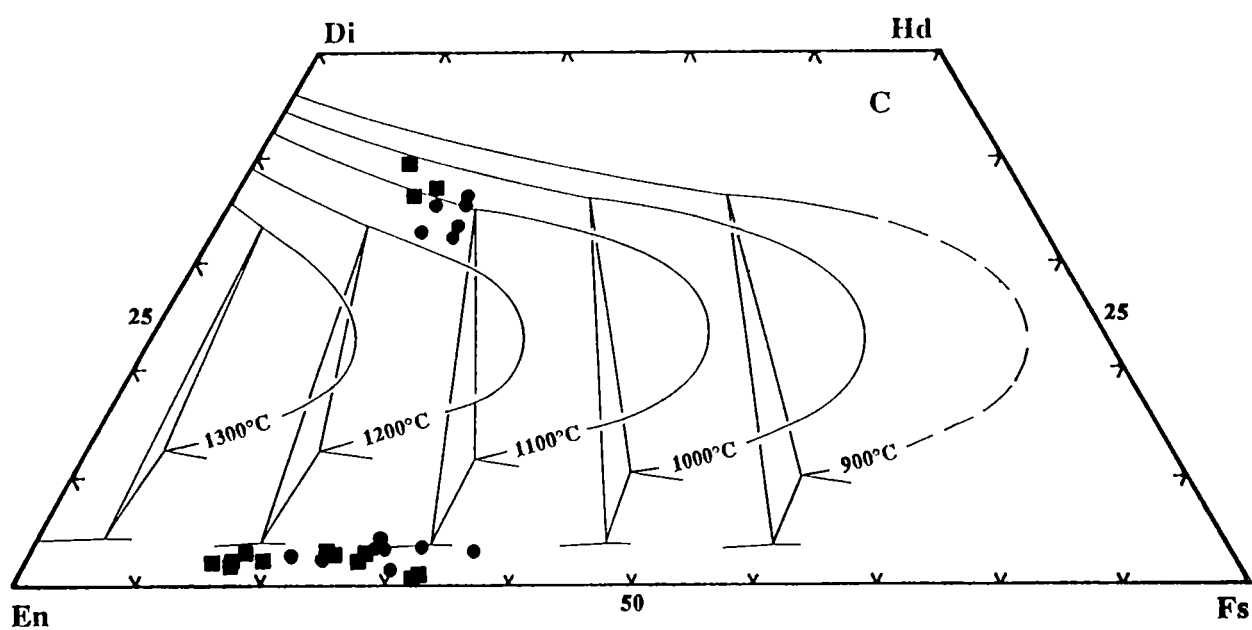
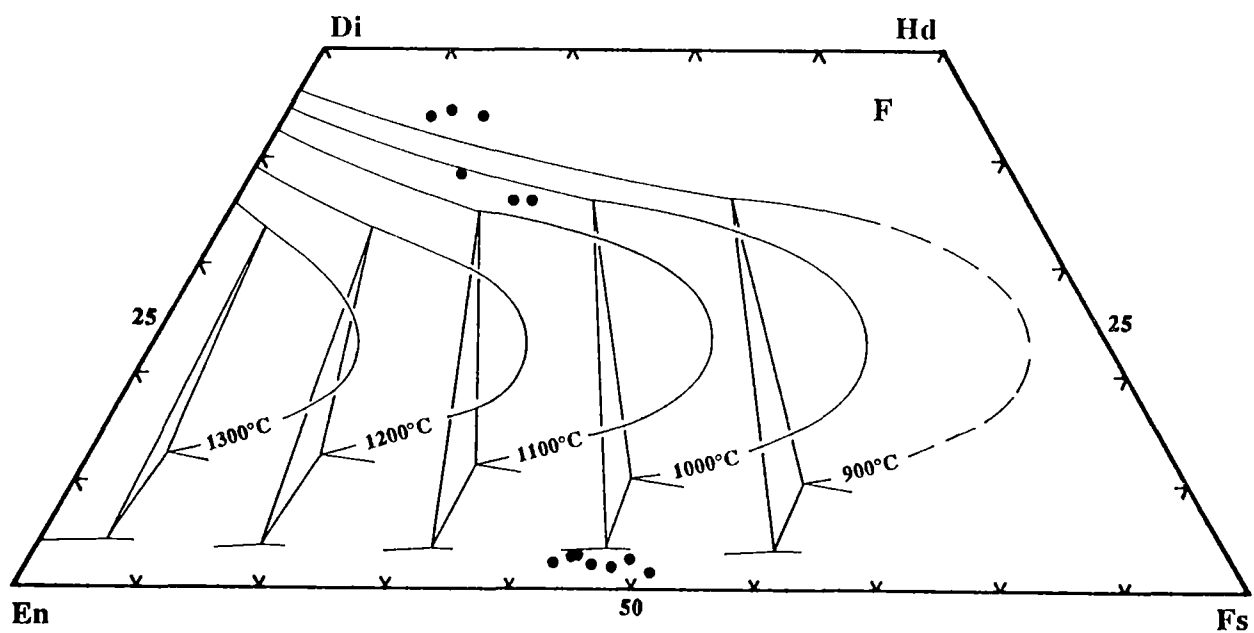
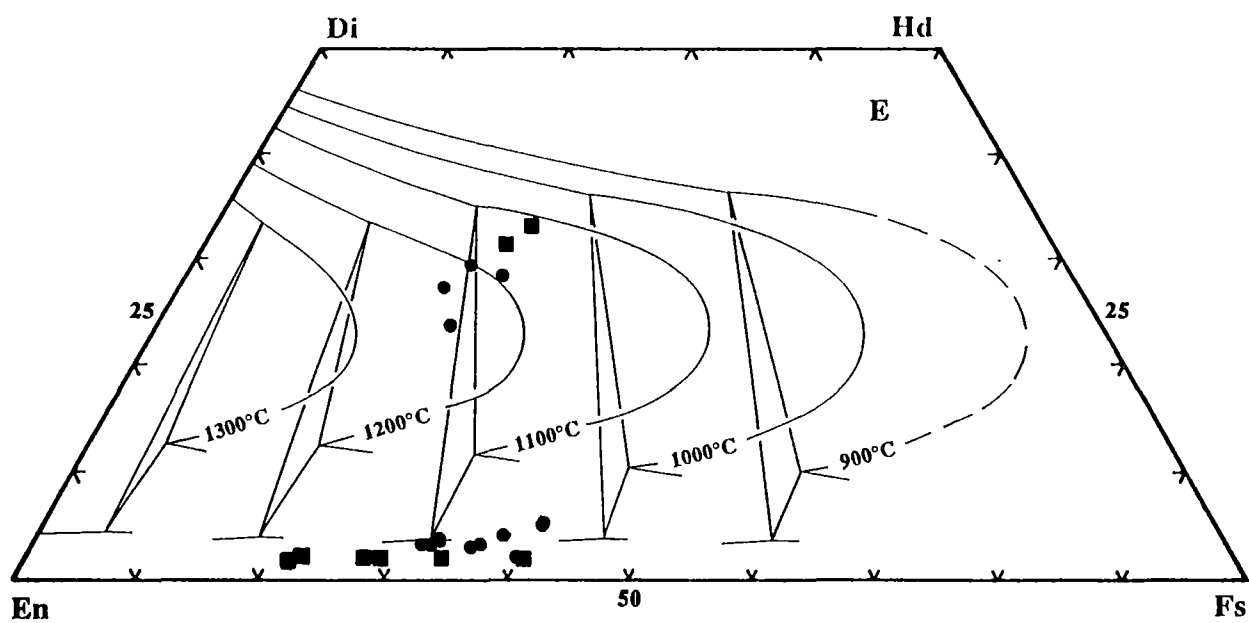


Figure 4.4

The graphical geothermometer of Lindsley (1983) (5 kbar projection) applied to coexisting orthopyroxene and clinopyroxene assemblages of (A) *Homogeneous Norite* (70667), (B) *Mottled Norite* (70661), (C) *Rubbly Norite* (70707), (D) *Rubbly Norite* hosting the enstatite nodules, (E) fine grained dykes associated with the norite (70709) and (F) coexisting intercumulus pyroxenes in *Homogeneous Norite*.





THERMOMETRY OF NORITE

Sample No. 70793				
Rock Type: H-Norite				
	cpx	opx	Thermometers	T°C
Si	1.958	1.963		
Ti	0.007	0.000	Bertrand & Mercier	1212
Al	0.081	0.058	Wells	1204
Cr	0.015	0.008	Kretz (>1080)	1224
Fe2+	0.332	0.547		
Fe3+	0.000	0.000		
Mn	0.009	0.008		
Mg	0.946	1.339		
Ca	0.642	0.081		
Na	0.000	0.000		
Sum	3.990	4.004		
Mg#	74.0	71.0		
Sample No. 70661				
Rock Type: M-Norite				
	cpx	opx	Thermometers	T°C
Si	1.945	1.974		
Ti	0.006	0.000	Bertrand & Mercier	1254
Al	0.096	0.034	Wells	1239
Cr	0.015	0.009	Kretz (>1080)	1269
Fe2+	0.309	0.455		
Fe3+	0.000	0.000		
Mn	0.000	0.007		
Mg	1.012	1.481		
Ca	0.610	0.052		
Na	0.000	0.000		
Sum	3.992	4.009		
Mg#	76.6	76.5		
Sample No. 70653				
Rock Type: R-Norite				
	cpx	opx	Thermometers	T°C
Si	1.947	1.951		
Ti	0.010	0.006	Bertrand & Mercier	1233
Al	0.089	0.061	Wells	1223
Cr	0.012	0.013	Kretz (>1080)	1240
Fe2+	0.316	0.540		
Fe3+	0.000	0.000		
Mn	0.000	0.007		
Mg	0.979	1.359		
Ca	0.639	0.069		
Na	0.000	0.000		
Sum	3.992	4.006		
Mg#	75.6	71.6		
Sample No. 70709				
Rock Type: FG-Dyke (opx-phyric tholeiite)				
	cpx	opx	Thermometers	T°C
Si	1.957	1.942		
Ti	0.008	0.007	Bertrand & Mercier	1251
Al	0.105	0.081	Wells	1234
Cr	0.000	0.011	Kretz (>1080)	1248
Fe2+	0.491	0.775		
Fe3+	0.000	0.000		
Mn	0.008	0.017		
Mg	0.884	1.062		
Ca	0.538	0.098		--
Na	0.000	0.000		
Sum	3.991	3.993		
Mg#	64.3	57.8		

Table 4.1

Temperatures calculated for coexisting orthopyroxene and clinopyroxene pairs using thermometers of Wells (1977), Kretz (1982) and Bertrand & Mercier (1985).

Orthopyroxene and clinopyroxene pairs in the fine grained dykes, which are associated with the norite, indicate emplacement temperatures of 1175° to 1245° C using the thermometers of Wells (1977), Kretz (1982) and Lindsley (1983). These temperatures are in good agreement with temperature estimates for orthopyroxene - clinopyroxene pairs from the norite bodies (see Table 4.1).

In Chapter 2 pressure estimates were made, using the Ellis geobarometer (Ellis, 1980), for a single dyke which occurs *ca.* 7 km to the south of the norite complex. In this section pressures were estimated for the emplacement of the norite itself. The only direct pressure estimate able to be made for the norite units, is based on aluminium exchange between plagioclase and clinopyroxene (Ellis, 1980). This geobarometer gives variable results which have been shown to be dependent on rates of cooling (see Chapter 2). Despite the wide range of pressures derived, the highest obtained can be considered as an upper limit for the pressure of emplacement .

Best estimates for the pressure of emplacement can be calculated from clinopyroxene - plagioclase pairs from the slowly cooled interior of the norite complex (see Chapter 2). Values obtained range from 2 - 4.5 kbars, indicating a maximum crystallization pressure of 4.5 kbar. Averaged Ca-Tschermaks content in clinopyroxene and anorthite content in plagioclase indicate a pressure of 3.5 kb, which is in agreement with estimates obtained for the crystallization of the olivine + orthopyroxene-phyric high-Mg tholeiite dykes in the central Vestfold Hills (see Chapter 2).

Based on these results the norite complex is believed to have been emplaced into the upper crust at ≤ 3.5 kbar and possibly as low as 2 kbar. Temperatures of 1200° - 1250° C are appropriate for liquidus temperatures of this type of magma.

--

4.5 LAYERING IN THE HOMOGENEOUS NORITE

4.5.1 Introduction

Layering is observed as colour variations, with thin, darker 'layers' occurring within lighter-coloured matrix. Layering occurs only in the *Homogeneous Norite* where it is observed in nearly all outcrops, particularly in the northern outcrops (*Bandits Island*, SE of *Barrier Island* on the land spit where *Tryne Fjord* narrows, and in the outcrops north of *Tryne Fjord*; see dyke base map Appendix).

Two principal layering types occur: (1) subvertical layering which can be subdivided into continuous linear layering and non-linear or cylindrical layering types, and (2) moderately inclined rhythmic layering.

The dominant layering type observed is subvertical layering.

Subvertical Layering

Subvertical layers occur as thin, 1 cm, and occasionally up to 20 cm wide bands which can extend up to 50 m, but more typically are between 5 and 20 m long. At their terminations the layer ends tend to fade into the *Homogeneous Norite* or curve into and join another layer. These layers never crosscut one another. They are usually inclined at near vertical angles between 80° and 90°.

Several different types of subvertical layering can be distinguished. The most abundant is a continuous layering, often occurring as parallel layer-sets of varying width and layer numbers. Layers in these sets sometimes curve and may coalesce (Figure 4.1 J). The distance between successive layers may be only a few to tens of centimetres, but generally spacings are about 15 - 20 cm.

Curving and cylindrical layers are less common and are randomly distributed through the *Homogeneous Norite*. Cylindrical layering (*ca.* 1m in diameter) comprising multiple, near vertical, often intersecting layers are also-observed. The outermost layers break away from the cylinder, as they migrate and fade into the

Homogeneous Norite (Figure 4.1). Similar layering (orbicular or circular structures) have been observed in other intrusions (e.g. Mitchell & Platt, 1982).

Layers may approach each other either at high- or low - angles but coalescing intersections are marked only by low-angle junctions. These layer junctions are characterized by enrichment in granophyric intergrowths (Figure 4.5). Lenses of granophyric intergrowth occur both at layer margins and within the layers themselves, showing elongation parallel to the layer as are crystals aligned within the layer margins.

Mineralogical features of the layers are consistent throughout the norite outcrops. In addition to the features noted above the layers in the *Homogeneous Norite* are notably finer grained than the norite. Zones marginal to the layers, within 1 to 5 cm, often exhibit a gradation in quartz-feldspar granophyre content, with late-stage fluids concentrating on the layer side facing the centre of the intrusion. The amount of granophyric intergrowth within the norite then decreases towards the next layer and, if the layer spacing is wide enough (more than 0.5 m), it may grade into a zone virtually free of late-stage granophyre. Where layers are in close proximity, less than 20 cm apart, late-stage granophyres become relatively enriched between the layers and grading of granophyre content is not observed.

Rhythmic Layering

Rhythmic layering is a subordinate layer variety, which in contrast to the subvertical layering is flat lying to moderately inclined and related to varying amounts of plagioclase, pyroxenes, and quartz-feldspar intergrowth. It is always poorly developed and often not an obvious feature. The layers occur as cycles in close succession with spacings between 2 and 4 cm.

--

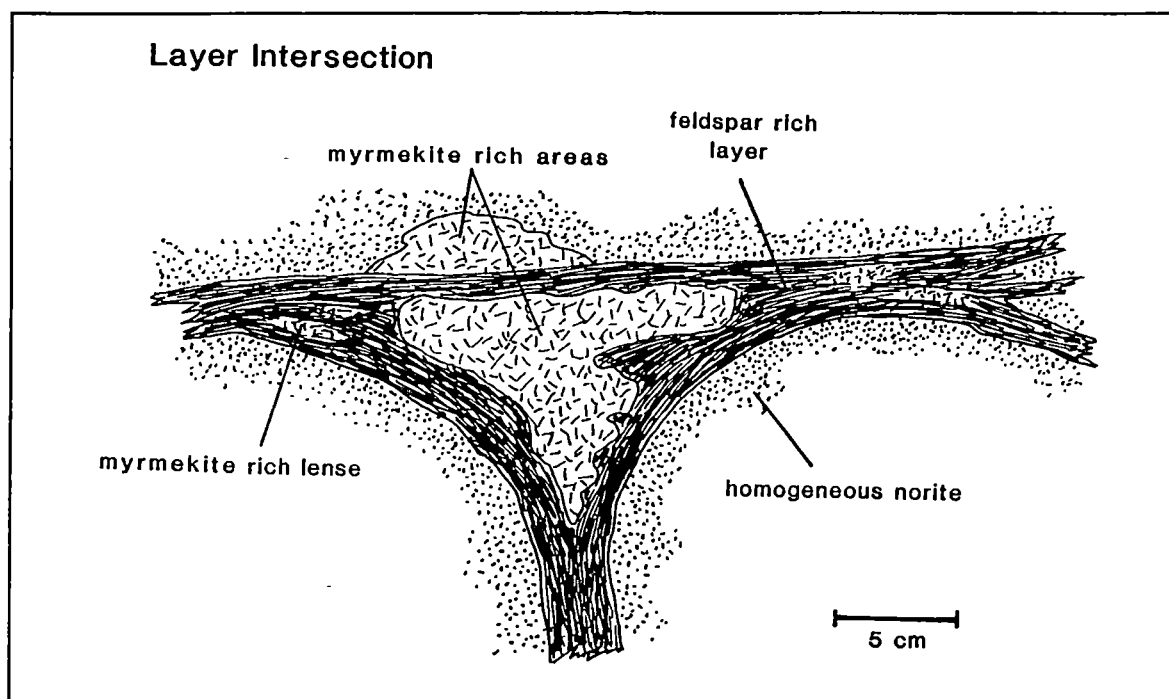


Figure 4.5

Schematic view of intersecting plagioclase-rich layers within the *Homogeneous Norite*.

4.5.2 Layer Orientation

The subvertical layering in the *Homogeneous Norite* has a consistent distribution and orientation in each outcrop area (Figure 4.6). In general, layering is not developed in marginal regions of the complex but rather is most abundant within 15 and 50 m from the intrusion margin. The layer sets are consistently orientated, the strike directions of which correspond to the strike direction of the ring-dyke structure. Rosediagrams in Figure 4.6 show that layer directions mainly strike between 130° and 140° (SE/NW) on *Bandits Island* and between 40° and 50° (NE/SW) in the *Rybnaya Bay* region, in both cases parallel to the intrusion margins at these places. The steep dips of the layers also parallel the steep dips of the intrusion margins.

4.5.3 Petrography and Mineral Chemistry

A comparison of mineral modes in the layers and the host *Homogeneous Norite* reveals the layers to have a much greater plagioclase content. Abundant opaque inclusions in plagioclase give the dark grey colour to the layers.

Modal mineral variations across a layer and into the host *Homogeneous Norite* is shown in Figure 4.7. Plagioclase in the *Homogeneous Norite* increases from ~ 40 to 50 vol% at the contact with the layer and reaching 75 and 80 vol% within the layer. Corresponding with this increase of plagioclase, orthopyroxene decreases from 25 vol% in the norite to *ca.* 15 vol% in the contact zone, and is less than 5 vol% within the layer.

Cloudy Plagioclase

The dark brown to grey plagioclase laths within the layers have an average length of 1 mm, though larger (2 mm) crystals are also common. The dust-like opaque inclusions in these plagioclase occur usually as equant crystals ~ 1 µm in diameter, or as fine needles up to 5 µm long. They are evenly distributed throughout the plagioclase, apart from narrow bands about crystal rims (5 - 25 µm wide) which are virtually free of inclusions. Similar inclusion-rich plagioclase are commonly observed

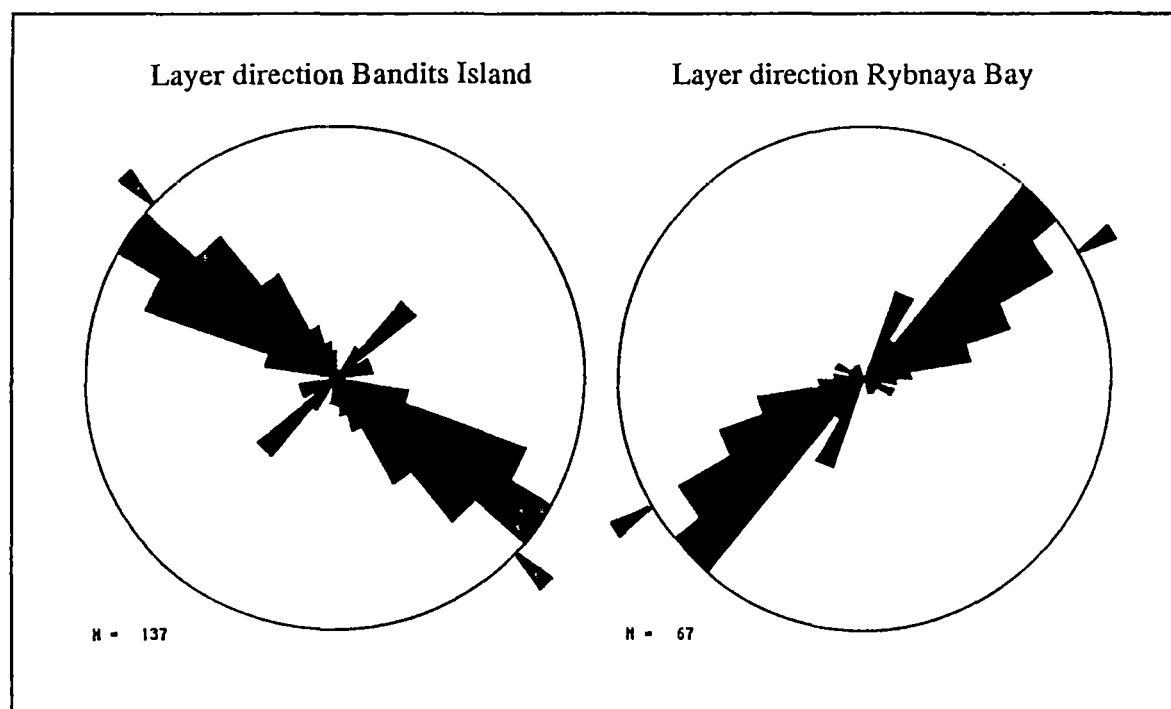


Figure 4.6

Layer directions at various points of the norite complexes (on *Bandits Island* and near *Rybnaya Bay*). Arrows at the outer side of the rose diagram indicate the strike of the ring complex at this location.

MINERAL DISTRIBUTION IN LAYERED NORITE

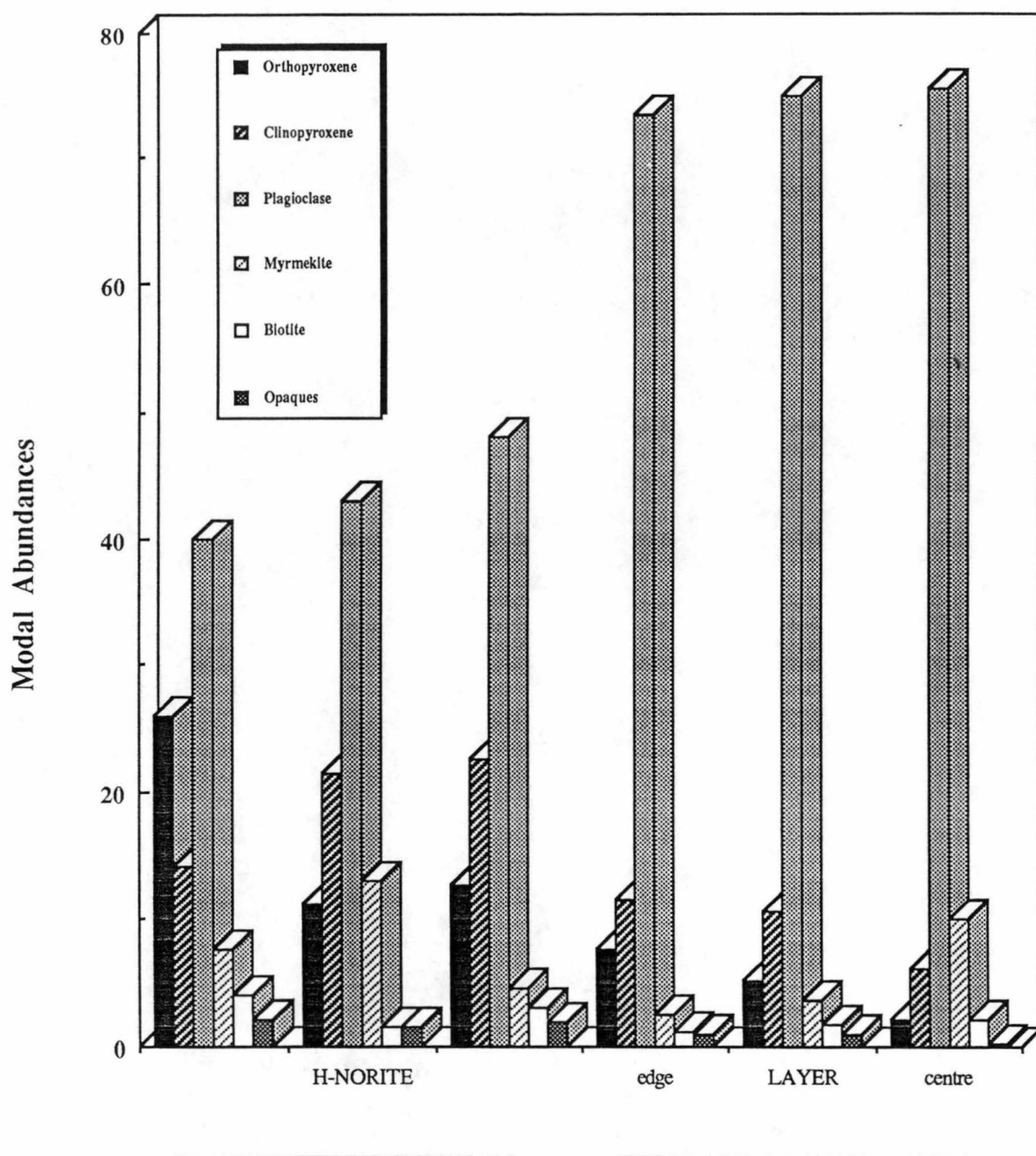


Figure 4.7

Mineral distribution in the *Homogeneous Norite* and in the plagioclase-rich layer occurring within this unit. Modal mineral abundances given in vol% were determined by point counting. Scale across diagram: 5 cm.

in the dykes of the Vestfold Hills, occurring in both the old 2350 Ma and younger 1350 Ma tholeiitic dykes. Microprobe analyses show these plagioclase to have high Fe content (up to 1.6 wt%), which may reflect the presence of an iron-bearing phase (magnetite or hematite).

Cloudy plagioclase has been described previously by a number of authors (e.g. Shand, 1945; Poldervaart et al., 1954; Whitney, 1972; Wass, 1973). The most frequent observed inclusion phases are opaques, spinel and rutile, with occasional garnet and hornblende. Magnetite inclusions are also known to occur in plagioclase (e.g. Adirondack Highlands (Poldervaart et al., 1954)), and Herz (1951) was able to separate finely crushed cloudy plagioclase cores and inclusion free rims into a more and less magnetic fraction. Experimental work on iron-bearing alkali-feldspars (Faust, 1936; Rosenqvist, 1951) indicates that Fe^{3+} may substitute for Al^{3+} in the feldspar lattice, and that it may exsolve upon slow cooling as magnetite or hematite. This mechanism was proposed for the development of cloudy plagioclase by Poldervaart et al. (1954).

Another possible cause of plagioclase clouding may be thermal overprinting. MacGregor (1931) attributed clouding of plagioclase to later heating (thermal metamorphism) resulting in the exsolution of iron originally contained in plagioclase in solid solution.

Dykes of the northern Vestfold Hills show no petrographic evidence for thermal overprinting (e.g. absence of metamorphic mineral assemblages), and an origin by slow cooling is supported by the presence of clear, inclusion free or poor plagioclase in dyke chilled margins. Inclusions become more abundant with increasing host crystal size and in plagioclase in the dyke interiors. If thermal overprinting were the cause of dusting of plagioclase, then plagioclase in both, chilled margins and dyke interiors should exhibit similar inclusion-rich textures. The clouding of plagioclase in the tholeiitic suites of the Vestfold Hills is therefore consistent with an origin by exsolution of Fe from iron-rich plagioclase formed under magmatic conditions.

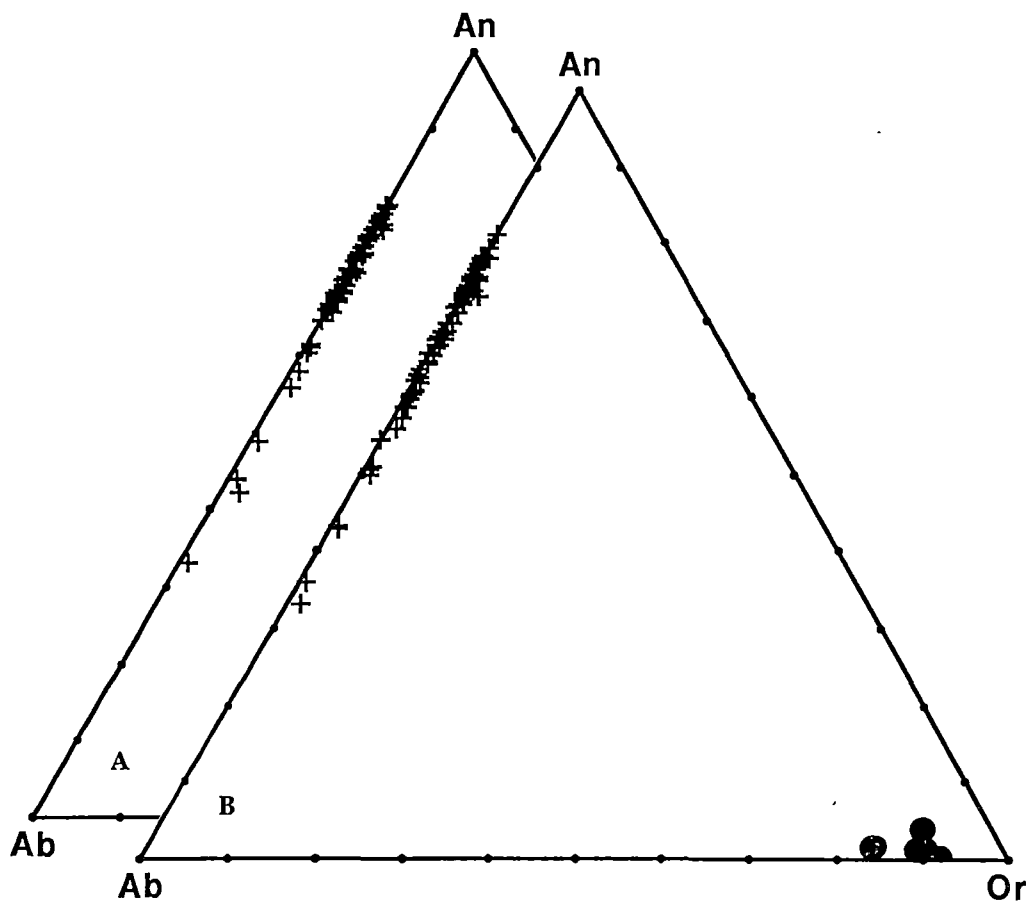


Figure 4.8

Composition of plagioclase compositions within the (A) Layer and (B) *Homogeneous Norite*.

Plagioclase crystals in the layers and in the *Homogeneous Norite* have a similar compositional range and are strongly zoned from An₈₁ cores to An₃₃ rims (Figure 4.8). Whereas orthopyroxene is cumulus phase in the *Homogeneous Norite*, plagioclase is a cumulus phase in the layers. Interstices between plagioclase crystals are occupied largely by quartz and minor amounts of quartz-alkali-feldspar intergrowth. Solitary orthopyroxene and clinopyroxene crystals (up to 0.5 - 1.5 mm) do occur within the layers, but are generally extensively altered and rimmed by biotite, chlorite and opaques. These orthopyroxenes have compositions between Mg# 75 cores and Mg# 49 rims and are compositionally much more evolved than orthopyroxene in the *Homogeneous Norite*. Clinopyroxene in contact with orthopyroxene range from Mg# 70 to Mg# 56.

Temperatures based on orthopyroxene and clinopyroxene pairs indicate closing temperatures between 900° and 750° C (calculated following Wells (1977), Kretz (1982) and Lindsley (1983)).

4.5.4 Layer Genesis

Layering in magmatic intrusions can originate in many ways, including: (1) crystal settling, (2) re-injection of liquids into a semicrystalline body, (3) slumping of cumulates, (4) turbulent currents and/or convective overturns, (5) flow differentiation and (6) static diffusion, to mention a few possibilities (e.g. Wager et al., 1960; McBirney & Noyes, 1979; Irvine, 1980; Parsons & Butterfield, 1981; Mitchell & Platt, 1982)

The vertical orientation of the layering makes a crystal settling origin, driven by density contrasts, an unlikely explanation in this case. The re-injection of liquids (to form the layers) into the semi-crystalline dyke is not supported by textural variations (e.g. grain size variations from the margin to the centre in the layer and the fact that one would expect a generally fine-grained layer). The absence of any alignment of crystals in the layer is evidence against flow differentiation. Furthermore, if flow differentiation were the responsible mechanism, multiple pulses of magma would be required to

explain the multiple layering throughout the dyke and these pulse would have to have an identical composition to explain the homogeneous nature of the host norite. Thus flow differentiation is also considered an unlikely mechanism in this case.

Two models are discussed below as possible mechanisms of layer formation. One model is based on the action of convection caused by different pulses of magma and the other model is based on migration of intercumulus liquid from the host norite.

Convection Model

A semi-crystalline margin within the crystallizing norite body may create a surface for the nucleation and crystallization of mineral upon influx of a new pulse of magma. If the new pulses of magma are saturated in both pyroxene and plagioclase, plagioclase which is known to be a poor 'nucleator' (e.g. Lofgren, 1980, 1983; Dowty, 1980) would continue to grow on pre-existing plagioclase at the semi-crystalline surface to form large crystals. Pyroxenes, in comparison, nucleate readily and new crystals will form nuclei in the new pulse of magma resulting in abundant relatively small crystals compared to plagioclase. The large plagioclase will grow *in situ* on the margin surface (or crystallization front), whereas small pyroxene nuclei may crystallize within the convecting magma and be carried away. This process could yield a coarse plagioclase rich 'skin' on the crystallization front and thus produce a layer relatively enriched in plagioclase over pyroxenes. This process necessarily only occurs at the onset of a new magma pulse, where there is an interface between more crystalline and less crystalline magma before the conditions which crystallize the *Homogeneous Norite*.

Disadvantages of the model outlined are, (1) the predicted gradational change on the 'inner side' (towards the dyke centre facing) of the layer is not observed (Figure 4.9) and (2) each magma pulse has to have the same composition as the *Homogeneous Norite* to form the parallel sequences of texturally and compositionally similar layers.

Intercumulus Model

This model proposes two stages of development. During the first stage, intercumulus liquid migrates into 'veins', which develop by shear movement between more crystalline cooler margins and less crystalline, hotter dyke interiors or by contraction induced by cooling. As the norite intercumulus liquid is known to be plagioclase saturated, this process can explain the sudden change in the apparent liquidus phases, from being orthopyroxene dominated in the *Homogeneous Norite* to being plagioclase dominated in the layer. The concentration of a liquid component and its separation from *Homogeneous Norite* is supported by the lack of crystal orientation and by the similar plagioclase compositions occurring in the layer and in the host norite. The late stage development is also indicated by the compositional differences in the pyroxene compositions (being more evolved in the layer), and the low temperatures calculated from pyroxene pairs.

In the second and final stage, evolved liquids from the layer migrate towards the less crystalline areas of the norite, adjacent to the plagioclase layer, where they pond and crystallize (see Figure 4.9).

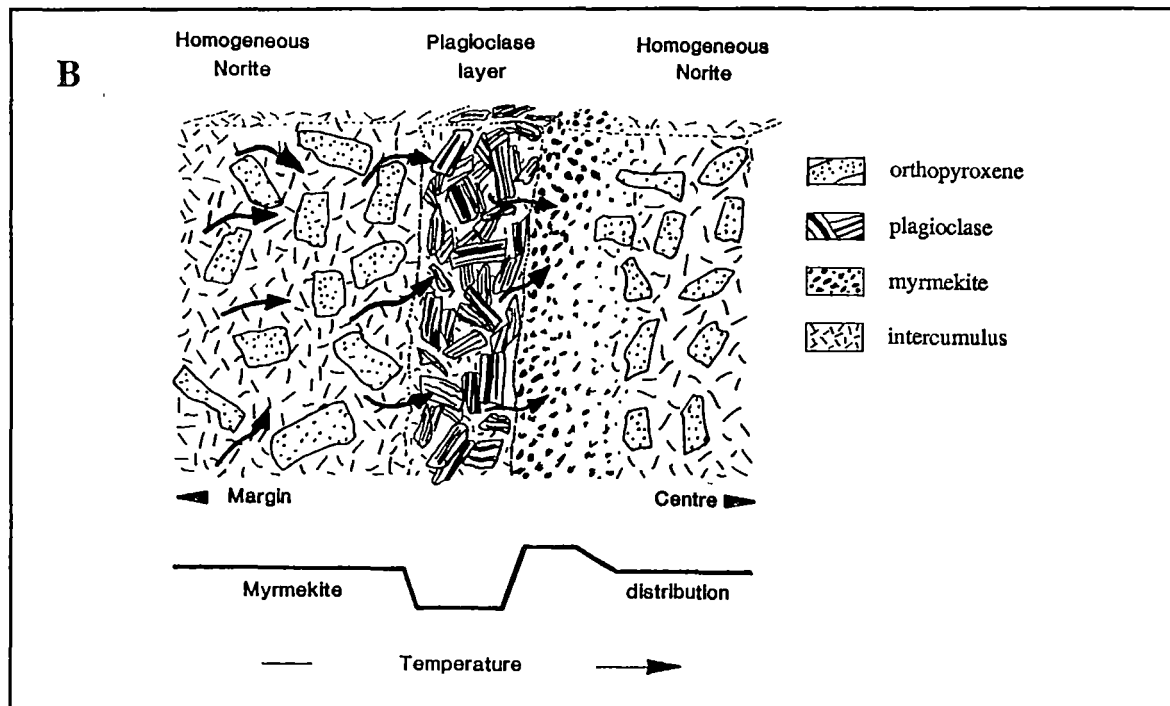
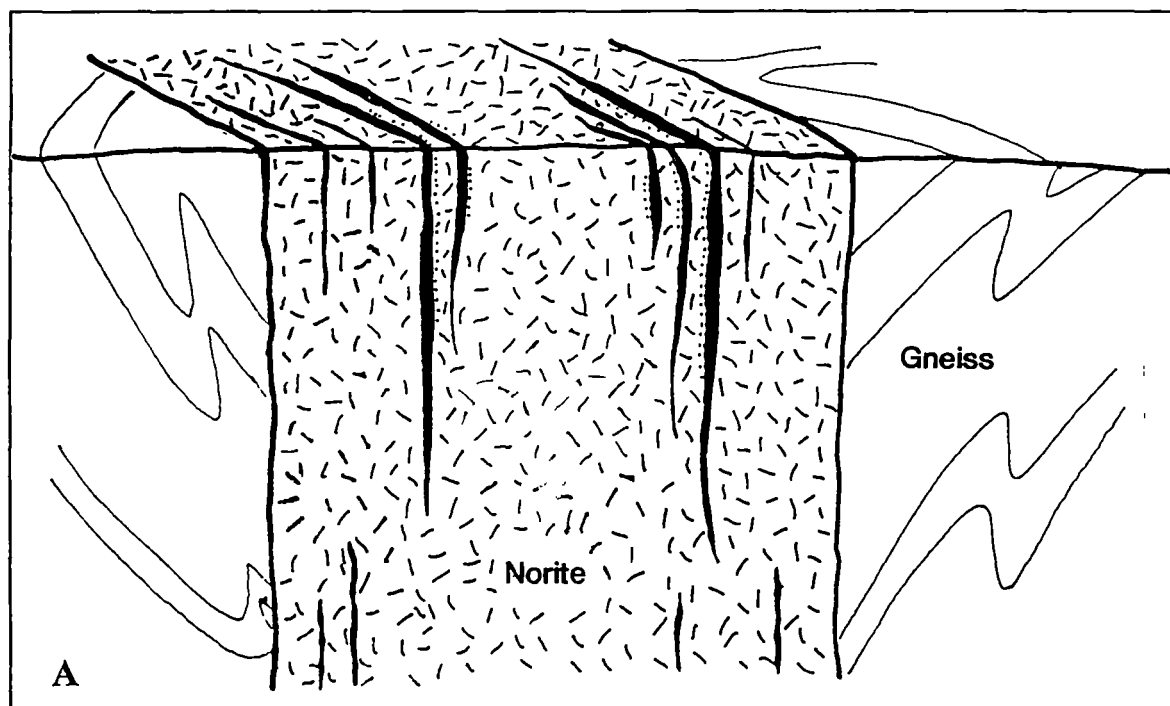


Figure 4.9

Schematic view of subvertical layering within the *Homogeneous Norite* in (A) outcrop (dyke width varies between 50 and 400 m) and (B) on microscopic scale (cross-section is ca. 5 cm). Arrows point towards the margin and the centre of the intrusion.

4.6 MAJOR AND TRACE ELEMENT GEOCHEMISTRY

Twenty four samples from the noritic ring dyke and seven from the associated fine grained dykes have been analyzed for major and trace elements. These samples have high SiO₂, MgO, and low TiO₂ contents, consistent with Siliceous High Magnesian Basalts (SHMB), using the classification of Glikson (1983) and Redman & Keays (1985). All samples are silica saturated and vary from 55.1 wt% to 56.7 wt% SiO₂ (3.8 to 10.8 CIPW normative Quartz). MgO content varies from 7.0 to 18.8 wt% and TiO₂ is less than 0.8% (0.38 - 0.74 wt%). Sample 70796 is a late stage segregation which is considerably more evolved, with 61.4 wt% SiO₂, and only 2.2 wt% MgO (representative whole rock analyses are listed in Table 4.2).

Major and minor element variations in the norite and associated dykes are plotted against MgO content in Figure 4.10. When considered together, these rocks form a coherent geochemical trend of increasing SiO₂, Al₂O₃, CaO, TiO₂ and K₂O, and decreasing FeO with decreasing MgO content. There are notable systematic differences between the rock types: with a progression of decreasing MgO contents in the sequence *Rubbly Norite*, *Mottled Norite*, to the *Homogeneous Norite*. The fine grained dyke compositions are identical to the *Homogeneous Norite*.

The normative compositions of various norite units and associated fine grained dykes projected from diopside onto the Ol, Qtz and Jd+CaTs plane and from plagioclase onto the Ol, Di and Qtz plane of the basalt tetrahedron in Figure 4.11. The quartz normative, norite types plot in a continuum and define a trend along a hypersthene control-line. Compositions become progressively less hypersthene normative from the *Rubbly Norite* through the *Mottled Norite* to the *Homogeneous Norite*. This is consistent with a model of progressive orthopyroxene fractionation (or accumulation) which is supported by mineral modes revealing an decrease in orthopyroxene content from 40 vol% in the *Rubbly Norite* to *ca.* 30 vol% in the *Homogeneous Norite*. Fine grained dykes associated with the norite plot in the same field as the *Homogeneous Norite*, and have similar modal orthopyroxene abundances.

REPRESENTATIVE NORITE WHOLE ROCK ANALYSES

Sample No. Rock Type	70688 HN	70801 HN	70653 RN	70766 RN	70661 MN	70704 MN	70796 LS	70709 FGD	71889 FGD
Major Elements									
SiO ₂	55.40	55.14	55.84	54.93	55.97	56.72	61.45	55.92	56.15
TiO ₂	0.56	0.52	0.39	0.44	0.55	0.64	1.24	0.74	0.71
Al ₂ O ₃	10.51	11.12	6.81	8.26	9.30	10.33	13.68	13.00	12.64
Fe ₂ O ₃	11.47	12.42	12.67	12.77	11.87	11.82	9.53	11.39	11.37
FeO	0.00	0.00	0.00	0.00	0.00	0.00	0.00	0.00	0.00
MnO	0.16	0.19	0.19	0.19	0.19	0.18	0.10	0.17	0.16
MgO	12.17	11.00	18.77	15.91	14.27	12.26	2.17	7.56	8.33
CaO	6.78	7.45	4.74	5.41	5.78	6.11	6.06	7.93	7.71
Na ₂ O	1.32	1.71	0.81	0.93	1.20	1.36	2.52	1.72	1.77
K ₂ O	0.96	0.96	0.62	0.72	0.92	1.09	2.42	1.33	1.21
P ₂ O ₅	0.09	0.09	0.04	0.07	0.08	0.11	0.23	0.13	0.12
LOI	-0.04	-0.06	-0.12	0.24	-0.19	-0.23	0.40	0.16	0.06
Total	98.35	99.42	99.62	98.72	98.87	99.33	98.94	100.05	100.23
Mg#	67.8	63.7	74.6	71.2	70.4	67.3	31.1	56.8	59.2
CIPW Norm wt%									
Qtz	7.41	5.26	4.94	5.84	7.04	8.66	18.80	9.22	8.88
Or	5.67	5.67	3.66	4.25	5.44	6.44	14.30	7.86	7.15
Ab	11.17	14.47	6.85	7.87	10.15	11.51	21.32	14.55	14.98
An	19.92	19.83	13.11	16.24	17.27	18.86	18.87	23.82	22.97
Lc									
Ne									
Cpx	10.64	13.47	8.15	8.19	8.78	8.70	8.22	12.05	11.87
Di	7.36	8.76	6.14	5.91	6.30	5.98	2.88	7.09	7.26
Hd	3.27	4.72	2.00	2.28	2.49	2.71	5.35	4.95	4.60
Opx	40.63	37.77	60.33	53.23	47.41	42.21	12.76	28.01	30.02
En	26.90	23.34	43.91	36.89	32.63	27.76	4.07	15.54	17.38
Fs	13.73	14.43	16.43	16.34	14.78	14.44	8.69	12.46	12.64
Ol									
Fo									
Fa									
Mt	1.66	1.80	1.84	1.85	1.72	1.72	1.38	1.65	1.65
Il	1.06	0.99	0.74	0.84	1.04	1.22	2.36	1.41	1.35
Ap	0.21	0.21	0.09	0.17	0.19	0.26	0.54	0.31	0.28
Trace Elements									
Ba	216	202	131	159	201	245	515	292	286
Rb	41	40	37	43	51	61	127	72	64
Nb	6	5	5	6	8	8	13	6	7
Sr	90	98	50	71	77	94	150	115	107
Zr	85	78	50	69	83	104	213	122	113
Y	19	14	11	11	21	19	38	22	22
La	15	14	8	11	16	17	36	22	21
Ce	33	28	16	23	31	34	77	42	44
Nd	14	12	9	7	12	15	33	19	17
Ni	332	253	1395	452	360	294	32	199	179
Cr	1152	836	2104	1431	1509	1169	22	524	615
V	213	215	187	216	201	208	232	221	213
Sc	31	35	28	32	30	30	29	34	33

Table 4.2

Selected Norite whole rock analyses showing various groups, including Homogeneous Norite (HN), Rubbly Norite (RN), Mottled Norite (MN), Late Stage Segregation (LS) and Fine Grained Dykes (FGD).

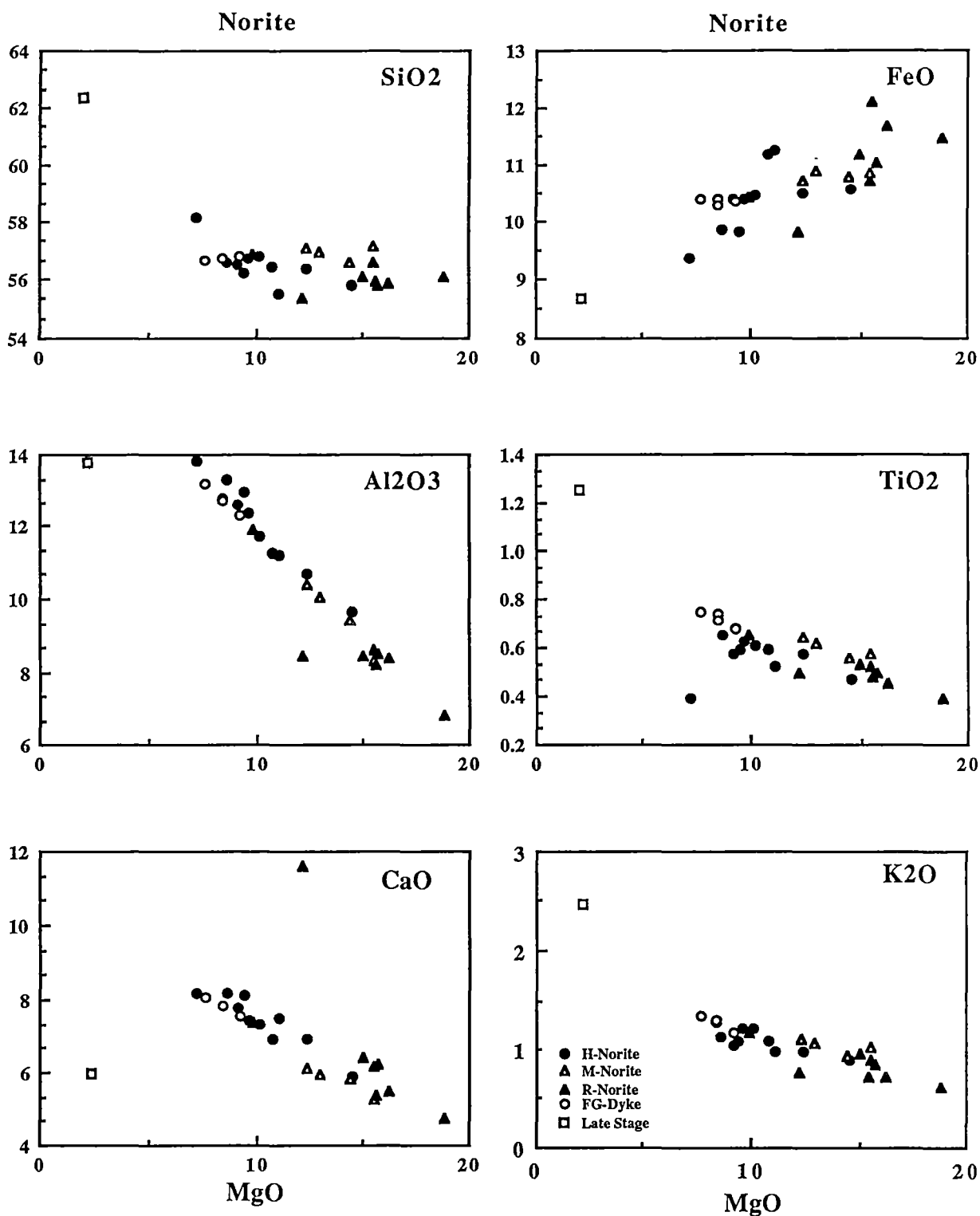


Figure 4.10

Major elements plotted against MgO. Before plotting major elements were recalculated to 100% volatile free and total Fe as FeO.

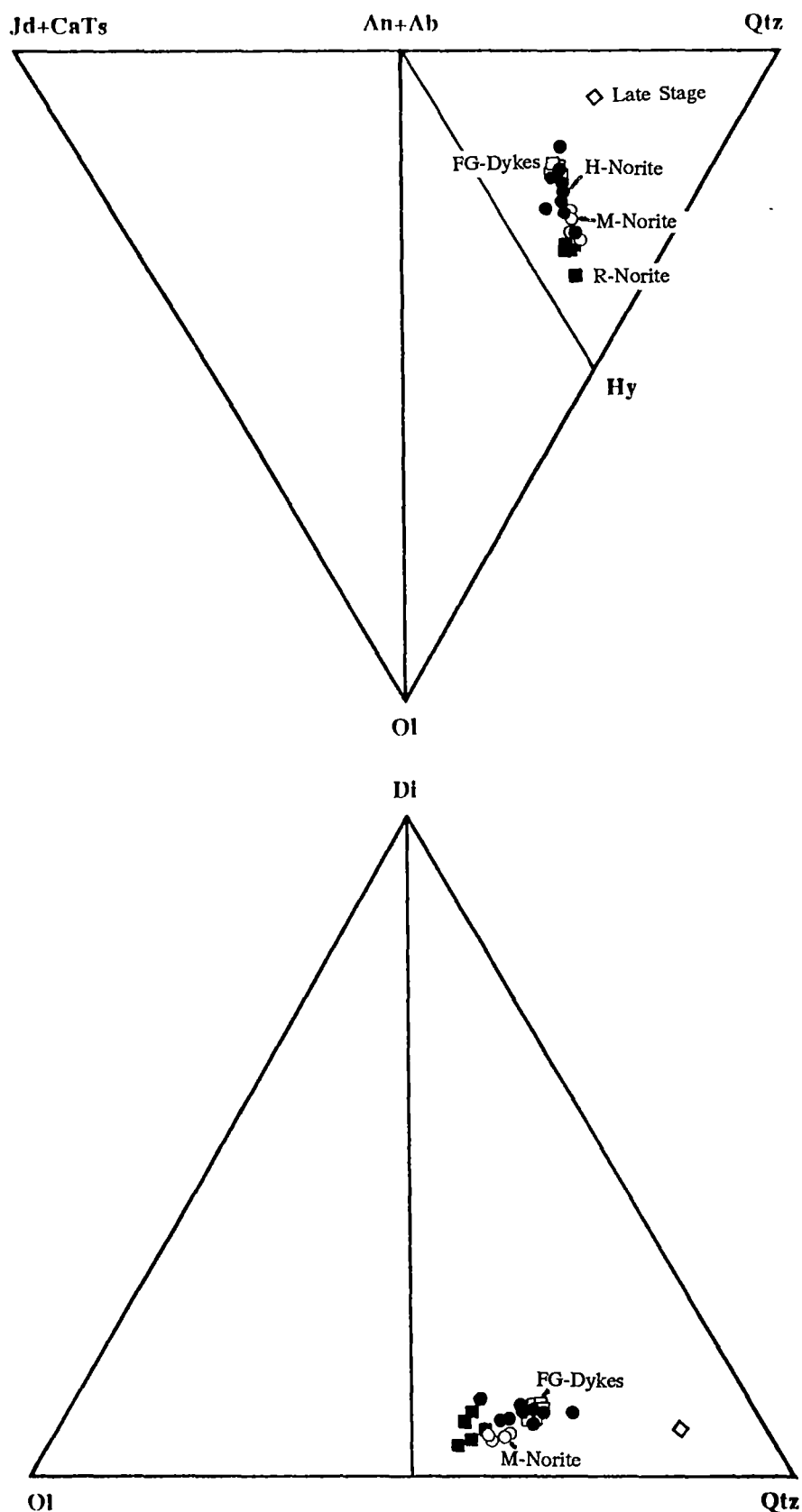


Figure 4.11

Compositions of the *Homogeneous Norite*, *Mottled Norite*, *Rubbly Norite* and fine grained dykes are projected from diopside onto the plane Jd+CaTs - Ol - Qtz of the basalt tetrahedron following Green (1970) ($\text{Fe}_2\text{O}_3/\text{FeO} = 0.1$).

Variations in major elements between the *Homogeneous*-, *Mottled Norite* and the *Rubbly Norite* (Table 4.3 A and B) can be explained by orthopyroxene accumulation. GENMIX modelling (Le Maitre, 1980) shows that the *Mottled Norite* and *Rubbly Norite* major element compositions may be explained by 13% and 40% orthopyroxene accumulation respectively in a *Homogeneous Norite* composition (Table 4.3 A and B). The difference in composition between the *Homogeneous Norite* and associated fine grained dykes has also been modelled, and shows that 22% orthopyroxene fractionation is required to produce the composition of sample 70709.

The incompatible trace elements (Sr, Ba, Rb and Nb) are positively correlated with Zr, whereas Ni and Cr decrease with increasing Zr. Apart from orthopyroxene accumulation, the accumulation of Fe-Ni-Cu sulphides within the *Rubbly Norite* is evident from petrographic observations (see Chapter 5). This is supported by Ni variations plotted versus Zr (Figure 4.12), the very high Ni contents in the *Rubbly Norite* are inconsistent with orthopyroxene accumulation alone and require an additional Ni-rich phase, which is consistent with the high modal sulphide content in this rock.

Trace element concentrations, normalized to primitive mantle (Sun et al., 1989) are plotted in multi element diagrams in Figure 4.13. Identical trace element patterns are observed in all samples including the late stage segregations, which show significant trace element enrichment over the other norite units. The fine grained dykes 70623, 70709 and 71984 also have slightly higher concentrations of these elements than the norite units, except for Nb, which is similar to normalized abundances in the *Rubbly Norite*. Notable Ba, Nb, Sr, P and Ti anomalies occur relative to neighbouring elements in all the samples.

Chondrite-normalized REE patterns show relatively strong enrichment of LREE over HREE (Figure 4.14). The various norite types and fine grained dykes have similar abundances, whereas the late stage segregation has similar degree of LREE and HREE fractionation but at double concentration levels observed in the other samples. With the exception of the *Rubbly Norite*, all the norite types and associated rocks have

A				Estimated	
Sample No.	Reactant	Product A	Product B	Reactant	Difference
Description	70661	70688	Opx		
	M-Norite	H-Norite	phenocryst		
SiO ₂	55.97	55.40	54.84	55.33	0.64
TiO ₂	0.55	0.56	0.12	0.50	0.05
Al ₂ O ₃	9.30	10.51	1.79	9.36	-0.06
FeO	10.67	10.30	11.49	10.46	0.21
MgO	14.27	12.17	28.97	14.39	-0.12
CaO	5.78	6.78	2.36	6.20	-0.42
Na ₂ O	1.20	1.32	0.00	1.15	0.05
K ₂ O	0.92	0.96	0.00	0.83	0.09
P ₂ O ₅	0.08	0.09	0.00	0.08	0.00
Total	98.74	98.09	99.57	98.30	0.44
Mass%	100.00	86.77	13.23		
Sum of squares					0.8146

B				Estimated	
Sample No.	Reactant	Product A	Product B	Reactant	Difference
Description	70653	70688	Opx		
	R-Norite	H-Norite	phenocryst		
SiO ₂	55.84	55.40	54.84	55.17	0.67
TiO ₂	0.39	0.56	0.12	0.38	0.01
Al ₂ O ₃	6.81	10.51	1.79	6.99	-0.18
FeO	11.40	10.30	11.49	10.78	0.62
MgO	18.77	12.17	28.97	18.95	-0.18
CaO	4.74	6.78	2.36	5.00	-0.26
Na ₂ O	0.81	1.32	0.00	0.79	0.02
K ₂ O	0.62	0.96	0.00	0.57	0.05
P ₂ O ₅	0.04	0.09	0.00	0.05	-0.01
Total	99.42	98.09	99.57	98.68	0.74
Mass%	100.00	59.65	40.35		
Sum of squares					0.9805

C				Estimated	
Sample No.	Reactant	Product A	Product B	Reactant	Difference
Description	70688	70709	Opx		
	H-Norite	FG-Dyke	phenocryst		
SiO ₂	55.40	55.92	54.84	55.69	-0.29
TiO ₂	0.56	0.74	0.12	0.61	-0.05
Al ₂ O ₃	10.51	13.00	1.79	10.57	-0.06
FeO	10.30	10.25	11.49	10.52	-0.22
MgO	12.17	7.56	28.97	12.20	-0.03
CaO	6.78	7.93	2.36	6.72	0.06
Na ₂ O	1.32	1.72	0.00	1.35	-0.03
K ₂ O	0.96	1.33	0.00	1.04	-0.08
P ₂ O ₅	0.09	0.13	0.00	0.10	-0.01
Total	98.09	98.58	99.57	98.80	-0.71
Mass%	100.00	78.34	21.66		
Sum of squares					0.3835

Table 4.3

Least-squares mixing GENMIX (Le Maitre, 1980). In Tables A - C various norite types and fine grained dyke have been modelled from Homogeneous Norite by the accumulation of orthopyroxene (A and B) and from fine grained dykes (C).

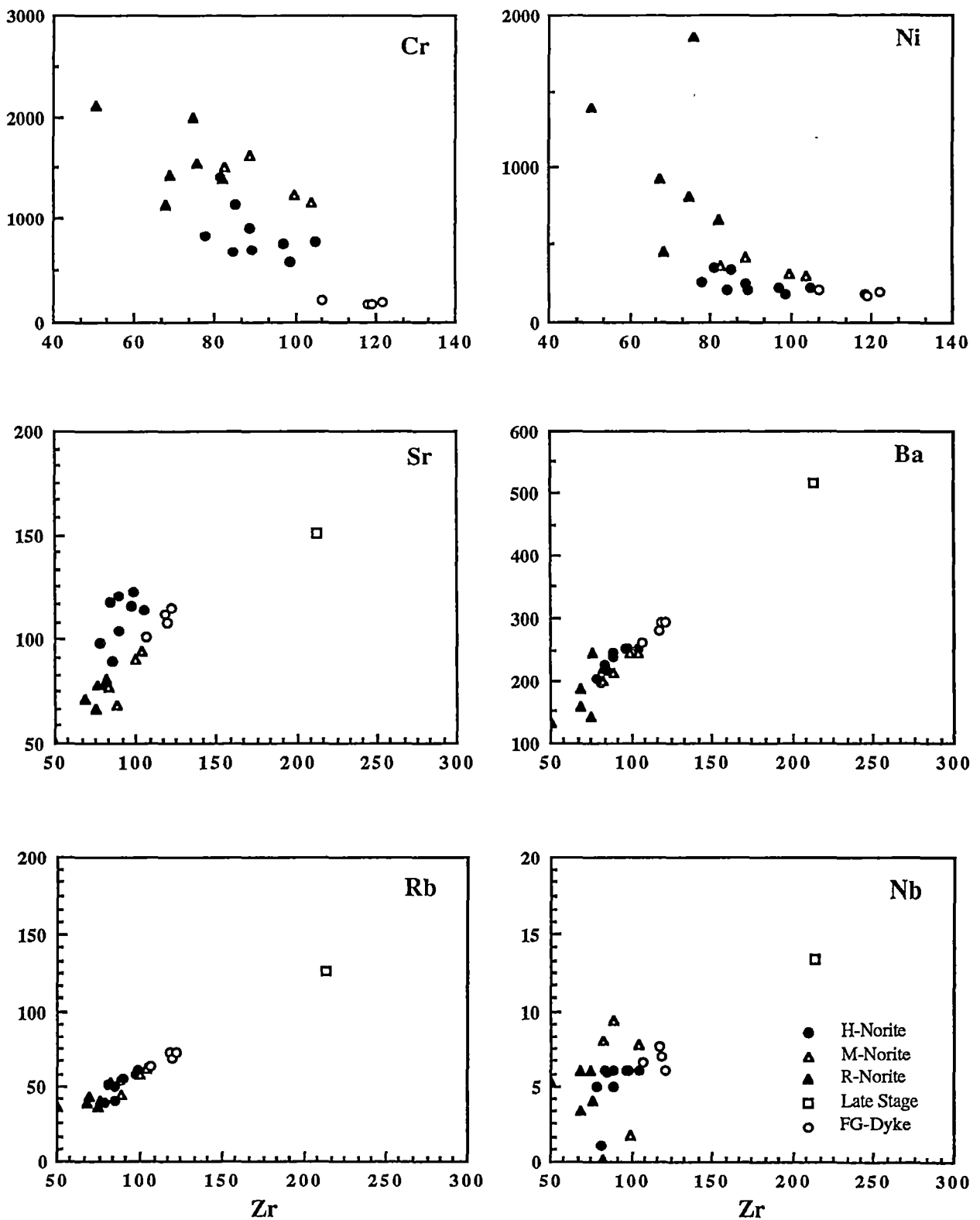


Figure 4.12

Selected trace elements plotted against Zr. Note the distinct chemistry of the various norite types and the associated fine grained dykes.

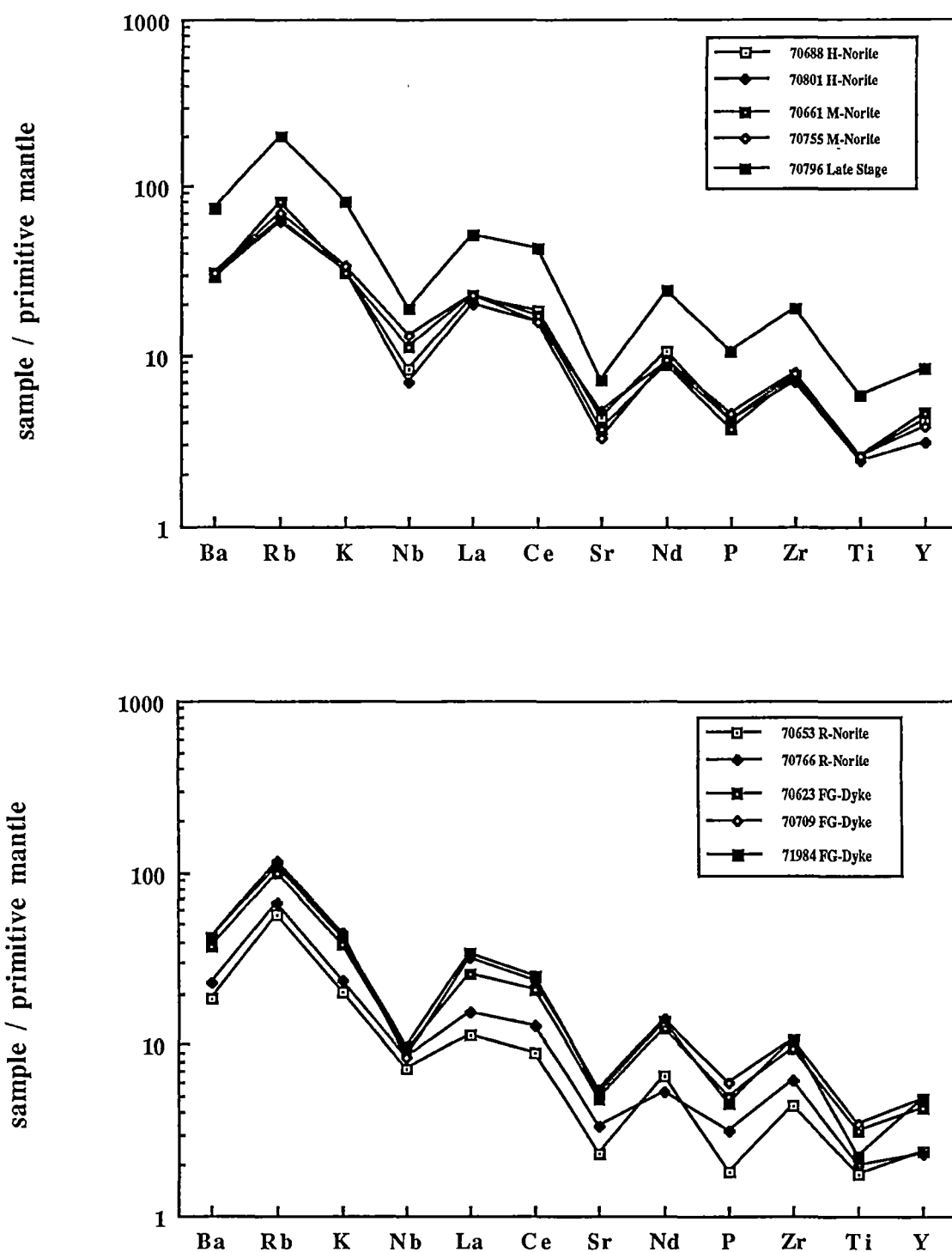


Figure 4.13

Incompatible element 'spidergrams' of various norite types and associated fine grained dykes, normalized to primitive mantle composition (Sun et al., 1989).

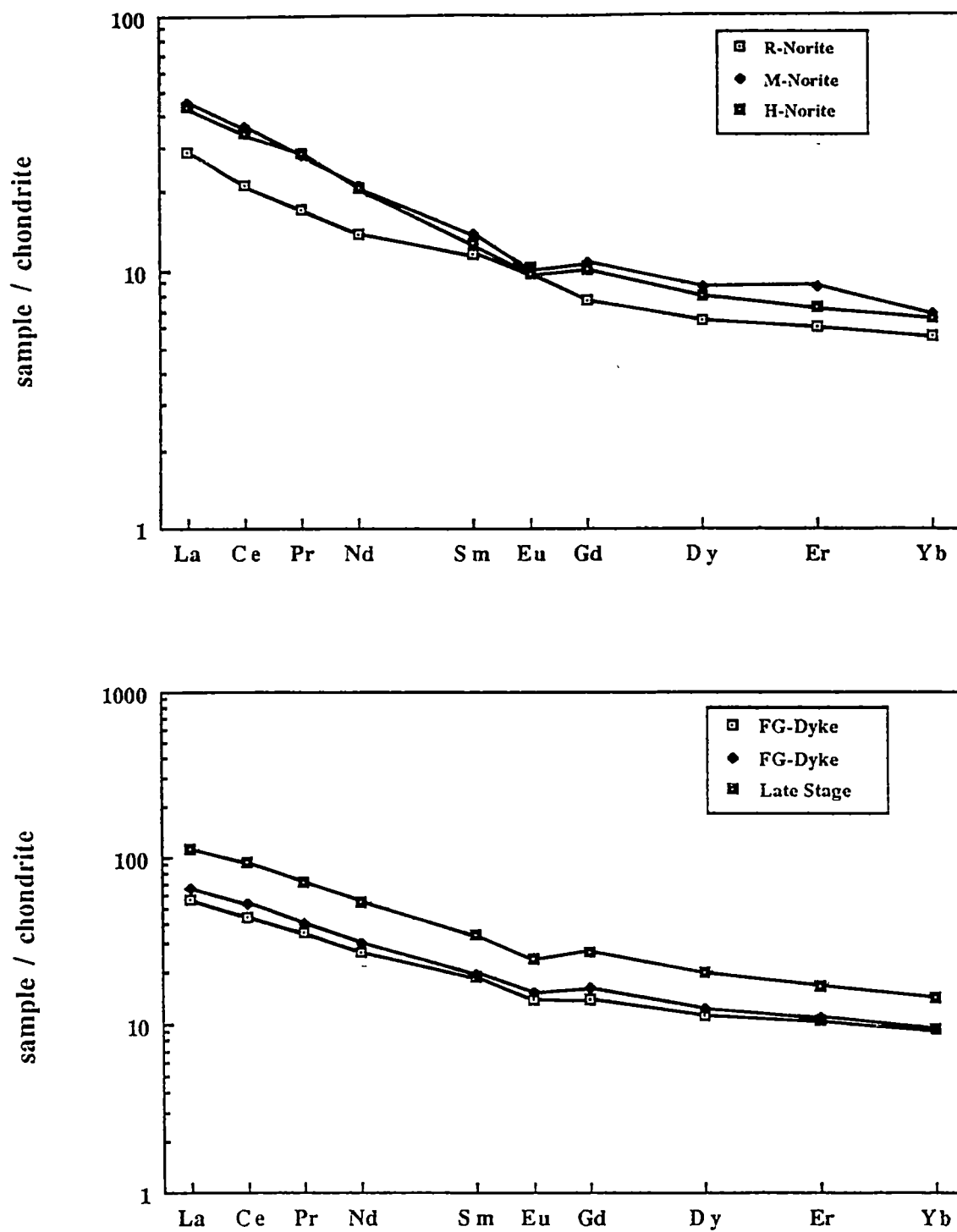


Figure 4.14
Chondrite normalized REE patterns (Leedy/1.2; Masuda et al. 1973; Taylor & Gorton, 1977) of various norite samples.

REE ANALYSES FROM NORITES AND FINE GRAINED DYKES

Sample No. Rock Type	70661 MN	70801 HM	70796 LS	70653 RN	70623 FGD	70709 FGD	71889 FGD
REE / ppm							
La	14.4	13.8	35.8	9.1	17.6	20.7	19.6
Ce	29.5	28.2	77.0	17.6	35.7	42.1	40.2
Pr	3.3	3.3	8.2	2.0	4.0	4.6	4.5
Nd	12.8	12.4	32.7	8.3	15.9	18.0	18.1
Sm	2.6	2.5	6.6	2.2	3.7	3.8	4.0
Eu	0.8	0.7	1.8	0.8	1.0	1.1	1.0
Gd	2.8	2.6	7.0	2.0	3.6	4.2	3.9
Dy	2.8	2.6	6.5	2.1	3.7	4.1	4.1
Er	1.8	1.5	3.5	1.3	2.3	2.3	2.3
Yb	1.4	1.4	3.0	1.2	1.9	2.0	2.1
La/Yb	10.1	10.1	11.8	7.7	9.1	10.5	9.3

Table 4.4

Rare earth abundances in norites and fine grained dykes from the Vestfold Hills. Analyses were done following the method of Robinson et al. (1986). Concentrations given in ppm, were normalized to chondritic values (Leedey /1.2, Taylor & Gorton, 1977). Abbreviations: HN - Homogeneous Norite, MN - Mottled Norite, RN - Rubbly Norite, FGD - fine grained dykes, LS - late stage segregation.

a small negative Eu anomaly. The *Rubbly Norite*, has a distinct pattern compared to other norite types with LREE and HREE being relatively depleted to these in the *Homogeneous* and *Mottled Norite*, and the fine grained dykes.

Trace element variations in the norites and fine grained dykes have been modelled assuming Rayleigh fractionation, and 40% orthopyroxene fractionation (from the *Rubbly-* to *Homogeneous Norite*) and 22% orthopyroxene fractionation (from the *Homogeneous Norite* to the fine grained dykes), as constrained GENMIX calculations (Table 4.3). The calculated incompatible trace element variations compare well with the observed trace element concentrations (Figure 4.15). As a compatible element Cr variations place a useful constraint on models. A model fractionating 40% and 22% orthopyroxene requires a D^{Cr}_{Opx} of 2.2 and 4.2, respectively. This is feasible considering published $K_D^{Cr}_{Opx}$ (e.g. Cox et al. (1979) listed $K_D^{Cr}_{Opx} = 2$ for basaltic rocks), though much higher K_D 's (8 - 10) are reported (Ewart & Taylor, 1969; Jenner, pers. comm., respectively). Mineral partition coefficients used in the crystal fractionation model are listed in Table 4.5.

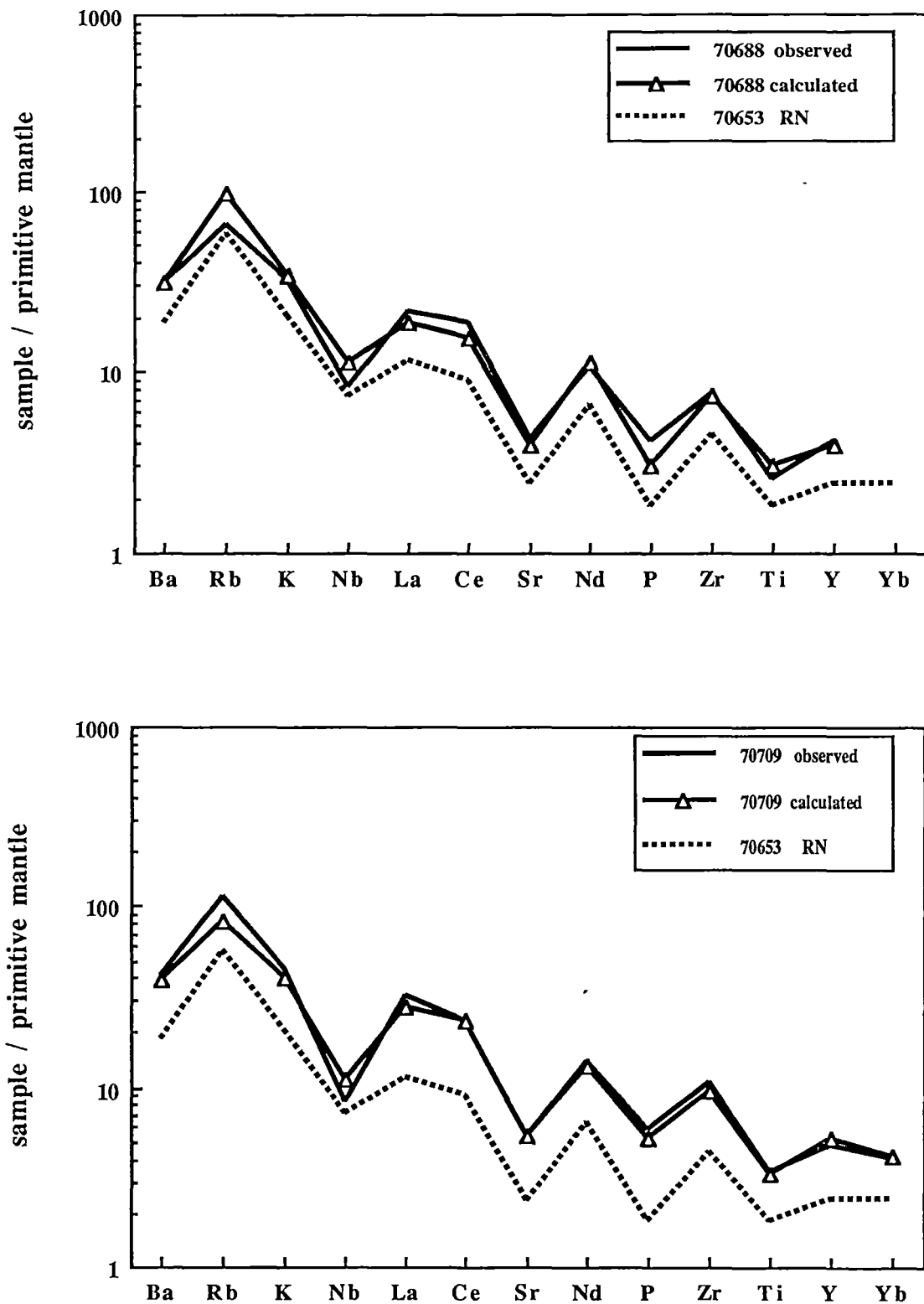


Figure 4.15

Incompatible element fractional crystallization-model. All compositions were normalized to primitive mantle, showing abundances in the natural rock and those calculated using Rayleigh fractionation.

MINERAL-MELT PARTITION COEFFICIENTS

	Olivine	Clinopyroxene	Orthopyroxene	Plagioclase
Elements				
Ba	0.0001	0.0011	0.0010	0.2300
Rb	0.0002	0.0011	0.0060	0.1000
K	0.0002	0.0020	0.0010	0.1700
Nb	0.0004	0.0150	0.0040	0.0100
La	0.0005	0.0200	0.0005	0.1800
Ce	0.0008	0.0400	0.0009	0.1200
Sr	0.0002	0.0670	0.0070	1.8000
Nd	0.0013	0.0900	0.0019	0.0810
P	0.0013	0.0900	0.0019	0.0810
Zr	0.0020	0.1200	0.0030	0.0100
Ti	0.0020	0.2000	0.0040	0.0450
Y	0.0050	0.2000	0.0300	0.0250
Yb	0.0230	0.5200	0.1100	0.0670
Ni	14.000	3.0000	4.0000	0.0400
Cr	2.1000	8.4000	10.000	0.0400

Table 4.5

Mineral-melt partition coefficients used in crystal fractionation modelling. Partition coefficients were taken from compilation (Jenner, pers. comm.).

4.7 SUMMARY

The noritic ring complex in the northern Vestfold Hills was intruded into upper crustal levels (≤ 3.5 kbar) at *ca.* 2350 Ma. Three distinct intrusive units occur: (1) *Homogeneous Norite*, (2) *Mottled Norite* and (3) *Rubbly Norite*. The *Rubbly Norite* is the final emplacement phase. Contemporaneous with the emplacement of the *Homogeneous* and *Mottled Norite* are fine grained dykes. These link several discrete norite bodies which comprise the ring complex. Petrographic evidence indicates a cumulative origin for at least the *Rubbly Norite* which contains up to 70 vol% orthopyroxene phenocrysts. Beside the accumulation of orthopyroxene, cognate enstatite nodules and sulphides are concentrated within the *Rubbly Norite*. Compositional variations in major and trace elements are consistent with differentiation controlled largely by orthopyroxene fractionation/accumulation and with an accumulation of orthopyroxene as well as Ni-Cu and Fe-sulphides for the *Rubbly Norite*.

It is suggested that *Rubbly* and *Mottled Norite* have been originated from the *Homogeneous Norite*, by the accumulation of up to 40% orthopyroxene, whereas the fine grained dykes evolved from the *Homogeneous Norite* by the fractionation of *ca.* 20% orthopyroxene.

TABLE 4.6

SELECTED ORTHOPYROXENE MICROPROBE ANALYSES

Sample No.	70667					70793				70661		
Pos. of Anal.	core	core	rim-plag	rim-opx	rim-cpx	rim	rim	rim		core	rim-cpx	rim-cpx
Rock Type	H-Norite					H-Norite - Layer				M-Norite		
SiO ₂	56.10	55.54	52.98	54.41	52.61	51.49	50.65	50.32		56.27	54.85	51.99
TiO ₂	0.00	0.00	0.19	0.00	0.27	0.39	0.26	0.30		0.00	0.00	0.42
Al ₂ O ₃	0.97	0.86	1.18	1.23	0.88	1.21	1.00	0.94		0.87	0.80	1.34
Cr ₂ O ₃	0.58	0.48	0.22	0.34	0.22	0.19	0.15	0.04		0.48	0.30	0.00
FeO	10.50	12.80	20.08	16.23	20.52	25.98	30.75	29.05		10.38	15.11	23.66
NiO	0.00	0.00	0.00	0.00	0.50	0.037	0.000	0.040		0.00	0.00	0.00
MnO	0.00	0.00	0.45	0.00	0.52	0.40	0.67	0.62		0.00	0.00	0.45
MgO	30.77	29.26	23.25	26.75	22.30	19.08	16.28	16.39		30.91	27.60	20.39
CaO	1.08	1.06	1.63	1.03	2.18	1.34	0.82	1.39		1.09	1.34	1.75
Total	100.00	100.00	99.98	99.99	100.00	100.14	100.58	99.11		100.00	100.00	100.00
Cations (6 ox)												
Si	1.975	1.976	1.958	1.967	1.963	1.956	1.956	1.965		1.980	1.973	1.956
Ti	0.000	0.000	0.005	0.000	0.008	0.011	0.008	0.009		0.000	0.000	0.012
Al	0.040	0.036	0.052	0.053	0.039	0.054	0.046	0.044		0.036	0.034	0.060
Cr	0.016	0.014	0.006	0.010	0.006	0.006	0.005	0.001		0.013	0.009	0.000
Fe ²⁺	0.309	0.381	0.604	0.486	0.627	0.819	0.972	0.941		0.305	0.442	0.740
Fe ³⁺	0.000	0.000	0.016	0.004	0.013	0.006	0.022	0.007		0.000	0.012	0.004
Mn	0.000	0.000	0.014	0.000	0.016	0.013	0.022	0.021		0.000	0.000	0.014
Mg	1.614	1.551	1.280	1.441	1.240	1.080	0.937	0.954		1.620	1.479	1.143
Ca	0.041	0.040	0.065	0.040	0.087	0.055	0.034	0.058		0.041	0.052	0.071
Sum	3.996	3.999	4.000	4.000	4.000	4.000	4.000	4.000		3.996	4.000	4.000
Mg#	83.9	80.3	67.9	74.8	66.4	56.9	49.1	50.3		84.1	77.0	60.7
Endmembers												
enstatite	82.2	78.6	65.1	73.1	63.0	55.1	47.7	48.6		82.4	74.5	58.4
ferrosilite	15.7	19.3	31.6	24.9	32.5	42.1	50.6	48.4		15.5	22.9	38.0
wollastonite	2.1	2.0	3.3	2.0	4.4	2.8	1.7	3.0		2.1	2.6	3.6

SELECTED ORTHOPYROXENE MICROPROBE ANALYSES

Sample No.	70653				71952			70709				
Pos. of Anal.	rim	rim	core	rim	core	core	core	core	rim	rim	rim	core
Rock Type	R-Norite				R-Norite	enstatite	nodule	Fine grained dyke				
SiO ₂	53.91	52.36	56.10	53.57	57.45	56.81	55.46	55.26	52.11	52.15	52.10	
TiO ₂	0.00	0.42	0.00	0.00	0.00	0.06	0.04	0.00	0.00	0.19	0.00	
Al ₂ O ₃	1.24	1.14	1.07	1.43	0.68	1.18	1.92	0.84	2.19	1.86	0.97	
Cr ₂ O ₃	0.38	0.00	0.57	0.43	0.19	0.59	0.73	0.46	0.44	0.44	0.58	
FeO	17.24	22.54	11.01	18.51	8.25	6.99	6.45	14.11	20.51	22.06	25.00	
NiO	0.00	0.00	0.00	0.00	0.00	0.06	0.17	0.00	0.00	0.00	0.00	
MnO	0.00	0.34	0.00	0.00	0.00	0.09	0.11	0.00	0.29	0.34	0.31	
MgO	25.82	21.31	30.07	24.55	33.05	33.91	33.66	28.25	22.48	21.35	19.94	
CaO	1.41	1.89	1.18	1.51	0.37	0.39	0.75	1.08	1.98	1.60	1.11	
Total	100.00	100.00	100.00	100.00	99.99	100.07	99.29	100.00	100.00	99.99	100.01	
Cations (6 ox)												
Si	1.959	1.959	1.979	1.961	1.994	1.966	1.933	1.978	1.929	1.948	1.970	
Ti	0.000	0.012	0.000	0.000	0.000	0.002	0.001	0.000	0.000	0.005	0.000	
Al	0.053	0.050	0.045	0.062	0.029	0.048	0.079	0.036	0.096	0.082	0.043	
Cr	0.011	0.000	0.016	0.012	0.005	0.016	0.020	0.013	0.013	0.013	0.017	
Fe ²⁺	0.506	0.696	0.325	0.563	0.239	0.202	0.155	0.422	0.601	0.689	0.790	
Fe ³⁺	0.018	0.009	0.000	0.004	0.000	0.000	0.033	0.000	0.033	0.000	0.000	
Mn	0.000	0.011	0.000	0.000	0.000	0.003	0.003	0.000	0.009	0.011	0.010	
Mg	1.398	1.188	1.581	1.339	1.709	1.749	1.748	1.507	1.240	1.188	1.124	
Ca	0.055	0.076	0.045	0.059	0.014	0.014	0.028	0.041	0.079	0.064	0.045	
Sum	4.000	4.000	3.990	4.000	3.990	4.000	4.000	3.997	4.000	4.000	4.000	
Mg#	73.4	63.0	83.0	70.4	87.7	89.6	91.9	78.1	67.3	63.3	58.7	
Endmembers												
enstatite	70.7	60.3	81.1	68.2	87.1	89.0	89.0	76.5	63.5	61.2	57.4	
ferrosilite	26.5	35.8	16.7	28.8	12.2	10.3	9.6	21.4	32.5	35.5	40.4	
wollastonite	2.8	3.8	2.3	3.0	0.7	0.7	1.4	2.1	4.0	3.3	2.3	

Selected mineral analyses from various norite types. Mg# (silicates) = 100 Mg/(Mg + Fe total). Mg# (spinel) = 100 Mg/(Mg + Fe²⁺), Cr# = 100 Cr/(Cr + Al), Fe determination as FeO: Fe³⁺ and Fe₂O₃ calculated from stoichiometry.

SELECTED CLINOPYROXENE MICROPROBE ANALYSES

Sample No.	70667					70793				70661	
Pos. of Anal.	core	rim-ox	rim-ox	rim-plag	rim-ox	rim-ox	rim-ox	rim-ox		core	rim-ox
Rock Type	H-Norite					H-Norite	- Layer			M-Norite	
SiO2	52.44	52.53	54.01	52.33	52.87	53.34	51.00	50.34		52.55	51.68
TiO2	0.30	0.00	0.00	0.37	0.29	0.18	0.45	0.52		0.29	0.75
Al2O3	2.34	1.89	0.80	1.90	1.98	0.97	2.05	1.38		2.70	2.16
Cr2O3	0.45	0.36	0.00	0.20	0.37	0.06	0.27	0.08		0.55	0.38
FeO	9.14	12.79	6.89	13.15	10.70	8.42	10.63	21.78		9.46	12.08
NiO	0.00	0.00	0.00	0.00	0.00	0.11	0.12	0.00		0.00	0.00
MnO	0.00	0.00	0.00	0.00	0.00	0.15	0.21	0.31		0.00	0.00
MgO	16.77	16.93	15.59	16.07	16.76	15.40	13.03	15.35		17.27	15.85
CaO	18.57	15.51	22.71	15.98	17.03	22.04	21.40	9.33		17.18	17.10
Na2O	0.00	0.00	0.00	0.00	0.00	0.22	0.32	0.13		0.00	0.00
Total	100.01	100.01	100.00	100.00	100.00	100.89	99.48	99.23		100.00	100.00
Cations (6 ox)											
Si	1.936	1.953	1.991	1.952	1.956	1.963	1.928	1.940		1.934	1.928
Ti	0.008	0.000	0.000	0.010	0.008	0.005	0.013	0.015		0.008	0.021
Al	0.102	0.083	0.035	0.084	0.086	0.042	0.092	0.063		0.117	0.095
Cr	0.013	0.011	0.000	0.006	0.011	0.002	0.008	0.002		0.016	0.011
Fe2+	0.282	0.397	0.212	0.410	0.331	0.224	0.293	0.668		0.291	0.377
Fe3+	0.000	0.000	0.000	0.000	0.000	0.035	0.043	0.034		0.000	0.000
Mg	0.922	0.938	0.856	0.893	0.923	0.844	0.734	0.882		0.947	0.881
Ca	0.734	0.618	0.897	0.638	0.675	0.869	0.867	0.385		0.677	0.684
Na	0.000	0.000	0.000	0.000	0.000	0.015	0.024	0.010		0.000	0.000
Sum	3.998	4.000	3.992	3.993	3.990	4.000	4.000	4.000		3.991	3.997
Mg#	76.6	70.2	80.1	68.5	73.6	76.5	68.6	55.7		76.5	70.0
Endmembers											
Mg2Si2O6	46.1	46.9	42.8	44.7	46.2	42.2	36.7	44.1		47.4	44.1
Fe2Si2O6	14.1	19.9	10.6	20.5	16.5	11.2	14.6	33.4		14.6	18.8
Ca2Si2O6	33.9	28.5	44.4	30.0	31.9	41.9	40.3	17.1		31.0	31.6
CaAl2SiO6	3.4	3.6	0.9	2.2	1.9	0.5	1.9	0.3		3.4	1.8
CaFeAlSiO6	0.0	0.0	0.0	0.0	0.0	2.2	2.8	2.6		0.0	0.0
CaCrAlSiO6	1.3	1.1	0.0	0.6	1.1	0.0	0.0	0.0		1.6	1.1
CaTiAl2O6	0.8	0.0	0.0	1.0	0.8	0.5	1.3	1.5		0.8	2.1

SELECTED CLINOPYROXENE MICROPROBE ANALYSES

Sample No.	70661		70653				70623				
Pos. of Anal.	rim-ox	rim-plag	core	rim-ox	rim-ox	rim	exolution	rim-ox	rim-ox	exol-ox	
Rock Type	M-Norite		R-Norite				Fine grained dyke				
SiO2	52.88	51.50	52.52	52.89	52.05	51.85	51.57	51.99	52.67	51.93	
TiO2	0.28	0.72	0.00	0.35	0.35	0.22	0.44	0.31	0.20	0.00	
Al2O3	1.98	2.37	2.81	2.06	2.15	0.97	2.18	2.77	2.40	0.83	
Cr2O3	0.37	0.22	0.75	0.40	0.43	0.00	0.23	0.39	0.44	0.00	
FeO	10.70	13.13	7.93	10.27	11.02	19.73	14.37	13.69	12.84	23.05	
NiO	0.00	0.00	0.00	0.00	0.00	0.00	0.00	0.00	0.00	0.00	
MnO	0.00	0.00	0.00	0.00	0.00	0.25	0.00	0.00	0.22	0.35	
MgO	16.76	14.06	16.61	17.83	16.44	18.35	14.25	16.53	19.44	15.70	
CaO	17.03	17.62	19.38	16.19	17.56	8.64	16.97	14.31	11.78	8.14	
Na2O	0.00	0.38	0.00	0.00	0.00	0.00	0.00	0.00	0.00	0.00	
Total	100.00	100.00	100.00	99.99	100.00	100.01	100.01	99.99	99.99	100.00	
Cations (6 ox)											
Si	1.955	1.933	1.933	1.948	1.933	1.952	1.942	1.935	1.942	1.988	
Ti	0.008	0.020	0.000	0.010	0.010	0.006	0.012	0.009	0.006	0.000	
Al	0.086	0.105	0.122	0.090	0.094	0.043	0.097	0.122	0.105	0.038	
Cr	0.011	0.007	0.022	0.012	0.013	0.000	0.007	0.011	0.013	0.000	
Fe2+	0.331	0.403	0.244	0.316	0.334	0.580	0.452	0.426	0.396	0.738	
Fe3+	0.000	0.009	0.000	0.000	0.008	0.041	0.000	0.000	0.000	0.000	
Mg	0.923	0.786	0.911	0.978	0.910	1.029	0.799	0.917	1.068	0.896	
Ca	0.675	0.709	0.764	0.639	0.699	0.348	0.684	0.571	0.465	0.334	
Na	0.000	0.028	0.000	0.000	0.000	0.000	0.00	0.00	0.00	0.00	
Sum	3.989	4.000	3.995	3.992	4.000	4.000	3.994	3.99	3.994	3.993	
Mg#	73.6	65.6	78.9	75.6	72.7	62.4	63.9	68.3	73.0	54.8	
Endmembers											
Mg2Si2O6	46.2	39.3	45.5	48.9	45.5	51.5	40.0	45.8	53.4	44.8	
Fe2Si2O6	16.5	20.2	12.2	15.8	16.7	29.0	22.6	21.3	19.8	36.9	
Ca2Si2O6	31.9	33.1	34.8	29.8	32.1	15.3	31.9	25.7	20.6	16.1	
CaAl2SiO6	1.9	2.6	4.6	2.1	2.7	0.5	2.7	3.6	3.4	1.2	
CaFeAlSiO6	0.0	0.0	0.0	0.0	0.8	4.1	0.0	0.0	0.0	0.0	
CaCrAlSiO6	1.1	0.0	2.2	1.2	1.3	0.0	0.7	1.1	1.3	0.0	
CaTiAl2O6	0.8	2.0	0.0	1.0	1.0	0.6	1.2	0.9	0.6	0.0	

SELECTED OLIVINE MICROPROBE ANALYSES

Sample No.	71952								
Pos of Anal.	core	core	rim	core	core	rim	core	core	rim
Rock Type	R-Norite enstatite nodule								
SiO ₂	40.86	39.91	39.98	39.72	40.11	40.59	39.70	40.20	39.74
Cr ₂ O ₃	0.00	0.00	0.03	0.00	0.04	0.00	0.00	0.01	0.02
FeO	9.70	13.27	13.99	15.27	12.41	13.00	15.30	13.38	13.38
NiO	0.38	0.44	0.45	0.40	0.58	0.52	0.40	0.50	0.58
MnO	0.16	0.21	0.00	0.08	0.06	0.09	0.70	0.14	0.09
MgO	49.21	45.35	44.62	44.53	46.78	46.44	44.44	46.68	45.82
Total	100.31	99.18	99.06	100.00	99.98	100.63	100.00	100.91	99.63
Cations (4 ox)									
Si	0.999	1.004	1.009	0.999	0.997	1.003	0.999	0.994	0.996
Cr	0.000	0.000	0.000	0.000	0.000	0.000	0.000	0.000	0.000
Fe	0.198	0.279	0.295	0.321	0.258	0.269	0.320	0.277	0.280
Ni	0.009	0.010	0.011	0.009	0.013	0.012	0.009	0.012	0.014
Mn	0.003	0.004	0.000	0.002	0.001	0.002	0.002	0.003	0.002
Mg	1.792	1.699	1.677	1.669	1.733	1.711	1.670	1.720	1.711
Sum	3.001	2.996	2.991	3.001	3.003	2.997	3.001	3.006	3.004
Mg#	90.0	85.9	85.0	83.9	87.0	86.4	84.0	86.1	85.9

SELECTED SPINEL MICROPROBE ANALYSES

Sample No.	71952								
Pos. of Anal.	core	core	rim	core	rim	rim	core	core	rim
Rock Type	R-Norite enstatite nodule								
SiO ₂	0.00	0.07	0.01	0.05	0.07	0.09	0.06	0.32	0.02
TiO ₂	0.17	0.04	0.01	0.29	0.32	0.23	0.05	0.02	0.07
Al ₂ O ₃	36.86	37.18	36.15	13.38	13.54	14.88	41.81	32.17	24.37
Cr ₂ O ₃	26.80	27.55	26.74	48.26	48.43	48.06	21.85	31.32	40.33
Fe ₂ O ₃	2.58	2.21	8.53	4.70	5.10	3.34	1.69	1.57	1.69
FeO	16.13	16.37	10.56	20.53	21.01	20.17	14.85	17.39	19.44
MnO	0.00	0.24	0.12	0.18	0.18	0.25	0.10	0.16	0.16
NiO	0.32	0.29	0.31	0.18	0.08	0.16	0.25	0.15	0.18
MgO	13.32	13.17	17.43	7.86	7.89	8.18	14.33	11.54	9.76
Total	96.18	97.12	99.87	95.44	96.62	95.37	94.99	94.64	96.02
Cations									
Ti	0.004	0.001	0.000	0.007	0.008	0.006	0.001	0.000	0.002
Al	1.301	1.303	1.215	0.546	0.546	0.602	1.453	1.188	0.928
Cr	0.633	0.646	0.602	1.317	1.307	1.300	0.508	0.774	1.028
Fe ₃₊	0.058	0.049	0.183	0.122	0.131	0.086	0.037	0.037	0.041
Fe ₂₊	0.403	0.406	0.251	0.593	0.600	0.577	0.365	0.455	0.524
Mn	0.000	0.006	0.003	0.005	0.005	0.007	0.002	0.004	0.004
Ni	0.008	0.007	0.007	0.005	0.002	0.004	0.006	0.004	0.005
Mg	0.593	0.582	0.739	0.404	0.401	0.417	0.628	0.538	0.469
Sum	3.000	3.000	3.000	3.000	3.000	3.000	3.000	3.000	3.000
Mg #	59.5	58.9	74.6	40.6	40.1	42.0	63.2	54.2	47.2
Chrome #	32.7	33.1	33.1	70.7	70.5	68.4	25.9	39.4	52.5
Ferric #	12.6	10.8	42.1	17.1	17.9	13.0	9.3	7.5	7.2

SELECTED PLAGIOCLASE MICROPROBE ANALYSES

Sample No.	70667					70793					
Pos. of Anal.	core	core	rim-myrm	rim-myrm		rim	rim	rim	rim-cpx	rim	rim-qtz
Rock Type	H-Norite					H-Norite - Layer					
SiO ₂	48.76	49.82	52.97	53.13		47.68	49.01	50.18	53.71	57.02	59.71
Al ₂ O ₃	32.93	32.11	29.91	29.71		32.82	32.07	31.54	29.35	27.40	25.60
FeO	0.00	0.83	0.40	0.27		1.58	0.99	0.47	0.24	0.00	0.00
CaO	15.81	13.96	12.22	12.22		15.88	15.14	14.47	11.81	9.13	6.93
Na ₂ O	2.50	3.13	4.35	4.67		2.04	2.67	3.22	4.73	6.30	7.51
K ₂ O	0.00	0.14	0.15	0.00		0.00	0.12	0.12	0.16	0.15	0.25
Total	100.00	99.99	100.00	100.00		100.00	100.00	100.00	100.00	100.00	100.00
Cations											
Si	2.226	2.282	2.403	2.408		2.211	2.257	2.294	2.431	2.554	2.659
Al	1.776	1.738	1.603	1.591		1.798	1.745	1.704	1.569	1.450	1.347
Ca	0.773	0.685	0.594	0.593		0.789	0.747	0.709	0.573	0.438	0.331
Na	0.221	0.278	0.383	0.410		0.183	0.238	0.285	0.415	0.547	0.648
K	0.000	0.008	0.009	0.000		0.000	0.007	0.007	0.009	0.009	0.014
Sum	4.997	4.992	4.991	5.002		4.982	4.994	5.000	4.997	4.998	4.999
Endmembers											
An	77.8	70.5	60.3	59.1		81.1	75.3	70.8	57.4	44.1	33.3
Ab	22.2	28.6	38.8	40.9		18.9	24.0	28.5	41.6	55.1	65.3
Or	0.0	0.8	0.9	0.0		0.0	0.7	0.7	0.9	0.9	1.4

SELECTED PLAGIOCLASE MICROPROBE ANALYSES

Sample No.	70653			70707			71952			70623		
Pos. of Anal.	core	rim		core	rim-nod.		rim-ol			core	rim	rim
Rock Type	R-Norite			R-Norite	enstatite nodule					Feeder Dyke		
SiO ₂	52.39	53.12		49.89	54.73		48.03			52.80	54.48	54.90
Al ₂ O ₃	30.60	30.08		31.86	28.97		33.16			30.24	29.13	28.41
FeO	0.00	0.22		0.00	0.00		0.25			0.00	0.00	0.74
CaO	13.32	12.39		0.35	0.00		17.26			0.00	0.00	0.00
Na ₂ O	3.69	4.06		14.88	10.99		1.95			12.84	11.43	10.76
K ₂ O	0.00	0.13		3.01	5.17		0.03			4.12	4.96	5.18
Total	100.00	100.00		99.99	99.99		100.76			100.00	100.00	99.99
Cations												
Si	2.370	2.403		2.279	2.464		2.193			2.384	2.450	2.480
Al	1.636	1.608		1.720	1.541		1.789			1.617	1.552	1.522
Ca	0.645	0.600		0.728	0.530		0.844			0.622	0.552	0.523
Na	0.324	0.356		0.267	0.451		0.172			0.361	0.434	0.455
K	0.000	0.008		0.000	0.008		0.002			0.006	0.008	0.012
Sum	4.974	4.975		4.994	4.995		5.000			4.991	4.995	4.993
Endmembers												
An	66.6	62.3		73.2	53.6		82.9			62.9	55.6	52.8
Ab	33.4	36.9		26.8	45.6		16.9			36.5	43.6	46.0
Or	0.0	0.8		0.0	0.8		0.2			0.6	0.8	1.2

CHAPTER 5

BASE METAL SULPHIDES AND PLATINUM GROUP MINERAL OCCURRENCES IN THE RUBBLY NORITE

5.1. INTRODUCTION

In the previous chapter the noritic ring complex, of the northern Vestfold Hills, was discussed in detail. Three major rock units were distinguished: i.e. homogeneous, mottled and rubbly units, the latter of which is characterized by cognate pyroxenite nodules and mineralization of base-metal sulphide (BMS). Finely dispersed sulphides and oxides, are present in all norite units but are more abundant in the *Rubbly Norite*. Sulphide mineralization within the *Rubbly Norite* is not confined to a particular zone but is randomly distributed throughout this unit.

The aim of this chapter is to describe the sulphide mineralization and associated platinum group minerals (PGM). Data are compared with other high-Mg tholeiites from the Vestfold Hills and with PGE (platinum group elements) enriched mafic intrusives described in the literature.

Sulphur and PGE data obtained from selected samples are presented and discussed in section 5.3.

5.2 PETROGRAPHY AND MINERAL CHEMISTRY

Modal abundances of ore minerals increase from 2 vol% in the *Homogeneous Norite* and *Mottled Norite* to approximately 8 vol% in the *Rubbly Norite* (Table 5.1). While oxide minerals, ilmenite and magnetite, are the dominant opaque phases in the homogeneous and mottled variety, sulphides are prominent in the *Rubbly Norite*. Base-metal sulphides (BMS) occur as disseminated accessory blebs (*ca.* 0.1 - 0.2 mm in size) throughout this rock unit, but globular patches also commonly occur, often associated with pyroxenite nodules. These globular patches are always irregularly shaped and can reach 2 - 3 cm in diameter. Sulphides occur as intercumulus assemblages, surrounded by cumulus orthopyroxene, but more commonly by plagioclase and late stage quartz - alkali feldspar granophyric intergrowths. Sulphides are observed to enclose magnetite and ilmenite (Figure 5.1). Textural relationships between sulphides, silicates and oxides clearly indicate late crystallization of the sulphides. Intercumulus sulphide globules are always composites of chalcopyrite, pentlandite, pyrrhotite and bravoite. Modal abundances of sulphides can vary between different samples. Averaged concentrations from seven samples reveal that pyrrhotite is the most abundant phase, followed by chalcopyrite and pentlandite, whereas bravoite is a minor non-ubiquitous phase. Where present, bravoite occurs as fine 10 to 20 μm wide borders between pyrrhotite and pentlandite. Opaque mineral assemblages and abundances are listed in Table 5.1.

Microprobe analyses of the major BMS (Table 5.2) reveal stoichiometry close to their ideal formulae (pyrrhotite is commonly non-stoichiometric at Fe_7S_8 to Fe_8S_9). Whereas pentlandite and pyrrhotite show no trace element enrichment, some chalcopyrites contain up to 0.15 wt% platinum.

Sulpharsenides and tellurides also have been found in the more sulphide-rich samples. Minute blebs, up to 20 μm in diameter, are present in the globular sulphides. They occur as inclusions in chalcopyrite and pyrrhotite, or between sulphide grain boundaries. Sulpharsenides are solid solutions (ss) between arsenopyrite (FeAsS), gersdorffite (NiAsS) and cobaltite (CoAsS). Microprobe analyses reveal Co-rich

		Ideal formula	Average abundance (vol%)*
Base Metal Sulphides			
Pyrrhotite	(po)	Fe_{1-x}S	3.3
Pentlandite	(pn)	$(\text{Fe},\text{Ni})_9\text{S}_8$	1.5
Chalcopyrite	(cc)	CuFeS_2	2.3
Bravoite		$(\text{Ni},\text{Fe},\text{Co})\text{S}_2$	< 0.1
Sulpharsenides			
Arsenopyrite		FeAsS	
Gersdorffite		NiAsS	< 0.1
Cobaltite		CoAsS	
Tellurides			
Michenerite		PdBiTe	< 0.1
Oxides			
Magnetite	(mt)	FeFe_2O_4	0.5
Ilmenite	(ilm)	FeTiO_3	1.1

Table 5.1.

Base metal sulphide (BMS), sulpharsenide, telluride and oxide mineral assemblages in *Rubbly Norite*. *Average volume percent (estimated) sulphide is given relative to the whole rock mineral abundances. Sulpharsenides always occur as solid solutions between the endmembers arsenopyrite, gersdorffite and cobaltite.

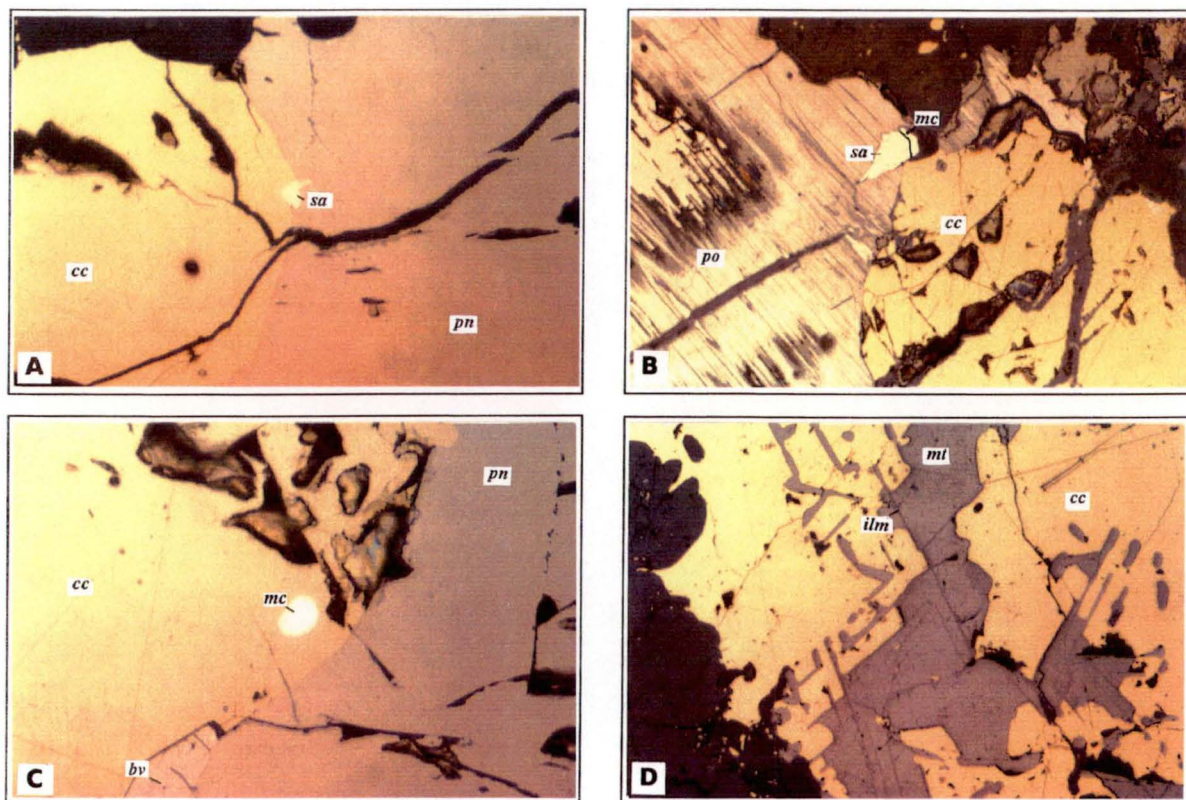


Figure 5.1

Photomicrographs of chalcopyrite (*cc*) and pentlandite (*pn*) with sulpharsenide (*sa*) (0.65 * 0.45 mm) (A), with chalcopyrite, pyrrhotite (*po*) and interstitial sulpharsenide partly mantled by michenerite (*mc*) (0.35 * 0.25 mm) (B). Michenerite inclusion in chalcopyrite - partial bravoite (*bv*) border between chalcopyrite and pentlandite (0.65 * 0.45 mm) (C) and ilmenite (*ilm*) exsolution lamellae parallel (111) in magnetite (*mt*) (1.3 * 0.95) (D).

character for the sulpharsenides (average $\text{Ni}_{0.25} \text{Co}_{0.60} \text{Fe}_{0.15}$) with one sulpharsenide being more Ni-rich ($\text{Ni}_{0.68} \text{Co}_{0.18} \text{Fe}_{0.16}$). While Fe content is virtually constant, variations in Co and Ni are more obvious. The system FeAsS - NiAsS - CoAsS has been studied in detail by Klemm (1965). He synthesized sulpharsenides and showed the effect of temperature on solid solutions in the system FeAsS - NiAsS - CoAsS. Sulpharsenides from this study are plotted in the ternary diagram FeAsS - NiAsS - CoAsS (Figure 5.2). With the exception of one example, all sulpharsenides plot in the high temperature range between 550° and 600° C, indicating no exsolution below this temperature.

Platinum group minerals (PGM) were found as discrete grains, up to 12 μm in diameter, commonly associated with sulpharsenides, but also as single inclusions in chalcopyrite. Michenerite, a palladium - bismuth - tellurium mineral, is the only observed PGM, and individual grains yield similar composition at $\text{Pd}_{0.34} \text{Bi}_{0.30} \text{Te}_{0.36}$. Microprobe analyses (Table 5.2) show that traces of platinum with up to 0.9 wt% seem to be real incorporations in Michenerite. In the sulpharsenides, traces of palladium and occasionally platinum occur, attaining 1.25 and 0.11 wt% respectively. The association with tellurides may indicate higher temperature solid solution between these tellurides and sulpharsenides, but the absence of tellurium and bismuth in the analyses of sulpharsenides, suggests that the traces of palladium and platinum are in solid solution in sulpharsenides rather than constituting an analytical relict due to very small telluride inclusions. Mineral parageneses are interpreted as a consequence of the separation of a complex Fe - Cu - Ni - As - S melt with dissolved PGE, followed by crystallization of sulphides, minor sulpharsenide and rare PGE-telluride minerals from the melt.

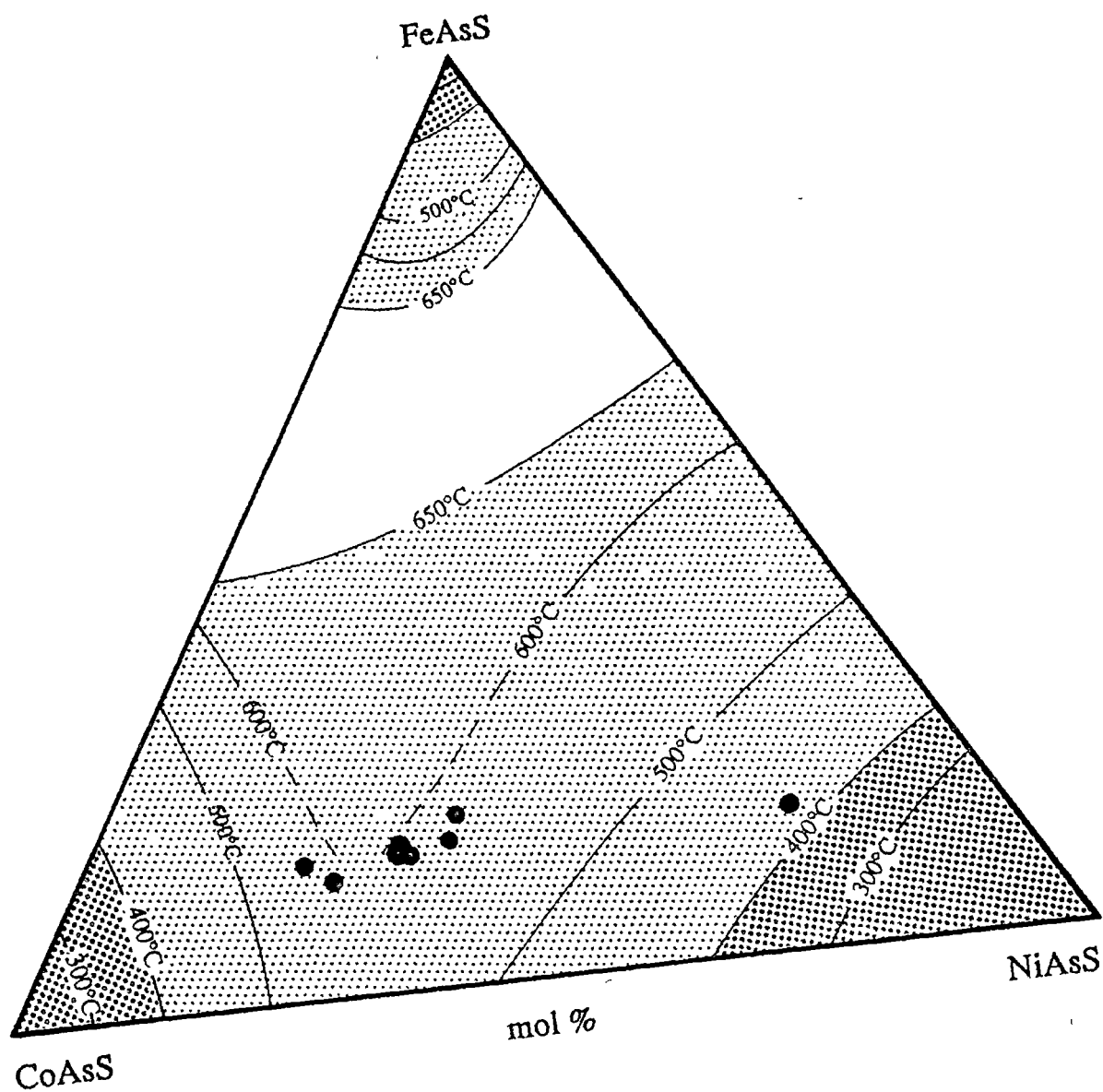


Figure 5.2
Sulpharsenide solid solutions (sample 70653) plotted in the system FeAsS - CoAsS - NiAsS after Klemm (1965).

5.3 PLATINUM GROUP ELEMENT ABUNDANCES IN ROCK UNITS

5.3.1 Introduction

Sixteen samples from the high-Mg tholeiitic suite have been analyzed for PGE, including two samples from the *Homogeneous Norite*, one from the *Mottled Norite* and eight from the *Rubbly Norite*, as well as two samples from related 'fine grained dykes' and three from high-Mg tholeiites which predate the norite. The elements sulphur, copper, nickel and zinc were also analyzed (data are listed in Table 5.3 and presented in Figures 5.8 to 5.9). In addition to measurement of PGE abundances the relative abundances amongst the PGE were compared to 'primitive' mantle PGE abundances i.e. a 'normalization' of PGE abundances.

Before normalization of PGE data, values were recalculated to 100% sulphides. Barnes et al. (1988) discussed the usage of 100% sulphide recalculated data and normalization to mantle or chondritic abundances. In this study values were normalized to chondrite C1 abundances as listed in Naldrett (1981) and Naldrett (1989) (also see Table 5.3). Mantle abundances of $0.00815 * C1$, as used by Barnes et al. (1988) and similar mantle values listed in Brüggmann et al. (1987) do not change the spidergram patterns when Ni is disregarded (multiplication of C1 with a constant factor). The metals are plotted in the order Os, Ir, Ru, Rh Pt, Pd, Au and Cu, according to their decreasing melting point (Naldrett et al., 1979; Naldrett, 1981). Samples from this study were analyzed for Os and Rh (data are listed in Table 5.3) but due to analytical uncertainties these elements have been omitted in the chondrite normalized plots.

In calculating element ratios e.g. Pd/Ir and Ni/Cu raw data rather than normalized figures were used.

5.3.2 Platinum Group Element Geochemistry

5.3.2.1 PGE Abundances in Basaltic Melts

High PGE contents are documented in some mantle - derived mafic to ultramafic magmas but others are low in PGE. For example mid ocean-ridge basalts (MORB) are strongly depleted in PGE but are inferred to be sulphur saturated (Keays, 1982; Hamlyn & Keays, 1986). To form a basaltic melt rich in PGE, it is argued that partial melting of the mantle must take place in the absence of a sulphide phase (Keays, 1981; Hamlyn & Keays, 1986). If a sulphide melt is present during partial melting and the degree of melting is not high enough to eliminate all sulphides, PGE will be retained in the mantle source due to their high partition coefficients for sulphides. Consequently the melt will be depleted in these elements (e.g. Hamlyn et al., 1985).

The geochemical affinities of noble metals determine their distribution in the earth's crust. In interpreting PGE data it is necessary to understand the behaviour of noble metals during partial melting and fractional crystallization, to evaluate geochemical problems such as mantle evolution and formation of magmatic sulphides. Noble metals can be grouped in various ways, according to their compatibility and their tendency to dissolve in or fractionate into a metallic (siderophile) or sulphidic phase (chalcophile). Barnes et al. (1985) discussed the origin of PGE fractionation and the distribution of noble metals, particularly in relation to Ni and Cu, during partial melting, crystal fractionation and alteration. Ni, and Cu to a lesser extent only, are strongly lithophile and, depending on the degree of partial melting, can become enriched or depleted relative to PGE abundances. Iridium, osmium, ruthenium and nickel behave as compatible elements, decreasing in concentration with olivine fractionation, whereas copper, gold and palladium are incompatible, increasing with fractionation. According to their compatibility, Barnes et al. (1985) divided PGE on the basis of fractionation into two groups: (1) The Iridium Group (IPGE), consisting of Ru, Os and Ir and (2) the Palladium Group (PPGE), consisting of Rh, Pt, Pd and Au. The compatible behaviour of Os, Ir and Ru, causing them to become depleted with

fractionation, is attributed to solid solution in chromite and olivine (Agiorgitis & Wolf, 1978; Naldrett & Barnes, 1986; Brüggmann, 1985; Brüggmann et al, 1987). On the other hand Keays & Campbell (1981), Keays (1982) and Barnes et al. (1985) suggested that IPGE's form primary magmatic alloys which fractionated early from mantle magmas. Estimates of distribution coefficients for PPGE between sulphide and silicate melts are greatly variable and not yet well established. Campbell et al. (1983) concluded that $D_{(Pd,Pt)}$ vary from 1,000 to more than 100,000 for various sulphides separating from mafic to ultramafic melts enriched in PPGE. It is apparent that knowledge of PGE element behaviour in silicate melts and their response to segregation of sulphide melt, remains a subject of debate with limited factual data.

5.3.2.2 PGE Abundances in the Vestfold Hills High-Mg Tholeiites

In addition to PGE concentrations in natural mafic rocks taken from the literature, abundances from the high-Mg tholeiite (SHMB: classification as siliceous high magnesian basalts; Glikson, 1983; Redman & Keays, 1985) from the Vestfold Hills are plotted in Figure 5.3. Concentrations represented here are from chilled margin samples which are considered to be liquid compositions. Average Pd values are *ca.* 15 ppb, which are slightly higher than Pd concentration in Archaean komatiites, and are overlapped by those grouped as Flood Basalts. Platinum abundances between 10 - 18 ppb are also similar to those from Stillwater chilled margin and Archaean komatiites. Iridium concentrations between 0.5 and 1 ppb overlap with OIB, Flood Basalt and with abundances in komatiites.

Variations of PGE concentrations within the high-Mg tholeiitic suite are shown in Figure 5.4. Pd and Pt concentrations in the *Rubbly Norite* are higher than those of to the *Homogeneous Norite*, *Mottled Norite* and 'fine grained dykes' (the dykes designated as 'fine grained dykes' (2 samples) are spatially and genetically linked to the norite intrusion and belong as the norite to the high-Mg tholeiite suite, see Chapter 4), but Ru, Rh, Ir, Os and Au are all similar. Sample 70653 has the highest PGE abundances of all *Rubbly Norite* samples, reaching ppm abundances for Pd. Palladium

PGE CONCENTRATIONS IN NATURAL SILICATE LIQUIDS

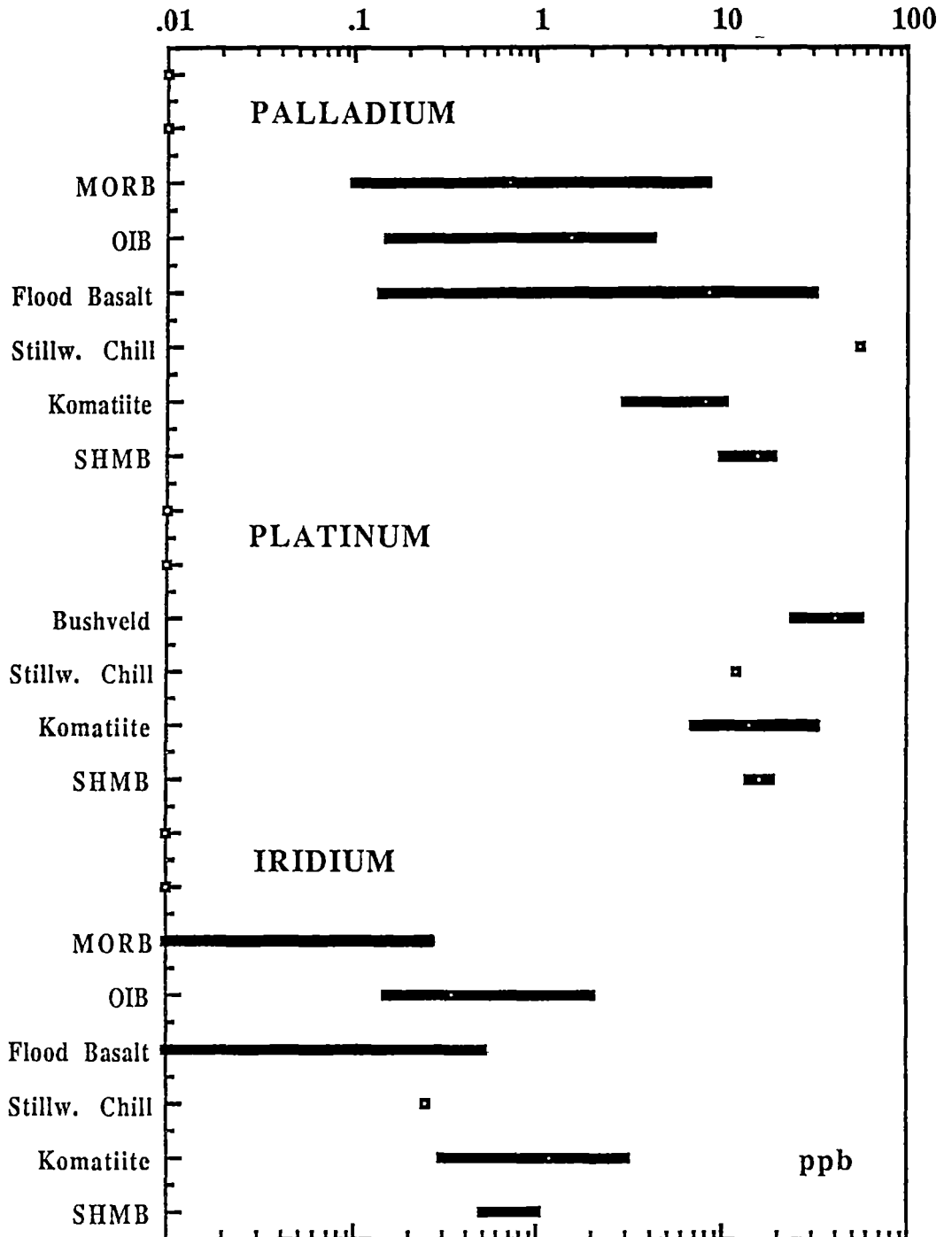


Figure 5.3

Pd, Pt and Ir in silicate magmas. Modified after Crocket (1981) and Campbell et al. (1983). Data on SHMB (siliceous high magnesian basalts) are from this study. Dots indicate averaged abundances

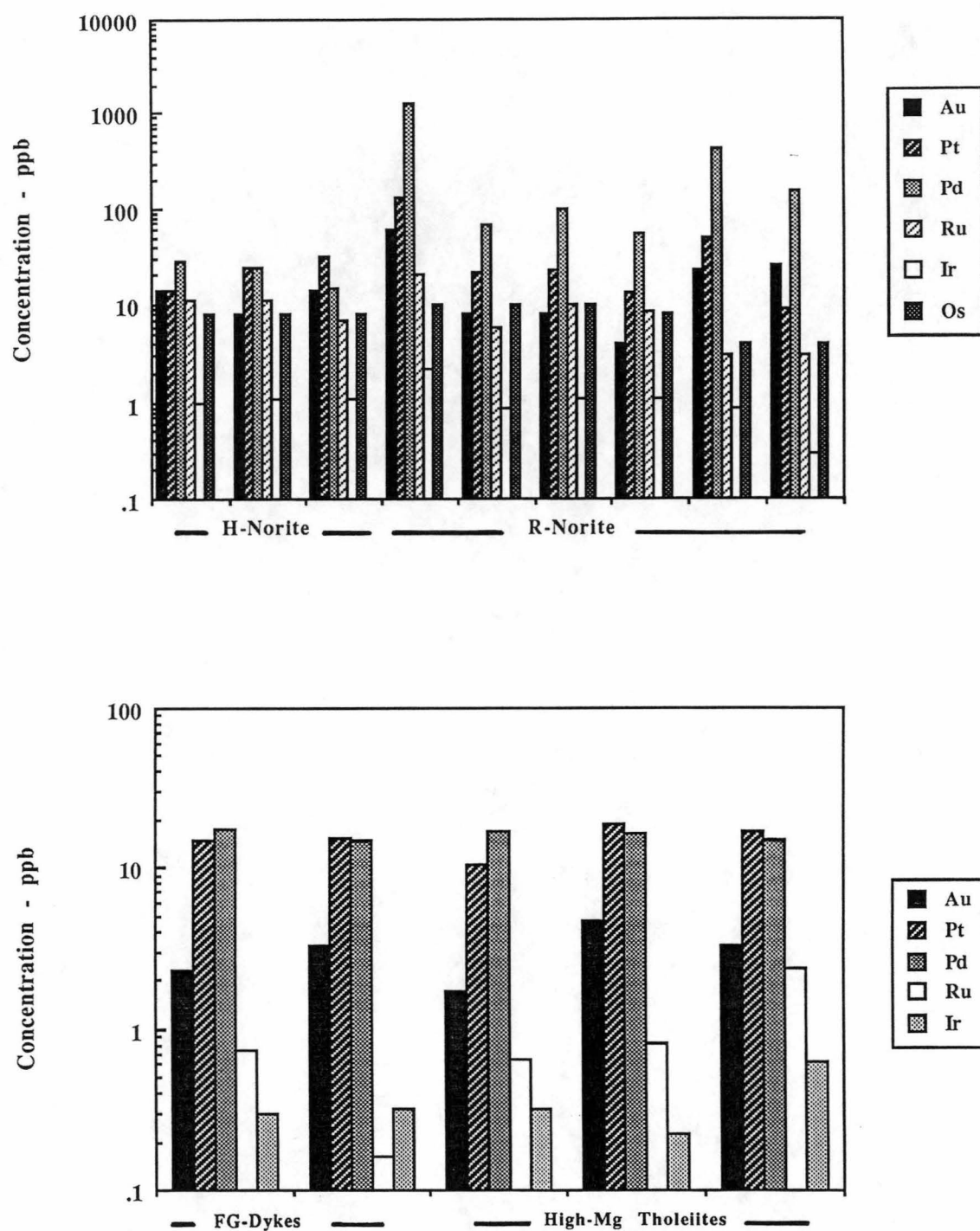


Figure 5.4

PGE abundances in high-Mg tholeiites, norites and associated 'fine grained dykes' from the Vestfold Hills.

is enriched in all *Rubbly Norite* samples, increasing from an averaged 22 ppb in the *Homogeneous Norite* and *Mottled Norite* to 60 - 1300 ppb in the *Rubbly Norite*. 'Fine grained dykes' and high-Mg tholeiites have Pd and Pt concentrations between 15 to 17 ppb and 10.5 to 18.5 ppb, respectively. These chilled margin samples represent liquid compositions from the three dyke generations in the high-Mg suite (compare whole rock data in Table 6.1 and Appendix). All five samples show very similar noble metal abundances. In comparison to these dykes, the *Homogeneous Norite* and *Mottled Norite* are slightly enriched in Pt and Pd ranging from 15 to 30 ppb.

In order to be able to recognize the controlling mechanisms of PGE variation within the various norite types and related high-Mg tholeiites, PGE abundances in whole rocks are plotted against S (Figure 5.5). Palladium shows a good positive correlation with sulphur (S). The *Homogeneous Norite* and *Mottled Norite* have S concentrations between 60 and 140 ppm corresponding to low Pd. Samples from the *Rubbly Norite* become enriched in Pd (60 - 130 ppb) with increasing S (250 - 4300 ppm). Two samples (71950 and 71986) which are low in S (79 - 164 ppm) exhibit significantly lower Pd abundances but still correlate positively with S. While samples from the norite show a positive correlation with sulphur, 'fine grained dykes' and high-Mg tholeiitic dykes have a constant, relatively low Pd content, showing no variation with increasing S (180 - 450 ppm).

In comparison to Pd, Pt is less well correlated with S. Samples with S content between 150 and 4300 ppm S appear to be positively correlated with Pt from 14 to 130 ppb. Three samples, including two from the *Rubbly Norite* (71950 and 71986), have low S content (62 - 164 ppm) but are enriched in Pt (24 - 31 ppb), relative to other low S-bearing samples. Platinum content in 'fine grained dykes' and related high-Mg tholeiitic dykes increase slightly with increasing S. However, no obvious correlation exists between Ir and S, or Ru and S. Related dykes contain lower Ir values than samples from the norite (Figure 5.5). In the norite, the positive correlation between Pd and S, and to a certain extent between Pt and S suggests concentration of these metals together with sulphides. The constant Pd and Pt abundances and lack of relationships

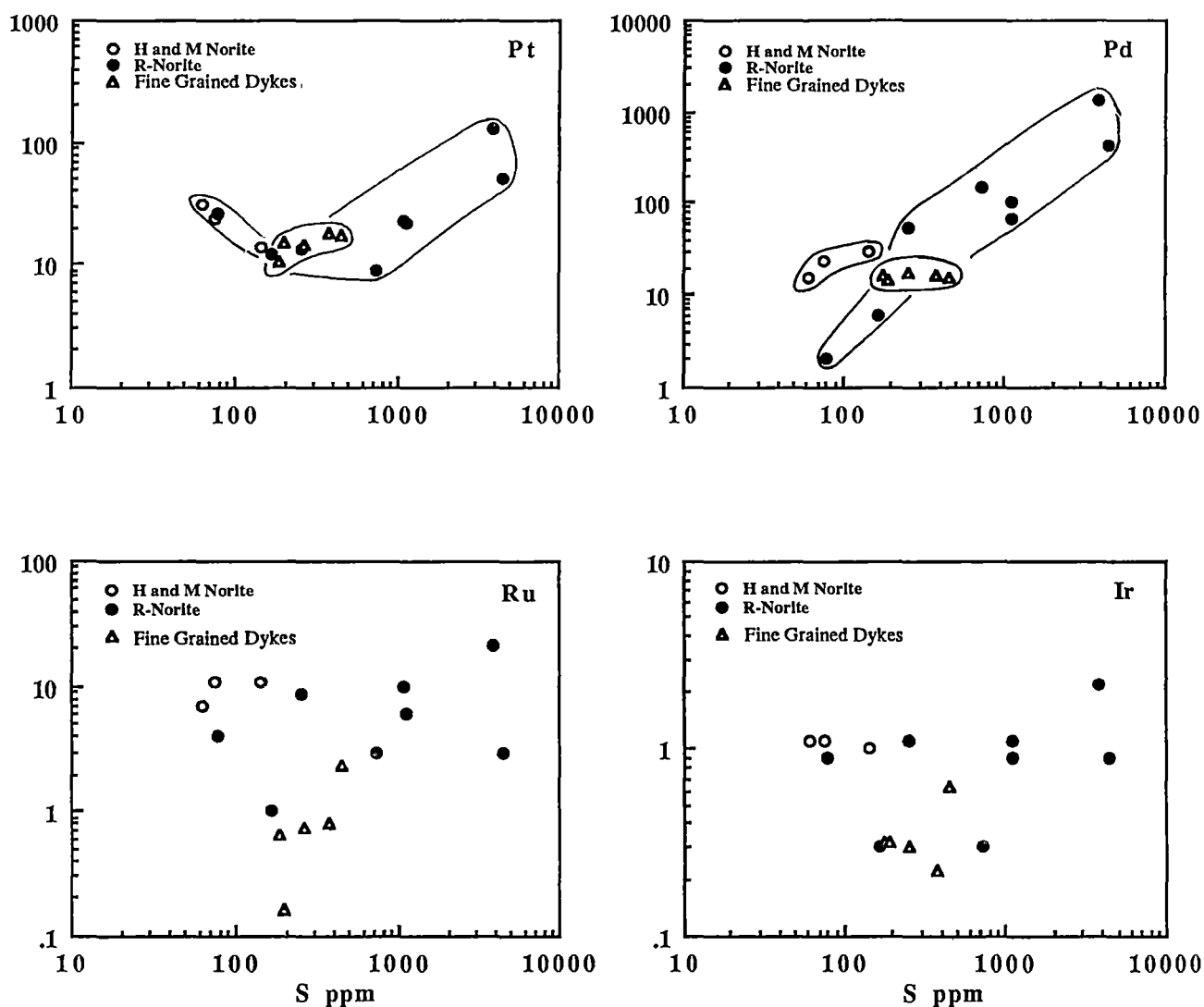


Figure 5.5

PGE's Pt, Pd, Ru and Ir (ppb) plotted versus S (ppm) from various norite types and associated fine grained dykes.

with S in the 'fine grained dykes' and high-Mg tholeiitic dykes imply segregation of magma with relatively low sulphur and constant Pt and Pd. Ruthenium and iridium are not correlated with S indicating that their concentrations are not controlled by sulphides.

Noting the ambivalence of the previous discussion it is nevertheless apparent that in the norite at least there is a correlation between S-content and Pd content. A common approach in considering PGE abundance data is to recalculate rock samples to a constant sulphur content (Naldrett et al., 1979). When PGE's are recalculated to 100% sulphide, assuming that they are collected by sulphide droplets, the effects caused by varying content of sulphides can be eliminated and it is possible to compare data from different deposits. The data are also conventionally compared, when recalculated to 100% sulphide, with chondritic abundance patterns.

The chondrite normalized patterns (Figure 5.6 A) all have steep positive trends, indicating strong fractionation of the noble metals, showing depletion of IPGE's relative to PPGE's. With the exception of one *Homogeneous Norite* and two *Rubbly Norite* samples, all samples have Pd > Pt in their PGE trends. Excluding samples from the *Homogeneous Norite* and *Mottled Norite*, Pd is enriched relative to Au. When normalized to 100% sulphide, it becomes apparent that the *Rubbly Norite* is not particularly enriched in PGE in comparison to 'fine grained dykes' and high-Mg tholeiites, whereas concentrations in *Homogeneous Norite* and *Mottled Norite* are one magnitude higher. IPGE's and Pt from the *Rubbly Norite* are depleted relative to abundances in associated 'fine grained dykes'. In most *Rubbly Norite* samples, Pd is strongly enriched relative to Pt but samples 71950 and 71986 show an inverse relationship with higher Pt and lower Pd concentrations (Figure 5.6 B). Chondrite normalized patterns show that PGE concentrations within the norite, 'fine grained dykes' and high-Mg tholeiites, are quite similar when recalculated to 100% sulphide. In Figure 5.7 chondrite normalized PGE patterns from the Vestfold Hills high-Mg tholeiites and norites (including the 'fine grained dykes') are compared to flood basalts, Merensky Reef, Stillwater, Sudbury and Proterozoic komatiites. Samples

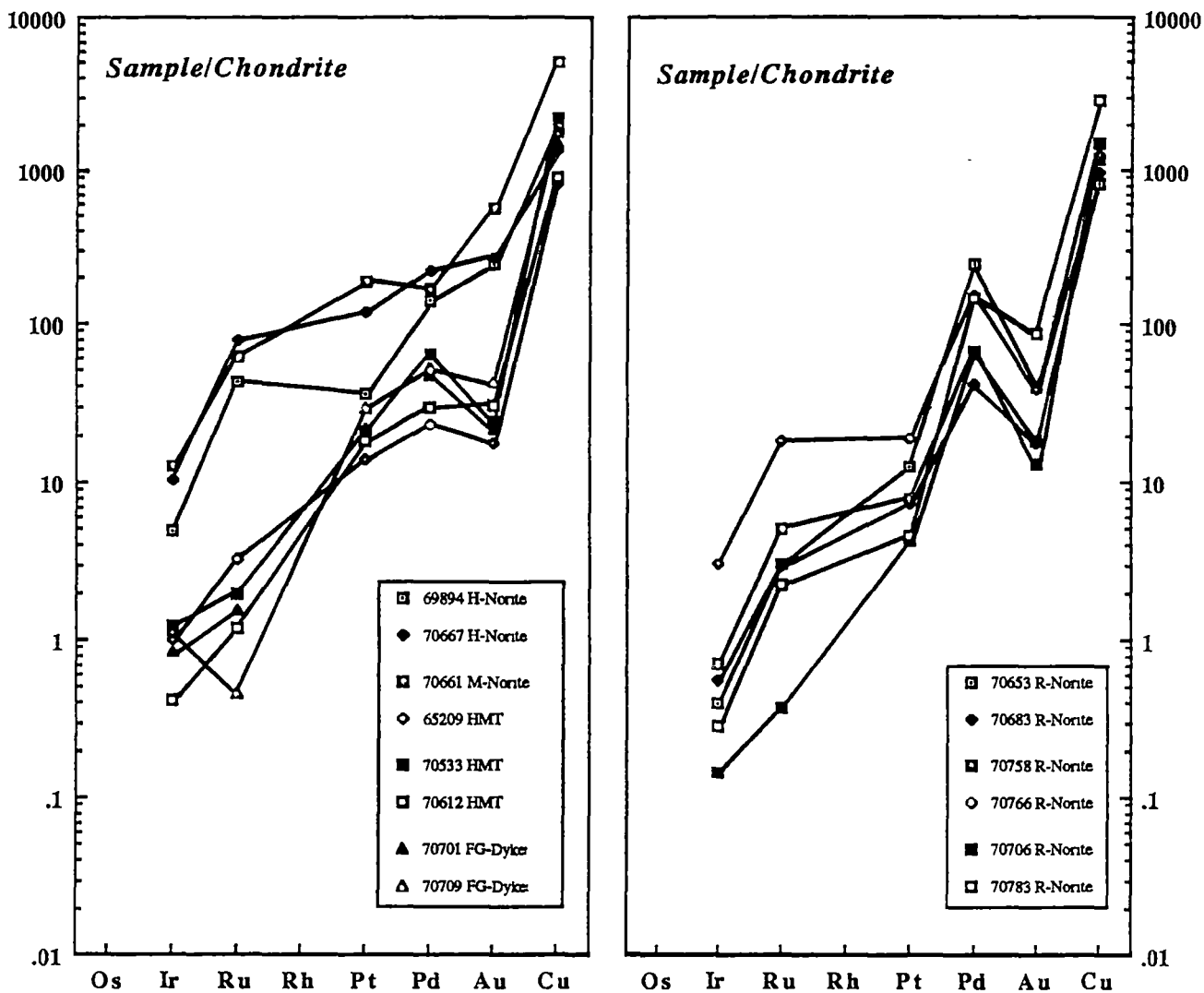


Figure 5.6 A

Chondrite normalized PGE patterns for high-Mg tholeiite, norite types and 'fine grained dykes' from the Vestfold Hills. Before plotting data were recalculated to 100% sulphide.

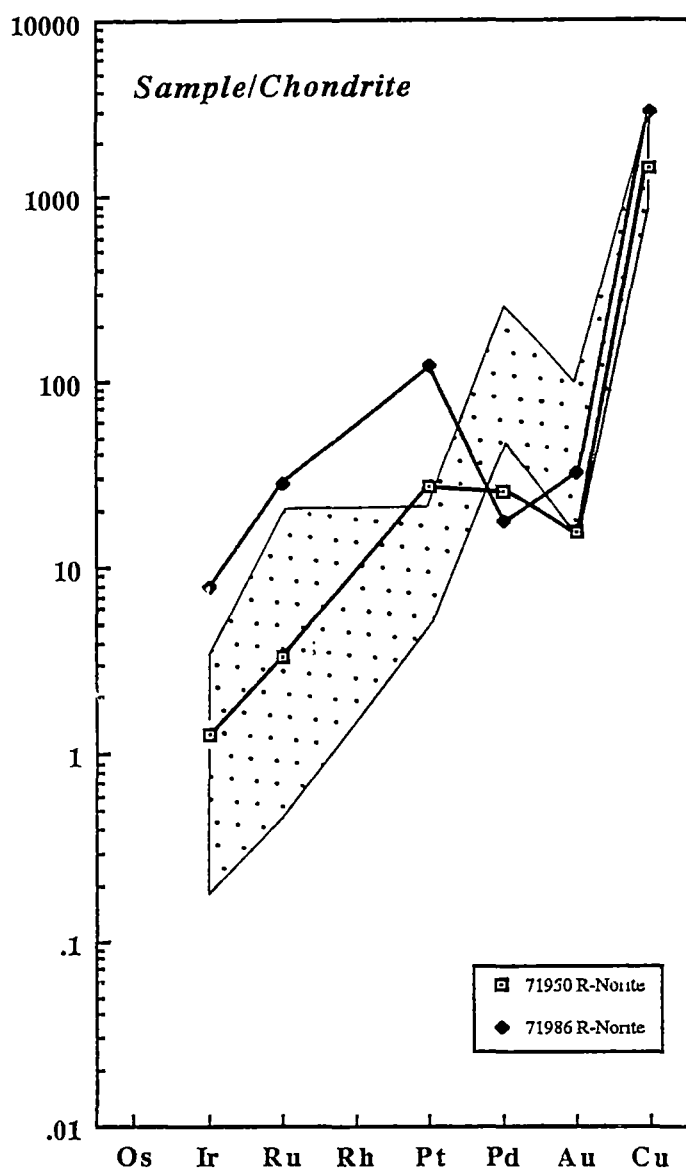


Figure 5.6 B

Chondrite normalized PGE patterns. Two Pt enriched samples from the *Rubbly Norite* (dotted area) are compared with patterns from the same norite unit from Figure 5.7 A. Before plotting data were recalculated to 100% sulphide.

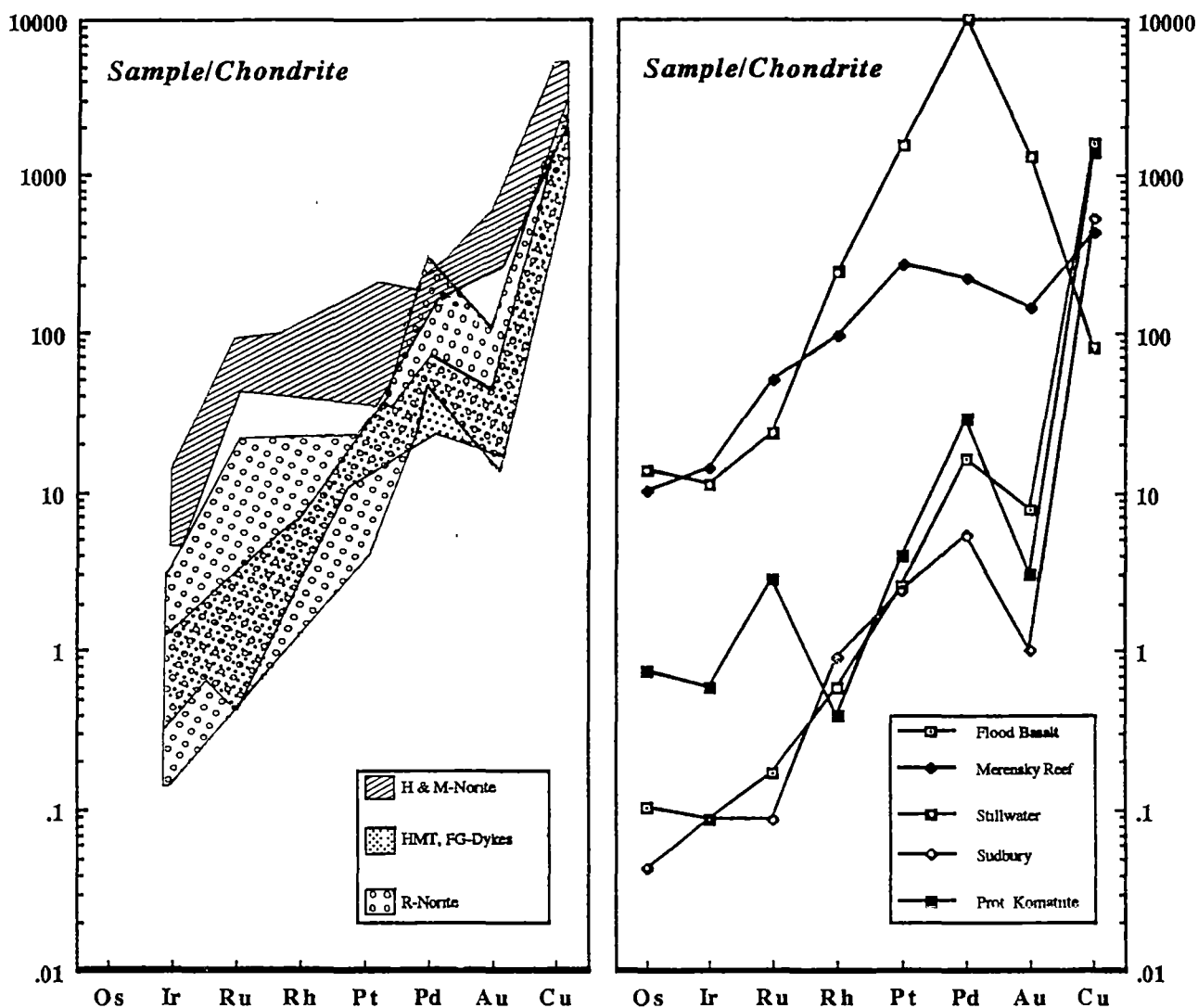


Figure 5.7

Chondrite normalized PGE patterns from the Vestfold Hills high-Mg tholeiite dykes and norites in comparison to Flood Basalt, Merensky Reef, Stillwater, Sudbury and Proterozoic komatiite. Data were taken from Naldrett (1981).

from the Vestfold Hills have similar patterns to flood basalt, Sudbury and Proterozoic komatiites, with characteristics such as $Pt < Pd$ and Au relatively depleted to Pd and Cu, but have higher PGE abundances. Patterns from the Merensky Reef and Stillwater are distinctly different to those from the Vestfold Hills, although sample 71950 (*Rubbly Norite*) has a similar pattern to Merensky Reef, exhibiting $Pt > Pd > Au$ (compare Figures 5.6 B and 5.7).

As pointed out previously, Os, Ir and Ru are compatible elements, decreasing in concentration with increasing olivine and chromite fractionation. Ratio diagrams were applied to show the degree of crystal fractionation or accumulation within high-Mg tholeiitic magma types and in relation to mantle source compositions. Ratios are listed in Table 5.3 and Pd/Ir is plotted against Ni/Cu in Figure 5.8. Moderately to slightly more fractionated patterns have Pd/Ir = 10 (peridotitic komatiite) and Pd/Ir = 20 - 30 (pyroxenitic komatiite), whilst continental tholeiites and ocean floor basalts have highly fractionated Pd/Ir = 100 - 200 (Barnes et al., 1985; Barnes et al., 1988). The ratios for high-Mg tholeiites of the Vestfold Hills, range between 23 to 74, whereas some samples from the *Rubbly Norite* have highly fractionated patterns (Pd/Ir up to 590). *Homogeneous* and *Mottled Norite* are moderately fractionated (Pd/Ir = 13 - 29). Barnes et al. (1988) pointed out that by using metal ratio diagrams (e.g. Pd/Ir versus Ni/Cu), various rock types can be effectively separated and effects of partial melting, sulphide segregation and crystal fractionation can be recognized. In Figure 5.8, Pd/Ir vs Ni/Cu, samples from this study are plotted together with ratios from the mantle, Archaean komatiites, SHMB (siliceous high magnesian basalts), layered intrusions and PGE Reefs (Barnes et al. 1988; Barnes & Often, 1990). 'Fine grained dykes', high-Mg tholeiites and most samples from the norite plot within the field defined by SHMB. Three *Rubbly Norite* samples with higher Pd/Ir ratios (470 - 590) plot within the field for PGE reefs, while one Pd-poor sample (71986) plots well below the average. With the exception of two samples low in Pd, samples from the *Rubbly Norite* have higher Pd/Ir ratios than associated 'fine grained dykes' and samples from the *Homogeneous Norite* and *Mottled Norite*. The majority of samples plot within the SHMB field and

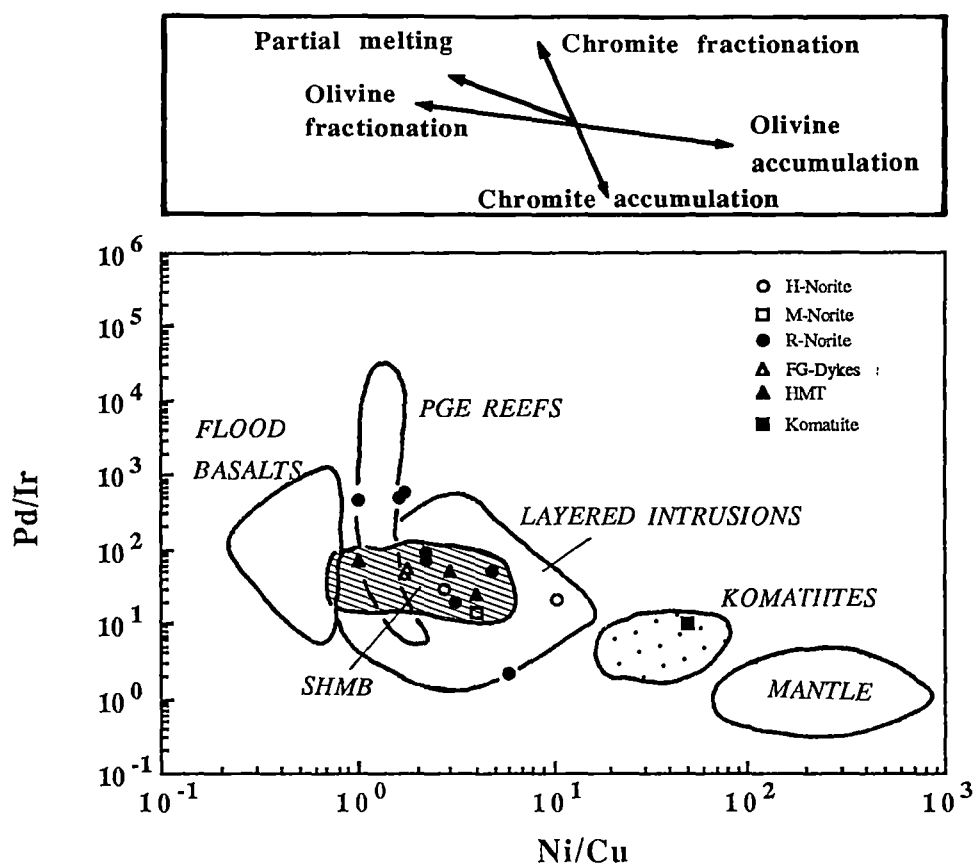


Figure 5.8

Metal ratio diagram of Pd/Ir versus Ni/Cu showing the Vestfold Hills samples and analyzed komatiite standard from this study with compositional fields of: mantle, komatiites, high-Mg basalts (SHMB), layered intrusions, flood basalts and PGE reefs. Modified after Barnes et al. (1988).

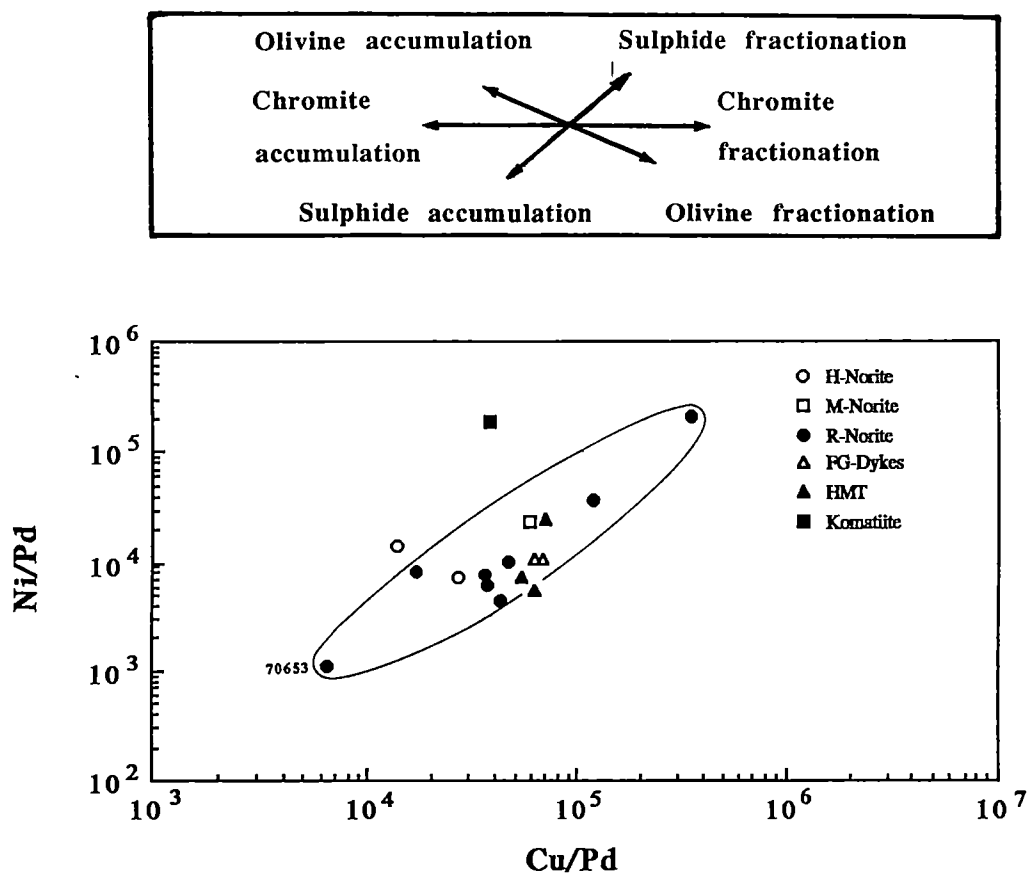


Figure 5.9

Metal ratio diagram of Ni/Pd versus Cu/Pd showing the Vestfold Hills samples. Arrows indicate fractionation and accumulation trends.

define a trend from a more primitive to a more evolved composition. Increasing Pd/Ir and decreasing Ni/Cu ratios indicate a control consistent with olivine fractionation (Figure 5.8). As the geochemistry of the norite is dominated by pyroxene accumulation, it is suggested that Ni concentrations in this example reflect orthopyroxene rather than olivine accumulation.

With the ratio plot Ni/Pd versus Cu/Pd, effects such as the segregation of sulphide liquid from a silicate melt becomes visible. The partition coefficients for Cu and Ni into sulphides are smaller than those for PGE's and during the segregation of sulphides Ni and Cu become depleted in sulphides relative to PGE's. Thus sulphide fractionation would increase Ni/Pd and Cu/Pd ratios in silicates, subsequently the accumulation of sulphides would shift compositions towards PGE enriched rocks. Metal ratio plot Ni/Pd versus Cu/Pd (Figure 5.9) shows a trend within the *Rubbly Norite* which is consistent with the accumulation/fractionation of sulphides, whereas the other *Homogeneous-*, *Mottled Norite*, 'fine grained dykes' and high-Mg tholeiite samples exhibit similar, intermediate ratios, suggesting that sulphide accumulation is not a prominent process.

5.4 DISCUSSION

Sulphide mineralization and PGM occurrences within the high-Mg tholeiite suite of the Vestfold Hills are believed to be of magmatic origin because there is no evidence for hydrothermal alteration, and because the compositional range of sulpharsenides indicate a high temperature origin. PGM's occur as inclusions in chalcopyrite and pentlandite. Microprobe analyses suggest solid solution of Pt and Pd within chalcopyrite and sulpharsenides, respectively. PGE's as solid solutions in sulphides have been described by Chyi & Crocket (1976) and Skinner et al. (1976), who showed that Pd can be concentrated in pentlandite and pyrrhotite, whereas Ir is evenly distributed amongst pentlandite, pyrrhotite and chalcopyrite. While IPGE's show poor correlation with S, PPGE's are clearly associated with sulphides, increasing with

increasing sulphur content. When recalculated to 100% sulphides, comparison with chondritic relative concentrations reveal that the sulphide-rich *Rubbly Norite* does not show further fractionation in PGE relative to high Mg tholeiites. Samples from the *Homogeneous* and *Mottled Norite* have higher PGE abundances (normalized to 100% sulphide) than associated 'fine grained dykes' and *Rubbly Norite*. It should be noted here, that the recalculation of sulphide - poor samples to 100% sulphides may cause uncertainties in relative PGE concentrations, because at low sulphur concentrations not all PGE may have entered the sulphide melt, or sulphur may have been mobilized during alteration. Therefore recalculated PGE concentrations for the sulphur-poor samples 70661 and 70667 may be less accurate than S-rich samples. Nevertheless, samples with similarly low sulphur concentrations from the 'fine grained dykes' and high Mg-tholeiites plot distinctively below the patterns to the *Homogeneous Norite* and *Mottled Norite* suggesting the relative enrichment of PGE in the latter. Pd in the *Rubbly Norite* is strongly enriched relative to other noble metals but also shows relative enrichment to *Homogeneous Norite*, *Mottled Norite* and associated 'fine grained dykes'. In Figure 5.7, chondrite normalized patterns are compared with patterns from Merensky Reef, flood basalts, Stillwater, Sudbury and Proterozoic komatiites. 'Fine grained dykes', high-Mg tholeiites and *Rubbly Norite* have similar patterns to Sudbury and flood basalts with a pronounced Pd peak and high Pd/Pt ratios (up to 16).

Samples from *Homogeneous* and *Mottled Norite* as well as samples 71950 and 71986 (*Rubbly Norite*) possess chondrite normalized patterns which are more similar to those of the Merensky Reef, with low Pd/Pt ratios (0.9). Patterns indicate strong fractionation of PGE with depletion of IPGE's relative to PPGE's. Ratios plot within the field defined by SHMB, showing trends which are controlled by olivine fractionation (Figure 5.8) and by sulphide accumulation/fractionation (Figure 5.9). This is in good agreement with petrography and geochemistry (Chapters 3 and 4). All high-Mg tholeiitic dykes, including the norite have fractionated olivine during their evolution. In addition to olivine fractionation, the norite has accumulated

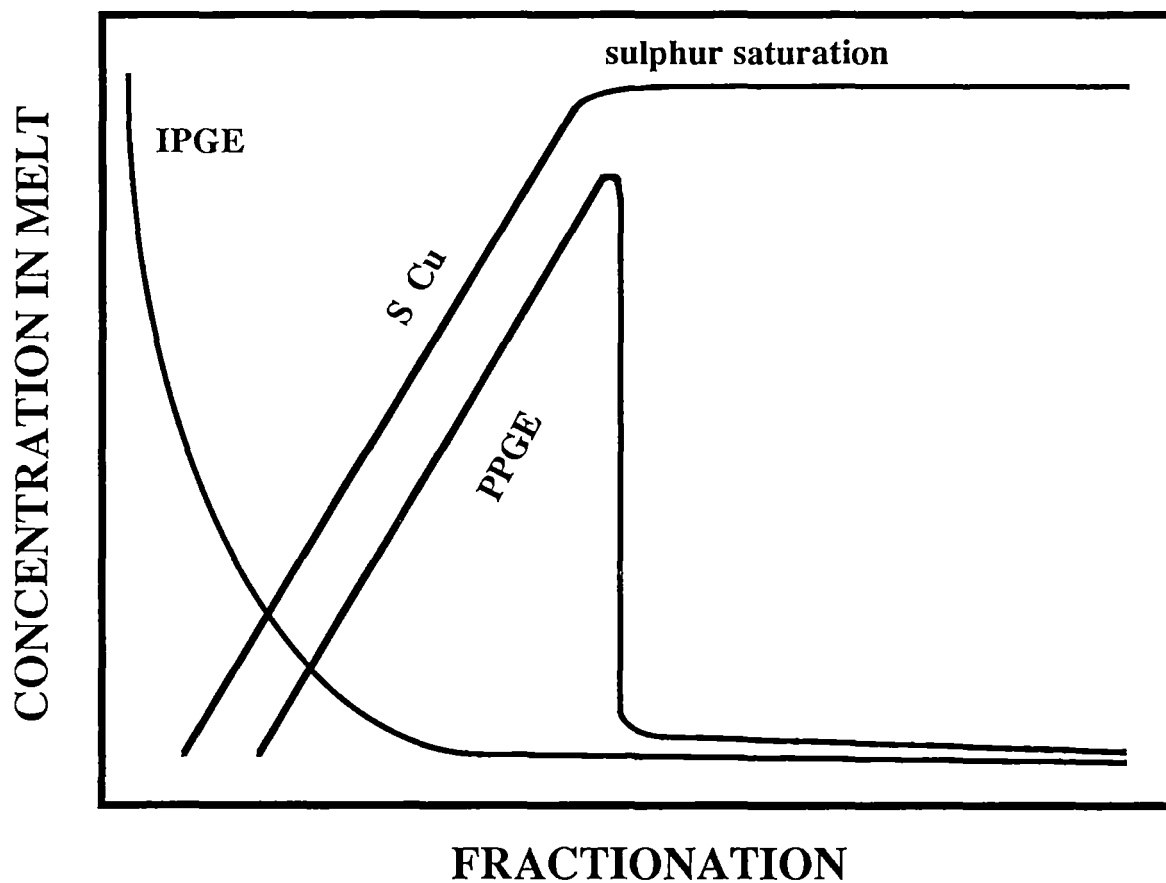


Figure 5.10

Schematic diagram showing the behaviour of IPGE, PPGE, S and Cu during fractionation.

orthopyroxene, increasing from *Homogeneous* to *Mottled* to *Rubby Norite*. In the *Rubby Norite*, sulphides were accumulated in various amounts, which is indicated by accumulation fractionation trend shown in Figure 5.9.

PGE concentrations in mafic to ultramafic melts are mainly dependent on the sulphur capacity of the magma. The sulphur solubility in a magma is determined by the magma composition, temperature, fO_2 and fS_2 (Haughton et al., 1974). A decrease in sulphur solubility will produce sulphur saturation and segregation of an immiscible sulphide liquid. Dependent on magma dynamics, the sulphide liquid remains suspended or will separate and accumulate. As soon as a magma becomes sulphur saturated, elements with high $D^{s/l}$ (sulphide to silicate melt) will partition into the sulphide liquid. In Figure 5.10 the behaviour of PPGE and IPGE with increasing fractionation is shown schematically. The concentration of Ir in a melt decreases with increasing fractionation, while Pd concentration increases. At the point of sulphur saturation, Pd partitions into the sulphide liquid. In other words, during crystallization of sulphur undersaturated ultramafic and mafic magmas Pd (and the other PPGE) will behave incompatibly and become concentrated in the residual silicate melt (Naldrett & Barnes, 1986; Brüggemann et al., 1987). At the point of sulphide liquid unmixing, these elements become compatible and partition into the sulphide phase. With respect to PGE abundances, sulphur saturation plays a significant role during the evolution of mafic and ultramafic melts. Hamlyn & Keays (1986) proposed a model for PGE enrichment of mantle sulphides, and suggested that at low to moderate degrees of partial melting of an undepleted mantle, melts will form which are sulphur-saturated at the time of segregation. Due to coexistence of a residual immiscible sulphide phase at low degree of partial melting these magmas (first stage melts) have low PGE concentrations. For example, mid-ocean ridge basalts (MORB) are considered to be S-saturated first stage melts, containing average sulphur concentrations of 800 ppm (Moore & Fabbi, 1971), and low Pd concentrations (< 0.83 ppb: Crocket & Teruta, 1977; Hertogen et al., 1980; Hamlyn & Keays, 1986), although higher concentrations were reported (Crocket, 1981; Campbell et al., 1983). Melts which form by partial melting of the

depleted mantle residue are sulphur undersaturated, low in TiO_2 , high in MgO and PGE, with abundances of < 54 ppm S and *ca.* 15 ppb Pd (Hamlyn & Keays, 1985). If such sulphur undersaturated, PGE-rich melts reach sulphur saturation (by e.g. temperature decrease, change in $f\text{O}_2$ and/or $f\text{S}_2$, silica-enrichment) the immiscible sulphide liquid can segregate and accumulate. In this model, initially S-undersaturated second stage melts, are the potential precursors of PGE deposits. SHMB have been regarded as Archaean analogues to Tertiary boninites (Redman & Keays, 1985) or contaminated komatiites (Sun et al., 1989). Boninite lavas are interpreted as second stage melts, derived from a strongly depleted mantle source (Sun & Nesbitt, 1978; Cameron et al., 1979; Coish et al., 1982; Hickey & Frey, 1982) and contain sulphur abundances of < 120 ppm (Ueda & Saki, 1984). However, although SHMB's have some geochemical and isotopic characteristics similar to boninites they do not appear to be associated with subduction environments and their siliceous and high MgO content may be ascribed to crustal contamination or shallow melting (< 12 kbar) of a metasomatized asthenosphere - continental lithosphere (Sun & Nesbitt, 1978; Jaques & Green, 1980; Green, 1981).

Chilled margin compositions from the Vestfold Hills high-Mg tholeiites have enriched PGE abundances and sulphur concentrations between 180 and 450 ppm. Samples 70533, 70709 and 70701, with 182, 194 and 256 ppm are likely to be sulphur undersaturated, while samples 70612 and 65209 with 375 and 449 ppm S are more likely to have reached sulphur saturation. Chilled margin sample 70533 is the most primitive composition (Mg# 68) of the examined dykes, whereas others are more evolved (Mg# ~ 57). Assuming that sample 70533 has a primary composition, its concentration of 182 ppm S indicates sulphur-undersaturation of the primary magma. Most norite sample have higher sulphur abundances, indicating early sulphur saturation and sulphide accumulation. If the low sulphur concentration in the chilled dyke margin samples is applicable to the norite intrusion as a whole, then sulphur saturation probably occurred at an intermediate stage of evolution of the high-Mg, high SiO_2 magma, possibly during the emplacement into the crust.

5.5 SUMMARY

Sulphides, and sulpharsenides and platinum group minerals precipitated from sulphide melts and accumulated in the *Rubbly Norite* in various amounts, resulting in high PGE abundances (up to ~ 1600 pbb total PGE) in this unit.

Microprobe analysis of sulphide-rich samples indicates that much of the PGE's occur in solid solution within sulpharsenides and sulphides, rather than in discrete PGM's.

High-Mg tholeiites from the Vestfold Hills, including the *Homogeneous-* and *Mottled Norite*, exhibit anomalously high PGE (30 - 90 ppb total PGE) and low sulphur concentrations, which are characteristics of SHMB's. High PGE and low sulphur concentrations indicate that these melts were not sulphur saturated. Combined with low TiO₂, high SiO₂ and high MgO, a derivation by melting of a previously depleted mantle source is inferred, although processes such as melt segregation at low pressure and crustal contamination may have modified these melts.

TABLE 5.2

BASE METAL MICROPROBE ANALYSES

Sample No. 70653									
Mineral	Chalcopyrite					Pyrrhotite		Pentlandite	
Pos. of Anal.	core	rim	core	core	rim	core	rim	core	rim
Rock Type	R-Norite								
S	34.80	34.96	34.92	34.58	34.66	39.22	38.89	32.97	32.59
Fe	30.71	30.71	30.77	30.57	35.33	58.95	59.34	30.19	30.06
Ni	0.00	0.02	0.03	0.01	0.04	1.37	1.55	36.02	36.01
Cu	33.48	33.51	33.54	33.37	29.88	0.01	0.01	0.07	0.06
As	0.00	0.09	0.09	0.04	0.08	0.00	0.02	0.08	0.01
Pd	0.00	0.01	0.03	0.02	0.00	0.00	0.00	0.00	0.01
Te	0.00	0.00	0.00	0.00	0.02	0.00	0.03	0.04	0.02
Co	0.00	0.00	0.00	0.00	0.00	0.00	0.01	0.56	0.54
Pt	0.15	0.10	0.12	0.04	0.00	0.08	0.00	0.02	0.00
Bi	0.03	0.02	0.03	0.23	0.19	0.18	0.02	0.09	0.00
Total	99.18	99.41	99.52	98.85	100.20	99.80	99.89	100.05	99.32
Atom proportions									
S	0.990	0.991	0.989	0.988	0.975	1.048	1.039	0.923	0.919
Fe	0.516	0.514	0.515	0.516	0.587	0.930	0.936	0.499	0.501
Ni	0.000	0.000	0.000	0.000	0.001	0.021	0.023	0.566	0.570
Cu	0.494	0.493	0.493	0.495	0.436	0.000	0.000	0.001	0.001
As	0.000	0.001	0.001	0.001	0.001	0.000	0.000	0.001	0.000
Pd	0.000	0.000	0.000	0.000	0.000	0.000	0.000	0.000	0.000
Te	0.000	0.000	0.000	0.000	0.000	0.000	0.000	0.000	0.000
Co	0.000	0.000	0.000	0.000	0.000	0.000	0.000	0.009	0.009
Pt	0.001	0.000	0.001	0.000	0.000	0.000	0.000	0.000	0.000
Bi	0.000	0.000	0.000	0.001	0.001	0.001	0.000	0.000	0.000
Sum	2.000	2.000	2.000	2.000	2.000	2.000	2.000	2.000	2.000

SULPHARSENIDES AND TELLURIDE MICROPROBE ANALYSES

Sample No. 70653									
Mineral	Gersdorffite - Arsenopyrite - Cobaltite ss					Michenerite			
Pos. of Anal.	core	core	rim	core	rim	core	core	core	rim
Rock Type	R-Norite								core
S	18.54	19.68	19.76	19.85	19.73	0.01	0.77	0.02	0.04
Fe	5.48	5.38	5.15	5.19	6.30	0.76	1.66	1.66	1.68
Ni	23.70	11.72	10.32	7.50	11.58	0.01	0.63	0.26	0.29
Cu	0.67	0.14	0.11	0.12	0.10	0.86	0.51	0.60	0.36
As	43.67	42.63	43.15	42.73	43.02	0.00	0.00	0.00	0.00
Pd	0.17	1.06	0.77	0.47	1.25	25.27	23.85	24.64	24.99
Te	0.01	0.01	0.00	0.00	0.01	29.61	32.10	33.90	33.58
Co	6.74	17.41	19.60	23.06	16.78	0.00	1.26	0.13	0.18
Pt	0.02	0.00	0.04	0.11	0.00	0.89	0.59	0.57	0.67
Bi	0.00	0.00	0.00	0.00	0.00	44.03	37.51	38.09	38.69
Total	99.00	98.04	98.91	99.04	98.77	101.44	98.88	99.88	100.48
Atom proportions									
S	0.951	1.012	1.007	1.008	1.008	0.000	0.031	0.001	0.002
Fe	0.166	0.163	0.155	0.156	0.190	0.019	0.040	0.041	0.041
Ni	0.683	0.338	0.295	0.214	0.332	0.000	0.014	0.006	0.007
Cu	0.018	0.004	0.003	0.003	0.003	0.019	0.011	0.013	0.008
As	0.986	0.965	0.968	0.955	0.967	0.000	0.000	0.000	0.000
Pd	0.003	0.017	0.012	0.007	0.020	0.333	0.298	0.318	0.321
Te	0.000	0.000	0.000	0.000	0.000	0.326	0.335	0.364	0.360
Co	0.193	0.501	0.559	0.655	0.480	0.000	0.028	0.003	0.004
Pt	0.000	0.000	0.000	0.001	0.000	0.006	0.004	0.004	0.005
Bi	0.000	0.000	0.000	0.000	0.000	0.296	0.239	0.250	0.253
Sum	3.000	3.000	3.000	3.000	3.000	1.000	1.000	1.000	1.000

Selected Microprobe Analyses from Base Metal Sulphides, Sulpharsenides and Platinum Group Minerals from Rubbly Norite.
 Number of atoms calculated for 2, 3 and 1 atom per formula unit. Analytical conditions: CAMECA Microprobe, 20 kv - 100 nA.

TABLE 5.3

PGE, SULPHUR AND TRACE ELEMENT ANALYSES

Sample No Rock Type	69894 H-Norite	70667 M-Norite	70653	70683	70758	70766 R-Norite	70706	70783	71950	71986
PGE ppb										
Os	8	8	10	10	10	8	4	4	4	4
Ir	1	1.1	2.2	0.9	1.1	1.1	0.9	0.3	0.3	0.9
Ru	11	11	21	6	10	8.5	3	3	1	4
Rh	5	4.5	65	5	14	4.5	15	6	1	2
Pt	14	24	130	22	23	13	50	9	12	26
Pd	29	24	1300	66	100	54	420	150	6	2
Au	14	8	62	8	8	4	23	25	1	1
PGE normalized to chondrite **										
Os	41.4	77.9	1.9	6.6	6.8	23.3	0.7	4.1	18.0	37.5
Ir	4.9	10.2	0.4	0.6	0.7	3.0	0.1	0.3	1.3	8.0
Ru	42.4	79.8	3.0	3.0	5.0	18.4	0.4	2.3	3.4	27.9
Rh	66.4	112.6	32.4	8.5	24.4	33.7	6.5	15.7	11.6	48.1
Pt	36.5	117.7	12.7	7.3	7.9	19.1	4.3	4.6	27.3	122.7
Pd	141.4	220.3	237.9	41.2	63.9	148.3	67.2	143.7	25.5	17.7
Au	244.8	263.3	40.7	17.9	18.3	39.4	13.2	85.9	15.3	31.7
Cu	1884.7	1357.3	805.5	980.6	1184.2	1283.5	1497.1	2810.7	1442.6	3034.9
Ratios										
Pd/Ir	29.0	21.8	590.9	73.3	90.9	49.1	466.7	500.0	20.0	2.2
Ni/Cu	2.8	10.4	1.7	2.2	2.2	4.9	1.0	1.6	3.2	5.9
Ni/Pd	7362	14313	1081	10009	8020	8185	4420	6060	37333	200000
Cu/Pd	26414	13750	6462	46515	35800	16667	42810	37133	116667	340500
Pt/Pd	0.48	1.00	0.10	0.33	0.23	0.24	0.12	0.06	2.00	13.00
Mg#										
Mg#	62.3	71.0	74.6	70.4	72.0	71.2	69.6	68.8	62.8	71.8
Sulphur and Trace Elements										
S	143	76	3813	1118	1092	254	4358	728	164	79
Ni	214	344	1405	661	802	442	1857	909	224	400
Cu	77	33	840	307	358	90	1798	557	70	68
Zn	84	87	92	111	92	95	142	76	86	105

Sample No. Rock Type	65209 High-Mg Tholeiite	70533	70612	70701 Fine Grained Dykes	70709	Standard Komatiite	Chondrite C1*
PGE ppb (except C1 = ppb relative to 100% sulphide)							
Os	n.d.	n.d.	n.d.	n.d.	n.d.	n.d.	514
Ir	0.6	0.3	0.2	0.3	0.3	0.8	540
Ru	2.6	0.6	0.8	0.7	0.2	3	690
Rh	n.d.	n.d.	n.d.	n.d.	n.d.	n.d.	200
Pt	17.1	10.5	18.4	14.8	15.2	8	1021
Pd	15.0	16.7	16.2	17.3	14.8	8	545
Au	3.2	1.7	4.6	2.3	3.3	0.6	152
PGE normalized to chondrite **							
Os						24.1	
Ir	1.0	1.2	0.4	0.8	1.1	2.3	
Ru	3.2	1.9	1.2	1.6	0.5	6.7	
Rh						23.2	
Pt	14.2	21.4	18.3	21.6	29.3	12.1	
Pd	23.3	64.1	30.0	47.1	53.2	22.7	
Au	17.9	23.9	30.7	22.1	42.5	6.1	
Cu	803.7	2214.9	904.1	1489.4	1789.4	433.6	
Ratios							
Pd/Ir	24	53	73	57	47	10	
Ni/Cu	4	3	1	2	2	49	
Ni/Pd	25331	18541	5573	10809	12314	184638	
Cu/Pd	68470	53828	61300	61272	66712	37875	
Pt/Pd	1.13	0.63	1.14	0.86	1.03	1.00	
Mg#							
Mg#	68.6	67.8	57.0	59.4	56.8	81.7	
Sulphur and Trace Elements ppm (except C1 = % sulphide)							
S	449	182	375	256	194	246	10.8
Ni	379	310	90	187	182	1477	
Cu	103	90	99	106	99	30	0.0108
Zn	88	85	75	89	88	55	

PGE, sulphur and trace element analyses from various norite types and associated dykes. Ni abundance* for C1 is from Palme et al. (1978) and PGE concentrations* (* recalculated to 100% sulphide) are from Naldrett & Duke (1980). PGE and Au determined by fire assay and NAA; S determined by LECO iodate titration and trace elements determined by XRF. (n.d. = not determined). ** Before normalized to chondrite PGE were recalculated to 100% sulphide, assuming 38% S in sulphide liquid.

CHAPTER 6

GEOCHEMISTRY AND PETROGENESIS OF THE HIGH-MG THOLEIITES : PRIMARY MAGMAS OR PRODUCTS OF CRUSTAL CONTAMINATION ?

6.1 INTRODUCTION

High-Mg tholeiites intruded deep granulitic crust (10 - 15 km) of the Vestfold Hills at ~ 2350 Ma, forming dykes and a large noritic ring complex. At least three separate intrusive events can be recognized from crosscutting relationships. The oldest event comprises olivine- and orthopyroxene-phyric dykes (Chapter 3), which are crosscut by two younger sets of solely orthopyroxene-phyric dykes. The *Rubbly Norite* unit of the noritic ring complex, and associated 'fine grained dykes', can be related to the last of these intrusive events (Chapter 4). The olivine-, and orthopyroxene-phyric dykes have distinctive geochemistry. Kuehner (1986, 1989) subdivided the olivine + orthopyroxene-phyric dykes from the orthopyroxene-phyric dykes based on relatively enriched and depleted Sr abundances respectively, and identified two separate Sr-depleted, orthopyroxene-phyric dyke groups, one relatively Rb-rich and the other Rb-poor.

High SiO₂ and MgO, low TiO₂, enrichments in platinum group elements and gold are characteristic features of this dyke suite from the Vestfold Hills. These are general characteristics of siliceous high magnesian basalts (SHMB; Glikson, 1983; Redman & Keays, 1985) and observed in many continental basement terranes (Kuehner, 1989). This chapter examines whether these characteristics are primary, and

if so, what is the nature of their mantle source, or whether they are a product of magma modification involving assimilation of continental crust.

It has been suggested by Cattell (1987), Barley (1986), and by Arndt & Jenner (1986) that SHMB elsewhere have been derived from komatiitic parent magmas by crustal contamination, involving combined assimilation and fractional crystallization (AFC) processes (after DePaolo, 1981). Elsewhere Sparks (1986) and Longhi et al. (1983) have proposed an origin for Bushveld U-type parent magmas (Barnes, 1989), which are geochemically similar to the SHMB suite, by combined 30 - 50% crustal contamination and 35% olivine fractionation of a komatiitic parent with 28 wt% MgO.

Alternatively, SHMB have been considered as Archaean and Proterozoic analogues of Tertiary boninites (Redman & Keays, 1985). This interpretation implies second-stage melting of a refractory harzburgitic mantle source, and that melting is induced either by fluids/hydrous melts derived from subducting oceanic crust (e.g. Sun & Nesbitt, 1978) or by anomalously high mantle temperatures (Crawford et al., 1981).

A variant of this latter model invokes magma generation by melting and melt segregation from metasomatized but still refractory mantle (sub-continental lithosphere) at shallow depths, probably < 12 kbar (Sun & Nesbitt, 1978 b; Jaques & Green, 1980; Green, 1981; Weaver & Tarney, 1981; Fisk, 1986; McCallum, 1987).

This chapter establishes and evaluates the origin of geochemical diversity within the Vestfold Hills high-Mg tholeiites and addresses the origin of these magmas in terms of the models outlined above.

6.2. WHOLE ROCK GEOCHEMISTRY

6.2.1 Major and Trace Element Geochemistry

The Vestfold Hills high-Mg tholeiite dykes have relatively high SiO₂ (52 -57 wt%) and MgO (7 -18 wt%), and low TiO₂ (0.38 - 0.74 wt%). Compositions vary from olivine normative (9.1 wt%) to quartz normative (10.8 wt%) (see Table 6.1). The compositional spectrum extends from olivine and orthopyroxene phyric dykes with > 9% MgO to include orthopyroxene phyric 'fine grained dykes' (see Chapter 4) with ~ 7 - 8% MgO, interpreted as cogenetic with the norite complex. This compositional spectrum is illustrated in Figure 6.1 where all analyzed samples are projected from diopside onto the base of the basalt tetrahedron, following Green (1971).

Three distinct compositional groups are apparent in Figure 6.1: one group straddling the boundary between olivine and quartz normative fields, and two separate quartz normative groups, one of which forms a linear array aligned through orthopyroxene. These groups correspond to those distinguished earlier on the basis of phenocryst mineralogy and major element geochemistry (see Figure 6.1).

Chemical differences between the three compositional groups are further illustrated by plotting incompatible element concentrations on multi-element diagrams (Figure 6.2 A - C). Within each of the dyke groups, trace element characteristics are very similar, whereas between group differences may be marked (Figure 6.2. A, B and C). All trace element patterns show enrichment of LILE (Ba, Rb, K) and LREE relative to the high-field strength elements, Nb and Ti. All groups exhibit pronounced negative anomalies in Nb, P and Ti, when normalized against 'primitive mantle' as inferred by Sun et al. (1989). The negative Nb anomaly is a feature common to many continental tholeiites (e.g. Dupuy & Dostal, 1984). The absence of a negative Sr anomaly readily distinguishes *Group I* from the *Group II*, *Ila* and *III* dykes. The *Group II* and *Ila* dykes in turn, can be separated from *Group III* by Rb-enrichment relative to Ba and K in *Group II* and *Ila* dykes, with primitive mantle normalized

REPRESENTATIVE HIGH-MG THOLEIITE WHOLE ROCK ANALYSES

Sample No.	65209	70533	70536	70612	70634	70653	70661	70667	70709	71735	71889
Rock Type	HMT	HMT	HMT	HMT	HMT	RN	MN	HN	FGD	HMT	FGD
Main Group	1	1	1	1	1	3	3	3	3	3	3
Group	Ia	I	I	Ia	I	Ila	II	II	II	III	II
Major Elements											
SiO ₂	53.67	51.80	52.83	54.58	50.59	55.84	55.97	55.63	55.92	52.01	56.15
TiO ₂	0.71	0.60	0.55	0.67	0.57	0.39	0.55	0.47	0.74	0.47	0.71
Al ₂ O ₃	8.33	11.36	11.52	13.28	11.00	6.81	9.30	9.65	13.00	11.89	12.64
Fe ₂ O ₃	12.08	11.60	11.17	10.61	11.13	12.67	11.87	11.71	11.39	10.95	11.37
FeO	0.00	0.00	0.00	0.00	0.00	0.00	0.00	0.00	0.00	0.00	0.00
MnO	0.18	0.19	0.19	0.16	0.19	0.19	0.19	0.19	0.17	0.16	0.16
MgO	13.45	12.36	12.13	7.09	12.33	18.77	14.27	14.49	7.56	12.34	8.33
CaO	9.23	9.28	9.37	9.67	8.99	4.74	5.78	5.85	7.93	8.99	7.71
Na ₂ O	1.65	1.74	1.63	2.25	2.18	0.81	1.20	1.06	1.72	1.53	1.77
K ₂ O	0.75	0.59	0.61	0.96	0.71	0.62	0.92	0.89	1.33	0.60	1.21
P ₂ O ₅	0.09	0.10	0.10	0.11	0.11	0.04	0.08	0.10	0.13	0.06	0.12
LOI	-0.03	0.14	-0.10	0.27	2.04	-0.12	-0.19	-1.00	0.16	0.79	0.06
Total	100.11	99.76	100.00	99.65	99.84	99.62	98.87	100.04	100.05	99.79	100.23
Mg#	68.6	67.8	68.3	56.9	68.7	74.6	70.4	71.0	56.8	69.0	59.2
CIPW Norm wt%											
Qtz	1.14		1.31	5.58		4.94	7.04	8.20	9.22	1.07	8.88
Or	4.43	3.49	3.60	5.67	4.20	3.66	5.44	5.26	7.86	3.55	7.15
Ab	13.96	14.72	13.79	19.04	18.45	6.85	10.15	8.97	14.55	12.95	14.98
An	13.11	21.44	22.32	23.30	18.13	13.11	17.27	18.94	23.82	23.80	22.97
Lc											
Ne											
Cpx	25.96	19.39	19.04	19.67	20.83	8.15	8.78	2.86	12.05	16.50	11.87
Di	18.24	13.44	13.25	11.60	14.60	6.14	6.30	2.06	7.09	11.66	7.26
Hd	7.72	5.95	5.79	8.07	6.23	2.00	2.49	0.80	4.95	4.83	4.60
Opx	37.21	34.95	36.13	22.09	23.19	60.33	47.41	50.74	28.01	37.37	30.02
En	25.05	23.17	24.07	12.28	15.57	43.91	32.63	35.14	15.54	25.33	17.38
Fs	12.17	11.79	12.06	9.81	7.63	16.43	14.78	15.60	12.46	12.04	12.64
Ol		1.52			9.04						
Fo		0.97			5.87						
Fa		0.55			3.17						
Mt	1.77	1.68	1.62	1.54	1.62	1.84	1.72	1.70	1.65	1.59	1.65
Il	1.35	1.14	1.04	1.27	1.08	0.74	1.04	0.89	1.41	0.89	1.35
Ap	0.21	0.24	0.24	0.26	0.26	0.09	0.19	2.37	0.31	0.14	0.28
Trace Elements											
Ba	174	212	219	336	195	131	201	196	292	232	286
Rb	31	20	22	40	25	37	51	51	72	17	64
Nb	5	3	3	4	3	5	8	1	6	4	7
Sr	209	160	159	267	152	50	77	78	115	92	107
Zr	69	54	56	76	52	50	83	81	122	75	113
Y	41	18	15	15	16	11	21	15	22	18	22
La	9	8	9	14	7	8	16	14	22	17	21
Ce	17	16	14	32	15	16	31	30	42	29	44
Nd	10	10	9	14	8	9	12	11	19	12	17
Ni	377	311	262	92	301	1395	360	345	199	389	179
Cr	1600	1225	1093	373	1199	2104	1509	1406	524	1363	615
V	218	238	220	218	230	187	201	195	221	312	213
Sc	31	39	39	35	41	28	30	29	34	40	33

Table 6.1
Representative High-Mg Tholeiite (HMT) whole rock analyses showing various groups, including Homogeneous Norite (HN), Rubbly Norite (RN), Mottled Norite (MN) and Fine Grained Dykes (FGD). Data for sample 65209 was taken from Kuehner (1986).

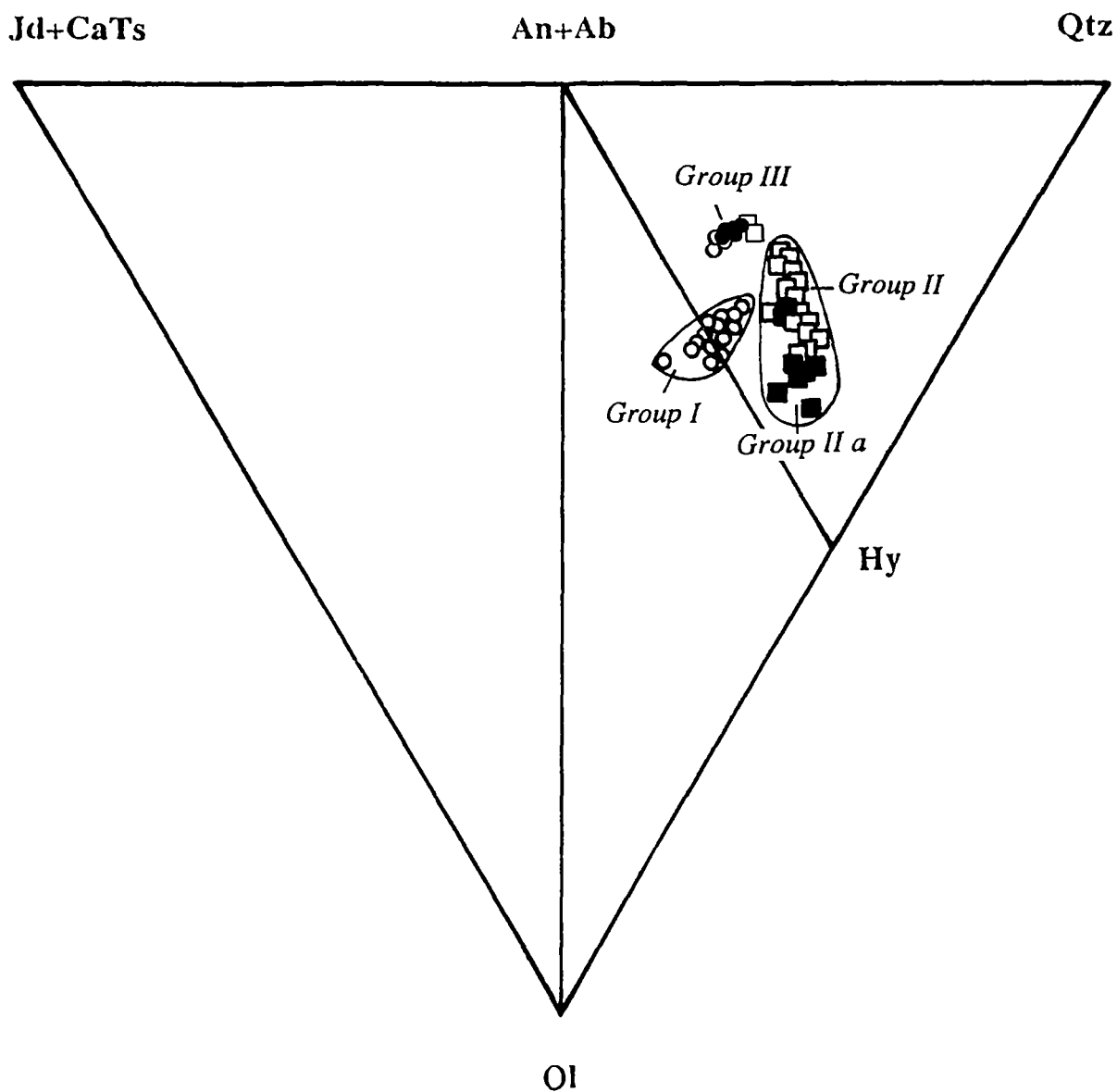


Figure 6.1

Compositions of various high-Mg tholeiites from the Vestfold Hills including the norite types and 'fine grained dykes' are projected from diopside onto the plane Jd+CaTs - Ol - Qtz of the basalt tetrahedron following Green (1970) ($\text{Fe}_2\text{O}_3/\text{FeO} = 0.1$). Circles - *Group I*, open squares - *Group II*, filled squares - *Group II a*, dots - *Group III*.

(Rb/Ba)_N ratios ranging from 0.8 to 0.9 for *Group III*, and between 1.2 and 2.5, and between 1.1 and 1.5 for *Group II* and *Ila* respectively (Figure 6.3). *Group III* has different (Sr/Nd)_N ratios to *Group I*, but similarly low (Sr/Nd)_N ratios compared to *Group II* and *Ila*.

The rare earth element (REE) concentrations of eleven high-Mg tholeiite dykes, analyzed using the ion-exchange XRF method of Robinson et al. (1986), are listed in Table 6.2. The REE patterns of each of the groups are quite similar, with slightly fractionated heavy rare earth elements and intermediate to strongly enriched light rare earth elements (LREE). The LREE in *Group II*, *Ila* and *III* are slightly more enriched than in *Group I*, with these dykes having (La/Yb)_{CN} > 8 and ≤ 7, respectively. The presence of small negative Eu anomalies further distinguishes *Group II*, *Ila* and *III* dykes from *Group I*. The only exception to these systematics is sample 70653, an orthocumulate from the *Rubbly Norite* (Chapter 4), which exhibits a similar REE pattern to the *Group I* tholeiites but is otherwise equivalent to the *Group Ila* tholeiites (cf. Figure 6.4).

To summarize, the following subdivision of the Vestfold Hills high-Mg tholeiites can be made on the basis of geochemistry, mineralogy and crosscutting relationships:

<i>HIGH-MG THOLEIITE GROUPS</i>	
<i>Group I</i>	olivine and orthopyroxene phyric tholeiite, these are the oldest dykes from this suite
<i>Group II</i>	orthopyroxene phyric tholeiites including the <i>Homogeneous-Mottled Norite</i> and associated fine grained dykes
<i>Group Ila</i>	orthopyroxene phyric tholeiites including the <i>Rubbly Norite</i>
<i>Group III</i>	orthopyroxene phyric tholeiite

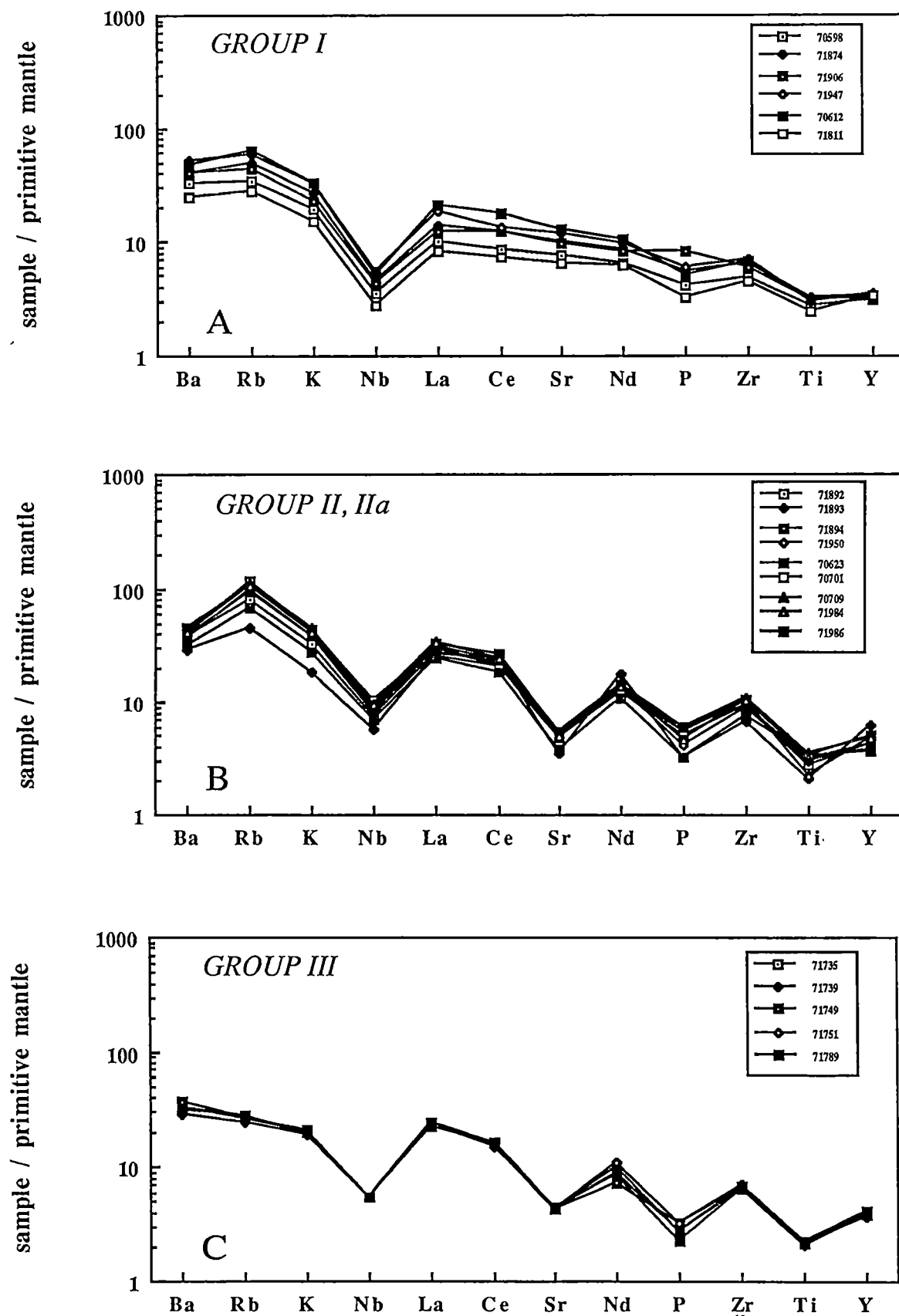


Figure 6.2

Incompatible element 'spidergrams' distinguishing between *Group I, II, IIa* and *III* high-Mg tholeiites. Before plotting data were normalized to primitive mantle after Sun et al. (1989).

GROUP I, II, IIa, III HIGH-MG THOLEIITES

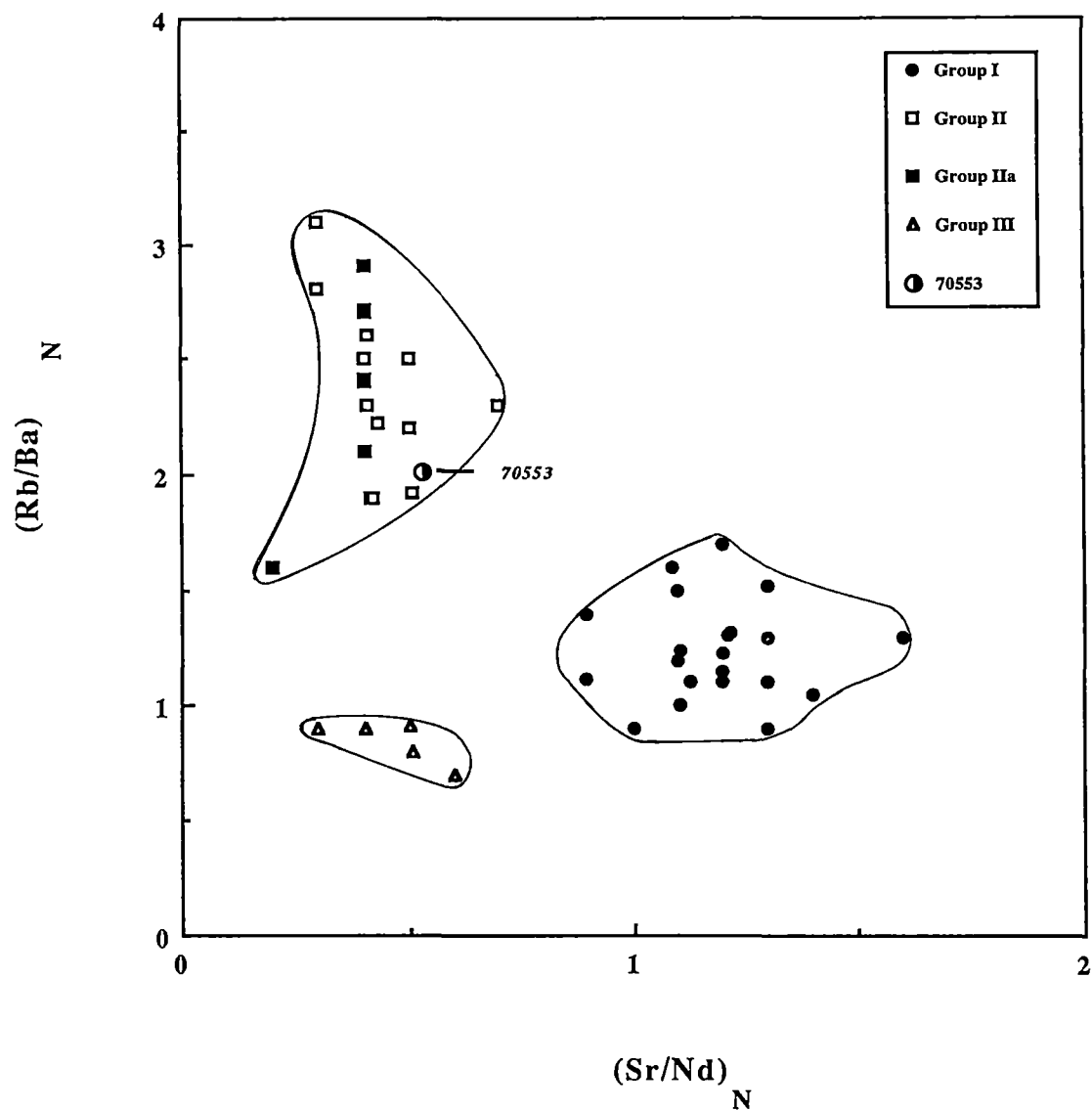


Figure 6.3

$(Rb/Ba)_N$ plotted against $(Sr/Nd)_N$ distinguishing between *Group I, II, IIa* and *III* high-Mg tholeiites.

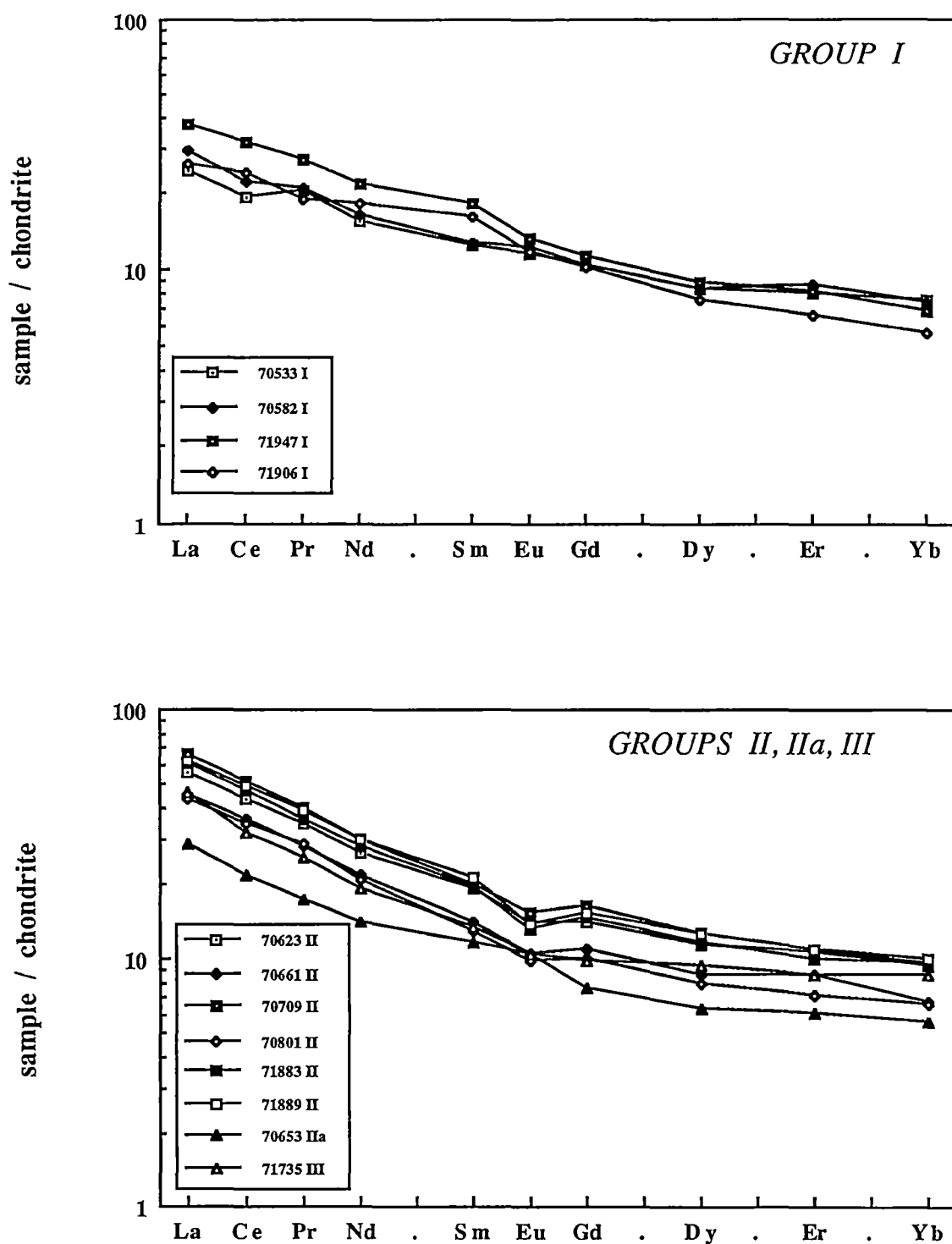


Figure 6.4

Chondrite normalized REE patterns (Leedy/1.2; Masuda et al. 1973; Taylor & Gorton, 1977) of various norite samples.

REE ANALYSES FROM HIGH-MG THOLEIITES

Sample No.	70533	70536	70582	70583	71906	71947	71735
Rock Type	HMT	HMT	HMT	HMT	HMT	HMT	HMT
Group	I	I	I	I	I	I	III
REE / ppm							
La	7.8	8.9	9.4	9.9	8.3	11.8	14.5
Ce	15.6	17.2	18.0	19.0	19.7	26.2	26.1
Pr	2.4	2.1	2.4	2.5	2.2	3.1	2.9
Nd	9.3	9.1	9.8	10.1	10.8	13.0	11.4
Sm	2.4	2.2	2.4	2.5	3.1	3.5	2.6
Eu	0.8	0.7	0.9	0.9	0.9	1.0	0.8
Gd	2.7	2.3	2.7	2.7	2.6	2.9	2.6
Dy	2.7	2.4	2.7	2.8	2.5	2.9	3.0
Er	1.7	1.4	1.8	1.7	1.4	1.7	1.8
Yb	1.6	1.3	1.5	1.4	1.2	1.4	1.8
La/Yb	5.0	6.8	6.1	7.1	7.2	8.2	8.1
Sample No.	70661	70801	71883	70623	70709	71889	70653
Rock Type	MN	HN	HMT	FGD	FGD	FGD	RN
Group	II	II	II	II	II	II	IIa
REE / ppm							
La	14.4	13.8	19.2	17.6	20.7	19.6	9.1
Ce	29.5	28.2	38.6	35.7	42.1	40.2	17.6
Pr	3.3	3.3	4.2	4.0	4.6	4.5	2.0
Nd	12.8	12.4	17.0	15.9	18.0	18.1	8.3
Sm	2.6	2.5	3.8	3.7	3.8	4.0	2.2
Eu	0.8	0.7	0.9	1.0	1.1	1.0	0.8
Gd	2.8	2.6	3.8	3.6	4.2	3.9	2.0
Dy	2.8	2.6	3.8	3.7	4.1	4.1	2.1
Er	1.8	1.5	2.2	2.3	2.3	2.3	1.3
Yb	1.4	1.4	2.0	1.9	2.0	2.1	1.2
La/Yb	10.1	10.1	9.7	9.1	10.5	9.3	7.7

Table 6.2

Rare earth abundances in a high-Mg tholeiitic dykes from the Vestfold Hills. Analyses were done following the method of Robinson et al. (1986). Concentrations are given in ppm.

Abbreviations: HMT - high-Mg tholeiite, HN - Homogeneous Norite, MN - Mottled Norite, RN - Rubbly Norite, FGD - fine grained dykes.

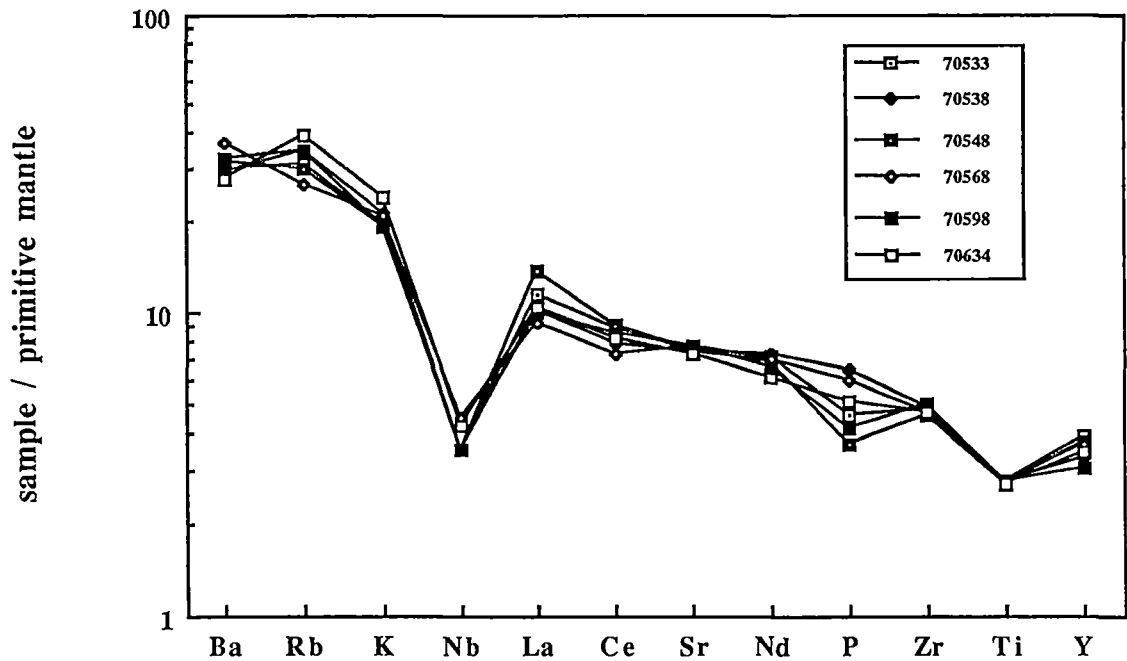
While *Group I*, *II* and *IIa* were emplaced in succession (becoming younger with increasing number), *Group III* tholeiites are younger than *Group I* but their relationship to *Groups II* and *IIa* has not yet been established.

6.3 CHEMICAL VARIATIONS WITHIN THE HIGH-MG THOLEIITIC SUITE

Kuehner (1986, 1989) has suggested that the two major groups (i.e. *Groups I* and *II*) were derived from two separate and geochemically distinct mantle source regions, modified by different incompatible - element enrichments. He further showed that variations in trace elements (including REE abundances) between *Group II* and *III* could be explained by fractional crystallization, with variation in CaO/Al₂O₃ ratios requiring the fractionation of a CaO-rich phase. However this model was excluded (Kuehner, 1986) for no suitable Ca-rich phenocryst phases (i.e. clinopyroxene or plagioclase) was observed in these dykes.

Geochemical variation documented within a single *Group I* dyke (Chapter 3) offers an apparent solution to the problem of intragroup geochemical differences. The trace element variation occurring in this dyke is shown again in Figure 6.5, with chilled margin and dyke interior samples being plotted separately. The point to note is that the trace element pattern of the most evolved sample (70553), from the interior of this *Group I* dyke, is almost identical to that of the *Group II* dykes, cf. Rb/Ba and Sr/Nd ratios. This sample was interpreted to be the product of *in situ* differentiation following dyke emplacement (Chapter 3), and the development of the large negative Sr_N anomaly to be a result of plagioclase fractionation, associated with the migration and accumulation of residual liquids. Further evidence for plagioclase fractionation, is given by the presence of a small negative Eu_{CN} - anomaly, which is typical for *Group II*, *IIa* and *III*.

HIGH-MG THOLEIITE - CHILLED MARGINS



HIGH-MG THOLEIITE - DYKE INTERIORS

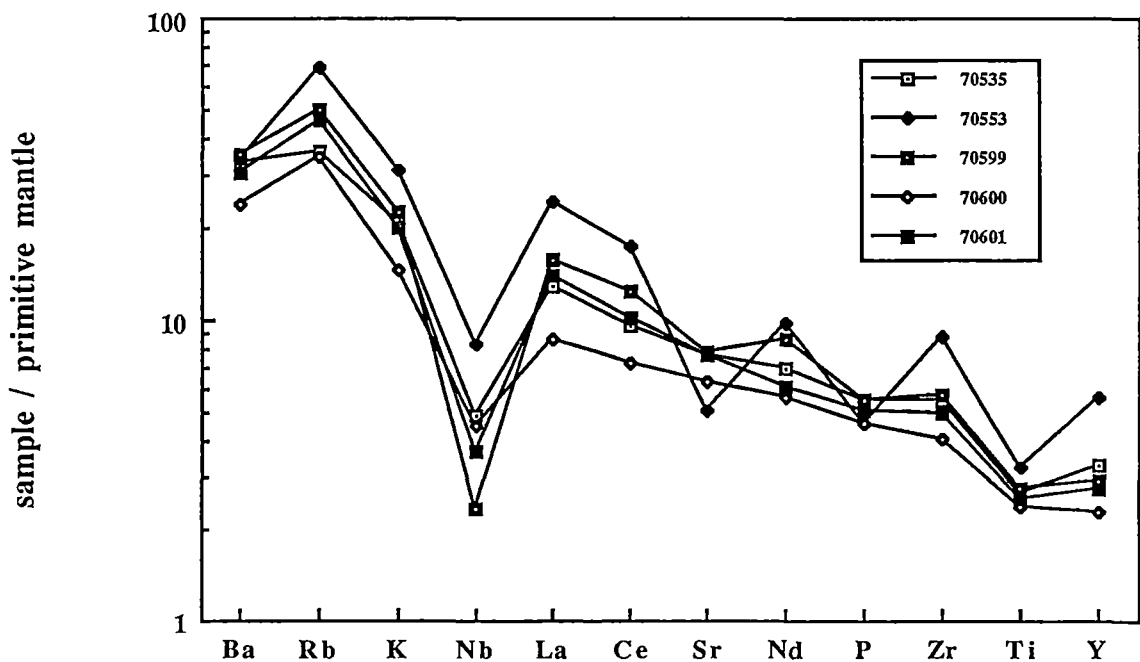


Figure 6.5

Incompatible element 'spidergrams' showing chilled margin and dyke interior compositions from one *Group I* high-Mg tholeiitic dyke (compare Chapter 3). Before plotting data were normalized to primitive mantle after Sun et al. (1989.) Note that 70598 is plotted in both Figure 6.2 (i.e. it is a typical *Group I* high-Mg tholeiite) and Figure 6.5).

The origin of geochemical differences between the dyke suites is re-examined here, with close scrutiny given to the possible role of crystal fractionation, contamination by crustal material and partial melting processes.

6.4 CRYSTAL FRACTIONATION

Geochemical variations within the dyke groups have been assessed in detail in Chapters 3 and 4. It was shown that variation in *Group I* dykes could be ascribed largely to olivine and orthopyroxene fractionation, apart from the most evolved members of this group which requires further orthopyroxene, clinopyroxene and plagioclase fractionation. Variation within *Group II* and *IIa* was found to be consistent with varying amounts of orthopyroxene fractionation/accumulation. The extent to which fractionation processes can account for variation between the dyke groups is examined below using the least squares mixing program "GENMIX" (Le Maitre, 1980).

To test possible crystal fractionation links between *Group I*, *II*, *IIa*, and *III* dykes, representative phenocryst and whole-rock compositions for each of these dyke groups have been selected for least squares modelling. Rb/Sr ratio plotted against Sr was used as the criterion, for endmembers of each group as depicted schematically in Figure 6.6 and also in 6.7. Letters along side lines refer to the least square mixing calculations listed in Table 6.3 A - E.

The least squares modelling demonstrates that for major elements within *Group I*, the most evolved dyke can be related to the most primitive dyke by *ca.* 13 wt% olivine fractionation (Table 6.3 A). *Group II* dykes may be derived by relatively large amounts (28 to 38 wt%) of fractionation from primitive *Group I* magmas of an assemblage comprising 13 wt% olivine 15.5 wt% clinopyroxene and 9.5 wt% plagioclase (Table 6.3 D, E) although the 'fits' of model and actual compositions are not perfect. Some *Group III* dykes are very similar geochemically to evolved *Group I*

The origin of geochemical differences between the dyke suites is re-examined here, with close scrutiny given to the possible role of crystal fractionation, contamination by crustal material and partial melting processes.

6.4 CRYSTAL FRACTIONATION

Geochemical variations within the dyke groups have been assessed in detail in Chapters 3 and 4. It was shown that variation in *Group I* dykes could be ascribed largely to olivine and orthopyroxene fractionation, apart from the most evolved members of this group which requires further orthopyroxene, clinopyroxene and plagioclase fractionation. Variation within *Group II* and *Ila* was found to be consistent with varying amounts of orthopyroxene fractionation/accumulation. The extent to which fractionation processes can account for variation between the dyke groups is examined below using the least squares mixing program "GENMIX" (Le Maitre, 1980).

To test possible crystal fractionation links between *Group I*, *II*, *Ila*, and *III* dykes, representative phenocryst and whole-rock compositions for each of these dyke groups have been selected for least squares modelling. Rb/Sr ratio plotted against Sr was used as the criterion, for endmembers of each group as depicted schematically in Figure 6.6 and also in 6.7. Letters along side lines refer to the least square mixing calculations listed in Table 6.3 A - E.

The least squares modelling demonstrates that for major elements within *Group I*, the most evolved dyke can be related to the most primitive dyke by *ca.* 13 wt% olivine fractionation (Table 6.3 A). *Group II* dykes may be derived by relatively large amounts (28 to 38 wt%) of fractionation from primitive *Group I* magmas of an assemblage comprising 13 wt% olivine 15.5 wt% clinopyroxene and 9.5 wt% plagioclase (Table 6.3 D, E) although the 'fits' of model and actual compositions are not perfect. Some *Group III* dykes are very similar geochemically to evolved *Group I*

GROUP I, II, III - HIGH-MG THOLEIITES

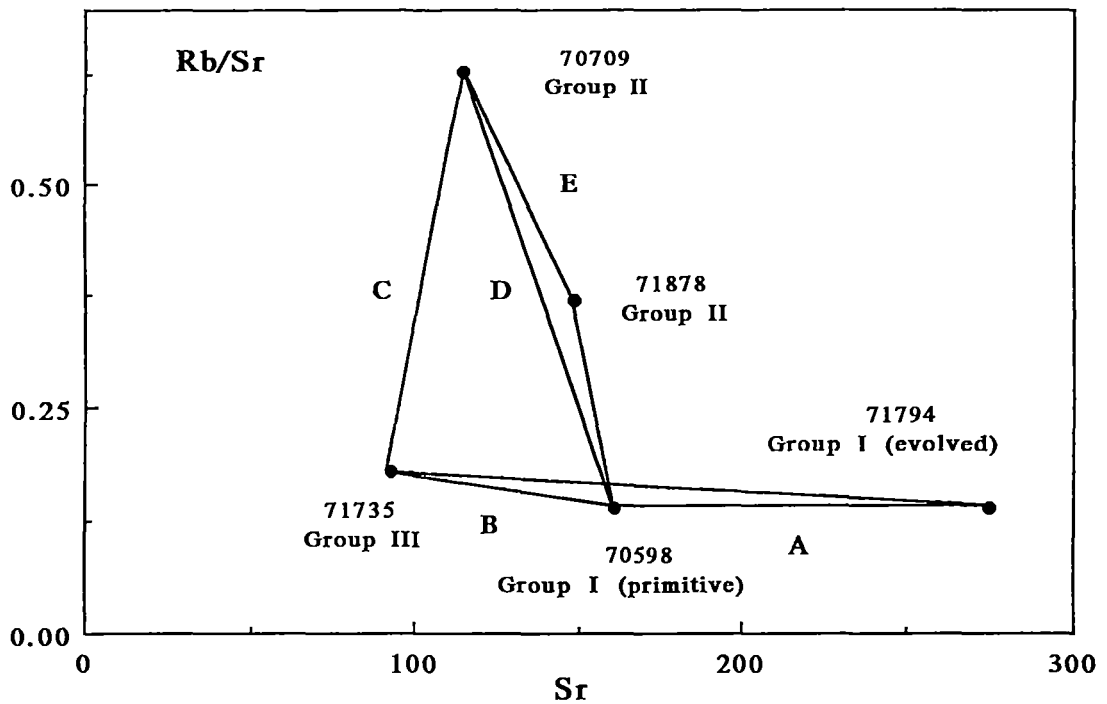


Figure 6.6

Rb/Sr plotted against Sr showing end-members of *Group I, II* and *III* high-Mg tholeiites. Lines between various samples indicate the Rb and Sr variations for endmember samples for which major elements have been modelled using least-squares mixing (Table 6.3 A to E).

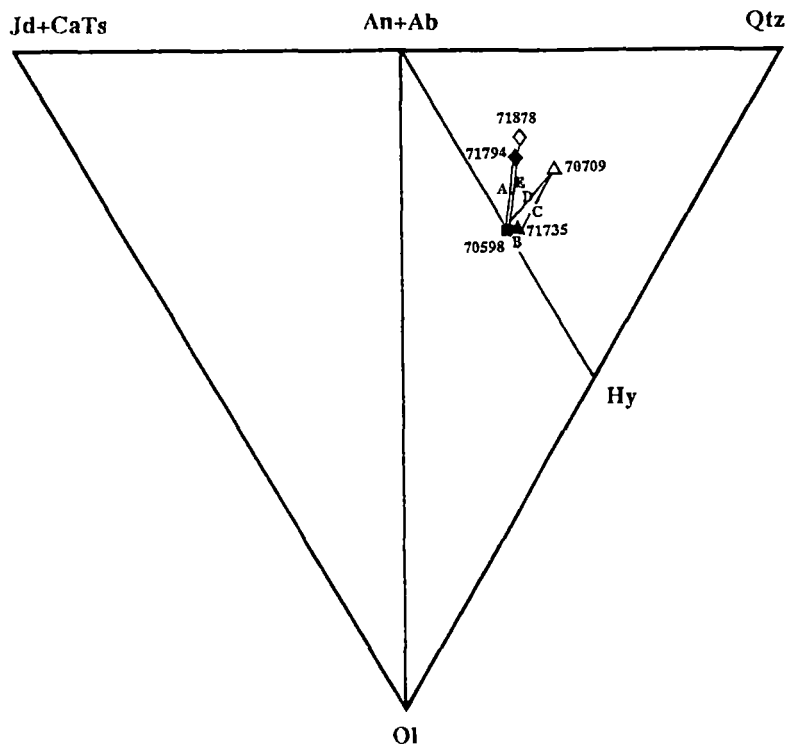


Figure 6.7

Comparison of dykes modelled in terms of possible crystal fractionation c.f. Figure 6.1 and Table 6.3.

A				Estimated	
Sample No.	Reactant	Product A	Product B	Reactant	Difference
Description	70598	71794	Olivine		
Group	primitive	evolved	phenocryst		
	I	I			
SiO2	51.98	54.22	39.57	52.29	-0.31
TiO2	0.59	0.64	0.00	0.56	0.03
Al2O3	11.43	13.19	0.00	11.45	-0.02
FeO	10.17	9.42	14.31	10.07	0.10
MgO	12.25	7.25	45.02	12.24	0.01
CaO	9.17	9.82	0.00	8.52	0.65
Na2O	1.73	2.24	0.00	1.94	-0.21
K2O	0.57	0.93	0.00	0.81	-0.24
P2O5	0.09	0.10	0.00	0.09	0.00
Total	97.98	97.81	98.90	97.97	0.01
Mass%	100.00	86.80	13.20		
Sum of squares					0.6225

B					Estimated	
Sample No.	Reactant	Product A	Product B	Product C	Reactant	Difference
Description	70598	71735	Opx	Cpx		
Group	primitive	ol+opx ph.	phenocryst	microphen.		
	I	III				
SiO2	51.98	52.01	54.84	50.48	51.98	0.00
TiO2	0.59	0.47	0.12	0.57	0.47	0.12
Al2O3	11.43	11.89	1.79	4.15	11.67	-0.24
FeO	10.17	9.86	11.49	9.29	9.85	0.32
MgO	12.25	12.34	28.97	14.10	12.44	-0.19
CaO	9.17	8.99	2.36	20.92	9.26	-0.09
Na2O	1.73	1.53	0.00	0.50	1.50	0.23
K2O	0.57	0.60	0.00	0.00	0.58	-0.01
P2O5	0.09	0.06	0.00	0.00	0.06	0.03
Total	97.98	97.75	99.57	100.01	97.81	0.17
Mass%	100.00	97.21	0.32	2.47		
Sum of squares						0.2572

C						Estimated	
Sample No.	Reactant	Product A	Product B	Product C	Product D	Reactant	Difference
Description	71735	70709	Olivine	Cpx	Plag		
Group	ol+opx ph.	opx-ph.	phenocryst	microphen.	groudmass		
	III	II					
SiO2	52.01	55.92	39.57	50.48	49.96	52.07	-0.06
TiO2	0.47	0.74	0.00	0.57	0.00	0.56	-0.09
Al2O3	11.89	13.00	0.00	4.15	30.14	11.88	0.01
FeO	9.86	10.25	14.31	9.29	0.40	9.75	0.11
MgO	12.34	7.56	45.02	14.10	0.18	12.39	-0.05
CaO	8.99	7.93	0.00	20.92	14.06	9.01	-0.02
Na2O	1.53	1.72	0.00	0.50	3.73	1.54	-0.01
K2O	0.60	1.33	0.00	0.00	0.05	0.89	-0.29
P2O5	0.06	0.13	0.00	0.00	0.00	0.09	-0.03
Total	97.75	98.58	98.90	100.01	98.52	98.18	-0.43
Mass%	100.00	66.53	12.65	11.70	9.12		
Sum of squares							0.1100

D						Estimated	
Sample No.	Reactant	Product A	Product B	Product C	Product D	Reactant	Difference
Description	70598	70709	Olivine	Cpx	Plag		
Group	primitive	opx-ph.	phenocryst	microphen.	groudmass		
	I	II					
SiO ₂	51.98	55.92	39.57	50.48	54.02	52.79	-0.81
TiO ₂	0.59	0.74	0.00	0.57	0.00	0.55	0.04
Al ₂ O ₃	11.43	13.00	0.00	4.15	28.80	11.45	-0.02
FeO	10.17	10.25	14.31	9.29	0.31	9.68	0.49
MgO	12.25	7.56	45.02	14.10	0.04	12.69	-0.44
CaO	9.17	7.93	0.00	20.92	11.63	9.28	-0.11
Na ₂ O	1.73	1.72	0.00	0.50	4.83	1.60	0.13
K ₂ O	0.57	1.33	0.00	0.00	0.33	0.86	-0.29
P ₂ O ₅	0.09	0.13	0.00	0.00	0.00	0.08	0.01
Total	97.98	98.58	98.90	100.01	99.96	98.98	-1.00
Mass%	100.00	62.02	12.88	15.57	9.52		
Sum of squares							1.1777

E						Estimated	
Sample No.	Reactant	Product A	Product B	Product C	Product D	Reactant	Difference
Description	70598	71878	Olivine	Opx	Cpx		
Group	ol+opx-ph.	opx-ph.	phenocryst	phenocryst	microphen.		
	I	II					
SiO ₂	51.98	54.83	39.57	54.84	50.48	52.29	-0.31
TiO ₂	0.59	0.59	0.00	0.12	0.57	0.49	0.10
Al ₂ O ₃	11.43	15.85	0.00	1.79	4.15	11.97	-0.54
FeO	10.17	8.90	14.31	11.49	9.29	9.78	0.39
MgO	12.25	5.59	45.02	28.97	14.10	12.72	-0.47
CaO	9.17	10.07	0.00	2.36	20.92	9.52	-0.35
Na ₂ O	1.73	2.04	0.00	0.00	0.50	1.53	0.20
K ₂ O	0.57	1.11	0.00	0.00	0.00	0.80	-0.23
P ₂ O ₅	0.09	0.11	0.00	0.00	0.00	0.08	0.01
Total	97.98	99.09	98.90	99.57	100.01	99.18	-1.20
Mass%	100.00	72.44	13.74	3.62	10.21		
Sum of squares							0.9733

Table 6.3

Least - squares mixing (GENMIX, Le Maitre, 1980) between various endmembers of Group I, II and III tholeiites. Sample 70598 represents a primitive member of Group I, while 71794 is the most evolved sample in this group. Samples 70709 and 71878 belong to Group II and sample 71735 represents Group III.

dykes (Table 6.3 B), and thus, the *Group II* dykes may be related to *Group I* or *Group III* by similar modelled crystal fractionation (Table 6.3 C, D, E).

Using the modelled major element relationships of Table 6.3 the trace element variation between the various dyke groups may be evaluated assuming Rayleigh crystal fractionation:

$$C_1/C_0 = F(D - 1) \quad (6.1)$$

where F is the degree of crystallization determined from least squares modelling, D is the bulk distribution coefficient for the fractionating phases, and C_1 and C_0 are trace element concentrations in the derivative and parent magmas, respectively.

Trace element models were constrained using the results of GENMIX calculation as listed in Table 6.3. The observed and calculated trace element concentrations are plotted in Figure 6.8 A - B (letters refer to least squares calculations in Table 6.3). Partition coefficients used in the fractionation model are listed in Table 4.5 (Chapter 4). In Figure 6.8 A trace element variations within *Group I* are modelled, showing no close fit between observed and calculated LILE and LREE abundances, while P, Zr, Ti, and Y exhibit a better fit. Calculated concentrations in model 6.8 B (between *Group I* and *III*) and D (between *Group I* and *II*) exhibit large differences for nearly all elements. In modelling variation between *Group II* and *III* a better fit is obtained, with the exception of Rb, K and P, which show much higher concentrations in the natural rock than in the derivative liquid predicted from the calculation (Figure 6.8 C).

6.4.1 Summary

Fractionation of observed phenocryst phases can account for differences in major element geochemistry between *Group I* and *II* and *Group I* and *III* but not their trace element abundances. Even within *Group I*, trace element variations cannot be explained solely by crystal fractionation. For instance the incompatible element Sr,

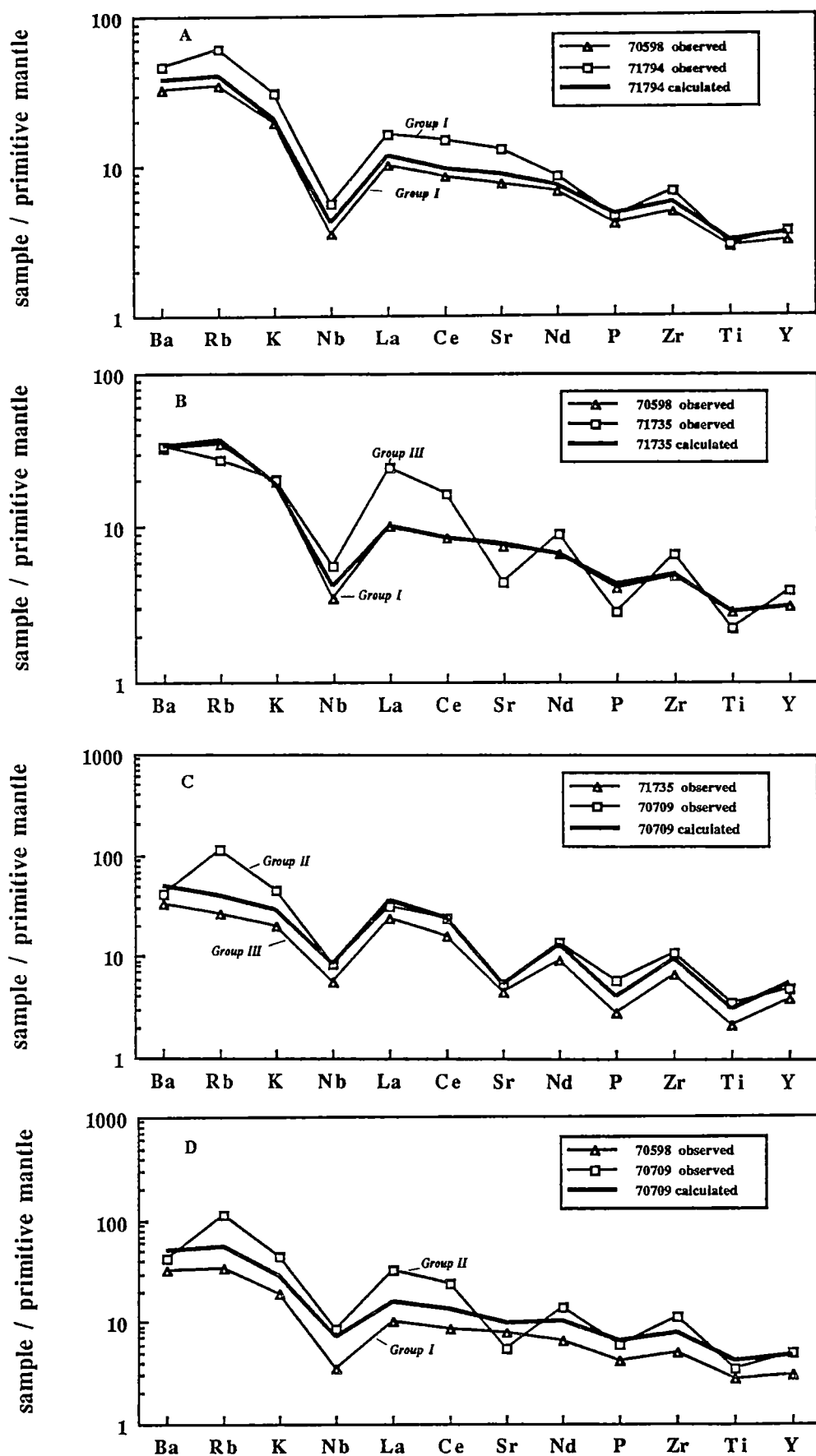


Figure 6.8

Incompatible element abundances predicted by fractional crystallization models. All compositions were normalized to primitive mantle, showing abundances in the natural rock and those calculated using Rayleigh fractionation. (A) within *Group I*, (B) between *Group I* and *III*, (C) between *Group II* and *II* and (D) between *Group I* and *II*.

undergoes a threefold increase in abundances from the most primitive to the most evolved *Group I* sample. This requires more than 50% fractionation and conflicts directly with least squares modelling which suggests olivine fractionation has not exceeded *ca.* 13 vol% (Table 6.3 A).

Differences between observed and calculated Rb (twofold higher in the observed compositions compared to calculated concentrations) and K concentrations of *Group II* also are inconsistent with crystal fractionation alone.

The results of the above modelling suggest that neither of the three Groups are related by simple crystal fractionation. Even when plagioclase is included as a fractionating phase variations in Sr cannot be modelled. Accordingly, processes other than fractional crystallization (e.g. partial melting, crustal contamination) are required to explain the different geochemistry of the individual dyke groups.

6.5 CRUSTAL CONTAMINATION

6.5.1 Introduction

The role of crustal contamination within the high-Mg tholeiitic dyke suite of the Vestfold Hills has been investigated by Sheraton & Black (1981), Collerson & Sheraton (1986). These authors concluded from low initial $^{87}\text{Sr}/^{86}\text{Sr}$ values of 0.7019 ± 0.0011 that contamination of these magmas with crustal-derived radiogenic ^{87}Sr was negligible. Furthermore, they showed that high-Mg tholeiites from the Napier Complex (1000 km to the west of the Vestfold Hills) have virtually identical trace element characteristics and low initial $^{87}\text{Sr}/^{86}\text{Sr}$ (0.7020 ± 0.0008). This isotopic consistency over such a considerable area was considered to be good evidence against widespread crustal assimilation, and accordingly geochemically variations were ascribed to mantle source characteristics (Kuehner, 1986).

The low initial $^{87}\text{Sr}/^{86}\text{Sr}$ values reported by Sheraton & Black (1981) and Collerson & Sheraton (1986), however, are not necessarily evidence for the absence of crustal contamination as unradiogenic Sr-isotope ratios may be a feature of the lower crust (Weaver & Tarney, 1981). Sun et al. (1989), for example, have modelled crustal contamination of a hypothetical parental Kambalda komatiite by AFC, using an initial $^{87}\text{Sr}/^{86}\text{Sr}$ value of 0.7007 for the magma and 0.7027 for the crustal contaminant, resulting in an initial $^{87}\text{Sr}/^{86}\text{Sr}$ of 0.7020 for the product SHMB.

The attempt to model major and trace element variations of the high-Mg tholeiites from the Vestfold Hills by crustal assimilation processes was considered for two reasons: (1) trace element variations within *Group I* and between the three high-Mg tholeiitic groups are not consistent with fractional crystallization of observed phenocrysts and (2) the high-Mg tholeiites have trace element characteristics, such as LILE-enrichment, Nb, Sr, P and Ti depletion, characteristics which are common for crustal rocks, suggesting crustal assimilation as a possible process.

Crustal contamination models were considered to model variations (1) within *Group I* (2) between *Group I* and *II*, (3) between *Group I* and *III* and (4) the

derivation of *Group I* from an uncontaminated parent. The last approach recognizes that *Group I* high-Mg tholeiites are the oldest dykes of this suite but that they may not be primary, possibly having been contaminated during emplacement through continental crust.

6.5.2 Assimilation-Fractional Crystallization Model

To assess the possibility of crustal contamination of the high-Mg tholeiitic magma, crustal contamination was modelled using the coupled assimilation-fractional crystallization model (AFC) proposed by De Paolo (1981). AFC considers assimilation of wall-rock to be driven by the heat of crystallization. De Paolo (1981) derives two equations to describe the process mathematically when: (1) the assimilated mass (M_a) is equal the mass crystallized (M_c) ($M_a = M_c$) and (2) $M_a \neq M_c$.

(1) For $r = 1$ ($r = M_a/M_c$)

$$C_m/C_m^0 = (C_a/DC_m^0) (1 - \exp(-DM_a/M_m)) \quad (6.2)$$

where C_m^0 is the starting concentration in the magma, M_m is the mass of magma, C_m the concentration of an element in the magma, C_a the concentration in the assimilant and D the bulk solid/liquid partition coefficient.

(2) For $r \neq 1$

$$C_m/C_m^0 = F^{-z} (r/(r - 1)) (C_a/zC_m^0) (1 - F^{-z}) \quad (6.3)$$

where $F = M_m/M_m^0$ (liquid remaining) and $z = (r + D - 1)/(r - 1)$.

6.5.3 Choice of Assimilant

The Archaean crust of the Vestfold Hills is composed dominantly of felsic orthogneisses. The most abundant gneiss unit is the Crooked Lake Gneiss, a felsic orthogneisses, which intruded the Vestfold Hills terrane at about 2450 Ma (Collerson & Sheraton, 1986). In the late Archaean and early Proterozoic the gneisses, now exposed, were at considerable depths (25 - 33 km), as they have undergone a granulite-facies metamorphic event indicating pressures between 8 - 10 kbar (Collerson et al., 1983 b). Any AFC processes, could then involve the assimilation of the felsic gneisses by the high-Mg tholeiitic magma at these depths.

The Crooked Lake Gneiss is variable in composition, exhibiting a range in composition from granitic compositions (73.5 wt% SiO₂) to dioritic compositions with 53 wt% SiO₂ (Collerson & Sheraton, 1986). In Figure 6.9 various Archaean and Proterozoic gneisses (Sheraton & Black, 1988) from the East Antarctic shield are plotted for comparison, exhibiting common features such as Nb, Sr and Ti depletion. The gneisses show differences mainly in Rb and Sr and in Nb to a minor extent only.

In modelling crustal contamination two granitic gneiss compositions were chosen: a felsic Crooked Lake Gneiss and a felsic gneiss composition from the Napier complex, the latter exhibiting a higher Rb and lower Sr concentrations in comparison to the Crooked Lake Gneiss. These composition were chosen for a number of reasons: (1) the felsic Crooked Lake Gneiss is an abundant rock type in the Vestfold Hills; (2) assimilation of crust is most likely to occur, when the melting point of the assimilant is significantly lower than the magma temperature, in other words, in comparison to mafic rocks, siliceous material (such as the selected compositions) can be more easily assimilated by a basaltic magma; (3) the greater LILE abundances in felsic material relative to mafic material means that a much smaller amount of felsic material (Sheraton & Black, 1988, see Table 6.4) needs to be assimilated for the same geochemical effect and (4) trace element characteristics such as Nb, P, Ti depletion in the Crooked Lake Gneiss as well as Sr depletion and Rb enrichment relative to adjacent elements on the

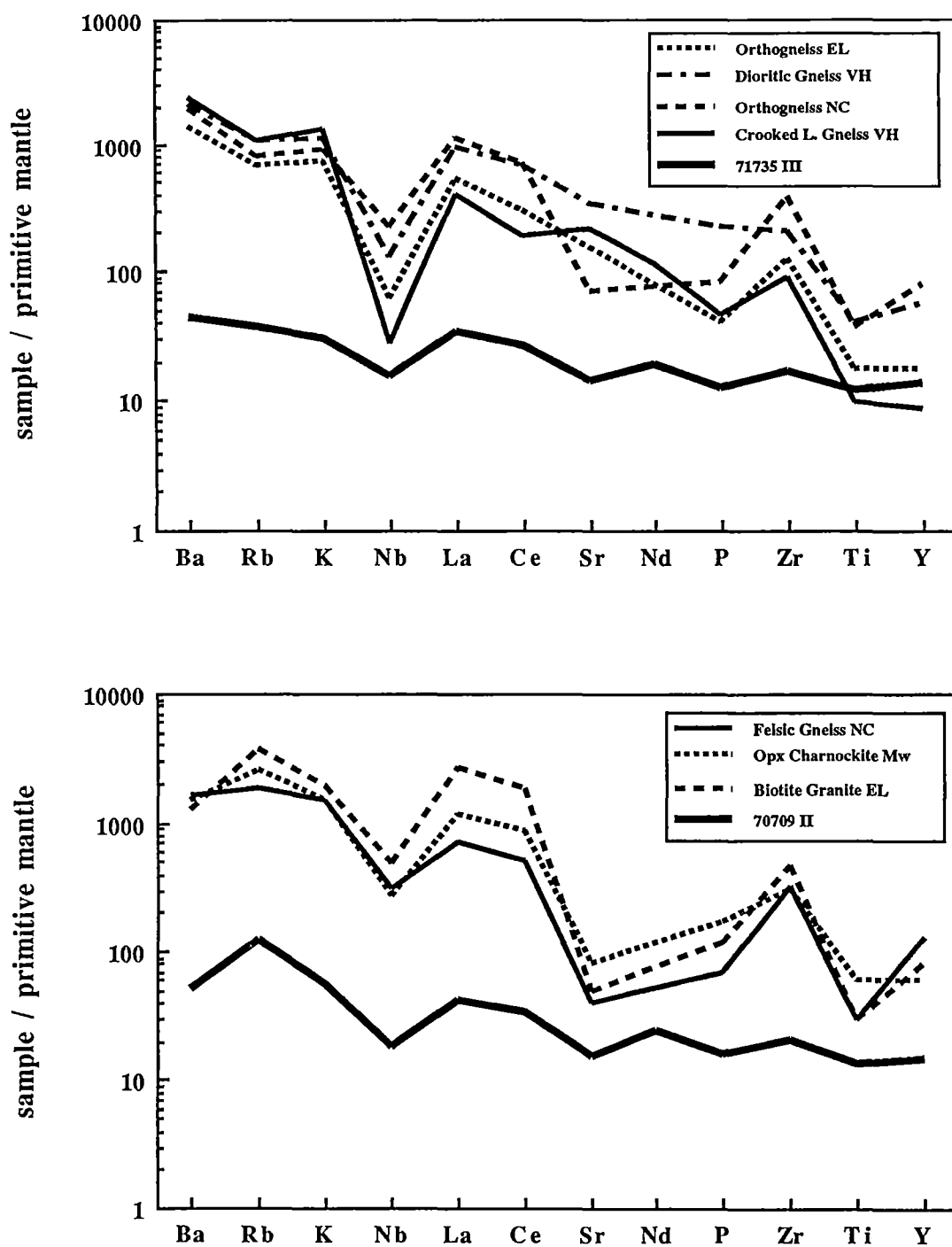


Figure 6.9

'Spidergram' of incompatible trace elements (primitive mantle normalized following Sun et al. 1989) of various gneisses, granulites and granites from the East Antarctic shield in comparison to *Group II* and *III* high-Mg tholeiites. Abbreviations: EL - Enderby Land, VH - Vestfold Hills, NC - Napier Complex, Mw - Mawson.

PARENT MAGMA AND CRUSTAL ASSIMILANT COMPOSITIONS

Sample Rock Type Locality	70598 HMT VH	Crooked Lake Gneiss VH	Felsic Gneiss NC
Major elements wt%			
SiO ₂	52.98	73.50	70.53
TiO ₂	0.60	0.21	0.75
Al ₂ O ₃	11.65	13.33	12.42
FeO	10.33	1.62	4.98
MnO	0.17	0.02	0.06
MgO	12.48	0.78	0.85
CaO	9.35	2.25	2.31
Na ₂ O	1.76	3.42	2.93
K ₂ O	0.58	4.02	4.54
P ₂ O ₅	0.09	0.10	0.15
Total	99.99	99.25	99.52
Mg#	68.3	46.2	23.3
Ba	227	1644	1131
Rb	22	67	117
Nb	3	2	22
Sr	161	442	76
La	7	27	48
Ce	15	33	90
Nd	9	15	-
Zr	55	97	358
Y	14	4	61
Cr	1224	16	35
Ni	310	9	15

Table 6.4

Starting composition (70598) represents Group I high-Mg tholeiites in AFC modelling with Crooked Lake Gneiss from the Vestfold Hills (VH) and felsic gneiss from the Napier Complex (NC). Data for the gneisses are taken from Sheraton & Black (1988).

spidergram (Figure 6.9) in the felsic gneiss from the Napier complex, are similar features which the high-Mg tholeiites from the Vestfold Hills have.

6.5.4 Modelling

The trace and incompatible minor element results from AFC modelling are shown in Figure 6.10 A - D with model parameters given in Table 6.6. Contamination of the high-Mg tholeiitic magma may have occurred prior to the emplacement of the first high-Mg *Group I* dykes and/or between the first and following magmatic events from this suite. An 'uncontaminated' parent magma (Figure 6.10 A) was reproduced sample 70598 (*Group I*) by modelling with the two granitic gneiss assimilant compositions. For the AFC parameters $r = 0.4$, $F = 0.75$ and K_D 's as shown in Table 4.5, parent magma compositions were obtained exhibiting SiO_2 content of 49.2 and 49.9 wt%, low TiO_2 (0.4 and 0.43 wt%) and high MgO (19.8 and 20.8 wt%). The estimated parent liquid compositions are compared to some high-Mg basaltic compositions from the literature in Table 6.5. Major element concentrations of these model parent compositions are similar to basaltic komatiites from Belingwe Greenstone Belt (Nisbet et al., 1977) and basaltic komatiite from Yakabindie (Naldrett & Turner, 1977). Compared to a picritic composition from Karoo (Duncan et al., 1984) all major elements show a close fit with the exception of TiO_2 , which is 2.5 wt% higher in the Karoo picrite average. Incompatible trace element concentrations of the Karoo picrite are also unlike abundances calculated for a *Group I* parent (Table 6.5).

Variations in major and minor elements within *Group I* were obtained by modelling the evolved sample 71794 by adding the crustal component to sample 70598, the primitive endmember in this group and fractionating olivine and orthopyroxene. Mantle normalized trace element patterns exhibit a close fit between calculated and observed concentrations (Figure 6.10 B). This is consistent with Ni and Cr concentrations which vary from 310 ppm Ni and 1224 ppm Cr in sample 70598 to 100 ppm Ni and 438 ppm Cr in sample 71794 (Figure 6.11). The variations from high

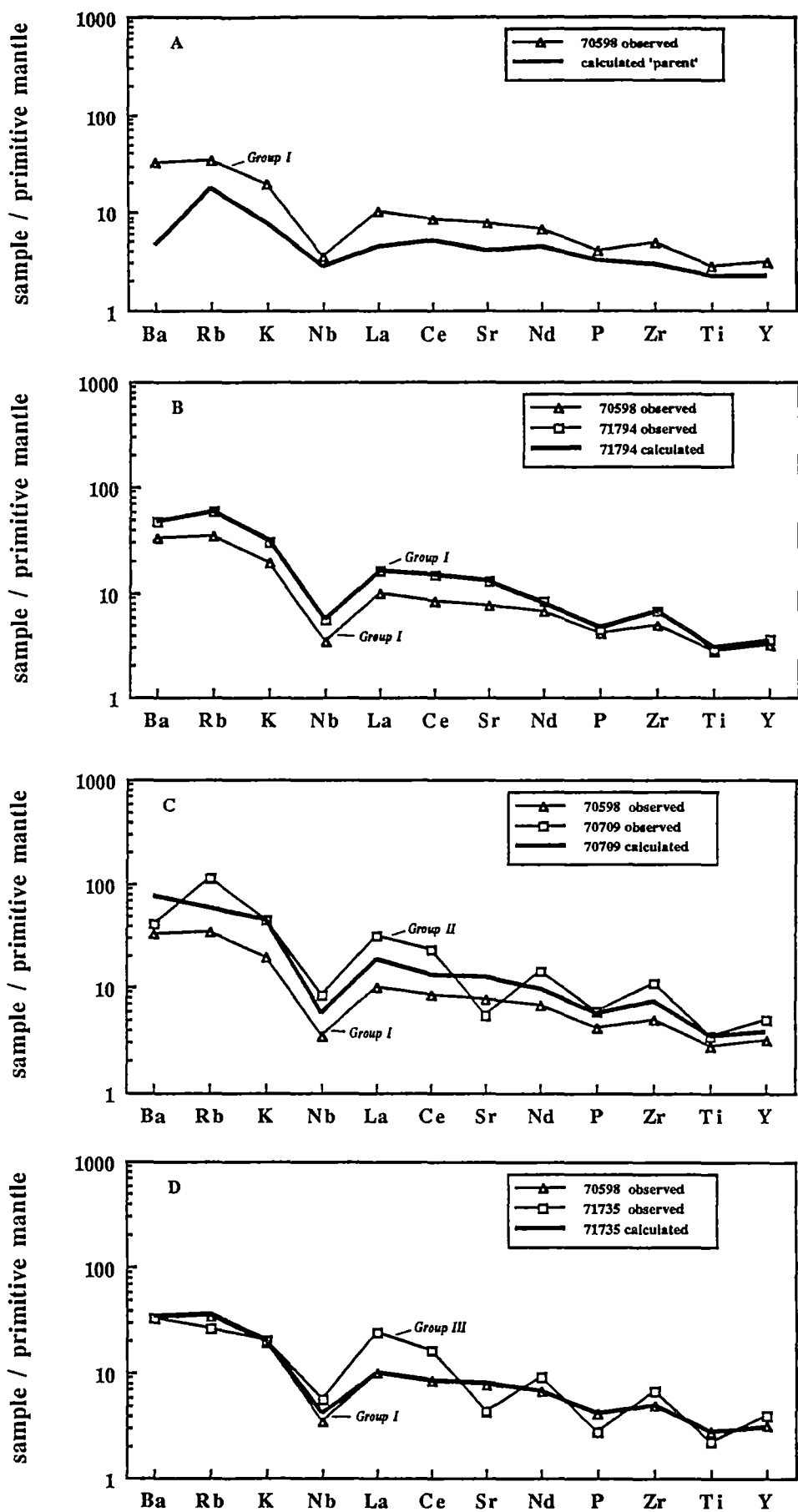


Figure 6.10

'Spidergram' of primitive mantle normalized (Sun et al., 1989) incompatible trace elements showing various AFC models (see text for discussion).

PARENTAL MAGMA COMPOSITIONS

Sample Rock Type	A basaltic komatiite	B basaltic komatiite	C Karoo picrite	D calculated	E calculated
Major elements wt%					
SiO ₂	49.90	49.00	49.97	49.43	49.22
TiO ₂	0.43	0.52	3.07	0.44	0.43
Al ₂ O ₃	8.18	9.73	8.22	8.84	8.66
FeO	11.92	11.40	10.80	11.52	11.60
MnO	0.21	0.24	0.16	0.19	0.19
MgO	19.70	17.80	15.52	20.26	20.77
CaO	8.87	8.71	7.07	7.98	7.89
Na ₂ O	0.25	1.18	1.43	1.21	1.17
K ₂ O	0.15	0.06	2.10	0.04	0.01
P ₂ O ₅	0.04	0.00	0.45	0.06	0.06
Total	99.65	98.64	98.79	99.97	100.00
Mg#	74.7	73.6	71.9	75.8	76.1
Ba			917	1	33
Rb			55	1	11
Nb			19	2	2
Sr			1000	108	84
Zr			402	1	33
Y			28	1	10
Cr			804	7550	4961
Ni			827	10770	5000

Table 6.5

Data taken from Nisbet et al. (1977) for composition A (estimated parental composition), from Naldrett & Turner (1977) for composition B and (C) an average of picrites from Karoo Province (Duncan et al., 1984). Data in D and E are estimated compositions from this study, using felsic gneiss from the Napier Complex (D) and Crooked Lake Gneiss (E).

WHOLE ROCK COMPOSITIONS MODELLED BY AFC

Sample	70709 observed	70709 calculated	71735 observed	71735 calculated	71794 observed	71794 calculated
modelling	Group I to II		Group I to III		Group I to I	
AFC parameters	r=0.45, F=0.83		r=0.4, F=0.99		r=0.26, F=0.84	
Major elements wt%						
SiO2	56.74	57.33	53.12	53.11	55.35	54.73
TiO2	0.75	0.71	0.48	0.60	0.65	0.68
Al2O3	13.19	12.74	12.14	11.76	13.46	13.65
FeO	10.40	10.05	10.06	10.28	9.62	9.58
MnO	0.17	0.20	0.17	0.17	0.15	0.16
MgO	7.67	7.88	12.60	12.20	7.40	7.67
CaO	8.05	7.68	9.18	9.40	10.02	10.42
Na2O	1.54	2.16	1.56	1.78	2.29	2.15
K2O	1.35	1.13	0.61	0.60	0.95	0.85
P2O5	0.13	0.13	0.06	0.09	0.10	0.11
Total	100.00	100.00	100.00	100.00	100.00	100.00
Mg#	56.8	58.3	69.1	67.9	57.8	58.8

Table 6.6

Comparison of observed and by AFC modelled whole rock compositions. A primitive Group I sample (70598) was used as starting composition, felsic Crooked Lake Gneiss as contaminant and olivine and orthopyroxene were fractionating phases. AFC parameters are give for each calculated composition (s.o.). Partition coefficients used in AFC model are listed in Table 4.19.

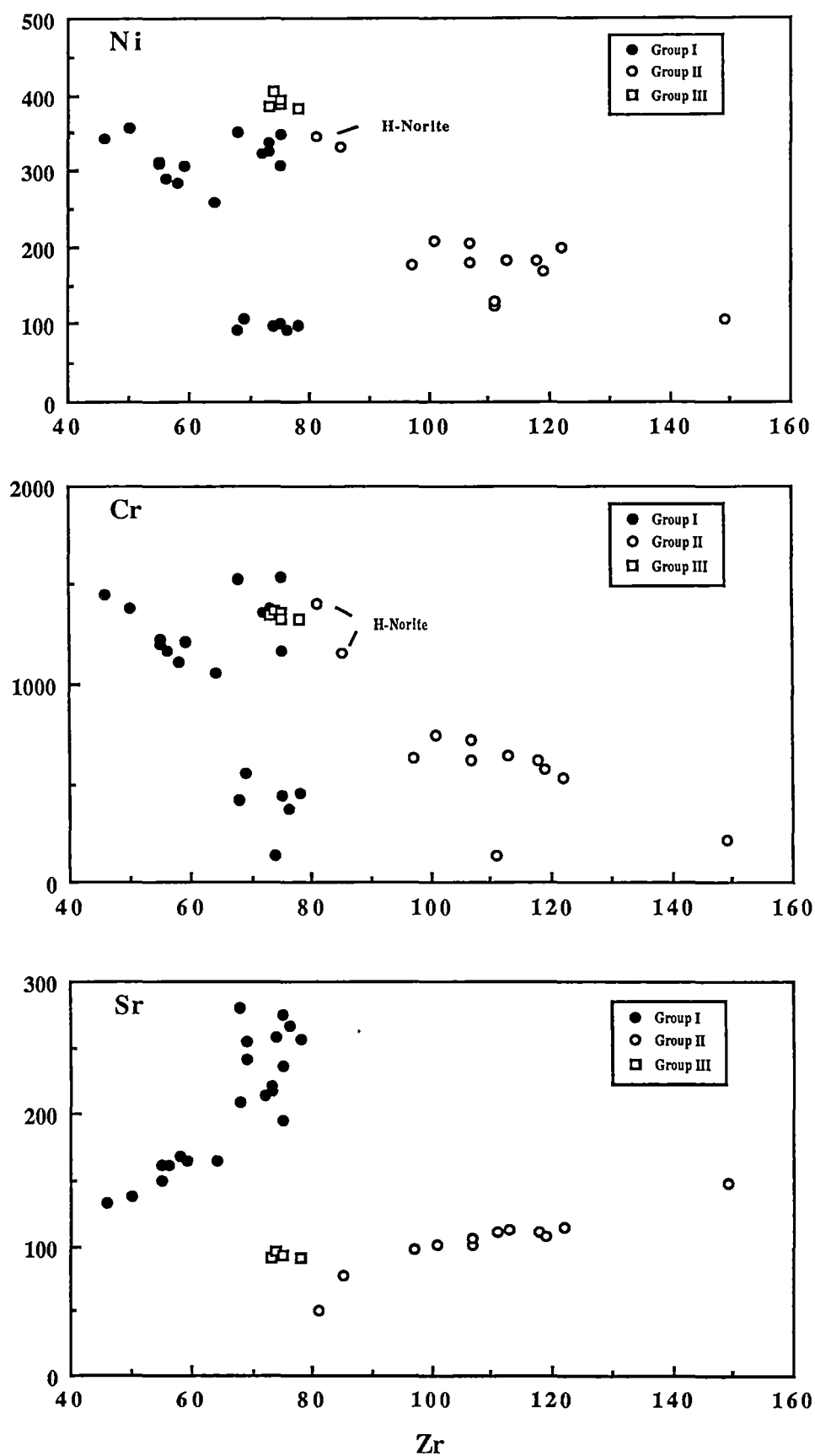


Figure 6.11

Ni, Cr and Sr plotted against Zr as fractionation index distinguishing between *Group I*, *II* and *III* tholeiites (see text for discussion).

Cr and Ni and low LREE and Sr in primitive samples to low Cr and Ni and high LREE and Sr in evolved samples, is consistent throughout *Group I*. It is suggested here that trace element variations within *Group I* are consistent with the assimilation and crystal fractionation (AFC) model. This result leads to the possible subdivision of *Group I* into a primitive *Group I* and evolved and contaminated *Group Ia*.

In modelling trace element variations between *Group I* and *II* and between *Group I* and *III*, the results show strong differences between calculated and observed compositions, particularly for elements such as LREE, Sr, P and Ti (Figure 6.10).

6.5.5 Discussion

A model of coupled assimilation of felsic crust and fractional crystallization (AFC) model may account for observed variations in *Group I*. Variations in major and minor elements between *Groups I, II* and *III* are not consistent with the process of assimilation of crustal material combined with fractional crystallization of olivine and orthopyroxene or olivine, clinopyroxene and plagioclase (Table 6.6, Figure 6.10). The assimilation of Sr-rich felsic crust cannot produce the negative Sr anomalies which are characteristic for *Group II* and *III* tholeiites, even when plagioclase fractionation is considered. To produce such Sr depletion a contaminant with much lower Sr than observed crust would be required. The modelling of LREE enrichment and depletion in P and Ti, features which the high-Mg tholeiites and the Crooked Lake Gneiss have in common, seem not to be the result of the AFC process. It is, however, suggested that as AFC can explain the within *Group I* chemical variation, it may also account for the composition of the more primitive *Group I* as derivatives by AFC from uncontaminated primary magmas which are geochemically similar (major elements) to basaltic komatiites.

The similarities of trace element patterns in 'spidergrams' comparing Archaean felsic crust and Proterozoic high-Mg tholeiites, both exhibiting large negative Nb-anomalies, depletion in P and Ti and high contents of incompatible LILE, may argue for crustal contamination as a likely process. However, this model has two major

disadvantages: (1) the enrichment of the melt in LILE and LREE would require crustal assimilation of more than 50 - 60%, which (2) requires a large amount of excess energy. Even considering a hot (1500 - 1600° C) komatiitic magma, such extensive assimilation of crustal material is most unlikely to occur. Moreover, there are some inconsistencies which suggest that crustal contamination is not an important process in the genesis of high-Mg tholeiites. In the case of the Vestfold Hills tholeiites the observed negative Sr-anomalies in *Group II* and *Group III*, as well as the low Sr_I of 0.7002 (Sheraton & Black, 1981; Collerson & Sheraton, 1986) do not support crustal contamination, as both the magma and the contaminant would require very low Sr_I .

A further argument against significant assimilation of crust is provided by the high abundance of PGE's concentrations (platinum group elements) in the high-Mg tholeiites. PGE's are sensitive to crustal contamination, as this process would lead to changes in silica activity, fO_2 and fS_2 . For instance increased crustal contamination would increase silica-activity and fO_2 and decrease fS_2 which would have the effect of achieving sulphur saturation in a previously undersaturated basaltic magma. PGE's would immediately partition strongly into the sulphide melt and the remaining silicate melt would be impoverished in these elements. Assuming separation of a sulphide phase from the silicate melt (e.g. crystallization of sulphides followed by crystal settling and accumulation on the magma chamber floor), the remaining magma would be depleted in PGE's. On the other hand, if the sulphide phase does not separate from the silicate melt, depletion in PGE concentrations would not occur and consequently crustal contamination, postulated to trigger the sulphur saturation in a basaltic magma, would not be detectable. Considering the much greater density of a sulphide phase to a silicate melt, however, sulphide separation is most likely.

It was shown that chilled margin samples of various high-Mg tholeiite dykes, including *Group I*, *II* and *III*, have similar PGE abundances. If crustal contamination is responsible for the variations between these magmatic episodes, then it is likely that the different groups would exhibit variations in PGE concentrations. The fact that variations in PGE concentrations are not observed suggests that crustal contamination

was not significant. As already pointed out by previous workers (Sheraton & Black, 1981; Collerson & Sheraton, 1986), the consistency of trace element abundances as well as initial $^{87}\text{Sr}/^{86}\text{Sr}$ over a large area, is also evidence for the minor role of crustal contamination.

6.6 HIGH-MG THOLEIITES, PRIMARY MAGMAS ?

Previous sections have considered whether high-Mg tholeiites are primary magmas or modified from more primitive 'komatiitic magmas' by secondary processes. This section seeks to evaluate evidence for primary characteristics among the spectrum of high-Mg tholeiite compositions from the Vestfold Hills.

Compatible trace elements such as Cr and Ni have been used to identify primary magmas (e.g. Frey et al., 1978). It was argued that crystal fractionation of olivine and pyroxenes in a basaltic magma would decrease abundances of compatible elements, so that liquids with high compatible trace element abundances have not undergone major crystal fractionation and are therefore inferred to be primary magmas.

Criteria such as $\text{Al}_2\text{O}_3/\text{CaO}$ and high Mg# of the whole rock can provide information of a magma being primary or not. $\text{Al}_2\text{O}_3/\text{CaO}$ of the upper mantle is believed to be close to that of chondrites (~ 1.2) (Frey et al., 1978). On the other hand, liquids derived from a primitive mantle with compositions of Mg# 88 - 89 have Mg# between 68 - 75 (Frey et al., 1978) for up to 30% melting (using $K_D^{\text{Fe/Mg}}_{\text{ol/liq}} = 0.3$, Roeder & Emslie, 1970; Jaques & Green, 1979). Applying these criteria to the various high-Mg tholeiitic groups it becomes apparent that only primitive (uncontaminated) *Group I* (*Group Ia* is excluded) and *Group III* tholeiite dykes have compositions consistent with being primary melts, showing high Mg# 66 - 70, high Ni 250 - 350 ppm and chondritic $\text{Al}_2\text{O}_3/\text{CaO}$ ratios (Figure 6.12).

In comparison to *Group I*, the more evolved *Group Ia* exhibits lower Mg# (57 - 61), Ni (90 - 110) as well as low Cr concentrations (Figure 6.12). A similar variation can be observed within *Group II* and *Ila* (latter indicated as 'Norites' in Figure 6.12)

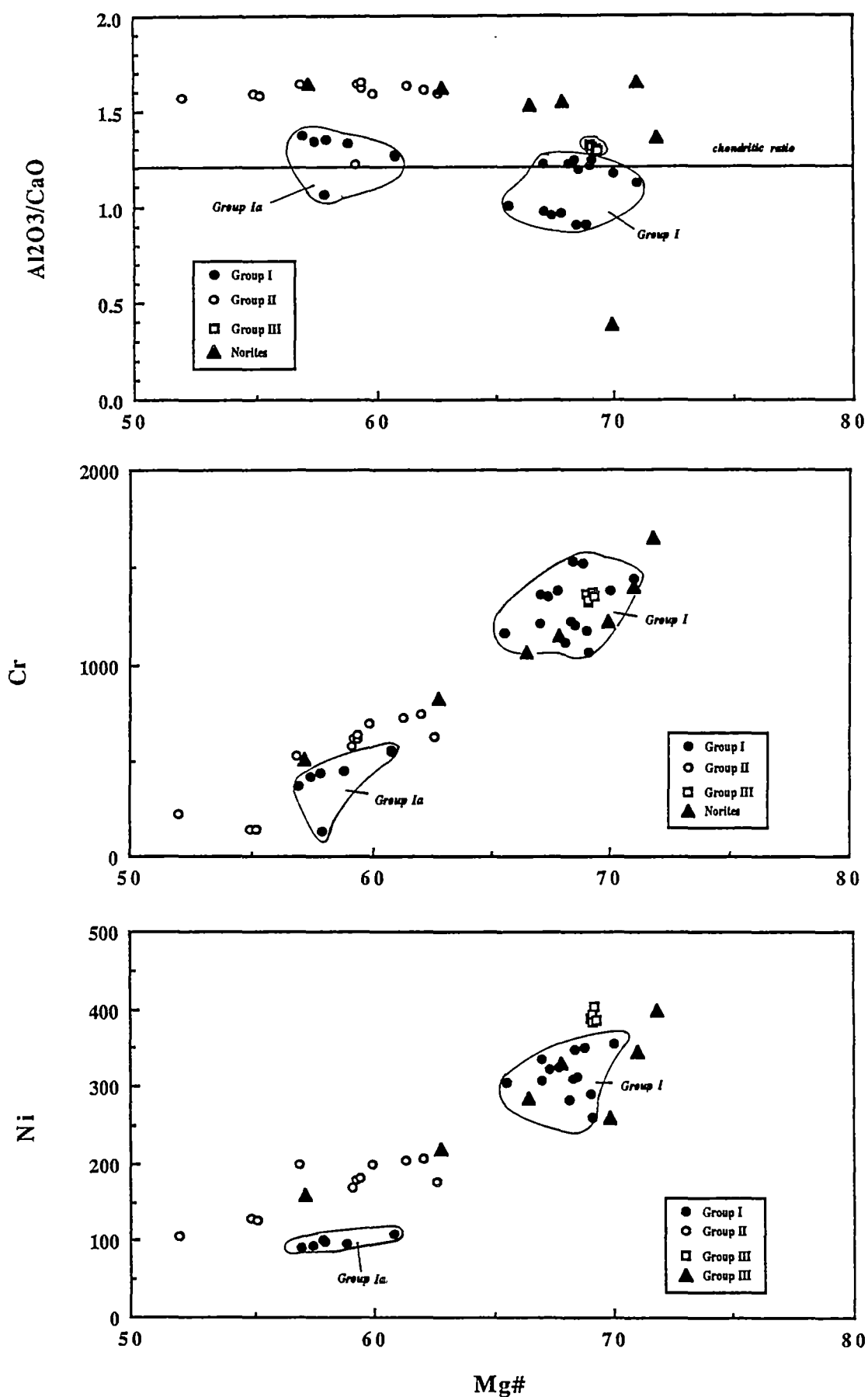


Figure 6.12

Ni, Cr and Al₂O₃/CaO plotted against Mg# as fractionation index distinguishing between *Group I, Ia* and *II* (including the norites) and *III* tholeiites (see text for discussion).

where Ni ranges from 180 - 420 ppm, Cr from 500 - 1700 ppm and Mg# from 52 - 72 (Figure 6.12). It was argued (Chapter 4) that variations within and between *Groups II* and *Ila* (norites and associated 'fine grained dykes') are the result of orthopyroxene accumulation and fractionation as well as the accumulation of sulphides (*Rubbly Norite*), a conclusion which was supported by geochemistry and petrography. Petrographical evidence suggests that variations in Cr and Ni between *Group I* and *Ia* are not the result of accumulation of observed phenocryst phases alone but are consistent with the more Mg-rich compositions being parental. The high Cr concentrations in *Group I* are accompanied by the presence of Cr-spinel inclusions in olivine and orthopyroxene phenocrysts (Chapter 3). Petrographical observations indicate a primary status of the Cr-spinels. The low Mg# of the chromites from *Group I* (~ 24), however, is inconsistent with their occurrence in bulk rock composition of Mg# > 65. This may indicate extensive subsolidus Fe/Mg re-equilibration between chromites and mafic silicates (Irvine, 1967; Roeder et al., 1979; Ozawa, 1983). In contrast to the inferred Fe/Mg exchange and re-equilibration, most chromites appear to have retained their Cr content and Cr# (c.f. Roeder et al., 1979).

Chromite saturation in basaltic liquids commonly occurs at levels of 200 - 300 ppm Cr (Hill & Roedder, 1974; Sigurdsson & Schilling, 1976) but is very sensitive to fO_2 (Ballhaus et al., 1991). The restriction of chromite inclusions to within the phenocryst phases, while the whole rock contains up to 1500 ppm Cr (*Group I*) suggests low fO_2 conditions.

In summary: high-Cr concentrations in *Group I* and *Group III* are considered primary characteristics indicating a Cr-rich mantle source. These groups also show high Mg# and chondritic Al_2O_3/CaO ratios suggesting primary nature of these melts. In contrast *Group Ia, II* and *Ila* have geochemical characteristic which show they are not primary.

Kuehner (1986, 1989) also concluded that *Group I* tholeiites may represent primary magmas, which have fractionated olivine and orthopyroxene only. Following this he estimated the depth of magma segregation for the high-Mg tholeiites, in using

the most primitive orthopyroxene composition in this suite and calculating a liquid composition in equilibrium with the orthopyroxene. Using a $K_D^{opx_{cryst}/liq} = 0.3$ (Jaques & Green, 1979), orthopyroxene (Mg# 91.2) requires a liquid of Mg# ~ 75. Using an observed composition of Mg# 71, Kuehner argued that this liquid had only experienced minor fractionation and calculated a parental or primary liquid with Mg# ~ 75. The estimated liquid composition was compared with experimental studies of Falloon & Green (1987, 1988), which are reversals of the anhydrous peridotite melting studies of Jaques & Green (1980). The calculated liquid composition (Mg# ~ 75) plots between the 10 and 15 kbar olivine - orthopyroxene cotectics (Kuehner, 1989). This pressure was interpreted to represent the depth of magma segregation, in melting a primitive peridotitic mantle and leaving a harzburgitic residue. Thus it is possible to support the primary character of *Group I* melts on the grounds that their major element geochemistry suggests equilibration at mantle P,T conditions.

6.7 PARTIAL MELTING

6.7.1 Introduction

In this section the role of partial melting in producing the geochemical characteristics of the Vestfold Hills high-Mg tholeiites is examined.

It has been suggested in section 6.6 that *Group I* and *Group III* tholeiites are consistent with them approaching primary melt compositions. *Group I* and *Group III* tholeiites have geochemical characteristics such as LILE- and Sr-depletion in *Group III* relative to *Group I*, and it was suggested that geochemical variations between these groups are inconsistent with crystal fractionation or AFC processes. If the variations in *Group I* and *Group III* are the result of partial melting of the same compositional source then the presence of Sr-depletion in *Group III* suggests that plagioclase is a residual phase and the absence of Sr-depletion in *Group I* indicates a higher degree of melting of a plagioclase-bearing source in comparison to lower degree of melting for

Group III. Alternatively the two Groups may be derived from different mantle compositions. Melting of a plagioclase-bearing source to produce high-Mg tholeiitic magmas is supported by estimates of magma segregation which is considered to be relatively shallow depths around 33 - 50 km (Kuehner, 1986, 1989, see section 6.1). It is also well accepted that tholeiitic magmas derived from depth between 10 and 20 kbar may be a consequence of relatively large degree of melting (15 - 20%) (Green, 1971).

Partial melting models are poorly constrained with respect to source compositions and their mineralogy, degree of melting, mineral/melt partition coefficients, as well as the physical processes of melting and melt dynamics (e.g. melt retention, migration and extraction). For example McKenzie (1984) and Ribe (1985) pointed out that melts with a volume greater than a few percent (3%) are unlikely to be retained in the mantle. In contrast Richter (1986) estimated the volume of melt to be retained in the mantle to be around 10%.

Partial melting has been modelled in various ways and for example Gast (1968) and Shaw (1970) derived different equations describing trace element behaviour assuming (1) equilibrium or batch melting, in which a melt equilibrates with its source at the final degree of melting prior to removal or (2) fractional (Rayleigh) melting where melting proceeds while melt fractions are continuously removed from the source (Shaw, 1970).

For non-modal equilibrium melting the concentration of a trace element in the melt (C_1) relative to the original composition in the source (C_0) is expressed by:

$$C_1/C_0 = 1/(D_0 + F (1 - P)) \quad (6.4)$$

where D_0 is the bulk distribution coefficient, F the melt fraction and P is the bulk partition coefficient based on the phase proportions entering the melt.

Rayleigh melting is expressed by the equation:

$$C_l/C_o = 1/D_o (1 - PF/D_o)^{(1/P - 1)} \quad (6.5)$$

6.7.2 Partial Melting Modelling

In this study partial melting was modelled assuming non-modal equilibrium melting and it is considered that the poor constraints on partial melting (e.g. source composition) far outweigh any differences due to choice of partial melting equation.

Mineral/melt partition coefficients are given in Table 6.7 and mineral and melting modes of the mantle used in the partial melting model are listed in Table 6.8.

In a first approach trace element concentrations in a source were modelled assuming (a) that sample 70533 (*Group I*) is derived by 15% melting of a primitive mantle with a composition of 55.2 vol% olivine, 17.8 vol% clinopyroxene, 24.7 vol% orthopyroxene and 2.3 vol% spinel (Table 6.8 A; Kelemen et al., 1990) and (b) derived by 15% melting of a plagioclase lherzolite with 63 vol% olivine, 10 vol% clinopyroxene 19 vol% orthopyroxene and 8 vol% plagioclase. The results were normalized to primitive mantle (Sun et al., 1989) and are plotted in 'spidergram' (Figure 6.13). Calculated trace element abundances for the source assuming that sample 70533 is derived by 15% melting are near identical for both mantle mineralogies, a spinel lherzolite and plagioclase lherzolite. In comparison to primitive mantle abundances (Sun et al., 1989) trace element concentrations of these sources show flat HREE patterns, are enriched in LILE and LREE (La, Ce) and depleted in Nb, P and Ti (Figure 6.13). The estimated source composition is compared with various mantle compositions in Figure 6.14 (observed and calculated source compositions are listed in Table 6.9. Trace element abundances observed in metasomatized spinel lherzolite from Western Victoria (Yaxley pers. comm.) and peridotite nodules from South Africa (Erlank et al., 1987) have features such as Nb, Sr, Ti depletion and are enriched in LILE and LREE relative to HREE. However, none

MINERAL DISTRIBUTION COEFFICIENTS

Elements	Olivine	Cpx	Opx	Spinel	Plagioclase
Ba	0.0010	0.0500	0.0010	0.0001	0.2300
Rb	0.0010	0.0500	0.0010	0.0001	0.1000
K	0.0010	0.0500	0.0010	0.0001	0.1700
Nb	0.0010	0.1000	0.1500	0.0001	0.0100
La	0.0020	0.0690	0.0010	0.0006	0.1800
Ce	0.0005	0.0980	0.0030	0.0006	0.1200
Sr	0.0010	0.2000	0.0100	0.0001	1.8000
Nd	0.0010	0.1800	0.0065	0.0006	0.0810
P	0.0010	0.0100	0.0010	0.0006	0.0810
Zr	0.0010	0.1000	0.0300	0.0700	0.0100
Ti	0.0100	0.3000	0.1000	0.1500	0.0450
Y	0.0010	0.3000	0.0400	0.0001	0.0250
Sm	0.0013	0.2600	0.0100	0.0006	0.0670
Eu	0.0015	0.3100	0.0130	0.0006	0.3400
Gd	0.0015	0.3000	0.0160	0.0006	0.0630
Dy	0.0015	0.3000	0.0220	0.0015	0.0550
Yb	0.0015	0.2800	0.0490	0.0045	0.0670

Table 6.7

Mineral distribution coefficient of trace elements used in partial melting models. Distribution coefficients were taken from compilation of Cox et al. (1984), Dy from Hanson (1980) for spinel from Kelemen et al. (1990) (REE only and trace elements were assumed to be highly incompatible) and from Jenner (pers. comm.) for plagioclase.

MINERAL AND MELTING MODES

Minerals	A		B	
	Spinel Lherzolite vol%	F	Plagioclase Lherzolite vol%	F
Olivine	55.2	0.1	63.0	0.0
Clinopyroxene	17.8	0.4	10.0	0.4
Orthopyroxene	24.7	0.3	19.0	0.2
Spinel	2.3	0.2	-	-
Plagioclase	-	-	8.0	0.4
Total	100.0	1.0	100.0	1.0

Table 6.8

Mineral and melting modes of mantle used in the melting models. Data for spinel lherzolite (A) and were taken from Kelemen et al. (1990) and for plagioclase lherzolite (B) was estimated.

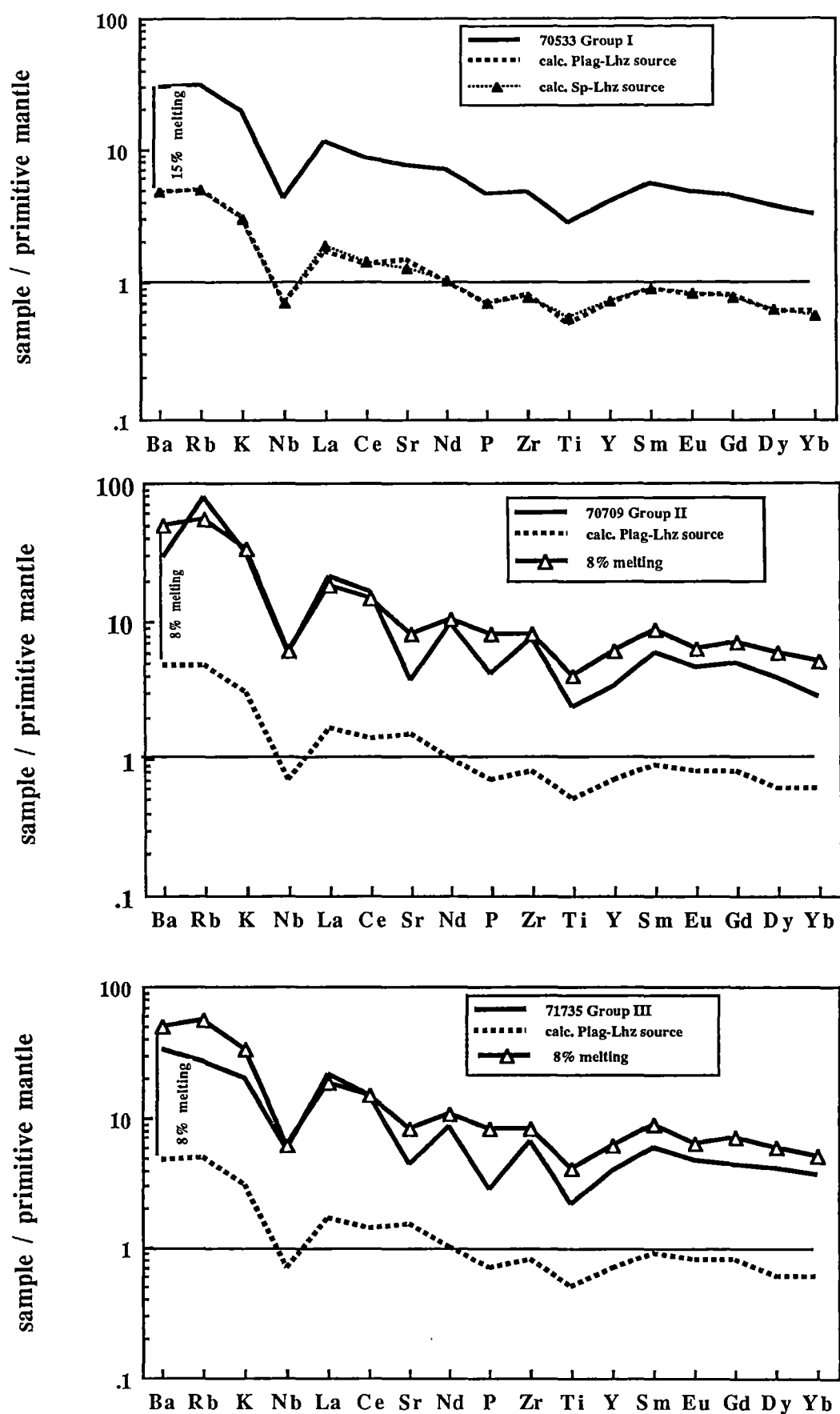


Figure 6.13

'Spidergram' of primitive mantle normalized (Sun et al., 1989) incompatible trace elements showing partial melting models (see text for discussion).

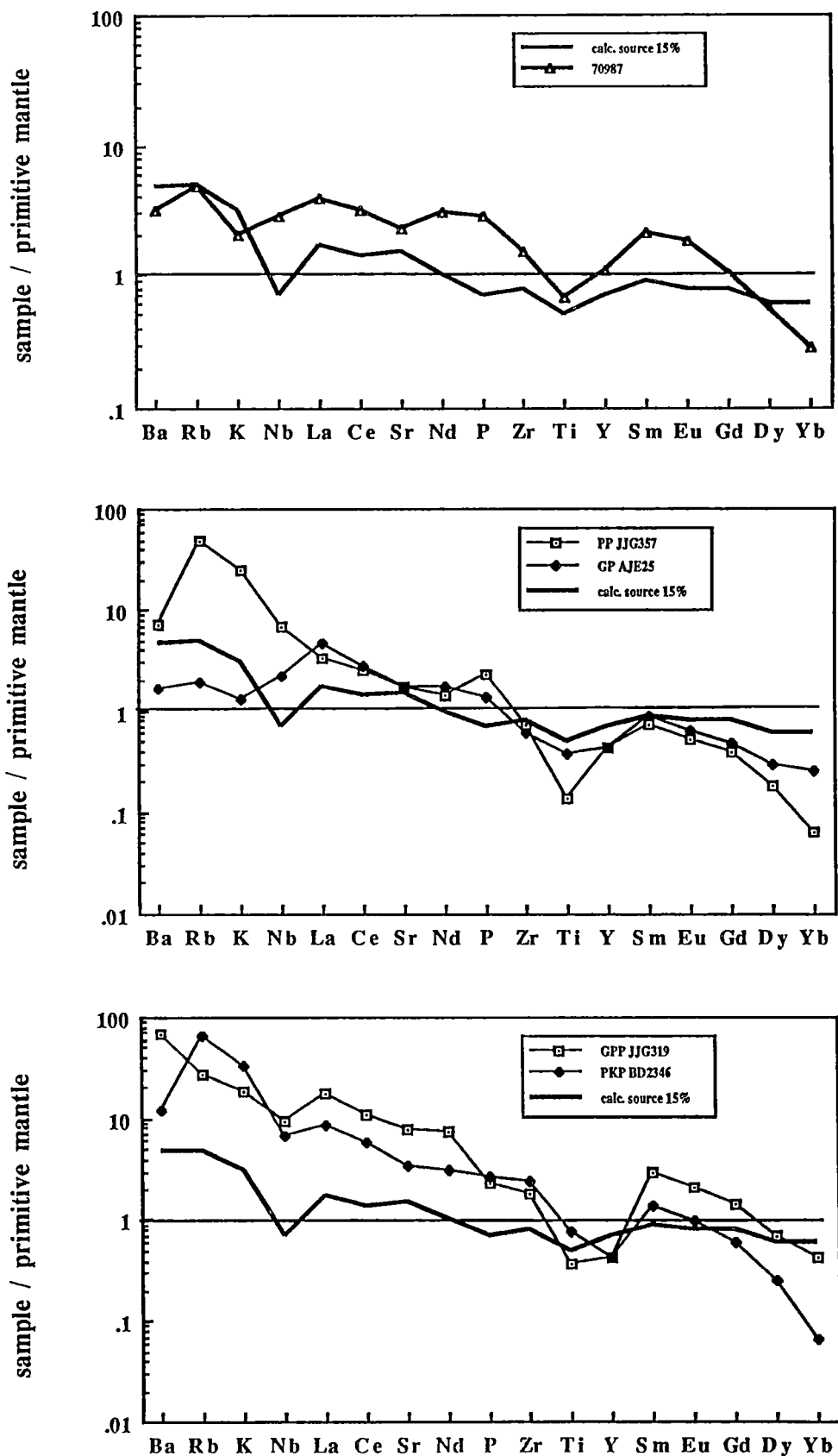


Figure 6.14

Comparison of primitive mantle normalized source compositions with estimated *Group I* source composition. Sample 70987 - Western Victoria (Yaxley, pers. comm.), PP JJG357 (phlogopite peridotite), GP AJE25 (garnet peridotite), GPP JJG319 (garnet phlogopite peridotite) and PKP BD2346 (phlogopite K-richterite peridotite) are taken from (Erlank, 1987).

OBSERVED AND ESTIMATED SOURCE COMPOSITIONS

Sample Group	70987	70533 I	70533 I	70709 II	71735 III
Source Type	Sp-Lhz observed	Sp - Lhz calculated 15% melting	Plag - Lhz calculated 15% melting	Plag - Lhz calculated 15% melting	Plag - Lhz calculated 15% melting
Ba	22.0	32.7	29.6	32.1	36.5
Rb	3.0	3.1	3.0	7.8	2.7
Nb	2.0	0.5	0.5	0.7	0.7
La	2.7	1.3	1.2	2.2	2.3
Ce	5.5	2.5	2.4	4.5	4.1
Sr	47.0	26.6	8.7	15.9	18.0
Nd	4.0	1.4	1.4	2.1	1.8
Zr	16.7	8.8	8.7	13.5	11.9
Y	5.0	3.3	3.1	2.5	3.0
Sm	0.9	0.4	0.4	0.4	0.4
Eu	0.3	0.1	0.1	0.1	0.1
Gd	-	0.5	0.4		
Dy	-	0.5	0.4		
Yb	0.1	0.3	0.3	0.2	0.3

Table 6.9

Estimated source composition for Group I, II and III high-Mg tholeiites, assuming 15% melting of a spinel lherzolite and plagioclase lherzolite (compare Table 6.18). Trace element concentrations for observed spinel lherzolite from Western Victoria (sample 70987) were taken from Yaxley (pers. comm.).

of the selected sources has identical trace element patterns to the calculated abundances in the estimated high-Mg tholeiitic source (Figure 6.14).

In a second approach trace element concentrations of sample 71735 (*Group III*) were modelled assuming the trace element concentrations of a plagioclase lherzolite source, which was the modelled source for *Group I* (70533). The presence of negative Sr anomaly in *Group III* tholeiites suggests plagioclase as a residual phase, which implies lower degree of melting. In modelling trace element concentrations for this sample (*Group III*), 8% melting of a plagioclase lherzolite was assumed. Calculated and observed trace element concentrations, normalized to primitive mantle (Sun et al., 1989) are compared in Figure 6.13, exhibiting similar patterns for K, Nb, LREE, HREE and Ti, but different patterns for Sr, P and LILE. However, partial melts derived at low degrees of melting (8%) from a plagioclase-bearing mantle, leaving plagioclase in the residue, are relatively depleted in Sr and Eu, as both elements are compatible. Compared to calculated melts the Sr-depletion in the natural melts of *Group III* is significantly more pronounced. Assumption of smaller degree of partial melting would increase the Sr and Eu anomaly but diminish the agreement between calculated and observed K, Nb, LREE and Zr abundances.

6.7.3 Implications for Source Compositions

Low TiO_2 , P_2O_5 and Sr, characteristics of *Group I*, *II* and *III* tholeiites, may suggest that high-Mg magmas were derived by partial melting of a depleted source. However, highly enriched incompatible trace elements (Ba, Rb and K) in the magma preclude melting of a uniformly depleted mantle source. Modelling trace element concentrations of *Group I* and *III* high-Mg tholeiites, assuming a common plagioclase bearing source, has shown that *Group I* and *III* cannot be related by variations in degree of melting. This suggests that these magma types were derived from a heterogeneous or different mantle sources which are variably enriched in incompatible LILE and LREE and depleted in Nb, Sr and P.

A model which suggests melting of a refractory mantle is consistent with high PGE and MgO and low TiO₂ concentrations. First stage melts, derived by low to moderate degrees of melting of a primitive mantle would have been sulphur saturated with low PGE concentrations, whereas melts derived from a refractory mantle, in which PGE's were retained during a previous melting event, are sulphur undersaturated and enriched in PGE's (see Chapter 5).

6.7 SUMMARY

High-Mg tholeiite dykes from the Vestfold Hills were emplaced during at least 3 magmatic events. Three main groups were distinguished (*Group I, II and III*), while *Groups I and II* were further subdivided into *Group I and Ia* and *Group II and IIa* on the basis of crosscutting relationships and geochemistry.

The high-Mg tholeiites have some similar geochemical characteristics to felsic crust, which may indicate an involvement of crust in the petrogenesis of these tholeiites. It was shown that crustal contamination is capable of generating the more primitive members and the variations within high-Mg tholeiitic magmas via assimilation of granitic crust by a basaltic komatiitic magma.

Modelling fractional crystallization, assimilation and partial melting has shown that the distinct characteristics of *Group I, II and III* are not simply related by either of these processes or their combination. Variations within *Group I* are explained by an AFC process; contamination with granitic crust and fractionation of olivine and orthopyroxene. PGE concentrations may be a criteria to detect contamination, and it is argued here that the similar PGE concentration between the various groups implies that crustal assimilation has not played a major role in accounting for their differences.

Thus, it is be concluded that the variations between the groups probably reflect their mantle sources. Partial melting models, require sources with low TiO₂ concentrations, suggesting melting of a depleted source which has been enriched in

some incompatible elements (LILE and LREE), but not in Nb relative to primitive mantle.

High-Mg tholeiites from the Vestfold Hills (including *Group Ia* and *III*) have characteristics, such as chondritic $\text{Al}_2\text{O}_3/\text{CaO}$ ratios, high bulk-rock Mg# (68 - 71) which suggest that these melts are primary melts. The other groups have features which are inconsistent with them being primary melts.

CHAPTER 7

LAMPROPHYRE DYKES

7.1 INTRODUCTION

Lamprophyric rocks of various types and different ages occur in Antarctica, including Tertiary (*ca.* 15 Ma) *Lamprophyre* dykes on *Alexander Island* (Horne & Thompson, 1967) and Cretaceous (110 Ma) dyke swarms in *MacRobertson Land* (Ravich et al., 1985). A notable example of Recent but now dormant alkaline (potassic) volcanism is Gaussberg, which occurs on the east Antarctic coastline between the *Vestfold Hills* and the *Bunger Hills* (Sheraton & Cundari, 1980). Occurrences of older lower Cambrian to early Ordovician *Lamprophyres* are known from the *Bunger Hills* (Sheraton et al., 1990), and approximately 500 Ma *Lamprophyric* dykes have been recognized in the *Rauer Islands* (Collerson & Sheraton, 1986).

Lamprophyric dykes also occur in the *Vestfold Hills* and have been correlated with petrologically and geochemically similar dykes in Enderby Land (Sheraton, 1983; Sheraton & England, 1980). It was suggested previously that the *Vestfold Hills* *Lamprophyric* magmatism is related to pre-Permian rifting of the *Lambert-Prydz Bay* Graben (Wellman & Tingey, 1976; Federov et al., 1982). This would require a post-Proterozoic age for this magmatism but fieldwork by Kuehner (1986), Mikhalsky & Andronikov (1990), and this study, clearly demonstrates that *Vestfold Hills* *Lamprophyre* dykes are mid-Proterozoic in age.

The *Lamprophyres* are volumetrically subordinate compared to the tholeiitic dykes but nevertheless they are common throughout the Vestfold Hills. The *Lamprophyre* dykes are typically only a couple of centimetres to decimetres wide and seldom exceed 1m in width. They are laterally continuous for up to 1 to 2 km and consistently strike N - S to NNE - SSW (see dyke base map), parallel to the trend of the mid Proterozoic Fe-rich tholeiites, which makes crosscutting relationships between these dyke suites rare. Petrographically the *Lamprophyric* dykes are very similar and this similarity, together with their consistent strike direction, suggests that they belong to the same intrusive phase. This is supported by field relationships which demonstrate that these dykes are contemporaneous with the 1350 Ma Fe-rich tholeiite event: the tholeiite dykes crosscut and are crosscut by the *Lamprophyric* dykes. Furthermore, all *Lamprophyre* dykes in the southern *Vestfold Hills*, have been affected by an 1100 Ma tectonothermal event (Kuehner, 1986) indicating emplacement prior to this time.

Lamprophyre dykes occurring in the nearby *Rauer Islands*, postdate an 1100 Ma metamorphic event and are of probable Cambrian age (Collerson & Sheraton, 1986) and these dykes may have a yet undiscovered equivalent in the *Vestfold Hills*.

7.2 PETROGRAPHY AND MINERAL CHEMISTRY

Phenocryst assemblages in the *Vestfold Hills Lamprophyre* dykes contain variable proportions of olivine, clinopyroxene, and sometimes phlogopite, with orthopyroxene phenocrysts also appearing in the more silica-rich compositions. The groundmass is composed of phlogopite, clinopyroxene, plagioclase, K-feldspar, dolomite, calcite, opaques \pm nepheline.

Olivine phenocrysts occur in abundances up to 30 vol% and clinopyroxene from 5 to 15 vol%, the latter increasing in abundance as the former decreases. Orthopyroxene only occurs as a phenocryst phase in the more olivine-poor samples (usually \sim 5 vol%), increasing up to 20 vol% in samples which are olivine and clinopyroxene-free. All *Lamprophyres* contain abundant phlogopite, sometimes as

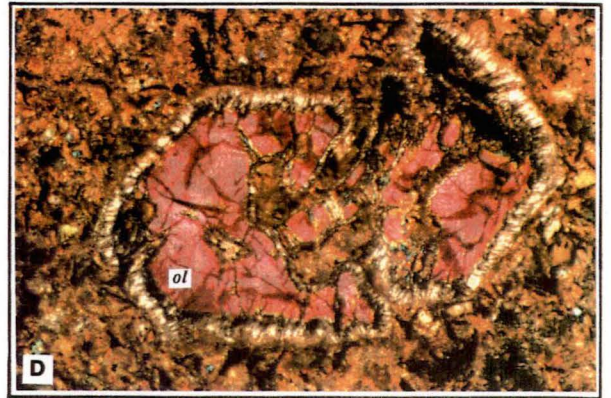
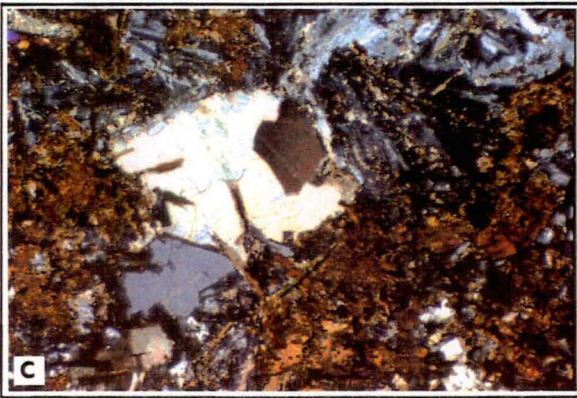
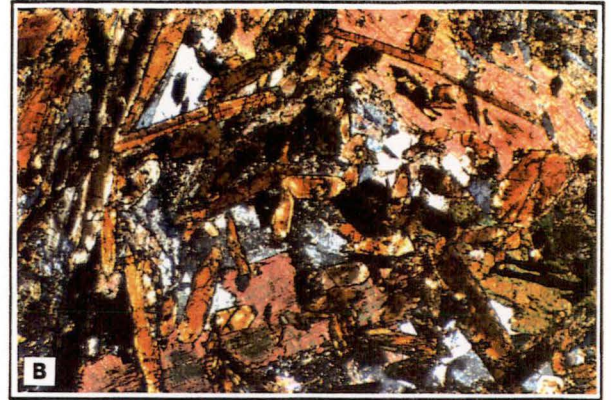
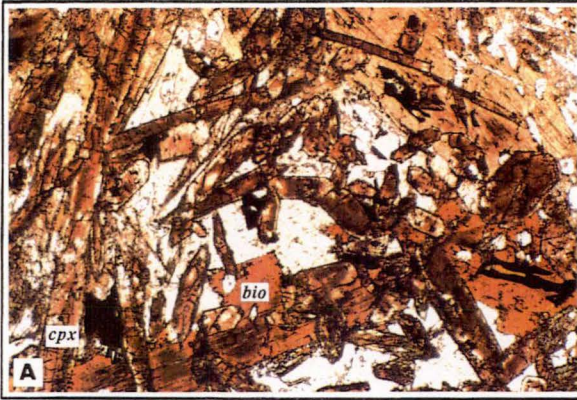


Figure 7.1

Photomicrographs of *Ultramafic Lamprophyre* with titano-augite and phlogopite phenocrysts (2.6 * 1.9 mm) (A and B), carbonate ocelli (1.3 * 0.95 mm) (C), olivine with kelyphitic rim (1.3 * 0.95) (D).

phenocrysts and always as a groundmass phase. A decrease in the modal abundance of phlogopite (from a *max.* of 45 vol% to 10 vol%; phenocrysts and groundmass inclusive) is accompanied a decrease in olivine phenocryst content.

Olivines occur mostly as single euhedral crystals, which are strongly zoned with cores up to Mg# 88 and rims down to Mg# 73. Many olivine phenocrysts are rimmed by orthopyroxene and in some samples olivine has been entirely replaced by opaques (Figure 7.1).

Clinopyroxene occurs in clusters of 2 to 6 euhedral to subhedral crystals ranging in size from 0.5 to 1.5 mm (Figure 7.1). The individual crystals have colourless cores and brownish tinted rims, and display strong chemical zonation from Mg-rich (Mg# 87) and Ti-poor (0.6 - 0.9 wt%) cores to Mg-poor (Mg# 76) and Ti-rich (up to 1.7 wt% TiO₂) rims (see Table 7.7). In some cases this zoning is reversed, from Mg# 80 core to Mg# 84 rims. Clinopyroxene microphenocrysts are typically more Fe-rich with rims of Mg# 65. Unusually Ti-rich (to 3 wt% TiO₂) clinopyroxene phenocrysts, are characterized by abundant minute opaque needles (probably rutile) exsolved from the host crystal, were observed in the olivine-rich samples.

Euhedral to subhedral orthopyroxene phenocrysts (to 3 mm) often occur in clusters. The individual crystals are normally zoned from Mg# 85 cores to Mg# 72 rims, though in some samples these rims may be considerably more Fe-rich (to Mg# 58). Fine grained (0.02 mm) inverted pigeonite occasionally rims orthopyroxene phenocrysts.

Phlogopite phenocrysts (up to 1.5 mm in length) with compositions between Mg# 55 and 63 (see Table 7.7) occur in the olivine-rich *Lamprophyres*. They form mostly euhedral to subhedral laths, but anhedral patches occur as well. Platey microphenocrysts (0.1 - 0.5 mm in length) are present in all the *Lamprophyre* dykes.

The fine to medium-grained, seriate-textured groundmass implies rapid cooling and comprises clinopyroxene, phlogopite, plagioclase, alkali-feldspar, carbonate, and ilmenite. Plagioclase abundances range from only a few percent (*ca.* 5 vol%) to about 20 vol%, and increases with decreasing olivine phenocryst content. The small (0.1 -

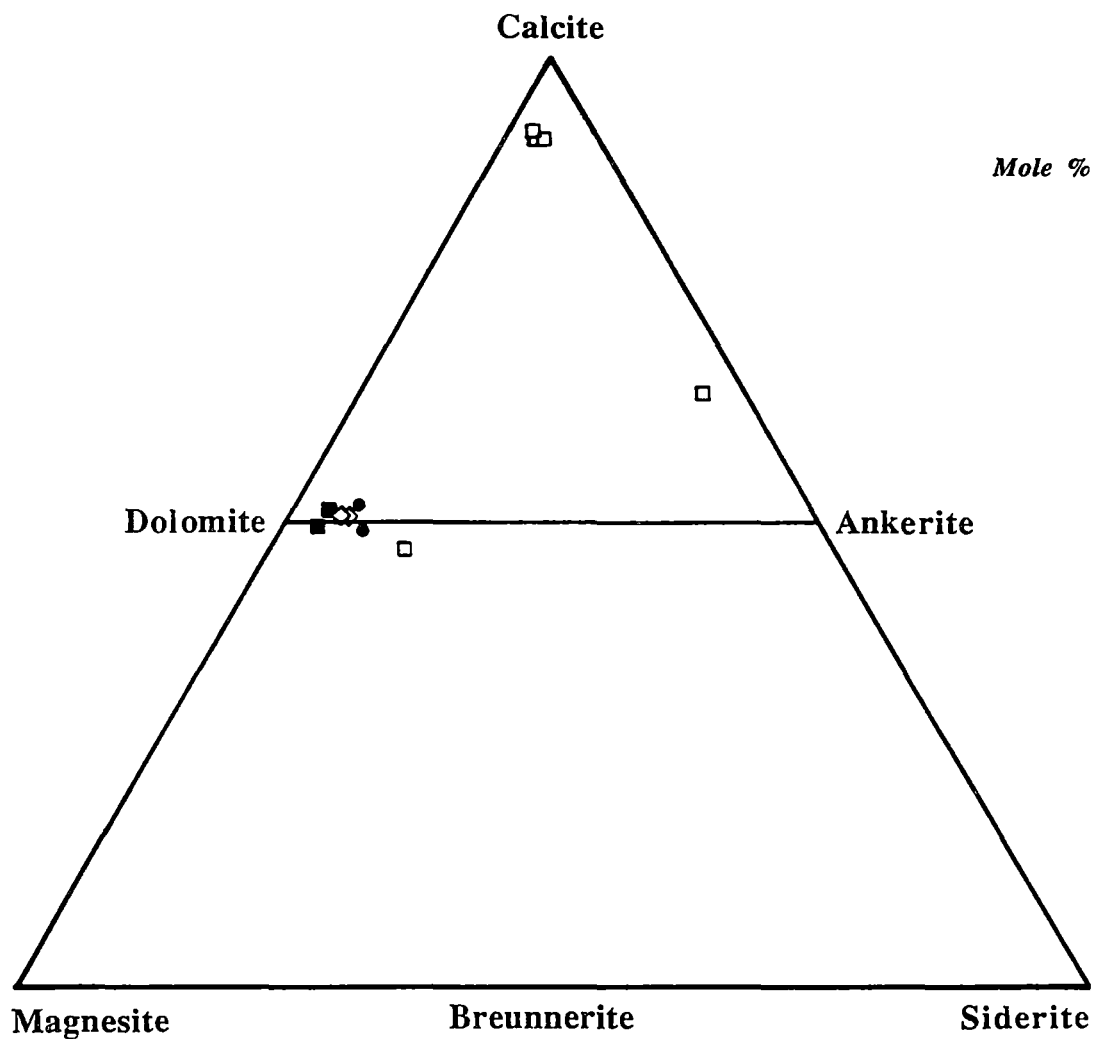


Figure 7.2

Carbonate compositions (mole%) from Vestfold Hills *Lamprophyres*.

Symbols: ■ 71928 (ULM), □ 71760 (AL), ● 71766 (ULM), ◇ 65041 (AL).

0.4 mm) plagioclase laths have compositions from An₅₈ to An_{1.3} (see Table 7.7), alkali-feldspars range between Or_{77.8} Ab_{21.7} An_{0.5} and Or_{49.7} Ab₄₆ An_{3.8}. Dolomite and calcite are the main carbonate phases present, occurring as ocelli (to 2.5 mm in diameter) and dispersed throughout the groundmass. Ankerite occurs in at least one sample, together with dolomite and calcite. The compositions of these carbonates are plotted in Figure 7.2. The highest abundance of carbonate (up to *ca.* 10 vol%) occurs in the more primitive, olivine-rich samples.

Mineral chemistry may be used to estimate magmatic temperatures. Coexisting clinopyroxene and orthopyroxene phenocrysts which occur within the olivine-poor dykes allow estimation of the temperatures at which these dykes were emplaced. All the temperature estimates herein are based on rim compositions of adjacent orthopyroxene and clinopyroxene from chilled margins, using the geothermometers of Wells (1977), Kretz (1982), and Bertrand & Mercier (1985). The temperatures obtained are consistent and range between 1187° and 1205° C for one pair and from 1077° to 1130° C for a second pair of pyroxenes (see Table 7.1). The graphical thermometer of Lindsley (1983) gives rim temperatures of 1080° to 1200° C for the orthopyroxene limb and 960° to 1210° C for the clinopyroxene limb (Figure 7.3). The observed wide spread of clinopyroxene rim compositions is consistent with partial re-equilibration at lower temperatures.

Core compositions of coexisting pyroxenes indicate temperatures between 1200° and 1300° C (Figure 7.3), which are higher than rim temperatures and are assumed to reflect higher magmatic temperatures during initial crystallization.

Sample No. 65407
Rock Type: Lamprophyre

	cpx	opx	Thermometers	T°C
Si	1.886	1.935		
Ti	0.025	0.006	Bertrand & Mercier	1202
Al	0.180	0.072	Wells	1187
Cr	0.007	0.013	Kretz (>1080)	1205
Fe2+	0.344	0.613		
Fe3+	0.020	0.032		
Mn	0.000	0.014		
Mg	0.881	1.212		
Ca	0.628	0.102		
Na	0.029	0.000		
Sum	4.000	4.000		
Mg#	70.8	65.3		

Sample No. 65041
Rock Type: Lamprophyre

	cpx	opx	Thermometers	T°C
Si	1.906	1.968		
Ti	0.020	0.005	Bertrand & Mercier	1077
Al	0.151	0.047	Wells	1097
Cr	0.006	0.008	Kretz (>1080)	1130
Fe2+	0.337	0.587		
Fe3+	0.014	0.000		
Mn	0.000	0.000		
Mg	0.831	1.297		
Ca	0.711	0.088		
Na	0.023	0.000		
Sum	3.999	4.000		
Mg#	70.3	68.8		

Table 7.1

Temperatures calculated from coexisting orthopyroxene and clinopyroxene pairs.
 Temperatures are calculated after Wells (1977), Kretz (1982) and Bertrand & Mercier (1985).

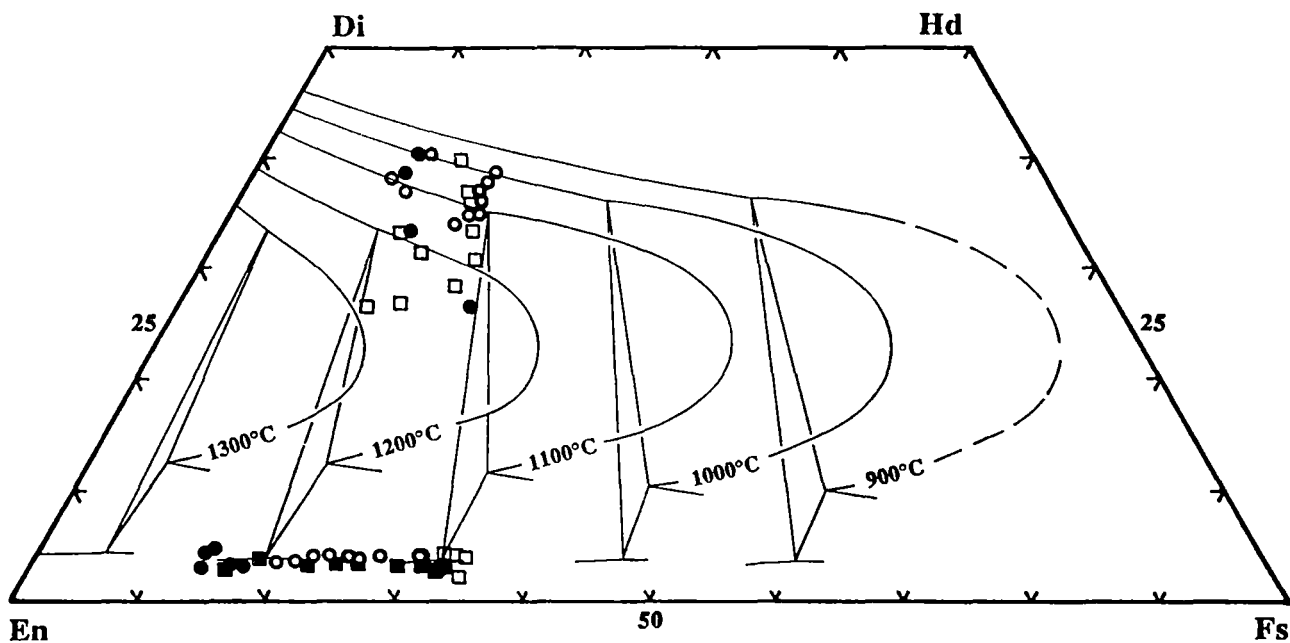


Figure 7.3

Graphical thermometer after Lindsley (1983): 5 kbar projection showing coexisting clinopyroxene and orthopyroxene from olivine-poor *Lamprophyres*. Various symbols indicate separate samples, whereas open circles, triangles and squares indicate rim compositions, the solid ones indicate core compositions.

7.3 GEOCHEMISTRY

Forty representative samples were chosen for major and trace element analysis, of which selected compositions are listed in Table 7.2 and a complete data set are listed in Appendix 10.2. All samples are olivine normative and some contain up to 11 wt% nepheline in their norm. The *Lamprophyre* dykes encompass a wide range in SiO₂ content and in total alkalis (from 2.8 - 6.5 wt% combined alkalis) and plot in the fields for foidite, basanite, trachybasalt and basalt in the TAS - diagram (Total Alkalis versus SiO₂, Figure 7.4) (Le Bas et al., 1986). An alternative classification by Rock (1987) would simply divide the lamprophyres into ULM and AL (Figure 7.4).

Variations in major elements versus SiO₂ are shown in Figure 7.5. MgO, K₂O and TiO₂ are negatively correlated with SiO₂, whereas Al₂O₃ and Na₂O are positively correlated. CaO, K₂O and P₂O₅ are scattered and show only a weak negative correlation with SiO₂ content. The occurrence of linear trends in most oxide - oxide plots suggests that the various *Lamprophyre* dykes are related by a systematic petrogenetic process or processes.

The occurrence of two sets of cross-cutting dykes gives some idea of the secular variation of geochemistry and it seems that the younger dykes have a more evolved composition (e.g. lower MgO, higher SiO₂, Figure 7.5).

Trace elements plotted against Zr in Figure 7.6 also display systematic variation, apart from Sc and V which maintain constant values (not shown). The incompatible trace elements (Ba, Rb, Nb, La, Ce, Nd) as well as Y and Sr are positively correlated and the highly compatible elements (Ni and Cr) are negatively correlated with Zr. However, most significantly there seems little consistency between major and trace elements (Figure 7.7): primitive dykes may have enriched or depleted incompatible element contents. This is further emphasized by considering the two set of cross-cutting dykes on Figure 7.6 which display enrichments and depletions with time for La, Ce and Sr. Thus, trace and major elements in these rocks appear to be decoupled.

Chondrite normalized REE patterns, plotted in Figure 7.8, display depletion of HREE relative to LREE and this degree of depletion tends to increase with increasing

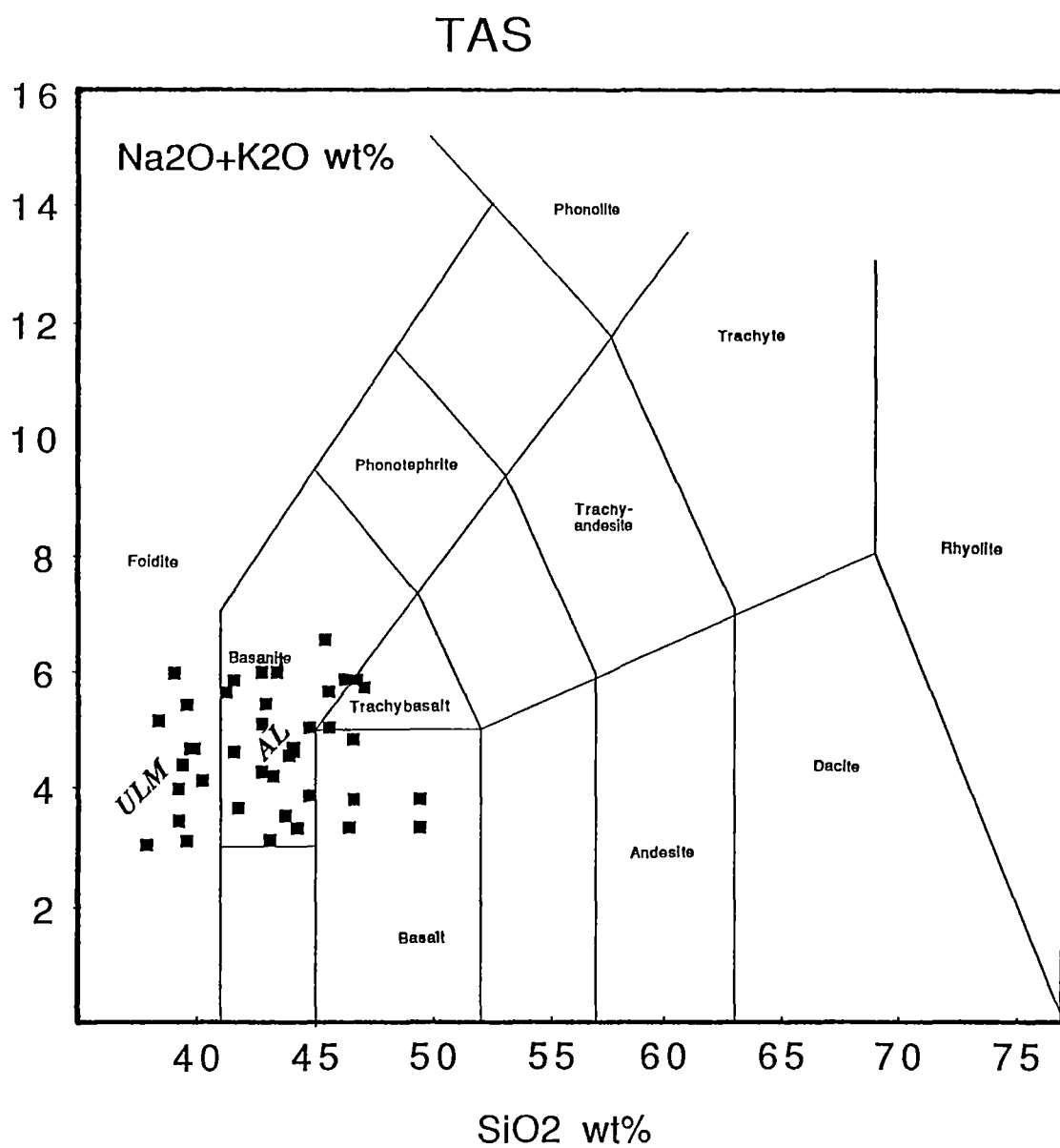


Figure 7.4

TAS-plot after Le Bas et al. (1986) showing the compositional variations within the *Lampropyresuite*.

REPRESENTATIVE LAMPROPHYRE WHOLE ROCK ANALYSES

Sample No. Rock Type	71753 AL	71760 AL	71761 UML	71768 AL	71865 UML	71869 UML	71888 AL
Major Elements							
SiO ₂	45.59	46.66	41.54	49.37	37.87	41.51	47.10
TiO ₂	3.95	4.25	4.88	1.67	2.97	3.72	3.52
Al ₂ O ₃	9.00	9.35	8.50	11.19	4.76	9.10	10.81
Fe ₂ O ₃	12.57	13.05	14.88	12.42	16.25	15.56	13.50
FeO	0.00	0.00	0.00	0.00	0.00	0.00	0.00
MnO	0.15	0.15	0.17	0.15	0.20	0.20	0.15
MgO	9.75	9.27	11.22	10.59	21.88	11.09	8.76
CaO	8.33	8.53	9.58	8.96	7.23	8.72	7.93
Na ₂ O	2.42	2.44	1.87	2.59	1.20	1.91	2.57
K ₂ O	3.24	3.44	3.98	1.21	1.87	2.72	3.18
P ₂ O ₅	0.99	0.99	0.70	0.41	0.62	0.94	0.84
LOI	3.54	1.89	2.09	1.56	5.21	4.22	1.30
Total	98.40	98.85	98.07	99.00	100.06	99.69	99.66
Mg#	60.6	58.4	59.9	62.8	72.7	58.5	56.2
CIPW Norm wt%							
Qtz							
Or	19.15	20.33	9.97	7.15		16.07	18.79
Ab	15.03	15.54	0.00	21.92		5.57	18.47
An	4.13	4.40	3.04	15.33	2.08	8.22	8.57
Lc			10.63		8.66		
Ne	2.95	2.77	8.57		5.50	5.74	1.78
Cpx	24.84	25.46	32.25	21.48	22.94	23.49	20.59
Di	17.62	17.71	22.87	14.37	17.75	15.59	13.40
Hd	7.22	7.75	9.38	7.11	5.19	7.90	7.19
Opx				11.63			
En				7.42			
Fs				4.21			
Ol	17.15	16.20	18.46	14.01	44.42	23.46	18.36
Fo	11.30	10.43	12.16	8.62	32.42	14.29	10.94
Fa	5.85	5.77	6.31	5.39	12.00	9.17	7.42
Mt	1.83	1.89	2.16	1.80	2.36	2.26	1.96
Il	7.50	8.07	9.27	3.17	5.64	7.07	6.69
Ap	2.34	2.34	1.66	0.97	1.47	2.23	1.99
Trace Elements							
Ba	1193	1271	1556	806	662	1280	1246
Rb	57	61	120	32	49	78	85
Nb	59	61	92	30	63	95	70
Sr	1477	1518	977	594	736	1087	1121
Zr	387	406	420	139	289	458	449
Y	38	40	28	31	24	38	33
La	107	109	66	45	55	94	85
Ce	239	248	146	98	124	198	188
Nd	119	125	77	46	61	92	92
Ni	336	308	352	373	870	397	283
Cr	351	315	550	475	1063	330	279
V	218	217	275	208	199	237	198
Sc	17	18	21	21	18	22	18

Table 7.2

Representative Lamprophyre whole rock analyses showing the compositional range of the Vestfold Hills Lamprophyres. Abbreviations: ULM - Ultramafic Lamprophyre, AL - Alkaline Lamprophyre. Note: 71760 crosscuts 71761.

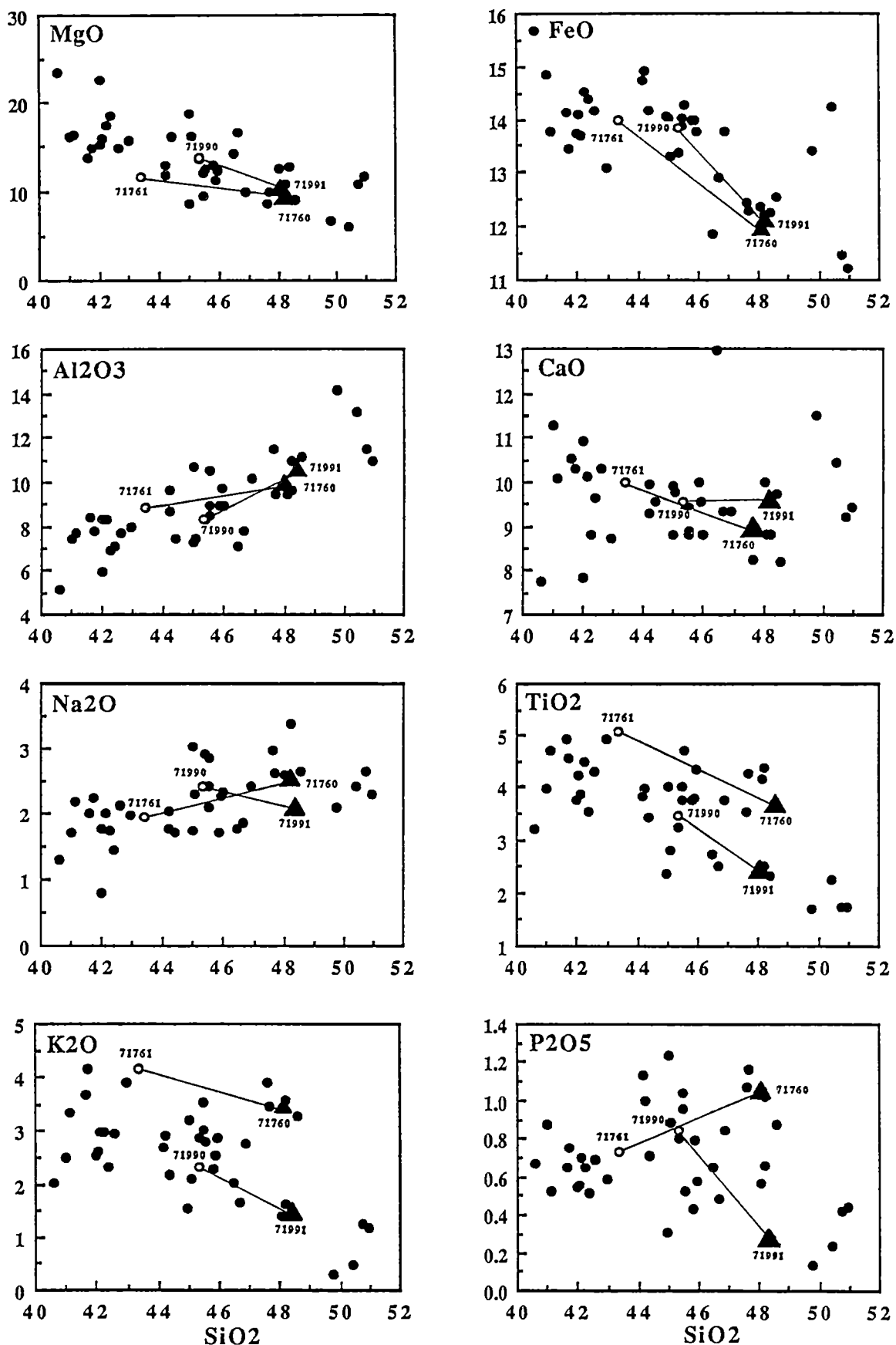


Figure 7.5

Major elements plotted against MgO. Before plotting major elements were recalculated to 100% volatile free and total Fe as FeO. *Lamprophyres* with crosscutting relationships are indicated by open circles (older) and solid triangles (younger).

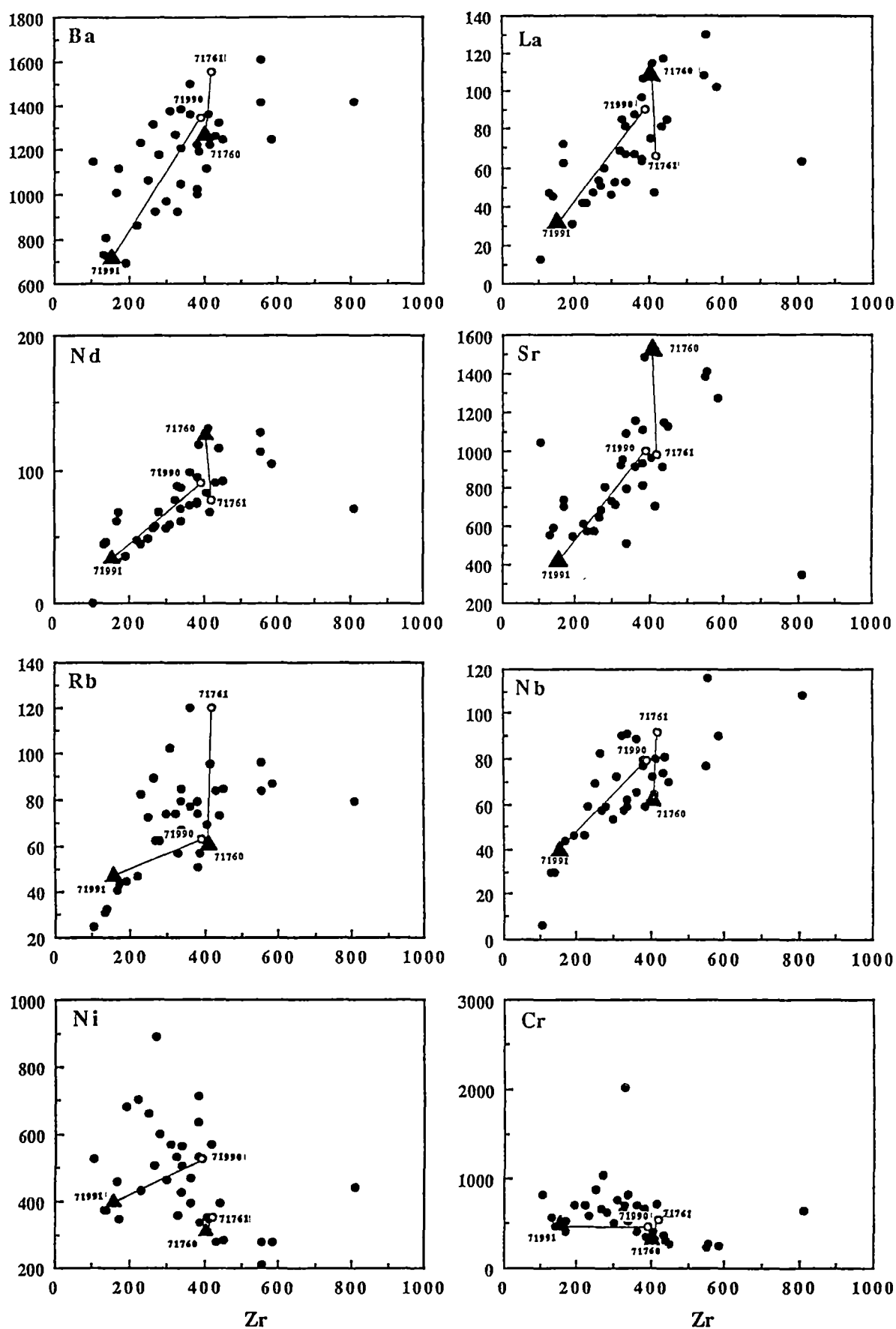


Figure 7.6

Selected trace elements plotted against Zr as a fractionation index. *Lamprophyres* with crosscutting relationships are indicated by open circles (older) and solid triangles (younger).

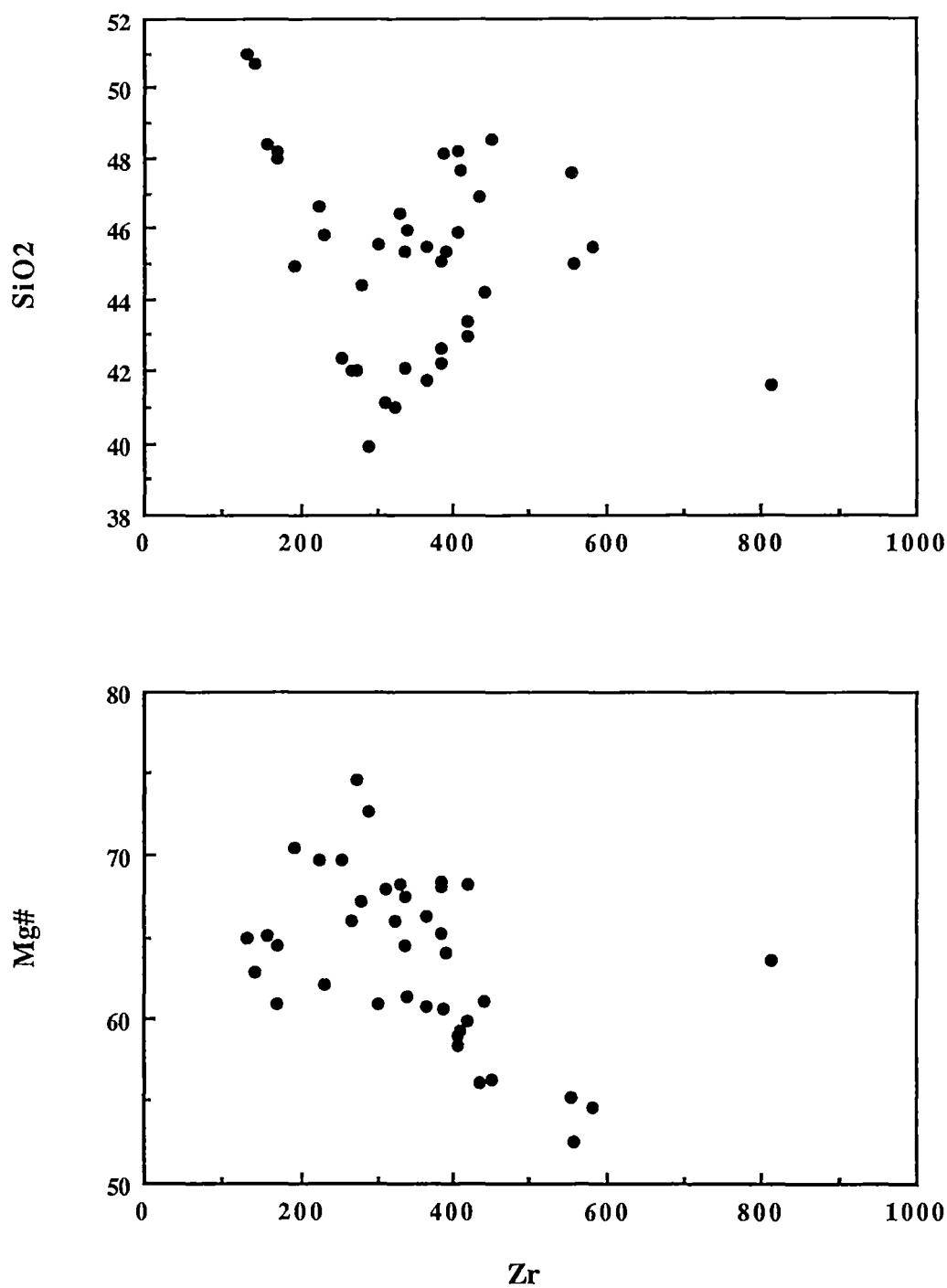


Figure 7.7

SiO₂ and Mg# versus Zr, showing wide compositional range of *Lamprophyre* suite (see text for discussion).

LAMPROPHYRES

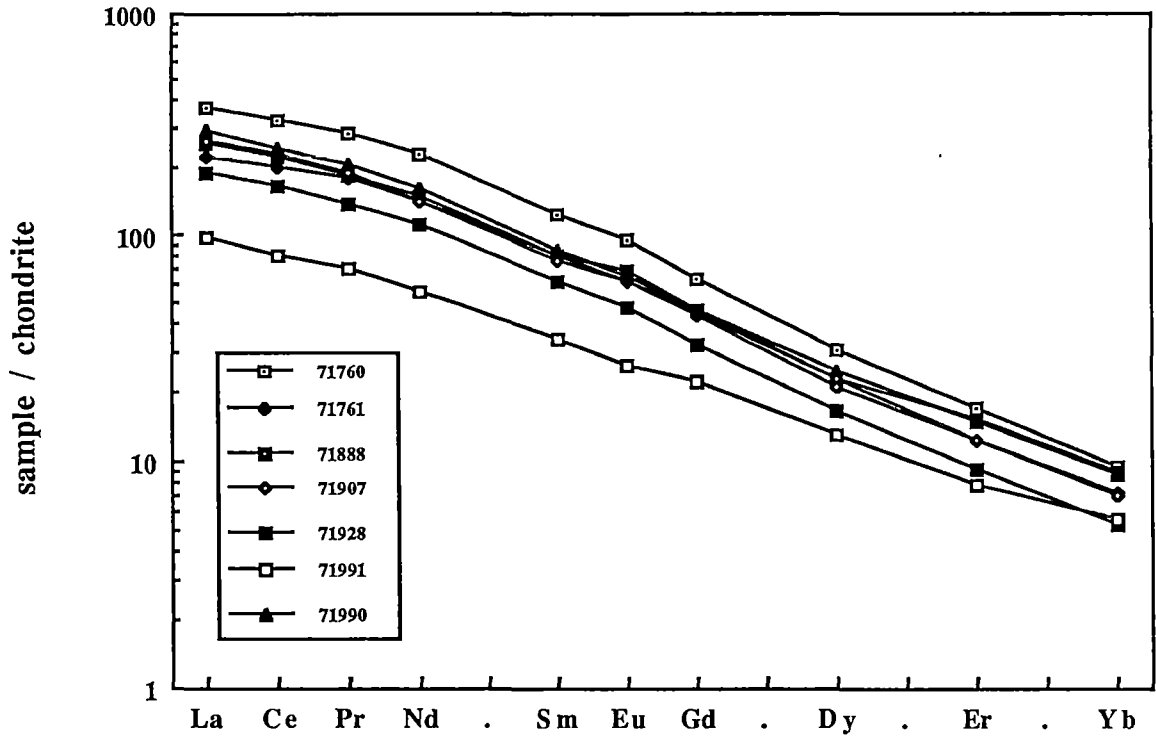


Figure 7.8

Chondrite normalized REE patterns (Leedy/1.2; Masuda et al. 1973; Taylor & Gorton, 1977) of various Vestfold Hills *Lamprophyres*.

REE ANALYSES FROM LAMPROPHYRES

Sample No. Rock Type	71760 AL	71761 ULM	71888 AL	71907 AL	71928 ULM	71990 AL	71991 AL
REE / ppm							
La	116.0	70.4	80.3	81.8	59.8	30.3	91.5
Ce	265.0	162.0	181.0	184.0	134.0	64.8	199.0
Pr	32.7	20.5	21.5	21.7	16.0	8.0	23.7
Nd	138.0	85.5	88.9	85.6	67.0	33.2	96.4
Sm	23.6	15.4	15.7	14.8	11.8	6.5	16.5
Eu	6.8	4.5	5.0	4.5	3.4	1.9	4.7
Gd	16.4	11.5	12.0	11.2	8.4	5.8	12.0
Dy	9.9	7.5	7.5	6.9	5.4	4.3	8.1
Er	3.6	2.6	3.3	2.6	2.0	1.7	3.2
Yb	2.0	1.5	1.9	1.5	1.1	1.2	1.8
La/Yb	58.0	46.9	42.5	56.4	55.4	26.3	49.7

Table 7.3

Rare earth abundances in Lamprophyres from the Vestfold Hills. Analyses were done following the method of Robinson et al. (1986). Concentrations are given in ppm. Abbreviations: ULM - Ultramafic Lamprophyre, Al - Alkaline Lamprophyre.

LREE abundances (i.e. La/Yb ratios increase with increasing La). There are no obvious systematic variations between older and younger *Lamprophyre* dykes.

7.4 PETROGENESIS

7.4.1 Crystal Fractionation

The relatively constant CaO content which accompanies increasing Al_2O_3 (Figure 7.8), suggests a possible control of chemical variation by the combined fractionation of clinopyroxene with olivine and perhaps orthopyroxene which is consistent with the dominance of these phases in the phenocryst assemblage. In addition the secular variation (Figure 7.5) is consistent with progressive fractional crystallization.

To test more rigorously whether the major element compositional variation trends are consistent with crystal fractionation of observed phenocrysts, samples representing the compositional spectrum have been modelled using least - squares methods (Le Maitre, 1980). The results of this modelling suggest that fractional crystallization may account for much of the major element variation, certainly within the resolution that the spread of the data permits (Table 7.4). However, as pointed out above, incompatible trace elements are decoupled from major elements and such a model cannot possibly account for the spectrum of trace element abundances (Figure 7.6). This is further emphasized by considering trace element ratios which exhibit a substantial variation in these dykes (Figure 7.10) which cannot be produced by fractional crystallization.

7.4.2 Mixing

The systematic variation of some trace element ratios (e.g. K/La vs La/Nb, Figure 7.10) may be produced by mixing. However, it is difficult to envisage a mixing process which would decouple major and trace elements to the extent observed and thus this model is not considered realistic.

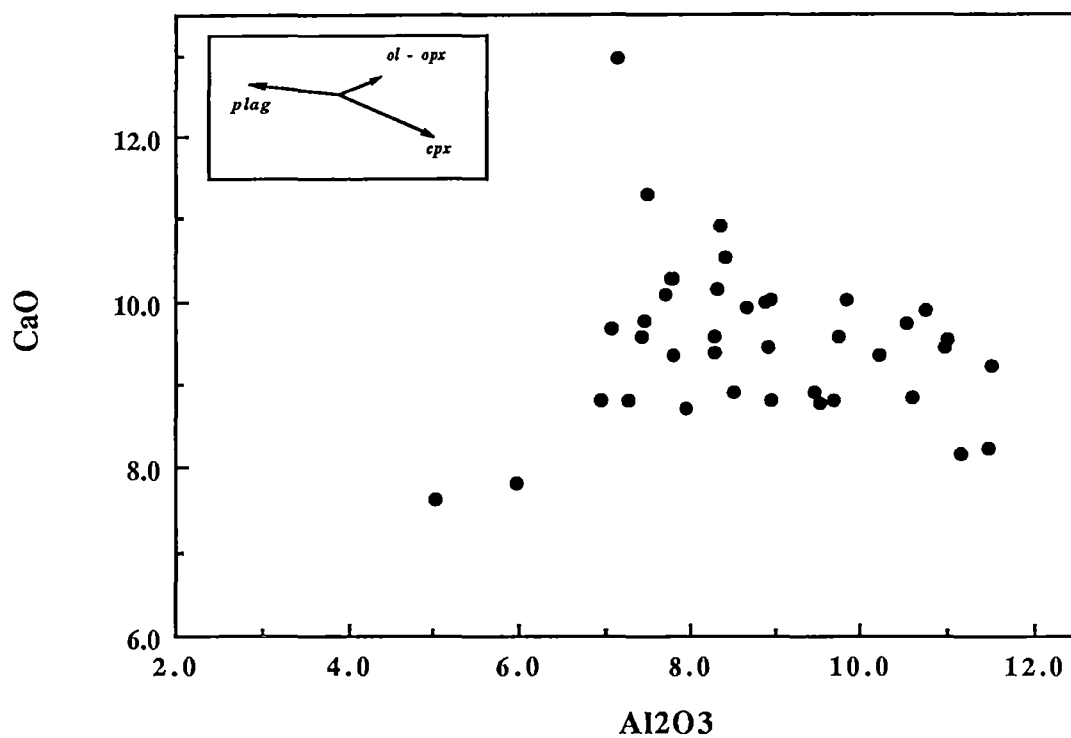


Figure 7.9

CaO versus Al₂O₃ showing the compositional range within the *Lamprophyre* suite and possible fractionation trends (see text for discussion).

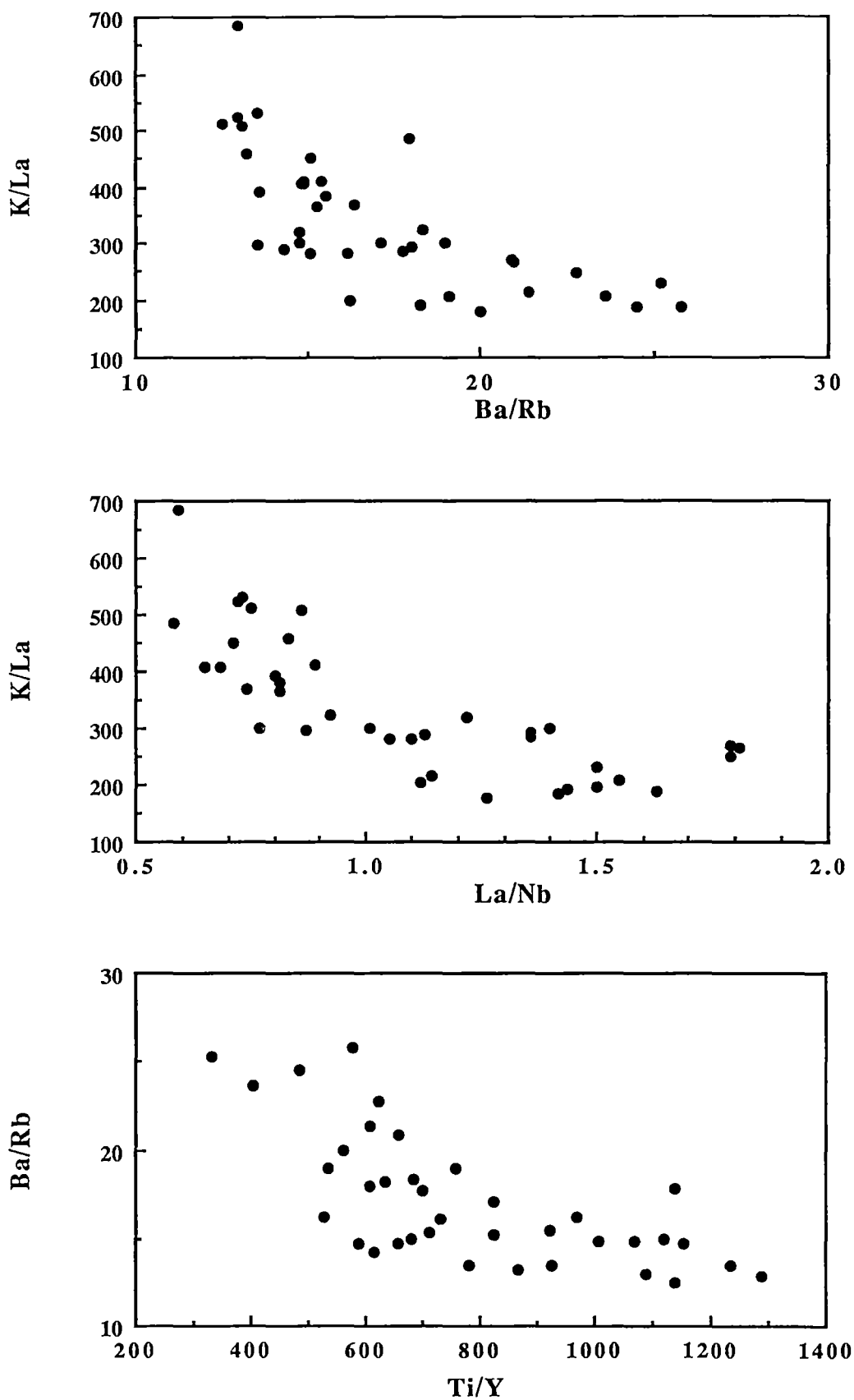


Figure 7.10

Ratio - ratio plots showing the compositional range of the *Lamprophyresuite* (see text for discussion).

A		Reactant	Product A	Product B	Product C	Product D	Product E	Estimated
Sample No.	71750		71898	OI	Cpx	Phlog	Ilm	Reactant Difference
Rock Type	ULM		AL					
SiO ₂	42.53		44.29	40.78	52.94	38.66	0.51	42.90
TiO ₂	4.31		3.94	0.00	0.96	4.86	50.02	4.90
Al ₂ O ₃	7.73		10.58	0.00	1.74	15.41	0.00	7.78
FeO	14.20		13.79	11.25	4.80	15.54	45.95	13.68
MgO	14.90		8.56	47.41	17.00	15.54	0.46	14.81
CaO	9.75		9.74	0.00	22.80	0.00	0.71	9.25
Na ₂ O	2.13		2.99	0.00	0.00	0.00	0.00	2.00
K ₂ O	2.77		3.15	0.00	0.00	9.74	0.00	2.43
P ₂ O ₅	0.68		1.22	0.00	0.00	0.00	0.00	0.80
Total	99.00		98.26	99.44	100.24	99.75	97.65	98.55
Mass%	100.00		65.63	13.69	12.96	3.69	4.02	
Sum of squares								1.1644

B		Reactant	Product A	Product B	Product C	Product D	Product E	Estimated
Sample No.	71750		71793	OI	Cpx	Phlog	Ilm	Reactant Difference
Rock Type	ULM		AL					
SiO ₂	42.53		46.80	40.78	52.94	38.66	0.51	43.67
TiO ₂	4.31		3.78	0.00	0.96	4.86	50.02	5.55
Al ₂ O ₃	7.73		10.20	0.00	1.74	15.41	0.00	7.77
FeO	14.20		13.74	11.25	4.80	15.54	45.95	13.85
MgO	14.90		9.83	47.41	17.00	15.54	0.46	14.98
CaO	9.75		9.32	0.00	22.80	0.00	0.71	9.10
Na ₂ O	2.13		2.40	0.00	0.00	0.00	0.00	1.31
K ₂ O	2.77		2.75	0.00	0.00	9.74	0.00	2.73
P ₂ O ₅	0.68		0.84	0.00	0.00	0.00	0.00	0.44
Total	99.00		99.66	99.44	100.24	99.75	97.65	99.40
Mass%	100.00		52.35	9.76	19.15	13.24	5.50	
Sum of squares								4.1317

Table 7.4

Least square mixing calculation (Le Maitre, 1980). Abbreviations: ULM - Ultramafic Lamprophyre, AL - Alkaline Lamprophyre.

7.4.3 Partial Melting

Partial melting may offer a mechanism to decouple major and trace elements. For instance the major element content of a melt may remain similar for different degrees of melting assuming multiple phase saturation during melting and the same residual mineralogy, whereas trace element content may vary considerably with degree of melting. Thus, the observed spectrum of major element compositions may be due to combination of variable partial melting together with fractional crystallization (as discussed above) and the incompatible element variations may be dominated by degree of partial melting - a more effective way of changing incompatible element abundances than crystal fractionation, assuming the melts represent small liquid fractions (e.g. Cox et al., 1979).

The REE are chosen to test such a model because of the constraints they give regarding the melting model. For instance the enrichment in LREE in the *lamprophyres* would require garnet as a residual phase from a source with a relatively flat REE pattern. This is consistent with the many geochemical studies which conclude garnet lherzolite is the mantle residue to SiO₂-undersaturated magma generation (e.g. alkali-basalts considered by Frey et al., 1978; Clague & Frey, 1982; Alibert et al., 1983; Chauvel & Jahn, 1984).

Two endmembers of the *Lamprophyre* suite are modelled, a primitive composition (*Ultramafic Lamprophyre*) with 38 wt% SiO₂ and Mg# 67.9 (sample 71928) and an evolved composition (*Alkaline Lamprophyre*) with 46.7 wt% SiO₂ and Mg# 58 (sample 71760). It was assumed that the composition of the *Ultramafic Lamprophyre* is primary, whereas the more evolved *Alkaline Lamprophyre* composition was recalculated to a primary composition until a Mg# of 68 was obtained, assuming that this sample has undergone mainly olivine and clinopyroxene fractionation in the proportions 2 : 1.

Non-modal equilibrium melting is assumed (see Chapter 6, equation 6.4) with partition coefficients listed in Table 7.5 and melting and source mineral modes given in Table 7.6.

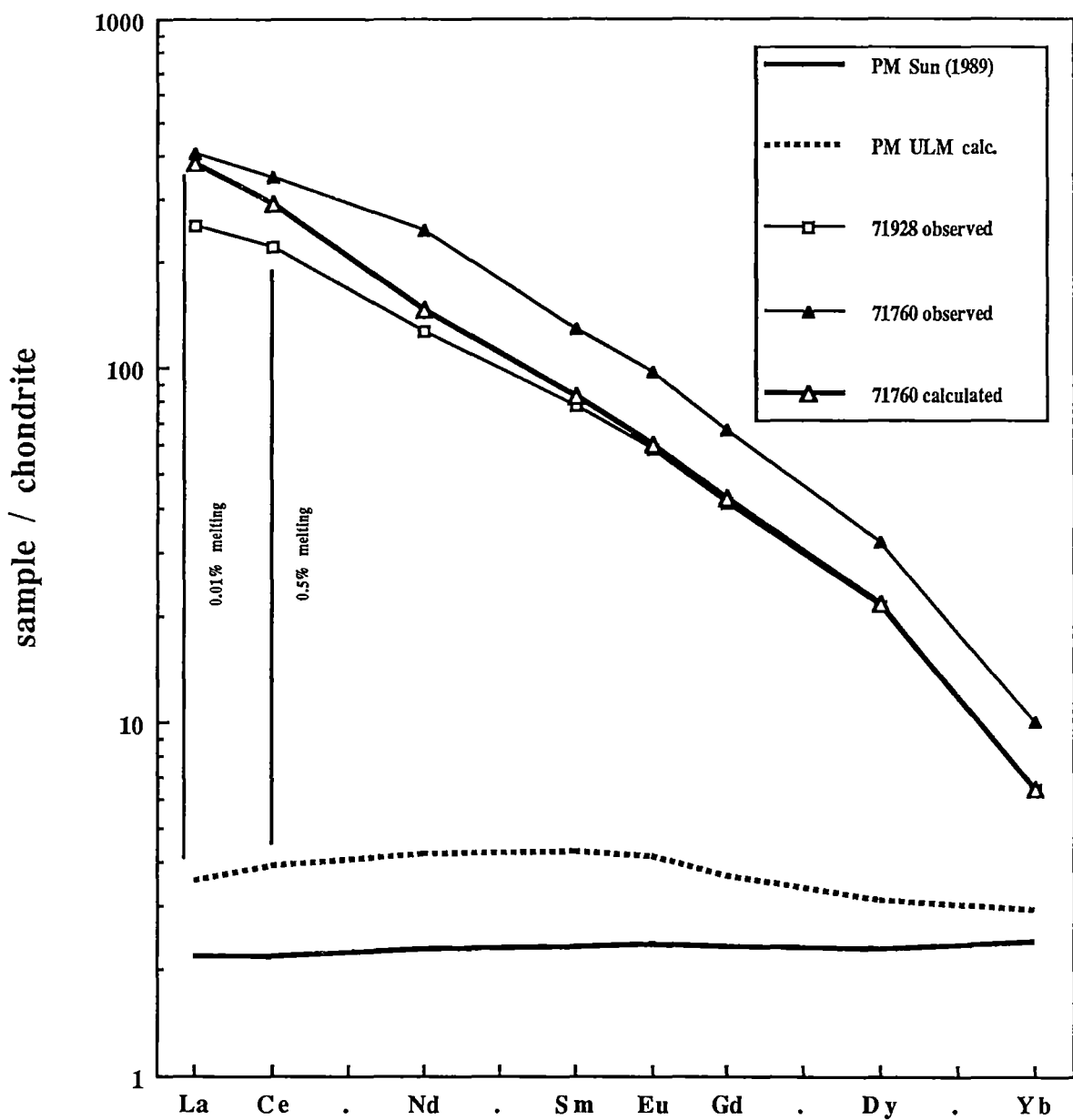


Figure 7.11

Chondrite normalized REE patterns (Leedy/1.2; Masuda et al. 1973; Taylor & Gorton, 1977) of various *Lamprophyres*, showing results from partial melting modelling for sample 71928 (*Ultramafic Lamprophyre*) and 71760 (*Alkaline Lamprophyre*).

Partial melting was modelled in two steps: (1) estimation of REE abundances in a garnet bearing 'primitive' source and (2) using the obtained source concentrations to derive the *Alkaline Lamprophyre* composition. In the first step the REE concentrations in the mantle source of the *Ultramafic Lamprophyre* (71928) was calculated assuming 0.5% melting of a peridotite source with 10% garnet. This produces a calculated mantle source with a relatively flat REE pattern, and abundances slightly above those of the Sun et al. (1989) primitive mantle estimate (Figure 7.11). This model clearly demonstrates that small degrees of melting are necessary to produce these *Lamprophyre* magmas (i.e. < 0.5%), if their mantle source is not substantially enriched in incompatible elements. An attempt was then made to model the REE concentrations of the *Alkaline Lamprophyre* by a smaller degree of melting (0.01%) of this model source and it is readily apparent that it is not possible to produce the overall enrichments in REE by such a mechanism: retaining garnet as a residual phase effectively anchors the HREE end of the spectrum.

If it supposed that garnet is not a residual phase then a source enriched in LREE over HREE would have to be assumed to produce the LREE/HREE enrichments observed. Even, if this were the case, however, Table 7.2 (selected analyses) and Figure 7.6 shows that enrichments in LREE (e.g. La, Nd) may not necessarily correspond to enrichments in other incompatible elements (e.g. Ba, Rb, Nb, Zr) as demonstrated by comparing the two crosscutting dyke pairs. Thus, it is apparent that the *Lamprophyric* dykes require a mantle source which is quite heterogeneous with respect to the abundances of the different incompatible trace elements considered here.

MINERAL DISTRIBUTION COEFFICIENTS

Elements	Olivine	Cpx	Opx	Garnet
La	0.0020	0.0690	0.0010	0.0100
Ce	0.0005	0.0980	0.0030	0.0210
Nd	0.0010	0.1800	0.0065	0.0800
Sm	0.0013	0.2600	0.0100	0.2170
Eu	0.0015	0.3100	0.0130	0.3200
Gd	0.0015	0.3000	0.0160	0.4980
Dy	0.0015	0.3000	0.0220	1.0600
Yb	0.0015	0.2800	0.0490	4.0300

Table 7.5

Mineral distribution coefficient of trace elements used in partial melting models. Distribution coefficients were taken from Cox et al. (1984) and Dy from Hanson, (1980).

MINERAL AND MELTING MODES OF MANTLE

Minerals		
	vol%	Garnet Lherzolite F
Olivine	50.0	0.1
Clinopyroxene	10.0	0.7
Orthopyroxene	30.0	0.1
Garnet	10.0	0.1
Total	100.0	1.0

Table 7.6

Mineral modes of mantle used in the melting models. Data for garnet lherzolite were taken from Cox (1983).

7.6 SUMMARY

Lamprophyre dykes from the Vestfold Hills have been emplaced during the Mid Proterozoic magmatic event which occurred between 1350 and 1150 Ma, showing crosscutting relationships within this rock suite but also between Fe-rich tholeiites which have been emplaced during the same magmatic episode. Younger alkaline magmatism, which is common in the East Antarctic shield has not been observed in the Vestfold Hills.

The *Lamprophyres* from the Vestfold Hills have a wide compositional range and have been classified in this study as *Ultramafic Lamprophyres* and *Alkaline Lamprophyres*. The uncommon crosscutting relationships between the *Lamprophyres* themselves and between *Lamprophyres* and Fe-rich tholeiites do not allow a link between geochemical variations and to particular magmatic events.

However, in modelling compositional variations within the suite the processes of crystal fractionation and partial melting were considered. Crystal fractionation of observed phenocryst phases, such as olivine, clinopyroxene and phlogopite may account for major element variations but cannot produce the observed incompatible trace element variations, suggesting that crystal fractionation is not the major process of magmatic differentiation for these rocks. In modelling REE concentration by partial melting it was shown that the abundances in the *Ultramafic Lamprophyres* and the *Alkaline Lamprophyre* are consistent with small (< 1%) but variable degrees of melting of heterogeneous garnet-bearing sources, with variable modal garnet.

The model favoured here is melting of heterogeneous garnet lherzolite sources, indicating pressures probably > 26 kbar. *Lamprophyric* magmas different in their primary composition subsequently undergone secondary differentiation processes, such as fractional crystallization.

In terms of Ba/Nb versus La/Nb variation (Figure 7.12) the Vestfold Hills *Lamprophyres* can be compared with the elevated values of Gough and Tristan da Cunha, being dispersed in arrays above the Ba/Nb values of both Primitive Mantle and N-MORB (values from Sun, 1980; and Sun et al., 1989).

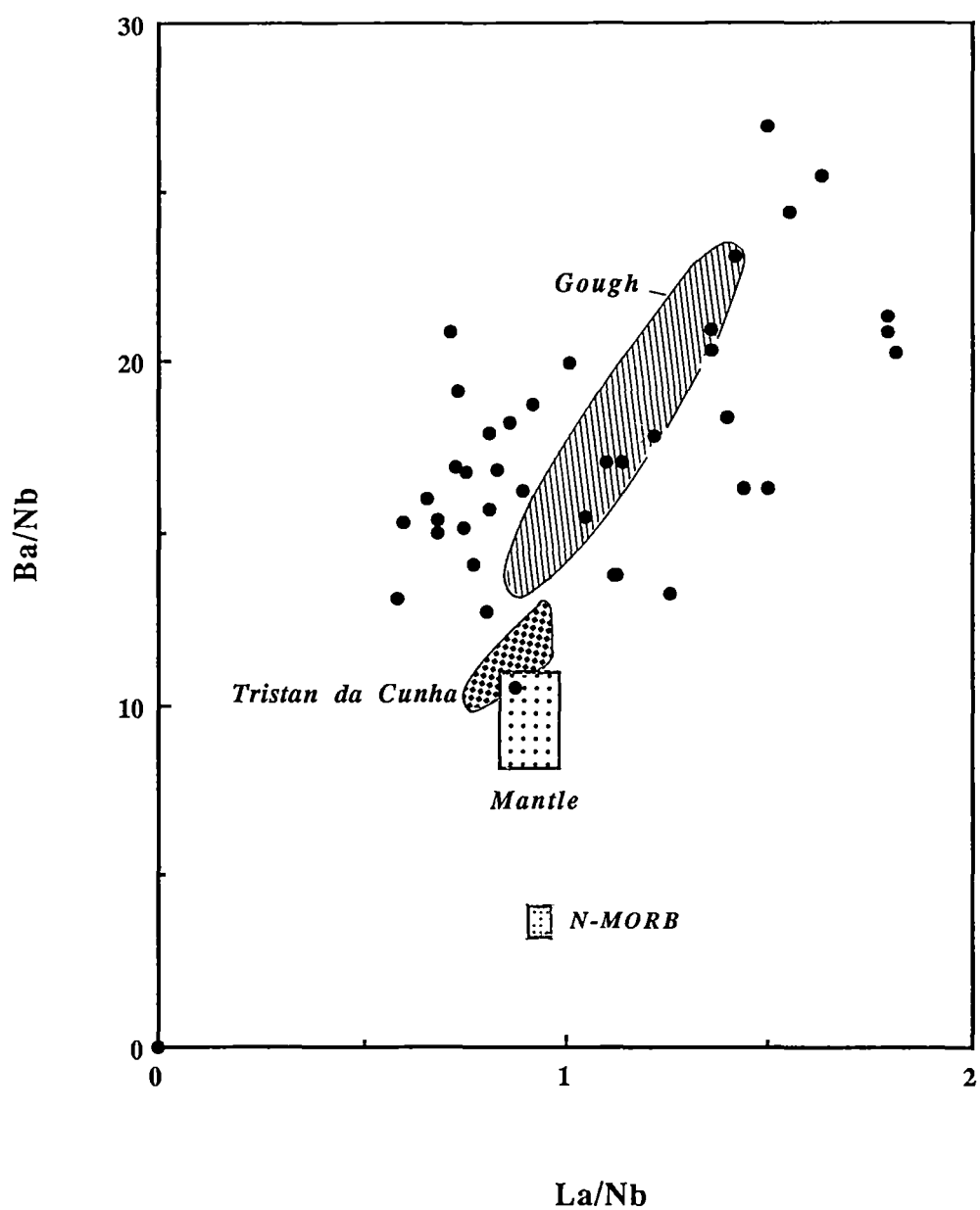


Figure 7.12

Plot of Ba/Nb versus La/Nb for *Lamprophyres* from the Vestfold Hills compared to Gough, Tristan da Cunha, primordial mantle and N-MORB (modified after Weaver et al, 1987).

TABLE 7.7

SELECTED CLINOPYROXENE MICROPROBE ANALYSES

Sample No.	71760	65030			65031	65041					
Pos. of Anal.	core	rim	pigeonite	pigeonite	core	rim	gm	core	core	rim	microph.
Rock Type	Lamprophyre										
SiO ₂	52.37	52.68	53.70	54.39	52.18	50.03	51.56	52.03	51.60	49.59	51.03
TiO ₂	0.85	0.95	0.35	0.36	0.65	0.93	0.67	0.73	0.96	1.72	0.77
Al ₂ O ₃	1.15	1.20	2.41	1.94	3.13	4.57	3.75	2.59	5.81	5.22	3.80
Cr ₂ O ₃	0.55	0.40	0.31	0.35	0.20	0.19	0.32	0.35	0.25	0.30	0.57
FeO	7.34	6.30	12.21	11.95	9.95	13.49	9.60	6.99	5.29	8.37	10.99
NiO	0.00	0.07	0.00	0.00	0.00	0.00	0.00	0.00	0.00	0.00	0.00
MnO	0.21	0.12	0.00	0.00	0.00	0.00	0.00	0.00	0.00	0.00	0.00
MgO	18.96	17.64	24.24	25.89	18.46	14.54	16.50	16.70	20.53	14.87	14.21
CaO	17.60	20.04	6.77	5.11	15.41	15.73	17.59	19.93	13.76	20.23	18.60
Na ₂ O	0.30	0.34	0.00	0.00	0.00	0.27	0.30	0.25	0.75	0.52	0.30
Total	99.32	99.72	99.99	99.99	99.98	99.75	100.29	99.57	98.95	100.82	100.27
Cations (6 ox)											
Si	1.929	1.937	1.939	1.952	1.915	1.877	1.896	1.918	1.866	1.818	1.899
Ti	0.024	0.026	0.010	0.010	0.018	0.026	0.019	0.020	0.026	0.047	0.022
Al	0.050	0.052	0.103	0.082	0.136	0.203	0.163	0.113	0.248	0.226	0.167
Cr	0.016	0.012	0.009	0.010	0.006	0.006	0.009	0.010	0.007	0.009	0.017
Fe ²⁺	0.175	0.159	0.369	0.359	0.305	0.419	0.275	0.198	0.148	0.185	0.342
Fe ³⁺	0.051	0.034	0.000	0.000	0.000	0.004	0.021	0.017	0.012	0.072	0.000
Mg	1.040	0.966	1.304	1.384	1.010	0.813	0.904	0.918	1.106	0.812	0.788
Ca	0.694	0.789	0.262	0.196	0.606	0.632	0.693	0.787	0.533	0.794	0.742
Na	0.021	0.024	0.000	0.000	0.000	0.020	0.021	0.018	0.053	0.037	0.022
Sum	4.000	4.000	3.995	3.993	3.996	4.000	4.000	4.000	4.000	4.000	3.998
Mg#	82.1	83.3	78.0	79.4	76.8	65.8	75.4	81.0	87.4	76.0	69.7
Endmembers											
Mg ₂ Si ₂ O ₆	52.0	48.3	65.2	69.2	50.5	40.6	45.2	45.9	55.3	40.6	39.4
Fe ₂ Si ₂ O ₆	8.8	8.0	18.4	17.9	15.3	20.9	13.7	9.9	7.4	9.2	17.1
Ca ₂ Si ₂ O ₆	32.3	37.6	10.5	7.9	27.0	26.8	30.4	36.3	21.3	33.0	33.1
NaAlSi ₂ O ₆	0.5	1.2	0.0	0.0	0.0	1.0	0.0	0.0	3.3	0.0	0.5
NaFeSi ₂ O ₆	1.6	1.2	0.0	0.0	0.0	0.4	1.2	0.8	1.2	2.8	0.0
NaCrSi ₂ O ₆	2.2	1.1	0.0	0.0	0.0	0.6	0.9	1.0	0.7	0.9	1.7
CaAl ₂ Si ₂ O ₆	4.6	2.2	3.3	1.9	4.3	7.0	5.9	3.1	8.2	4.4	5.8
CaFeAlSiO ₆	0.0	0.0	0.0	0.0	0.0	0.0	0.8	1.0	0.0	4.4	0.0
CaTiAl ₂ O ₆	2.4	2.6	1.0	1.0	1.8	2.6	1.9	2.0	2.6	4.7	2.2

SELECTED ORTHOPYROXENE MICROPROBE ANALYSES

Sample No.	65051	65407	65423			65030			65041		
Pos. of Anal.	kelyphit	rim	core	core	core	rim-cpx	microph.	ct rim	core	rim	microph.
Rock Type	Lamprophyre										
SiO ₂	54.76	50.70	53.19	52.56	52.43	53.49	51.81	55.03	56.39	53.18	51.81
TiO ₂	0.00	0.90	0.00	0.00	0.00	0.17	0.00	0.17	0.00	0.22	0.00
Al ₂ O ₃	0.00	0.00	1.22	0.40	0.37	1.08	0.43	1.25	1.17	1.71	0.43
Cr ₂ O ₃	0.00	2.48	0.32	0.00	0.00	0.28	0.00	0.00	0.36	0.42	0.00
FeO	17.23	23.79	19.12	26.02	26.16	19.09	27.02	14.33	9.29	18.50	27.02
NiO	0.00	0.00	0.00	0.00	0.00	0.00	0.00	0.00	0.00	0.00	0.00
MnO	0.40	0.48	0.37	0.61	0.63	0.00	0.40	0.00	0.00	0.00	0.40
MgO	27.11	20.31	23.87	20.46	20.15	23.66	20.12	27.97	31.03	24.84	20.12
CaO	0.31	1.34	1.92	0.27	0.26	2.23	0.21	1.22	1.77	2.03	0.21
Total	99.81	100.00	100.01	100.32	100.00	100.00	99.99	99.97	100.01	100.90	99.99
Cations (6 ox)											
Si	1.987	1.925	1.955	1.982	1.986	1.968	1.965	1.971	1.976	1.928	1.965
Ti	0.000	0.026	0.000	0.000	0.000	0.005	0.000	0.005	0.000	0.006	0.000
Al	0.000	0.000	0.053	0.018	0.017	0.047	0.019	0.053	0.048	0.073	0.019
Cr	0.000	0.074	0.009	0.000	0.000	0.008	0.000	0.000	0.010	0.012	0.000
Fe ²⁺	0.497	0.732	0.561	0.802	0.818	0.587	0.807	0.429	0.272	0.513	0.807
Fe ³⁺	0.026	0.024	0.027	0.018	0.011	0.000	0.050	0.000	0.000	0.048	0.050
Mn	0.012	0.015	0.012	0.019	0.020	0.000	0.013	0.000	0.000	0.000	0.013
Mg	1.466	1.149	1.308	1.150	1.138	1.297	1.137	1.493	1.621	1.342	1.137
Ca	0.012	0.055	0.076	0.011	0.011	0.088	0.009	0.047	0.066	0.079	0.009
Sum	4.000	4.000	4.000	4.000	4.000	4.000	4.000	3.998	3.994	4.000	4.000
Mg#	74.7	61.1	70.0	58.9	58.2	68.8	58.5	77.7	85.6	72.3	58.5
Endmembers											
enstatite	73.3	58.7	66.3	58.0	57.5	65.8	56.8	75.82	82.71	67.72	56.78
ferrosilite	26.1	38.6	29.8	41.4	41.9	29.8	42.8	21.80	13.90	28.30	42.79
wollastonite	0.6	2.8	3.8	0.6	0.5	4.5	0.4	2.38	3.39	3.98	0.43

Selected mineral analyses from Lamprophyres. Mg# = 100 Mg/(Mg + Fe total). Fe determined as FeO. Fe³⁺ and Fe₂O₃ calculated from stoichiometry.

SELECTED PLAGIOCLASE MICROPROBE ANALYSES								
Sample No.	65031		65041			65092	65407	65423
Pos. of Anal.	rim	core	rim	rim-opx	rim-opx	rim	core	rim
Rock Type	Lamprophyre							
SiO ₂	59.63	58.42	61.69	58.71	59.14	62.42	56.03	63.98
Al ₂ O ₃	27.04	27.88	24.21	26.71	26.22	25.07	27.73	23.88
FeO	0.00	0.00	0.00	0.00	0.22	0.00	0.29	0.00
MgO	0.00	0.00	0.00	0.00	0.00	0.00	0.18	0.00
CaO	8.59	9.58	5.64	8.25	7.75	6.07	9.97	4.69
Na ₂ O	6.31	5.84	7.84	6.41	6.63	7.62	5.26	8.56
K ₂ O	0.00	0.00	0.20	0.12	0.27	0.00	0.32	0.25
Total	101.57	101.72	99.58	100.20	100.23	101.18	99.78	101.36
Cations								
Si	2.614	2.565	2.741	2.611	2.633	2.726	2.530	2.785
Al	1.401	1.447	1.271	1.404	1.380	1.294	1.479	1.228
Ca	0.403	0.451	0.268	0.393	0.370	0.284	0.482	0.219
Na	0.536	0.497	0.675	0.553	0.572	0.645	0.460	0.722
K	0.000	0.000	0.011	0.007	0.015	0.000	0.018	0.014
Sum	4.954	4.960	4.967	4.967	4.971	4.949	4.970	4.969
Endmembers								
An	42.9	47.5	28.1	41.3	38.6	30.6	50.2	22.9
Ab	57.1	52.5	70.7	58.0	59.8	69.4	47.9	75.6
Or	0.0	0.0	1.2	0.7	1.6	0.0	1.9	1.5

SELECTED PLAGIOCLASE AND ALKALI-FELDSPAR MICROPROBE ANALYSES										
Sample No.	71760									
Pos. of Anal.	core	core	core	core	core	core	core	core	core	core
Rock Type	Lamprophyre									
SiO ₂	67.26	64.41	67.87	69.10	69.50	69.88	68.09	69.11	68.24	69.34
Al ₂ O ₃	19.20	19.84	19.40	20.60	19.90	19.50	19.40	20.69	20.94	19.10
FeO	0.09	0.32	0.20	0.01	0.72	0.10	0.10	0.09	0.27	0.10
MgO	0.00	0.24	0.00	0.00	0.31	0.08	0.02	0.00	0.07	0.02
CaO	0.09	6.47	0.10	1.09	0.22	1.24	0.11	0.38	0.61	1.24
Na ₂ O	2.16	9.47	4.22	9.76	9.22	9.82	3.11	9.23	4.12	8.26
K ₂ O	11.81	0.11	8.77	0.15	0.14	0.22	9.96	1.49	6.68	1.99
Total	100.61	100.85	100.57	100.71	100.01	100.84	100.78	100.99	100.92	100.05
Cations										
Si	3.018	2.860	3.018	2.981	3.029	3.017	3.025	2.985	2.991	3.029
Al	1.018	1.041	1.019	1.050	1.025	0.995	1.019	1.056	1.085	0.986
Ca	0.004	0.308	0.005	0.050	0.010	0.057	0.005	0.018	0.028	0.058
Na	0.188	0.815	0.364	0.817	0.779	0.822	0.268	0.773	0.350	0.699
K	0.676	0.006	0.498	0.008	0.008	0.012	0.564	0.082	0.374	0.111
Sum	4.905	5.030	4.904	4.906	4.852	4.903	4.881	4.914	4.828	4.883
Endmembers										
An	0.5	27.3	0.6	5.8	1.3	6.4	0.6	2.0	3.8	6.7
Ab	21.7	72.2	42.0	93.3	97.8	92.2	32.0	88.6	46.5	80.5
Or	77.8	0.5	57.4	0.9	1.0	1.3	67.4	9.4	49.7	12.8

SELECTED OLIVINE MICROPROBE ANALYSES

Sample No.	65041		65051				65096 B		
Pos of Anal.	core	core	core	core	rim	ct keli	rim	core	rim
Rock Type	Lamprophyre								
SiO ₂	40.01	40.90	38.10	38.35	38.15		40.59	40.78	37.80
Cr ₂ O ₃	0.00	0.00	0.00	0.00	0.00		0.00	0.00	0.00
FeO	14.30	13.70	22.55	21.20	22.86		13.00	11.25	24.10
NiO	0.40	0.00	0.44	0.00	0.46		0.52	0.37	0.39
MnO	0.00	0.00	0.25	0.00	0.00		0.09	0.00	0.35
MgO	45.10	46.20	38.93	40.44	38.50		46.44	47.41	37.36
Total	99.81	100.80	100.27	99.99	99.97		100.63	99.81	100.00
Si	1.003	1.009	0.992	0.992	0.996		1.003	1.007	0.994
Cr	0.000	0.000	0.000	0.000	0.000		0.000	0.000	0.000
Fe	0.300	0.283	0.491	0.458	0.499		0.269	0.232	0.530
Ni	0.009	0.000	0.011	0.000	0.011		0.012	0.008	0.010
Mn	0.000	0.000	0.006	0.000	0.000		0.002	0.000	0.008
Mg	1.685	1.699	1.510	1.558	1.498		1.711	1.745	1.464
Sum	2.997	2.991	3.008	3.008	3.004		2.997	2.993	3.006
Mg#	84.9	85.7	75.5	77.3	75.0		86.4	88.2	73.4

SELECTED PHLOGOPITE MICROPROBE ANALYSES

Sample No.	65051		65092				65423		
Pos. of Anal.	core	core	core	core	core	core	core	core	core
Rock Type	Lamprophyre								
SiO ₂	44.31	40.38	37.68	38.66	38.05	39.92	38.63	38.64	38.64
TiO ₂	2.64	4.21	5.20	4.86	5.12	4.16	4.95	4.93	4.93
Al ₂ O ₃	12.42	15.80	15.38	15.50	15.16	15.62	15.21	15.21	15.21
FeO	11.52	10.17	17.58	15.55	16.75	10.06	15.93	15.93	15.93
MgO	19.55	19.38	14.31	15.55	14.80	19.16	15.32	15.32	15.32
CaO	3.90	0.74	0.00	0.00	0.31	0.73	0.22	0.23	0.23
K ₂ O	5.38	9.00	9.68	9.74	9.65	8.90	9.63	9.63	9.63
Na ₂ O	0.94	0.32	0.00	0.00	0.00	0.00	0.00	0.00	0.00
Cl	0.09	0.00	0.18	0.14	0.15	0.32	0.11	0.12	0.12
Total	100.75	100.00	100.00	99.99	99.99	98.87	99.99	100.00	100.00
Cations									
Si	6.023	5.578	5.434	5.509	5.465	6.023	5.556	5.516	5.557
Ti	0.270	0.437	0.564	0.521	0.553	0.270	0.545	0.529	0.546
Al	1.990	2.527	2.612	2.601	2.568	1.990	2.533	2.558	2.533
Fe	1.039	1.176	2.120	1.852	2.012	1.039	1.909	1.902	1.909
Mg	3.960	3.990	3.076	3.302	3.168	3.960	3.153	3.259	3.153
Ca	0.568	0.109	0.000	0.000	0.049	0.568	0.030	0.035	0.030
K	0.932	1.586	1.782	1.771	1.769	0.932	1.721	1.754	1.721
Na	0.248	0.087	0.000	0.000	0.000	0.248	0.085	0.000	0.085
Cl	0.009	0.000	0.044	0.033	0.036	0.010	0.031	0.029	0.031
Sum	15.039	15.488	15.632	15.589	15.619	15.040	15.563	15.581	15.565
Mg #	75.2	77.2	59.2	64.1	61.2	75.2	62.2	63.2	62.3

CHAPTER 8

ULTRAMAFIC XENOLITHS

8.1 INTRODUCTION

A variety of ultramafic xenoliths have been found the Vestfold Hills, particularly in the Long Peninsula and Lichen Valley areas, where ovoid bodies (approximately 2 m by 5 m), rich in ultramafic xenoliths are associated with lamprophyric dykes. These dykes are invariably the more primitive members (SiO_2 contents between 38 - 43 wt% and Mg# of ~ 68 ; i.e. samples 71752, 71907 and 71928) of the lamprophyre suite. The ultramafic xenoliths often occur in ovoid, xenolith-rich bodies which have no obvious connections with dyke emplacement, though lamprophyric dykes are invariably in close proximity. The ultramafic xenoliths are mainly *spinel harzburgites*, *spinel websterites* and *pyroxenites* but *spinel lherzolites* have also been found. Crustal xenoliths dominated by feldspar and quartz occur frequently with the ultramafic xenoliths.

The occurrence of mantle xenoliths in the Vestfold Hills lamprophyre dykes indicates a possible primary origin for these lamprophyres (Green & Ringwood, 1967). The ability of these lamprophyric magmas to transport deep seated mantle and crustal material to upper crustal levels, requires a high yield strength for these magmas (e.g. Kushiro et al. 1976; Sparks et al., 1977; Spera, 1980) and/or rapid rates of magma ascent.

This chapter examines petrography, mineralogy and relationships of the ultramafic mantle xenoliths to their lamprophyric host magmas. Due to the small size (2 - 6 cm) of the xenoliths no major and trace element analyse have been made.

8.2 XENOLITH EMPLACEMENT IN PIPELIKE - BODIES

In four localities the xenolith-bearing ovoid bodies are clearly associated with the emplacement of the 1350 Ma old lamprophyre dykes. These bodies form part of relatively narrow (< 1 m) *Lamprophyric* dykes, which have been inflated beyond the usual dyke width, forming roughly elliptical crosssections (*ca.* 5 by 2 m) with long axes parallel to the strike of the host dykes. The xenolith bearing bodies are subvertical and exhibit a pipe - like geometry similar to illustration in Figure 8.1.

The presence of ultramafic xenoliths in these dykes at crustal levels generally requires high magma flow and fracture propagation rates (e.g. Maaløe, 1987). The attainment of high magma velocities is more readily achieved in pipe - like conduits and diatremes than in thin dykes (Jackson & Shaw, 1985). This is evident in the Vestfold Hills as xenolith densities in the ovoid bodies far exceeds that of the often extremely narrow dykes. The dense concentration of xenoliths in these lamprophyre dykes is clearly illustrated in Figure 8.2, along with the composite nature of the xenoliths, which have been derived from the upper mantle, and lower and upper crust. The xenoliths are usually quite small, between 2 and 6 cm in diameter, but occasionally reach up to 15 cm. The xenoliths are mostly elongate, disc-shapes. The high concentration in pipe or lense-like bodies (in cross section) suggests that these represent channels of higher velocity magma flow than the normal dykes and further that there may have been settling of xenoliths or 'choking' of pipes by xenoliths.

XENOLITH BEARING PIPE

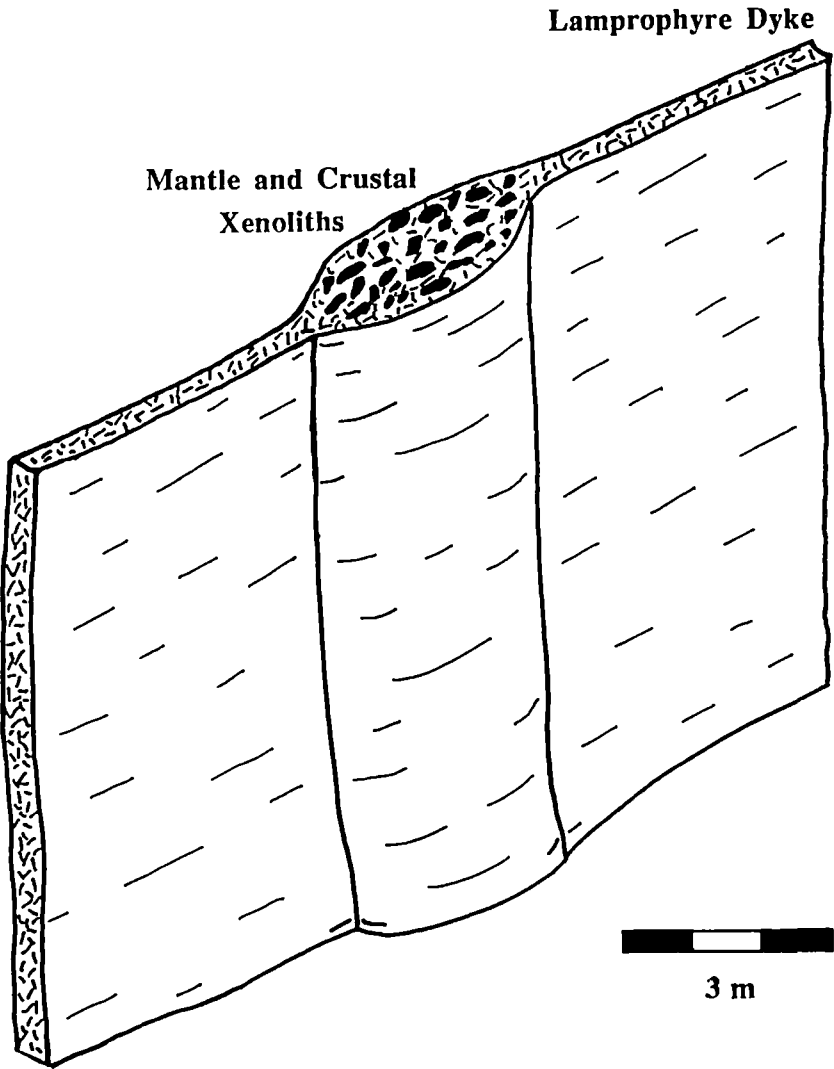


Figure 8.1
Schematic outline of a xenolith-bearing conduit within a narrow lamprophyre dyke.

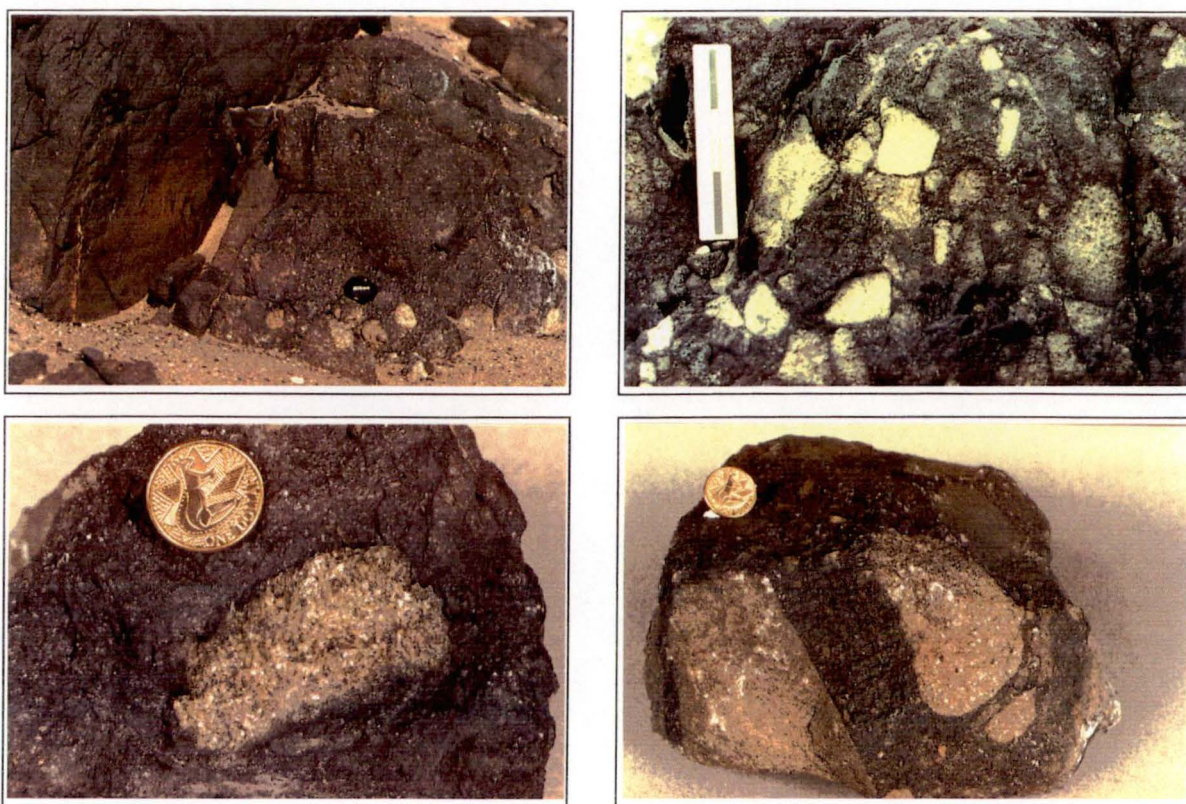


Figure 8.2

Photographs illustrating a variety of xenolith locations in the Vestfold Hills. Note the composite nature of the xenolith populations.

8.3 PETROGRAPHY AND MINERAL CHEMISTRY

Mantle xenoliths associated with the Vestfold Hills lamprophyre dykes include *spinel harzburgites*, *pyroxenites*, *spinel websterites* and *spinel lherzolites*. Many xenoliths have been altered by infiltrating fluids derived from host magmas, yet others remain remarkably fresh and show no significant interaction with their host magma. The six samples which were chosen for detailed examination in this study, were collected from six different xenolith bearing ovoid bodies. The size of these xenoliths ranges from approximately 2 * 3 cm to 5 * 7 cm. The composition of the host magma is known for two of these xenoliths, with xenolith 71766 occurring in sample 71752, xenolith 71928 occurring in dyke sample 71928.

In thin section, the contacts between the xenoliths and the lamprophyric host magma are sharp (Figure 8.2), though occasionally a thin reaction zone (up to 0.4 mm wide) is observed within the xenoliths. The host magma adjacent to the xenolith also has a finer grain size than the dyke proper, suggesting quenching of the host magma against the relatively cold xenoliths.

Spinel Harzburgites and Spinel Lherzolites

The *spinel harzburgite* and *spinel lherzolite* xenoliths usually have granoblastic but sometimes poikilitic textures. *Spinel Harzburgites* are composed of *ca.* 64 vol% olivine, 35 vol% orthopyroxene and 1 vol% spinel, while clinopyroxene occurs in the *spinel lherzolite* with *ca.* 5 vol%. Anhedral olivines reach up to 2.5 mm in size and occasionally show irregular, strained extinction. Core compositions are Mg# 94 (70621-II) whereas rims in contact with the host magma are Mg# 89 (70621-I). Anhedral orthopyroxene (up to 2 mm) in sample 70621-II has a similar Mg# (93 - 94) to coexisting olivine. Light brown and green spinels are \pm round and generally do not exceed 0.02 mm in size, although occasional spinels are up to 1 mm in size. Individual spinel grains are compositionally homogeneous, but differences may occur between spinels both in the same and different *spinel harzburgite* samples with variation ranging from Cr# (100 Cr/(Cr+Al)) 60 to Cr# 34 (Table 8.3). In sample 70621-II two

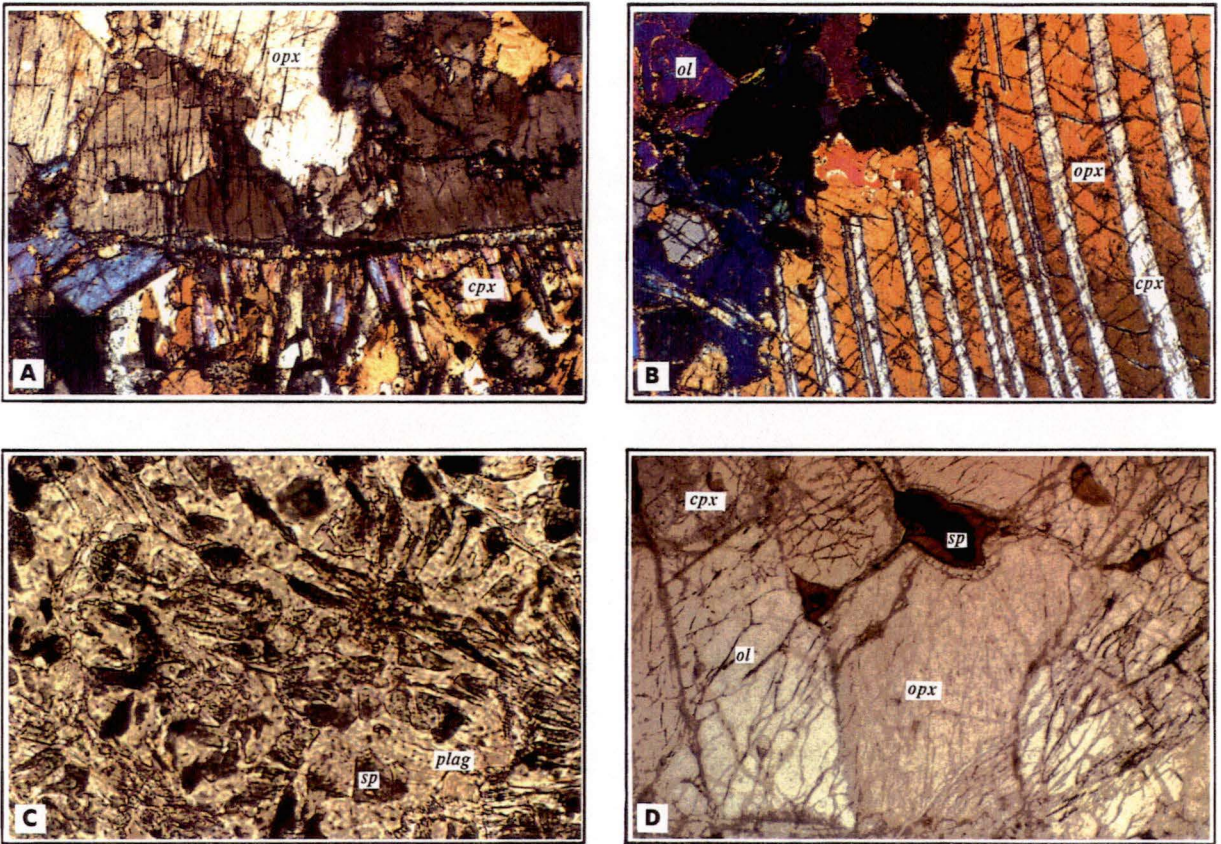


Figure 8.3

Photomicrographs of (A) *spinel harzburgite* xenolith rim in contact with host lamprophyre (2.6 * 1.9 mm), (B) clinopyroxene exsolution lamellae in orthopyroxene (1.3 * 0.95 mm), (C) spinel-plagioclase symplectite (0.65 * 0.45 mm), (D) *spinel lherzolite* (0.65 * 0.45 mm).

generations of spinel are observed; the first has Cr# of 34 - 40 and Mg# between 63 - 82, and the second has Cr# between 42 and 50 and Mg# between 63 and 60. The first generation is characterized by small (0.02 mm) light brown - greenish, rounded spinel, whereas the second spinel generation is characterized by euhedral to subhedral, brown - reddish spinels which reach up to 0.4 mm in size. While the first generation is considered to be primary, the second generation has crystallized due to the infiltration of the host magma into the xenolith. Olivines and orthopyroxenes which surround the second spinel generation are strongly altered and are embedded in a fine grained groundmass, consisting mainly of clinopyroxene.

Lath-shaped phlogopite, up to 0.4 mm long occurs in a single *spinel harzburgite* 72697. Mineral analyses (Table 8.3) exhibit an excess of cations, and high TiO₂ (up to 5.2 wt%) and high Na₂O content (1.5 wt%). Textural features and the high Mg# (96 - 96.7) indicate that this phlogopite is a primary phase.

Websterites and Spinel Websterites

Websterites, including *spinel websterites*, are the second most abundant type of ultramafic xenolith (e.g. samples 71766-I, 71766-II and 72683). They have granular textures and consist mainly of anhedral orthopyroxene and clinopyroxene in about equal amounts, along with minor olivine (*ca.* 5 vol%) and spinel (≤ 1 vol%). Orthopyroxene are up to 5 mm, and have core compositions of Mg# 90 and rims of Mg# 88.3, and clinopyroxenes have Mg# between 92 and 91.

Symplectic intergrowths of spinel, orthopyroxene and plagioclase occur in pyroxenite sample 71766-II (Figure 8.3). These spinels are anhedral spinels, and of irregular shape, with an average size of *ca.* 0.1 mm. They have compositions between Mg# 47 and 55 and low Cr# near 1. The intergrown orthopyroxene has a very narrow compositional range from Mg# 74 to 76, whereas the intergrown plagioclase has a relatively wide range, varying from An₇₂ to An₈₄.

Spinel intergrown with pyroxene or plagioclase is a relatively common feature of *spinel lherzolite* xenoliths (Dawson & Smith, 1975; Basu & MacGregor, 1975;

Morten, 1979; Garrison & Taylor, 1981; Morten et al. 1989). Jaques et al. (1990) has described similar symplectite assemblages in peridotites from Argyle, Western Australia, which have been interpreted as pseudomorphs after garnet. Spinel-pyroxene-plagioclase symplectites have also been observed in *spinel lherzolites* from SE Australia (Bullenmerri / Gnotuk) and attributed to the breakdown of garnet (Griffin et al., 1984). Alternatively, Garrison & Taylor (1981) suggest spinel intergrown with pyroxene may derive by subsolidus exsolution reactions from pyroxene solid solutions in the spinel peridotite field. On the other hand, symplectic intergrowth of spinel and orthopyroxene with plagioclase could represent a subsolidus reaction occurring in combination with the plagioclase lherzolite - spinel lherzolite transition, at pressures somewhere between 8 and 14 kbar depending on bulk composition (Green & Hibberson, 1970). In another interpretation, Morten et al. (1989) have interpreted such symplectic intergrowths with plagioclase to be reaction products formed between infiltrating basaltic liquid and xenolith spinels. Given the symplectic intergrowths occur only near the margins of the Vestfold Hills xenolith, it is concluded that they have formed by reaction between the xenolith and the host magma.

8.3.1 Mineral Compositions and their Variations between Xenoliths

Selected microprobe analyses of phases in the various ultramafic xenoliths are listed in Table 8.2 and compositional variations of olivine, orthopyroxene and clinopyroxene are shown in Figure 8.4 and for spinel in Figure 8.5. These diagrams reveal an overall consistency in mineral chemistry within individual xenoliths, but distinct differences between xenoliths.

Olivine

Olivine in most *spinel harzburgites* is highly magnesian (Mg# 92 - 95) and significantly more Mg-rich than the *spinel lherzolites* (Mg# 87 - 89) and *websterites* (Mg# 83 - 84). Within xenolith variations in olivine composition are minor (Figure 8.4) with for example, samples 70621-II and 72697 (*spinel harzburgites*) having

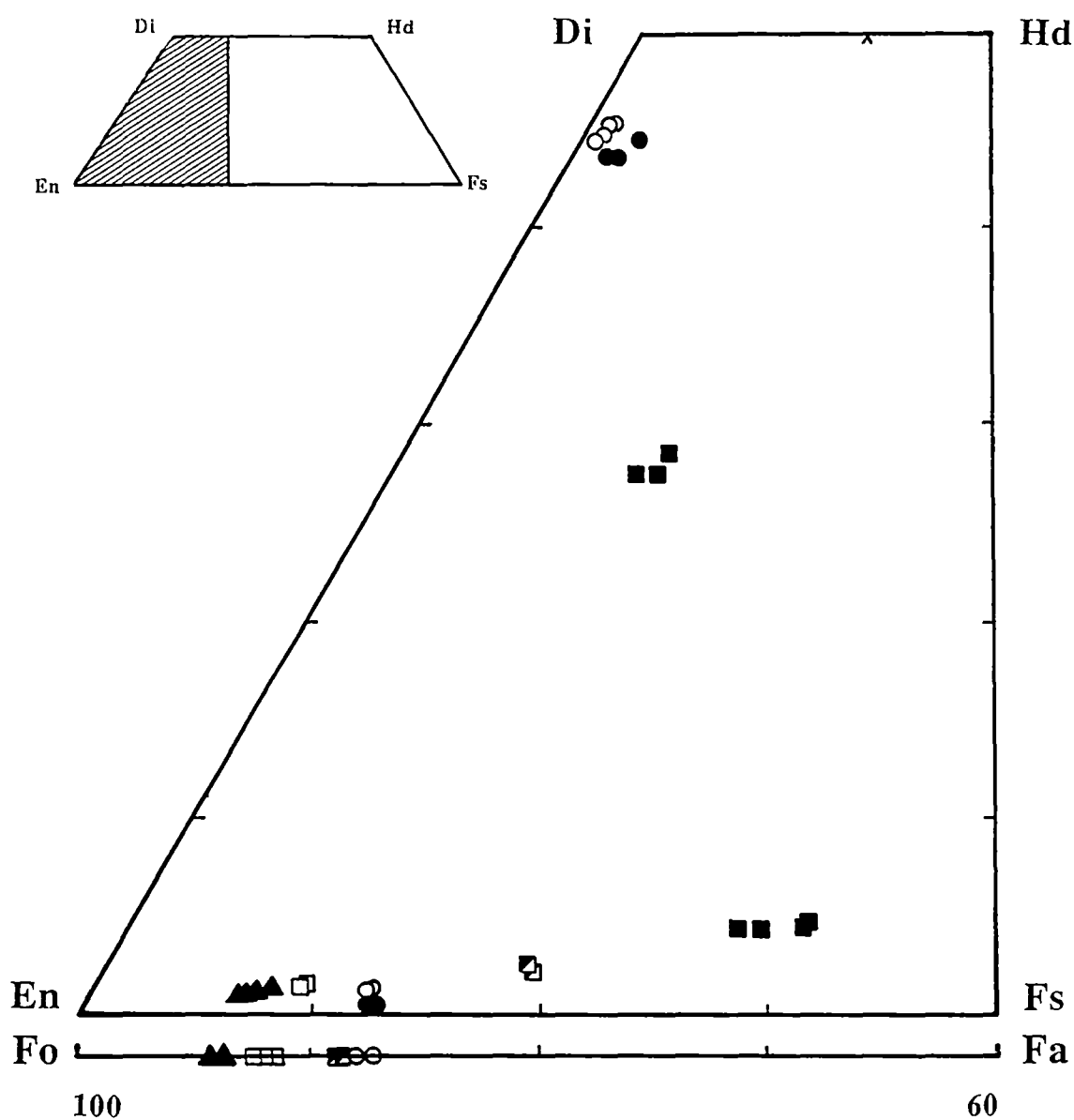


Figure 8.4

Coexisting olivine, orthopyroxene and clinopyroxene from Vestfold Hills ultramafic xenoliths plotted on the pyroxene quadrilateral. Symbols used are: ▲ *spinel harzburgite* 70621, ◼ *websterite* 71766-1, ■ *websterite* 71766-2, ○ *spinel ilherzolute* 72662, ● *spinel harzburgite* 72683 and ◻ *spinel harzburgite* 72697.

olivines of Mg# 94.8 - 94 and Mg# 93.9 - 92.5, respectively. Lower Mg-values are obtained from *spinel harzburgites* 70621-I (Mg# 89), 71766-I (Mg# 89.4 - 88.3) and *spinel lherzolite* 72662 (Mg# 88.3 - 87.1).

Pyroxenes

Orthopyroxenes in the *spinel harzburgites* (70621 and 72697) have compositions of Mg# 94 - 95 and Mg 93 respectively, and differ also in CaO content (0.4 - 0.6 wt% and 0.8 - 1.0 wt%, respectively). In the *spinel lherzolite* (72662) and *websterite* (72683), orthopyroxenes are more Fe-rich (Mg# 88 and Mg# 89 -90) with particularly low CaO content (0.2 - 0.25 wt%) in the *lherzolite* and moderate, variable CaO contents (0.57 - 1.79 wt%) in the *websterite*. Orthopyroxene in the *websterite* also has very low in Al₂O₃ contents (0.4 - 0.66 wt%), in contrast to those of the *spinel lherzolite* and *spinel harzburgite* samples (1.7 - 2.8 wt%). In sample 71766-I the olivine of a *harzburgitic* portion has Mg# 88 - 89 and is clearly out of equilibrium with orthopyroxene of Mg# 83.5 - 84 in a websteritic portion. In the symplectic intergrowth of orthopyroxene + plagioclase + spinel in this sample, orthopyroxene has Mg# 74 - 77. Clinopyroxene close to the symplectite has Mg 76.5 and is sub-calcic (15.4 wt% CaO) and aluminous (4.7 wt% Al₂O₃) in character.

Clinopyroxene in sample 72662, coexisting with olivine, orthopyroxene and spinel, is typical high pressure assemblages with, relatively high alumina content (2.0 - 2.9 wt%). The assemblage is notable for the very low CaO content of orthopyroxene and very high CaO content of clinopyroxene (24.8 -25.3 wt% CaO).

The clinopyroxene in the *websterite* is also highly calcic , i.e. 'low' temperature (23 - 24 wt% CaO) but is low in Al₂O₃ content (1.1 - 1.2 wt%).

Spinel

Spinel compositions in the various xenoliths (see Figure 8.5), exhibit a large range from Cr-poor to Cr-rich compositions. Within the individual xenoliths, variations are minor resulting in spinels from the different xenoliths plotting in distinct

groups. Spinel in the *websterites* (sample 71766-I and 71766-II, including the spinels intergrown with plagioclase and orthopyroxenes) are Cr-poor and have Mg# generally between 45 - 55. The more iron-rich *lherzolite* (sample 72662) contains spinels with Cr# between 6.5 and 12 and Mg# of 63 - 71. Spinel from the magnesian *harzburgite* (sample 72697) exhibit a narrow range in Cr# (47 - 50) but show a relatively wide range in Mg# (52 - 63). Spinel from the *harzburgite* (sample 71928) is similar, with the first generation anhedral spinel of *harzburgite* 70621 has higher Mg# (83 - 65) and lower Cr# (34 - 48). Spinel from *harzburgite* sample 70621 plot in two distinct fields, one with anhedral spinels often included in olivine and orthopyroxene having high Mg# and low Cr# (60 - 82 and 34 - 45), and euhedral intergranular spinels having low Mg# and high Cr# (19 - 23 and 88). This is consistent with the presence of two spinel generations in this sample (see section 8.3).

8.3.2 A Comparison with Spinel in Mantle Xenoliths Elsewhere

Spinel in *spinel lherzolite* xenoliths erupted in basaltic magmas form a well defined field from Mg# 85 to Mg# 70 and Cr# 7 to Cr# 60. Spinel in this field with low Cr# are characteristic of 'undepleted' or 'fertile peridotite' and those with higher Cr# occur in depleted or refractory *lherzolites* and *harzburgites*. Metasomatic effects may complicate this simple relationship as may reactions involving the host magma and also decompression melting of amphibole and phlogopite during xenolith ascent. In the latter case a second generation of spinels often develop as euhedral crystals in glass.

Spinel in *spinel lherzolite* 72662 are amongst the most aluminous occurring in *spinel lherzolites* but are distinct in their more Fe-rich compositions (i.e. Mg# 65 - 70 compared to Mg# 75 - 85). It is notable that coexisting olivine and orthopyroxene in this *spinel lherzolite* are not more Fe-rich than in other *spinel lherzolites*, thus suggesting a possible lower temperature of equilibration for this sample than is commonly found for *spinel lherzolite* xenoliths.

The symplectite spinels, particularly those in the *pyroxenite* sample, have very low Cr# and have Mg# lower than spinels in the *harzburgites*. A comparison can be

SPINEL COMPOSITIONS

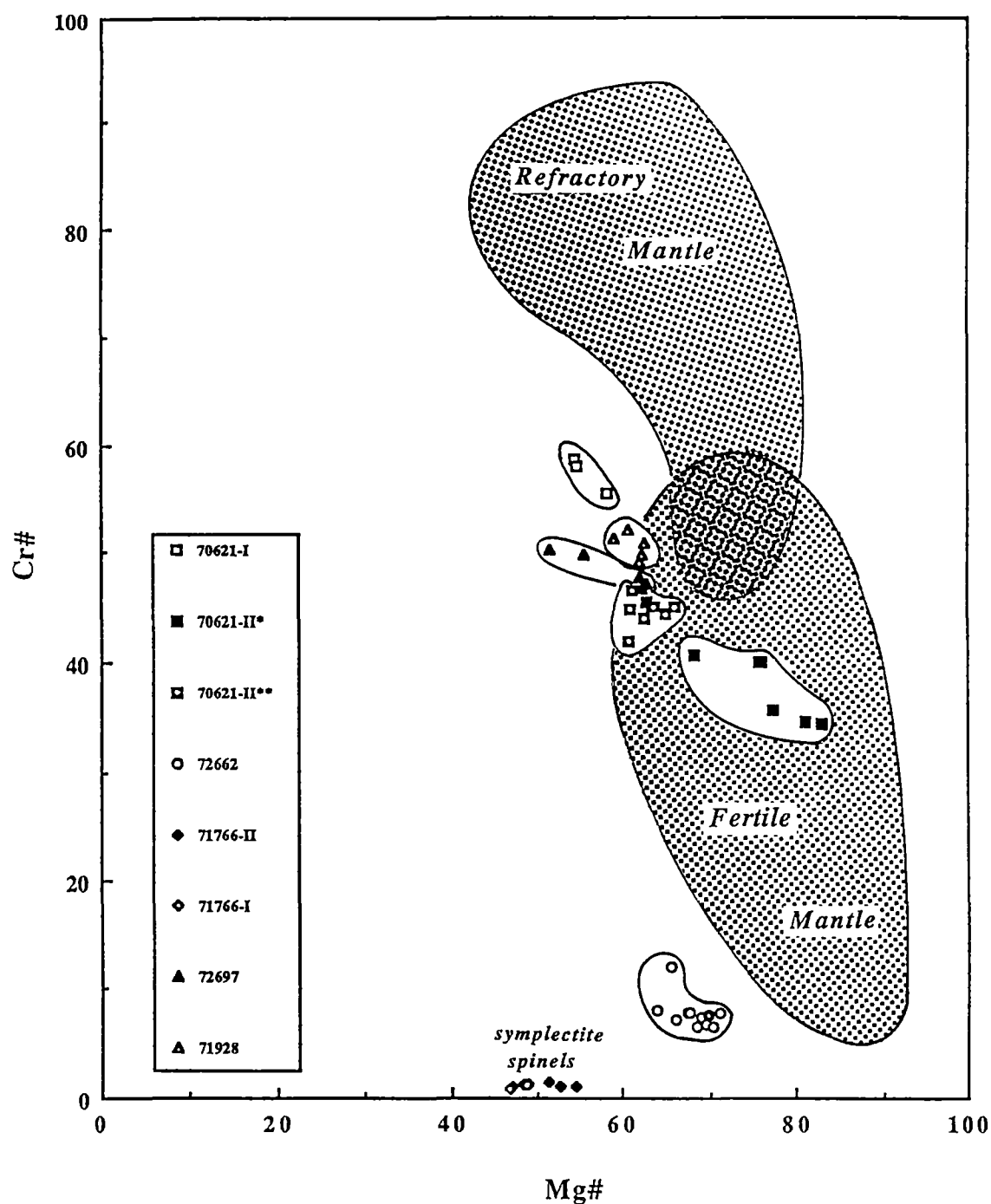


Figure 8.5

Cr# versus Mg# of spinels in Vestfold Hills mantle xenoliths, compared to spinels in fertile and refractory mantle xenoliths. Sample 70621-II* indicates the first generation spinel and 70621-II** the second generation. Data are taken from Griffin et al., 1984; Della Guista et al., 1986; Sachleben & Seck, 1980; Dawson & Smith, 1975; Winterburn et al., 1990; Kyser, 1981; Fuji & Scarfe, 1982; Preß et al., 1996; Brearley et al., 1984; Takahashi 1980, Rutter, 1987; Canil et al., 1990; Furnes et al., 1986; Erlank et al., 1987; Gutman, 1986; Francis, 1987; McGuire, 1988; Kurat et al., 1980; Jones et al., 1983; Reid et al., 1975.

made with similar symplectite spinels in olivine gabbros and peridotites from the Giles Complex, which have Mg# ~ 70 and Cr# between 0.5 and 4 (Ballhaus et al., 1989), which have formed by subsolidus reaction at deep crustal levels.

8.4 GEOTHERMOMETRY

Coexisting Ca-rich and Ca-poor pyroxenes in the ultramafic xenoliths can be used to estimate equilibration temperatures for these xenoliths. The geothermometers of Wells (1977), Kretz (1982) and Bertrand & Mercier (1985) have been applied using rim compositions of clinopyroxene and orthopyroxene only. Calculated temperatures range between 750° and 850° C for one pair, and 690° to 830° C for another pair (Table 8.1 A and B). Solvus temperatures calculated after Kretz (1977) are consistently lower than those obtained using the geothermometers of Bertrand & Mercier (1985) and Wells (1977) (by *ca.* 70° C and *ca.* 100° C, respectively). In a single *websterite* sample (72683) a large (1 cm) anhedral enstatite (Mg# 90) has exsolved lamellae of clinopyroxene (Mg# 92). Temperature calculated for all pyroxene pairs range between 775° and 921° C (Table 8.1 C), which is slightly lower than values obtained using pyroxene rim compositions. The texture of this sample indicates slow cooling from higher temperatures down to the calculated temperatures, and the lack of compositional zoning in all pyroxenes in the *websterites* suggests these xenoliths have remained at temperature near 700° - 900° C for a considerable period of time.

Temperatures calculated for the *spinel lherzolite* (72662) are much lower (i. e. 415° - 491° C) than these obtained from the *websterites* (see Table 8.1 D). Unfortunately, the accuracy of these particular estimates is unknown as the available geothermometers are either unsuitable at, or have not been calibrated at these low temperatures.

The equilibrium temperature of the spinel harzburgite and spinel lherzolite xenoliths have been calculated using the olivine - spinel Fe/Mg exchange geothermometers of Fabries (1979), O'Neill & Wall (1987) and Ballhaus et al. (1991).

THERMOMETRY OF XENOLITHS

A				
Sample No. 72683				
Rock Type: Websterite				
	cpx	opx	Thermometers	T°C
Si	1.964	1.981		
Ti	0.002	0.002	Bertrand & Mercier	816
Al	0.047	0.024	Wells	853
Cr	0.016	0.004	Kretz (<1080)	754
Fe2+	0.030	0.207		
Fe3+	0.050	0.004		
Mn	0.000	0.006		
Mg	0.939	1.749		
Ca	0.906	0.021		
Na	0.045	0.000		
Sum	4.000	4.000		
Mg#	92.6	89.3	Pressure estimate (kb):	15
B				
Sample No. 72683				
Rock Type: Websterite				
	cpx	opx	Thermometers	T°C
Si	1.979	1.976		
Ti	0.000	0.001	Bertrand & Mercier	752
Al	0.047	0.027	Wells	830
Cr	0.012	0.005	Kretz (<1080)	689
Fe2+	0.055	0.185		
Fe3+	0.025	0.013		
Mn	0.000	0.004		
Mg	0.926	1.754		
Ca	0.916	0.034		
Na	0.041	0.000		
Sum	4.000	4.000		
Mg#	92.3	89.9	Pressure estimate (kb):	15
C				
Sample No. 72683				
Rock Type: Websterite				
	cpx	opx	Thermometers	T°C
Si	1.985	1.967		
Ti	0.001	0.000	Bertrand & Mercier	842
Al	0.049	0.025	Wells	921
Cr	0.012	0.003	Kretz (<1080)	775
Fe2+	0.084	0.170		
Fe3+	0.000	0.037		
Mn	0.000	0.006		
Mg	0.943	1.768		
Ca	0.909	0.023		
Na	0.017	0.000		
Sum	4.000	3.999		
Mg#	91.8	89.7	Pressure estimate (kb):	15
D				
Sample No. 72662				
Rock Type: Spinel Lherzolite				
	cpx	opx	Thermometers	T°C
Si	1.985	1.967		
Ti	0.001	0.000	Bertrand & Mercier	491
Al	0.049	0.025	Wells	415
Cr	0.012	0.003	Kretz (<1080)	
Fe2+	0.084	0.170		
Fe3+	0.000	0.037		
Mn	0.000	0.006		
Mg	0.943	1.768		
Ca	0.909	0.023		
Na	0.017	0.000		
Sum	4.000	3.999		
Mg#	91.8	89.7	Pressure estimate (kb):	15

THERMOMETRY OF XENOLITHS

E					
Sample No. 70621					
Rock Type: Spinel Harzburgite					
	spinel		olivine	Thermometers	T°C
Ti	0.000	X Mg	0.850		
Al	1.134			O'Neill & Wall	912
Cr	0.818			Fabriès	950
Fe3+	0.048			Ballhaus	925
Fe2+	0.393				
Ni	0.000				
Mg	0.608				
Sum	3.001				
F					
Sample No. 72662					
Rock Type: Spinel Lherzolite					
	spinel		olivine	Thermometers	T°C
Ti	0.001	X Mg	0.880		
Al	1.797			O'Neill & Wall	578
Cr	0.147			Fabriès	672
Fe3+	0.055			Ballhaus	637
Fe2+	0.298				
Ni	0.013				
Mg	0.688				
Sum	2.999				
G					
Sample No. 72697					
Rock Type: Spinel Harzburgite					
	spinel		olivine	Thermometers	T°C
Ti	0.004	X Mg	0.931		
Al	1.017			O'Neill & Wall	646
Cr	0.896			Fabriès	704
Fe3+	0.079			Ballhaus	665
Fe2+	0.375				
Ni	0.004				
Mg	0.621				
Sum	2.996				
H					
Sample No. 72697					
Rock Type: Spinel Harzburgite					
	spinel		olivine	Thermometers	T°C
Ti	0.006	X Mg	0.929		
Al	1.016			O'Neill & Wall	662
Cr	0.905			Fabriès	716
Fe3+	0.067			Ballhaus	697
Fe2+	0.371				
Ni	0.002				
Mg	0.628				
Sum	2.995				

Table 8.1

Temperatures calculated after Wells (1977), Kretz (1982) and Bertrand & Mercier (1985), using pyroxene rim composition of coexisting orthopyroxene and clinopyroxene pairs (8.7 A and B). Temperatures calculated from exsolution lamellae are shown in 8.7 C.

Geothermometers based on the Fe - Mg partitioning between spinel and olivine, (Fabriès, 1979; O'Neill & Wall, 1987; Ballhaus, 1991) were applied to calculate temperatures for spinel-lherzolite and harzburgites. Temperatures for spinel lherzolite (72662), containing clinopyroxene - orthopyroxene pairs as well as olivine - spinel pairs, are shown in Table 8.7 D and F.

Temperatures obtained from Fabriès (1979) and Ballhaus (1991) are 20° - 50° C higher than those obtained using O'Neill & Wall (1987), giving temperatures between 578° - 672° C for the *spinel lherzolite* and 646° - 716° C for the *spinel harzburgite* (Table 8.1 F - G). Temperatures of 912° - 950° C were obtained for the second spinel generation in sample 70621-II, based on equilibrium with olivine of Mg# 85 (see Table 8.1 C). These values are about 200° C higher than the temperatures obtained for the first generation spinel.

Compared to the *websterite* two-pyroxene temperatures, the *harzburgite* olivine-spinel temperatures are lower by 50° - 100° C. This may reflect either the different closure temperatures of these different mineral pairs, or different thermal histories for these different xenolith types. The *spinel lherzolite* xenolith temperatures obtained from olivine - spinel pairs are slightly lower than these of the *spinel harzburgite*, but 100° - 200° C higher than the temperatures obtained from the pyroxene pairs. This discrepancy between these two different thermometers in this single sample could reflect a more rapid response of the olivine - spinel pairs to heating in the host magma, or may simply be an artifact of inaccuracies (systematic differences) in these geothermometers at low temperatures. The possibility that the low temperatures, implicated by these thermometers (i.e. 400° - 700° C), are the result of metamorphism within the crust can be ruled out by the differences in temperatures recorded in different xenoliths.

8.5 DISCUSSION

The spectrum of Vestfold Hills ultramafic xenoliths recorded here, provides evidence for the existence of complex and very heterogeneous upper-mantle and lower crust beneath the Vestfold Hills at 1350 Ma. The *pyroxenites* are likely to be cumulates associated with mafic intrusives in the deep crust (or upper mantle) which have equilibrated under granulite facies conditions. The *spinel harzburgites*, with their highly magnesian and Cr-rich phase assemblages, clearly represent fragments of very refractory mantle, and the occurrence of more fertile *spinel lherzolites* indicates this mantle is heterogeneous. The highly refractory nature of the *spinel harzburgites* is consistent with existing models for the nature of Archaean and early Proterozoic lithospheric mantle, formed by extraction of large volume of ultramafic melts. It further seems unlikely that this refractory mantle material could produce a source for the 1350 Ma lamprophyric magmas.

The lack of zoning in olivine, orthopyroxene and spinel in the most primitive xenoliths is consistent with these phases being in chemical equilibrium prior to entrainment in the lamprophyric host magmas, and indicate that rapid transportation to lower crustal levels has occurred with insufficient time for heating and re-equilibration in the host magma. Temperature estimates based on spinel - olivine and orthopyroxene - clinopyroxene pairs indicate unusually low upper mantle temperatures between 500° and 900° C, which is *ca.* 100 - 400° C lower than temperatures obtained for mantle xenoliths elsewhere (e.g. MacGregor & Basu, 1974; Mercier & Carter, 1975; Takahashi, 1980 a; Griffin et al., 1984; Stolz & Davies, 1988).

It is unlikely that the spinel - olivine and two pyroxene pairs have been reset to lower temperatures following emplacement. The host lamprophyric dykes have igneous mineral compositions and do not show any evidence of low temperature recrystallization. In addition, pyroxene pairs in alkaline lamprophyres, emplaced at the same time as the high-Mg lamprophyric magmas (ultramafic lamprophyres) in which the xenoliths occur, provide temperature estimates in the range of *ca.* 1100° - 1200° C (see Chapter 7). These temperatures have clearly not been reset by metamorphism

following dyke emplacement. The relatively high temperatures (920° C) obtained for the second spinel generation occurring in some xenoliths, which are affected by magma infiltration, are consistent with high temperature crystallization reactions involving the host lamprophyric magma. These relatively high temperatures provide additional evidence against low temperature recrystallization of the xenolith at crustal levels.

The low average temperatures (*ca.* 700° C) yielded by the spinel - olivine pairs are argued to record temperatures within the middle Proterozoic uppermost mantle beneath the Vestfold Hills at 1350 Ma. The very refractory and low temperature nature of the peridotite xenolith suggests these samples represent mantle which is residual after an earlier magma segregation event. It is notable that Kuehner (1986, 1989) has estimated shallow magma segregation depth for the 2350 Ma high-Mg tholeiites (between 10 and 15 kbar) leaving *harzburgite* residues. Clearly the highly refractory *spinel harzburgite* xenoliths and the high-Mg tholeiite magmas are potential complementary components of the 2350 Ma magma generation events beneath the Vestfold Hills. If correct the uppermost mantle must have cooled from the high-Mg tholeiite liquidus temperatures, at or > 1350° C, to less than 700° C over a period of 1100 Ma. A possible PT path of the uppermost mantle underlying the Vestfold Hills is shown in Figure 8.6.

8.6 CONCLUSIONS

Ultramafic xenoliths occurring in 1350 Ma lamprophyre dykes in the Vestfold Hills are fragments of a heterogeneous, uppermost Proterozoic mantle and lower crust. The highly refractory *spinel harzburgites* and *spinel lherzolites* can be argued to be the refractory residues, complementary to earlier magma generation events, which produced the 2350 Ma high-Mg tholeiites. Low calculated temperatures for these xenoliths (i.e. $\leq 700^{\circ}\text{C}$) indicate the presence of a cool, shallow (probably < 15 kbar) mantle at 1350 Ma. These low temperatures fall near present-day shield geotherms and may argue to require > 600° C cooling between 2350 and 1350 Ma.

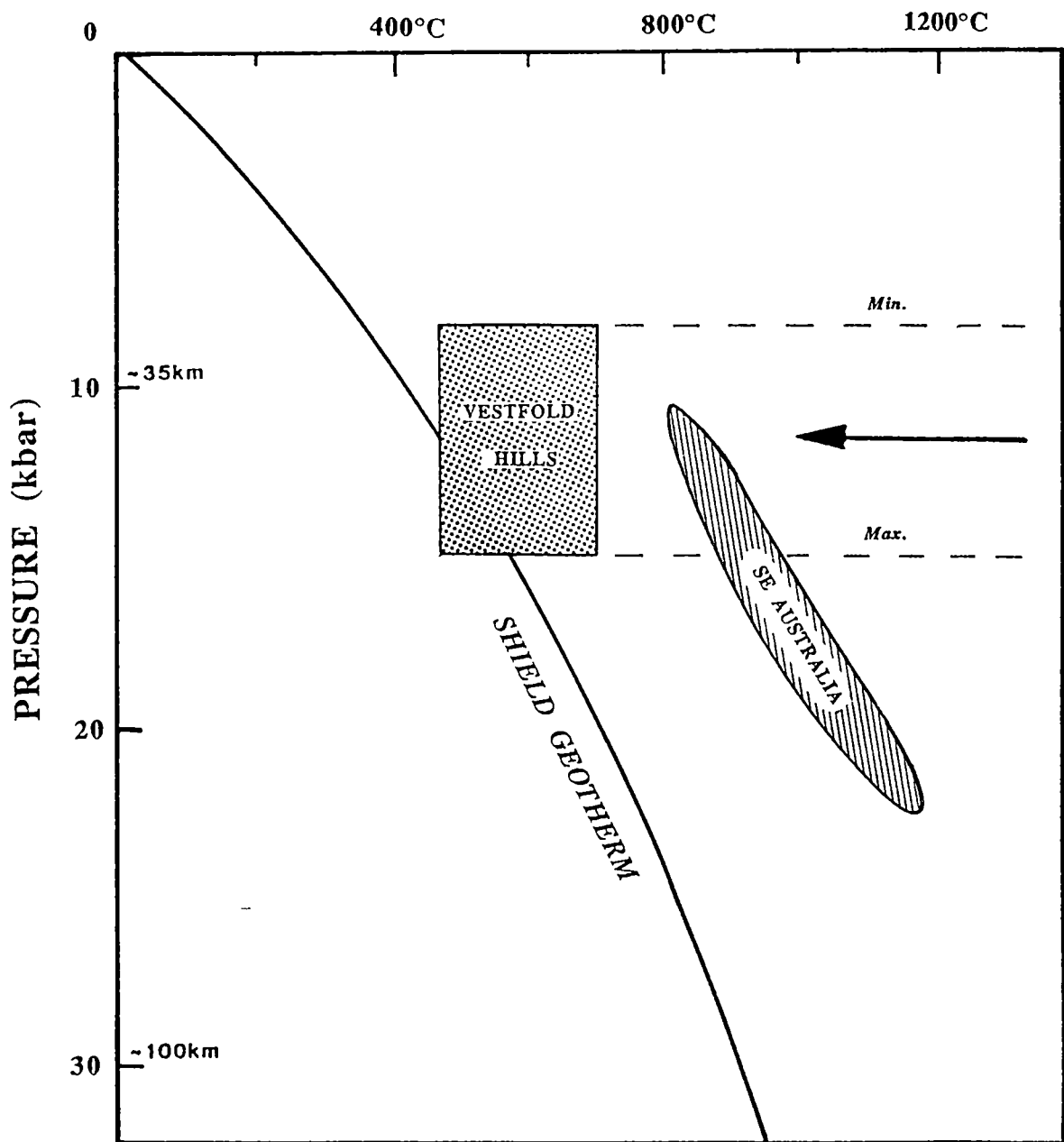


Figure 8.6

P-T estimates for *spinel harzburgite* and *spinel lherzolite* xenoliths in lamprophyres from the Vestfold Hills in relation to inclusions from SE Australia (Nickel & Green, 1985). Geotherm for shields after Clark & Ringwood (1964).

TABLE 8.2

SELECTED SPINEL MICROPROBE ANALYSES

Sample No. Pos.of Anal. Rock Type	70621-I core Spinel	70621-II core* Harzburgite	core*	core**	71766-I core Websterite	rim	71766-II symplectic intergr. Websterite	intergr.	72662 core Spinel	core
SiO ₂	0.07	0.08	0.01	0.02	0.17	0.00	0.09	0.17	0.01	0.00
TiO ₂	0.08	0.01	0.00	0.01	2.58	0.04	1.85	0.13	0.23	0.37
Al ₂ O ₃	23.73	34.55	38.43	32.54	57.98	57.57	57.97	61.41	53.81	50.57
Cr ₂ O ₃	44.22	34.48	30.16	35.09	0.83	7.02	0.95	0.89	6.74	6.69
Fe ₂ O ₃	0.82	1.53	2.54	2.14	0.55	2.75	2.21	2.03	6.61	9.74
FeO	15.90	9.99	7.29	15.93	24.48	13.48	23.96	20.31	14.22	15.61
MnO	0.17	0.00	0.00	0.00	0.20	0.10	0.25	0.07	0.01	0.04
NiO	0.00	0.00	0.00	0.00	0.14	0.61	0.20	0.10	0.70	0.73
MgO	2.41	17.64	19.79	13.83	12.02	17.47	11.96	13.74	16.66	15.48
Total	97.38	98.28	98.22	99.55	98.95	99.04	99.42	98.83	98.99	99.23
Cations										
Ti	0.002	0.000	0.000	0.000	0.053	0.001	0.038	0.003	0.005	0.008
Al	0.880	1.179	1.276	1.134	1.865	1.797	1.859	1.935	1.713	1.639
Cr	1.097	0.787	0.670	0.818	0.018	0.147	0.020	0.019	0.143	0.145
Fe ₃₊	0.019	0.033	0.054	0.048	0.011	0.055	0.045	0.041	0.134	0.201
Fe ₂₊	0.417	0.241	0.171	0.393	0.557	0.298	0.544	0.453	0.320	0.358
Mn	0.004	0.000	0.000	0.000	0.005	0.002	0.006	0.002	0.000	0.001
Ni	0.000	0.000	0.000	0.000	0.003	0.013	0.004	0.002	0.015	0.016
Mg	0.580	0.759	0.829	0.608	0.488	0.688	0.484	0.546	0.669	0.632
Sum	3.000	3.000	3.000	3.000	3.000	3.000	3.000	3.000	3.000	3.000
Mg #	58.2	75.9	82.9	60.7	46.7	69.8	47.1	54.6	67.6	63.9
Chrome #	55.5	40.0	34.4	41.9	0.9	7.5	1.1	1.0	7.7	8.1
Ferric #	4.4	12.1	23.9	10.8	2.0	15.5	7.7	8.3	29.5	36.0

SELECTED SPINEL MICROPROBE ANALYSES

Sample No. Pos.of Anal. Rock Type	72697 rim Spinel	rim Harzburgite	core	72662 core Spinel	core Lherzolite	near rim	rim	rim	core	core
SiO ₂	0.04	0.07	0.06	0.01	0.00	0.01	0.00	0.03	0.00	0.00
TiO ₂	0.17	0.20	1.08	0.23	0.37	0.16	0.04	0.00	0.00	0.07
Al ₂ O ₃	28.35	25.77	25.10	53.81	50.57	55.52	57.57	58.37	58.77	53.75
Cr ₂ O ₃	37.32	38.14	38.16	6.74	6.69	6.98	7.02	7.39	6.11	6.17
Fe ₂ O ₃	3.46	4.51	2.30	6.61	9.74	3.20	2.75	1.46	1.64	5.84
FeO	14.78	17.01	18.59	14.22	15.61	14.19	13.48	12.94	13.31	14.53
MnO	0.15	0.30	0.32	0.01	0.04	0.09	0.10	0.02	0.03	0.06
NiO	0.16	0.06	0.00	0.70	0.73	0.67	0.61	0.58	0.50	0.68
MgO	13.73	11.93	11.14	16.66	15.48	16.46	17.47	17.89	17.58	15.93
Total	98.17	97.99	96.75	98.99	99.23	97.28	99.04	98.68	97.94	97.03
Cations										
Ti	0.004	0.005	0.026	0.005	0.008	0.003	0.001	0.000	0.000	0.001
Al	1.017	0.947	0.939	1.713	1.639	1.779	1.797	1.817	1.839	1.743
Cr	0.896	0.938	0.955	0.143	0.145	0.150	0.147	0.154	0.128	0.134
Fe ₃₊	0.079	0.106	0.055	0.134	0.201	0.065	0.055	0.029	0.033	0.121
Fe ₂₊	0.375	0.442	0.492	0.320	0.358	0.322	0.298	0.285	0.295	0.333
Mn	0.004	0.008	0.009	0.000	0.001	0.002	0.002	0.000	0.001	0.001
Ni	0.004	0.001	0.000	0.015	0.016	0.015	0.013	0.012	0.011	0.015
Mg	0.621	0.553	0.525	0.669	0.632	0.665	0.688	0.702	0.694	0.651
Sum	3.000	3.000	3.000	3.000	3.000	3.000	3.000	3.000	3.000	3.000
Mg #	62.3	55.5	51.6	67.6	63.9	67.4	69.8	71.1	70.2	66.1
Chrome #	46.8	49.8	50.4	7.7	8.1	7.8	7.5	7.8	6.5	7.1
Ferric #	17.4	19.3	10.0	29.5	36.0	16.9	15.5	9.2	10.0	26.6

Mg#(spinel) = 100 Mg/(Mg + Fe₂₊), Cr# = 100 Cr/(Cr + Al), Fe determination as FeO: Fe₃₊ and Fe₂O₃ calculated from stoichiometry. Mg# (silicates) = 100 Mg/(Mg + Fe total). * First spinel generation, ** second spinel generation.

SELECTED ORTHOPYROXENE MICROPROBE ANALYSES

Sample No.	70621-II			72683		71766-I		71766-II		71928		72697		72662	
Pos. of Anal.	core	rim	ct ol	lamallae	rim-cpx	core	symp.	intergr.		core	core	core	rim	core	core
Rock Type	Sp. Harzburgite	Sp. Harzburgite	Sp. Harzburgite	Websterite	Websterite	Websterite	Websterite	Websterite	Websterite	Sp. Harzburgite	Sp. Harzburgite	Sp. Harzburgite	Sp. Harzburgite	Sp. Lhz	Sp. Lhz
SiO ₂	52.85	57.70		55.95	57.03	53.95	50.79	51.75	56.66	56.46	55.75	55.35	55.17		
TiO ₂	0.03	0.02		0.01	0.09	0.50	0.16	0.17	0.02	0.03	0.15	0.25	0.12		
Al ₂ O ₃	5.18	2.75		0.60	0.59	2.42	6.27	5.40	2.18	1.74	3.02	3.14	2.65		
Cr ₂ O ₃	2.78	0.49		0.12	0.14	0.07	0.10	0.05	0.67	0.35	0.69	0.84	0.10		
FeO	3.77	3.83		7.03	7.28	10.18	13.72	14.72	3.92	4.91	4.57	4.66	7.77		
NiO	0.00	0.00		0.11	0.12	0.08	0.10	0.03	0.05	0.05	0.06	0.20	0.00		
MnO	0.02	0.08		0.21	0.19	0.11	0.37	0.35	0.05	0.07	0.05	0.06	0.24		
MgO	33.64	35.43		33.75	33.79	29.88	25.41	25.74	34.91	34.69	34.43	34.48	34.50		
CaO	0.69	0.61		0.61	0.57	1.30	2.04	1.99	0.60	0.51	0.90	0.96	0.21		
Total	98.97	100.91		98.37	99.80	98.49	98.96	100.20	99.06	98.82	99.63	99.95	100.76		
Cations (6 ox)															
Si	1.835	1.949		1.967	1.981	1.931	1.843	1.858	1.954	1.960	1.921	1.904	1.889		
Ti	0.001	0.001		0.000	0.002	0.014	0.004	0.005	0.001	0.001	0.004	0.007	0.003		
Al	0.213	0.110		0.025	0.024	0.102	0.269	0.229	0.089	0.071	0.123	0.128	0.107		
Cr	0.076	0.013		0.003	0.004	0.002	0.003	0.001	0.018	0.010	0.019	0.023	0.003		
Fe ²⁺	0.069	0.108		0.170	0.207	0.298	0.383	0.398	0.113	0.142	0.122	0.106	0.117		
Fe ³⁺	0.040	0.000		0.037	0.004	0.007	0.034	0.044	0.000	0.000	0.009	0.028	0.105		
Mn	0.001	0.002		0.006	0.006	0.003	0.011	0.011	0.001	0.002	0.001	0.002	0.007		
Mg	1.740	1.784		1.768	1.749	1.593	1.374	1.378	1.794	1.794	1.767	1.768	1.760		
Ca	0.025	0.022		0.023	0.021	0.050	0.079	0.076	0.022	0.019	0.033	0.035	0.008		
Sum	4.000	3.989		4.000	4.000	4.000	4.000	4.000	3.992	3.999	4.000	4.000	4.000		
Mg#	94.3	94.3		89.7	89.2	84.0	76.9	75.9	94.1	92.6	93.1	93.1	89.3		
Endmembers															
enstatite	92.8	93.2		88.5	88.2	81.8	73.5	72.7	92.99	91.75	91.5	91.3	88.4		
ferrosilite	5.8	5.7		10.3	10.7	15.6	22.3	23.3	5.86	7.28	6.8	6.9	11.2		
wollastonite	1.4	1.1		1.2	1.1	2.6	4.2	4.0	1.15	0.96	1.7	1.8	0.4		

SELECTED CLINOPYROXENE MICROPROBE ANALYSES

Sample No.	71766-II		72662				72683						
Pos. of Anal.	core	core	core	core	core-rim	rim-opx	rim-opx	exol-opx	rim-opx	rim-opx	rim-opx	rim-opx	rim-opx
Rock Type	Websterite	Websterite	Spinel	Lherzolite	Lherzolite	Lherzolite	Lherzolite	Lherzolite	Websterite	Websterite	Websterite	Websterite	Websterite
SiO ₂	53.00	52.55	52.12	52.26	52.86	53.05	52.22	53.88	53.77	54.07	54.29	53.98	
TiO ₂	0.80	0.85	0.82	0.63	0.48	0.31	0.68	0.01	0.09	0.00	0.09	0.04	
Al ₂ O ₃	4.63	4.66	4.70	2.92	2.44	2.01	2.98	1.18	1.09	1.08	1.08	1.10	
Cr ₂ O ₃	0.14	0.13	0.17	0.09	0.10	0.10	0.08	0.46	0.54	0.40	0.46	0.49	
FeO	8.48	8.34	8.49	2.76	2.65	2.38	2.71	2.61	2.61	2.61	3.35	2.64	
NiO	0.01	0.06	0.07	0.02	0.02	0.05	0.04	0.00	0.11	0.06	0.20	0.04	
MnO	0.00	0.07	0.00	0.05	0.07	0.04	0.00	0.08	0.12	0.02	0.12	0.08	
MgO	15.63	15.22	15.51	16.66	16.73	16.91	16.32	17.18	17.26	16.97	20.47	17.19	
CaO	15.35	15.43	15.46	24.82	24.85	24.97	25.27	23.00	23.16	23.36	18.19	23.70	
Na ₂ O	1.97	1.91	1.90	0.27	0.24	0.21	0.24	0.66	0.64	0.58	0.67	0.61	
Total	100.00	99.21	99.26	100.48	100.44	100.04	100.55	99.07	99.38	99.16	98.93	99.86	
Cations (6 ox)													
Si	1.930	1.934	1.915	1.892	1.915	1.928	1.891	1.971	1.964	1.979	1.973	1.961	
Ti	0.022	0.023	0.023	0.017	0.013	0.008	0.019	0.000	0.002	0.000	0.003	0.001	
Al	0.199	0.203	0.204	0.125	0.105	0.086	0.127	0.051	0.047	0.047	0.047	0.047	
Cr	0.004	0.004	0.005	0.003	0.003	0.003	0.002	0.013	0.016	0.012	0.013	0.014	
Fe ²⁺	0.227	0.242	0.210	0.010	0.027	0.019	0.014	0.041	0.030	0.055	0.065	0.023	
Fe ³⁺	0.031	0.014	0.051	0.074	0.053	0.054	0.068	0.039	0.050	0.025	0.037	0.057	
Mg	0.848	0.835	0.849	0.898	0.903	0.916	0.881	0.937	0.939	0.926	1.108	0.931	
Ca	0.599	0.608	0.608	0.963	0.964	0.972	0.981	0.901	0.906	0.916	0.708	0.923	
Na	0.139	0.136	0.135	0.019	0.017	0.015	0.017	0.047	0.045	0.041	0.047	0.043	
Sum	4.000	4.000	4.000	4.000	4.000	4.000	4.000	4.000	4.000	4.000	4.000	4.000	
Mg#	76.7	76.5	76.5	91.5	91.8	92.7	91.5	92.1	92.2	92.1	91.6	92.1	
Endmembers													
Mg ₂ Si ₂ O ₆	42.4	41.7	42.5	44.9	45.1	45.8	44.0	46.8	47.0	46.3	55.4	46.5	
Fe ₂ Si ₂ O ₆	11.4	12.1	10.5	0.5	1.3	0.9	0.7	2.0	1.5	2.7	3.2	1.2	
Ca ₂ Si ₂ O ₆	27.6	28.3	27.3	43.6	44.6	45.4	44.5	43.6	43.6	44.7	34.2	44.3	
NaAlSi ₂ O ₆	10.4	11.8	7.9	0.0	0.0	0.0	0.0	0.0	0.0	0.0	0.0	2.9	
NaFeSi ₂ O ₆	3.1	1.4	5.1	1.6	1.4	1.2	1.5	3.3	3.0	2.5	3.4	1.4	
NaCrSi ₂ O ₆	0.4	0.4	0.5	0.3	0.3	0.3	0.2	1.3	1.6	1.2	1.3	0.8	
CaAl ₂ Si ₂ O ₆	2.6	1.9	4.0	1.7	1.9	1.4	1.9	2.2	1.1	2.1	1.9	2.8	
CaFeAlSiO ₆	0.0	0.0	0.0	5.7	3.9	4.2	5.3	0.6	2.0	0.0	0.3	0.0	
CaTiAl ₂ O ₆	2.2	2.3	2.3	1.7	1.3	0.8	1.9	0.0	0.0	0.0	0.0	0.0	

SELECTED PLAGIOCLASE MICROPROBE ANALYSES

Sample No. Pos. of Anal. Rock Type	71766-II symplectic intergrowth Websterite				
SiO ₂	44.24	44.96	46.72	47.96	48.65
Al ₂ O ₃	33.18	33.46	33.75	32.19	32.74
FeO	0.49	0.77	0.78	0.79	0.78
MgO	0.21	0.31	0.30	0.58	0.59
CaO	17.37	16.73	17.23	14.39	14.43
Na ₂ O	1.75	2.01	1.73	2.97	2.53
K ₂ O	0.02	0.00	0.05	0.05	0.05
Total	97.25	98.24	100.56	98.92	99.77
Cations					
Si	2.112	2.127	2.155	2.240	2.246
Al	1.872	1.871	1.840	1.776	1.786
Ca	0.888	0.848	0.852	0.720	0.714
Na	0.161	0.185	0.155	0.269	0.226
K	0.001	0.000	0.003	0.003	0.003
Sum	5.034	5.030	5.004	5.008	4.975
Endmembers					
An	84.5	82.1	84.4	72.6	75.7
Ab	15.4	17.9	15.3	27.1	24.0
Or	0.1	0.0	0.3	0.3	0.3

SELECTED PHLOGOPITE MICROPROBE ANALYSES

Sample No. Pos. of Anal. Rock Type	72697 core rim core rim rim Spinel Harzburgite				
SiO ₂	42.34	43.09	41.75	42.38	43.08
TiO ₂	3.54	3.61	5.17	4.74	3.62
Al ₂ O ₃	16.44	15.81	16.30	16.13	15.79
FeO	1.71	1.68	1.86	1.80	1.68
MgO	26.19	26.65	25.45	25.40	26.67
CaO	0.01	0.00	0.00	0.00	0.00
K ₂ O	8.41	7.90	8.11	8.03	7.91
Na ₂ O	1.35	1.27	1.36	1.51	1.26
Total	100.00	100.00	100.00	100.00	100.00
Cations					
Si	6.009	6.088	5.939	5.990	6.089
Ti	0.378	0.384	0.553	0.504	0.383
Al	2.750	2.633	2.732	2.687	2.631
Fe	0.203	0.198	0.222	0.213	0.198
Mg	5.539	5.612	5.397	5.351	5.614
Ca	0.002	0.000	0.000	0.001	0.000
K	1.523	1.423	1.472	1.448	1.425
Na	0.371	0.348	0.374	0.414	0.346
Sum	16.774	16.686	16.688	16.608	16.687
Mg #	96.5	96.6	96.1	96.2	96.7

SELECTED OLIVINE MICROPROBE ANALYSES

Sample No.	70621-I	70621-II	71766-I							71928
Pos of Anal.		rim-sp	incl-opx	core	rim	core	rim	rim	core	core
Rock Type	Spinel Harzburgite			Websterite						Sp Harzb.
SiO ₂	40.50	42.16	42.46	40.22	40.28	39.52	40.35	40.67	40.35	40.66
Cr ₂ O ₃	0.05	0.05	0.06	0.01	0.07	0.01	0.00	0.02	0.09	0.02
FeO	10.71	5.93	5.19	10.43	11.23	10.60	10.57	10.24	10.50	5.57
NiO	0.41	0.05	0.51	0.29	0.34	0.32	0.38	0.28	0.27	0.39
MnO	0.14	0.06	0.09	0.19	0.19	0.24	0.21	0.14	0.23	0.06
MgO	48.45	52.11	53.09	47.93	47.54	47.77	48.22	48.43	48.16	50.35
Total	100.24	100.36	101.41	99.06	99.65	98.45	99.74	99.76	99.60	97.05
Cations (4 ox)										
Si	0.996	1.009	1.005	0.999	0.999	0.991	0.997	1.001	0.998	1.007
Cr	0.000	0.000	0.000	0.000	0.000	0.000	0.000	0.000	0.001	0.000
Fe	0.220	0.119	0.103	0.217	0.233	0.222	0.218	0.211	0.217	0.115
Ni	0.009	0.001	0.011	0.007	0.008	0.007	0.009	0.006	0.006	0.009
Mn	0.003	0.001	0.002	0.004	0.004	0.005	0.004	0.003	0.005	0.001
Mg	1.775	1.860	1.873	1.774	1.757	1.784	1.775	1.777	1.775	1.859
Sum	3.004	2.990	2.995	3.001	3.001	3.009	3.003	2.999	3.002	2.992
Mg#	89.0	94.0	94.8	89.1	88.3	88.9	89.0	89.4	89.1	94.2

SELECTED OLIVINE MICROPROBE ANALYSES

Sample No.	72697						72662			
Pos of Anal.	core	rim	core	core	core	rim	core	rim-opx	core	rim
Rock Type	Spinel Harzburgite						Spinel Lherzolite			
SiO ₂	41.17	41.18	41.43	40.56	40.75	40.79	40.19	39.83	39.44	38.91
Cr ₂ O ₃	0.03	0.01	0.00	0.04	0.01	0.03	0.00	0.00	0.00	0.03
FeO	6.02	6.09	6.81	6.85	7.27	7.27	11.05	11.20	11.42	12.22
NiO	0.35	0.34	0.47	0.31	0.28	0.41	0.63	0.55	0.57	0.48
MnO	0.10	0.09	0.07	0.05	0.04	0.11	0.20	0.11	0.09	0.17
MgO	52.31	51.80	51.21	50.43	50.79	51.00	47.49	47.58	47.55	46.34
Total	99.98	99.51	100.00	98.24	99.14	99.62	99.54	99.26	99.07	98.16
Cations (4 ox)										
Si	0.994	0.998	1.002	0.999	0.997	0.994	0.998	0.993	0.987	0.987
Cr	0.000	0.000	0.000	0.000	0.000	0.000	0.000	0.000	0.000	0.000
Fe	0.122	0.123	0.138	0.141	0.149	0.148	0.229	0.233	0.239	0.259
Ni	0.008	0.008	0.011	0.007	0.006	0.009	0.014	0.013	0.013	0.011
Mn	0.002	0.002	0.002	0.001	0.001	0.002	0.004	0.002	0.002	0.004
Mg	1.881	1.871	1.846	1.851	1.851	1.852	1.757	1.767	1.773	1.752
Sum	3.006	3.002	2.998	3.000	3.003	3.006	3.002	3.007	3.013	3.013
Mg#	93.9	93.8	93.1	92.9	92.6	92.6	88.5	88.3	88.1	87.1

CHAPTER 9

SUMMARY

Mafic dyke swarms of mantle derivation are common in the Precambrian shields of all continents. The Vestfold Hills with its dense network of mafic dykes, provides a classic area for a detailed study of mantle and crustal evolution processes accompanying development of the Archaean and Proterozoic East Antarctic shield. Mafic dykes intruded into this terrane between earliest Proterozoic and mid-Proterozoic time (2350 - 1150 Ma). Based on crosscutting relationships, at least 9 different dyke sets are distinguished, which according to their major element geochemistry, can be divided into 3 major compositional groups: (1) high-Mg tholeiites, (2) lamprophyre magmas and (3) Fe-rich tholeiites. The high-Mg tholeiites were intruded in a major event at 2350 Ma, whereas Fe-rich tholeiites have been emplaced at 2350, 1350 Ma and possibly also at 1800 Ma. Lamprophyric magmas and associated mantle xenoliths were additionally intruded during the 1350 Ma magmatic episode.

The 2350 Ma high-Mg tholeiites have geochemical characteristics of high silica and MgO and low TiO₂ contents. In a re-evaluation of emplacement pressures of the high-Mg tholeiites (Chapter 2), using the mineral chemistry of coexisting clinopyroxene + plagioclase + quartz geobarometry (after Ellis, 1983), and olivine and orthopyroxene phenocryst compositions to constrain crystallization pressures, it is suggested that the tholeiites intruded upper crustal levels at pressures probably between 3 - 5 kbar, but possibly as low as 1 - 2 kbar. This emplacement represents periodic tapping of subjacent magma chambers whose depth, on the basis of olivine and orthopyroxene phenocrysts, was estimated as ~ 8 kbar. It is concluded that the presently exposed crustal level of the Vestfold Hills was uplifted from depths around

24 - 30 km to depths of probably < 10 km between the late Archaean and earliest Proterozoic, at a rate which is a considerably faster than previously proposed. The present crustal thickness of *ca.* 30 km (Kadmina et al. 1983), implies either major crustal thickening (to ~ 55 km) in the 2350 Ma metamorphic and deformation event or that there has been ~ 20 km of crustal underplating during this period of uplift.

Based on geochemical features and crosscutting relationships the high-Mg tholeiite suite is subdivided into 3 major groups and 2 subgroups. A noritic ring complex defines one of the major groups (*II*) and one of the subgroups (*IIa*). The norite consists of three units, a *Homogeneous*-, a *Mottled*-, and a *Rubbly Norite*. The variations of mineralogy, major and minor element geochemistry within the norite the units and associated 'fine grained dykes', are consistent with differentiation dominated by orthopyroxene fractionation/accumulation. In addition to the accumulation of orthopyroxene, Cu-Ni sulphides have been accumulated in the *Rubbly Norite*. Associated with the sulphides are platinoid minerals, considered to have precipitated from the sulphide melt. Due to the accumulation of sulphides and associated platinoids, this unit reveals higher total PGE abundances in comparison to *Homogeneous Norite*, *Mottled Norite* and the 'fine grained dykes'. Recalculation of PGE abundances to 100% sulphides reveals that all high Mg-tholeiite magmas, including the sulphide-rich *Rubbly Norite*, exhibit similar high PGE concentrations when compared to 'normal' basalts (e.g. MORB). A fundamental question concerning genesis of the high-Mg tholeiite magmas is whether their high PGE, MgO, SiO₂ and low TiO₂ concentrations are mantle signatures or result from crustal contamination. Some authors have argued that high Mg, high SiO₂, tholeiitic magmas in ancient shields are the product of high temperature komatiitic magmas and crustal assimilation processes. In Chapters 3 and 6 the role of crustal contamination in producing the geochemical characteristics of the high-Mg tholeiites was considered. Detailed examination of chemical and mineralogical variations in one of the largest high-Mg tholeiitic dykes in the Vestfold Hills reveals only minor contamination across and along dyke, attributed largely to *in situ* differentiation processes.

Within-suite variations, i.e. differences among the high-Mg tholeiite groups (*I, II and III*) noted above, are not consistent with crystal fractionation. With respect to trace element patterns, the high-Mg tholeiites have features, such as Nb, P, Ti and Sr depletions and enrichment in LILE, which may be characteristics of granitic crust. By using such a granitic crust composition from the Vestfold Hills it was possible to match variations within *Group I* high-Mg tholeiites by calculated compositions derived by AFC process. If the geochemical characteristics of the parental or more primitive high-Mg tholeiites are the result of crustal contamination then an uncontaminated mafic primary magma, would have affinities with basaltic komatiites. However, the assimilation of crustal material cannot account for the variations between the other high-Mg tholeiite groups (Chapter 6). The geochemical characteristics of the separate groups of the high-Mg tholeiite suite are interpreted in this study to be more probably signatures of at least two different mantle sources or of an highly heterogeneous mantle source.

In addition to the difficulties associated with understanding the causes for the separate geochemical differences between the 5 high-Mg tholeiite dyke suites, there is the additional complexity of the coeval emplacement of the Fe-rich tholeiite suite. Sheraton & Black (1981) and Kuehner (1986) came to the conclusion that high-Mg tholeiites and Fe-rich tholeiites are not related by simple crystal fractionation or partial melting processes and Kuehner (1986) suggested tapping of two different mantle sources.

There is convincing evidence for the presence of deep crustal cooling and magmatic evolution within the high-Mg tholeiite suite in the presence of olivine and orthopyroxene phenocrysts and microphenocrysts in the chilled margins of the dykes. The demonstration by Kuehner (1986) that equilibrium between quenched liquid and phenocrysts requires pressures of 7 - 8 kbar is re-interpreted (Chapter 2) here to represent the depth of magma chambers in which temporary storage, variable cooling and crystallization and possibly magma influx and mixing, took place. It is possible

that this is the environment in which crustal contamination is imposed but if so then this magma chamber imprint is very complex and not a simple AFC process.

Further evidence for deeper crustal storage and magmatic evolution is provided by the norite body. The pyroxenite nodules occurring in the *Rubbly Norite* are highly refractory in nature and are considered to be cognate to the parental norite magma which must have had $Mg\# > 75$. The association of these nodules with sulphur saturation and sulphide accumulation has also been used to indicate crustal contamination at depth, accompanying orthopyroxene crystallization. The preferred model for 2350 Ma magmatism is one of high temperature melt segregation from mantle sources at rather shallow depth (~ 35 km) and temporary magma storage at 7 - 8 kbar (20 - 25 km). This process produces periods of high temperature evolution from picritic or komatiite magmas at 7 - 8 kbar to high-Mg tholeiites with limited contamination of magmas during this process. Other magma batches fractionate by olivine separation to more Fe-rich tholeiite compositions. Emplacement of dykes and norite body from these subjacent magma chambers occur episodically giving inter woven sequences of dyke emplacement from high Mg, high SiO_2 types to more fractionated high Fe tholeiites.

Lamprophyres, volumetrically subordinate to the high-Mg tholeiites and Fe-rich tholeiites, have been emplaced synchronously with the 1350 Ma magmatic event. The emplacement of *lamprophyric* dykes in the Vestfold Hills is restricted to the mid Proterozoic time and no examples post-dating the 1100 Ma metamorphism were observed in the Vestfold Hills. The derivation of the *lamprophyric* magmas by partial melting of garnet-bearing mantle sources, is indicated by the fractionation of REE (LREE are enriched relatively to HREE), assuming such a source is not significantly LREE enriched. Variations in REE from the primitive to evolved members of the *lamprophyre* suite are consistent with small degrees of partial melting of geochemically heterogeneous, garnet bearing sources.

The near contemporaneity of the Fe-rich tholeiites and *lamprophyres* indicates magma segregation under two distinctly different mantle regimes. The coexistence of

lamprophyric - and Fe-rich tholeiitic magmas may indicate multistage melting of an upwelling mantle diapir (Frey & Green, 1974; Duncan & Green, 1980; 1987), a model which may suggest early magma segregation at pressures > 26 kbar and low degrees of melting to produce the *lamprophyric* magmas and subsequent melting at shallower depth (10 - 20 kbar), after the diapir has risen adiabatically, to produce Fe-rich tholeiites by high degree of melting (10 - 20%).

Mantle xenoliths hosted in the 1350 Ma by the *lamprophyric* magmas, including *spinel lherzolites*, *spinel harzburgites* and *spinel websterites*, represent fragments of heterogeneous uppermost mantle and lower crust underlying the Vestfold Hills at 1350 Ma. Geothermometry indicates the presence of unusually cool mantle at this time, at levels probably less than 15 kbar. The peridotite xenoliths may be the refractory mantle residues remaining following an earlier Proterozoic melting event, probably that which generated the 2350 Ma high Mg tholeiite magmas.

This study builds on earlier studies to provide what is a more comprehensive and better understanding of the complex history of the Vestfold Hills. Several questions remain, in particular the relationship between the 1800 Ma Fe-rich tholeiites and those emplaced at 2350 Ma and 1350 Ma. This particular problem will require further detailed geochemical studies, including confirmation of age relationships by radiometric dating. The possible occurrence of lamprophyric magmas < 1350 Ma also need to be established.

In regard to the high-Mg tholeiites it is still uncertain whether they are primary magmas or products of crustal contamination. A solution to this problem is not only fundamental to understanding their petrogenesis, including their unusual geochemistry, but also questions concerning the development of high PGE concentrations and potential PGE mineralization associated with this magma type. A detailed study of radiogenic isotopes in the magmas would offer a method to establish the relative contributions of mantle and crust to these magmas.

10 APPENDIX

ANALYTICAL TECHNIQUES AND DATA BASE

10.1 WHOLE ROCK CHEMICAL ANALYSES

Samples selected for major and trace element geochemistry were prepared by removing weathered surfaces using a diamond saw to produce fist-size samples with fresh surfaces. These samples were then ground on a tungsten carbide lap wheel to remove any trace of material from the saw blade and were washed in an ultrasonic bath following this procedure. Samples were then crushed to 0.5 - 1 cm pieces in a jaw-crusher and approximately 100 g of these rock chips were selected and powdered to *ca.* 325 mesh in a tungsten carbide swing mill.

Major and trace element analyses were determined by XRF spectrometry using an automated Philips PW 1410 spectrometer. For major elements fused glass discs were prepared following the methods of Norrish & Hutton (1969), and LOI (loss on ignition) was determined by calculating the percentage loss in weight after heating 2 - 3 g of each sample for *ca.* 12 hours at 1000° C.

Trace elements were analyzed using 4 - 5 g powder pellets cased in boric acid, following the method of Norrish & Chappell (1977), and trace element concentrations were determined using mass absorption coefficients calculated from major element analyses. REE concentrations have been determined by the ion-exchange-XRF spectrometry technique developed by Robinson et al. (1986). La, Ce and Nd were also analyzed using the methods of Norrish & Chappell (1977). Analyses determined by ion-exchange and those determined using pressed powder pellets are compared in Table 10.1. These show good agreement. Specpure compounds (oxides and silica) and

STANDARD ROCKS

Standard	TasBas			TasGran		
		$\pm \sigma\%$	$\sigma\%$		$\pm \sigma\%$	$\sigma\%$
Major Elements (wt%)						
SiO ₂	44.56	± 0.23	0.5	72.6	± 0.17	0.2
TiO ₂	2.31	± 0.04	1.7	0.29	± 0.01	3.4
Al ₂ O ₃	14.14	± 0.10	0.7	13.65	± 0.08	0.6
Fe ₂ O ₃	12.65	± 0.09	0.8	2.29	± 0.03	1.3
MnO	0.17	± 0.01	5.1	0.04	± 0.003	7.5
MgO	8.16	± 0.11	1.3	0.59	± 0.04	6.8
CaO	7.81	± 0.06	0.8	1.87	± 0.02	1.1
Na ₂ O	5.43	± 0.12	2.1	2.82	± 0.1	3.5
K ₂ O	1.86	± 0.03	1.6	4.61	± 0.04	0.9
P ₂ O ₅	0.97	± 0.03	2.6	0.12	± 0.002	1.7
Trace Elements (ppm)						
Ba	204	± 3.0	1.5	462	± 4.5	1.0
Rb	16.5	± 0.7	4.2	259	± 3.0	1.2
Nb	61.4	± 1.2	2.0	17	± 0.5	2.9
La	43.4	± 1.4	3.2	38.8	± 1.0	2.6
Ce	89	± 3.4	3.9	86.9	± 3.2	3.7
Sr	1025	± 11.2	1.1	152	± 1.5	1.0
Nd	41.2	± 2.4	5.8	37.4	± 1.8	4.8
Zr	260	± 4.3	1.7	157	± 2.5	1.6
Y	23.1	± 0.6	2.6	35	± 1.0	2.9
Sc	13.1	± 0.5	3.8	6.7	± 0.3	4.5
V	163	± 2.3	1.4	25.4	± 1.0	3.9
Cr	198	± 4.1	2.1	10	± 0.5	5.0
Ni	154	± 2.0	1.3	3.4	± 0.2	5.9
REE (analyzed by ion exchange technique*)						
La	43.2	± 1.25	2.9			
Ce	89.1	± 2.58	2.9			
Pr	10.34	± 0.28	2.7			
Nd	41.8	± 0.79	1.9			
Sm	8.15	± 0.10	1.2			
Eu	2.61	± 0.11	4.3			
Gd	7.01	± 0.10	1.5			
Dy	4.89	± 0.10	2.0			
Er	2.05	± 0.15	7.2			
Yb	1.26	± 0.06	4.6			

Table 10.1

Precision estimates determined for multiple analyses of Tasmania University standard rocks (TasBas and TasGran).

* After Robinson et al. (1986).

INSTRUMENTAL CONDITIONS FOR TRACE ELEMENT ANALYSIS

ROUTINE XRF AUTOMATED ANALYSIS

ELEMENT	LINE	TUBE	CRYSTAL*	COLLIMATOR	VACUUM	DETECTION LIMIT (ppm)	PRECISION
Sc	K (α)	Cr	200	C	YES	1	10 ± 1, 30 ± 1
V	K (α)	Au	220	F	YES	3	30 ± 2, 100 ± 1
Cr	K (α)	Au	200	F	YES	2	10 ± 2, 400 ± 4
Ni	K (α)	Au	200	F	YES	1	3 ± 0.5, 20 ± 0.5, 200 ± 2
Rb	K (α)	Rh	220	F		2	10 ± 1, 70 ± 1, 170 ± 2
Sr	K (α)	Rh	220	F		2	10 ± 1, 200 ± 2, 500 ± 5
Y	K (α)	Rh	220	F		1.5	10 ± 2, 20 ± 1, 100 ± 2
Zr	K (α)	Rh	220	F		1	100 ± 2, 250 ± 4, 500 ± 10
Nb	K (α)	Rh	220	F		1	10 ± 0.5, 20 ± 1
Ba	L (α)	Cr	200	F	YES	3	500 ± 5, 1200 ± 5
La	L (α)	Au	220	C	YES	2.5	20 ± 1, 40 ± 2, 100 ± 2
Ce	L (β)	Au	220	C	YES	5	30 ± 2, 80 ± 3, 150 ± 1
Nd	L (α)	Au	220	C	YES	3	15 ± 1, 30 ± 2, 50 ± 2

Table 10. 2

X-Ray Tube is operated at 60 kV 40 mA excepted for Ba, Sc, La, Ce and Nd where 50 kV 50 mA is used. Detection limits are 3 σ (99%) confidence levels. * Planes in LiF Crystal.

PGE STANDARD ROCK

LABORATORY	A	DETECTION LIMIT (ppb)	B	DETECTION LIMIT (ppb)	C	DETECTION LIMIT (ppb)
PGE (ppb)						
Au	0.6	0.01	4.0	2.0	5.0	1.0
Pt	8.0	0.20	8.0	0.5	6.0	1.0
Pd	8.0	0.20	15.0	0.5	8.0	1.0
Ru	3.0	0.10	13.0	0.5	6.0	1.0
Rh	n.d.	-	3.5	0.5	3.0	1.0
Ir	0.8	0.01	18.0	0.5	1.1	0.2
Os	n.d.	-	10.0	2.0	8.0	3.0
Re	n.d.	-	n.d.	-	3.0	1.0

Table 10.3

A: PGE analyses Melbourne (N.A.A.) ppb; B: PGE analyses Western Australia (FA + ICP-Mass Spectrometer) ppb; C: PGE analyses Canada (FA + P-Mass Spectrometer + NA) ppb.

international standards were used for calibration and precision was monitored by frequent analyses of 'in house' standards. Precision estimates and XRF run details are listed in Table 10.2.

10.2 WHOLE ROCK ANALYSES

Major and trace element analyses and CIPW norms (calculated based on total iron as FeO) of the dykes analyzed in this study are listed below. Major elements and CIPW norms are given in wt% and trace elements in ppm. Mg# was calculated base on FeO^{T} .

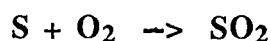
The analyses are arranged according to the identified dyke suites (e.g. high-Mg tholeiite suite), and sequenced according to sample numbers. Arabic numbers indicate dyke groups based on crosscutting relationships, roman numbers indicate geochemical subgroupings.

Whole rock analyses are listed in sequence as listed below:

1. High-Mg Tholeiites, *ca.* 2350 Ma
2. Lamprophyres, *ca.* 1350 Ma
3. Fe-rich Tholeiites, 2350, 1800 and 1350 Ma
4. Complete REE analyses of all dyke types

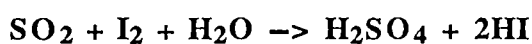
10.3 SULPHUR ANALYSES

Sulphur has been determined using the LECO automatic iodate titration method. Sulphur was combusted at high temperature (*ca.* 1200° C) to SO_2 and SO_3 in a induction furnace. The determination of sulphur by titration follows the combustion of S:



The products reduced by iodine, in starch-potassium iodide solution, to iodide and

destroys the blue starch-iodine complex:



The precision of this method is as low as 0.0001 % and sulphur concentration can be determined with an accuracy of 3 - 4 relative%.

Calibration was made using standards which were re-analyzed after every third analysis. Each sample was analyzed 2 - 3 times and the results were averaged. To increase resolution for samples with low sulphur concentrations (i.e. < 0.01%) the iodide solution was diluted to 0.0444 g/l.

10.4 PLATINUM GROUP ELEMENT (PGE) ANALYSES

Platinum group elements and Au were analyzed at the *University of Melbourne*¹ and by two commercial laboratories; (1) *Analytical Services (W. A.) Pty. Ltd*² and (2) *Nuclear Activation Services Ltd*³ (Ontario Canada). All laboratories preconcentrated PGE's and Au by fire assay (FA). The analytical techniques employed by the various laboratories were INAA³ (Instrumental Neutron Activation), RNAA¹ (Radiochemical Neutron Activation) and by ICP-MS² (Inductively Coupled Plasma Mass-Spectrometry)

A standard sample has been analyzed by all laboratories. Results and detection limits quoted by the various laboratories are listed in Table 10.3.

10.5 MICROPROBE ANALYSES

Mineral analyses were obtained by energy-dispersive methods using a Jeol-JXA 50 microprobe, operating at 15 kv and 20 nA (EDAX detector; calibrated on spec pure Cu) in spot mode with a 1 µm beam size. A CAMECA SX 50 electron microprobe, fitted with a wavelength dispersive analytical system was also used operating at a beam current of 20 nA and accelerating voltage of 15 kv for silicates, and 100 nA and 20 kv for sulphides.

10.6 SAMPLE CATALOGUE

A complete list of samples collected during 3 summer expeditions are listed below, showing University of Tasmania catalogue numbers, field numbers, rock description, co-ordinates of sample location or area and sample preparations. The abbreviation POW, PTS and PGE indicate rock powders prepared for whole rock geochemistry, polished thin sections and samples analyzed for platinum group elements, respectively.

10.7 DYKE BASE MAPS

Three dyke base maps are enclosed showing crosscutting relationships of the Proterozoic dyke suites. These are the results of a mapping program carried out during summer expeditions in 1987/88 and 1988/89 undertaken in a collaboration with the University of Uetrecht. Two of the three maps show detailed dyke crosscutting relationships observed in Lichen Valley area and Long Peninsula (see Figure 10.1 for location). Samples numbers indicate sample location of samples catalogued at the University of Tasmania and to whole rock analyses and sample descriptions referred in this thesis.

VESTFOLD HILLS

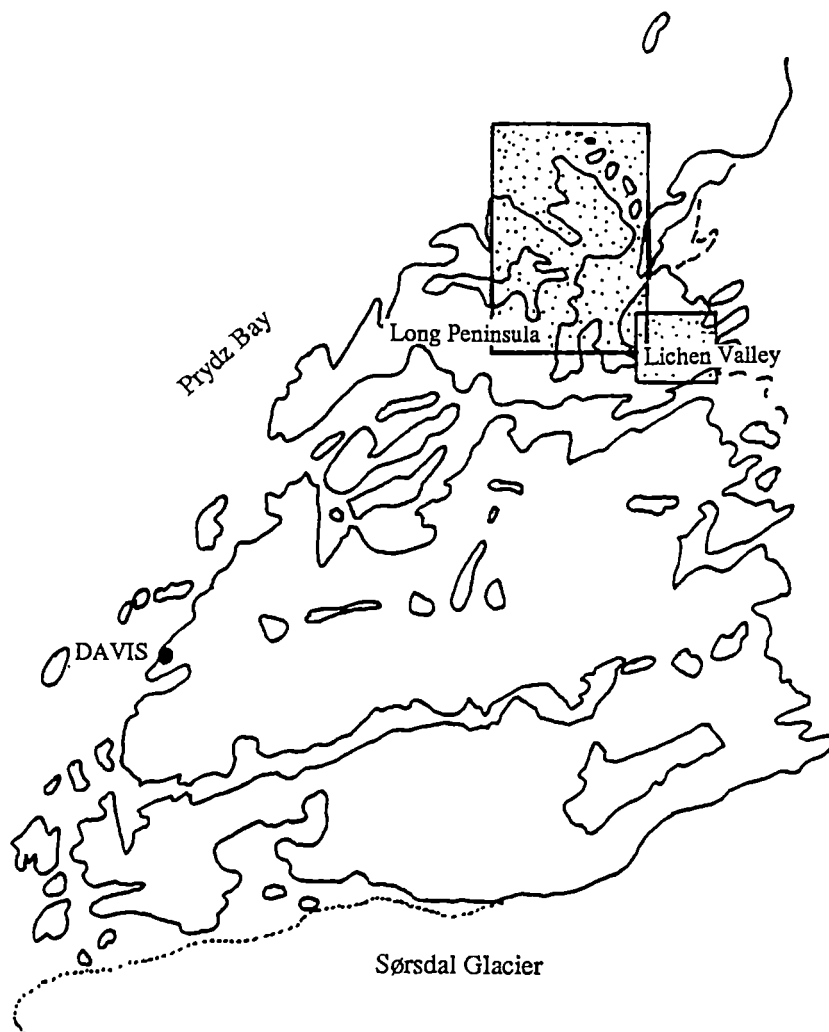


Figure 10.1

Map of the Vestfold Hills showing the areas of the more detailed dyke base maps (included in this thesis) from Lichen Valley and Long Peninsula area.

HIGH-MG THOLEIITE WHOLE ROCK ANALYSES

Sample No.	69892	69893	69894	69895	69896	69897	70533	70535	70536	70537
Rock Type	HN	HN	HN	HN	HN	HN	HMT	HMT	HMT	HMT
Main Group	3	3	3	3	3	3	I	I	I	I
Group	II	II	II	II	II	II	I	I	I	I
Major Elements										
SiO ₂	55.35	55.93	56.19	55.86	55.32	55.33	51.80	52.80	52.83	52.54
TiO ₂	0.64	0.58	0.62	0.60	0.56	0.58	0.60	0.57	0.55	0.59
Al ₂ O ₃	13.00	11.15	12.26	11.55	12.37	12.75	11.36	11.77	11.52	11.76
Fe ₂ O ₃	10.72	12.31	11.43	11.42	11.32	10.76	11.60	11.17	11.17	11.53
FeO	0.00	0.00	0.00	0.00	0.00	0.00	0.00	0.00	0.00	0.00
MnO	0.15	0.18	0.16	0.16	0.16	0.17	0.19	0.18	0.19	0.19
MgO	8.43	10.69	9.55	9.97	8.99	9.29	12.36	11.56	12.13	11.38
CaO	7.99	6.84	7.36	7.17	7.63	8.01	9.28	9.32	9.37	9.51
Na ₂ O	1.41	1.49	1.35	1.45	1.65	1.55	1.74	1.81	1.63	1.72
K ₂ O	1.10	1.07	1.20	1.20	1.02	1.06	0.59	0.62	0.61	0.64
P ₂ O ₅	0.06	0.07	0.08	0.07	0.08	0.06	0.10	0.12	0.10	0.12
LOI	0.81	0.04	0.06	0.60	0.35	0.19	0.14	-0.26	-0.10	-0.22
Total	98.70	99.24	99.23	99.02	98.43	98.78	99.76	99.66	100.00	99.76
Mg#	60.9	63.2	62.3	63.4	61.1	63.1	67.8	67.2	68.3	66.2
CIPW Norm wt%										
Qtz	9.79	7.97	9.60	8.75	8.35	7.98		1.19	1.31	1.14
Or	6.50	6.32	7.09	7.09	6.03	6.26	3.49	3.66	3.60	3.78
Ab	11.93	12.61	11.42	12.27	13.96	13.12	14.72	15.32	13.79	14.55
An	25.89	20.58	23.85	21.46	23.33	24.70	21.44	22.16	22.32	22.48
Lc										
Ne										
Cpx	10.91	10.51	9.90	11.12	11.43	11.93	19.39	18.88	19.04	19.41
Di	6.85	6.80	6.34	7.23	7.17	7.72	13.44	12.96	13.25	13.13
Hd	4.06	3.71	3.56	3.89	4.26	4.21	5.95	5.92	5.79	6.29
Opx	29.95	38.16	34.29	34.77	32.08	31.78	34.95	34.72	36.13	34.49
En	17.82	23.47	20.85	21.48	19.07	19.56	23.17	22.79	24.07	22.26
Fs	12.12	14.68	13.44	13.28	13.01	12.22	11.79	11.94	12.06	12.23
Ol							1.52			
Fo							0.97			
Fa							0.55			
Mt	1.56	1.79	1.66	1.66	1.64	1.56	1.68	1.62	1.62	1.67
Il	1.22	1.10	1.18	1.14	1.06	1.10	1.14	1.08	1.04	1.12
Ap	0.14	0.17	0.19	0.17	0.19	0.14	0.24	0.28	0.24	0.28
Trace Elements										
Ba	253	239	252	253	244	226	212	233	219	238
Rb	60	54	57	62	55	49	20	23	22	23
Nb	6	5	6	6	6	6	3	4	3	3
Sr	122	105	116	114	121	118	160	163	159	169
Zr	99	89	97	105	89	84	54	61	56	59
Y	20	19	18	19	18	18	18	15	15	17
La							8	9	9	9
Ce							16	17	14	17
Nd							10	9	9	9
Ni	182	251	215	219	212	203	311	250	262	250
Cr	588	902	757	779	699	668	1225	1042	1093	1018
V	203	201	200	201	200	198	238	225	220	218
Sc	34	32	31	31	35	33	39	40	39	40

Abbreviations: HMT - High-Mg Tholeiite, HN - Homogeneous Norite, MN - Mottled Norite, RN - Rubbly Norite, LS - Late Stage Segregation, FGD - Fine Grained Dyke.

HIGH-MG THOLEIITE WHOLE ROCK ANALYSES

Sample No.	70538	70548	70551	70552	70553	70568	70569	70570	70581	70582
Rock Type	HMT	HMT	HMT	HMT	HMT	HMT	HMT	HMT	HMT	HMT
Main Group	1	1	1	1	(1) 3	1	1	1	1	1
Group	I	I	I	I	(I) II	I	I	I	I	I
Major Elements										
SiO ₂	51.53	52.41	53.33	52.65	53.85	51.57	52.49	52.24	52.12	51.69
TiO ₂	0.59	0.58	0.59	0.60	0.69	0.59	0.58	0.49	0.60	0.57
Al ₂ O ₃	11.35	11.31	11.83	11.43	15.09	11.19	11.70	10.73	11.42	11.45
Fe ₂ O ₃	11.38	11.22	11.21	11.30	10.58	11.39	11.36	11.15	11.45	11.27
FeO	0.00	0.00	0.00	0.00	0.00	0.00	0.00	0.00	0.00	0.00
MnO	0.19	0.17	0.17	0.17	0.16	0.19	0.19	0.19	0.19	0.19
MgO	12.32	12.21	11.28	12.31	6.63	12.37	11.36	13.71	12.71	11.89
CaO	9.20	9.21	9.44	9.13	9.48	9.23	9.35	9.28	9.28	9.24
Na ₂ O	1.93	1.82	1.68	1.70	1.74	1.71	1.85	1.42	1.73	1.83
K ₂ O	0.64	0.57	0.65	0.56	0.93	0.62	0.64	0.48	0.59	0.63
P ₂ O ₅	0.14	0.08	0.07	0.07	0.10	0.13	0.11	0.09	0.11	0.14
LOI	0.63	-0.18	-0.29	-0.21	0.23	0.23	-0.20	-0.08	-0.11	1.00
Total	99.90	99.40	99.96	99.71	99.48	99.22	99.43	99.70	100.09	99.90
Mg#	68.2	68.3	66.6	68.3	55.4	68.3	66.4	70.9	68.7	67.6
CIPW Norm wt%										
Qtz		0.25	2.45	0.93	7.27		0.79	0.32		
Or	3.78	3.37	3.84	3.31	5.50	3.66	3.78	2.84	3.49	3.72
Ab	16.33	15.40	14.19	14.38	14.72	14.47	15.65	12.02	14.64	15.49
An	20.42	21.01	22.83	21.90	30.62	21.03	21.73	21.49	21.65	21.17
Lc										
Ne										
Cpx	19.68	19.56	19.10	18.56	12.97	19.36	19.42	19.34	19.15	19.25
Di	13.70	13.64	13.01	12.97	7.45	13.49	13.19	13.94	13.44	13.29
Hd	5.98	5.91	6.09	5.60	5.51	5.87	6.23	5.40	5.71	5.96
Opx	30.76	36.07	33.92	36.86	24.15	35.19	34.21	40.01	35.47	34.39
En	20.50	24.09	22.07	24.65	13.06	23.47	22.18	27.69	23.85	22.70
Fs	10.26	11.98	11.85	12.21	11.09	11.72	12.03	12.32	11.63	11.69
Ol	4.17					1.18			1.70	0.83
Fo	2.69					0.76			1.11	0.53
Fa	1.48					0.42			0.60	0.30
Mt	1.65	1.63	1.63	1.64	1.54	1.65	1.65	1.62	1.66	1.64
Il	1.12	1.10	1.12	1.14	1.31	1.12	1.10	0.93	1.14	1.08
Ap	0.33	0.19	0.17	0.17	0.24	0.31	0.26	0.21	0.26	0.33
Trace Elements										
Ba	208	223	250	213	236	257	233	189	226	228
Rb	22	19	23	19	43	17	22	16	21	23
Nb	3	3	3	3	6	3	3	3	3	3
Sr	157	158	168	150	108	162	168	145	164	167
Zr	54	51	60	58	99	53	57	47	56	60
Y	15	17	16	19	25	17	18	15	15	15
La	7	9	11	8	17	6	10	7	9	10
Ce	14	16	20	15	31	13	20	12	18	20
Nd	10	9	9	9	13	9	9	6	11	11
Ni	307	306	256	299	119	301	256	316	302	251
Cr	1216	1196	1037	1203	136	1200	1040	1294	1181	1039
V	230	233	224	222	246	231	227	219	227	219
Sc	40	41	40	40	44	41	40	42	39	40

HIGH-MG THOLEIITE WHOLE ROCK ANALYSES

Sample No.	70583	70584	70598	70599	70600	70601	70612	70613	70614	70623
Rock Type	HMT	HMT	HMT	HMT	HMT	HMT	HMT	HMT	HMT	FGD
Main Group	1	1	1	1	1	1	1	1	1	3
Group	I	I	I	I	I	I	Ia	Ia	Ia	II
Major Elements										
SiO ₂	52.92	52.72	51.98	52.90	52.37	52.84	54.58	54.71	55.08	55.88
TiO ₂	0.00	0.51	0.59	0.59	0.52	0.55	0.67	0.61	0.65	0.67
Al ₂ O ₃	11.70	11.12	11.43	11.71	10.50	11.38	13.28	12.67	13.16	12.14
Fe ₂ O ₃	11.26	11.16	11.27	10.10	11.36	11.05	10.61	10.26	10.43	11.33
FeO	0.00	0.00	0.00	0.00	0.00	0.00	0.00	0.00	0.00	0.00
MnO	0.19	0.19	0.17	0.18	0.19	0.19	0.16	0.16	0.16	0.16
MgO	11.58	12.56	12.25	11.40	14.02	12.43	7.09	8.04	7.25	9.08
CaO	9.33	9.37	9.17	9.38	9.33	9.37	9.67	9.99	9.69	7.43
Na ₂ O	1.61	1.47	1.73	1.55	1.64	1.78	2.25	2.34	2.33	1.63
K ₂ O	0.66	0.55	0.57	0.68	0.44	0.61	0.96	0.89	0.97	1.15
P ₂ O ₅	0.12	0.10	0.09	0.12	0.10	0.11	0.11	0.12	0.12	0.11
LOI	-0.17	-0.24	0.63	0.01	0.02	-0.03	0.27	0.49	0.32	0.67
Total	99.20	99.51	99.88	98.62	100.49	100.28	99.65	100.28	100.16	100.25
Mg#	67.1	69.0	68.3	69.1	71.0	69.0	56.9	60.8	57.9	61.3
CIPW Norm wt%										
Qtz	1.66	1.74	0.16	3.27		0.33	5.58	4.29	5.59	8.93
Or	3.90	3.25	3.37	4.02	2.60	3.60	5.67	5.26	5.73	6.80
Ab	13.62	12.44	14.64	13.12	13.88	15.06	19.04	19.80	19.72	13.79
An	22.75	22.12	21.74	22.99	19.99	21.26	23.30	21.44	22.59	22.41
Lc										
Ne										
Cpx	18.48	19.18	18.75	18.40	20.69	19.82	19.67	22.34	20.26	11.21
Di	12.42	13.48	13.08	13.00	14.94	13.95	11.60	13.99	12.13	7.09
Hd	6.06	5.70	5.67	5.40	5.75	5.87	8.07	8.34	8.13	4.12
Opx	36.02	37.19	36.61	33.03	36.90	36.33	22.09	22.81	21.99	32.25
En	23.09	25.04	24.45	22.37	25.58	24.50	12.28	13.54	12.43	19.33
Fs	12.93	12.16	12.16	10.66	11.31	11.83	9.81	9.27	9.56	12.92
Ol					2.52					
Fo					1.69					
Fa					0.82					
Mt	1.63	1.62	1.64	1.47	1.65	1.60	1.54	1.49	1.51	1.65
Il	0.00	0.97	1.12	1.12	0.99	1.04	1.27	1.16	1.23	1.27
Ap	0.28	0.24	0.21	0.28	0.24	0.26	0.26	0.28	0.28	0.26
Trace Elements										
Ba	230	205	227	248	168	214	336	291	326	261
Rb	24	21	22	31	22	29	40	45	46	63
Nb	5	2	3	2	3	3	4	4	4	7
Sr	166	155	161	165	132	162	267	242	258	102
Zr	60	51	55	64	46	56	76	69	74	107
Y	16	12	14	14	11	13	15	11	13	20
La	10	9	7	11	6	10	14	11	11	18
Ce	19	16	15	22	13	18	32	24	25	37
Nd	9	7	9	12	8	8	14	13	15	17
Ni	259	279	310	259	343	290	92	108	98	204
Cr	1056	1197	1224	1061	1446	1171	373	553	134	722
V	224	218	231	224	233	224	218	227	225	218
Sc	40	27	42	40	42	40	35	37	37	32

HIGH-MG THOLEIITE WHOLE ROCK ANALYSES

Sample No.	70634	70635	70636	70637	70653	70661	70667	70683	70688	70701
Rock Type	HMT	HMT	HMT	HMT	RN	MN	HN	RN	HN	FGD
Main Group	1	1	1	1	3	3	3	3	3	3
Group	I	I	I	I	IIa	II	II	IIa	II	II
Major Elements										
SiO ₂	50.59	53.37	51.51	51.80	55.84	55.97	55.63	55.48	55.40	56.24
TiO ₂	0.57	0.52	0.56	0.61	0.39	0.55	0.47	0.52	0.56	0.70
Al ₂ O ₃	11.00	11.12	11.30	11.24	6.81	9.30	9.65	8.32	10.51	12.65
Fe ₂ O ₃	11.13	10.68	10.89	11.39	12.67	11.87	11.71	12.31	11.47	11.33
FeO	0.00	0.00	0.00	0.00	0.00	0.00	0.00	0.00	0.00	0.00
MnO	0.19	0.17	0.17	0.18	0.19	0.19	0.19	0.19	0.16	0.17
MgO	12.33	12.29	11.41	12.41	18.77	14.27	14.49	14.80	12.17	8.38
CaO	8.99	9.11	8.99	9.24	4.74	5.78	5.85	6.35	6.78	7.79
Na ₂ O	2.18	1.65	1.97	1.58	0.81	1.20	1.06	1.20	1.32	1.66
K ₂ O	0.71	0.59	0.55	0.48	0.62	0.92	0.89	0.94	0.96	1.29
P ₂ O ₅	0.11	0.10	0.10	0.09	0.04	0.08	0.10	0.08	0.09	0.12
LOI	2.04	1.21	2.12	1.21	-0.12	-0.19	-1.00	-0.16	-0.04	0.18
Total	99.84	100.81	99.57	100.23	99.62	98.87	100.04	98.92	98.35	100.51
Mg#	68.7	69.5	67.5	68.3	74.6	70.4	71.0	70.4	67.8	59.4
CIPW Norm wt%										
Qtz		2.41	0.36	0.72	4.94	7.04	8.20	5.35	7.41	9.08
Or	4.20	3.49	3.25	2.84	3.66	5.44	5.26	5.55	5.67	7.62
Ab	18.45	13.96	16.67	13.37	6.85	10.15	8.97	10.16	11.17	14.05
An	18.13	21.19	20.37	22.16	13.11	17.27	18.94	14.54	19.92	23.26
Lc										
Ne										
Cpx	20.83	18.87	19.11	18.69	8.15	8.78	2.86	13.28	10.64	11.95
Di	14.60	13.37	13.18	13.05	6.14	6.30	2.06	9.50	7.36	7.34
Hd	6.23	5.50	5.93	5.64	2.00	2.49	0.80	3.77	3.27	4.62
Opx	23.19	35.94	33.84	37.19	60.33	47.41	50.74	47.24	40.63	30.09
En	15.57	24.41	22.31	24.86	43.91	32.63	35.14	32.46	26.90	17.47
Fs	7.63	11.52	11.52	12.33	16.43	14.78	15.60	14.78	13.73	12.62
Ol	9.04									
Fo	5.87									
Fa	3.17									
Mt	1.62	1.55	1.58	1.65	1.84	1.72	1.70	1.79	1.66	1.65
Il	1.08	0.99	1.06	1.16	0.74	1.04	0.89	0.99	1.06	1.33
Ap	0.26	0.24	0.24	0.21	0.09	0.19	2.37	0.19	0.21	0.28
Trace Elements										
Ba	195	198	241	190	131	201	196	220	216	281
Rb	25	19	21	17	37	51	51	52	41	73
Nb	3	2	3	1	5	8	1	0	6	8
Sr	152	155	167	142	50	77	78	81	90	112
Zr	52	50	58	55	50	83	81	82	85	118
Y	16	15	16	16	11	21	15	16	19	17
La	7	10	9	8	8	16	14	16	15	21
Ce	15	17	20	16	16	31	30	31	33	39
Nd	8	8	7	11	9	12	11	16	14	18
Ni	301	292	247	307	1395	360	345	661	332	182
Cr	1199	1235	1055	1234	2104	1509	1406	1393	1152	620
V	230	230	226	232	187	201	195	177	213	213
Sc	41	42	44	41	28	30	29	31	31	32

HIGH-MG THOLEIITE WHOLE ROCK ANALYSES

Sample No.	70704	70706	70709	70755	70758	70766	70771	70777	70783	70788
Rock Type	MN	RN	FGD	MN	RN	RN	HMT	HMT	RN	MN
Main Group	3	3	3	3	3	3	3	3	3	3
Group	II	IIa	II	II	IIa	IIa	I	II	IIa	II
Major Elements										
SiO ₂	56.72	54.65	55.92	56.44	55.22	54.93	51.70	52.27	54.83	56.26
TiO ₂	0.64	0.47	0.74	0.56	0.51	0.44	0.75	0.43	0.50	0.61
Al ₂ O ₃	10.33	8.03	13.00	8.22	8.39	8.26	8.59	4.36	8.34	9.93
Fe ₂ O ₃	11.82	13.00	11.39	11.91	11.61	12.77	12.27	18.30	10.72	11.99
FeO	0.00	0.00	0.00	0.00	0.00	0.00	0.00	0.00	0.00	0.00
MnO	0.18	0.19	0.17	0.17	0.17	0.19	0.19	0.32	0.18	0.20
MgO	12.26	15.18	7.56	15.27	15.09	15.91	12.67	13.23	12.06	12.78
CaO	6.11	5.25	7.93	5.18	6.03	5.41	9.54	5.81	11.48	5.86
Na ₂ O	1.36	1.13	1.72	1.06	1.00	0.93	1.90	0.89	1.08	1.28
K ₂ O	1.09	0.87	1.33	1.01	0.70	0.72	0.56	0.58	0.76	1.05
P ₂ O ₅	0.11	0.08	0.13	0.10	0.08	0.07	0.10	0.05	0.07	0.12
LOI	-0.23	0.66	0.16	0.32	0.01	0.24	1.42	3.22	0.15	-0.08
Total	99.33	98.45	100.05	99.17	97.77	98.72	99.69	99.46	99.29	98.92
Mg#	67.3	69.6	56.8	71.7	72.0	71.2	67.2	58.9	68.8	67.9
CIPW Norm wt%										
Qtz	8.66	5.31	9.22	7.71	7.16	5.84		6.01	5.38	8.31
Or	6.44	5.14	7.86	5.97	4.14	4.25	3.31	3.43	4.49	6.20
Ab	11.51	9.56	14.55	8.97	8.46	7.87	16.08	7.53	9.14	10.83
An	18.86	14.27	23.82	14.69	16.34	16.24	13.26	6.19	15.66	18.25
Lc										
Ne										
Cpx	8.70	9.10	12.05	8.35	10.52	8.19	27.08	18.30	33.03	8.13
Di	5.98	6.43	7.09	6.10	7.70	5.91	18.66	10.92	23.16	5.63
Hd	2.71	2.67	4.95	2.25	2.82	2.28	8.42	7.38	9.87	2.50
Opx	42.21	51.42	28.01	50.14	48.30	53.23	31.94	49.54	28.75	44.09
En	27.76	34.83	15.54	35.21	34.02	36.89	21.04	27.89	19.30	29.22
Fs	14.44	16.59	12.46	14.93	14.29	16.34	10.90	21.65	9.44	14.87
Ol							2.06			
Fo							1.31			
Fa							0.75			
Mt	1.72	1.90	1.65	1.73	1.69	1.85	1.78	2.65	1.57	1.74
Il	1.22	0.89	1.41	1.06	0.97	0.84	1.42	0.82	0.95	1.16
Ap	0.26	0.19	0.31	0.24	0.19	0.17	0.24	0.12	0.17	0.28
Trace Elements										
Ba	245	246	292	212	143	159	225	199	188	246
Rb	61	41	72	44	36	43	20	28	39	57
Nb	8	4	6	9	6	6	1	2	3	2
Sr	94	78	115	69	66	71	214	60	71	90
Zr	104	76	122	89	75	69	61	80	68	100
Y	19	14	22	17	18	11	15	31	18	16
La	17		22	15	13	11	9	13		16
Ce	34		42	28	23	23	22	30		31
Nd	15		19	13	10	7	12	21		15
Ni	294	1857	199	416	816	452	343	302	926	305
Cr	1169	1543	524	1634	1991	1431	1452	1060	1140	1235
V	208	179	221	197	191	216	250	210	249	206
Sc	30	30	34	29	32	32	40	49	54	31

HIGH-MG THOLEIITE WHOLE ROCK ANALYSES

Sample No.	70796	70801	71735	71739	71749	71751	71789	71790	71794	71804
Rock Type	LS	HN	HMT	HMT	HMT	HMT	HMT	HMT	HMT	HMT
Main Group	3	3	3	3	3	3	3	1	1	1
Group	II	II	III	III	III	III	III	Ia	Ia	I
Major Elements										
SiO ₂	61.45	55.14	52.01	52.35	51.82	52.54	52.66	54.05	54.22	52.11
TiO ₂	1.24	0.52	0.47	0.45	0.49	0.50	0.50	0.63	0.64	0.58
Al ₂ O ₃	13.68	11.12	11.89	11.87	11.86	11.80	12.00	13.09	13.19	11.18
Fe ₂ O ₃	9.53	12.42	10.95	11.06	10.89	11.00	11.06	10.47	10.47	11.52
FeO	0.00	0.00	0.00	0.00	0.00	0.00	0.00	0.00	0.00	0.00
MnO	0.10	0.19	0.16	0.17	0.17	0.16	0.17	0.15	0.15	0.18
MgO	2.17	11.00	12.34	12.60	12.31	12.42	12.53	7.45	7.25	12.64
CaO	6.06	7.45	8.99	9.14	9.02	8.97	9.17	9.82	9.82	9.34
Na ₂ O	2.52	1.71	1.53	1.49	1.55	1.62	1.48	2.18	2.24	1.57
K ₂ O	2.42	0.96	0.60	0.59	0.63	0.62	0.61	0.91	0.93	0.49
P ₂ O ₅	0.23	0.09	0.06	0.06	0.07	0.07	0.05	0.10	0.10	0.07
LOI	0.40	-0.06	0.79	0.08	0.65	0.24	-0.01	1.06	0.47	0.04
Total	98.94	99.42	99.79	99.86	99.46	99.94	100.22	98.97	98.54	98.68
Mg#	31.1	63.7	69.0	69.3	69.1	69.1	69.2	58.5	57.8	68.5
CIPW Norm wt%										
Qtz	18.80	5.26	1.07	0.87	0.65	0.92	1.18	5.02	5.08	0.50
Or	14.30	5.67	3.55	3.49	3.72	3.66	3.60	5.38	5.50	2.90
Ab	21.32	14.47	12.95	12.61	13.12	13.71	12.52	18.45	18.95	13.28
An	18.87	19.83	23.80	23.96	23.54	23.09	24.30	23.24	23.19	22.01
Lc										
Ne										
Cpx	8.22	13.47	16.50	16.98	16.78	16.94	16.88	20.34	20.40	19.32
Di	2.88	8.76	11.66	11.96	11.81	11.93	11.89	12.29	12.20	13.50
Hd	5.35	4.72	4.83	5.02	4.97	5.01	4.99	8.05	8.20	5.81
Opx	12.76	37.77	37.37	38.28	37.34	37.67	38.08	22.53	21.97	37.70
En	4.07	23.34	25.33	25.84	25.19	25.41	25.70	12.86	12.40	25.23
Fs	8.69	14.43	12.04	12.44	12.15	12.26	12.38	9.67	9.57	12.47
Ol										
Fo										
Fa										
Mt	1.38	1.80	1.59	1.61	1.58	1.60	1.61	1.52	1.52	1.67
Il	2.36	0.99	0.89	0.85	0.93	0.95	0.95	1.20	1.22	1.10
Ap	0.54	0.21	0.14	0.14	0.17	0.17	0.12	0.24	0.24	0.17
Trace Elements										
Ba	515	202	232	207	265	231	224	302	323	199
Rb	127	40	17	16	17	18	18	38	38	16
Nb	13	5	4	4	4	4	4	5	4	3
Sr	150	98	92	91	93	90	95	260	275	150
Zr	213	78	75	73	75	78	74	69	75	55
Y	38	14	18	17	19	17	18	15	16	15
La	36	14	17	17	16	17	16	11	11	8
Ce	77	28	29	28	29	29	29	22	26	15
Nd	33	12	12	14	10	15	12	15	11	10
Ni	32	253	389	386	394	383	404	101	100	313
Cr	22	836	1363	1353	1331	1328	1374	460	438	1203
V	232	215	312	208	209	214	210	222	224	230
Sc	29	35	40	39	40	36	38	33	35	37

HIGH-MG THOLEIITE WHOLE ROCK ANALYSES

Sample No.	71809	71811	71816	71834	71844	71867	71874	71875	71876	71877
Rock Type	HMT	HMT	HMT	HMT	HMT	HMT	HMT	HMT	HMT	HMT
Main Group	I	I	3	3	3	3	I	I	I	I
Group	I	I	II	II	II	II	I	I	I	I
Major Elements										
SiO ₂	52.00	52.14	54.33	54.38	50.83	54.10	52.69	52.95	53.07	52.77
TiO ₂	0.57	0.53	0.71	0.69	0.46	0.70	0.72	0.73	0.74	0.77
Al ₂ O ₃	11.40	10.56	15.23	15.41	14.21	15.43	8.68	8.18	8.96	9.33
Fe ₂ O ₃	11.33	11.47	10.89	10.91	9.12	10.93	12.05	12.05	12.20	12.36
FeO	0.00	0.00	0.00	0.00	0.00	0.00	0.00	0.00	0.00	0.00
MnO	0.18	0.17	0.16	0.17	0.15	0.17	0.18	0.18	0.18	0.18
MgO	12.23	13.88	6.76	6.70	12.11	6.64	12.52	13.19	12.48	11.85
CaO	9.24	8.97	9.65	9.67	10.95	9.67	9.10	9.03	9.18	9.32
Na ₂ O	1.90	1.50	1.93	1.74	1.61	1.68	1.95	1.79	2.00	2.12
K ₂ O	0.61	0.45	0.95	0.93	0.30	0.92	0.82	0.78	0.79	0.80
P ₂ O ₅	0.11	0.07	0.10	0.09	0.04	0.10	0.12	0.12	0.11	0.12
LOI	0.17	0.44	-0.29	-0.43	0.31	-0.34	0.65	0.54	0.13	0.08
Total	98.72	99.15	99.44	99.28	99.27	100.00	99.48	99.54	99.84	99.70
Mg#	68.1	70.6	55.1	54.9	72.4	54.6	67.3	68.4	67.0	65.5
CIPW Norm wt%										
Qtz			6.12	7.06		7.19		0.48		
Or	3.60	2.66	5.61	5.50	1.77	5.44	4.85	4.61	4.67	4.73
Ab	16.08	12.69	16.33	14.72	13.62	14.22	16.50	15.15	16.92	17.94
An	20.78	20.75	30.09	31.49	30.66	31.84	12.51	11.98	13.14	13.58
Lc										
Ne										
Cpx	19.71	18.80	14.10	13.09	18.84	12.75	25.81	25.91	25.68	25.88
Di	13.71	13.51	8.08	7.45	13.89	7.22	17.81	18.18	17.65	17.43
Hd	6.00	5.29	6.02	5.64	4.95	5.52	7.99	7.74	8.03	8.45
Opx	33.21	40.76	24.30	24.74	27.47	24.77	34.52	36.36	34.46	31.46
En	22.10	28.12	13.09	13.24	19.50	13.19	22.79	24.43	22.64	20.22
Fs	11.11	12.64	11.21	11.51	7.97	11.58	11.74	11.93	11.83	11.24
Ol	2.19	0.20			4.30		0.16		0.30	1.38
Fo	1.41	0.14			2.96		0.10		0.19	0.86
Fa	0.78	0.07			1.33		0.06		0.11	0.52
Mt	1.65	1.66	1.58	1.58	1.32	1.59	1.75	1.75	1.77	1.79
Il	1.08	1.01	1.35	1.31	0.87	1.33	1.37	1.39	1.41	1.46
Ap	0.26	0.17	0.24	0.21	0.09	0.24	0.28	0.28	0.26	0.28
Trace Elements										
Ba	246	175	257	259	79	247	286	287	300	314
Rb	22	18	44	45	12	43	31	29	33	31
Nb	3	2	6	6	2	6	3	3	4	3
Sr	168	139	111	111	92	108	214	196	220	236
Zr	58	50	98	98	38	98	72	75	73	75
Y	15	15	23	22	12	21	15	16	16	17
La	8	6	14	18	6	21	10	11	11	11
Ce	17	13	34	31	10	37	22	26	23	21
Nd	9	8	16	16	4	17	12	13	13	11
Ni	284	357	125	128	274	122	323	348	336	306
Cr	1115	1383	135	135	847	128	1358	1536	1367	1167
V	220	233	234	259	203	246	233	229	247	249
Sc	36	36	41	42	37	41	36	34	33	34

HIGH-MG THOLEIITE WHOLE ROCK ANALYSES

Sample No.	71878	71883	71889	71892	71893	71894	71906	71921	71947	71948
Rock Type	HMT	HMT	FGD	RN	RN	RN	HMT	HMT	HMT	HMT
Main Group	3	3	3	3	3	3	1	3	1	1
Group	II	II	II	IIa	IIa	IIa	I	II	Ia	Ia
Major Elements										
SiO ₂	54.83	55.32	56.15	55.13	52.72	56.20	52.72	54.65	54.77	54.85
TiO ₂	0.59	0.67	0.71	0.60	0.46	0.73	0.68	0.57	0.65	0.63
Al ₂ O ₃	15.85	11.99	12.64	10.21	5.10	12.98	8.35	13.44	13.04	12.82
Fe ₂ O ₃	9.88	11.37	11.37	11.83	12.23	11.30	12.00	10.63	10.50	10.23
FeO	0.00	0.00	0.00	0.00	0.00	0.00	0.00	0.00	0.00	0.00
MnO	0.14	0.16	0.16	0.17	0.19	0.16	0.18	0.16	0.16	0.16
MgO	5.59	9.37	8.33	11.83	14.34	7.58	13.34	8.98	7.56	8.01
CaO	10.07	7.43	7.71	6.67	13.00	7.90	9.24	8.42	9.74	10.03
Na ₂ O	2.04	1.64	1.77	1.59	0.82	1.72	1.85	1.65	2.30	2.36
K ₂ O	1.11	1.17	1.21	1.01	0.55	1.29	0.70	0.92	1.00	0.95
P ₂ O ₅	0.11	0.11	0.12	0.14	0.07	0.13	0.10	0.10	0.13	0.13
LOI	0.06	0.18	0.06	0.46	0.61	-0.03	0.86	0.08	0.22	0.18
Total	100.27	99.41	100.23	99.64	100.09	99.96	100.02	99.60	100.07	100.35
Mg#	52.8	62.0	59.2	66.4	69.9	57.1	68.8	62.6	58.8	60.8
CIPW Norm wt%										
Qtz	7.10	7.89	8.88	6.33	1.13	9.70		7.02	4.85	4.11
Or	6.56	6.91	7.15	5.97	3.25	7.62	4.14	5.44	5.91	5.61
Ab	17.26	13.88	14.98	13.45	6.94	14.55	15.65	13.96	19.46	19.97
An	30.81	21.90	22.97	17.74	8.61	23.89	12.41	26.55	22.30	21.58
Lc										
Ne										
Cpx	15.21	11.62	11.87	11.71	44.79	11.87	26.51	11.88	20.62	22.33
Di	8.34	7.42	7.26	7.96	31.78	7.02	18.65	7.63	12.52	14.00
Hd	6.87	4.20	4.60	3.75	13.01	4.85	7.86	4.25	8.10	8.33
Opx	19.56	32.82	30.02	39.73	30.84	28.00	35.12	30.86	22.70	22.66
En	10.06	19.90	17.38	25.78	20.99	15.63	23.67	18.83	13.03	13.46
Fs	9.50	12.92	12.64	13.95	9.86	12.38	11.45	12.03	9.67	9.20
Ol							0.98			
Fo							0.64			
Fa							0.34			
Mt	1.43	1.65	1.65	1.72	1.78	1.64	1.74	1.54	1.52	1.49
Il	1.12	1.27	1.35	1.14	0.87	1.39	1.29	1.08	1.23	1.20
Ap	0.26	0.26	0.28	0.33	0.17	0.31	0.24	0.24	0.31	0.31
Trace Elements										
Ba	261	272	286	276	202	314	283	228	355	325
Rb	55	61	64	52	29	68	28	46	37	38
Nb	5	6	7	5	4	6	3	5	4	3
Sr	149	101	107	111	74	116	209	97	256	254
Zr	97	108	113	103	76	117	68	88	78	69
Y	20	21	22	20	28	23	15	19	16	15
La	18	19	21	20	19	23	9	18	13	11
Ce	37	38	44	41	44	47	22	31	24	22
Nd	15	15	17	19	25	20	11	13	13	13
Ni	106	207	179	285	261	160	350	176	97	108
Cr	217	746	615	1063	1222	506	1523	631	447	549
V	200	211	213	217	223	212	222	205	220	223
Sc	33	32	33	31	58	31	34	38	37	38

HIGH-MG THOLEIITE WHOLE ROCK ANALYSES

Sample No.	71949	71950	71958	71962	71978	71982	71984	71986	71987
Rock Type	HMT	RN	HMT	HMT	HMT	HMT	FGD	RN	HMT
Main Group	1	3	1	1	3	3	3	3	3
Group	Ia	IIa	Ia	I	II	II	II	IIa	II
Major Elements									
SiO ₂	54.44	55.88	55.98	52.59	55.30	52.26	55.90	55.13	53.20
TiO ₂	0.65	0.64	0.71	0.59	0.58	0.50	0.73	0.49	0.74
Al ₂ O ₃	13.31	11.74	12.60	11.38	14.03	12.15	12.62	8.41	8.82
Fe ₂ O ₃	10.72	11.38	11.41	11.67	10.28	10.97	11.41	12.11	12.15
FeO	0.00	0.00	0.00	0.00	0.00	0.00	0.00	0.00	0.00
MnO	0.17	0.17	0.17	0.18	0.17	0.17	0.17	0.19	0.18
MgO	7.31	9.72	8.41	12.41	8.69	12.13	8.31	15.54	12.85
CaO	9.87	7.23	7.61	9.32	8.28	9.14	7.71	6.17	9.17
Na ₂ O	2.36	1.45	1.69	1.61	1.32	1.50	1.56	1.10	1.96
K ₂ O	1.10	1.16	1.26	0.55	1.01	0.62	1.26	0.85	0.75
P ₂ O ₅	0.12	0.09	0.10	0.08	0.08	0.06	0.10	0.07	0.10
LOI	0.04	-0.03	0.31	-0.25	-0.07	0.17	-0.09	-0.32	0.27
Total	100.09	99.43	100.25	99.08	98.83	99.67	98.65	98.65	99.10
Mg#	57.4	62.8	59.4	67.8	62.4	68.7	59.1	71.8	67.7
CIPW Norm wt%									
Qtz	3.82	9.17	8.88	0.78	9.35	1.27	9.48	4.90	
Or	6.50	6.85	7.45	3.25	5.97	3.66	7.45	5.02	4.43
Ab	19.97	12.27	14.30	13.62	11.17	12.69	13.20	9.31	16.59
An	22.48	22.10	23.07	22.20	29.37	24.59	23.71	15.50	13.05
Lc									
Ne									
Cpx	21.10	10.74	11.48	19.05	9.12	16.48	11.37	11.81	25.74
Di	12.52	6.94	7.04	13.19	5.84	11.53	6.95	8.60	17.87
Hd	8.57	3.81	4.44	5.85	3.28	4.95	4.42	3.21	7.87
Opx	22.15	34.22	30.48	37.43	31.12	37.13	30.25	49.57	35.34
En	12.40	21.00	17.68	24.80	18.94	24.87	17.48	34.72	23.48
Fs	9.74	13.22	12.80	12.63	12.19	12.26	12.77	14.85	11.86
Ol									0.27
Fo									0.17
Fa									0.10
Mt	1.56	1.65	1.66	1.69	1.51	1.59	1.66	1.76	1.76
Il	1.23	1.22	1.35	1.12	1.10	0.95	1.39	0.93	1.41
Ap	0.28	0.21	0.24	0.19	0.19	0.14	0.24	0.17	0.24
Trace Elements									
Ba	335	269	287	241	242	217	295	223	296
Rb	39	59	66	19	51	21	69	44	31
Nb	4	6	7	3	7	4	7	5	3
Sr	280	108	113	165	105	95	108	82	217
Zr	68	102	113	59	97	75	119	84	73
Y	16	20	21	15	18	17	22	17	15
La	10	21	19	8	15	17	23	17	12
Ce	23	38	36	15	31	28	44	33	22
Nd	14	18	16	8	17	11	19	15	13
Ni	94	220	183	307	161	344	169	398	327
Cr	418	827	636	1213	507	1257	573	1649	1381
V	225	205	216	232	209	207	206	190	230
Sc	36	29	30	37	35	35	29	30	32

LAMPROPHYRE WHOLE ROCK ANALYSES

Sample No. Rock Type Main Group	71736 AL 6	71740 AL 6	71750 UML 6	71752* UML 6	71753 AL 6	71760 AL 8	71761 UML 6	71768 AL 6	71788 AL 6	71791 UML 6
Major Elements										
SiO ₂	49.38	46.27	39.74	39.35	45.59	46.66	41.54	49.37	44.25	41.70
TiO ₂	1.70	4.14	4.03	4.17	3.95	4.25	4.88	1.67	2.38	3.20
Al ₂ O ₃	10.61	9.16	7.22	6.46	9.00	9.35	8.50	11.19	7.40	6.95
Fe ₂ O ₃	12.10	13.27	14.70	15.05	12.57	13.05	14.88	12.42	13.60	14.79
FeO	0.00	0.00	0.00	0.00	0.00	0.00	0.00	0.00	0.00	0.00
MnO	0.15	0.14	0.17	0.18	0.15	0.15	0.17	0.15	0.17	0.18
MgO	11.28	9.73	13.93	16.24	9.75	9.27	11.22	10.59	15.79	15.31
CaO	9.15	8.65	9.60	8.22	8.33	8.53	9.58	8.96	8.86	8.98
Na ₂ O	2.22	2.54	1.99	1.62	2.42	2.44	1.87	2.59	1.76	1.62
K ₂ O	1.12	3.34	2.73	2.78	3.24	3.44	3.98	1.21	1.56	2.04
P ₂ O ₅	0.43	1.13	0.64	0.61	0.99	0.99	0.70	0.41	0.46	0.67
LOI	1.48	1.13	5.34	4.71	3.54	1.89	2.09	1.56	3.19	4.82
Total	98.53	98.31	98.77	98.04	98.40	98.85	98.07	99.00	98.20	98.93
Mg#	64.9	59.2	65.2	68.1	60.6	58.4	59.9	62.8	69.7	67.2
CIPW Norm wt%										
Qtz										
Or	6.62	19.74	4.19	7.10	19.15	20.33	9.97	7.15	9.22	12.06
Ab	18.79	14.50			15.03	15.54	0.00	21.92	11.94	4.59
An	15.68	3.73	2.71	2.14	4.13	4.40	3.04	15.33	7.68	5.67
Lc			9.37	7.31			10.63			
Ne		3.79	9.12	7.43	2.95	2.77	8.57		1.60	4.94
Cpx	21.80	25.74	32.81	27.81	24.84	25.46	32.25	21.48	26.76	27.80
Di	15.05	17.95	24.14	21.16	17.62	17.71	22.87	14.37	19.92	20.41
Hd	6.75	7.79	8.68	6.65	7.22	7.75	9.38	7.11	6.84	7.38
Opx	18.13							11.63		
En	11.96							7.42		
Fs	6.16							4.21		
Ol	10.06	17.27	23.96	30.01	17.15	16.20	18.46	14.01	30.24	29.28
Fo	6.42	11.15	16.47	21.47	11.30	10.43	12.16	8.62	21.09	20.09
Fa	3.64	6.12	7.49	8.54	5.85	5.77	6.31	5.39	9.16	9.19
Mt	1.76	1.93	2.13	2.18	1.83	1.89	2.16	1.80	1.97	2.15
Il	3.23	7.86	7.65	7.92	7.50	8.07	9.27	3.17	4.52	6.08
Ap	1.02	2.68	1.52	1.44	2.34	2.34	1.66	0.97	1.09	1.59
Trace Elements										
Ba	732	1365	1225	1003	1193	1271	1556	806	861	1176
Rb	31	60	79	74	57	61	120	32	47	62
Nb	30	64	78	79	59	61	92	30	46	59
Sr	554	1519	810	934	1477	1518	977	594	614	802
Zr	130	410	384	382	387	406	420	139	223	279
Y	26	41	28	29	38	40	28	31	22	27
La	47	115	64	63	107	109	66	45	42	60
Ce	97	256	150	147	239	248	146	98	99	134
Nd	45	131	75	76	119	125	77	46	47	68
Ni	370	346	528	711	336	308	352	373	700	595
Cr	578	330	709	673	351	315	550	475	699	620
V	200	225	276	265	218	217	275	208	25	244
Sc	24	16	23	22	17	18	21	21	22	22

Abbreviations: UML - Ultramafic Lamprohyre, AL - Alkaline Lamprohyre.
* indicates xenoliths bearing dykes.

LAMPROPHYRE WHOLE ROCK ANALYSES

Sample No. Rock Type Main Group	71793 AL 6	71814 AL 6	71825 AL 6	71848 AL 6	71865 UML 6	71869 UML 6	71888 AL 6	71896 AL 6	71898 AL 6	71907* AL 6
Major Elements										
SiO2	45.50	44.64	44.06	43.06	37.87	41.51	47.10	42.64	43.29	43.77
TiO2	3.63	4.21	3.63	2.27	2.97	3.72	3.52	3.69	3.86	2.56
Al2O3	9.92	8.70	9.34	6.94	4.76	9.10	10.81	8.35	10.35	6.72
Fe2O3	14.84	14.88	14.93	14.98	16.25	15.56	13.50	15.80	14.98	12.42
FeO	0.00	0.00	0.00	0.00	0.00	0.00	0.00	0.00	0.00	0.00
MnO	0.19	0.16	0.21	0.18	0.20	0.20	0.15	0.18	0.18	0.17
MgO	9.56	11.93	10.81	17.96	21.88	11.09	8.76	12.47	8.37	13.46
CaO	9.06	8.56	9.18	8.45	7.23	8.72	7.93	9.59	9.52	12.22
Na2O	2.34	2.24	2.17	1.66	1.20	1.91	2.57	1.70	2.92	1.66
K2O	2.67	2.77	2.44	1.48	1.87	2.72	3.18	2.59	3.08	1.91
P2O5	0.82	0.56	0.76	0.30	0.62	0.94	0.84	1.09	1.19	0.61
LOI	1.51	1.01	2.73	2.24	5.21	4.22	1.30	1.17	2.23	4.77
Total	98.71	98.32	98.92	98.17	100.06	99.69	99.66	99.27	99.97	100.27
Mg#	56.1	61.4	58.9	70.4	72.7	58.5	56.2	61.0	52.5	68.2
CIPW Norm wt%										
Qtz										
Or	15.78	16.37	14.42	8.75		16.07	18.79	15.31	18.20	11.29
Ab	13.94	9.58	10.66	6.68		5.57	18.47	5.40	6.00	2.64
An	8.68	5.52	8.54	7.11	2.08	8.22	8.57	7.50	6.04	5.24
Lc					8.66					
Ne	3.17	5.06	4.17	3.99	5.50	5.74	1.78	4.87	10.13	6.18
Cpx	25.20	26.92	26.04	26.42	22.94	23.49	20.59	26.72	27.35	41.37
Di	16.19	18.99	17.39	19.67	17.75	15.59	13.40	18.29	16.81	30.61
Hd	9.01	7.93	8.65	6.75	5.19	7.90	7.19	8.43	10.53	10.76
Opx										
En										
Fs										
Ol	19.47	22.40	21.54	35.79	44.42	23.46	18.36	25.06	16.40	19.58
Fo	11.43	14.66	13.22	24.96	32.42	14.29	10.94	15.83	9.15	13.55
Fa	8.04	7.75	8.32	10.83	12.00	9.17	7.42	9.23	7.25	6.02
Mt	2.15	2.16	2.17	2.17	2.36	2.26	1.96	2.29	2.17	1.80
Il	6.89	8.00	6.89	4.31	5.64	7.07	6.69	7.01	7.33	4.86
Ap	1.94	1.33	1.80	0.71	1.47	2.23	1.99	2.58	2.82	1.44
Trace Elements										
Ba	1262	1043	1112	691	662	1280	1246	1324	1604	924
Rb	84	79	69	45	49	78	85	73	84	57
Nb	74	62	72	46	63	95	70	81	116	57
Sr	917	796	956	550	736	1087	1121	1145	1404	952
Zr	433	339	407	192	289	458	449	441	555	328
Y	33	30	31	20	24	38	33	36	45	31
La	81	52	75	31	55	94	85	117	130	85
Ce	186	115	164	72	124	198	188	255	280	188
Nd	90	62	82	35	61	92	92	116	128	87
Ni	279	424	350	683	870	397	283	392	209	358
Cr	375	520	403	708	1063	330	279	308	277	2019
V	240	237	261	190	199	237	198	203	230	205
Sc	23	18	21	18	18	22	18	21	18	38

LAMPROPHYRE WHOLE ROCK ANALYSES

Sample No. Rock Type Main Group	71908 UML 6	71911 AL 6	71913 AL 6	71914 AL 6	71916 AL 6	71925 AL 6	71927 UML 6	71928* UML 6	71930 AL 6	71933 UML 6
Major Elements										
SiO ₂	39.09	45.35	42.84	46.49	42.75	44.02	39.59	38.43	43.22	41.18
TiO ₂	4.27	3.36	3.07	2.35	3.76	4.57	4.70	4.42	2.69	4.75
Al ₂ O ₃	7.29	10.92	7.82	9.53	9.93	8.24	8.01	7.18	7.13	7.62
Fe ₂ O ₃	13.99	13.17	14.04	13.30	14.63	15.35	14.92	14.30	14.20	13.92
FeO	0.00	0.00	0.00	0.00	0.00	0.00	0.00	0.00	0.00	0.00
MnO	0.18	0.15	0.17	0.17	0.17	0.16	0.18	0.16	0.18	0.16
MgO	13.91	8.21	12.86	12.22	8.93	12.06	13.14	15.29	15.47	15.11
CaO	9.64	7.83	8.87	9.70	8.30	8.62	10.03	9.43	9.38	8.36
Na ₂ O	2.11	2.84	2.76	2.50	2.67	2.03	1.91	2.05	2.20	1.88
K ₂ O	3.88	3.72	2.69	1.34	3.33	2.70	3.51	3.11	1.99	3.74
P ₂ O ₅	0.70	1.02	0.76	0.55	0.98	0.51	0.62	0.49	0.85	0.57
LOI	5.15	3.31	3.55	1.85	2.56	1.85	3.42	5.07	2.78	2.68
Total	100.21	99.88	99.43	100.00	98.01	100.11	100.03	99.93	100.09	99.97
Mg#	66.3	55.2	64.5	64.5	54.7	60.9	63.6	67.9	68.3	68.2
CIPW Norm wt%										
Qtz										
Or		21.98	15.90	7.92	19.68	15.96			11.76	7.50
Ab		11.76	3.14	18.26	6.54	9.04			5.50	
An		6.06	1.00	10.82	5.28	5.40	2.92	1.20	3.70	1.31
Lc	17.98						16.26	14.41		11.45
Ne	8.61	6.65	10.95	1.57	8.70	4.41	8.75	9.40	7.10	8.62
Cpx	24.39	21.30	30.73	27.28	24.07	27.52	30.47	26.16	30.02	29.17
Di	18.23	13.62	21.84	19.04	15.29	19.45	22.40	20.14	22.11	22.83
Hd	6.16	7.68	8.89	8.24	8.78	8.07	8.07	6.02	7.91	6.35
Opx										
En										
Fs										
Ol	26.20	16.97	23.26	23.43	18.33	22.46	22.80	27.77	28.79	25.63
Fo	18.36	9.91	15.35	15.14	10.62	14.73	15.66	20.15	19.82	18.96
Fa	7.84	7.06	7.91	8.28	7.71	7.73	7.14	7.62	8.97	6.67
Mt	1.17	1.91	2.04	1.93	2.12	2.23	2.17	2.07	2.06	2.02
Il	8.11	6.38	5.83	4.46	7.14	8.68	8.93	8.39	5.11	9.02
Ap	1.66	2.42	1.80	1.30	2.32	1.21	1.47	1.16	2.01	1.35
Trace Elements										
Ba	1497	1414	1206	1004	1243	966	1415	1378	1020	1223
Rb	120	96	67	41	87	74	79	102	51	95
Nb	89	77	59	44	90	53	108	72	77	80
Sr	918	1382	1090	744	1270	732	347	708	1102	700
Zr	363	552	336	169	583	299	810	309	384	417
Y	24	36	32	30	39	26	26	23	30	23
La	67	108	81	62	102	46	63	52	97	47
Ce	148	242	180	134	224	106	143	123	210	122
Nd	73	114	86	61	105	56	70	59	94	68
Ni	468	280	504	458	276	464	441	568	633	564
Cr	703	233	540	534	246	509	655	758	633	729
V	282	184	218	231	207	263	307	299	203	284
Sc	19	17	18	22	21	19	22	27	19	19

LAMPROPHYRE WHOLE ROCK ANALYSES

Sample No. Rock Type Main Group	71935 AL 6	71938 UML 6	71939 AL 6	71940 AL 6	71941 UML 6	71942 UML 6	71945 UML 6	71956 UML 6	71990 AL 6	71991 AL 8
Major Elements										
SiO ₂	44.63	39.82	46.62	42.67	39.26	40.12	39.55	39.16	43.81	46.33
TiO ₂	3.64	3.67	2.43	3.51	3.27	4.05	3.52	3.80	3.34	2.23
Al ₂ O ₃	8.73	7.86	10.64	8.38	6.54	7.96	5.61	7.15	8.01	10.08
Fe ₂ O ₃	15.15	14.41	13.15	14.45	14.81	14.94	14.36	15.78	14.86	13.05
FeO	0.00	0.00	0.00	0.00	0.00	0.00	0.00	0.00	0.00	0.00
MnO	0.18	0.16	0.16	0.17	0.18	0.19	0.18	0.19	0.18	0.17
MgO	12.55	15.12	10.34	11.25	17.22	14.59	21.38	15.39	13.36	12.28
CaO	9.75	9.59	9.24	8.86	8.95	10.42	7.37	10.80	9.25	9.32
Na ₂ O	1.67	1.90	3.26	2.26	1.33	1.68	0.74	1.63	2.33	1.96
K ₂ O	2.21	2.81	1.56	2.82	2.14	2.48	2.37	2.39	2.24	1.36
P ₂ O ₅	0.42	0.66	0.64	0.90	0.47	0.53	0.52	0.83	0.81	0.27
LOI	0.93	3.87	1.73	4.11	6.00	2.52	4.55	2.30	1.32	2.52
Total	99.86	99.87	99.77	99.38	100.17	99.48	100.15	99.42	99.51	99.57
Mg#	62.1	67.5	60.9	60.7	69.7	65.9	74.7	65.9	64.0	65.1
CIPW Norm wt%										
Qtz										
Or	13.06		9.22	16.66	3.74		6.96		13.24	8.04
Ab	9.13		18.99	6.38					7.68	16.59
An	9.80	4.62	9.79	4.39	5.55	6.85	5.00	5.13	4.78	14.69
Lc		13.02			6.98	11.49	5.52	11.07		
Ne	2.71	8.71	4.66	6.90	6.10	7.70	3.38	7.47	6.52	
Cpx	29.00	30.62	25.90	27.31	28.73	33.13	22.48	29.36	28.95	24.10
Di	20.21	22.94	17.27	18.70	21.77	24.52	18.12	21.44	20.52	16.90
Hd	8.79	7.68	8.63	8.61	6.96	8.61	4.36	7.91	8.43	7.20
Opx										4.23
En										2.84
Fs										1.39
Ol	23.78	26.97	20.29	21.46	32.28	25.28	40.99	29.18	25.30	21.47
Fo	15.34	18.94	12.44	13.56	22.99	17.50	31.43	19.90	16.65	13.95
Fa	8.44	8.03	7.86	7.90	9.30	7.78	9.56	9.29	8.65	7.52
Mt	2.20	2.09	1.91	2.10	2.15	2.17	2.08	2.29	2.16	1.89
Il	6.91	6.97	4.62	6.67	6.21	7.69	6.69	7.22	6.34	4.24
Ap	0.99	1.56	1.52	2.13	1.11	1.26	1.23	1.97	1.92	0.64
Trace Elements										
Ba	1230	1381	1119	1360	1063	1314	924	1267	1345	715
Rb	82	85	43	77	72	89	62	74	63	47
Nb	59	91	44	65	69	82	57	90	79	40
Sr	576	514	707	1150	575	644	685	925	1000	424
Zr	231	336	170	363	251	266	270	322	390	156
Y	20	24	26	32	21	22	21	29	34	17
La	42	67	72	88	47	53	51	69	90	32
Ce	93	151	151	200	103	122	113	157	191	65
Nd	44	71	68	98	49	56	57	77	90	34
Ni	429	559	348	395	658	502	892	531	522	391
Cr	596	816	402	415	887	670	1043	652	467	479
V	319	288	222	236	269	327	228	270	237	217
Sc	25	28	20	19	24	24	20	25	15	23

FE-RICH THOLEIITE WHOLE ROCK ANALYSES

Sample No.	71729	71730	71731	71732	71733	71734	71738	71742	71746	71747
Rock Type	FRT	FRT	FRT	FRT	FRT	FRT	FRT	FRT	FRT	FRT
Main Group	5	5	9	4	7	5	9	4	5	5
Major Elements										
SiO ₂	49.97	50.06	48.50	49.04	50.29	48.70	50.68	50.53	49.58	49.87
TiO ₂	1.19	1.33	1.55	1.77	1.64	1.62	1.96	1.23	1.22	1.16
Al ₂ O ₃	14.95	15.46	14.57	12.40	14.32	14.38	13.29	14.22	14.54	14.74
Fe ₂ O ₃	12.95	13.20	13.27	17.05	14.05	13.67	15.43	13.68	13.21	12.98
FeO	0.00	0.00	0.00	0.00	0.00	0.00	0.00	0.00	0.00	0.00
MnO	0.20	0.20	0.20	0.26	0.21	0.21	0.24	0.20	0.21	0.21
MgO	6.88	6.72	7.49	5.39	6.19	7.26	5.24	6.75	7.02	7.15
CaO	11.76	10.07	11.35	10.22	10.49	11.28	9.47	10.89	11.71	11.80
Na ₂ O	2.27	2.32	2.20	2.61	2.19	2.22	2.58	2.22	2.18	2.39
K ₂ O	0.26	0.41	0.40	0.19	0.53	0.40	0.66	0.18	0.23	0.24
P ₂ O ₅	0.11	0.14	0.15	0.15	0.16	0.17	0.23	0.11	0.12	0.12
LOI	-0.25	0.01	0.15	-0.07	-0.25	0.02	-0.20	-0.01	-0.42	-0.17
Total	99.13	98.73	98.64	99.01	98.56	98.70	98.19	100.00	98.41	99.32
Mg#	51.3	50.2	52.8	38.5	46.6	51.3	40.2	49.4	51.3	52.2
CIPW Norm wt%										
Qtz		0.17			1.37		2.00	1.24		
Or	1.54	2.42	2.36	1.12	3.13	2.36	3.90	1.06	1.36	1.42
Ab	19.21	19.63	18.62	22.09	18.53	18.79	21.83	18.79	18.45	20.22
An	29.84	30.56	28.70	21.56	27.68	28.09	22.73	28.30	29.21	28.78
Lc										
Ne										
Cpx	22.96	15.29	21.94	23.67	19.37	22.09	19.05	20.71	23.22	23.92
Di	12.45	8.18	12.40	9.88	9.76	12.17	8.43	10.84	12.59	13.16
Hd	10.51	7.11	9.53	13.79	9.61	9.91	10.62	9.87	10.63	10.75
Opx	18.82	25.87	14.36	22.63	23.20	15.82	22.38	24.10	19.71	15.47
En	9.56	12.95	7.63	8.70	10.89	8.18	9.15	11.79	10.02	7.99
Fs	9.26	12.92	6.73	13.93	12.31	7.64	13.23	12.31	9.70	7.49
Ol	2.62		7.30	0.29		6.07			2.37	5.30
Fo	1.27		3.70	0.11		2.99			1.14	2.61
Fa	1.35		3.60	0.19		3.08			1.22	2.70
Mt	1.88	1.91	1.93	2.47	2.04	1.98	2.24	1.99	1.92	1.88
Il	2.26	2.53	2.94	3.36	3.11	3.08	3.72	2.34	2.32	2.20
Ap	0.26	0.33	0.36	0.36	0.38	0.40	0.54	0.26	0.28	0.28
Trace Elements										
Ba	75	113	110	58	134	114	148	68	87	70
Rb	5	16	12	2	22	13	30	3	4	3
Nb	5	8	7	4	6	7	12	4	6	4
Sr	140	147	159	92	156	161	141	109	136	138
Zr	80	118	102	109	113	108	175	79	86	79
Y	29	34	33	41	37	33	49	27	29	29
La	6	13	9	6	12	9	16	4	7	4
Ce	13	23	20	16	28	27	29	13	18	15
Nd	10	16	15	14	18	16	18	11	11	12
Ni	83	99	90	56	52	85	46	100	74	89
Cr	151	136	371	68	136	319	73	198	172	172
V	290	302	308	799	341	328	400	378	311	304
Sc	47	41	50	52	47	47	51	49	49	49

Abbreviation: FRT - Fe-rich Tholeiite

FE-RICH THOLEIITE WHOLE ROCK ANALYSES

Sample No. Rock Type Main Group	71748 FRT 5	71755 FRT 5	71757 FRT 4	71758 FRT 4	71759 FRT 7	71764 FRT 5	71767 FRT 5	71769 FRT 7	71770 FRT 5	71773 FRT 4
Major Elements										
SiO ₂	48.05	46.51	50.49	50.09	50.61	49.46	48.26	50.90	47.82	49.04
TiO ₂	1.39	1.58	1.22	1.16	1.99	1.20	1.86	1.80	1.64	1.90
Al ₂ O ₃	15.56	15.65	14.19	14.27	13.02	14.89	13.80	13.48	15.40	12.65
Fe ₂ O ₃	14.27	16.12	13.75	13.52	15.53	13.11	16.35	15.13	14.97	16.99
FeO	0.00	0.00	0.00	0.00	0.00	0.00	0.00	0.00	0.00	0.00
MnO	0.21	0.24	0.21	0.19	0.24	0.21	0.25	0.23	0.21	0.26
MgO	7.27	7.55	6.80	6.69	5.53	6.88	6.74	5.87	7.08	5.07
CaO	10.39	10.10	10.94	10.70	9.78	11.88	10.51	9.94	9.94	10.08
Na ₂ O	2.45	2.55	2.43	2.14	2.52	2.20	2.27	2.33	2.56	2.63
K ₂ O	0.29	0.18	0.16	0.20	0.65	0.20	0.32	0.60	0.40	0.21
P ₂ O ₅	0.12	0.13	0.10	0.11	0.20	0.10	0.18	0.18	0.18	0.18
LOI	-0.07	-0.53	-0.33	0.87	0.23	-0.14	-0.65	-0.31	-0.02	-0.03
Total	98.65	98.63	99.96	99.94	98.90	98.81	98.42	98.79	98.83	98.98
Mg#	50.2	48.1	49.5	49.5	41.4	51.0	44.9	43.4	48.4	37.1
CIPW Norm wt%										
Qtz			0.06	1.45	1.56			2.08		0.40
Or	1.71	1.06	0.95	1.18	3.84	1.18	1.89	3.55	2.36	1.24
Ab	20.73	21.58	20.56	18.11	21.33	18.59	19.21	19.72	21.66	22.25
An	30.60	30.73	27.34	28.74	22.29	30.18	26.52	24.55	29.35	22.09
Lc										
Ne										
Cpx	16.68	15.37	21.77	19.57	20.84	23.24	20.35	19.67	15.57	22.51
Di	8.90	7.89	11.40	10.24	9.47	12.52	9.90	9.30	8.09	9.14
Hd	7.77	7.49	10.37	9.33	11.37	10.71	10.46	10.37	7.48	13.37
Opx	12.85	5.41	23.81	24.37	22.31	18.24	18.43	23.50	11.80	22.49
En	6.42	2.59	11.65	11.92	9.38	9.20	8.33	10.31	5.73	8.39
Fs	6.43	2.82	12.16	12.45	12.93	9.03	10.10	13.19	6.07	14.10
Ol	11.15	19.36				3.11	6.34		12.40	
Fo	5.30	8.80				1.49	2.71		5.72	
Fa	5.85	10.56				1.62	3.63		6.68	
Mt	2.07	2.34	1.99	1.96	2.25	1.90	2.37	2.20	2.17	2.47
Il	2.64	3.00	2.32	2.20	3.78	2.28	3.53	3.42	3.11	3.61
Ap	0.28	0.31	0.24	0.26	0.47	0.24	0.43	0.43	0.43	0.43
Trace Elements										
Ba	81	37	51	61	162	72	126	150	104	66
Rb	13	2	2	2	27	5	7	25	17	2
Nb	6	2	4	5	8	5	7	8	9	6
Sr	148	149	105	156	143	140	129	154	154	94
Zr	107	91	78	70	146	81	92	127	132	117
Y	36	37	29	28	44	31	36	38	40	41
La	9	3	4	4	21	4	10	13	11	8
Ce	20	10	12	11	35	13	20	31	25	19
Nd	15	10	10	9	14	11	14	19	17	15
Ni	101	107	98	98	40	87	70	38	108	45
Cr	157	157	202	201	40	171	175	92	123	46
V	279	269	381	369	420	298	350	385	288	494
Sc	43	41	52	54	49	45	50	51	40	50

FE-RICH THOLEIITE WHOLE ROCK ANALYSES

Sample No.	71776	71779	71780	71781	71782	71783	71784	71802	71803	71805
Rock Type	FRT	FRT	FRT	FRT	FRT	FRT	FRT	FRT	FRT	FRT
Main Group	4	5	5	7	4	7	4	7	4	7
Major Elements										
SiO ₂	48.65	50.85	47.88	50.06	48.31	50.14	50.26	48.95	45.83	50.68
TiO ₂	1.78	2.09	1.26	1.65	2.35	1.95	1.23	2.45	2.99	1.54
Al ₂ O ₃	12.36	13.39	16.32	14.16	12.74	13.31	14.15	12.85	13.36	14.22
Fe ₂ O ₃	16.83	15.86	13.99	13.79	18.15	15.43	13.57	16.89	18.04	13.57
FeO	0.00	0.00	0.00	0.00	0.00	0.00	0.00	0.00	0.00	0.00
MnO	0.27	0.24	0.21	0.21	0.26	0.23	0.21	0.25	0.25	0.20
MgO	5.35	5.20	7.85	6.19	7.79	5.47	7.01	5.92	6.25	6.05
CaO	10.12	9.59	10.36	10.40	9.67	9.75	11.06	10.10	9.75	10.76
Na ₂ O	2.50	2.40	2.39	2.31	2.41	2.44	2.14	2.38	2.29	2.28
K ₂ O	0.23	0.60	0.23	0.45	0.25	0.66	0.15	0.52	0.52	0.56
P ₂ O ₅	0.15	0.21	0.08	0.14	0.22	0.19	0.11	0.26	0.37	0.15
LOI	1.02	-0.10	0.00	0.54	0.05	-0.15	0.25	-0.29	-0.21	-0.08
Total	99.26	98.90	99.31	98.66	102.20	98.03	100.14	98.76	97.82	98.71
Mg#	38.6	39.4	52.6	47.1	45.9	41.3	50.6	41.0	40.7	46.9
CIPW Norm wt%										
Qtz	0.25	2.91		1.14		1.43	0.98			1.43
Or	1.36	3.55	1.36	2.66	1.48	3.90	0.89	3.07	3.07	3.31
Ab	21.15	20.31	20.22	19.55	20.39	20.65	18.11	20.14	19.38	19.29
An	21.82	23.99	33.12	26.94	23.21	23.42	28.56	22.84	24.64	26.91
Lc										
Ne										
Cpx	23.02	18.62	14.64	19.70	19.38	19.83	21.17	21.37	17.81	21.16
Di	9.65	8.11	8.13	10.04	9.73	8.98	11.32	9.76	8.21	10.71
Hd	13.38	10.51	6.51	9.67	9.65	10.85	9.84	11.61	9.59	10.45
Opx	22.94	22.86	11.69	22.66	18.80	22.57	24.40	23.12	13.77	21.42
En	8.85	9.19	6.09	10.77	8.79	9.46	12.21	9.77	5.89	10.10
Fs	14.09	13.67	5.59	11.90	10.01	13.11	12.19	13.35	7.89	11.32
Ol			13.66		9.64			0.80	10.20	
Fo			6.79		4.28			0.32	4.12	
Fa			6.87		5.37			0.48	6.08	
Mt	2.44	2.30	2.03	2.00	2.63	2.24	1.97	2.45	2.62	1.97
Il	3.38	3.97	2.39	3.13	4.46	3.70	2.34	4.65	5.68	2.92
Ap	0.36	0.50	0.19	0.33	0.52	0.45	0.26	0.62	0.88	0.36
Trace Elements										
Ba	71	158	58	119	47	51	51	164	194	156
Rb	3	28	7	17	4	31	6	18	16	24
Nb	6	11	3	7	7	8	4	10	19	7
Sr	94	137	157	151	126	159	106	142	173	159
Zr	11	175	61	109	149	134	70	167	207	117
Y	39	51	23	35	46	40	27	51	55	33
La	5	15	5	19	7	14	5	15	21	13
Ce	16	36	10	30	23	35	13	38	43	30
Nd	14	24	8	11	18	20	8	24	29	19
Ni	59	49	126	54	57	37	104	67	85	50
Cr	68	68	152	164	59	63	232	126	127	89
V	511	420	312	371	544	408	378	446	432	347
Sc	54	49	42	56	85	167	55	52	42	51

FE-RICH THOLEIITE WHOLE ROCK ANALYSES

Sample No. Rock Type Main Group	71807 FRT 7	71808 FRT 9	71810 FRT 2	71815 FRT 4	71817 FRT 9	71818 FRT 9	71819 FRT 9	71820 FRT 7	71821 FRT 4	71822 FRT 7
Major Elements										
SiO2	50.74	47.69	48.41	50.05	48.90	48.84	49.55	50.55	50.27	50.86
TiO2	1.96	1.26	2.25	1.39	1.46	1.41	2.24	1.79	1.58	1.41
Al2O3	13.11	16.68	11.77	13.47	14.56	14.80	13.11	13.40	13.45	13.55
Fe2O3	16.21	12.43	19.14	15.82	13.91	13.47	15.88	14.93	15.76	14.31
FeO	0.00	0.00	0.00	0.00	0.00	0.00	0.00	0.00	0.00	0.00
MnO	0.24	0.18	0.28	0.23	0.22	0.21	0.24	0.24	0.21	0.22
MgO	5.31	8.24	5.29	5.63	6.87	7.48	5.76	5.80	5.57	5.89
CaO	9.53	11.37	9.95	10.11	11.43	11.79	9.99	10.04	9.86	10.30
Na2O	2.53	2.07	2.54	2.46	2.38	2.23	2.45	2.27	2.44	2.27
K2O	0.67	0.22	0.23	0.18	0.22	0.21	0.58	0.61	0.43	0.54
P2O5	0.21	0.09	0.25	0.13	0.12	0.11	0.25	0.17	0.31	0.12
LOI	-0.33	0.02	0.03	0.36	-0.48	-0.12	-0.22	-0.14	0.21	-0.28
Total	98.72	99.13	98.42	98.41	98.34	99.22	98.40	98.32	98.67	97.90
Mg#	39.4	56.8	35.4	41.3	49.4	52.4	41.8	43.5	41.2	44.9
CIPW Norm wt%										
Qtz	1.68			1.30			0.48	2.13	1.64	2.22
Or	3.96	1.30	1.36	1.06	1.30	1.24	3.43	3.60	2.54	3.19
Ab	21.41	17.52	21.49	20.82	20.14	18.87	20.73	19.21	20.65	19.21
An	22.44	35.57	20.04	25.18	28.40	29.75	23.06	24.57	24.48	25.19
Lc										
Ne										
Cpx	19.69	16.60	23.36	20.21	22.79	23.11	20.77	20.12	18.77	20.94
Di	8.50	9.96	9.10	8.92	12.04	12.88	9.63	9.52	8.34	10.07
Hd	11.19	6.64	14.26	11.29	10.75	10.23	11.14	10.60	10.43	10.87
Opx	23.31	11.77	22.85	24.24	14.87	13.91	23.01	22.86	24.37	22.41
En	9.29	6.67	8.17	9.89	7.35	7.28	9.89	10.03	10.01	10.01
Fs	14.03	5.11	14.68	14.35	7.53	6.63	13.13	12.82	14.36	12.40
Ol		11.94	1.65		6.25	7.57				
Fo		6.48	0.55		2.93	3.77				
Fa		5.47	1.10		3.31	3.79				
Mt	2.35	1.80	2.78	2.30	2.02	1.96	2.31	2.17	2.29	2.08
Il	3.72	2.39	4.27	2.64	2.77	2.68	4.25	3.40	3.00	2.68
Ap	0.50	0.21	0.59	0.31	0.28	0.26	0.59	0.40	0.73	0.28
Trace Elements										
Ba	171	64	58	58	70	62	158	157	157	123
Rb	32	7	5	4	7	7	28	28	15	28
Nb	11	4	7	5	4	3	11	7	7	7
Sr	139	166	110	108	150	150	148	160	133	136
Zr	152	70	145	90	88	81	175	135	117	102
Y	51	26	48	34	33	30	53	41	38	34
La	15	11	8	3	6	6	14	13	12	10
Ce	35	14	22	13	16	16	35	30	25	22
Nd	23	5	23	13	11	14	24	17	18	14
Ni	48	172	82	73	89	100	65	37	88	42
Cr	62	229	83	99	221	297	145	87	109	71
V	407	273	577	414	353	336	431	329	380	369
Sc	52	42	48	51	53	53	51	52	40	51

FE-RICH THOLEIITE WHOLE ROCK ANALYSES

Sample No.	71823	71824	71829	71830	71831	71832	71833	71835	71836	71837
Rock Type	FRT	FRT	FRT	FRT	FRT	FRT	FRT	FRT	FRT	FRT
Main Group	9	4	9	9	7	9	7	7	7	9
Major Elements										
SiO ₂	50.29	48.45	46.82	49.18	50.87	49.06	50.85	49.41	49.32	49.52
TiO ₂	1.57	2.26	1.82	1.67	1.97	2.21	1.63	2.89	1.76	1.27
Al ₂ O ₃	14.88	12.11	14.74	14.87	13.15	13.60	13.80	12.58	13.27	14.34
Fe ₂ O ₃	13.87	18.04	15.65	14.01	15.58	15.27	13.99	17.46	14.93	13.52
FeO	0.00	0.00	0.00	0.00	0.00	0.00	0.00	0.00	0.00	0.00
MnO	0.21	0.25	0.24	0.21	0.24	0.24	0.21	0.25	0.24	0.21
MgO	5.81	5.50	6.96	6.30	5.64	6.31	6.35	4.75	6.80	7.08
CaO	10.37	10.07	10.47	10.99	9.97	10.51	10.65	9.05	11.00	11.90
Na ₂ O	2.54	2.32	2.60	2.17	2.48	2.46	2.36	2.32	2.38	2.11
K ₂ O	0.53	0.21	0.33	0.33	0.61	0.57	0.60	0.84	0.53	0.20
P ₂ O ₅	0.17	0.18	0.19	0.15	0.21	0.24	0.18	0.36	0.19	0.11
LOI	-0.11	0.03	0.08	-0.22	-0.40	-0.18	-0.28	-0.29	-0.48	-0.40
Total	98.88	97.80	98.49	98.40	98.92	98.92	99.08	98.05	98.60	98.64
Mg#	45.3	37.6	46.8	47.1	41.8	45.0	47.3	35.0	47.4	50.9
CIPW Norm wt%										
Qtz	0.12	0.61			1.67		0.83	2.60		
Or	3.13	1.24	1.95	1.95	3.60	3.37	3.55	4.96	3.13	1.18
Ab	21.49	19.63	21.97	18.36	20.99	20.82	19.97	19.63	20.14	17.85
An	27.64	22.01	27.59	29.86	22.95	24.38	25.29	21.43	23.96	29.07
Lc										
Ne										
Cpx	18.89	22.51	19.19	19.66	21.01	21.77	21.88	17.78	24.37	24.18
Di	9.26	9.36	9.71	10.02	9.62	10.82	11.19	7.15	12.48	13.04
Hd	9.63	13.14	9.48	9.63	11.39	10.95	10.69	10.64	11.89	11.14
Opx	22.33	24.44	5.49	23.24	22.61	17.98	22.29	23.06	16.40	19.83
En	10.18	9.36	2.59	11.05	9.59	8.32	10.63	8.52	7.84	10.01
Fs	12.15	15.08	2.90	12.19	13.02	9.66	11.66	14.55	8.56	9.81
Ol			16.04			3.80			5.12	2.30
Fo			7.18			1.67			2.32	1.11
Fa			8.86			2.13			2.80	1.19
Mt	2.01	2.62	2.27	2.03	2.26	2.22	2.03	2.53	2.17	1.96
Il	2.98	4.29	3.46	3.17	3.74	4.20	3.10	5.49	3.34	2.41
Ap	0.40	0.43	0.45	0.36	0.50	0.57	0.43	0.85	0.45	0.26
Trace Elements										
Ba	141	56	126	99	160	174	157	214	165	72
Rb	26	3	10	13	27	29	26	41	20	7
Nb	11	7	6	8	10	12	12	13	8	5
Sr	141	111	140	154	150	156	159	150	147	137
Zr	154	141	102	123	147	159	123	230	117	85
Y	42	46	35	39	44	50	37	64	39	31
La	13	6	8	10	24	14	13	21	14	6
Ce	28	17	26	24	32	34	27	49	29	15
Nd	19	17	17	17	14	24	18	32	16	10
Ni	74	86	79	93	49	69	62	42	61	86
Cr	119	124	154	166	53	198	112	83	285	170
V	343	585	340	373	420	410	374	515	385	332
Sc	46	47	47	50	51	53	50	46	60	51

FE-RICH THOLEIITE WHOLE ROCK ANALYSES

Sample No. Rock Type Main Group	71838 FRT 9	71839 FRT 7	71840 FRT 7	71841 FRT 7	71842 FRT 9	71845 FRT 4	71849 FRT 2	71850 FRT 4	71851 FRT 9	71852 FRT 4
Major Elements										
SiO ₂	49.40	48.06	50.98	50.42	48.93	50.07	50.01	49.53	47.76	50.12
TiO ₂	1.93	2.83	1.74	1.36	1.42	1.01	1.61	1.27	1.54	1.43
Al ₂ O ₃	13.97	12.90	13.72	13.53	15.49	14.35	13.14	14.40	15.47	13.49
Fe ₂ O ₃	15.01	16.68	14.46	14.27	13.33	13.53	16.10	14.37	13.88	15.12
FeO	0.00	0.00	0.00	0.00	0.00	0.00	0.00	0.00	0.00	0.00
MnO	0.24	0.25	0.23	0.22	0.21	0.21	0.22	0.21	0.20	0.21
MgO	6.96	5.78	6.27	6.31	7.15	7.13	5.61	6.73	7.59	6.08
CaO	11.53	10.20	10.44	10.59	11.34	10.90	9.82	10.67	10.57	10.06
Na ₂ O	2.12	2.42	2.28	2.20	2.07	2.44	2.55	2.34	2.19	2.35
K ₂ O	0.29	0.59	0.61	0.47	0.29	0.20	0.43	0.22	0.34	0.37
P ₂ O ₅	0.06	0.28	0.17	0.11	0.13	0.09	0.32	0.13	0.15	0.27
LOI	-0.88	-0.52	-0.46	-0.47	-0.35	-0.27	-0.10	0.01	-0.27	-0.31
Total	99.28	97.97	99.14	97.73	98.81	98.44	99.71	99.88	99.42	99.19
Mg#	47.9	40.7	46.2	46.7	51.5	51.1	40.8	48.1	52.0	44.3
CIPW Norm wt%										
Qtz			1.47	1.39			0.82			1.36
Or	1.71	3.49	3.60	2.78	1.71	1.18	2.54	1.30	2.01	2.19
Ab	17.91	20.48	19.29	18.62	17.52	20.65	21.58	19.80	18.53	19.89
An	27.76	22.59	25.40	25.65	32.12	27.61	23.14	28.14	31.38	25.17
Lc										
Ne										
Cpx	24.08	21.87	21.01	21.75	19.23	21.40	19.68	19.87	16.56	19.16
Di	12.53	10.11	10.52	10.82	10.56	11.45	8.67	10.14	9.21	9.09
Hd	11.55	11.76	10.48	10.93	8.67	9.96	11.01	9.74	7.35	10.07
Opx	19.83	18.56	23.02	23.10	19.68	20.66	24.46	22.68	15.31	24.84
En	9.64	7.95	10.74	10.70	10.14	10.34	9.96	10.79	7.99	10.93
Fs	10.20	10.61	12.28	12.40	9.55	10.32	14.51	11.89	7.32	13.91
Ol	2.88	3.05			3.97	3.11		1.98	9.36	
Fo	1.33	1.24			1.95	1.48		0.90	4.66	
Fa	1.55	1.82			2.02	1.63		1.09	4.70	
Mt	2.18	2.42	2.10	2.07	1.94	1.96	2.34	2.09	2.01	2.19
Il	3.67	5.37	3.30	2.58	2.70	1.92	3.06	2.41	2.92	2.72
Ap	0.14	0.66	0.40	0.26	0.31	0.21	0.76	0.31	0.36	0.64
Trace Elements										
Ba	81	207	153	104	82	59	158	68	46	141
Rb	4	19	24	22	10	3	12	5	12	11
Nb	6	14	8	4	5	5	7	5	5	6
Sr	145	210	147	135	155	109	131	107	156	123
Zr	57	173	126	90	90	71	121	85	105	104
Y	28	46	39	31	32	27	41	30	34	37
La	5	18	12	10	6	7	17	11	9	8
Ce	11	37	27	20	16	15	29	17	18	21
Nd	8	25	17	14	12	10	18	13	12	16
Ni	42	49	42	70	90	115	84	101	139	95
Cr	259	148	110	78	170	214	108	199	140	148
V	436	452	369	344	321	330	378	363	308	366
Sc	54	54	55	52	49	52	41	50	91	45

FE-RICH THOLEIITE WHOLE ROCK ANALYSES

Sample No.	71853	71854	71857	71858	71859	71860	71861	71862	71863	71866
Rock Type	FRT	FRT	FRT	FRT	FRT	FRT	FRT	FRT	FRT	FRT
Main Group	4	7	7	4	4	7	9	7	7	7
Major Elements										
SiO ₂	50.31	49.23	50.24	49.78	48.34	49.52	49.23	48.30	48.18	46.78
TiO ₂	1.54	2.70	1.91	1.02	2.16	1.94	1.37	2.34	3.48	2.44
Al ₂ O ₃	14.75	11.96	13.38	14.09	12.22	13.24	14.48	12.09	12.54	13.53
Fe ₂ O ₃	14.84	19.60	14.98	13.10	18.50	14.93	12.47	18.81	17.65	17.95
FeO	0.00	0.00	0.00	0.00	0.00	0.00	0.00	0.00	0.00	0.00
MnO	0.20	0.30	0.23	0.20	0.27	0.23	0.20	0.27	0.25	0.26
MgO	4.55	4.62	6.06	7.57	5.36	6.40	7.86	5.23	5.17	6.41
CaO	9.72	9.29	10.11	11.62	9.96	10.51	11.85	9.83	9.27	9.65
Na ₂ O	2.57	2.63	2.40	2.14	2.30	2.28	2.07	2.43	2.46	2.08
K ₂ O	0.45	0.52	0.57	0.13	0.23	0.43	0.35	0.17	0.81	0.53
P ₂ O ₅	0.33	0.27	0.17	0.09	0.19	0.18	0.12	0.21	0.45	0.24
LOI	0.06	-0.83	-0.31	0.10	-0.12	-0.43	-0.14	-0.22	-0.48	-0.54
Total	99.32	100.29	99.74	99.84	99.41	99.23	99.86	99.46	99.78	99.33
Mg#	37.8	31.8	44.5	53.4	36.5	45.9	55.5	35.5	36.7	41.4
CIPW Norm wt %										
Qtz	2.48	0.54	0.94		0.42	0.45		0.31	0.39	
Or	2.66	3.07	3.37	0.77	1.36	2.54	2.07	1.00	4.79	3.13
Ab	21.75	22.25	20.31	18.11	19.46	19.29	17.52	20.56	20.82	17.60
An	27.38	19.29	24.05	28.46	22.34	24.62	29.19	21.58	20.78	26.02
Lc										
Ne										
Cpx	15.72	21.21	20.81	23.58	21.76	21.89	23.66	21.77	18.68	16.97
Di	6.45	7.60	10.12	13.18	8.72	10.97	13.96	8.56	8.05	7.78
Hd	9.26	13.61	10.69	10.40	13.04	10.91	9.71	13.21	10.62	9.20
Opx	22.09	24.39	23.02	21.64	25.29	23.25	16.77	25.10	22.99	19.84
En	8.34	7.98	10.40	11.36	9.31	10.86	9.32	9.06	9.14	8.42
Fs	13.75	16.40	12.62	10.29	15.98	12.39	7.44	16.04	13.84	11.42
Ol				1.95			4.99			6.90
Fo				0.97			2.65			2.76
Fa				0.97			2.33			4.13
Mt	2.15	2.85	2.17	1.90	2.69	2.17	1.81	2.73	2.56	2.61
Il	2.92	5.13	3.63	1.94	4.10	3.68	2.60	4.44	6.61	4.63
Ap	0.78	0.64	0.40	0.21	0.45	0.43	0.28	0.50	1.07	0.57
Trace Elements										
Ba	155	183	150	54	127	127	96	49	239	196
Rb	13	13	26	5	17	17	13	5	29	19
Nb	7	9	8	6	7	7	7	7	18	13
Sr	145	129	148	97	158	158	157	111	212	131
Zr	130	161	138	130	121	121	88	136	243	159
Y	44	62	42	46	39	39	32	46	55	54
La	12	18	13	4	10	10	8	6	25	18
Ce	27	36	30	16	24	24	21	17	51	43
Nd	20	26	20	16	19	19	17	15	35	27
Ni	64	36	58	71	54	54	92	82	43	74
Cr	88	37	111	72	136	136	383	74	81	146
V	286	421	403	538	403	403	314	556	463	348
Sc	38	53	52	48	55	55	52	47	49	52

FE-RICH THOLEIITE WHOLE ROCK ANALYSES

Sample No. Rock Type Main Group	71870 FRT 7	71873 FRT 7	71879 FRT 7	71880 FRT 7	71881 FRT 7	71884 FRT 4	71886 FRT 9	71897 FRT 9	71899 FRT 4	71901 FRT 7
Major Elements										
SiO ₂	49.97	50.01	47.01	47.82	50.21	51.40	49.44	49.23	50.52	51.31
TiO ₂	1.66	1.66	2.78	2.87	1.62	1.49	1.38	1.37	1.37	2.06
Al ₂ O ₃	13.63	13.53	13.16	12.95	13.71	13.72	14.36	14.59	13.56	14.33
Fe ₂ O ₃	14.01	14.25	18.85	16.67	14.09	14.56	12.67	12.47	15.76	12.26
FeO	0.00	0.00	0.00	0.00	0.00	0.00	0.00	0.00	0.00	0.00
MnO	0.22	0.23	0.27	0.26	0.22	0.22	0.21	0.20	0.24	0.19
MgO	6.46	6.42	5.74	5.70	6.44	5.03	7.63	7.81	5.73	5.82
CaO	10.70	10.80	9.49	10.10	10.55	9.47	11.51	11.84	10.20	9.97
Na ₂ O	2.66	2.43	2.17	2.61	2.25	2.39	2.15	2.04	2.72	3.02
K ₂ O	0.51	0.52	0.64	0.62	0.53	0.65	0.39	0.33	0.19	1.07
P ₂ O ₅	0.17	0.16	0.29	0.31	0.17	0.14	0.13	0.14	0.12	0.27
LOI	0.21	-0.03	-0.16	0.24	0.24	0.37	0.08	0.03	-0.08	0.17
Total	100.20	99.98	100.24	100.15	100.03	99.44	99.95	100.05	100.33	100.47
Mg#	47.7	47.1	37.6	40.4	47.5	40.6	54.4	55.4	41.9	48.5
CIPW Norm wt%										
Qtz					0.89	3.83			0.18	
Or	3.01	3.07	3.78	3.66	3.13	3.84	2.30	1.95	1.12	6.32
Ab	22.51	20.56	18.36	22.09	19.04	20.22	18.19	17.26	23.02	25.55
An	23.74	24.47	24.28	21.79	25.74	24.79	28.38	29.68	24.23	22.39
Lc										
Ne										
Cpx	23.41	23.29	17.56	21.97	21.14	17.83	22.92	23.11	21.42	20.92
Di	12.07	11.85	7.43	10.10	10.84	7.82	13.26	13.60	9.56	11.30
Hd	11.34	11.44	10.13	11.87	10.31	10.01	9.66	9.52	11.86	9.62
Opx	16.69	20.64	20.73	14.40	23.05	21.97	18.15	17.87	23.84	15.96
En	8.03	9.80	8.08	6.13	11.02	8.90	9.89	9.91	9.84	8.07
Fs	8.66	10.85	12.65	8.27	12.03	13.06	8.27	7.96	14.00	7.89
Ol	3.78	1.09	5.31	5.90			4.01	4.28		1.73
Fo	1.73	0.49	1.95	2.37			2.08	2.27		0.83
Fa	2.05	0.60	3.36	3.53			1.92	2.01		0.89
Mt	2.03	2.07	2.74	2.42	2.04	2.11	1.84	1.81	2.29	1.78
Il	3.15	3.15	5.28	5.45	3.08	2.83	2.62	2.60	2.60	3.91
Ap	0.40	0.38	0.69	0.73	0.40	0.33	0.31	0.33	0.28	0.64
Trace Elements										
Ba	132	128	222	204	148	162	110	108	286	309
Rb	18	22	25	20	23	33	16	13	64	44
Nb	7	6	14	13	8	7	8	6	7	24
Sr	160	156	129	215	148	143	155	162	107	293
Zr	112	114	186	173	113	110	97	92	113	211
Y	34	35	55	44	35	34	31	31	22	39
La	10	13	23	17	12	14	9	9	21	26
Ce	21	24	49	42	29	28	22	20	44	50
Nd	14	16	28	26	18	17	14	14	17	31
Ni	53	49	59	48	44	26	86	87	179	79
Cr	136	139	135	139	105	22	337	358	615	184
V	371	377	387	459	354	345	318	307	213	307
Sc	51	51	46	48	50	47	48	48	33	33

FE-RICH THOLEIITE WHOLE ROCK ANALYSES

Sample No.	71902	71904	71905	71910	71912	71915	71917	71918	71919	71920
Rock Type	FRT	FRT	FRT	FRT	FRT	FRT	FRT	FRT	FRT	FRT
Main Group	7	7	9	4	4	9	9	7	9	7
Major Elements										
SiO ₂	50.13	47.51	48.28	49.97	52.06	49.69	49.03	47.59	49.81	49.21
TiO ₂	1.83	1.18	2.21	1.38	1.64	2.31	2.11	1.22	2.32	1.46
Al ₂ O ₃	13.67	15.86	13.89	13.41	13.70	13.18	13.11	15.70	13.16	13.86
Fe ₂ O ₃	14.79	13.76	15.92	15.86	15.49	15.84	15.49	14.01	15.84	13.84
FeO	0.00	0.00	0.00	0.00	0.00	0.00	0.00	0.00	0.00	0.00
MnO	0.23	0.20	0.24	0.25	0.23	0.24	0.25	0.21	0.25	0.21
MgO	6.12	8.27	5.99	5.64	4.89	5.98	6.05	8.15	5.89	7.15
CaO	10.49	10.86	10.23	10.17	9.47	10.34	10.65	10.96	10.34	11.40
Na ₂ O	2.44	2.18	2.38	2.58	2.55	2.35	2.55	2.12	2.44	2.24
K ₂ O	0.55	0.23	0.41	0.25	0.77	0.47	0.54	0.24	0.53	0.29
P ₂ O ₅	0.18	0.12	0.21	0.13	0.17	0.26	0.20	0.13	0.26	0.16
LOI	-0.27	-0.10	-0.36	0.17	-0.27	-0.32	-0.32	-0.04	-0.36	-0.29
Total	100.16	100.07	99.40	99.81	100.70	100.34	99.66	100.29	100.48	99.53
Mg#	45.0	54.3	42.7	41.3	38.5	42.8	43.6	53.5	42.4	50.6
CIPW Norm wt%										
Qtz	0.10			0.32	3.10	0.80			0.44	
Or	3.25	1.36	2.42	1.48	4.55	2.78	3.19	1.42	3.13	1.71
Ab	20.65	18.42	20.14	21.83	21.58	19.89	21.58	17.94	20.65	18.95
An	24.72	32.83	26.01	24.27	23.66	24.03	22.73	32.61	23.39	26.91
Lc										
Ne										
Cpx	21.75	16.68	19.50	21.22	18.66	21.32	24.00	17.23	21.86	23.64
Di	10.67	9.53	9.20	9.36	7.80	10.13	11.52	9.71	10.31	12.76
Hd	11.09	7.15	10.30	11.87	10.87	11.19	12.48	7.52	11.56	10.88
Opx	22.58	11.33	20.18	23.85	22.26	23.13	16.18	12.38	22.63	18.50
En	10.30	6.09	8.83	9.71	8.57	10.20	7.21	6.55	9.89	9.35
Fs	12.28	5.24	11.35	14.14	13.70	12.93	8.97	5.83	12.73	9.15
Ol		13.79	3.09				4.18	12.84		3.70
Fo		7.07	1.28				1.76	6.48		1.78
Fa		6.71	1.81				2.42	6.35		1.92
Mt	2.15	2.00	2.31	2.30	2.25	2.30	2.25	2.03	2.30	2.01
Il	3.48	2.24	4.20	2.62	3.11	4.39	4.01	2.32	4.41	2.77
Ap	0.43	0.28	0.50	0.31	0.40	0.62	0.47	0.31	0.62	0.38
Trace Elements										
Ba	153	79	110	91	167	142	150	77	149	97
Rb	24	8	17	7	39	20	22	9	20	10
Nb	8	5	7	4	8	11	10	5	11	6
Sr	164	121	151	109	146	161	155	121	165	140
Zr	125	66	141	84	123	159	145	70	164	82
Y	38	28	47	34	37	47	46	29	47	32
La	13	9	12	6	15	14	12	6	14	9
Ce	25	17	27	15	30	32	28	15	32	18
Nd	16	11	19	11	20	23	21	10	23	12
Ni	46	137	88	70	26	69	50	134	65	84
Cr	110	171	102	110	24	105	104	173	113	312
V	375	263	448	406	359	411	402	278	416	338
Sc	51	41	52	48	46	52	52	47	54	56

FE-RICH THOLEIITE WHOLE ROCK ANALYSES

Sample No. Rock Type Main Group	71922 FRT 9	71923 FRT 7	71926 FRT 9	71931 FRT 9	71934 FRT 7	71937 FRT 7	71944 FRT 7	71955 FRT 7	71957 FRT 7	71964 FRT 9
Major Elements										
SiO ₂	49.55	47.11	48.72	49.46	46.46	49.91	47.24	45.15	49.34	49.33
TiO ₂	2.15	2.51	1.72	2.23	2.62	3.16	2.50	4.13	1.79	2.23
Al ₂ O ₃	13.05	13.43	13.75	12.99	13.52	12.45	13.41	13.14	13.36	12.95
Fe ₂ O ₃	15.68	17.59	14.76	15.75	18.21	18.09	17.52	19.07	15.33	15.82
FeO	0.00	0.00	0.00	0.00	0.00	0.00	0.00	0.00	0.00	0.00
MnO	0.24	0.25	0.22	0.25	0.25	0.27	0.26	0.28	0.24	0.24
MgO	5.89	5.75	7.13	5.81	6.15	4.07	6.01	5.03	6.35	5.80
CaO	10.15	9.58	11.49	10.09	9.72	8.51	9.64	8.82	10.66	9.94
Na ₂ O	2.67	2.27	2.14	2.43	2.12	2.53	2.40	2.46	2.29	2.36
K ₂ O	0.59	0.69	0.29	0.54	0.56	1.19	0.71	1.02	0.38	0.60
P ₂ O ₅	0.23	0.28	0.15	0.27	0.30	0.47	0.31	0.75	0.17	0.24
LOI	-0.35	0.12	-0.26	-0.36	-0.30	-0.34	-0.37	-0.34	-0.09	-0.39
Total	99.85	99.58	100.11	99.46	99.61	100.31	99.63	99.51	99.82	97.70
Mg#	42.7	39.3	48.9	42.2	40.1	30.8	40.5	34.3	45.1	42.1
CIPW Norm wt%										
Qtz				0.60		2.56				0.73
Or	3.49	4.08	1.71	3.19	3.31	7.03	4.20	6.03	2.25	3.55
Ab	22.59	19.21	18.11	20.56	17.94	21.41	20.31	20.82	19.38	19.97
An	21.88	24.42	27.06	22.94	25.72	19.10	23.72	21.80	25.05	22.97
Lc										
Ne										
Cpx	22.50	17.83	23.98	21.16	17.19	16.98	18.47	14.35	22.24	20.68
Di	10.60	7.82	12.64	9.90	7.69	6.11	8.32	5.92	10.86	9.64
Hd	11.91	10.01	11.34	11.26	9.50	10.87	10.15	8.43	11.38	11.05
Opx	18.80	18.49	17.52	22.79	18.22	22.21	15.17	14.03	23.13	23.10
En	8.21	7.49	8.63	9.88	7.54	7.30	6.32	5.33	10.50	9.98
Fs	10.59	11.00	8.89	12.90	10.68	14.91	8.85	8.71	12.63	13.12
Ol	2.63	5.88	4.89		7.57		8.55	8.76	0.46	
Fo	1.09	2.25	2.29		2.96		3.36	3.13	0.20	
Fa	1.54	3.63	2.60		4.62		5.19	5.63	0.26	
Mt	2.28	2.55	2.14	2.28	2.64	2.63	2.54	2.77	2.23	2.30
Il	4.08	4.77	3.27	4.24	4.98	6.00	4.75	7.84	3.40	4.24
Ap	0.54	0.66	0.36	0.64	0.71	1.11	0.73	1.78	0.40	0.57
Trace Elements										
Ba	157	97	93	144	200	1230	240	438	119	166
Rb	23	10	7	20	20	82	25	35	12	27
Nb	13	6	6	12	13	59	13	36	6	12
Sr	149	140	140	160	129	576	131	213	122	148
Zr	157	82	81	162	170	231	188	420	110	172
Y	48	32	33	45	54	20	54	76	39	52
La	16	9	8	16	21	42	24	43	10	16
Ce	39	18	18	39	46	93	53	103	23	37
Nd	23	12	13	25	26	44	29	58	17	24
Ni	50	84	93	67	66	429	55	47	62	61
Cr	100	312	338	114	130	596	131	67	186	145
V	412	338	420	408	365	319	358	402	379	428
Sc	53	56	58	52	48	25	50	42	51	50

FE-RICH THOLEIITE WHOLE ROCK ANALYSES

Sample No. Rock Type Main Group	71965 FRT 7	71966 FRT 7	71968 FRT 7	71969 FRT 7	71970 FRT 9	71973 FRT 7	71974 FRT 7	71975 FRT 4	71976 FRT 7	71977 FRT 9
Major Elements										
SiO ₂	50.57	50.34	50.12	49.44	49.20	49.12	49.31	50.81	49.44	51.04
TiO ₂	1.92	2.05	1.72	2.17	2.10	1.91	3.46	1.17	1.46	2.05
Al ₂ O ₃	13.21	13.18	12.61	13.08	12.95	13.83	12.29	14.46	13.87	14.09
Fe ₂ O ₃	15.33	15.70	15.78	15.90	15.56	15.23	18.24	13.55	13.19	11.98
FeO	0.00	0.00	0.00	0.00	0.00	0.00	0.00	0.00	0.00	0.00
MnO	0.24	0.24	0.23	0.25	0.24	0.24	0.26	0.20	0.21	0.18
MgO	6.09	5.62	6.33	6.00	5.97	6.03	4.45	6.98	7.04	5.77
CaO	10.24	9.88	10.87	10.46	10.41	10.42	8.87	10.84	11.55	9.88
Na ₂ O	2.29	2.30	2.05	2.55	2.43	2.25	2.22	2.11	2.10	2.45
K ₂ O	0.60	0.62	0.48	0.55	0.51	0.59	0.94	0.17	0.38	1.07
P ₂ O ₅	0.19	0.20	0.12	0.22	0.21	0.18	0.36	0.09	0.13	0.28
LOI	-0.24	-0.34	-0.20	-0.22	0.11	0.02	-0.39	-0.40	0.04	0.65
Total	99.06	98.38	98.69	98.97	98.29	98.45	98.37	99.98	98.22	98.36
Mg#	44.0	41.5	44.3	42.8	43.2	43.9	32.6	50.5	51.4	48.8
CIPW Norm wt%										
Qtz	1.42	2.05	1.31				3.39	1.67		2.38
Or	3.55	3.66	2.84	3.25	3.01	3.49	5.55	1.00	2.25	6.32
Ab	19.38	19.46	17.35	21.58	20.54	19.04	18.79	17.85	17.77	20.73
An	23.99	23.81	23.79	22.62	22.94	25.89	20.79	29.48	27.30	24.29
Lc										
Ne										
Cpx	21.30	19.98	24.47	23.22	22.79	20.52	17.61	19.61	24.07	18.91
Di	10.24	9.12	11.70	10.95	10.84	9.85	6.77	10.46	13.23	10.31
Hd	11.06	10.86	12.77	12.27	11.95	10.67	10.84	9.15	10.84	8.60
Opx	23.35	23.11	23.29	18.77	21.71	22.57	22.55	25.13	20.89	18.78
En	10.42	9.77	10.34	8.21	9.58	10.06	7.95	12.54	10.76	9.59
Fs	12.92	13.34	12.95	10.56	12.13	12.51	14.61	12.59	10.12	9.19
Ol				2.81	0.45	0.67			0.92	
Fo				1.16	0.19	0.28			0.45	
Fa				1.65	0.26	0.38			0.47	
Mt	2.23	2.28	2.29	2.31	2.26	2.21	2.65	1.97	1.91	1.74
Il	3.65	3.89	3.27	4.12	3.99	3.63	6.57	2.22	2.77	3.89
Ap	0.45	0.47	0.28	0.52	0.50	0.43	0.85	0.21	0.31	0.66
Trace Elements										
Ba	151	168	112	158	167	189	245	49	109	290
Rb	24	27	20	23	23	25	45	5	14	44
Nb	9	10	6	11	11	9	15	4	6	23
Sr	146	150	124	152	157	156	146	104	163	285
Zr	138	153	99	157	155	134	227	70	96	204
Y	42	46	34	45	45	39	63	26	32	35
La	13	17	9	16	14	13	23	3	10	25
Ce	33	39	22	31	35	32	53	10	22	49
Nd	18	23	14	20	23	20	36	9	15	32
Ni	54	47	45	48	49	52	34	95	66	78
Cr	103	75	104	99	95	201	41	201	203	178
V	398	406	468	410	388	376	519	361	331	307
Sc	50	49	54	51	47	49	47	50	51	35

FE-RICH THOLEIITE WHOLE ROCK ANALYSES

Sample No.	71979	71980	71981	71988
Rock Type	FRT	FRT	FRT	FRT
Main Group	9	7	9	7
Major Elements				
SiO2	49.54	49.13	49.33	50.64
TiO2	1.33	1.99	1.41	1.84
Al2O3	14.53	13.92	14.47	13.47
Fe2O3	12.42	15.43	12.69	15.04
FeO	0.00	0.00	0.00	0.00
MnO	0.20	0.24	0.21	0.24
MgO	7.70	5.67	7.52	5.66
CaO	11.91	10.06	11.65	9.79
Na2O	1.90	2.51	2.05	2.36
K2O	0.35	0.70	0.35	0.62
P2O5	0.13	0.21	0.12	0.16
LOI	0.11	-0.08	-0.13	-0.16
Total	100.12	99.78	99.67	98.31
Mg#	55.1	42.1	54.0	42.7
CIPW Norm wt%				
Qtz				2.14
Or	2.07	4.14	2.07	3.66
Ab	16.08	21.24	17.35	19.97
An	30.08	24.65	29.25	24.33
Lc				
Ne				
Cpx	23.13	19.95	22.84	19.36
Di	13.53	9.23	13.13	9.03
Hd	9.60	10.72	9.71	10.34
Opx	21.45	19.14	19.55	22.95
En	11.82	8.20	10.58	9.91
Fs	9.63	10.94	8.97	13.03
Ol	1.44	2.84	2.80	
Fo	0.76	1.15	1.45	
Fa	0.68	1.69	1.35	
Mt	1.80	2.24	1.84	2.18
Il	2.53	3.78	2.68	3.49
Ap	0.31	0.50	0.28	0.38
Trace Elements				
Ba	127	211	108	158
Rb	14	28	15	29
Nb	8	13	5	7
Sr	158	158	159	155
Zr	90	147	95	128
Y	30	44	31	37
La	10	18	9	14
Ce	22	37	21	27
Nd	14	23	14	17
Ni	88	48	86	39
Cr	378	151	334	77
V	306	361	312	374
Sc	51	46	34	49

REPRESENTATIVE REE ANALYSES

Sample No.	70533	70536	70582	70583	70623	70653	70661	70709
Rock Type	HMT	HMT	HMT	HMT	HMT	RN	MN	HMT
Main Group	I	I	I	I	3	3	3	3
Group	I	I	I	I	II	II	II	II

REE (ppm)

La	7.8	8.9	9.4	9.9	17.6	9.1	14.4	20.7
Ce	15.6	17.2	18.0	19.0	35.7	17.6	29.5	42.1
Pr	2.4	2.1	2.4	2.5	4.0	2.0	3.3	4.6
Nd	9.3	9.1	9.8	10.1	15.9	8.3	12.8	18.0
Sm	2.4	2.2	2.4	2.5	3.7	2.2	2.6	3.8
Eu	0.8	0.7	0.9	0.9	1.0	0.8	0.8	1.1
Gd	2.7	2.3	2.7	2.7	3.6	2.0	2.8	4.2
Dy	2.7	2.4	2.7	2.8	3.7	2.1	2.8	4.1
Er	1.7	1.4	1.8	1.7	2.3	1.3	1.8	2.3
Yb	1.6	1.3	1.5	1.4	1.9	1.2	1.4	2.0
Tb	-	-	-	-	-	-	-	-

Sample No.	70796	70801	71735	71883	71889	71894	71906	71947	71978
Rock Type	LS	HN	HMT	HMT	FGD	RN	HMT	HMT	HMT
Main Group	3	3	3	3	3	3	1	1	1
Group	II	II	III	II	II	IIa	I	Ia	II

REE (ppm)

La	35.8	13.8	14.5	19.2	19.6	6.0	8.3	11.8	17.2
Ce	77.0	28.2	26.1	38.6	40.2	14.6	19.7	26.2	35.9
Pr	8.2	3.3	2.9	4.2	4.5	2.0	2.2	3.1	4.0
Nd	32.7	12.4	11.4	17.0	18.1	11.4	10.8	13.0	16.1
Sm	6.6	2.5	2.6	3.8	4.0	3.6	3.1	3.5	3.4
Eu	1.8	0.7	0.8	0.9	1.0	1.2	0.9	1.0	0.9
Gd	7.0	2.6	2.6	3.8	3.9	4.8	2.6	2.9	3.2
Dy	6.5	2.6	3.0	3.8	4.1	5.5	2.5	2.9	3.3
Er	3.5	1.5	1.8	2.2	2.3	3.5	1.4	1.7	1.8
Yb	3.0	1.4	1.8	2.0	2.1	3.2	1.2	1.4	1.7
Tb	-	-	-	-	-	-	-	-	-

Abbreviations: HMT - High-Mg Tholeiite, HN - Homogeneous Norite, MN- Mottled Norite, RN - Rubbly Norite, FGD - Fine Grained Dyke, FRT - Fe-rich Tholeiite, ULM - Ultramafic Lamprophyre, AL - Alkaline Lamprophyre.

REPRESENTATIVE REE ANALYSES

Sample No.	71886	71904	71905	71934	71955	71873	71975	71979
Rock Type	FRT	FRT	FRT	FRT	FRT	FRT	FRT	FRT
Main Group	9	7	9	7	7	7	4	9

REE (ppm)

La	8.2	6.8	9.4	18.5	40.8	11.1	4.9	8.7
Ce	20.7	14.6	25.1	44.0	99.4	25.6	12.9	21.9
Pr	2.8	2.1	3.6	5.7	12.3	3.6	1.9	2.8
Nd	14.2	10.6	18.6	25.9	56.9	17.6	10.0	14.3
Sm	4.3	3.5	6.0	7.0	13.4	5.2	3.2	4.1
Eu	1.5	1.3	2.1	2.2	3.9	1.7	1.0	1.5
Gd	5.2	4.5	7.5	8.6	14.5	6.2	4.2	5.2
Dy	5.7	5.0	8.3	9.7	14.2	6.5	4.6	5.6
Er	3.5	3.0	4.9	6.1	8.2	4.0	2.9	3.2
Yb	3.0	2.6	4.1	5.3	6.6	3.3	2.7	2.7
Tb	-	-	-	-	-	-	-	-

Sample No.	71980	71760	71761	71888	71907	71928	71990	71991
Rock Type	FRT	AL	AL	AL	AL	AL	AL	AL
Main Group	7	8	6	6	6	6	6	8

REE (ppm)

La	16.0	116.0	70.4	80.3	81.8	59.8	91.5	30.3
Ce	38.5	265.0	162.0	181.0	184.0	134.0	199.0	64.8
Pr	5.0	32.7	20.5	21.5	21.7	16.0	23.7	8.0
Nd	23.2	138.0	85.5	88.9	85.6	67.0	96.4	33.2
Sm	6.1	23.6	15.4	15.7	14.8	11.8	16.5	6.5
Eu	1.9	6.8	4.5	5.0	4.5	3.4	4.7	1.9
Gd	7.4	16.4	11.5	12.0	11.2	8.4	12.0	5.8
Dy	8.0	9.9	7.5	7.5	6.9	5.4	8.1	4.3
Er	4.8	3.6	2.6	3.3	2.6	2.0	3.2	1.7
Yb	4.1	2.0	1.5	1.9	1.5	1.1	1.8	1.2
Tb	-	2.0	1.5	-	-	-	1.6	-

VESTFOLD HILLS - ANTARCTICA 1987/88

CAT. NO.	FIELD NO.	ROCK DESCRIPTION	LOCALITY	COORDS	PREPS
70506	1	High-Mg tholeiite dyke, centre	South of Platcha	LJ 961 921	
70507	2	High-Mg tholeiite dyke, chilled margin	South of Platcha	LJ 958 969	
70508	3	High-Mg tholeiite dyke, 2m from margin	South of Platcha	LJ 958 969	
70509	4	Crooked Lake Gneiss	South of Platcha	LJ 958 969	
70510	5	Crooked Lake Gneiss	South of Platcha	LJ 958 969	
70511	6	High-Mg tholeiite dyke, centre	South of Platcha	LJ 958 969	
70512	7	High-Mg tholeiite dyke, chilled margin	South of Platcha	LJ 958 969	
70513	8	Crooked Lake Gneiss	South of Platcha	LJ 958 969	
70514	9	Crooked Lake Gneiss	South of Platcha	LJ 958 969	
70515	10	High-Mg tholeiite dyke, centre	South of Platcha	LJ 964 972	
70516	11	High-Mg tholeiite dyke, centre	South of Platcha	LJ 947 972	
70517	12	High-Mg tholeiite dyke, chilled margin	South of Platcha	LJ 947 972	
70518	13	High-Mg tholeiite dyke, chilled margin	South of Platcha	LJ 947 972	
70519	14	High-Mg tholeiite dyke, 2m from margin	South of Platcha	LJ 947 972	
70520	15	Crooked Lake Gneiss	South of Platcha	LJ 947 972	
70521	16	Crooked Lake Gneiss	South of Platcha	LJ 947 972	
70522	17	Crooked Lake Gneiss	South of Platcha	LJ 947 972	
70523	18	High-Mg tholeiite dyke, chilled margin	South of Platcha	LJ 949 972	
70524	19	High-Mg tholeiite dyke, 2m from margin	South of Platcha	LJ 949 972	
70525	20	High-Mg tholeiite dyke, centre	South of Platcha	LJ 949 972	
70526	21	Crooked Lake Gneiss	South of Platcha	LJ 949 972	
70527	22	Crooked Lake Gneiss	South of Platcha	LJ 949 972	
70528	23	High-Mg tholeiite dyke, chilled margin	South of Platcha	LJ 952 973	
70529	24	High-Mg tholeiite dyke, 2m from margin	South of Platcha	LJ 952 973	
70530	25	High-Mg tholeiite dyke, centre	South of Platcha	LJ 952 973	
70531	26	Crooked Lake Gneiss	South of Platcha	LJ 952 973	
70532	27	Crooked Lake Gneiss	South of Platcha	LJ 952 973	
70533	28	High-Mg tholeiite dyke chilled margin	South of Platcha	LJ 955 971	PTS,POW,PGE
70534	29	Contact between dyke and gneiss	South of Platcha	LJ 955 971	POW
70535	30	High-Mg tholeiite dyke, 2m from margin	South of Platcha	LJ 955 971	PTS,POW
70536	31	High-Mg tholeiite dyke, 15m from margin	South of Platcha	LJ 955 971	POW,PTS
70537	32	High-Mg tholeiite dyke, 10m from margin	South of Platcha	LJ 955 971	POW,PTS
70538	33	High-Mg tholeiite dyke, chilled margin	South of Platcha	LJ 955 971	PTS
70539	34	Crooked Lake Gneiss	South of Platcha	LJ 955 971	
70540	35	High-Mg tholeiite dyke, chilled margin	South of Platcha	LJ 957 971	
70541	36	Gneiss in contact with dyke	South of Platcha	LJ 957 971	
70542	37	High-Mg tholeiite dyke, 2m from margin	South of Platcha	LJ 957 971	
70543	38	High-Mg tholeiite dyke, 10m from margin	South of Platcha	LJ 957 971	
70544	39	High-Mg tholeiite dyke, centre	South of Platcha	LJ 957 971	
70545	40	High-Mg tholeiite dyke, 2m from margin	South of Platcha	LJ 957 971	
70546	41	Crooked Lake Gneiss	South of Platcha	LJ 957 971	
70547	42	Crooked Lake Gneiss	South of Platcha	LJ 957 971	
70548	43	High-Mg tholeiite dyke, chilled margin	South of Platcha	LJ 964 974	PTS,POW
70549	44	Crooked Lake Gneiss	South of Platcha	LJ 964 974	
70550	45	Crooked Lake Gneiss	South of Platcha	LJ 964 974	
70551	46	High-Mg tholeiite dyke, 10m from margin	South of Platcha	LJ 964 974	POW
70552	47	High-Mg tholeiite dyke, centre	South of Platcha	LJ 964 974	POW
70553	48	High-Mg tholeiite dyke, centre	South of Platcha	LJ 953 972	POW
70554	49	Crooked Lake Gneiss	South of Platcha	LJ 952 972	
70555	50	High-Mg tholeiite dyke, chilled margin	South of Platcha	LJ 952 972	
70556	51	High-Mg tholeiite dyke, 5m from margin	South of Platcha	LJ 952 972	
70557	52	High-Mg tholeiite dyke, 1m from margin	South of Platcha	LJ 949 972	
70558	53	High-Mg tholeiite dyke, 2m from margin	South of Platcha	LJ 947 972	
70559	54	Crooked Lake Gneiss	South of Platcha	LJ 944 972	
70560	55	High-Mg tholeiite dyke, chilled margin	South of Platcha	LJ 944 972	
70561	56	High-Mg tholeiite dyke, 10m from margin	South of Platcha	LJ 944 972	
70562	57	High-Mg tholeiite dyke, margin	South of Platcha	LJ 943 972	
70563	58	High-Mg tholeiite dyke, 10m from margin	South of Platcha	LJ 943 972	

VESTFOLD HILLS - ANTARCTICA 1987/88

CAT. NO.	FIELD NO.	ROCK DESCRIPTION	LOCALITY	COORDS	PREPS
70564	59	High-Mg tholeiite dyke, centre	South of Platcha	LJ 943 972	
70565	60	High-Mg tholeiite dyke, margin	South of Platcha	LJ 943 972	
70566	61	Crooked Lake Gneiss	South of Platcha	LJ 941 972	
70567	62	Dyke (vein) in gneiss	South of Platcha	LJ 941 972	
70568	63	High-Mg tholeiite dyke, chilled margin	South of Platcha	LJ 941 972	PTS,POW
70569	64	High-Mg tholeiite dyke, 7m from margin	South of Platcha	LJ 941 972	POW
70570	65	High-Mg tholeiite dyke, centre	South of Platcha	LJ 941 972	POW
70571	66	Crooked Lake Gneiss	South of Platcha	LJ 941 972	
70572	67	Crooked Lake Gneiss	South of Platcha	LJ 928 972	
70573	68	High-Mg tholeiite dyke, 2m from margin	South of Platcha	LJ 928 972	
70574	69	High-Mg tholeiite dyke, 15m from margin	South of Platcha	LJ 928 972	
70575	70	High-Mg tholeiite dyke, 10m from margin	South of Platcha	LJ 928 972	
70576	71	High-Mg tholeiite dyke, chilled margin	South of Platcha	LJ 928 972	
70577	72	Crooked Lake Gneiss	South of Platcha	LJ 928 972	
70578	73	Crooked Lake Gneiss	South of Platcha	LJ 928 972	
70579	74	Crooked Lake Gneiss	South of Platcha	LJ 925 973	
70580	75	Crooked Lake Gneiss	South of Platcha	LJ 925 973	
70581	76	High-Mg tholeiite dyke, chilled margin	South of Platcha	LJ 925 973	PTS,POW
70582	77	High-Mg tholeiite dyke, 2m from margin	South of Platcha	LJ 925 973	POW
70583	78	High-Mg tholeiite dyke, centre	South of Platcha	LJ 925 973	POW
70584	79	High-Mg tholeiite dyke, 15m from margin	South of Platcha	LJ 925 973	POW
70585	80	Crooked Lake Gneiss	South of Platcha	LJ 918 973	
70586	81	Mixing ('Schlieren') gneiss/dyke	South of Platcha	LJ 918 973	
70587	82	High-Mg tholeiite dyke, chilled margin	South of Platcha	LJ 918 973	
70588	83	High-Mg tholeiite dyke, 10m from margin	South of Platcha	LJ 918 973	
70589	84	High-Mg tholeiite dyke, centre	South of Platcha	LJ 918 973	
70590	85	High-Mg tholeiite dyke, centre	SW of Lake Vereteno	LJ 918 973	
70591	86	High-Mg tholeiite dyke, 15m from margin	SW of Lake Vereteno	LJ 918 973	
70592	87	High-Mg tholeiite dyke, 2m from margin	SW of Lake Vereteno	LJ 918 973	
70593	88	High-Mg tholeiite dyke, chilled margin	SW of Lake Vereteno	LJ 918 973	
70594	89	Crooked Lake Gneiss	SW of Lake Vereteno	LJ 918 973	
70595	90	Crooked Lake Gneiss	SW of Lake Vereteno	LJ 916 973	
70596	91	Mixing of gneiss and tholeiite	SW of Lake Vereteno	LJ 916 973	
70597	92	Crooked Lake Gneiss	SW of Lake Vereteno	LJ 916 973	
70598	93	High-Mg tholeiite dyke, chilled margin	SW of Lake Vereteno	LJ 916 973	PTS,POW
70599	94	High-Mg tholeiite dyke, 2m from margin	SW of Lake Vereteno	LJ 916 973	POW
70600	95	High-Mg tholeiite dyke, centre	SW of Lake Vereteno	LJ 916 973	PTS,POW
70601	96	High-Mg tholeiite dyke, 5m from margin	SW of Lake Vereteno	LJ 916 973	POW
70602	97	Crooked Lake Gneiss	SW of Lake Vereteno	LJ 912 973	
70603	98	Crooked Lake Gneiss	SW of Lake Vereteno	LJ 912 973	
70604	99	High-Mg tholeiite dyke chilled margin	SW of Lake Vereteno	LJ 912 973	
70605	100	High-Mg tholeiite dyke, 2m from margin	SW of Lake Vereteno	LJ 912 973	
70606	101	High-Mg tholeiite dyke, 10m from margin	SW of Lake Vereteno	LJ 912 973	
70607	102	Mossel Gneiss	Long Peninsula	LK 905 032	
70608	103	Mossel Gneiss	Long Peninsula	LK 905 032	
70609	104	Mossel Gneiss; showing assimilation	Long Peninsula	LK 905 032	
70610	105	Mossel Gneiss; showing assimilation	Long Peninsula	LK 905 032	
70611	106	Mossel Gneiss; showing assimilation	Long Peninsula	LK 905 032	PTS
70612	107	High-Mg tholeiite dyke chilled margin	Long Peninsula	LK 905 032	PTS,POW,PGE
70613	108	High-Mg tholeiite dyke, centre	Long Peninsula	LK 905 032	POW
70614	109	High-Mg tholeiite dyke, 1m from margin	Long Peninsula	LK 905 032	POW
70615	110	Mossel Gneiss	Long Peninsula	LK 905 032	
70616	111	Mossel Gneiss	Long Peninsula	LK 905 032	
70617	112	Mossel Gneiss	Long Peninsula	LK 905 032	
70618	113	Late stage vein in Homogeneous Norite	Long Peninsula	LK 909 041	
70619	114	Rhythmic layering	Long Peninsula	LK 931 055	
70620	115	Norite (layered)	Long Peninsula	LK 911 044	
70621	116	Spinel Harzburgite xenolith	Long Peninsula	LK 909 045	PTS

VESTFOLD HILLS - ANTARCTICA 1987/88

CAT. NO.	FIELD NO.	ROCK DESCRIPTION	LOCALITY	COORDS	PREPS
70622	117	Enstatite nodule	Long Peninsula	LK 932 000	
70623	118	Orthopyroxene-phyric tholeiitic dyke	Long Peninsula	LK 909 039	PTS,POW
70624	119	Norite	Long Peninsula	LK 909 039	
70625	120	Norite	Long Peninsula	LK 909 039	
70626	121	Rubbly Norite + xenolith	Long Peninsula	LK 909 040	
70627	122	Rubbly Norite + sulphides	Long Peninsula	LK 909 040	
70628	123	Rubbly Norite + sulphides	Long Peninsula	LK 909 040	
70629	124	Rubbly Norite	Long Peninsula	LK 909 041	
70630	125	Mottled Norite	Long Peninsula	LK 909 041	
70631	126	Mottled Norite	Long Peninsula	LK 909 042	
70632	127	Rubbly Norite + enstatite nodule	Long Peninsula	LK 909 042	
70633	128	Mossel gneiss	NE of Ekho Lake	LJ 908 972	
70634	129	High-Mg tholeiite dyke, chilled margin	NE of Ekho Lake	LJ 908 972	PTS,POW
70635	130	High-Mg tholeiite dyke, 2m from margin	NE of Ekho Lake	LJ 908 972	
70636	131	High-Mg tholeiite dyke, centre	NE of Ekho Lake	LJ 908 972	POW
70637	132	High-Mg tholeiite dyke, 10m from margin	NE of Ekho Lake	LJ 908 972	POW
70638	133	Crooked Lake Gneiss	NE of Ekho Lake	LJ 908 972	
70639	134	Garnet-bearing gneiss Chelnok Supracrustals	NE of Ekho Lake	LJ 899 967	
70640	135	High-Mg tholeiite dyke, chilled margin	NE of Ekho Lake	LJ 899 967	
70641	136	High-Mg tholeiite dyke, 2m from margin	NE of Ekho Lake	LJ 899 967	
70642	137	High-Mg tholeiite dyke, 10m from margin	NE of Ekho Lake	LJ 899 967	
70643	138	High-Mg tholeiite dyke, chilled margin	NE of Ekho Lake	LJ 899 967	
70644	139	High-Mg tholeiite dyke, 2m from margin	NE of Ekho Lake	LJ 897 967	
70645	140	High-Mg tholeiite dyke, 10m from margin	NE of Ekho Lake	LJ 897 967	
70646	141	High-Mg tholeiite dyke, centre	NE of Ekho Lake	LJ 897 967	
70647	142	High-Mg tholeiite dyke	NE of Ekho Lake	LJ 894 966	
70648	143	High-Mg tholeiite dyke, chilled margin	NE of Ekho Lake	LJ 894 966	
70649	144	High-Mg tholeiite dyke, 5m from margin	NE of Ekho Lake	LJ 894 966	
70650	145	High-Mg tholeiite dyke, centre	NE of Ekho Lake	LJ 894 966	
70651	146	Rubbly Norite + xenolith + sulphides	Tanaya Bay	LK 892 031	
70652	147	Rubbly Norite + sulphides	Tanaya Bay	LK 892 031	
70653	148	Rubbly Norite + sulphides	"Black" Island	LK 892 038	PTS,POW,PGE
70654	149	Rubbly Norite + xenolith + sulphides	"Black" Island	LK 892 038	
70655	150	Rubbly Norite + xenolith + sulphides	"Black" Island	LK 892 038	
70656	151	Rubbly Norite + xenolith + sulphides	"Black" Island	LK 892 038	
70657	152	Rubbly Norite + xenolith + sulphides	"Black" Island	LK 892 038	
70658	153	Rubbly Norite + xenolith + sulphides	"Black" Island	LK 892 038	
70659	154	Rubbly Norite + xenolith + sulphides	"Black" Island	LK 892 038	
70660	155	Rubbly Norite + xenolith + sulphides	"Black" Island	LK 892 038	
70661	156	Mottled Norite	"Black" Island	LK 892 038	PTS,POW,PGE
70662	157	Xenolith in Rubbly Norite	"Black" Island	LK 892 038	
70663	158	Mottled Norite	"Black" Island	LK 892 038	
70664	159	Tholeiite	"Black" Island	LK 892 038	
70665	160	Homogeneous Norite (layered)	"Black" Island	LK 892 038	
70666	161	Homogeneous Norite	"Black" Island	LK 892 038	
70667	162	Homogeneous Norite	"Black" Island	LK 892 038	PTS,POW,PGE
70668	163	Homogeneous Norite + late stage	"Black" Island	LK 892 038	
70669	164	Sapphirine xenolith in norite	"Black" Island	LK 892 038	
70670	165	Mottled Norite	Tanaya Bay	LK 912 042	
70671	166	Homogeneous Norite	Tanaya Bay	LK 912 042	
70672	167	Plagioclase xenolith	Tanaya Bay	LK 912 042	
70673	168	Mottled Norite	Tanaya Bay	LK 912 042	
70674	169	Mottled Norite	Tanaya Bay	LK 912 042	
70675	170	Mottled Norite	Tanaya Bay	LK 912 042	
70676	171	Homogeneous Norite	Tanaya Bay	LK 912 042	
70677	172	Opx-phyric tholeiitic dyke	Tanaya Bay	LK 908 039	PTS
70678	173	Homogeneous Norite	Tanaya Bay	LK 888 031	
70679	174	Homogeneous Norite	Tanaya Bay	LK 885 030	

VESTFOLD HILLS - ANTARCTICA 1987/88

CAT. NO.	FIELD NO.	ROCK DESCRIPTION	LOCALITY	COORDS	PREPS
70680	175	Gabbro + sulphides	Long Peninsula	LK 898 016	
70681	176	Gabbro + sulphides	Long Peninsula	LK 898 016	
70682	177	Rubbly Norite	Tanaya Bay	LK 887 024	PTS, POW, PGE
70683	178	Rubbly Norite	Tanaya Bay	LK 887 024	
70684	179	Rubbly Norite	Tanaya Bay	LK 889 029	
70685	180	Rubbly Norite	Tanaya Bay	LK 889 029	
70686	181	Sapphirine xenolith	Tanaya Bay	LK 889 029	
70687	182	Mottled Norite	Tanaya Bay	LK 889 029	
70688	183	Homogeneous Norite	Tanaya Bay	LK 885 028	PTS, POW
70689	184	Rubbly Norite	Tanaya Bay	LK 885 025	
70690	185	Rubbly Norite	Tanaya Bay	LK 912 042	
70691	186	Homogeneous Norite	Tanaya Bay	LK 911 043	
70692	187	Homogeneous Norite	Tanaya Bay	LK 911 043	
70693	188	Tholeiite	Tanaya Bay	LK 911 043	
70694	189	Homogeneous Norite	Tanaya Bay	LK 907 044	
70695	190	Homogeneous Norite	Tanaya Bay	LK 898 043	
70696	191	Homogeneous Norite	Tanaya Bay	LK 895 045	
70697	192	Homogeneous Norite	Tanaya Bay	LK 901 044	
70698	193	Homogeneous Norite	Tanaya Bay	LK 903 045	
70699	194	Mixing norite/gneiss	Tanaya Bay	LK 904 045	
70700	195	Pegmatitic xenolith	Tanaya Bay	LK 908 038	PTS
70701	196	Opx-phyric tholeiitic dyke	Tanaya Bay	LK 907 036	PTS, POW, PGE
70702	197	Opx-phyric tholeiite chilled margin	Tanaya Bay	LK 907 034	PTS
70703	198	Homogeneous Norite	East of Rybnaya Bay	LK 918 051	PTS, POW
70704	199	Mottled Norite	East of Rybnaya Bay	LK 918 051	
70705	200	Homogeneous Norite	East of Rybnaya Bay	LK 918 051	
70706	201	Rubbly Norite	East of Rybnaya Bay	LK 918 051	POW, PGE
70707	202	Xenolith in Rubbly Norite	East of Rybnaya Bay	LK 918 051	PTS
70708	203	Contact between Rub.- and Homog. Norite	East of Rybnaya Bay	LK 918 051	PTS
70709	204	Opx-phyric tholeiitic	East of Rybnaya Bay	LK 918 051	PTS, POW, PGE
70710	205	Homogeneous Norite	East of Rybnaya Bay	LK 921 050	
70711	206	Pyroxenite	East of Rybnaya Bay	LK 918 051	
70712	207	Homogeneous Norite	East of Rybnaya Bay	LK 920 050	
70713	208	Homogeneous Norite	East of Rybnaya Bay	LK 924 051	
70714	209	Mottled Norite	East of Rybnaya Bay	LK 925 052	
70715	210	Tryne Metavolcanics	East of Rybnaya Bay	LK 925 052	
70716	211	Tryne Metavolcanics	East of Rybnaya Bay	LK 925 052	PTS
70717	212	Homogeneous Norite	East of Rybnaya Bay	LK 926 053	
70718	213	Rubbly Norite	East of Rybnaya Bay	LK 926 053	
70719	214	Homogeneous Norite	East of Rybnaya Bay	LK 926 053	
70720	215	Homogeneous Norite	East of Rybnaya Bay	LK 931 055	
70721	216	Homogeneous Norite (+ layering)	East of Rybnaya Bay	LK 932 057	
70722	217	Homogeneous Norite	East of Rybnaya Bay	LK 932 057	
70723	218	Homogeneous Norite	East of Rybnaya Bay	LK 932 057	
70724	219	Homogeneous Norite	East of Rybnaya Bay	LK 932 057	
70725	220	Homogeneous Norite	East of Rybnaya Bay	LK 932 057	
70726	221	Homogeneous Norite	East of Rybnaya Bay	LK 932 057	
70727	222	Homogeneous Norite (+ layering)	East of Rybnaya Bay	LK 932 057	
70728	223	Homogeneous Norite	East of Rybnaya Bay	LK 932 057	
70729	224	Homogeneous Norite	East of Rybnaya Bay	LK 932 057	
70730	225	Rubbly Norite	East of Rybnaya Bay	LK 932 057	PTS
70731	226	Homogeneous Norite (+ layering)	East of Rybnaya Bay	LK 932 057	
70732	227	Mafic gneiss	East of Rybnaya Bay	LK 932 055	
70733	228	Tholeiitic dyke + chilled margin	East of Rybnaya Bay	LK 932 057	
70734	229	Tholeiitic dyke centre	East of Rybnaya Bay	LK 932 057	
70735	230	Mylonitized Homogeneous Norite	East of Rybnaya Bay	LK 932 057	
70736	231	Homogeneous Norite / late stage	East of Rybnaya Bay	LK 932 057	PTS
70737	232	Homogeneous Norite / late stage	East of Rybnaya Bay	LK 932 057	PTS

VESTFOLD HILLS - ANTARCTICA 1987/88

CAT. NO.	FIELD NO.	ROCK DESCRIPTION	LOCALITY	COORDS	PREPS
70738	233	Homogeneous Norite	East of Rybnaya Bay	LK 932 057	
70739	234	Actinolitic Homogeneous Norite	East of Rybnaya Bay	LK 932 057	PTS
70740	235	Homogeneous Norite (+ layering)	East of Rybnaya Bay	LK 932 057	
70741	236	Tholeiite (cryptocrystalline)	East of Rybnaya Bay	LK 928 056	PTS
70742	237	Tholeiite (cryptocrystalline)	East of Rybnaya Bay	LK 928 056	PTS
70743	238	Tholeiite (cryptocrystalline)	East of Rybnaya Bay	LK 929 057	PTS
70744	239	Tholeiite (cryptocrystalline)	East of Rybnaya Bay	LK 929 057	PTS
70745	240	Tholeiite (cryptocrystalline)	East of Rybnaya Bay	LK 930 055	PTS
70746	241	Tholeiite (cryptocrystalline)	East of Rybnaya Bay	LK 930 055	PTS
70747	242	Tholeiite (cryptocrystalline)	East of Rybnaya Bay	LK 930 055	PTS
70748	243	Mylonite	East of Rybnaya Bay	LK 932 057	
70749	244	Homogeneous Norite (+ layering)	Barrier Island	LK 932 070	
70750	245	Late stage segregation	Barrier Island	LK 932 071	
70751	246	Late stage segregation	Barrier Island	LK 932 071	
70752	247	Late stage segregation	Barrier Island	LK 931 071	PTS
70753	248	Homogeneous Norite	Barrier Island	LK 932 070	
70754	249	Homogeneous Norite (+ layering)	Barrier Island	LK 932 069	
70755	250	Mottled Norite	Barrier Island	LK 932 066	PTS,POW
70756	251	Grey vein in norite	Barrier Island	LK 932 066	
70757	252	Rubbly Norite	Barrier Island	LK 932 066	PTS
70758	253	Rubbly Norite	Barrier Island	LK 932 066	PTS,POW,PGE
70759	254	Homogeneous Norite	Barrier Island	LK 932 066	
70760	255	Homogeneous Norite	Barrier Island	LK 932 066	
70761	256	Homogeneous gneiss	East of Rybnaya Bay	LK 932 057	
70762	257	Gneiss - norite mixing	East of Rybnaya Bay	LK 932 057	
70763	258	Norite close to mixing zone	East of Rybnaya Bay	LK 932 057	
70764	259	Opx-phyric tholeiite (in shear zone)	East of Rybnaya Bay	LK 932 057	
70765	260	Opx-phyric tholeiite (middle of dyke)	East of Rybnaya Bay	LK 932 057	
70766	261	Rubbly Norite	East of Rybnaya Bay	LK 932 057	PTS,POW,PGE
70767	262	Amphibolite (surface coloured by alteration)	East of Rybnaya Bay	LK 932 057	PTS
70768	263	Norite (Rubbly-zone)	East of Rybnaya Bay	LK 932 057	
70769	264	Contact tholeiitic dyke/norite	East of Rybnaya Bay	LK 932 057	PTS
70770	265	Tholeiitic dyke	East of Rybnaya Bay	LK 932 057	PTS
70771	266	Tholeiitic dyke, centre	East of Rybnaya Bay	LK 932 057	PTS,POW
70772	267	Tholeiitic dyke (margin to gneiss)	East of Rybnaya Bay	LK 932 057	PTS
70773	268	Opx-phyric tholeiite (chilled margin)	East of Rybnaya Bay	LK 932 057	
70774	269	Opx-phyric tholeiite (middle)	East of Rybnaya Bay	LK 932 057	
70775	270	High-Mg tholeiite	East of Rybnaya Bay	LK 932 057	PTS
70776	271	High-Mg tholeiite	East of Rybnaya Bay	LK 932 057	PTS
70777	272	High-Mg tholeiite	East of Rybnaya Bay	LK 932 057	PTS
70778	273	Xenolith in pyroxenite	East of Rybnaya Bay	LK 932 057	
70779	274	Tryne Metavolcanics	East of Rybnaya Bay	LK 931 054	
70780	275	Tryne Metavolcanics	East of Rybnaya Bay	LK 931 054	
70781	276	Tryne Metavolcanics	East of Rybnaya Bay	LK 928 057	
70782	277	Alkaline Lamprophyre	West of Snezhnyy Bay	LK 936 058	
70783	278	Rubbly Norite	West of Snezhnyy Bay	LK 936 058	PTS,POW,PGE
70784	279	Rubbly Norite	West of Snezhnyy Bay	LK 936 058	PTS
70785	280	Amphibolite (surface coloured by alteration)	West of Snezhnyy Bay	LK 936 058	
70786	281	Rubbly Norite	West of Snezhnyy Bay	LK 936 058	
70787	282	Rubbly Norite	West of Snezhnyy Bay	LK 936 058	
70788	283	Mottled Norite	West of Snezhnyy Bay	LK 936 058	PTS,POW
70789	284	Flacky gneiss	West of Snezhnyy Bay	LK 936 058	
70790	285	Rubbly Norite	West of Snezhnyy Bay	LK 936 058	PTS
70791	286	Homogeneous Norite (layering)	West of Snezhnyy Bay	LK 944 059	
70792	287	Rubbly Norite	West of Snezhnyy Bay	LK 941 065	
70793	288	Homogeneous Norite (layering)	Bandits Island	LK 926 075	PTS
70794	289	Late stage segregation in Homog. Norite	Bandits Island	LK 926 075	
70795	290	Late stage segregation in Homog. Norite	Bandits Island	LK 926 075	

VESTFOLD HILLS - ANTARCTICA 1987/88

CAT. NO.	FIELD NO.	ROCK DESCRIPTION	LOCALITY	COORDS	PREPS
70796	291	Late stage segregation in Homog. Norite	Bandits Island	LK 926 075	PTS,POW
70797	292	Homogeneous Norite (layering)	Bandits Island	LK 926 075	PTS
70798	293	Homogeneous Norite (layering)	Bandits Island	LK 926 075	PTS
70799	294	Homogeneous Norite (layering)	Bandits Island	LK 926 075	
70800	295	Homogeneous Norite (layering)	Bandits Island	LK 926 075	
70801	296	Homogeneous Norite (layering)	Bandits Island	LK 926 075	PTS,POW
70802	297	Homogeneous Norite (layering)	Bandits Island	LK 926 075	
70803	298	Homogeneous Norite/layer intersection	Bandits Island	LK 926 075	
70804	299	Homogeneous Norite/layer intersection	Bandits Island	LK 926 075	
70805	300	Orthopyroxene-phyrlic tholeiite	Bandits Island	LK 923 078	
70806	301	Felsic material in dyke	Bandits Island	LK 926 075	
70807	302	Felsic material in dyke	Bandits Island	LK 926 075	
70808	303	Tholeiite in contact with felsic norite	Bandits Island	LK 926 075	
70809	304	Orthopyroxene-rich tholeiite	Bandits Island	LK 926 075	
70810	305	Orthopyroxene-rich tholeiite	Bandits Island	LK 924 077	
70811	306	Tension gashes in norite	Bandits Island	LK 926 075	
70812	307	Homogeneous Norite + rhythmic layering	Bandits Island	LK 926 075	
70813	308	Norite with crosscutting dyke	East of Rybanaya Bay	LK 932 057	
70814	309	Homogeneous Norite	Tryne Islands		PTS
70815	310	Calcsilicate	Elephant Is., Rauer Gp		PTS
70816	311	Garnet-bearing granulite	Elephant Is., Rauer Gp		
70817	312	Deformed dyke	Elephant Is., Rauer Gp		
70818	313	Metapelite	Elephant Is., Rauer Gp		
70819	314	Mafic granulite	Elephant Is., Rauer Gp		
70820	315	Alkaline dyke	Dyke Island		PTS
70821	316	Alkaline dyke	Hopp Island		
70822	317	Calcsilicate	Hopp Island		
70823	318	Mylonite in metasediment	Hopp Island		
70824	319	Epidote (float)	Hopp Island		
70825	88-250	Alkaline dyke (30 cm thick)	Flag Island		
70826	88-251	Alkaline dyke	Flag Island		
70827	88-252	Alkaline dyke	Flag Island		
70828	88-282	Alkaline dyke	Flag Island		

Abbreviations: POW - rock powder for whole rock geochemistry; PTS - polished thin section; PGE - analyzed for platinum group elements.

VESTFOLD HILLS - ANTARCTICA 1988/89

CAT. NO.	FIELD NO.	ROCK DESCRIPTION	LOCALITY	COORDS	PREPS
71729	320	Dolerite, chilled margin + centre	Lichen Valley	LK 950 008	POW
71730	321	Dolerite	Lichen Valley	LK 950 008	POW
71731	322	Tholeiitic dyke	Lichen Valley	LK 950 008	POW
71732	323	Opx-phyric tholeiite	Lichen Valley	LK 950 008	POW
71733	324	Opx-phyric tholeiite	Lichen Valley	LK 950 008	POW
71734	325	Opx-phyric tholeiite	Lichen Valley	LK 950 008	POW
71735	326	Tholeiitic dyke	Lichen Valley	LK 950 008	POW
71736	327	Alkaline Lamprophyre	Lichen Valley	LK 950 008	POW
71737	328	Tholeiite	Lichen Valley	LK 950 008	
71738	329	Tholeiitic dyke	Lichen Valley	LK 950 008	POW
71739	330	Opx-phyric tholeiite	Lichen Valley	LK 950 008	POW
71740	331	Alkaline Lamprophyre	Lichen Valley	LK 950 008	POW
71741	332	Lamprophyre	Lichen Valley	LK 950 008	
71742	333	Tholeiite	Lichen Valley	LK 950 008	POW
71743	334	Alkaline Lamprophyre	Lichen Valley	LK 950 008	
71744	335	Opx-phyric tholeiite	Lichen Valley	LK 950 008	
71745	336	Calcsilicate	Lichen Valley	LK 950 008	
71746	337	Dolerite	Lichen Valley	LK 950 008	POW
71747	338	Dolerite	Lichen Valley	LK 950 008	POW
71748	339	Dolerite	Lichen Valley	LK 950 008	POW
71749	340	Opx-phyric tholeiite	Lichen Valley	LK 950 008	POW
71750	341	Alkaline Lamprophyre	Lichen Valley	LK 950 008	POW,PTS
71751	342	Opx-phyric tholeiite	Lichen Valley	LK 950 008	POW,PTS
71752	343	Alkaline Lamprophyre	Lichen Valley	LK 950 008	POW
71753	344	Alkaline Lamprophyre	Lichen Valley	LK 950 008	POW
71754	345	Dolerite	Lichen Valley	LK 950 008	
71755	346	Opx-phyric dolerite	Lichen Valley	LK 950 008	POW
71756	347	Opx-phyric tholeiite	Lichen Valley	LK 950 008	
71757	348	Dolerite	Lichen Valley	LK 950 008	POW
71758	349	Dolerite	Lichen Valley	LK 950 008	POW
71759	350	Dolerite	Lichen Valley	LK 950 008	POW
71760	351	Alkaline Lamprophyre	Lichen Valley	LK 950 008	POW
71761	352	Alkaline Lamprophyre	Lichen Valley	LK 950 008	POW
71762	353	Dolerite	Lichen Valley	LK 950 008	
71763	354	Deformed dyke	Lichen Valley	LK 950 008	
71764	355	Dolerite	Lichen Valley	LK 950 008	POW
71765	356	Alkaline Lamprophyre	Lichen Valley	LK 950 008	PTS
71766	357	Lamprophyre with xenoliths	Lichen Valley	LK 950 008	7 PTS
71767	358	Dolerite	Lichen Valley	LK 950 008	POW
71768	359	Alkaline Lamprophyre	Lichen Valley	LK 950 008	POW
71769	360	Dolerite	Lichen Valley	LK 950 008	POW
71770	361	Olivine-phyric dolerite	Lichen Valley	LK 950 008	POW
71771	362	Tholeiite - 20 kg for dating	Lichen Valley	LK 950 008	
71772	363	Calcsilicate	Lichen Valley	LK 950 008	
71773	364	Tholeiite	Lichen Valley	LK 950 008	POW
71774	365	Opx-phyric tholeiite	Lichen Valley	LK 950 008	
71775	366	Opx-phyric dolerite	Lichen Valley	LK 950 008	
71776	367	Opx-phyric dolerite	Lichen Valley	LK 950 008	POW
71777	368	Olivine-phyric dolerite	Lichen Valley	LK 950 008	
71778	369	Tholeiite	Lichen Valley	LK 950 008	
71779	370	Dolerite	Lichen Valley	LK 950 008	POW
71780	371	Olivine-phyric dolerite	Lichen Valley	LK 950 008	POW
71781	372	Olivine-phyric dolerite	Lichen Valley	LK 950 008	POW
71782	373	Dolerite	Lichen Valley	LK 950 008	POW
71783	374	Dolerite	Lichen Valley	LK 950 008	POW
71784	375	Dolerite	Lichen Valley	LK 950 008	POW
71785	376	Dolerite	Lichen Valley	LK 950 008	
71786	377	Dolerite	Lichen Valley	LK 950 008	

VESTFOLD HILLS - ANTARCTICA 1988/89

CAT. NO.	FIELD NO.	ROCK DESCRIPTION	LOCALITY	COORDS	PREPS
71787	378	Alkaline Lamprophyre	Lichen Valley	LK 950 008	POW
71788	379	Alkaline Lamprophyre	Lichen Valley	LK 950 008	POW
71789	380	Dolerite	Lichen Valley	LK 950 008	POW
71790	381	Dolerite	Lichen Valley	LK 950 008	POW
71791	382	Alkaline Lamprophyre	Lichen Valley	LK 950 008	POW
71792	383	Garnet-sapphirine-quartz gneiss	Lichen Valley	LK 950 008	
71793	384	Alkaline Lamprophyre	Lichen Valley	LK 950 008	POW
71794	385	Dolerite	Lichen Valley	LK 950 008	POW
71795	386	Alkaline Lamprophyre	Lichen Valley	LK 950 008	
71796	387	Opx-phyric tholeiite - 20 kg for dating	Lichen Valley	LK 950 008	
71797	388	Tholeiite - 20 kg for dating	Lichen Valley	LK 950 008	
71798	389	Opx-phyric tholeiite - 20 kg for dating	Lichen Valley	LK 950 008	
71799	390	Alkaline Lamprophyre - 20 kg for dating	Lichen Valley	LK 950 008	
71800	391	Dolerite - 20 kg for dating	Lichen Valley	LK 950 008	
71801	392	Chilled margin-contact bet. 2 dykes	Partizan Island	LJ 845 975	
71802	393	Tholeiite	Partizan Island	LJ 845 975	POW
71803	394	Dolerite	Partizan Island	LJ 845 975	POW
71804	395	Opx-phyric dolerite	Partizan Island	LJ 845 975	POW
71805	396	Tholeiite	Partizan Island	LJ 845 975	POW
71806	397	Tholeiite	Partizan Island	LJ 845 975	
71807	398	Tholeiite	Partizan Island	LJ 845 975	POW
71808	399	Olivine-phyric tholeiite	Partizan Island	LJ 845 975	POW
71809	400	Opx-phyric tholeiite	Partizan Island	LJ 845 975	POW
71810	401	Dolerite	Partizan Island	LJ 845 975	POW
71811	402	Opx-phyric tholeiite	Partizan Island	LJ 845 975	POW
71812	403	Opx-phyric tholeiite	Partizan Island	LJ 845 975	
71813	404	Dolerite	Partizan Island	LJ 845 975	
71814	405	Alkaline Lamprophyre	Lake Zvezda	LJ 845 975	POW
71815	406	Dolerite	Lake Zvezda	LJ 845 975	POW
71816	407	Opx-phyric dolerite	Lake Zvezda	LJ 845 975	POW
71817	408	Olivine-phyric dolerite	Lake Zvezda	LJ 845 975	POW
71818	409	Dolerite	Lake Zvezda	LJ 845 975	POW
71819	410	Dolerite	Lake Zvezda	LJ 845 975	POW
71820	411	Dolerite	Lake Zvezda	LJ 845 975	POW
71821	412	Opx-phyric tholeiite	Lake Zvezda	LJ 845 975	POW
71822	413	Dolerite	Lake Zvezda	LJ 845 975	POW
71823	414	Dolerite	Lake Zvezda	LJ 845 975	POW
71824	415	Dolerite	Lake Zvezda	LJ 845 975	POW
71825	416	Alkaline Lamprophyre	Lake Zvezda	LJ 845 975	
71826	417	6 samples fr. dyke+crust. xenolith	Lake Zvezda	LJ 845 975	
71827	418a	Brecciated dolerite	Crooked Lake	LJ 970 880	
71828	418b	Brecciated dolerite	Crooked Lake	LJ 970 880	
71829	419	Tholeiite	Crooked Lake	LJ 970 880	POW
71830	420	Olivine-phyric tholeiite	Crooked Lake	LJ 970 880	POW
71831	421	Tholeiite	Crooked Lake	LJ 970 880	POW
71832	422	Dolerite	Crooked Lake	LJ 970 880	POW
71833	423	Dolerite	Crooked Lake	LJ 970 880	POW
71834	424	Opx-phyric tholeiite	Crooked Lake	LJ 970 880	POW
71835	425	Dolerite	Tyne Crossing	LJ 900 997	POW
71836	426	Opx-phyric tholeiite	East of Ellis Rapids	LJ 895 885	POW
71837	427	Leucocratic "dolerite"	East of Ellis Rapids	LJ 895 885	POW
71838	428	Olivine-phyric tholeiite	East of Ellis Rapids	LJ 895 885	POW
71839	429	Tholeiite	East of Ellis Rapids	LJ 895 885	POW
71840	430	Tholeiite	East of Ellis Rapids	LJ 895 885	POW
71841	431	Dolerite, sulphide bearing	East of Ellis Rapids	LJ 895 885	POW
71842	432	Tholeiite	East of Ellis Rapids	LJ 895 885	POW
71843	433	Dolerite	East of Ellis Rapids	LJ 895 885	
71844	434	Opx-phyric tholeiite	East of Ellis Rapids	LJ 895 885	POW

VESTFOLD HILLS - ANTARCTICA 1988/89

CAT. NO.	FIELD NO.	ROCK DESCRIPTION	LOCALITY	COORDS	PREPS
71845	435	Dolerite	East of Ellis Rapids	LJ 895 885	POW
71846	436	Tholeiite garnet-bearing	East of Ellis Rapids	LJ 895 885	
71847	437	Dolerite	East of Ellis Rapids	LJ 895 885	
71848	438	Alkaline Lamprophyre	Brookes Hut	LJ 845 941	POW
71849	439	Dolerite - garnet-bearing	Brookes Hut	LJ 845 941	POW,PTS
71850	440	Opx-phyric tholeiite	Brookes Hut	LJ 845 941	POW
71851	441	Opx-olivine-phyric tholeiite	Brookes Hut	LJ 845 941	POW
71852	442	Opx-phyric tholeiite	Brookes Hut	LJ 845 941	POW
71853	443	Opx-phyric tholeiite	Brookes Hut	LJ 845 941	POW
71854	444	Tholeiite	Brookes Hut	LJ 845 941	POW
71855	445	Gabbroic dyke	Brookes Hut	LJ 845 941	POW
71856	446	Gabbroic dyke	Brookes Hut	LJ 845 941	
71857	447	Opx-phyric tholeiite	Brookes Hut	LJ 845 941	POW
71858	448	Tholeiite	Brookes Hut	LJ 845 941	POW
71859	449	Dolerite	Brookes Hut	LJ 845 941	POW
71860	450	Garnet-bearing tholeiite	Brookes Hut	LJ 845 941	POW
71861	451	Opx-phyric tholeiite	Brookes Hut	LJ 845 941	POW,PTS
71862	452	Tholeiite	Brookes Hut	LJ 845 941	POW
71863	453	Dolerite	Brookes Hut	LJ 845 941	POW
71864	454	Dolerite dyke	Brookes Hut	LJ 845 941	
71865	455	Alkaline Lamprophyre	Lebed Lake	LJ 865 850	POW
71866	456	Dolerite	Lebed Lake	LJ 865 850	POW,PTS
71867	457	Gabbroic dyke	Lebed Lake	LJ 865 850	POW
71868	458	Dolerite	Lebed Lake	LJ 865 850	POW
71869	459	Alkaline Lamprophyre	NE of Ekho Lake	LJ 902 965	POW
71870	460	Dolerite	NE of Ekho Lake	LJ 902 965	POW
71871	461	Alkaline Lamprophyre	NE of Ekho Lake	LJ 902 965	
71872	462	Dolerite	NE of Ekho Lake	LJ 902 965	
71873	463	Dolerite	SE of Taynaya Bay	LK 903 030	POW
71874	464	Dolerite	SE of Taynaya Bay	LK 903 030	POW,PTS
71875	465	Dolerite	SE of Taynaya Bay	LK 903 030	POW,PTS
71876	466	Homogeneous Norite	SE of Taynaya Bay	LK 903 030	POW
71877	467	Homogeneous Norite	SE of Taynaya Bay	LK 903 030	POW,PTS
71878	468	Homogeneous Norite	SE of Taynaya Bay	LK 903 030	POW,PTS
71879	469	Dolerite	SE of Taynaya Bay	LK 903 030	POW
71880	470	Dolerite	SE of Taynaya Bay	LK 903 030	POW
71881	471	Dolerite	SE of Taynaya Bay	LK 903 030	POW
71882	472	Alkaline Lamprophyre	SE of Taynaya Bay	LK 903 030	POW,PTS
71883	473	Opx-phyric dolerite	SE of Taynaya Bay	LK 903 030	POW
71884	474	Dolerite	SE of Taynaya Bay	LK 903 030	POW
71885	475	Fldsp + Qtz xenoliths in tholeiite	SE of Taynaya Bay	LK 903 030	
71886	476	Dolerite	SE of Taynaya Bay	LK 903 030	POW
71887	477	Mantle xenolith	SE of Taynaya Bay	LK 903 030	2 PTS
71888	478	Alkaline Lamprophyre	SE of Taynaya Bay	LK 903 030	POW
71889	479	Opx-phyric dolerite	SE of Taynaya Bay	LK 903 030	POW
71890	480	Rubbly Norite	SE of Taynaya Bay	LK 903 030	5 PTS
71891	481	Xenolith in tholeiitic norite	SE of Taynaya Bay	LK 903 030	2 PTS
71892	482a	Opx phyric tholeiite, link to norite	SE of Taynaya Bay	LK 903 030	POW,PTS
71893	482b	Opx phyric tholeiite, link to norite	SE of Taynaya Bay	LK 903 030	POW,PTS
71894	482c	Opx phyric tholeiite, link to norite	SE of Taynaya Bay	LK 903 030	POW,PTS
71895	483	Opx-phyric dolerite - 20 kg for dating	SE of Taynaya Bay	LK 903 030	
71896	484	Alkaline Lamprophyre	SE of Taynaya Bay	LK 903 030	POW,PTS
71897	485	Dolerite	SE of Taynaya Bay	LK 903 030	POW
71898	486	Alkaline Lamprophyre	SE of Taynaya Bay	LK 903 030	POW
71899	487	Dolerite	SE of Taynaya Bay	LK 903 030	POW
71900	488	Alkaline Lamprophyre	SE of Taynaya Bay	LK 903 030	POW
71901	489	Dolerite	SE of Taynaya Bay	LK 903 030	POW
71902	490	Dolerite	SE of Taynaya Bay	LK 903 030	POW

VESTFOLD HILLS - ANTARCTICA 1988/89

CAT. NO.	FIELD NO.	ROCK DESCRIPTION	LOCALITY	COORDS	PREPS
71903	491	Chilled margin between 71901/71902	SE of Taynaya Bay	LK 903 030	
71904	492	Dolerite	SE of Taynaya Bay	LK 903 030	POW
71905	493	Dolerite	SE of Taynaya Bay	LK 903 030	POW
71906	494	Opx-phyric dolerite	SE of Taynaya Bay	LK 903 030	POW
71907	495	Alkaline Lamprophyre	SE of Taynaya Bay	LK 903 030	POW
71908	496	Alkaline Lamprophyre	SE of Taynaya Bay	LK 903 030	POW
71909	497	Alkaline Lamprophyre + xenolith	SE of Taynaya Bay	LK 903 030	
71910	498	Dolerite	SE of Taynaya Bay	LK 903 030	POW
71911	499	Alkaline Lamprophyre	SE of Taynaya Bay	LK 903 030	POW
71912	500	Dolerite	SE of Taynaya Bay	LK 903 030	POW
71913	501	Alkaline Lamprophyre	SE of Taynaya Bay	LK 903 030	POW
71914	502	Alkaline Lamprophyre	SE of Taynaya Bay	LK 903 030	POW
71915	503	Dolerite	SE of Taynaya Bay	LK 903 030	POW
71916	504	Alkaline Lamprophyre	SE of Taynaya Bay	LK 903 030	POW
71917	505	Dolerite	SE of Taynaya Bay	LK 903 030	POW
71918	506	Dolerite	SE of Taynaya Bay	LK 903 030	POW
71919	507	Tholeiite	SE of Taynaya Bay	LK 903 030	POW
71920	508	Dolerite	SE of Taynaya Bay	LK 903 030	POW
71921	509	Opx-phyric tholeiite	SE of Taynaya Bay	LK 903 030	POW
71922	510	Dolerite	SE of Taynaya Bay	LK 903 030	POW
71923	511	Dolerite	SE of Taynaya Bay	LK 903 030	POW
71924	512	Chilled margin between 71922/71923	SE of Taynaya Bay	LK 903 030	
71925	513	Lamprophyric body	SE of Taynaya Bay	LK 903 030	POW
71926	514	Dolerite	SE of Taynaya Bay	LK 903 030	POW
71927	515	Alkaline Lamprophyre	SE of Taynaya Bay	LK 903 030	POW
71928	516	Alkaline Lamprophyre + xenolith	SE of Taynaya Bay	LK 903 030	POW
71929	517	Alkaline Lamprophyre	SE of Taynaya Bay	LK 903 030	POW
71930	518	Alkaline Lamprophyre	SE of Taynaya Bay	LK 903 030	POW
71931	519	Dolerite - fine grained	SE of Taynaya Bay	LK 903 030	POW,PTS
71932	520	Dolerite	SE of Taynaya Bay	LK 903 030	POW
71933	521	Alkaline Lamprophyre	SE of Taynaya Bay	LK 903 030	POW
71934	522	Dolerite - fine grained	SE of Taynaya Bay	LK 903 030	POW
71935	523	Alkaline Lamprophyre	SE of Taynaya Bay	LK 903 030	POW
71936	524	Alkaline Lamprophyre	SE of Taynaya Bay	LK 903 030	POW
71937	525	Dolerite	SE of Taynaya Bay	LK 903 030	POW
71938	526	Lamprophyre	SE of Taynaya Bay	LK 903 030	POW
71939	527	Alkaline Lamprophyre	SE of Taynaya Bay	LK 903 030	POW
71940	528	Alkaline Lamprophyre	SE of Taynaya Bay	LK 903 030	POW
71941	529	Alkaline Lamprophyre	SE of Taynaya Bay	LK 903 030	POW
71942	530	Alkaline Lamprophyre	SE of Taynaya Bay	LK 903 030	POW
71943	531	felsic segregation in tholeiite-20 kg for dating	SE of Taynaya Bay	LK 903 030	
71944	532	Dolerite	SE of Taynaya Bay	LK 903 030	POW
71945	533	Alkaline Lamprophyre	SE of Taynaya Bay	LK 903 030	POW
71946	534	Dolerite	SE of Taynaya Bay	LK 903 030	POW
71947	535	Opx-phyric tholeiite	SE of Taynaya Bay	LK 903 030	POW,PTS
71948	536	Opx-phyric tholeiite	SE of Taynaya Bay	LK 903 030	POW,PTS
71949	537	Opx-phyric tholeiite, link to norite	SE of Taynaya Bay	LK 903 030	POW,PTS
71950	538	Rubbly Norite	SE of Taynaya Bay	LK 903 030	POW,PTS,PGE
71951	539	Contact betw. Rubbly and Homo. Norite	SE of Taynaya Bay	LK 903 030	
71952	540	Xenolith in Rubbly Norite	SE of Taynaya Bay	LK 903 030	2 PTS
71953	541	Dolerite	SE of Taynaya Bay	LK 903 030	
71954	542	Deformed dyke (relict)	SE of Taynaya Bay	LK 903 030	
71955	543	Dolerite	SE of Taynaya Bay	LK 903 030	POW
71956	544	Alkaline Lamprophyre	SE of Taynaya Bay	LK 903 030	POW
71957	545	Dolerite	SE of Taynaya Bay	LK 903 030	POW
71958	546	Opx-phyric dolerite	SE of Taynaya Bay	LK 903 030	POW
71959	547	Dolerite	SE of Taynaya Bay	LK 903 030	
71960	548	Dolerite	SE of Taynaya Bay	LK 903 030	

VESTFOLD HILLS - ANTARCTICA 1988/89

CAT. NO.	FIELD NO.	ROCK DESCRIPTION	LOCALITY	COORDS	PREPS
71961	549	Dolerite	SE of Taynaya Bay	LK 903 030	
71962	550	Opx-phyric tholeiite	Soldat Island	LJ 845 965	POW
71963	551	Dolerite	Soldat Island	LJ 845 965	
71964	552	Dolerite	SE of Taynaya Bay	LK 903 030	POW
71965	553	Dolerite	SE of Taynaya Bay	LK 903 030	POW
71966	554	Dolerite	SE of Taynaya Bay	LK 903 030	POW
71967	555	Tholeiite	SE of Taynaya Bay	LK 903 030	POW
71968	556	Dolerite	SE of Taynaya Bay	LK 903 030	POW
71969	557	Dolerite	SE of Taynaya Bay	LK 903 030	POW
71970	558	Dolerite	SE of Taynaya Bay	LK 903 030	POW
71971	559	Rubbly Norite	SE of Taynaya Bay	LK 903 030	POW,PTS
71972	560	Dolerite dyke from norite	SE of Taynaya Bay	LK 903 030	
71973	561	Dolerite	Rybnaya Bay	LK 920 052	POW
71974	562	Dolerite	Rybnaya Bay	LK 920 052	POW
71975	563	Dolerite	Rybnaya Bay	LK 920 052	POW
71976	564	Opx-phyric tholeiite	Rybnaya Bay	LK 920 052	POW
71977	565	Dolerite	Rybnaya Bay	LK 920 052	POW
71978	566	Opx-phyric tholeiite	Rybnaya Bay	LK 920 052	POW
71979	567	Oi-phyric dolerite & sulphide	Rybnaya Bay	LK 920 052	POW
71980	568	Xenolithic dyke	Rybnaya Bay	LK 920 052	POW,PTS
71981	569	Dolerite	Rybnaya Bay	LK 920 052	POW,PTS
71982	570	Dolerite	Rybnaya Bay	LK 920 052	POW
71983	571	Augen gneiss	Rybnaya Bay	LK 920 052	
71984	572	Dolerite (coming from norite)	SE of Taynaya Bay	LK 903 030	POW
71985	573	Dolerite (same dyke as 71984)	SE of Taynaya Bay	LK 903 030	
71986	574	Rubbly Norite	Snezhnyy Bay	LK 938 060	POW,PTS,PGE
71987	575	Opx-phyric dolerite	Snezhnyy Bay	LK 938 060	POW
71988	576	Dolerite	Snezhnyy Bay	LK 938 060	POW
71989	577	Pseudotachylyte	Snezhnyy Bay	LK 938 060	
71990	578	Alkaline Lamprophyre	SE of Taynaya Bay	LK 903 030	POW,PTS
71991	579	Alkaline Lamprophyre	SE of Taynaya Bay	LK 903 030	POW,PTS
71992	580	Charnockite	Mawson		

Abbreviations: POW - rock powder for whole rock geochemistry; PTS - polished thin section; PGE - analyzed for platinum group elements.

VESTFOLD HILLS - ANTARCTICA 1989/90

CAT. NO.	FIELD NO.	ROCK DESCRIPTION	LOCALITY	COORDS	PREPS
72556	593	Dolerite	Bandits Is. W part	LK 926 075	
72557	594	Dyke 593 runs inside this one	Bandits Is. W part	LK 926 075	
72558	595	Dyke xcutting 596	Bandits Is. W part	LK 926 075	
72559	596	Dyke xcut by 595	Bandits Is. centre	LK 926 075	
72560	597	Dolerite	Bandits Is. centre	LK 926 075	
72561	598	Dolerite	Bandits Is. centre	LK 926 075	
72562	599	Dolerite	Bandits Is. centre	LK 926 075	
72563	600	Dolerite, chilled margin	Bandits Is. centre	LK 926 075	
72564	601	Same as 600, centre	Bandits Is. centre	LK 926 075	
72565	602	Youngest dyke, chilled margin	Island N of Bandits	LK 926 083	
72566	603	Same as 602, centre	Island N of Bandits	LK 926 083	
72567	604	Same as 603, coarser	Island N of Bandits	LK 926 083	
72568	605	Dolerite	Island N of Bandits	LK 926 083	
72569	606	Little vesiculated dyke	Island N of Bandits	LK 926 083	
72570	607	Dolerite, chilled margin	Bandits Is. centre	LK 926 075	
72571	608	Same as 607, centre	Bandits Is. centre	LK 926 075	
72572	609	Plagioclase layering in norite	Bandits Is. centre	LK 926 075	PTS
72573	610	Dolerite - for dating	Taynaya Bay	LK 900 020	
72574	611	Contact dyke 610 - norite, altered	Taynaya Bay	LK 900 020	
72575	612	Same as 611, not altered	Taynaya Bay	LK 900 020	
72576	613	Dolerite	Taynaya Bay	LK 900 020	
72577	614	Dolerite	Taynaya Bay	LK 900 020	
72578	615	Dolerite, 20 kg for dating	Taynaya Bay	LK 900 020	
72579	616	Dolerite, 20 kg for dating	Taynaya Bay	LK 900 020	
72580	617	Dolerite	Taynaya Bay	LK 900 020	
72581	618	Dolerite, centre	Taynaya Bay	LK 900 020	
72582	619	Dolerite, centre	Taynaya Bay	LK 900 020	
72583	620	Dolerite, centre	Taynaya Bay	LK 900 020	
72584	621	S-rich material in Rubbly Norite	Taynaya Bay	LK 900 020	
72585	622	Rubbly Norite	Taynaya Bay	LK 900 020	
72586	623	Tholeiitic dyke - 20 kg for dating	Taynaya Bay	LK 900 020	
72587	624	Alkaline dyke, centre	Taynaya Bay	LK 900 020	
72588	625	Same as 624, chilled margin	Taynaya Bay	LK 900 020	
72589	626	Tholeiitic dyke, for dating	Taynaya Bay	LK 900 020	
72590	627	Tholeiitic dyke, centre	Taynaya Bay	LK 900 020	
72591	628	Alkaline dyke, centre	Taynaya Bay	LK 900 020	
72592	629	Same as 628, chilled margin	Taynaya Bay	LK 900 020	
72593	630	Tholeiitic dyke, centre	Taynaya Bay	LK 900 020	
72594	631	Tholeiitic dyke, centre + chilled margin	Taynaya Bay	LK 900 020	
72595	632	Rubbly Norite	Taynaya Bay	LK 900 020	
72596	633	Dyke, centre	Taynaya Bay	LK 900 020	
72597	634	Same as 633, chilled margin	Taynaya Bay	LK 900 020	
72598	635	Dyke, centre + chilled margin	Taynaya Bay	LK 900 020	
72599	636	Same as 635	Taynaya Bay	LK 900 020	
72600	637	Rubbly Norite, xenoliths/sulph.-rich	Taynaya Bay	LK 900 020	
72601	638	Rubbly Norite, xenoliths/sulph.-rich	Taynaya Bay	LK 900 020	
72602	639	Rubbly Norite, xenoliths/sulph.-rich	Taynaya Bay	LK 900 020	
72603	640	Rubbly Norite, xenoliths/sulph.-rich	Taynaya Bay	LK 900 020	
72604	641	Rubbly Norite, xenoliths/sulph.-rich	Taynaya Bay	LK 900 020	
72605	642	Rubbly Norite, xenoliths/sulph.-rich	Taynaya Bay	LK 900 020	
72606	643	Rubbly Norite, xenoliths/sulph.-rich	Taynaya Bay	LK 900 020	
72607	644	Rubbly Norite, xenoliths/sulph.-rich	Taynaya Bay	LK 900 020	
72608	645	Rubbly Norite	Taynaya Bay	LK 900 020	
72609	646	Rubbly Norite/Crooket Lake Gneiss	Taynaya Bay	LK 900 020	
72610	647	Tholeiitic dyke - 20 kg for dating	Taynaya Bay	LK 900 020	
72611	648	Tholeiitic dyke - 20 kg for dating	Taynaya Bay	LK 900 020	
72612	649	Dolerite, centre	Taynaya Bay	LK 900 020	
72613	650	Dolerite	Taynaya Bay	LK 900 020	

VESTFOLD HILLS - ANTARCTICA 1989/90

CAT. NO.	FIELD NO.	ROCK DESCRIPTION	LOCALITY	COORDS	PREPS
72614	651	Xenoliths in alkaline lamprophyre	Taynaya Bay	LK 900 020	PTS
72615	652	Xenolith in gneiss	Taynaya Bay	LK 900 020	
72616	653	Dolerite, centre	Taynaya Bay	LK 900 020	
72617	654	Dolerite, centre, xcutting 653	Taynaya Bay	LK 900 020	
72618	655	Dolerite, centre, xcutting 653	Taynaya Bay	LK 900 020	
72619	656	Dolerite, centre, xcutting 659	Taynaya Bay	LK 900 020	
72620	657	Dolerite, centre	Taynaya Bay	LK 900 020	
72621	658	Dolerite, centre, same as 660	Taynaya Bay	LK 900 020	
72622	659	Dolerite, centre, xcut by 656,660,661	Taynaya Bay	LK 900 020	
72623	660	Dolerite, centre, xcutting 659	Taynaya Bay	LK 900 020	
72624	661	Dolerite dyke, inside 660	Taynaya Bay	LK 900 020	
72625	662	Dolerite, centre	Taynaya Bay	LK 900 020	
72626	663	High-Mg tholeiitic dyke, centre	Taynaya Bay	LK 900 020	
72627	664	Rubbly Norite	Taynaya Bay	LK 900 020	
72628	665	'Youngest' dolerite, chilled margin	Bandits Is.	LK 926 075	PTS
72629	666	Same as 665, 1.5m from chilled margin	Bandits Is.	LK 926 075	PTS
72630	667	Same as 665, 7m from chilled margin	Bandits Is.	LK 926 075	
72631	668	Same as 665, centre	Bandits Is.	LK 926 075	PTS
72632	669	Same as 665, 6m from chilled margin	Bandits Is.	LK 926 075	
72633	670	Same as 665, 1m from chilled margin	Bandits Is.	LK 926 075	PTS
72634	671	Same as 665, chilled margin E	Bandits Is.	LK 926 075	
72635	672	'Youngest' dolerite, chilled margin	near Ekho Lake	LJ 885 965	
72636	673	Same as 672, 1m from chilled margin	near Ekho Lake	LJ 885 965	
72637	674	Same as 672, 5m from chilled margin	near Ekho Lake	LJ 885 965	
72638	675	Same as 672, centre	near Ekho Lake	LJ 885 965	
72639	676	Same as 672, 5m from chilled margin	near Ekho Lake	LJ 885 965	
72640	677	Same as 672, 1m from chilled margin	near Ekho Lake	LJ 885 965	
72641	678	Same as 672, chilled margin	near Ekho Lake	LJ 885 965	
72642	679	'Youngest' dolerite, chilled margin	near Tassie Lake	LJ 865 945	
72643	680	Same as 679, 1m from chilled margin	near Tassie Lake	LJ 865 945	
72644	681	Same as 679, 5m from chilled margin	near Tassie Lake	LJ 865 945	
72645	682	Same as 679, centre	near Tassie Lake	LJ 865 945	
72646	683	Same as 679, 5m from chilled margin	near Tassie Lake	LJ 865 945	
72647	684	Same as 679, 1m from chilled margin	near Tassie Lake	LJ 865 945	
72648	685	Same as 679, chilled margin	near Tassie Lake	LJ 865 945	
72649	686	Dyke, margin	N of Deep Lake	LJ 855 928	
72650	687	Same as 686, centre	N of Deep Lake	LJ 855 928	
72651	688	Dolerite xcut by 690 xcutting 686,687	N of Deep Lake	LJ 855 928	
72652	689	Dolerite xcutting 687 and 687	N of Deep Lake	LJ 855 928	
72653	690	Dolerite xcutting 688,686?,687?	N of Deep Lake	LJ 855 928	
72654	691	'Youngest' dolerite, chilled margin	Deep Lake, S shore	LJ 855 915	PTS
72655	692	Same as 691, 1.5m from chilled margin	Deep Lake, S shore	LJ 855 915	PTS
72656	693	Same as 691, centre	Deep Lake, S shore	LJ 855 915	PTS
72657	694	Same as 691, 1m from chilled margin	Deep Lake, S shore	LJ 855 915	
72658	695	Same as 691, ch. marg. E	Deep Lake, S shore	LJ 855 915	
72659	696	'Youngest' dolerite, 20 kg for dating	Tryne Fjord	LK 902 005	
72660	697	Alkaline lamprophyre - for dating	Tryne Fjord	LK 902 005	
72661	698	Alkaline lamprophyre - for dating	Tryne Fjord	LK 902 005	
72662	699	Xenoliths from alkaline lamprophyre	Taynaya Bay	LK 900 020	PTS
72663	700	Rubbly Norite	Long Peninsula	LK 885 025	
72664	701	Tryne Metavolcanics	Long Peninsula	LK 885 025	
72665	702	Similar to 701	Long Peninsula	LK 885 025	
72666	703	Tryne Metavolcanics	Long Peninsula	LK 885 025	
72667	704	Tryne Metavolcanics	Long Peninsula	LK 885 025	
72668	705	Dolerite, centre	N of Rybnaya Bay	LK 910 065	
72669	706	Xenoliths in central part of 705	N of Rybnaya Bay	LK 910 065	
72670	707	Dolerite, centre	N of Rybnaya Bay	LK 910 065	
72671	708	Same as 707, chilled margin	N of Rybnaya Bay	LK 910 065	

VESTFOLD HILLS - ANTARCTICA 1989/90

CAT. NO.	FIELD NO.	ROCK DESCRIPTION	LOCALITY	COORDS	PREPS
72672	709	Dolerite, centre fine grained	N of Rybnaya Bay	LK 910 065	
72673	710	Same as 709	N of Rybnaya Bay	LK 910 065	
72674	711	Dolerite xcutting 710	N of Rybnaya Bay	LK 910 065	
72675	712	Dolerite inside a big tholeiitic one	N of Rybnaya Bay	LK 910 065	
72676	713	Dolerite xcutting 714	N of Rybnaya Bay	LK 910 065	
72677	714	Dolerite	N of Rybnaya Bay	LK 910 065	
72678	715	Dolerite xcutting 714	N of Rybnaya Bay	LK 910 065	
72679	716	Dolerite, centre	N of Rybnaya Bay	LK 910 065	
72680	717	Dolerite xcutting? 716, centre/margin	N of Rybnaya Bay	LK 910 065	
72681	718	Dolerite similar to 717	N of Rybnaya Bay	LK 910 065	
72682	719	Dolerite xcutting 718	N of Rybnaya Bay	LK 910 065	
72683	720	Xenoliths from dyke similar to 719	N of Rybnaya Bay	LK 910 065	PTS
72684	721	Dolerite, centre	N of Rybnaya Bay	LK 910 065	
72685	722	Little dyke inside Tryne Metavolcanics	N of Rybnaya Bay	LK 910 065	
72686	723	Rubbly Norite	N of Rybnaya Bay	LK 910 065	
72687	724	Dolerite, centre	N of Rybnaya Bay	LK 910 065	
72688	725	Dolerite, centre, xcutting 724	N of Rybnaya Bay	LK 910 065	
72689	726	Tryne Metavolcanics	N of Rybnaya Bay	LK 910 065	
72690	727	Dolerite, centre	N of Rybnaya Bay	LK 910 065	
72691	728	Dolerite xcutting 727	N of Rybnaya Bay	LK 910 065	
72692	729	Dolerite	N of Rybnaya Bay	LK 910 065	
72693	730	Dolerite, centre, same as 709	Long Peninsula, N	LK 915 065	
72694	731	Tryne Metavolcanics	Long Peninsula, N	LK 915 065	
72695	732	Late stage segregation in norite-for dating	Bandits Is.	LK 926 075	
72696	733	Plagioclase layering in norite	Bandits Is.	LK 926 075	
72697	734	Xenoliths from dyke	Tryne Fjord	LK 925 065	
72698	735	Allochthonous xenolith - big block	Tryne Fjord	LK 925 065	
72699	736	'Youngest' dolerite, chilled margin	Tryne Fjord	LK 925 065	PTS
72700	737	Same as 736, 1m from chilled margin	Tryne Fjord	LK 925 065	
72701	738	Same as 736, 5m from chilled margin	Tryne Fjord	LK 925 065	
72702	739	Same as 736, centre	Tryne Fjord	LK 925 065	
72703	740	Same as 736, 5m from chilled margin	Tryne Fjord	LK 925 065	
72704	741	Same as 736, 1m from chilled margin	Tryne Fjord	LK 925 065	
72705	742	Same as 736, chilled margin	Tryne Fjord	LK 925 065	

Abbreviations: POW - rock powder for whole rock geochemistry; PTS - polished thin section; PGE - analyzed for platinum group elements.

REFERENCES

- Agiorgitis G., Wolf R.* (1978) Aspects of osmium, ruthenium and iridium contents in some greek chromites. *Chem. Geol.*, 23, 267-272.
- Alibert C., Michard A., Alberede F.* (1983) The transition from alkali basalts to kimberlites: isotopes and trace element evidence from melilitites. *Contrib. Mineral. Petrol.*, 82, 176-186.
- Arndt N. T., Jenner G. A.* (1986) Crustally contaminated komatiites and basalts from Kambalda, Western Australia. *Chem. Geol.*, 56, 229-255.
- Arriens P. A.* (1975) Precambrian geochronology of Antarctica. *First Australian Geological Convention, Abstracts*, 97-98.
- Ballhaus C. G., Glikson A. Y.* (1989) Magma mixing and intraplutonic quenching in the Wingellina Hills Intrusion, Giles Complex, Central Australia. *J. Petrol.*, 30, 1443-1469.
- Ballhaus C., Berry R. F., Green D. H.* (1991) High pressure experimental calibration of the olivine-orthopyroxene-spinel oxygen geobarometer: Implications for the oxidation state of the upper mantle. *Contrib. Mineral. Petrol.*, 107, 27-40.
- Barley M. E.* (1986) Incompatible-element enrichment in Archaean basalts: a consequence of contamination by older sialic crust rather than mantle heterogeneity. *Geology*, 14, 947-950.
- Barnes S. J.* (1989) Are Bushveld U-type parent magmas boninites or contaminated komatiites? *Contrib. Mineral. Petrol.*, 101, 447-457.
- Barnes S. J., Boyd R., Korneliussen A., Nilsson L. P., Often M., Pederson R. B., Robins B.* (1988) The use of mantle normalized and metal ratios in discriminating between the effects of partial melting, crystal fractionation and sulphide segregation on platinum-group elements, gold, nickel and copper: examples from Norway. In: *H. M. Pichard, P. J. Plotts, J. F. W. Barles and S. J. Cribb, Geo-Platinum, Elsevier Applied Science*, 113-143.
- Barnes S. J., Naldrett A. J., Gorton M. P.* (1985) The origin of the fractionation of platinum-group elements in terrestrial magmas. *Chem. Geol.*, 53, 7-30.
- Barnes S. J., Often M.* (1990) Ti-rich komatiites from northern Norway. *Contrib. Mineral. Petrol.*, 105, 42-54.

- Barnes S. J. (1986) The effect of trapped liquid crystallization on cumulus mineral compositions. *Contrib. Mineral. Petrol.*, 93, 524-531.
- Basaltic Volcanism Study Project (1981) Basaltic Volcanism Study on the terrestrial planets. Pergamon Press, New York, 1286 pp.
- Basu A. R. , MacGregor I. D. (1975) Chromite spinels from ultramafic xenoliths. *Geochim. Cosmochim. Acta*, 39, 937-945.
- Bertrand P., Mercier J. C. (1985) The mutual solubility of coexisting ortho- and clinopyroxene: toward an absolute geothermometer for the natural system ? *Earth Planet. Sci. Lett.*, 76, 109-122.
- Black L. P., Kinny P. D., Sheraton J. W. (1990) A revised chronology for the Vestfold Block based on ion-probe zircon ages. *10th Australian Geological Convention, Geol. Soc. Am., Abstracts*, 25, 253-253.
- Bravo M. S., O'Hara M. J. (1975) Partial melting of phlogopite-bearing synthetic spinel- and garnet-lherzolites. *Phys. Chem. Earth*, 9, 845-854.
- Brearley M., Scarfe C. M., Fujii T. (1984) The petrology of ultramafic xenoliths from Summit Lake, near Prince George, British Columbia. *Contrib. Mineral. Petrol.*, 88, 53-63.
- Brey G. Green D. H. (1976) CO₂ solubility and solubility mechanisms in silicate melts at high pressures. *Contrib. Mineral. Petrol.*, 57, 215-221.
- Brey G. P., Green D. H. (1975) The role of CO₂ in the genesis of olivine melilitite. *Contrib. Mineral. Petrol.*, 49, 93-103.
- Brügmann G. E. (1985) Geochemistry of noble metals and lithophile elements in komatiite flows from Alexo, Canada and Gorgona, Colombia. *Ph.D. thesis, Johannes Gutenberg-Universität, Mainz, F.R.G.*, 261p.,
- Brügmann G. E., Arndt N. T., Hofmann A. W., Tobschall H. J. (1987) Noble metal abundances in komatiite suite from Alexo, Ontario, and Gorgona Island, Colombia. *Geochim. Cosmochim. Acta*, 51, 2159-2169.
- Cameron W. E., Nisbet E. G., Dietrich V. J. (1979) Boninites, komatiites and ophiolitic basalts. *Nature*, 280, 550-553.
- Campbell I. H., Naldrett A. J., Barnes S. J. (1983) A model for the origin of the platinum-rich sulfide horizons in the Bushveld and Stillwater Complexes. *J. Petrol.*, 24, 133-165.

- Campbell I. H., Turner J. S. (1985) Turbulent mixing between fluids with different viscosities. *Nature*, 313, 39-42.
- Campbell I. H., Turner J. S. (1986) The influence of viscosity in fountains in magma chambers. *J. Petrol.*, 27, 1-30.
- Canil D., Virgo D., Scarfe C. M. (1990) Oxidation state of mantle xenoliths from British Columbia, Canada. *Contrib. Mineral. Petrol.*, 104, 453-462.
- Cattell A. (1987) Enriched komatiitic basalts from Newton, Township Ontario: their genesis by crustal contamination of depleted komatiite magma. *Geol. Mag.*, 124, 303-309.
- Chauvel C., Jahn B. (1984) Nd-Sr isotope and REE geochemistry of alkali basalts from the Massif Central, France. *Geochim. Cosmochim. Acta*, 48, 93-110.
- Chyi L. L., Crocket J. H. (1976) Partition of platinum, palladium, iridium and gold among coexisting minerals from deep ore zone Srathcona Mine, Sudbury, Ontario. *Econ. Geol.*, 71, 1196-1205.
- Clague D. A., Frey F. A. (1982) Petrology and trace element geochemistry of the Honolulu Volcanics, Oahu. Implications of the oceanic mantle beneath Hawaii. *J. Petrol.*, 23, 447-504.
- Clark S. P., Ringwood A. E. (1964) Density distribution and constitution of the mantle. *Rev. Geophys.*, 2, 35-88.
- Coish R. A., Hickey R., Frey F. A. (1982) Rare earth element geochemistry of the Betts Cove ophiolite, Newfoundland: complexities in ophiolite formation. *Geochim. Cosmochim. Acta*, 46, 2117-2134.
- Collerson K. D., Arriens P. A. (1979) Rb-Sr isotope systematics in high-grade gneisses from the Vestfold Hills, East Antarctica. *J. Geol. Soc. Aust. (Abstr.)*, 26, 267-268.
- Collerson K. D., Sheraton J. W., Arriens P. A. (1983 b) Granulite facies Metamorphic conditions during the Archaean evolution and late Proterozoic reworking of the Vestfold Block, Eastern Antarctica. 6 (sixth) Australian Geological Convention, Canberra, (Abst.), 53 -54.
- Collerson K. D., Reid E., Millar D., McCulloch M. T. (1983 a) Lithological and Sr-Nd isotopic relationships in the Vestfold Block: implications for Archaean and Proterozoic crustal evolution in the East Antarctic Shield. In: Oliver, R.L., James, P.R. and Jago, J.B. (Eds.) *Antarctic Earth Science*, Australian Academy of Science, Canberra, 77-84.

- Collerson K. D., Sheraton J. W. (1986 a) Bedrock geology and crustal evolution of the Vestfold Hills. In: *Pickard, J. The Antarctic Oasis: Terrestrial Environments and History of the Vestfold Hills, chapter 2*, 21-62.
- Collerson K. D., Sheraton J. W. (1986 b) Age and geochemical characteristics of mafic dyke swarms in the Archaean Vestfold Block, Antarctica: Inferences about Proterozoic dyke emplacement in Gondwanaland. *J. Petrol.*, 27, 853-886.
- Cox K. G. (1983) The Karoo Province of Southern Africa: origin of trace element enrichment patterns. In: *Continental Basalts and Mantle Xenoliths*. C. J. Hawkesworth and M. J. Norry (Eds.), Shiva, Nantwich, 272 pp.
- Cox K. G., Duncan A. R., Bristow J. W., Taylor S. R. & Erlank A. J. (1984) Petrogenesis of the basic rocks of the Lebombo. *Spec. Pub. Geol. Soc. S. Afr.*, 13, 149-170.
- Cox K. G., Bell J. D., Pankhurst R. J. (1979) The interpretation of igneous rocks. *George Allen & Unwin (Publishers)*, pp 450.
- Crawford A. J., Baccaluva L., Serri G. (1981) Tectono-magnetic evolution on the West Philippine-Mariana region and the origin of boninites. *Earth Planet. Sci. Lett.*, 54, 346-356.
- Crocket J. H. (1981) Geochemistry of the platinum group elements. In: *Cabri L.J. (Ed.) Platinum Group Elements. Mineralogy, Geology and Exploration. Can. Inst. Min. Met. Spec. Volume*, 47-64.
- Crocket J. H., Teruta Y. (1977) Palladium, iridium and gold contents of mafic and ultramafic rocks drilled from the Mid-Atlantic Ridge, leg 37, Deep Sea Drilling Project. *Can. J. Earth Sci.*, 14, 777-784.
- Dawson J. B., Smith J. V. (1975) Chromite-silicate intergrowths in upper-mantle peridotites. *Phys. Chem. Earth*, 9, 339-350.
- Della Guista A., Princivale F., Carbonin S. (1986) Crystal chemistry of natural Cr-bearing spinels with $0.15 < Cr < 1.07$. *Neues Jahrb. Mineral. Abh.*, 155, 319-330.
- DePaolo D. J. (1981) Trace element and isotopic effects of combined wallrock assimilation and fractional crystallization. *Earth Planet. Sci. Lett.*, 53, 189-202.
- Dowty E. (1980) Crystal growth and nucleation theory and the numerical simulation of igneous crystallization. In: *Physics of magmatic processes*, R. B. Hargraves (Ed.), Princeton University Press, New Jersey, 419-485.

Drake M. J., Weill D. F. (1975) Partition of Sr, Ba, Ca, Y, Eu²⁺, Eu³⁺, and other REE between plagioclase feldspar and magmatic liquid: an experimental study. *Geochim. Cosmochim. Acta*, 39, 689-712,

Duncan A. R., Erlank A. J., Marsh J. S. (1984) Regional geochemistry of the Karoo igneous province. In: *Petrogenesis of the Volcanic Rocks of the Karoo Province*. A. J. Erlank (Ed.) *Spec. Publ. Geol. Soc. S Africa*, 13, 355-388.

Duncan R. A., Green D. H. (1980) Role of multistage melting in the formation of oceanic crust. *Geology*, 8, 22-26.

Duncan R. A., Green D. H. (1987) The genesis of refractory melts in the formation of oceanic crust. *Contrib. Mineral. Petrol.*, 96, 326-342.

Dupuy C., Dostal, J. (1984) Trace element geochemistry of some continental tholeiites. *Earth Planet. Sci. Lett.*, 67, 61-69.

Ellis D. J. (1980) Osumulite - sapphirine - quartz granulites from Enderby Land, Antarctica: P-T conditions of metamorphism, implications for garnet - cordierite equilibria and the evaluation of the deep crust. *Contrib. Mineral. Petrol.*, 74, 201-210.

Ellis D. J., Green D. H. (1985) Garnet-forming reactions in mafic granulites from Enderby-Land, Antarctica - Implications for geothermometry and geobarometry. *J. Petrol.*, 26, 633-662.

Erlank A. J. (1984) ED.: Petrogenesis of the volcanic rocks of the Karoo Igneous Province. *Spec. Pub. Geol. Soc. S. Afr.*, 13, 395 pp.

Erlank A. J., Waters F. G., Hawkesworth C. J., Haggerty S. E., Allsopp H. L., Rickard R. S., Menzies M. A. (1987) Evidence for mantle metasomatism in peridotite nodules from the Kimberley pipes, South Africa. In: C.J. Hawkesworth and Menzies (Eds.), *Mantle Metasomatism*, Academic Press, 472 pp.

Ewart A., Bryan W. B., Gill J. B. (1973) Mineralogy and geochemistry of the younger volcanic islands of Tonga, SW Pacific. *J. Petrol.*, 14, 3, 429-465.

Ewart A., Taylor S. R. (1969) Trace element geochemistry of the rhyolitic volcanic rocks, Central North Island, New Zealand. Phenocryst data. *Contrib. Mineral. Petrol.*, 22, 127-146.

Fabries J. (1979) Spinel-olivine geothermometry in peridotites from ultramafic complexes. *Contrib. Mineral. Petrol.*, 69, 329-36.

- Falloon T. J., Green D. H. (1987) Anhydrous partial melting of MORB pyrolite and other peridotite compositions at 10 kbar: Implications for the origin of primitive MORB glasses. Mineral. Petrol., 37, 181-219.*
- Falloon T. J., Green D. H. (1988) Anhydrous partial melting of peridotite from 8 to 35 kb and the petrogenesis of MORB. J. Petrol., Special Lithosphere Issue, 379-414.*
- Faust G. T. (1936) The fusion relations of iron-orthoclase. Am. Mineral., 21, 735-763.*
- Federov L. V., Ravich M., Hofmann J. (1982) Geological comparison of southeastern peninsular India and Sri Lanka with a part of East Antarctica (Enderby Land, Mac Robertson Land and Princess Elizabeth Land). In: Caddock, C (Ed.) Antarctic Geoscience Univ. Wisconsin Press, Madison, 552 pp.*
- Fisk M. R. (1986) Basalt magma interaction with harzburgite and the formation of high-magnesian andesites. Geophys. Res. Lett., 13, 467-470.*
- Flower M. F. J. (1971) Evidence for the role of phlogopite in the genesis of alkali basalt. Contrib. Mineral. Petrol., 32, 126-137.*
- Foley S. E., Venturelli G., Green D. H., Toscani L. (1987) The ultrapotassic rocks: characteristics, classification and constraints for petrogenetic models. Earth Sci. Rev., 24, 81-134.*
- Foley S. F. (1986) The genesis of lamproitic magmas in a reduced, fluorine-rich mantle. In: Fourth International Kimberlite Conference, Abstract, 16, 173-175.*
- Francis D. (1987) Mantle-melt interaction recorded in spinel lherzolite xenoliths from the Alligator Lake volcanic complex, Yukon, Canada. J. Petrol., 28, 569-597.*
- Frey F. A., Green D. H. (1974) The mineralogy, geochemistry and origin of lherzolite inclusions in Victorian basanites. Geochim. Cosmochim. Acta, 38, 1023-1059.*
- Frey F. A., Green D. H., Roy S. D. (1978) Integrated models of basalt petrogenesis: a study of quartz tholeiites to olivine melilitites from South Eastern Australia utilizing geochemical experimental petrological data. J. Petrol., 19, 3, 463-513.*
- Fujii T., Scarfe C. M. (1982) Petrology of ultramafic nodules from West Kettle River, near Kelowna, southern British Columbia. Contrib. Mineral. Petrol., 80, 297-306.*

- Furnes H., Pedersen R. B., Maaløe S. (1986) Petrology and geochemistry of spinel peridotite nodules and host basalt, Vertspitsbergen. *Norsk Geol Tidssk*, 66, 53-68.
- Garrison J. R. jr, Taylor L. A. (1981) Petrogenesis of pyroxene-oxide intergrowths from kimberlite cumulate rocks: co-precipitation or exsolution? *Am. Mineral.*, 66, 723-740.
- Gast P. W. (1968) Trace element fractionation and the origin of tholeiitic and alkaline magma types. *Geochim. Cosmochim. Acta*, 32, 1057-1086.
- Glikson A. Y. (1983) Geochemistry of Archaean tholeiitic basalt and high-Mg to peridotite komatiite suites, with petrogenetic implications. *Mem. Geol. Soc. India*, 4, 183-219.
- Goode A. D. T., Moore A. C. (1975) High pressure crystallization of the Ewarara, Kalka and Gosse Pile Intrusions, Giles Complex, Central Australia. *Contrib. Mineral. Petrol.*, 51, 77-97.
- Green D. H. (1971) Composition of basaltic magmas as indicators of conditions of origin: application to oceanic volcanism. *Phil. Trans. R. Soc. London*, 268, 707-25.
- Green D. H., Hibberson W. O., Jaques A. L. (1979) Petrogenesis of mid-ocean ridge basalts. In: McElhinny, M.W. (Ed.), *The Earth: Its origin, structure and evolution*, London, Academic Press, 265-290.
- Green D.H., Hibberson W. (1970) The stability of plagioclase in peridotite at high pressure. *Lithos*, 3, 209-221.
- Green D. H. (1970) The origin of basaltic and nephelinitic magmas. *Leicester Literary & Philosophical Soci. Trans. Leicester Lit. Phil. Soc.*, 64, 28-54.
- Green D. H. (1981) Petrogenesis of Archaean ultramafic magmas and implications for Archaean tectonics. In: Kroner, A. *Precambrian Plate Tectonics*. Elsevier:, 469-489.
- Green D. H., Ringwood A. E. (1967) The genesis of basaltic magmas. *Contrib. Mineral. Petrol.*, 15, 103-190.
- Griffin W. L., Wass S. Y., Hollis J. D. (1984) Ultramafic xenoliths from Bullenmerri and Gnotuk Maars, Victoria, Australia. Petrology of a sub-continental crust-mantle transition. *J. Petrol.*, 25, 53-87.
- Gutmann J. T. (1986) Origin of four- and five-phase ultramafic xenoliths from Sonora, Mexico. *Am. Mineral.*, 71, 1076-1084.

- Hamlyn P. R., Keays R. P. (1986) Sulfur saturation and second stage-melts: Applications to the Bushveld platinum metal deposits. *Econ. Geol.*, 81, 1431-1445.
- Hamlyn P. R., Keays R. R., Cameron W. E., Crawford A. J. & Waldron H. M. (1985) Precious metals in magnesian low-Ti lavas: implications for metallogenesis and sulfur saturation in primary magmas. *Geochim. Cosmochim. Acta*, 49, 1797-1811.
- Hanson G. N. (1980) Rare earth elements in petrogenetic studies of igneous systems. *Annu. Rev. Earth Planet. Sci. Lett.*, 40, 203-219.
- Hanson G. N. (1977) Evolution of the sub-oceanic mantle. *J. Geol. Soc. London*, 134, 235-253.
- Haughton D. R., Roeder P. L., Skinner B. J. (1974) Solubility of sulfur in mafic magmas. *Econ. Geol.*, 69, 457-467.
- Hart S. R., Davis K. E. (1978) Nickel partitioning between olivine and silicate melt. *Earth Planet. Sci. Lett.*, 40, 203-219.
- Harte B. (1983) Mantle peridotites and processes - the kimberlite sample. In: Hawkesworth and M.J. Norry (Eds.). *Continental basalts and mantle xenoliths*, Shiva, Nantwich., 46-91.
- Helz R. T. (1987) Differentiation behavior of Kilauea Iki lava lake, Kilauea volcano, Hawaii: An overview of past and current work. *The Geochem. Soc., Special Publication*, 1, 241-258.
- Hertogen J., Janssen M. J., Palme H. (1980) Trace elements in ocean ridge basalt glasses: implications for fractionation during mantle evolution and petrogenesis. *Geochim. Cosmochim. Acta*, 44, 2125-2143.
- Herz N. (1951) Petrology of the Baltimore gabbro, Maryland. *Geol. Soc. Am. Bull.*, 62, 979-1016.
- Herzberg C. T. (1978) The bearing of phase equilibria in simple and complex systems on the origin and evolution of some well-documented garnet-websterites. *Contrib. Mineral. Petrol.*, 66, 375-382.
- Hickey R. L., Frey F. A. (1982) Geochemical characteristics of boninite series volcanics: implications for their source. *Geochim. Cosmochim. Acta*, 46, 2099-2115.
- Hill R., Roeder P. L. (1974) The crystallisation of spinel from basaltic liquid as a function of oxygen fugacity. *J. Geol.*, 82, 709-29.

- Hoek J. D. (1991) A classification of dyke-fracture geometry with examples of Precambrian dyke swarms in the Vestfold Hill, Antarctica. *Geologische Rundschau*, (in press),
- Horne R. R., Thompson M. R. A. (1967) Post-Aptian camptonite dykes in SE Alexander Island. *Bulletin British Antarctic Survey.*, 14, 15-24.
- Huppert H. E., Sparks R. S. J., Arndt N. T. (1985) Reply to contaminated komatiites. *Nature*, 313, 247-248
- Huppert H. E., Sparks R. S. J. (1985) Cooling and contamination of mafic and ultramafic magmas during ascent through continental crust. *Earth Planet. Sci. Lett.*, 74, 371-386.
- Irvine T. N. (1967) Chromian spinel as a petrogenetic indicator. *Part 2 Petrologic applications: Canad. J. Earth Sci.*, 4, 71-103.
- Irvine T. N. (1980) Magmatic infiltration metasomatism, double-diffusive fractional crystallisation, and adcumulus growth in the Muskox intrusion and other layered intrusions. *in: Hargraves R.B. (Ed.) Physics of Magmatic Processes. Princeton: Princeton University Press*, 325-83.
- Jackson E. D., Shaw H. R. (1975) Stress field in central portions of the Pacific plate, delineated in time by linear volcanic chains. *J. Geophys. Res.*, 80, 1861-1874.
- James P.R., Tingey R. J. (1983) The precambrian geological evolution of the East Antarctic metamorphic shield - a review. *In: Oliver, R.L., James, P.R., Jago, J.B. (Eds.): Antarctic Earth Science, Australian Academy of Science*, 5-10.
- Jaques A. L., Lewis J. D., Smith C. B. (1986) The kimberlites and lamproites of Western Australia. *Geol. Surv. West. Aust. Bull.*, 132, pp 268.
- Jaques A. L., O'Neill H. St. C., Smith C. B., Moon J., Chappell B. W. (1990) Diamondiferous peridotite xenoliths from the Argyle (Ak 1) Lamproite pipe, Western Australia. *Contrib. Mineral. Petrol.*, 104, 255-276.
- Jaques A. L., Green D. H. (1979) Determination of liquid compositions in high-pressure melting of peridotite. *Am. Mineral.*, 64, 1312-1321.
- Jaques A. L., Green D. H. (1980) Anhydrous melting of peridotite at 0-15 kb pressure and the genesis of tholeiitic basalts. *Contrib. Mineral. Petrol.*, 73, 287-310.
- Jones A. P., Smith J. V., Dawson J. B. (1983) Glasses in mantle xenoliths from Olmani, Tanzania. *J. Geol.*, 91, 167-178.

- Kadmina I. N., Kurumin R. G., Masolov V. N., Grilurov, G. E. (1983) Antarctic crustal structure from geophysical evidence: a review. In: Oliver, R. L., James, P. R. & Jago J. B. (Eds.): *Antarctic Earth Science*, 498-502.
- Kalsbeck F., Taylor P. N. (1986) Chemical and isotopic homogeneity of a 400 km long basic dyke in central west Greenland. *Contrib. Mineral. Petrol.*, 93, 439-448.
- Keays R. R. (1982) Palladium and irridium in kamatiites and associated rocks, application to petrogenetic problems. In: N.T. Arndt and E.G. Nisbet (Eds.), *Komatiites*, Allen, London, pp 435-438.
- Keays R. R., Campbell I. H. (1981) Precious metals in the Jimberlana Intrusion, Western Australia. Implications for genesis of platiniferous ores in layered intrusions. *Econ. Geol.*, 76, 1118-1141.
- Kelemen P. B., Johnson K. T. M., Kinzler R. J., Irving A. J. (1990) High-fiel-strength element depletions in arc basalts due to mantle-magma interaction. *Nature*, 345, 521-524.
- Kinny P. D., Black L. P. (1990) Zircon ages and the distribution of Archaean and Proterozoic rocks in the Rauer Islands. *10th Australian Geological Convention, Geological Society of Australia, Abstracts*, 25, 251-251.
- Klemm D. D. (1965) Synthesen und Analysen in den Dreiecksdiagrammmen FeAsS - CoAsS - NiAsS und FeS₂ - CoS₂ - NiS₂. *Neues Jahrbuch Mineralogische Abhandlungen*, 103, 3, 205-255.
- Kretz R. (1982) Transfer and exchange equilibria in a portion of the pyroxene quadrilateral as deduced from natural and experimental data. *Geochim. Cosmochim. Acta*, 46, 411-421.
- Kuehner S. M. (1987) Mafic dykes of the East Antarctic Shield: a note on the Vestfold Hills and Mawson Coast occurrences. In: *Mafic Dyke swarms*. H. C. Hall and W. F. Fahrig (Eds.), *Geological Association of Canada, Special Paper*, 34, 429-430.
- Kuehner S. M. (1989) Petrology and Geochemistry of early Proterozoic high-Mg dykes from the Vestfold Hills, Antarctica. In: A. R. Crawford (Ed.), *Boninites and related Rocks*, Unwin Hyman, London, 208-231.
- Kuehner S. M. (1986) Mafic dykes in the East Antarctic shield: experimental, geochemical and petrological studies focusing on the Proterozoic evolution of the crust and mantle. *Unpubl. Ph. D. Thesis, University of Tasmania, Hobart*.

- Kurat G., Palme H., Spettel B., Baddenhausen H., Hofmeister H., Palme C., Wänke H. (1980) Geochemistry of ultramafic xenoliths from Kufstein, Austria: evidence from a variety of upper mantle processes. *Geochim. Cosmochim. Acta*, 44, 45-60.
- Kushiro I., Yoder H. S., Mysen B. O. (1976) Viscosities of basalts and andesite melts at high pressures. *J. Geophys. Res.*, 81, 6351-6356.
- Kyser T. K., O'Neil J. R., Carmichael I. S. W. E. (1981) Oxygen isotope thermometry of basic lavas and mantle nodules. *Contrib. Mineral. Petrol.*, 77, 11-23.
- Langmuir C. H. (1980) A major and trace element approach to basalts. Unpublished Ph.D. thesis, State University of New York at Stony Brook. 330 pp.
- Le Bas M. J., Le Maitre R. W., Streckeisen A., Zanettin A. (1986) A chemical classification of volcanic rocks based on the total alkali silica diagram. *J. Petrol.*, 27, 745-750.
- Le Maitre R. W. (1980) GENMIX: a new generalized petrological mixing program. *Contrib. Mineral. Petrol.*, 71, 133-137.
- Le Roex A. P. (1980) Geochemistry and mineralogy of Atlantic Ocean basalts. *Unpubl. Ph D thesis, University of Cape Town.*
- Lindsley D. H. (1983) Pyroxene thermometry. *Am. Mineral.*, 68, 4779-493.
- Lofgren G. (1980) Experimental studies on the dynamic crystallization of silicate melts. In: *Physics of Magmatic Processes*, R. B. Hargraves (Ed.), Princeton University Press, New Jersey, 487-551.
- Lofgren G. E. (1983) Effect of heterogeneous Nucleation on basaltic textures: a dynamic crystallization study. *J. Petrol.*, 24, 3, 229-255.
- Longhi J., Wooden J. L., Coppinger K. D. (1983) The petrology of high-Mg dikes from the Beartooth Mountains, Montana: a search for the parent magma of the stillwater complex. *J. Geophys. Res.*, 88, B 53-89.
- Maaløe S. (1987) The generation of feeder dykes from mantle sources. *Contrib. Mineral. Petrol.*, 96, 47-55.
- MacGregor A. G. (1931) Clouded feldspars and thermal metamorphism. *Min. Mag.*, 22, 524-538.
- MacGregor I. D., Basu A. R. (1974) Thermal structure of the lithosphere: A petrologic model. *Science*, 185, 1007-1011.

- MacGregor I. D., Basu A. R. (1974) Thermal structure of the lithosphere: A petrologic model. *Science*, 185, 1007-1011.
- MacKenzie W. S., Donaldson C. H., Guilford C. (1982) Atlas of igneous rocks and their textures. *Longman*, 148 pp.
- Marsh B. (1987) Magmatic processes. *Reviews of Geophysics*, 25, 5, 1043-1053.
- Mason R. A. (1982) Trace element distribution between the perthite phase of alkali feldspars from pegmatites. *Mineral. Mag*, 45, 101-106.
- Masuda A., et al (1973) Fine structures of mutually normalized rare-earth patterns of chondrites. *Geochim. Cosmochim. Acta*, 37, 239-248.
- Matsui Y., Nishizawa O. (1974) Iron (II)-magnesium exchange equilibrium between olivine and calcium free pyroxene over a temperature range of 800° C to 1300° C. *Bull. Soc. fr. Mineral. Cristallogr.*, 97, 122-130.
- Mc Callum I. S. (1987) Petrology of the igneous rocks. *Rev. Geophys.*, 25, 5, 1021-1042.
- McBirney A.R., Noyes R.M. (1979) Crystallization and layering of the Skaergaard intrusion. *J. Petrol.*, 20, 487-554.
- McGuire A. V. (1988) Petrology of mantle xenoliths from Harrat al Kishb: The mantle beneath Western Saudi Arabia. *J. Petrol.*, 29, 1, 73-92.
- McKenzie D. (1984) The generation and compaction of partially molten rock. *J. Petrol.*, 25, 3, 713-765.
- McLeod J. R., Harding R. R. (1967) Age of dolerite dykes in the Vestfold Hills, Antarctica. *Nature*, 215, 149-151.
- Menzies M. (1983) Mantle ultramafic xenoliths in alkaline magmas: Evidence for mantle heterogeneity modified by magmatic activity. In C.J. Hawkesworth and M.J. Norry (Eds.), *Continental basalts and mantle xenoliths*. Shiva, Nantwich, 92-110.
- Mercier J-C. C., Carter N. L. (1975) Pyroxene geotherms. *J. Geophys. Res.*, 80, 3349-3362.
- Mikhalsky E. V., Andronokov A. V. (1990) Petrology of late Proterozoic alkaline lamprophyres of Vestfold Block, East Antarctica. *Second International Dyke Conference, Mafic Dykes and Emplacement Mechanisms, Abstracts*, 28.

- Mitchell R. H., Platt R. G. (1982) Mineralogy and petrology of nepheline syenites from the Coldwell Alkaline Complex, Ontario, Canada. *J. Petrol.*, 23, 2, 186-214.
- Moore J.G., Fabbi B. (1971) An estimate of the juvenile sulfur content of basalts. *Contrib. Mineral. Petrol.*, 33, 118-127.
- Mori T., Green D. H. (1978) Laboratory duplication of phase equilibria observed in natural garnet lherzolite. *J. Geol.* 86, 83-97.
- Morten L. (1979) Sialic, mafic and ultramafic inclusions and megacrysts in basaltic rocks from M. Lessini, Veneto Region, North Italy. *Period. Miner.*, 48, 75-91.
- Morten L., Taylor L. A., Durazzo A. (1989) Spinel in harzburgite and lherzolite inclusions from the San Giovanni ilarione quarry, Lessini Mountains, Venete Region, Italy. *Mineral. Petrol.*, 40, 73-89.
- Naldrett A. J. (1981) Platinum-group element deposits. *Can. Inst. Min. Metall., Spec. Iss.*, 23, 197-232.
- Naldrett A. J. (1989) Magmatic sulfide deposits. A. J. Naldrett (Ed.) Oxford University Press, 186 pp.
- Naldrett A. J., Barnes S. J. (1986) The fractionation of platinum-group elements with special reference to the composition of sulphide ores. *Fortsch. Mineral. Petrol.*, 64, 113-133.
- Naldrett A. J., Duke J. M. (1980) Pt metals in magmatic sulfide ores; the occurrence of these metals is discussed in relation to the formation and importance of these ores. *Science*, 208, 1417-1424.
- Naldrett A. J., Hoffmann E. L., Green A. H., Chou C. L., Naldrett S. R. (1979) The composition of Ni-sulfide ores with particular reference to their content of PGE and An. *Canad. Mineral.*, 17, 403-415.
- Naldrett A. J., Turner A. R. (1977) The geology and petrogenesis of a greenstone belt and related nickel sulfide mineralisation at Yakabindie, Western Australia. *Precambrian Research*, 5, 43-103.
- Nesbitt R. W. (1971) Skeletal crystal forms in the ultramafic rocks of the Yilgarn Block, Western Australia: evidence for an Archaean ultramafic liquid. *Spec. Publs. Geol. Soc. Australia*, 3, 331-347.

- Nickel K. G., Green D. H. (1985) Experimental geothermobarometry for garnet peridotites and implications for the nature of the lithosphere, kimberlites and diamonds. *Earth and Planet. Sci. Lett.*, 73, 158-170.
- Nisbet E. G., Bickel M. J., Martin A. (1977) The mafic and ultramafic lavas of the Belingwe Greenstone Belt, Rhodesia. *J. Petrol.*, 18, 521-566.
- Norrish K, Chappell B. W. (1977) X-ray fluorescence spectrometry. in: Zussman J. (Ed.) *Physical Methods of Determinative Mineralogy*, Academic Press, 201-272.
- Norrish K, Hutton J. T. (1969) An accurate X-ray spectrographic method for the analysis of a wide range of geological samples. *Geochim. Cosmochim. Acta*, 33, 431-453.
- O'Hara M. J. (1977) Thermal history of excavation of Archaean gneisses from the base of the continental crust. *J. Geol. Soc. Lond.*, 134, 185-200.
- O'Neill H. St. C., Wall V. J. (1987) The olivine-orthopyroxene-spinel oxygen geobarometer, the nickel precipitation curve and the oxygen fugacity of the earth's upper mantle. *J. Petrol.*, 28, 1169-91.
- Oliver R. L., James P. R., Collerson K. D., Ryan A. B. (1982) Precambrian Geological relationships in the Vestfold Hills, Antarctica. In: Craddock, C. (Eds.), *Antarctic Geoscience: University of Wisconsin Press, Madison, Wis., U.S.A.*, 435-444.
- Ozawa K. (1983) Evaluation of olivine - spinel geothermometry as an indicator of thermal history for peridotites. *Contrib. Mineral. Petrol.*, 82, 52-65.
- Parker A. J., James P. R., Mielnik V. and Oliver R. L. (1983) Structure, fabric development and metamorphism in Archaean gneisses of the Vestfold Hills, East Antarctica. In: R.L. Oliver, P.R. James and J.B. Jago (Eds.), *Antarctic Earth Science. Aust. Acad. Sci., Canberra*, 85-90.
- Parsons I., Butterfield A. W. (1981) Sedimentary features of the Nunarssuit and Klokken syenites, S. Greenland. *J. Geol. Soc. Lond.*, 138, 289-306.
- Passchier C. W., Hoek J. D., Bekendam R. F., De Boorder H. (1990) Ductile reactivation of Proterozoic brittle fault rocks; an example from the Vestfold Hills, East Antarctica. *Precambrian Research*, 47, 3-16.
- Poldervaart A., Gilkey A. K. (1954) On clouded plagioclase. *Am. Mineral.*, 39, 75-91.

- Preß S., Witt G., Seck H. A., Eonov D., Kovalenko V. L. (1986) Spinel peridotite xenoliths from the Tariat depression, Mongolia. I: Major element chemistry and mineralogy of primitive mantle xenolith suite. *Geochim. Cosmochim. Acta*, 50, 2587-2599.
- Ravich M. G., Solov'ev D. S., Federov L. V. (1985) Geological structure of MacRobertson Land. *Russian Translation Series, No. 24, Rotterdam: Balkema*, pp 247.
- Redman B. A., Keays R. R. (1985) Archaean basic volcanism in the Eastern Goldfields Province, Yilgarn Block, Western Australia. *Precambrian Res.*, 30, 113-152.
- Reid A. M., Donaldson C. H., Brown R. W., Ridley W. I., Dawson J. B. (1975) Mineral chemistry of peridotite xenoliths from the Lashain volcano, Tanzania. *Phys. Chem. Earth*, 9, 525-543.
- Ribe N. M. (1985) The generation and compaction of partial melts in the Earth's mantle. *Earth Planet. Sci. Lett.*, 73, 361-376.
- Richter F. M. (1986) Simple models for trace element fractionation during melt segregation. *Earth Planet. Sci. Lett.*, 77, 323-344.
- Robinson P., Higgins N. C., Jenner G. A. (1986) Determination of rare-earth elements, Yttrium and Scandium rocks by an ion exchange-X-R fluorescence technique. *Chem. Geol.*, 55, 121-137.
- Rock N. M. S. (1984) The nature and origin of calc-alkaline lamprophyres: minettes, vogesites, kersantites and spessartites. *Trans. R. Soc. Edinb.*, 74, 193-227.
- Rock N. M. S. (1986) The nature and origin of ultramafic lamprophyres: alnöites and allied rocks. *J. Petrol.*, 27-1, 155-196.
- Rock N. M. S. (1987) The nature and origin of lamprophyres: an overview. In: *Fitton, J.G & Upton, B.G.J (Eds.). Alkaline Igneous Rocks, Geological Society Special Publication*, 30, 191-226.
- Rock N. M. S. (1987) The need for standardization of normalized multi-element diagrams in geochemistry: a comment. *Geochem. Journal*, 21, 75-84.
- Roeder P. L., Campbell I. H., Jamieson H. E. (1979) A re-evaluation of the olivine-spinel thermometer. *Contrib. Mineral. Petrol.*, 68, 325-34.
- Roeder P. L., Emslie R. F. (1970) Olivine-liquid equilibrium. *Contrib. Mineral. Petrol.*, 29, 275-289.

- Rosenqvist I. Th.* (1951) Investigations in the crystal chemistry of silicates. III. The relation haematite-microcline. *Norsk. Geol. Tidsskr.*, 29, 65-76.
- Rutter M. J.* (1987) The nature of lithosphere beneath the Sardinian continental block: mantle and deep crustal inclusions in mafic alkaline lavas. *Lithos*, 20, 225-234.
- Sachtleben T., Seck H. A.* (1981) Chemical control of Al-solubility in orthopyroxene and its implications on pyroxene geothermometry. *Contrib. Mineral. Petrol.*, 78, 157-65.
- Sack R. O., Walker D., Carmichael I. S. E.* (1987) Experimental petrology of alkali lavas: constraints on cotectics of multiple saturation in natural basic liquids. *Contrib. Mineral. Petrol.*, 96, 1-23.
- Shand S. J.* (1945) Coronas and coronites. *Geol. Soc. Am., Bull.*, 56, 247-266.
- Shaw D. M.* (1970) Trace element fractionation during anatexis. *Geochim. Cosmochim. Acta*, 34, 237-243.
- Sheraton J. W.* (1983) Geochemistry of mafic igneous rocks of the Northern Prince Charles Mountains, Antarctica. *J. Geol. Soc. Australia*, 30, 295-304.
- Sheraton J. W., Black L. P.* (1988) Chemical evolution of granitic rocks in the East Antarctic Shield, with particular reference to post-orogenic granites. *Lithos*, 21, 37-52.
- Sheraton J. W., Black L. P., McCulloch M. T., Oliver R. L.* (1990) Age and origin of a compositionally varied mafic dyke swarm in the Bunger Hills, East Antarctica. *Chem. Geol.*, 85, 215-246.
- Sheraton J. W., Black, L. P., McCulloch, M. T.* (1984) Regional geochemical and isotopic characteristics of high - grade metamorphics of the Prydz Bay Area: the existent of proterozoic reworking of archaean continental crust in East Antarctica. *Precambrian Research*, 26, 169-198.
- Sheraton J. W., Collerson K. D.* (1984) Geochemical evolution of Archaean granulite-facies gneisses in the Vestfold Block and comparisons with other Archaean gneiss complexes in the East Antarctic Shield. *Contrib. Mineral. Petrol.*, 87, 51-64.
- Sheraton J. W., Cundari A.* (1980) Leucitites from Gaussberg, Antarctica. *Contrib. Mineral. Petrol.*, 71, 417-427.
- Sheraton J. W., England R. U.* (1980) Highly potassic dykes from Antarctica. *J. Geol. Soc. Australia*, 27, 129-135.

- Sheraton J. W., Black L. P.* (1981) Geochemistry and geochronology of proterozoic tholeiite dykes of East Antarctica: Evidence for mantle metasomatism. *Contrib. Mineral. Petrol.*, 78, 305-317.
- Sheraton J. W., Collerson K.D.* (1983) Archaean and Proterozoic geological relationships in the Vestfold Hills - Prydz Bay area, Antarctica. *BMR J. Australian Geol. Geophys.*, 8, 119-128.
- Sigurdsson H., Schilling J. G.* (1976) Spinel in mid-atlantic ridge basalts: chemistry and occurrence. *Earth Planet. Sci. Lett.*, 29, 7-20.
- Skinner B. J., Luce F. D., Dill J. A., Ellis P. E., Hagan H. A., Lewis D. M., Odell D. A., Sverjensky D. A. & Williams N.* (1976) Phase relationships in ternary portions of the system Pt-Pd-Fe-As-S. *Econ. Geol.*, 71, 1469-1475.
- Smith J. V.* (1983) Some chemical properties of feldspars. In: *Feldspar Mineralogy*, *Ribbe, P.H., (Ed.), Reviews in Mineralogy Vol. 2*, 281-296.
- Sparks R. S. J., Pinkerton H., MacDonald R.* (1977) The transport of xenoliths in magmas. *Earth Planet. Sci. Lett.*, 35, 234-238.
- Spera F. J.* (1980) Aspects of magma transport. in: *Hargreaves R.B. (Ed.), Physics of Magmatic Processes. Princeton University Press, Princeton NJ.*, pp 265-232.
- Stolz A. J., Davies G. R.* (1988) Chemical and isotopic evidence from spinel lherzolite xenoliths for episodic metasomatism of the upper mantle beneath Southwest Australia. *J. Petrol., Spec. Lithosphere Issue*, 303-330.
- Sun S.-S.* (1980) Lead isotopic study of young volcanic rocks from mid-ocean ridges, ocean islands, and island arcs. *Phil. Trans R. Soc. London, Ser. A.*, 297, 409-45.
- Sun S.-S., Nesbitt R. W.* (1978) Petrogenesis of Archaean ultrabasic and basic volcanics: evidence from rare earth elements. *Contrib. Mineral. Petrol.*, 65, 301-325.
- Sun S.-S., Nesbitt R. W., McCulloch M. T.* (1989) Geochemistry and petrogenesis of archaean and early proterozoic siliceous high magnesian basalts. In: *Crawford A. (Ed.) Boninites and related rocks. Allen and Unwin.*, pp 148-173.
- Takahashi E.* (1980) Melting relations on alkali-olivine basalt to 30 kbar and their bearing on the origin of alkali basaltic magmas. *Carnegie Inst. Washington Yearbook*, 79, 271-276.

- Taylor S. R., Gorton M. K. (1977) Geochemical application of spark-source mass spectrometry. III: element sensitivity, precision and accuracy. *Geochim. Cosmochim. Acta*, 41, 1375-1380.
- Ueda A., Sakai H. (1984) Sulfur isotope study of Quaternary volcanic rocks from the Japanese islands arc. *Geochim. Cosmochim. Acta*, 48, 1837-1848.
- Wager L. R., Brown G. M., Wadsworth W. I. (1960) Types of igneous cumulates. *J. Petrol.*, 1, 1, 73-85.
- Wass S. Y. (1973) Plagioclase-spinel intergrowths in alkali basaltic rocks from the Southern Highlands, N.S.W. *Contrib. Mineral. Petrol.*, 38, 167-175.
- Weaver B. L., Tarney J. (1981) The Scourie Dyke Suite: Petrogenesis and geochemical nature of the Proterozoic sub-continental mantle. *Contrib. Mineral. Petrol.*, 78, 175-188.
- Weaver B. L., Wood D. A., Tarney J., Joron J. L. (1987) Geochemistry of ocean island basalts from the South Atlantic: Ascensio, Bouvet, St. Helena, Gough and Tristan da Cunha. In: Fitton J.G. & Upton B.G.J. (Eds.). *Alkaline Igneous Rocks. Geol. Soc. Spec. Publ.*, 30, 253-267.
- Wellman P., Tingey R. J. (1976) Gravity evidence for a major crustal fracture in east Antarctica. *BMR (Bur. Mineral. Resour.) J. Aust. Geol. Geophys.*, 1, 105-108.
- Wells P. R. A. (1977) Pyroxene thermometry in simple and complex systems. *Contrib. Mineral. Petrol.*, 62, 129-139.
- Whitney P. R. (1972) Spinel inclusions in plagioclase of meta-gabbros from the Adirondack Highlands. *Am. Mineral.*, 57, 1429-1436.
- Winterburn P. A., Harte B., Gurney J. J. (1990) Peridotite xenoliths from the Jagerfontein kimberlite pipe: I. Primary and primary metasomatic mineralogy. *Geochim. Cosmochim. Acta*, 54, 329-341.